EMERGING INFECTIOUS DISEASES®

CDC
Centers for Disease Control and Prevention

Coronavirus

September 2020

Artist Unknown. Relief showing Helios, sun god in the Greco-Roman mythology (detail) (c.390 BCE). Marble. 33.8 in × 33.9 in × 8 5/8 in/85.8 cm × 86.3 cm. From Wikimedia Commons. Holding institution: Pergamon-Museum, Berlin, Germany.

EMERGING INFECTIOUS DISEASES®

Emerging Infectious Diseases is published monthly by the Centers for Disease Control and Prevention, 1600 Clifton Rd NE, Mailstop H16-2, Atlanta, GA 30329-4027, USA. Telephone 404-639-1960; email, eideditor@cdc.gov

EMERGING INFECTIOUS DISEASES®

Coronaviruses **September 2020**

On the Cover

Artist Unknown. Relief showing Helios, sun god in the Greco-Roman mythology (detail) (c.390 BCE). Marble. 33.8 in × 33.9 in × 8 5/8 in/85.8 cm × 86.3 cm. From Wikimedia Commons. Holding institution: Pergamon-Museum, Berlin, Germany.

About the Cover p. 2304

Perspectives

Synopses

Research

Dispatches

EMERGING INFECTIOUS DISEASES®
September 2020

EMERGING INFECTIOUS DISEASES®
September 2020

Research Letters

Comment Letters

About the Cover

Etymologia

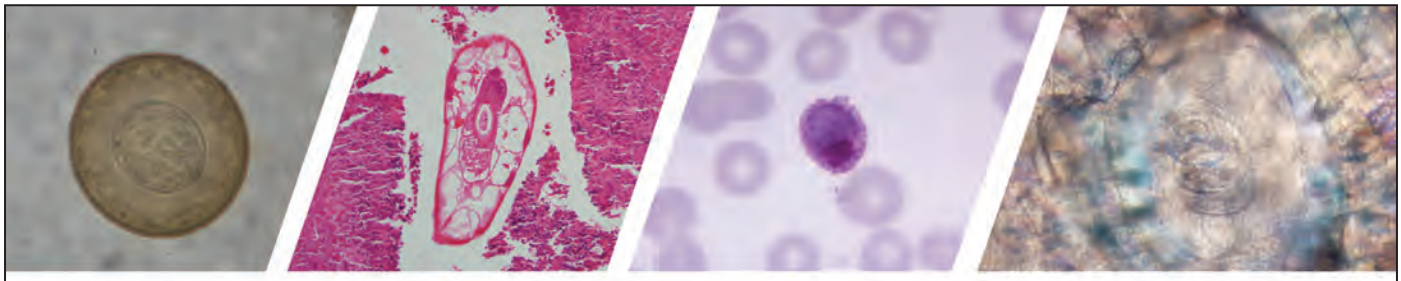

DPDx

Diagnostic Assistance and Training in Laboratory Identification of Parasites

A free service of CDC available to laboratorians, pathologists, and other health professionals in the United States and abroad

- Diagnosis from photographs of worms, histological sections, fecal, blood, and other specimen types
- Expert diagnostic review
- Formal diagnostic laboratory report
- Submission of samples via secure file share

Visit the DPDx website for information on laboratory diagnosis, geographic distribution, clinical features, parasite life cycles, and training via Monthly Case Studies of parasitic diseases.

www.cdc.gov/dpdx
dpdx@cdc.gov

U.S. Department of Health and Human Services
Centers for Disease Control and Prevention

CS272346-DE

Disparate Effects of Invasive Group A *Streptococcus* on Native Americans

Ryan M. Close, James B. McAuley

Active surveillance of invasive group A *Streptococcus* (iGAS) disease indicates that its incidence in the US general population is low, but limited studies show rates for American Indians and Alaska Natives (AI/AN) are severalfold higher. Major disparities in rates of iGAS exist between Indigenous and non-Indigenous populations of Australia, New Zealand, and Canada, but much less is understood about iGAS among AI/AN in the United States. Although complex host–pathogen interactions influence the rates of iGAS, including strain variation and virulence, the number and type of concurrent conditions, and socioeconomic status, the relative contribution of each remains unclear. We highlight the poor correlation between the substantial effect of iGAS among Indigenous persons in industrialized countries and the current understanding of factors that influence iGAS disease in these populations. Prospective, large-scale, population-based studies of iGAS are needed that include AI/AN as a necessary first step to understanding the effects of iGAS.

Streptococcus pyogenes (group A *Streptococcus* [GAS]) causes a range of pyogenic, toxigenic, and immunologic diseases with varying degrees of severity, from pharyngitis and impetigo to necrotizing fasciitis and streptococcal toxic shock syndrome (*1*). Improved sanitation and increased availability of antimicrobial drugs have led to a decline in GAS incidence and virulence (*2*), but concern about invasive GAS (iGAS) has increased in recent decades (*3*).

Each year, ≈500,000 deaths occur worldwide from GAS; 160,000 of these are from invasive infections, of which 97% occur in resource-limited countries (*4*). Some of the highest rates of iGAS occur in Indigenous populations within industrialized countries (*5*), most likely as a consequence of health disparities between general populations and marginalized peoples, in addition to a poorly understood host–pathogen relationship. In the United States, American Indians and Alaska Natives (AI/AN) suffer from high rates of iGAS, but epidemiologic and clinical data on GAS among these Indigenous populations is more sparse than it is in other industrialized nations (*6*). We highlight discordance between the substantial effect of iGAS on AI/AN and understanding of factors that influence iGAS disease in these vulnerable US populations and in other Indigenous persons.

Author affiliations: University of Pennsylvania, Philadelphia, Pennsylvania, USA (R.M. Close); Indian Health Service Hospital, Whiteriver, Arizona, USA (R.M. Close, J.B. McAuley); Rush University, Chicago, Illinois, USA (J.B. McAuley)

DOI: https://doi.org/10.3201/eid2609.181169

iGAS in the United States

During the 1980s, the first reports of streptococcal toxic shock–like syndrome resulted in a resurgence in concern about GAS disease. A population-based study of iGAS in the United States found a stable annual incidence rate of 4.3 cases/100,000 population during 1985–1990 (*7*). Despite this stable rate, GAS disease increased, and multiorgan dysfunction and hypotension signaled an increase in GAS severity.

This study prompted the Centers for Disease Control and Prevention (CDC) to add iGAS to the Active Bacterial Core surveillance (ABCs) program. The first survey, which assessed iGAS in the United States during 1995–1999, found an annual incidence of 2.2–4.8 iGAS cases/100,000 population (*3*). Rates were stable in 2 follow-up epidemiologic studies that showed iGAS incidence of 3.5 cases/100,000 population for 2000–2004 and 3.8 cases/100,000 population for 2005–2012 (*1*,*8*).

The CDC reports suggested stability with unchanging rates and disease distribution. Each report concluded that iGAS incidence had been stable not only intrastudy but also across decades, starting with the work of Hoge et al. (*7*). The researchers referenced higher rates of iGAS among Indigenous populations of other countries, and ABCs data indicated that AI/AN make up <2% of the country but contributed 4% of iGAS cases during 2000–2012 (*1*,*8*). This finding provides at least inferential evidence of higher rates of iGAS among AI/AN that warrants further investigation.

Incidence varies by region. For example, Utah reported an iGAS incidence significantly higher than country averages for 2002–2010: 6.3 cases/100,000 Utah residents. The study noted an increased relative risk among Native Hawaiians/Pacific Islanders (3.3% vs. 1.2%), but this observation was not explored further (*9*). More recent data from the ABCs program indicated an increase in iGAS incidence in the general population; rates rose in 2014 to 4.8 cases/100,000 population and in 2016 to 5.8 cases/100,000 population (*10*,*11*). Although this recent increase is notable, it is marginal, and overall rates remain substantially lower than those reported among AI/AN.

These studies highlight the stable pattern of iGAS in the general US population. However, they fail to highlight the limited but important evidence that suggests higher iGAS rates among AI/AN.

iGAS among AI/AN

Hoge et al. reported an overall iGAS incidence of 4.3 cases/100,000 population but found an age-adjusted incidence of 46.0 cases/100,000 population for AI (*7*). Heightened concern for iGAS among AI led Benjamin et al. to review all cultures positive for GAS from sterile sites at a hospital serving Zuni Indians during the same period (1982–1991) (*12*). The annualized incidence rate for iGAS of 13.3 cases/100,000 population (95% CI 8.3–33.2) for Zuni Indians contrasted with a rate of 1.7 cases/100,000 population in a neighboring county of predominantly Hispanic and non-Hispanic White residents. The authors noted that during a time when the medical community was focused on suspected rising rates in the general population that remained in single digits, the rate of iGAS among Zuni AI patients was, and had been, substantially higher.

The findings are consistent with more recent studies and case series that described iGAS among AI/AN. Rudolph et al. evaluated iGAS in Alaska during 2001–2013, and although only 20% of the state's population was AN, this group represented 46% of the state's 516 iGAS cases. The rates of iGAS were 13.7 for AN and 3.9 for non-AN persons per 100,000 population (*6*). The Arizona Department of Health Services reported iGAS incidence rates for AI/AN that were 2–5 times higher than those for the general population and an increase in rates in recent years (*13*). However, this information has not reached the broader public health or medical literature that mostly comprises smaller, local reports of iGAS clusters involving AI communities (*14*,*15*).

A Disease of Displaced Indigenous Populations

Other high-resource countries with more recent iGAS population-based studies among Indigenous populations can provide insight for an explanatory model for iGAS among Indigenous persons in the United States. Although evidence is limited on the true incidence of iGAS globally, Indigenous populations of industrialized nations have the highest recorded rates of both epidemic and endemic iGAS disease (*4*).

Canada

After an iGAS outbreak swept through Canada, researchers conducted an epidemiologic review of iGAS cases in northwestern Ontario for 2001–2013 at the health center, metropolitan, and provincial levels (*16*). First Nations Canadians accounted for 41% of iGAS cases despite making up only 8% of the population. The rate of iGAS at the health center where most of this population obtains care ranged from 9.8 to 18.1 cases/100,000 population, a rate 2–7 times higher than the largely nonnative metropolitan and provincial populations. In a more focused follow-up study of 22,000 First Nations Canadians among 26 communities in the same region, Bocking et al. reported an iGAS annualized rate of 56.0 cases/100,000 population for 2009–2014, >10 times higher the rate for the general population during the same period (*17*).

Australia

The rates of GAS and poststreptococcal sequelae are substantially higher for Aboriginal Australians than for the general population of Australia, for which GAS disease has declined (*18*). In a retrospective 6-year study of all cases of GAS bacteremia in the Northern Territory, Carapetis et al. noted that >50% of cases occurred in Aboriginal Australians, who make up only one quarter of the population (*19*). Two separate sequential studies in neighboring Queensland spanning 1996–2009 supported these findings; rates of iGAS for Aboriginal Australians were 3–8 times higher than for non-Indigenous Australians (Appendix, https://wwwnc.cdc.gov/EID/article/26/9/18-1169-App1.pdf).

New Zealand

In nearby New Zealand, Safar et al. conducted a population-based study of iGAS to anticipate coverage of potential GAS vaccines in development (*20*). In the diverse city of Auckland (population ≈1.3 million), 11% were Indigenous Māori. Yet, this group accounted for 31% of all iGAS infections over a 2-year period, and the incidence rate for Māori was 5 times higher than for New Zealand residents of European and Asian descent. The disparity was more dramatic at the ends of the age spectrum for Indigenous Māori. iGAS incidence rates per 100,000

population were 40.9 for children <1 year of age and 146.8 for persons ≥65 years of age.

The disparity in iGAS between Indigenous and non-Indigenous populations spans geography and cultures (Table). However, the extent and reasons for that disparity remain poorly understood.

Influencing Factors in iGAS

The relationship between GAS and Indigenous populations most likely involves complex interactions between pathogens and humans. Numerous studies have contributed to a long list of influencers of GAS incidence but a lack of rigorous analyses has yielded few prevention strategies (*21*). The high rates of iGAS among Indigenous persons may represent unique circumstances that combine pathogen characteristics, population dynamics, and individual risk factors that all contribute to varying degrees.

A high incidence of noninvasive GAS disease and postinfectious sequelae is well described in the Indigenous populations of industrialized countries and coincides with elevated rates of iGAS (*5*). Among Indigenous Australian children, the prevalence of pyoderma was reported as high as 90% (*18*), and incidence rates were 4–10 times higher than in other resource-limited settings (*22*). Rates of acute rheumatic fever for Indigenous Australians are as high as 194 cases/100,000 population and for Māori in New Zealand, 78 cases/100,000 population (*5*). These rates are down from estimated rates of 374–508 cases/100,000 population during the 1980s, but remain higher than rates for local non-Indigenous groups (1.1–7.2/100,000) (*5*). Finally, Indigenous Australians have the highest reported rates of acute poststreptococcal glomerulonephritis worldwide (239 cases/100,000 population) (*23*).

Less is known about noninvasive GAS and post-GAS sequelae among AI/AN in recent decades. Studies among AI children in Minnesota during the 1960s and 1970s showed high rates of poststreptococcal glomerulonephritis in addition to a >80% prevalence of pyoderma (*24*,*25*). Despite national declines in rheumatic heart disease, limited reports reveal rates of rheumatic heart disease in AI nearly 5 times national estimates (4.6 vs. <1.0 cases/1,000 population) (*26*) along with higher rates of rheumatic heart disease–related death (*27*). These observations require a broader appreciation of GAS among Indigenous persons, including AI/AN.

Socioeconomic Status

Socioeconomic status (SES) is a commonly asserted but poorly studied explanation for the high rates of iGAS among Indigenous persons. Few studies have directly measured SES when comparing iGAS rates between Indigenous and non-Indigenous populations, and the evidence is conflicting. In 1 study from Australia, half of iGAS cases occurred in the lowest socioeconomic quintile, in which Indigenous persons were overrepresented (*20*). Yet, a study in Fiji that specifically looked for a relationship with SES found that Indigenous Fijians had higher rates of iGAS despite a higher SES than did Indo-Fijians (*28*). Although this study was limited by small sample sizes, it is an example of the difficulty in understanding how SES indicators relate to iGAS incidence. Yet, of all the potential influencers, SES seems to be the most obvious commonality between displaced Indigenous persons of different industrialized nations.

According to US national health statistics, 23.9% of AI/AN lived below the poverty level during 2014–2016 (*29*), whereas 12.7% of all persons and 11.0% of White persons lived below the poverty level (*29*). According to Akee et al., AI/AN experience substantial income inequality and immobility. Along with Blacks and Hispanic persons, AI/AN are consistently at the lower end of income distribution in the United States and are the least likely to move percentiles in their lifetime (*30*). Of the top 10% of US income earners, 84% were White, whereas only 0.3% were AI/AN (*30*).

For numerous health indicators, AI/AN are worse off as well and have some of the highest age-adjusted death rates secondary to chronic liver disease and cirrhosis, diabetes, unintentional injuries, septicemia, and alcohol-related deaths (*29*). Although the overall age-adjusted death rate for AI/AN is lower than that for all races (591 vs. 729/100,000 population), the years of potential life lost before age 75 years is 10% higher for AI/AN than for White persons (i.e., AI/AN lose 645 more years of life per 100,000 persons before age 75 years) (*29*). Infant mortality is a "fundamental indicator of … community health status, and the availability and use of appropriate health care," and from 2005 to 2015, infant mortality rates decreased >10% for every racial group except AI/AN, for whom infant mortality rates did not improve (*29*).

For some conditions, however, AI/AN have lower death rates than the US general population and for White Americans. These conditions include heart disease, cerebrovascular disease, malignancies, and chronic lower respiratory disease (*29*). Misclassification and incomplete data for racial groups other than White and Black explains some of the reason for these lower death rates.

Although AI/AN experience socioeconomic and health disparities, linking the 2 causally is complicated. The relationship between SES overall, specific SES indicators (e.g., income or education), and health outcomes varies by race (*31*). Furthermore, Black Americans have near equivalent rates of poverty (22.0% in 2016) to AI/AN and have some of the largest health disparities of any racial group (*29*). The all-cause age-adjusted death rate is highest for Black persons (857/100,000 population), and Black persons have higher death rates for heart disease, cerebrovascular disease, malignancies, diabetes, and homicides than persons of all other races (*29*). Although Black Americans have worse health indicators than AI/AN for many conditions, the rates of iGAS among Blacks are more similar to those among Whites than for AI/AN. In the most recent comprehensive report by CDC, the rate of iGAS among Blacks was 4.7 cases/100,000 population and increased to 6.2 cases/100,000 population in the 2016 update (*1*,*11*).

For these reasons, we caution against attributing substantial disparities in iGAS among AI/AN compared with the general population to SES alone. Although SES undoubtedly plays a major role, more information is needed on which SES indicators most strongly predict iGAS in AI/AN and the general population. Such information will best guide public health interventions beyond oversimplified suggestions to improve hygiene and ameliorate poverty.

Perhaps the reason SES fails to accurately capture which, and how, certain SES indicators most affect Indigenous persons is that the colonization, displacement, assimilation practices, and subsequent intergenerational historical trauma experienced by Indigenous populations fundamentally differentiate them from other impoverished groups. The health effects of centuries of denying and denigrating Indigenous culture have only recently been appreciated, but much needs to be done to promote healing (*32*). The displacement and discrimination experienced by AI/AN is difficult to measure and correlate with health outcomes. Furthermore, the experiences of Indigenous persons have shaped migration, their interactions with non-Indigenous communities, and relationships with institutions such as the education and healthcare systems. These factors have led to social, economic, and political disparities not captured in typical epidemiologic studies and may contribute to the confusion in how SES is linked to health disparities among AI/AN. Recognizing these historical differences for AI/AN is critical for better understanding health disparities, such as iGAS, and might be the most important and least understood aspect of disparities in Indigenous health.

Microbiological Factors

Although strain novelty and virulence play important roles in iGAS outbreaks, their differential contribution remains unclear. Some studies have postulated that strain prevalence and novelty, rather than innate virulence potential, was the predominant reason a specific strain would emerge as a cause of iGAS (*33*). That is, upsurges in both iGAS and noninvasive GAS disease could occur when a predominant strain is supplanted with a new *emm*-type to which the population lacks sufficient immunity (*21*,*34*). Outbreaks can occur within specific risk groups that may implicate interaction between strain-type and host irrespective of virulence (e.g., the spread of severe GAS infections among intravenous drug users in the United Kingdom) (*35*).

Yet, hypervirulent strains also have contributed to outbreaks of iGAS (*36*,*37*). A well-described outbreak of iGAS in Canada resulted from a single, recently emerged, hypervirulent strain of *emm59*, which then migrated to the United States; genetically diversified; and led to *emm59* outbreaks in Montana, Wyoming, and Arizona (*15*,*38*,*39*). During the outbreak in Canada, Tyrrel et al. noted that a relatively modest proportion of iGAS cases (5%) in Ontario was attributable to *emm59*. Yet, they observed that 56 (83%) of Ontario's 68 *emm59* cases occurred in an area with a high proportion of First Nations Canadians (*37*). This observation supported by the findings of Athey et al. that reported a disproportionate number of iGAS cases among Indigenous Canadians in Ontario, particularly in the Thunder Bay region, where *emm59* caused 44% of iGAS in 2008 (*16*). An *emm59* outbreak in a northern Arizona hospital cited Native American race as a primary risk factor for infection. Eighteen (62%) of 29 iGAS cases were identified as *emm59*, 15 (83%) of which occurred in AI (*15*). A phylogenetic analysis of 67 *emm59* strains known to cause outbreaks of iGAS in the United States revealed that AIs had the highest proportion of invasive *emm59* infections (*40*). However, without more detailed community epidemiologic data, the relative contribution of novelty versus virulence was difficult to discern. Genetic studies of invasive streptococcal outbreaks in the United States suggest that a progenitor pathogen makes its way into a population (e.g., AI/AN) and then spreads quickly from person to person if the dynamics are favorable (*15*,*16*,*39*,*40*). Novelty and virulence most likely work together to intensify iGAS epidemics in

Indigenous communities. Where a new pathogen might lead to an increase in iGAS overall because of population susceptibility, a particularly virulent new pathogen leads to dramatically increased rates of disease. It is entirely plausible that population-specific dynamics and pathogen virulence work together in amplifying outbreaks.

Host Factors: Concurrent Conditions and Immunologic Vulnerability

Evidence suggests a strong relationship between iGAS and the prevalence of concurrent conditions (*19*). Diabetes, skin disease, chronic kidney disease, heart disease, and alcoholism are consistently associated with iGAS (*1*,*17*,*20*,*28*). Although some studies found Indigenous persons with iGAS were more likely than non-Indigenous persons to have diabetes, chronic kidney disease, or both (*7*,*19*), evidence demonstrating no association in the number or type of concurrent conditions was equally limited (*20*,*28*). This observation reflects the limitations of the research and the poor understanding of how concurrent conditions contribute to iGAS. Indigenous populations clearly have more such conditions and acquire them at a younger age (*41*,*42*). The quantity of concurrent conditions, in addition to the specific conditions (e.g., diabetes), might explain why Indigenous persons, including AI/AN, are overrepresented among iGAS cases and is supported by the higher rates of all-cause infectious disease–related death, including from iGAS, in AI/AN (*43*). However, this approach would be an oversimplification that neither accounts for the role of pathogen virulence and host factors nor provides insight into how such conditions specifically contribute to iGAS. Furthermore, attributing markedly elevated rates of iGAS to overall vulnerability cannot explain the variability in findings on the effects of concurrent conditions among surveys. Concurrent conditions appear to play an integral but incomplete role in the incidence of iGAS among Indigenous populations. Prospective studies to interpret the effects of specific conditions on the incidence of iGAS are needed to better identify persons at highest risk within vulnerable populations.

The potential contribution of host genetics is the least understood of variables. Evidence suggests genetic conservation among AI/AN (*44*), and a genetic basis for several conditions prevalent among AI/AN has been explored or established, including asthma (*45*), diabetes (*46*), and rheumatoid arthritis (*47*). Evolutionary bottlenecks and founder effects have led to an overall decrease in allele diversity, and tribal structure of reservation life has led to semi-independent gene pools (*44*,*48*). Such gene pools provide a potentially more homogenous widespread susceptibility that could partly explain the vulnerability of all AI/AN populations to invasive infections caused by encapsulated organisms (*Haemophilus influenzae, Streptococcus pneumoniae*) that is well described but incompletely understood (*49*). A similar mechanism could be involved with GAS disease. The application of more recently developed techniques that measure host immune response to bacterial infections may offer additional insights, which can guide future efforts at GAS vaccine development and control (*50*).

Given the disparity in iGAS among AI/AN, it is reasonable to consider a host genetic predisposition to invasive infections. In a world of rapidly evolving techniques for genetic and epigenetic testing and the emerging potential for gene-targeted therapies, exploring the possibility of a genetic predisposition seems prudent to guide potential therapies for this marginalized population.

Conclusions

The medical and public health communities need to address the effects of iGAS among the ≈3 million AI/AN in the United States. The first step should address the lack of population-based studies of Indigenous Americans. The Indian Health Service needs to support further investigations into iGAS to fulfill its mission "[t]o raise the physical, mental, social, and spiritual health of American Indians and Alaska Natives to the highest level" (https://www.ihs.gov/aboutihs).

We recommend mandatory reporting of iGAS in regions with substantial numbers of AI/AN. This reporting would encourage smaller healthcare facilities to monitor iGAS outbreaks and improve surveillance in smaller, vulnerable populations. Greater capture of isolates is integral to using population-based epidemiologic studies to better identify risk factors for iGAS specific to AI/AN. We also propose large-scale sequencing and phylogenetic studies of GAS *emm* types to clarify the migration of strains within and among AI/AN and determination of unique host immune responses to GAS among AI/AN to guide control efforts. A tailored approach might be necessary for AI/AN or individual tribes, but better evidence would inform community-based interventions to reduce the incidence of iGAS and lay the foundation for multivalent GAS vaccines to protect communities from the most harmful GAS strains.

The opinions expressed by authors contributing to this journal do not necessarily reflect the opinions of the Indian Health Service or the institutions with which the authors are affiliated. There are no sources of funding to disclose for either author.

About the Authors

Dr. Close is an internist and pediatrician working as a clinician and public health officer with the Indian Health Service at Whiteriver Hospital in eastern Arizona. His research interests are anemia in children, the underutilization of vaccines in complex emergencies, and the effects of GAS and poststreptococcal sequelae in Native American populations.

Dr. McAuley is an internist and pediatrician and an adult and pediatric infectious disease specialist serving the Clinical Director of the Indian Health Service Whiteriver Indian Hospital in Arizona. His research interests include parasitology, tuberculosis, and health disparities in vulnerable populations.

References

1. Nelson GE, Pondo T, Toews KA, Farley MM, Lindegren ML, Lynfield R, et al. Epidemiology of invasive group A streptococcal infections in the United States, 2005–2012. Clin Infect Dis. 2016;63:478–86. https://doi.org/10.1093/cid/ciw248
2. Quinn RW. Epidemiology of group A streptococcal infections—their changing frequency and severity. Yale J Biol Med. 1982;55:265–70.
3. O'Brien KL, Beall B, Barrett NL, Cieslak PR, Reingold A, Farley MM, et al. Epidemiology of invasive group A *Streptococcus* disease in the United States, 1995–1999. Clin Infect Dis. 2002;35:268–76. https://doi.org/10.1086/341409
4. Carapetis JR, Steer AC, Mulholland EK, Weber M. The global burden of group A streptococcal diseases. Lancet Infect Dis. 2005;5:685–94. https://doi.org/10.1016/S1473-3099(05)70267-X
5. Sims Sanyahumbi A, Colquhoun S, Wyber R, Carapetis JR. Global disease burden of group A *Streptococcus*. In: Ferretti JJ, Stevens DL, Fischetti VA, editors. *Streptococcus pyogenes*: basic biology to clinical manifestations. Oklahoma City (OK): University of Oklahoma Health Sciences Center; 2016. p. 661–704.
6. Rudolph K, Bruce MG, Bruden D, Zulz T, Reasonover A, Hurlburt D, et al. Epidemiology of invasive group A streptococcal disease in Alaska, 2001 to 2013. J Clin Microbiol. 2016;54:134–41. https://doi.org/10.1128/JCM.02122-15
7. Hoge CW, Schwartz B, Talkington DF, Breiman RF, MacNeill EM, Englender SJ. The changing epidemiology of invasive group A streptococcal infections and the emergence of streptococcal toxic shock-like syndrome. A retrospective population-based study. JAMA. 1993;269:384–9. https://doi.org/10.1001/jama.1993.03500030082037
8. O'Loughlin RE, Roberson A, Cieslak PR, Lynfield R, Gershman K, Craig A, et al.; Active Bacterial Core Surveillance Team. The epidemiology of invasive group A streptococcal infection and potential vaccine implications: United States, 2000–2004. Clin Infect Dis. 2007;45:853–62. https://doi.org/10.1086/521264
9. Stockmann C, Ampofo K, Hersh AL, Blaschke AJ, Kendall BA, Korgenski K, et al. Evolving epidemiologic characteristics of invasive group a streptococcal disease in Utah, 2002–2010. Clin Infect Dis. 2012;55:479–87. https://doi.org/10.1093/cid/cis422
10. Centers for Disease Control and Prevention. Active Bacterial Core Surveillance report, Emerging Infections Program Network, group A *Streptococcus*, 2014 [cited 2018 May 9]. http://www.cdc.gov/abcs/reports-findings/survreports/gas14.pdf
11. Centers for Disease Control and Prevention. Active Bacterial Core Surveillance report, Emerging Infections Program Network, group A *Streptococcus*, 2016 [cited 2019 Feb 22]. http://www.cdc.gov/abcs/reports-findings/survreports/gas16.pdf
12. Benjamin EM, Gershman M, Goldberg BW. Community-acquired invasive group A beta-hemolytic streptococcal infections in Zuni Indians. Arch Intern Med. 1992;152:1881–4. https://doi.org/10.1001/archinte.1992.00400210103017
13. Infectious Disease Epidemiology 2008–2013 Report: Office of Infectious Disease Services, Bureau of Epidemiology and Disease Control, Arizona Department of Health Services [cited 2018 Jun 22]. http://www.azdhs.gov/documents/preparedness/epidemiology-disease-control/disease-data-statistics-reports/annual-reports-archive/infectious-disease-epidemiology-report-2008-2013.pdf
14. Harris AM, Yazzie D, Antone-Nez R, Dinè-Chacon G, Kinlacheeny JB, Foley D, et al. Community-acquired invasive GAS disease among Native Americans, Arizona, USA, winter 2013. Emerg Infect Dis. 2015;21:177–9. https://doi.org/10.3201/eid2101.141148
15. Engelthaler DM, Valentine M, Bowers J, Pistole J, Driebe EM, Terriquez J, et al. Hypervirulent *emm59* clone in invasive group A *Streptococcus* outbreak, southwestern United States. Emerg Infect Dis. 2016;22:734–8. https://doi.org/10.3201/eid2204.151582
16. Athey TB, Teatero S, Sieswerda LE, Gubbay JB, Marchand-Austin A, Li A, et al. High incidence of invasive group A *Streptococcus* disease caused by strains of uncommon *emm* types in Thunder Bay, Ontario, Canada. J Clin Microbiol. 2016;54:83–92. https://doi.org/10.1128/JCM.02201-15
17. Bocking N, Matsumoto CL, Loewen K, Teatero S, Marchand-Austin A, Gordon J, et al. High incidence of invasive group A streptococcal infections in remote indigenous communities in northwestern Ontario, Canada. Open Forum Infect Dis. 2016;4:ofw243. https://doi.org/10.1093/ofid/ofw243
18. Ralph AP, Carapetis JR. Group A streptococcal diseases and their global burden. In: Chhatwal GS, editor. Host-pathogen interactions in streptococcal diseases. Berlin: Springer; 2013. p. 1–27.
19. Carapetis JR, Walker AM, Hibble M, Sriprakash KS, Currie BJ. Clinical and epidemiological features of group A streptococcal bacteraemia in a region with hyperendemic superficial streptococcal infection. Epidemiol Infect. 1999;122:59–65. https://doi.org/10.1017/S0950268898001952
20. Safar A, Lennon D, Stewart J, Trenholme A, Drinkovic D, Peat B, et al. Invasive group A streptococcal infection and vaccine implications, Auckland, New Zealand. Emerg Infect Dis. 2011;17:983–9. https://doi.org/10.3201/eid/1706.100804
21. Efstratiou A, Lamagni T. Epidemiology of *Streptococcus pyogenes*. In: Ferretti JJ, Stevens DL, Fischetti VA, editors. *Streptococcus pyogenes*: basic biology to clinical manifestations. Oklahoma City (OK): University of Oklahoma Health Sciences Center; 2016. p. 601–28.

22. Andrews RM, Kearns T, Connors C, Parker C, Carville K, Currie BJ, et al. A regional initiative to reduce skin infections amongst aboriginal children living in remote communities of the Northern Territory, Australia. PLoS Negl Trop Dis. 2009;3:e554. https://doi.org/10.1371/journal.pntd.0000554
23. Jackson SJ, Steer AC, Campbell H. Systematic review: estimation of global burden of non-suppurative sequelae of upper respiratory tract infection: rheumatic fever and post-streptococcal glomerulonephritis. Trop Med Int Health. 2011;16:2–11. https://doi.org/10.1111/j.1365-3156.2010.02670.x
24. Anthony BF, Kaplan EL, Wannamaker LW, Chapman SS. The dynamics of streptococcal infections in a defined population of children: serotypes associated with skin and respiratory infections. Am J Epidemiol. 1976;104:652–66. https://doi.org/10.1093/oxfordjournals.aje.a112344
25. Dajani AS, Ferrieri P, Wannamaker L. Endemic superficial pyoderma in children. Arch Dermatol. 1973;108:517–22. https://doi.org/10.1001/archderm.1973.01620250005001
26. Schaffer WL, Galloway JM, Roman MJ, Palmieri V, Liu JE, Lee ET, et al. Prevalence and correlates of rheumatic heart disease in American Indians (the Strong Heart Study). Am J Cardiol. 2003;91:1379–82. https://doi.org/10.1016/S0002-9149(03)00338-2
27. Becker TM, Wiggins CL, Key CR, Samet JM. Ethnic differences in mortality from acute rheumatic fever and chronic rheumatic heart disease in New Mexico, 1958–1982. West J Med. 1989;150:46–50.
28. Steer AC, Jenney A, Kado J, Good MF, Batzloff M, Waqatakirewa L, et al. Prospective surveillance of invasive group A streptococcal disease, Fiji, 2005–2007. Emerg Infect Dis. 2009;15:216–22. https://doi.org/10.3201/eid15/2.080558
29. National Center for Health Statistics. Health, United States, 2017: with special feature on mortality [cited 2019 Feb 20]. http://www.cdc.gov/nchs/data/hus/hus17.pdf
30. Akee R, Jones MR, Porter SR. Adding insult to injury: racial disparity in an era of increasing income inequality [cited 2019 Feb 10]. http://www.census.gov/library/working-papers/2017/adrm/carra-wp-2017-01.html
31. Braveman PA, Cubbin C, Egerter S, Chideya S, Marchi KS, Metzler M, et al. Socioeconomic status in health research: one size does not fit all. JAMA. 2005;294:2879–88. https://doi.org/10.1001/jama.294.22.2879
32. Archibald L. Decolonization and healing: indigenous experiences in the United States, New Zealand, Australia, and Greenland: Aboriginal Healing Foundation; 2006 [cited 2019 Feb 10]. https://www.cwis.org/document/decolonization-and-healing-indigenous-experiences-in-the-united-states-new-zealand-australia-and-greenland/
33. Rogers S, Commons R, Danchin MH, Selvaraj G, Kelpie L, Curtis N, et al. Strain prevalence, rather than innate virulence potential, is the major factor responsible for an increase in serious group A *Streptococcus* infections. J Infect Dis. 2007;195:1625–33. https://doi.org/10.1086/513875
34. Turner CE, Abbott J, Lamagni T, Holden MT, David S, Jones MD, et al. Emergence of a new highly successful acapsular group A *Streptococcus* clade of genotype *emm89* in the United Kingdom. MBio. 2015;6:e00622. https://doi.org/10.1128/mBio.00622-15
35. Lamagni TL, Neal S, Keshishian C, Alhaddad N, George R, Duckworth G, et al. Severe *Streptococcus pyogenes* infections, United Kingdom, 2003–2004. Emerg Infect Dis. 2008;14:202–9. https://doi.org/10.3201/eid1402.070888
36. Afshar B, Turner CE, Lamagni TL, Smith KC, Al-Shahib A, Underwood A, et al. Enhanced nasopharyngeal infection and shedding associated with an epidemic lineage of *emm3* group A *Streptococcus*. Virulence. 2017;8:1390–400. https://doi.org/10.1080/21505594.2017.1325070
37. Tyrrell GJ, Lovgren M, St Jean T, Hoang L, Patrick DM, Horsman G, et al. Epidemic of group A *Streptococcus M/emm59* causing invasive disease in Canada. Clin Infect Dis. 2010;51:1290–7. https://doi.org/10.1086/657068
38. Fittipaldi N, Olsen RJ, Beres SB, Van Beneden C, Musser JM. Genomic analysis of *emm59* group A *Streptococcus* invasive strains, United States. Emerg Infect Dis. 2012;18:650–2. https://doi.org/10.3201/eid1804.111803
39. Brown CC, Olsen RJ, Fittipaldi N, Morman ML, Fort PL, Neuwirth R, et al. Spread of virulent group A S*treptococcus* type *emm59* from Montana to Wyoming, USA. Emerg Infect Dis. 2014;20:679–81. https://doi.org/10.3201/eid2004.130564
40. Olsen RJ, Fittipaldi N, Kachroo P, Sanson MA, Long SW, Como-Sabetti KJ, et al. Clinical laboratory response to a mock outbreak of invasive bacterial infections: a preparedness study. J Clin Microbiol. 2014;52:4210–6. https://doi.org/10.1128/JCM.02164-14
41. Health, United States, 2016: with chartbook on long-term trend in health. Hyattsville, MD: National Center for Health Statistics; 2017 [cited 2019 Feb 10]. http://www.cdc.gov/nchs/data/hus/hus16.pdf
42. Statistics Canada. Table 105–0513: Health indicator profile, by aboriginal identity and sex, age-standardized rate, four year estimates, Canada, provinces and territories, occasional (rate), CANSIM (database) [cited 2019 Feb 20]. https://www150.statcan.gc.ca/t1/tbl1/en/tv.action?pid=1310009901
43. Cheek JE, Holman RC, Redd JT, Haberling D, Hennessy TW. Infectious disease mortality among American Indians and Alaska Natives, 1999–2009. Am J Public Health. 2014;104(Suppl 3):S446–52. https://doi.org/ 10.2105/AJPH.2013.301721
44. Mulligan CJ, Hunley K, Cole S, Long JC. Population genetics, history, and health patterns in Native Americans. Annu Rev Genomics Hum Genet. 2004;5:295–315. https://doi.org/10.1146/annurev.genom.5.061903.175920
45. Best LG, Azure C, Segarra A, Enright KJ, Hamley S, Jerome D, et al. Genetic variants and risk of asthma in an American Indian population. Ann Allergy Asthma Immunol. 2017;119:31–36.e1. https://doi.org/10.1016/j.anai.2017.05.015
46. Yracheta JM, Lanaspa MA, Le MT, Abdelmalak MF, Alfonso J, Sánchez-Lozada LG, et al. Diabetes and kidney disease in American Indians: potential role of sugar sweetened beverages. Mayo Clin Proc. 2015;90:813–23. https://doi.org/ 10.1016/j.mayocp.2015.03.018
47. Scally SW, Law SC, Ting YT, Heemst JV, Sokolove J, Deutsch AJ, et al. Molecular basis for increased susceptibility of indigenous North Americans to seropositive rheumatoid arthritis. Ann Rheum Dis. 2017;76:1915–23. https://doi.org/10.1136/annrheumdis-2017-211300
48. Nei M, Maruyama T, Chakraborty R. The bottleneck effect and genetic variability in populations. Evolution. 1975;29:1–10. https://doi.org/10.1111/j.1558-5646.1975.tb00807.x
49. Weatherholtz R, Millar EV, Moulton LH, Reid R, Rudolph K, Santosham M, et al. Invasive pneumococcal disease a decade after pneumococcal conjugate vaccine use in an American Indian population at high risk for disease. Clin Infect Dis. 2010;50:1238–46. https://doi.org/10.1086/651680
50. Furman D, Davis MM. New approaches to understanding the immune response to vaccination and infection. Vaccine. 2015;33:5271–81. https://doi.org/10.1016/j.vaccine.2015.06.117

Address for correspondence Ryan M. Close, Indian Health Service Hospital, PO 860, 200 W Hospital Dr, Whiteriver, AZ 85941, USA; email: Ryan.M.Close@gmail.com

Seroepidemiologic Study Designs for Determining SARS-COV-2 Transmission and Immunity

Hannah Clapham, James Hay,[1] Isobel Routledge,[1] Saki Takahashi,[1] Marc Choisy,[2] Derek Cummings,[2] Bryan Grenfell,[2] C. Jessica E. Metcalf,[2] Michael Mina,[2] Isabel Rodriguez-Barraquer,[2] Henrik Salje,[2] Clarence C. Tam[2]

Serologic studies are crucial for clarifying dynamics of the coronavirus disease pandemic. Past work on serologic studies (e.g., during influenza pandemics) has made relevant contributions, but specific conditions of the current situation require adaptation. Although detection of antibodies to measure exposure, immunity, or both seems straightforward conceptually, numerous challenges exist in terms of sample collection, what the presence of antibodies actually means, and appropriate analysis and interpretation to account for test accuracy and sampling biases. Successful deployment of serologic studies depends on type and performance of serologic tests, population studied, use of adequate study designs, and appropriate analysis and interpretation of data. We highlight key questions that serologic studies can help answer at different times, review strengths and limitations of different assay types and study designs, and discuss methods for rapid sharing and analysis of serologic data to determine global transmission of severe acute respiratory syndrome coronavirus 2.

Serologic studies are crucial for understanding current and future dynamics of the coronavirus disease (COVID-19) pandemic. In the past few months, much discussion about serologic studies and key issues with their design and interpretation has occurred. In this article, we discuss the questions that could be answered with these studies at different points in the epidemic and summarize the features and issues regarding study design, implementation of studies during an ongoing epidemic, and interpretation of the results. Discussion on the use of severe acute respiratory syndrome coronavirus 2 (SARS-CoV-2) serologic studies has largely focused on 2 questions: first, what proportion of a population has been infected?; and second, what proportion of a population is immune to disease or infection?

First, for infections that elicit detectable antibody responses, serologic studies can detect past infection regardless of clinical symptoms. This capability is useful for understanding the extent of past transmission (Figure 1, panel A). By linking this information with data on symptomatic cases, severe disease, and death in the same population, these studies can provide information on asymptomatic proportion, and the ratio of infections to severe cases and deaths (i.e., infection fatality ratio). Such data are also useful for calibrating mathematical models.

Second, if measured antibody responses correlate with protection, serologic studies can be used to measure the proportion of the population that is immune. This information can be used to guide control policies, help identify populations that are still susceptible to epidemics, target treatment or vaccination trials, and target vaccination when available. Although much discussion around use of serologic testing to inform persons of their serologic status has occurred, crucial distinctions exist between the use of serologic information to estimate population-level versus person-level immunity. Person-level immunity information

Author affiliations: National University of Singapore Saw Swee Hock School of Public Health, Singapore (H. Clapham, C.C. Tam); Harvard University T.H. Chan School of Public Health, Boston, Massachusetts, USA (J. Hay, M. Mina); University of California San Francisco EPPIcenter Program, San Francisco, California, USA (I. Routledge, S. Takahashi, I. Rodriguez-Barraquer); University of California San Francisco Department of Medicine, San Francisco (I. Routledge, S. Takahashi, I. Rodriguez-Barraquer); Oxford University Clinical Research Unit–Vietnam, Ho Chi Minh City, Vietnam (M. Choisy); University of Florida Department of Biology, Gainesville, Florida, USA (D. Cummings); Princeton University, Princeton, New Jersey, USA (C.J.E. Metcalf, B. Grenfell); University of Cambridge, Cambridge, UK (H. Salje); London School of Hygiene and Tropical Medicine (C.C. Tam)

DOI: https://doi.org/10.3201/eid2609.201840

[1]These first authors contributed equally to this article.

[2]These authors contributed equally to this article.

is currently fraught with scientific, ethical, and legal uncertainties, which we do not address in this article.

SARS-CoV-2 Antibody Response

Serologic studies will help answer these questions, but key unknowns persist regarding SARS-CoV-2 immunity and assay interpretation. Although estimating the proportion of the population that has been infected seems straightforward, careful consideration must be given to assay characteristics, the possibility for cross-reactivity with related coronaviruses, and the timing and magnitude of antibody responses. Timing and magnitude of antibody responses is particularly critical during a rapidly evolving epidemic, given the recency of infection for many persons.

Understanding population- or person-level protective immunity requires knowledge of how protective immunity is related to past SARS-CoV-2 infection, the extent to which antibody types or levels correlate with protection, and how long immunity lasts. Serologic assays detect presence of antibodies but generally do not establish whether those antibodies protect

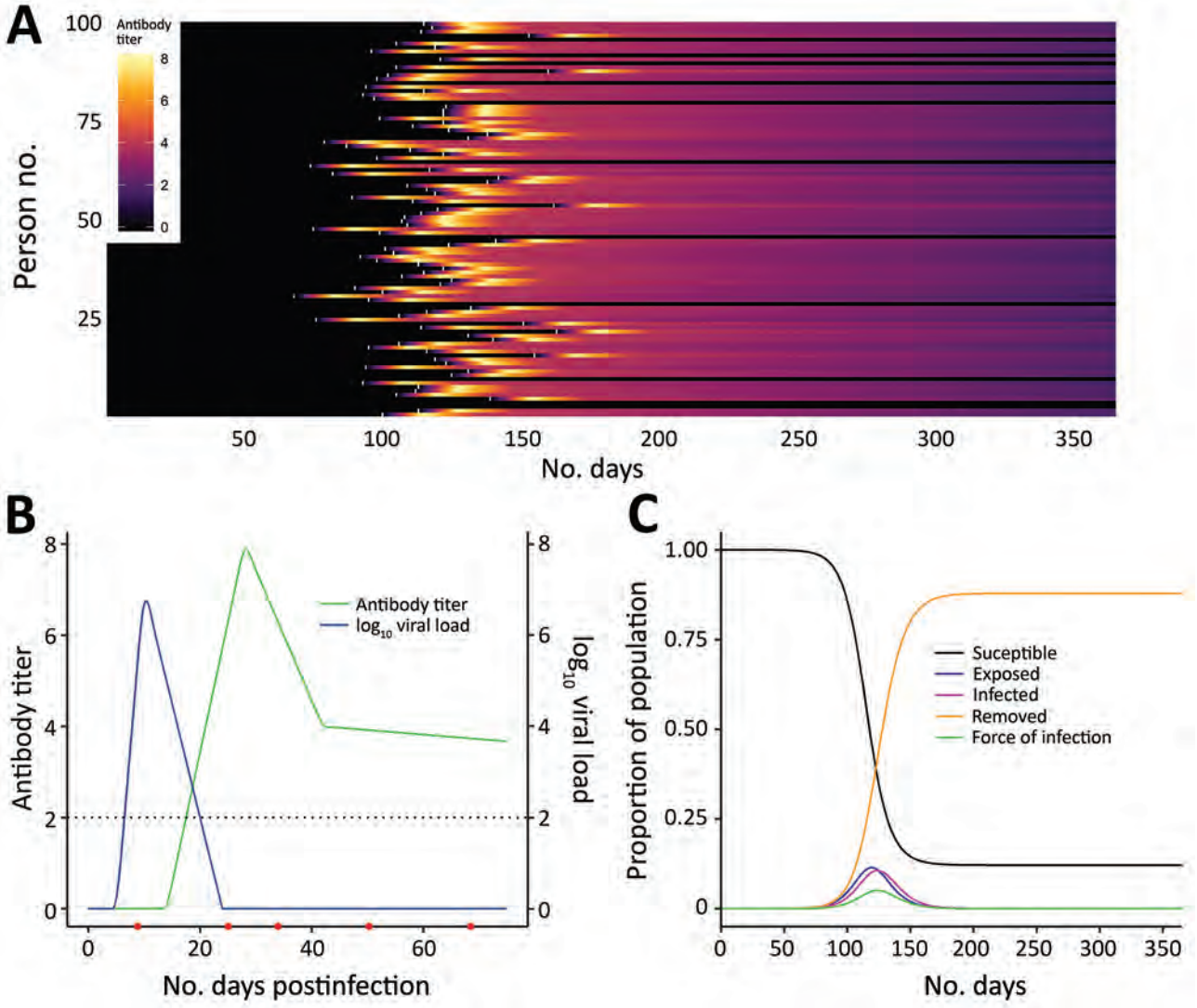

Figure 1. Link between severe acute respiratory syndrome coronavirus 2 infection dynamics and antibody levels in the population. A) Each line shows a person's antibody titer. After infection, each person's antibody levels undergo a dynamic process. A lag occurs from time of infection (white marks) to the generation of antibodies, which peaks several weeks postinfection and varies across persons depending on the time since infection and the parameters governing dynamics of the immune response. B) Antibody and virus dynamics in a person from time of infection. Frequent follow-up samples from the same person (indicated by red dots along the horizonal axis) would inform models of viral load and antibody kinetics. The dashed horizontal line represents the limit of detection of the assay. Early on, viral loads are more sensitive for diagnosing recent infection, whereas antibody titers become more sensitive once the humoral response is mounted and persons recover. C) Severe acute respiratory syndrome coronavirus 2 infections generated under an epidemic process (using a susceptible-exposed-infectious-removed model), modelling susceptible, exposed, infected, and recovered persons.

the person; neutralization assays are required to gain a deeper understanding of the functional role of antibodies in immune protection. Inferring protection from serologic tests is possible only after thresholds of protection have been established. Therefore, 3 additional intermediate questions need to be addressed to understand the benefits of conducting serologic studies and to interpret studies: 1) What is the antibody response observed after SARS-CoV-2 infections of different severity? 2) What is the extent of cross-reactivity in antibodies in different populations and in different assays? 3) Can we define a protective antibody response (a correlate of protection)?

A recent review summarized what is known regarding these questions for other coronaviruses (A.T. Huang et al., unpub. data, https://doi.org/10.1101/2020.04.14.20065771). For SARS-CoV-2, questions 2 and 3 can be answered with careful analysis of the types of seroepidemiologic studies proposed in this article, but question 1 requires a different type of study, one measuring antibody responses at multiple time points after acute infections of different severities (Figure 1, panel B). The first early studies on this subject suggest that some mild infections, or those in younger persons, might not lead to a measurable antibody response (F. Wu et al., unpub. data, https://doi.org/10.1101/2020.03.30.20047365), although more recent studies suggest that mild infections do lead to response (S. Fafi-Kremer et al., unpub. data, https://doi.org/10.1101/2020.05.19.20101832). This matter will be critical for inferring past infection from serologic tests and so requires continued study in different populations.

Characteristics and Interpretation of Serologic Assays

New SARS-CoV-2 serologic assays emerge regularly (*1–3;* C. Sun et al., unpub data, https://doi.org/10.1101/2020.02.16.951723). These assays mainly fall into 3 categories: rapid tests; ELISA; and neutralization assays, such as plaque-reduction neutralization tests (PRNTs), microneutralization, or pseudovirus neutralization. Rapid, point-of-care tests generally use lateral flow immunochromatography and yield a qualitative (positive or negative) result. Despite their speed, ease of use, and amenability to mass screening, currently available rapid tests for SARS-CoV-2 have questionable accuracy. The World Health Organization (WHO) currently recommends that SARS-CoV-2 seroepidemiologic studies use IgG ELISA followed by confirmation of positive results with a PRNT (*4*). PRNT is recommended because it is more specific than other tests. Moreover, like other neutralization assays, PRNT provides quantitative information on antibody titers that inhibit viral infection, at least in vitro. However, PRNTs require dedicated laboratory training and facilities. They are more difficult to standardize and perform at large volume, and the tests must be performed in a Biosafety Level (BSL) 3 capacity laboratory, whereas ELISAs can be performed in BSL-2 laboratories (*5*). BSL-3 laboratories are not available everywhere. For global comparisons of serologic data based on different assays, understanding their comparability is key (*1–3*).

High sensitivity and specificity is desired for all assays but might be prioritized differently depending on the specific objective. For example, an assay that detects past infection with higher sensitivity (e.g., one that can detect antibodies at lower titers) might be insufficiently specific to determine who in the population is immune (e.g., if antibody titers are related to protective immunity). Specificity also might be a particular issue when infection prevalence is low (i.e., when the number of false-positive results could be substantial and even outnumber true-positive results).

Even at the person level, interpretation of serologic testing is time-dependent because detectable antibody responses might only appear ≈2–3 weeks after infection. In an ongoing epidemic, a large proportion of persons will be recently infected and therefore will be negative by serologic testing. Conversely, a substantial proportion of previously infected persons might have detectable virus for several weeks (Figure 1, panel C) (*6*). Tracking the proportion of the population infected over time might thus require use of PCR assays to detect recent infections, in addition to serologic assays, to minimize false-negative serologic test results obtained soon after infection. However, this approach would require the collection of additional respiratory or salivary samples, and a period in which infected persons are PCR-negative and have undetectable antibodies might occur. The additional use of different antibody subclasses (e.g., IgA and IgM) that might develop at different times during infection and can be measured in serum might help (A.T. Huang et al., unpub. data), although the timing of IgG and IgM might be similar (B. Berriman et al., unpub. data, https://doi.org/10.1101/2020.05.15.20103275). The extent to which serologic testing missing current or very recent infections affects results will depend on the prevalence in the population and growth rate. The extra effort to collect a swab specimen might be necessary at epidemic peak but less necessary at the tail end of an epidemic.

For different study types, the important assay characteristics are what sample is needed (e.g., serum,

blood spot, nasopharyngeal swab, and nasal wash); where the assay can be performed (e.g., at home or in a laboratory); what resources, equipment, and reagents are needed; sample throughput and turnaround time; and cost. For public health, rapid and scalable approaches (e.g., point-of-care assays or laboratory testing of self-collected samples) are desirable. Such tests could also be useful for COVID-19 research in settings where restrictions on movement and social contact might limit the ability to collect samples. However, these methods need to be adequately validated before widespread use. The loss of information that comes with these tests might be offset by their ease of administration for some research questions but not for others.

Seroepidemiologic Study Designs and Uses

We assessed 3 seroepidemiologic study designs: cross-sectional studies, cohort studies, and targeted population studies. We also address the question of at-home or on demand testing. We provide a description of each type, the questions they could help answer, and issues with representativeness and implementation during the pandemic (Table).

Cross-Sectional Studies

Cross-sectional studies measure prevalence of antibody responses in a sample of the population at a single time point. These studies might be repeated at multiple time points (a repeated cross-sectional design) but not necessarily from the same persons. What inferences can be made about the wider population depends largely on how representative the study sample is. Studies with representative simple- or cluster-based random sampling of the population are the gold standard but require extensive planning, resources, and community engagement. Many other potential sources of serum samples for cross-sectional serologic studies are available, including residual serum samples from patients undergoing medical investigations and blood donation banks. These studies can be conducted more rapidly on routinely collected samples and might have access to historically collected, preepidemic samples available for analysis. However, they require different considerations of representativeness; residual serum samples reflect persons who are generally more ill than the general population and might come with biases inherent in clinical testing criteria, whereas blood donors tend to be healthier and do not include children. Moreover, routinely available blood samples might lack information beyond basic demographics, such as geographic information, underlying conditions, or potential risk factors for infection that could affect the epidemiology and transmission of SARS-CoV-2.

Table. Describing different study designs, questions they could answer, and issues with study design and execution during the coronavirus disease pandemic

Study type	Brief description	Questions study could answer	Issues with interpretation and representativeness	Issues with conducting during a pandemic
Cross-sectional	A sample of the population has serum samples collected at 1 time point	Background cross-reactivity (if started before pandemic); current proportion of population that have been infected; proportion of population that is immune (if a correlate of protection defined); infection fatality ratio (with information on cases or deaths in the same population)	For the different modes of collection (e.g., blood banks, residual sera, and volunteers), different issues can bias the sample included in the study that must be assessed	Blood banks might have fewer participants, residual sera studies in hospitals might have fewer samples or over representation of severe acute respiratory syndrome coronavirus 2 infections
Cohort	The same persons are followed up over time, with serum samples collected at regular intervals, and information on disease in intervening periods	Background cross-reactivity (if started before pandemic); ratio of asymptomatic to symptomatic infections; waning of antibody levels, correlates, and duration of protection; changes in infection dynamics over time	Attrition can make analysis and interpretation difficult, biases in which participants are retained across sampling rounds	Challenges in collecting and continuing cohort during outbreak; attrition
Targeted populations	Populations with particularly high exposures, such as those around index patients or healthcare workers, have serum samples taken either cross-sectionally or in a targeted cohort	Attack rates; ratio of asymptomatic to symptomatic infections; proportion of population infected, correlates, and duration of protection	Targeted populations because healthcare workers might have different infection exposure rates and intensity from the general population	Potentially logistically difficult to collect samples in household studies

Strict random sampling could also be relaxed by recruiting pragmatically through advertisements or from specific population groups but might be poorly representative and suffer from participation bias (e.g., if persons who think they have been previously exposed are more likely to participate). Invariably, a trade-off exists between ease of sampling and ease of interpretation, and studies employing more representative sampling strategies will yield more valuable information.

Prepandemic samples can be used to determine background non–SARS-CoV-2 coronavirus serologic profiles in populations. Repeated cross-sectional studies during the pandemic can give information on the proportion of a population infected, immune, or both at different time points and potentially different age groups (Figure 2, panels A–C). If compared with surveillance data, results of such studies can be used to estimate a reliable denominator of number of infections in the population for calculating infection fatality ratio. Studies conducted in different locations, particularly ones using the same assay or, after standardization of results, using different assays, will enable assessment of spatial heterogeneity in transmission.

During the pandemic, social distancing measures might restrict the ability to collect serum samples. Studies of residual serum samples might also be affected by reductions in hospital visits by noncritical patients, which will skew samples collected toward those from patients with substantial disease or COVID-19 patients. Blood banks might also have fewer donors during this period.

Cohort Studies

In cohort studies, the same persons are followed over time and samples collected periodically (Figure 2,

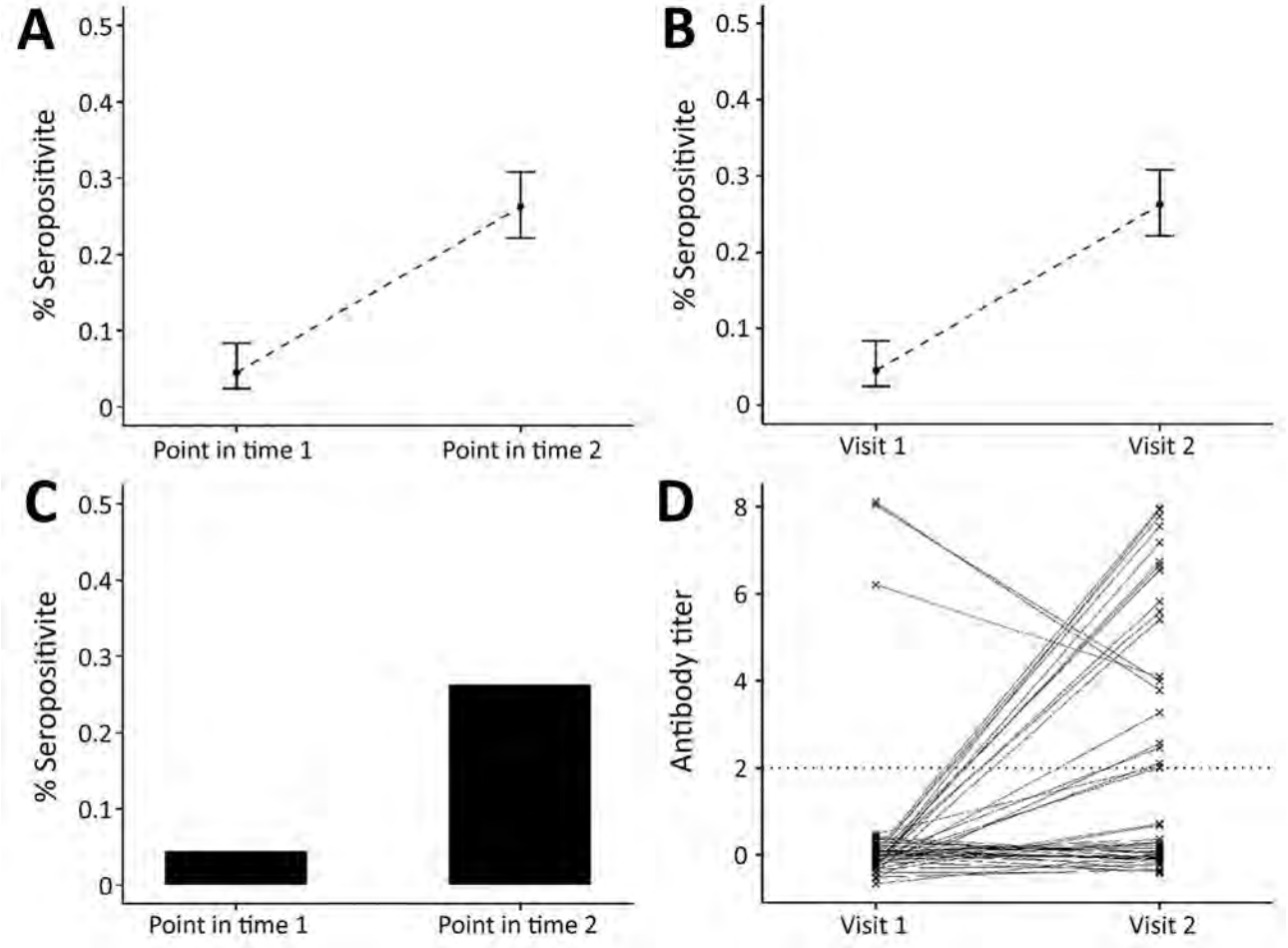

Figure 2. Link between severe acute respiratory syndrome coronavirus 2 infection dynamics and serologic analysis designs. A) Example of results from cross-sectional population study design, indicating percentage of study population who are seropositive at each sample time point. B) Example of results from a cohort study design: percentage of study population who are seropositive at each sample time point. The difference in the study designs is shown in panels C and D. C) In a cross-sectional design, we only know proportions in the population; however, panel D shows an example of each person's antibody titers over time, illustrating that in a cohort study we can follow the dynamics of antibody response over time (e.g., the proportion who seroconvert and person-to-person variability).

panel D) (*7*,*8*). During the intervening period, or at the point of sample collection, information might be collected on symptoms, healthcare use, and potential risk factors for infection. Cohort studies provide rich information but are expensive and labor-intensive to conduct. These studies might be conducted in communities, among specific populations (e.g., healthcare workers or pregnant women), or for biobanking. Cohorts can suffer from attrition, which causes issues in analyzing and interpreting the results. Therefore, during the pandemic, assessing whether cohorts should be collecting samples from, or information on, cohort participants who have died might be warranted.

Long-standing cohort studies might have historic serum samples to determine preepidemic non–SARS-CoV-2 coronavirus serologic profiles. In the short term, cohort studies can determine the incidence of infection. Concurrent symptom surveillance and acute illness sampling within cohorts can add considerable information and help determine the ratio of asymptomatic to clinically apparent infections. However, because of limits in cohort size, the number of severe cases might be insufficient to precisely estimate ratios of infection to severe illness and death.

Cohort studies might be useful to determine correlates of protection and the duration and waning of immunity. Depending on the size, demographics, and geographic distribution of the cohort, these studies might provide information on the serologic profile in different population subgroups. However, in some cases, these cohorts might be geographically or demographically restricted, so extrapolation to the whole population might not be possible.

Using existing cohorts, after making adjustments to ensure the cohorts capture information relevant to COVID-19, obviates the need to set up new cohorts. However, ongoing cohort studies might face restrictions on data and sample collection during the outbreak, and innovation might be needed.

Targeted Population Studies

Targeted population studies might be conducted by following populations with high infection risk or in whom infection has wider consequences, such as healthcare workers or households of case-patients. However, the exposure of healthcare workers might not be similar to that of the rest of the population.

As well as being of use for understanding infection rates in this important population, samples from healthcare workers and household members could be used to determine correlates of protection by comparing antibody profiles and subsequent infections. Fewer constraints on such collections would exist during an outbreak because healthcare workers will be coming to healthcare settings, where this type of study could be conducted.

Early in the pandemic, household studies might be useful to understand the proportion of infections that are asymptomatic; they are also useful in understanding age-specific infection rates because household members will vary in age but presumably will have exposure to any infectious person in the household. An advantage of these studies is that household contacts of a case-patient have greater exposure to infection at that time and that person's exposure within households would likely be fairly uniform. Similar to previous study designs, issues with collecting samples under movement restrictions might exist.

Persons Getting Tested for Their Own Personal Knowledge

Although not an epidemiologic study design, allowing persons to undertake home serologic tests to determine if they have been infected has generated interest recently. If a positive test result correlates well with immunity, then such tests could help determine which persons are no longer susceptible to infection and can safely resume normal activities. These samples might not be representative because persons might be more likely to request testing if they think they have been infected or if a family member or contact has been infected, and certain demographics might be overrepresented or underrepresented. The addition of a research component to such assay deployments, where persons are recruited randomly, could help overcome the limitation of information derived from this means of collection and provide valuable data.

Current tests are not sufficiently accurate for this use, and questions remain about the relationship between seropositivity and magnitude and duration of protection. However, such information could still have public health value. With additional demographic data on persons being tested, this approach could give information about the proportion of the population that has been infected (with caveats regarding the representativeness of the tested population). This approach might be less limited by restrictions on movements because of COVID-19.

Analytical Methods for Inferring Past Infection from Serologic Data

Recently, analytical methods for using serologic data to determine prevalence of past infection have progressed considerably, through an improved understanding of immunology and novel statistical methods.

A substantial body of literature now exists on statistical and mathematical modeling methods for antibody data, alongside off-the-shelf software packages. Antibody levels vary over time for each infected person in a population experiencing a COVID-19 epidemic (Figure 1). Existing methods to analyze this process fall into 2 broad categories. In the first category are methods that reduce assay results into binary metrics of seropositivity (a single reading above a specified threshold) (Figure 2, panels A and C) or seroconversion (an increase between 2 time points for the same person above a threshold) (Figure 2, panels B and D). In the second category are methods that incorporate full information on the magnitude or time series of antibody assay results (Figure 1, panel C).

If SARS-CoV-2 infection is found to generate stable, consistent antibody dynamics after infection, then binary metrics are likely to give accurate estimates of seroprevalence, albeit with considerations of assay variability and the sensitivity of the chosen threshold (*9*,*10*). The attack rate and force of infection (Figure 1, panel B), measures of transmission intensity, can then be calculated with existing serocatalytic models and software packages (*11*,*12*), with statistical adjustments for the (known) sensitivity and specificity of the chosen assay and the time lag between infection and seropositivity (*11*–*15*).

However, if antibody kinetics after SARS-CoV-2 infection follow a more complicated trajectory, then models that capture additional immunologic mechanisms (e.g., timing of development, antibody waning, cross-reactivity with other pathogens, or variation in person-level responses) will be required (*16*,*17*). The importance of these variables will depend on SARS-CoV-2 immunology, properties of the chosen assay (*3*), and the antibody isotype (*1*,*18*) being measured. Combining results from different assays and isotypes might be a powerful approach.

Methods for accounting for bias in the way samples are collected, and therefore who is in the study, must also be used, bearing in mind that for some study designs, fully accounting for biases will not be possible. The sensitivity and specificity and the proportion of the population that is infected are important for interpreting results. Methods for estimating population infection prevalence from serologic data are being developed, and one such method is described by Larremore et al. (*19*).

Analytical Methods to Infer Correlates of Protection

A recent review highlighted that, for the seasonal coronaviruses, only human challenge experiments have provided the level of data needed to identify a correlate of protection (A.T. Huang et al., unpub. data). Establishing a correlate of protection is difficult for any infectious disease, but challenges exist for novel pathogens, particularly during an outbreak with rapidly changing dynamics. When using the results from cohort studies as we have described, statistical analysis comparing preexposure immune responses in persons who subsequently have disease versus those that do not can provide information about whether an assay has characteristics that are useful for defining protective immunity or a correlate of protection. Similar work has been done for chikungunya and influenza viruses (*20*,*21*). However, potential confounders, such as differences in exposure risk over time, must be considered carefully in this type of analysis. Any measured level or correlate of protection will be specific to the assay used in the studies, as was the case for measles (*22*). Even for measles, where a correlate of protection has been used consistently, a recent review found little evidence to support the threshold used, suggesting this threshold needs refinement (*22*).

Comparing and Extrapolating Serologic Data across Studies and Geographic Regions

Studies will be useful for understanding situations in a particular population, place, and time. An important consideration is whether results can give information about transmission or immunity in other groups. Age, underlying conditions, or a combination of both have been shown to affect infection outcome and therefore should be considered carefully when extrapolating from one population to another. For the asymptomatic proportion, differences in reporting and surveillance systems between places and over time mean extrapolation should be done with care.

The use of various assays in different places shows the need to determine whether building methods to compare results from different assays in different populations is possible. Quantifying intra- and inter-laboratory variability of the same assay and between-assay variability will therefore be crucial.

Rapid Sharing and Comparative Analysis of Serologic Data

As proposed previously (*23*), rapid sharing and dissemination of serologic data are useful for clarifying infectious disease dynamics and have become even more vital given the urgency of questions in the current pandemic. Phylogenetic analysis has greatly benefited from development of the GISAID database (https://www.gisaid.org) to enable rapid sharing of

genomic data and from platforms like Nextstrain (*24*) for rapid analysis. Rapid sharing would enable comparison of assays across populations (including comparing prepandemic samples for understanding cross-reactivity in different populations). Rapid sharing would also enable pooled analyses, comparison of parameters of transmission, and gauging of the effect of interventions across place and time. If a database were to be developed, a core set of data would need to be collected on each sample and on each study and assay. WHO has proposed that all such data be shared with WHO and has issued standardized protocols (*4*), but even more open sharing would also enable rapid analysis and decision making. The rapid sharing of tools specifically to analyze SARS-CoV-2 serologic studies will also be useful. Even if data sharing is not possible, as results of seroepidemiologic studies are released, they need to clearly show how subjects were recruited, what inclusion criteria and which assay were used, and how the analysis was conducted.

Conclusions

Serologic studies at multiple stages of an epidemic could provide fundamental information for understanding the extent of past transmission, the current state of the epidemic, and future transmission. However, successful deployment of serologic testing will require optimization, validation, and proper interpretation of assays, which requires studies focused on these specific questions. Different types of epidemiologic study will be best and viable at different times during the outbreak and in different settings, and the biases of these study designs should be carefully taken into account in analysis and interpretation. Triangulation between multiple types of studies might also be of use. Current movement restrictions might constrain implementation of some study designs, so thought should be given to other study designs, although with consideration of their possible biases. The utility of serologic studies can be even greater if they are designed for optimal cross-location comparison. A platform to enable rapid data sharing, and therefore analyses across places and times, would also be very powerful.

About the Author

Dr. Clapham is an assistant professor in the Saw Swee Hock School of Public Health at the National University of Singapore. Her research covers mathematical modelling of infectious diseases, including the design and use of seroepidemiologic studies and surveillance to understand disease transmission.

References

1. Amanat F, Stadlbauer D, Strohmeier S, Nguyen THO, Chromikova V, McMahon M, et al. A serological assay to detect SARS-CoV-2 seroconversion in humans. Nat Med. 2020 May 12 [Epub ahead of print]. https://doi.org/10.1038/s41591-020-0913-5
2. Center for Health Security. Serology-based-tests-for-COVID-19 [cited 2020 Apr 3]. http://www.centerforhealthsecurity.org/resources/COVID-19/Serology-based-tests-for-COVID-19.html
3. Okba NMA, Müller MA, Li W, Wang C, GeurtsvanKessel CH, Corman VM, et al. Severe acute respiratory syndrome coronavirus 2–specific antibody responses in coronavirus disease 2019 patients. Emerg Infect Dis. 2020 Apr 8 [Epub ahead of print]. https://doi.org/10.3201/eid2607.200841
4. World Health Organization. Population-based age-stratified seroepidemiological investigation protocol for COVID-19 virus infection [cited 2020 Apr 6]. https://www.who.int/publications-detail/population-based-age-stratified-seroepidemiological-investigation-protocol-for-covid-19-virus-infection
5. World Health Organization. Laboratory biosafety guidance related to coronavirus disease 2019 (COVID-19): interim guidance [cited 2020 May 6]. https://apps.who.int/iris/bitstream/handle/10665/331138/WHO-WPE-GIH-2020.1-eng.pdf
6. Liu Y, Yan L-M, Wan L, Xiang T-X, Le A, Liu JM, et al. Viral dynamics in mild and severe cases of COVID-19. Lancet Infect Dis. 2020;20:656–7. https://doi.org/10.1016/S1473-3099(20)30232-2
7. Anderson KB, Chunsuttiwat S, Nisalak A, Mammen MP, Libraty DH, Rothman AL, et al. Burden of symptomatic dengue infection in children at primary school in Thailand: a prospective study. Lancet. 2007;369:1452–9. https://doi.org/10.1016/S0140-6736(07)60671-0
8. Tan KHX, Tan LWL, Sim X, Tai ES, Lee JJ, Chia KS, et al. Cohort profile: The Singapore Multi-Ethnic Cohort (MEC) study. Int J Epidemiol. 2018;47:699. https://doi.org/10.1093/ije/dyy014
9. Cauchemez S, Horby P, Fox A, Mai LQ, Thanh LT, Thai PQ, et al. Influenza infection rates, measurement errors and the interpretation of paired serology. PLoS Pathog. 2012;8:e1003061.
10. Zhao X, Siegel K, Chen MI-C, Cook AR. Rethinking thresholds for serological evidence of influenza virus infection. Influenza Other Respir Viruses. 2017;11:202–10. https://doi.org/10.1111/irv.12452
11. Hoze N. nathoze/Rsero: estimate the annual force of infection using serological data version 1.0 from GitHub [cited 2020 Apr 21]. https://rdrr.io/github/nathoze/Rsero
12. European Centre for Disease Prevention and Control. Seroincidence calculator tool [cited 2020 Apr 20]. https://www.ecdc.europa.eu/en/publications-data/seroincidence-calculator-tool
13. Wu JT, Ho A, Ma ESK, Lee CK, Chu DK, Ho PL, et al. Estimating infection attack rates and severity in real time during an influenza pandemic: analysis of serial cross-sectional serologic surveillance data. PLoS Med. 2011;8:e1001103. https://doi.org/10.1371/journal.pmed.1001103
14. Azman AS, Lessler J, Luquero FJ, Bhuiyan TR, Khan AI, Chowdhury F, et al. Estimating cholera incidence with cross-sectional serology. Sci Transl Med. 2020;11:eaau6242.
15. Salje H, Cauchemez S, Alera MT, Rodriguez-Barraquer I, Thaisomboonsuk B, Srikiatkhachorn A, et al. Reconstruction of 60 years of chikungunya epidemiology in the Philippines demonstrates episodic and focal transmission. J Infect Dis. 2016;213:604–10. https://doi.org/10.1093/infdis/jiv470

16. Teunis PF, van Eijkeren JC, de Graaf WF, Marinović AB, Kretzschmar MEPFT. Linking the seroresponse to infection to within-host heterogeneity in antibody production. Epidemics. 2016;16:33–9. https://doi.org/ 10.1016/j.epidem.2016.04.001
17. Zhao X, Ning Y, Chen MI-C, Cook AR. Individual and population trajectories of influenza antibody titers over multiple seasons in a tropical country. Am J Epidemiol. 2018;187:135–43. https://doi.org/10.1093/aje/kwx201
18. Zhao J, Yuan Q, Wang H, Liu W, Liao X, Su Y, et al. Antibody responses to SARS-CoV-2 in patients of novel coronavirus disease 2019. Clin Infect Dis. 2020 Mar 8 [Epub ahead of print].
19. Larremore DB, Fosdick BK, Bubar KM, Zhang S, Kissler S, Metcalf CJE, et al. Estimating SARS-CoV-2 seroprevalence and epidemiological parameters with uncertainty from serological surveys [cited 2020 Apr 20]. https://dash.harvard.edu/handle/1/42659939
20. Ranjeva S, Subramanian R, Fang VJ, Leung GM, Ip DKM, Perera RAPM, et al. Age-specific differences in the dynamics of protective immunity to influenza. Nat Commun. 2019;10:1660. https://doi.org/10.1038/s41467-019-09652-6
21. Yoon IK, Srikiatkhachorn A, Alera MT, Fernandez S, Cummings DAT, Salje H. Pre-existing chikungunya virus neutralizing antibodies correlate with risk of symptomatic infection and subclinical seroconversion in a Philippine cohort. Int J Infect Dis. 2020;95:167–73. https://doi.org/10.1016/j.ijid.2020.03.073
22. Bolotin S, Hughes SL, Gul N, Khan S, Rota PA, Severini A, et al. What is the evidence to support a correlate of protection for measles? A systematic review. J Infect Dis. 2020;221:1576–83. https://doi.org/10.1093/infdis/jiz380
23. Metcalf CJE, Farrar J, Cutts FT, Basta NE, Graham AL, Lessler J, et al. Use of serological surveys to generate key insights into the changing global landscape of infectious disease. Lancet. 2016;388:728–30. https://doi.org/10.1016/S0140-6736(16)30164-7
24. Hadfield J, Megill C, Bell SM, Huddleston J, Potter B, Callender C, et al. Nextstrain: real-time tracking of pathogen evolution. Bioinformatics. 2018;34:4121–3. https://doi.org/10.1093/bioinformatics/bty407

Address for correspondence: Hannah Clapham, Saw Swee Hock School of Public Health, National University of Singapore, 16 Medical Dr, Singapore, 117597; email: hannah.clapham@nus.edu.sg

Polyclonal *Burkholderia cepacia* Complex Outbreak in Peritoneal Dialysis Patients Caused by Contaminated Aqueous Chlorhexidine

Sally C.Y. Wong,[1] Shuk-Ching Wong, Jonathan H.K. Chen, Rosana W.S. Poon, Derek L.L. Hung, Kelvin H.Y. Chiu, Simon Y.C. So, Wing Shan Leung, Tak Mao Chan, Desmond Y.H. Yap, Vivien W.M. Chuang, Kwok-Yung Yuen,[2] Vincent C.C. Cheng[2]

Whether *Burkholderia cepacia* complex should be an objectionable organism in antiseptic solutions with acceptable total bacterial counts is controversial. By using next-generation sequencing, we documented a polyclonal *B. cepacia* complex outbreak affecting peritoneal dialysis patients in Hong Kong that was caused by contaminated chlorhexidine solutions. Epidemiologic investigations at a manufacturing site identified a semiautomated packaging machine as the probable source of contamination in some of the brands. Use of whole-genome sequencing differentiated the isolates into 3 brand-specific clonal types. Changes in exit site care recommendations, rapid recall of affected products, and tightening of regulatory control for chlorhexidine-containing skin antiseptics could prevent future similar outbreaks. Environmental opportunistic pathogens, including *B. cepacia* complex, might be included in regular surveillance as indicator organisms for monitoring environmental contamination.

Burkholderia cepacia is the type species of the genus *Burkholderia* and is a ubiquitous multidrug-resistant, motile, non–glucose-fermenting, gram-negative organism found in water and soil (*1*). The *B. cepacia* complex (BCC) contains ≥17 closely related species that require molecular methods for accurate differentiation (*2*). Previous typing methods, such as pulsed-field gel electrophoresis, restriction fragment-length polymorphism, or multilocus sequence typing (MLST), are ineffective and only enable differentiation into genome variants.

BCC is a major pathogen among patients with cystic fibrosis and an opportunistic pathogen affecting patients with indwelling medical devices and immunosuppression (*3*). Although >50 BCC-related nosocomial outbreaks associated with contaminated antiseptics or medications have been described, none of the skin disinfectant–related outbreaks were documented by next-generation genome sequencing as the typing method. The exact mode of contamination of commercial antiseptics was often not found (*4*,*5*). Implicated disinfectants and medications included intrinsically or extrinsically contaminated chlorhexidine (*4*–*11*), povidone–iodine (*12*,*13*), benzalkonium chloride (*14*–*16*), intravenous fluids or drugs (*17*–*20*), sodium docusate (*21*,*22*), eye drops (*23*), alcohol-free mouthwash, and nebulized salbutamol and albuterol (*24*–*26*).

There is a lack of consensus on whether *B. cepacia* should be considered an objectionable organism in nonsterile pharmaceutics according to guidelines for the United States and Europe (*27*–*30*). We report an outbreak involving ≥2 clusters of BCC strains among peritoneal dialysis patients caused by multiple brands of contaminated, prepackaged, single-use, 0.05% aqueous chlorhexidine (aqCHX) solutions.

Materials and Methods

Outbreak Investigation

On September 6, 2019, we conducted an investigation at the Queen Mary Hospital Dialysis Unit in

Author affiliations: Queen Mary Hospital, Hong Kong, China (S.C.Y. Wong, S.-C. Wong, J.H.K. Chen, R.W.S. Poon, D.L.L. Hung, K.H.Y. Chiu, S.Y.C. So, W.S. Leung, Vincent C.C. Cheng); The University of Hong Kong, Hong Kong (T.M. Chan, D.Y.H. Yap, K.Y. Yuen); Hospital Authority, Hong Kong (V.W.M. Chuang)

DOI: https://doi.org/10.3201/eid2609.191746

[1]Current affiliation: Queen Elizabeth Hospital, Hong Kong, China.

[2]These senior authors contributed equally to this article.

Hong Kong when a cluster of 4 dialysis patients had BCC isolated from their exit site. All 4 patients had recent-onset serous to bloody discharge from their exit site (3 peritoneal dialysis catheter exit sites and 1 hemodialysis catheter exit site). The hospital is a 1,700-bed university-affiliated tertiary referral center serving ≈270 peritoneal dialysis and 110 hemodialysis patients. Noting the unusual number of BCC among renal patients, we performed case finding and established baseline incidence rate of BCC during January 1, 2014–September 9, 2019, by using a laboratory information system (software system that records, manages, and stores data for clinical laboratories).

For the outbreak investigation, we defined a case-patient as a peritoneal dialysis patient who had BCC isolated from clinical specimens during March 13, 2018–October 30, 2019. The medical records of case-patients were reviewed by the infection control team as described (*31*). Epidemiologic investigation at the renal unit was performed, and nursing staff were interviewed and observed for any changes in their patient care practice; patients and their relatives, if available, were interviewed about their exit site care procedures. Environmental surveillance was conducted as described in the next section. Active surveillance was initiated for all peritoneal dialysis patients; we collected exit site swab specimens to screen for additional BCC cases. Ethics approval was obtained from the institutional review board of the University of Hong Kong/Hospital Authority Hong Kong West Cluster.

Environmental Surveillance

Air, water, and environmental samples from the peritoneal dialysis unit, together with various antiseptics used for exit site care from our hospital and the community, were collected and microbiologically analyzed as described (*31*,*32*) (Appendix, https://wwwnc.cdc.gov/EID/article/26/9/19-1746-App1.pdf). In brief, we collected surface specimens by using premoistened, Polywipe sponge swabs (Medical Wire & Equipment, https://www.mwe.co.uk). We sampled faucets and drains of sinks by using transport rayon swabs (Copan Diagnostics, https://www.copanusa.com). We collected tap water (250 mL) into labeled sterile bottles. We used an air sampler, SAS Super ISO 180 model 86834 (VWR International PBI Srl, https://it.vwr.com), to collect 1,000 liters of air onto MacConkey agar (CM 0507; Oxoid, http://www.oxoid.com) containing 0.0005% crystal violet (Merck KGaA, https://www.emdgroup.com) and 4 μg/mL gentamicin (CG-MAC). We collected in-use and unopened antiseptics in the hospital. Unopened 0.05% aqCHX was also obtained from other (outside) stores.

Tap water was filtered through a 0.45-μm membrane, which was then inoculated onto CG-MAC. Sponge swabs and transport rayon swabs were incubated in sterile selective brain heart infusion broth (CM1135; Oxoid) containing 4 μg/mL gentamicin, 15 μg/mL vancomycin, and 1 μg/mL amphotericin B (G3632, V2002, and A4888, respectively; Sigma-Aldrich, https://www.sigmaaldrich.com) at 37°C overnight before inoculation onto CG-MAC. All disinfectants and antiseptics were subjected to 1:10 dilution with neutralization broth (brain-heart infusion plus 2% Tween 80 [P1754; Sigma-Aldrich], 0.3% sodium thiosulphate pentahydrate [27910.260; VWR Chemicals, https://us.vwr.com], 0.4% potassium dihydrogen phosphate [26936.260; VWR Chemicals], and 0.5% lecithin). The suspension was left at room temperature for 5 min, then 100 μL of the suspension was spread onto blood agar (CM0331; Oxoid). Water and air samples were incubated at 37°C for 1 day, followed by room temperature for 5 days. Other specimens were incubated at 37°C for 5 days and examined daily for visible bacterial growth. Any bacterial growth was further speciated, and bacterial CFUs were also counted for air and antiseptic cultures.

Clinical Specimens

We processed all clinical specimens obtained before the outbreak investigation according to standard laboratory operating procedures. We performed active surveillance for BCC collected by swabbing catheter exit sites for all peritoneal dialysis patients. These swab specimens were inoculated onto CG-MAC for incubation at 37°C for 2 days. Patients with clinical symptoms suggestive of invasive catheter-related infection were investigated accordingly (e.g., peritoneal fluid or blood culture).

Field Investigation at Brand B Manufacturing Site

On September 19, 2019, a joint field investigation at brand B manufacturing site was conducted by a team of field epidemiologists, infection control professionals, and clinical microbiologists. The process of reconstitution, dilution, and packaging of 5% chlorhexidine solution into individually packed 25-mL volumes of 0.05% aqCHX was directly observed. Environmental samples and antiseptics were collected for microbiological investigations as described in the previous sections.

Identification by Matrix-Assisted Laser Desorption/Ionization Time-of-Flight Mass Spectrometry

We picked bacterial colonies from blood agar or CG-MAC for matrix-assisted laser desorption/

ionization time-of-flight (MALDI-TOF) mass spectrometry identification with bacterial colony protein extraction by using a direct transfer method. We measured mass spectra of isolates by using the MBT Smart Mass Spectrometer (Bruker Daltonik, https://www.bruker.com) and the Bruker MBT Database 9.0 (8326 spectra). Scores >2.0 were considered as showing high-confidence identification and scores of 1.7–2.0 as showing low-confidence identification.

Whole-Genome Sequencing and Bioinformatic Analysis

We further analyzed environmental and clinical BCC isolates by using the NovaSeq 6000 Sequencing System (Illumina Inc., https://www.illumina.com) at The University of Hong Kong Li Ka Shing Faculty of Medicine, Centre for PanorOmic Sciences, Genomics Core (Appendix). Two archived outbreak-unrelated BCC isolates were used as controls. We extracted MLST profiles from whole-genome assemblies by using BIGSdb, which is available on the BCC PubMLST website (*33*). We performed phylogenetic analysis according to single-nucleotide polymorphisms (SNPs) by using CSIPhylogeny version 1.4 with default settings (Appendix) (*34*). Results from CSIPhylogeny were subsequently imported into FigTree version 1.4.4 (http://tree.bio.ed.ac.uk) for visualizing the phylogenetic tree.

Statistical Analysis

We used the exact rate ratio test to compare exit site infection (ESI) rates between centers with and without routine chlorhexidine use. A p value <0.05 was considered statistically significant. We applied the Holm-Bonferroni correction for multiple comparisons to control the familywise error rate at 0.05. We used the R package rateratio.test (https://www.r-project.org) to perform calculations. We used an independent *t*-test to compare means of outbreak durations involving nonsterile and sterile sites. We used SPSS Statistics 20 (IBM, https://www.ibm.com) to perform this analysis.

Results

Epidemiologic Investigation

On September 6, 2019, we launched an outbreak investigation when BCC was isolated from 3 peritoneal dialysis catheter exit sites and 1 hemodialysis catheter exit site for 4 patients (2 women and 2 men; age range 49–90 years, median age 60.5 years). The exit site swab specimens were used for investigation of suspected ESI on September 4, 2019. Three patients had BCC isolated from previous exit site specimens, 1 from as early as September 24, 2018. The number of days from catheter insertion to first isolation of BCC ranged from 300 to 2,329 days (mean 1,084.5 days, median 854.5 days).

Retrospective case finding of BCC showed an increasing trend over time among nonduplicated dialysis patients since March 2018. During March 13, 2018–September 6, 2019, BCC was isolated from 53 renal patients, including 47 peritoneal dialysis catheter exit sites and 2 peritoneal fluid specimens (Table 1). The incidence rate of BCC isolated from peritoneal dialysis catheters during 2018–2019 was >2 SD from baseline (Figure 1), confirming an outbreak of BCC among peritoneal dialysis patients. Interviews with ward staff and observation of patient care practice found no recent changes or irregularity but showed that peritoneal dialysis patients purchased 0.05% aqCHX from community stores and used this solution for routine exit site care. Brands A and B were the commonest aqCHX bought by peritoneal dialysis patients because they were the most readily available brands in the community.

Environmental Surveillance

We collected 63 environmental and antiseptic specimens used in peritoneal dialysis catheter exit site care from the renal unit (Table 2). Different brands of aqCHX were purchased in the community (brands A–F) and collected in the hospital (brands G and H). All 77 aqCHX collected in the hospital were culture negative, but 103 of the 104 community aqCHX showed bacterial growth (Table 2). Brand A of aqCHX had an average bacterial load of 3.6×10^5, and brand B had a value of 5.9×10^4 CFU/mL. No BCC was isolated from environmental samples and other antiseptics collected from the renal unit.

Clinical Specimens

We collected peritoneal dialysis catheter exit site swab specimens from 275 patients for BCC surveillance. A total of 62 (22.5%) patients were positive for BCC, 33.9% (21/62) of whom had a genuine infection. A total of 29.0% (18/62) were among the 53 BCC-positive peritoneal dialysis patients identified from retrospective case finding.

Field Investigation at Brand B Manufacturing Site

We observed the entire process from dilution to packaging of aqCHX. In brief, 5% aqCHX was diluted with distilled water in the mixing compartment of a semiautomated packaging machine, which channeled and packed the diluted solution into

Table 1. Specimen types and demographic characteristics for 53 renal dialysis patients from whom *Burkholderia cepacia* complex was isolated, Hong Kong, China, March 13, 2018–September 6, 2019*

Characteristic	2018, 25 patients	2019, 28 patients	Total, 53 patients
Specimen type	23 PD catheter ES; 1 HD catheter ES; 1 ES swab specimen not otherwise specified	23 PD catheter ES; 2 HD catheter ES; 2 peritoneal fluid; 1 blood culture from HD catheter	46 PD catheter ES; 3 HD catheter ES; 2 peritoneal fluid; 1 blood culture from HD catheter; 1 ES swab specimen not otherwise specified
Age, y, mean (median, range)	60.1 (65, 24–81)	65.8 (66, 46–90)	63.1 (66, 24–90)
Sex ratio, F:M	16:9	13:15	29:24
Days from PD/HD catheter insertion until first isolation of *B. cepacia* complex, mean (median, range)	1,192 (648, 58–2,349)	1,140 (769.5, 70–6,098)	1,163, (713, 58–6,198)
B. cepacia complex peritonitis	1	4	5
Removal of PD catheter	1	3 (2 caused by renal transplant)	4
Previous infections			
ESI caused by other organisms	8	7	15
Peritonitis caused by other organisms	4	6	10
Antimicrobial drug use ≤1 y before isolation of *B. cepacian* complex	19	26	45
No. deaths†	2	2	4

*ES, exit site; ESI, exit site infection; HD, hemodialysis; PD, peritoneal dialysis.
†None of the 4 deaths were attributable to infection by *B. cepacia* complex.

25-mL sachets (Figure 2). Samples of antiseptics were taken before and after each step, together with additional environmental samples from the site. BCC was found in 19 of 29 environmental samples and antiseptics collected, and 3 freshly packed antiseptics also yielded *Achromobacter* species (Table 2). BCC was first detected at a low level after chlorhexidine was diluted with distilled water in the semi-automated machine, then at high level in all subsequent packaged aqCHX, implying that the machine was the probable source of contamination. No BCC was found in the distilled water, air samples, or samples taken from measuring beaker, mixing rod, and unused package material.

Identification by MALDI-TOF Mass Spectrometry

All isolates were identified correctly to the genus level and had scores ≥1.7. Further species identification within the BCC was not possible.

Whole-Genome Sequencing and Bioinformatic Analysis

A total of 80 isolates (52 patient isolates from active surveillance; 26 chlorhexidine-related isolates, including 5 isolates from the manufacturing site; and 2 outbreak-unrelated strains) were subjected to genome sequencing (Appendix Tables 1, 2). MLST analysis identified 2 predominant types. All BCC isolated from brands A, D, and E aqCHX (from the same company) were *B. cenocepacia* genomovar IIIA sequence

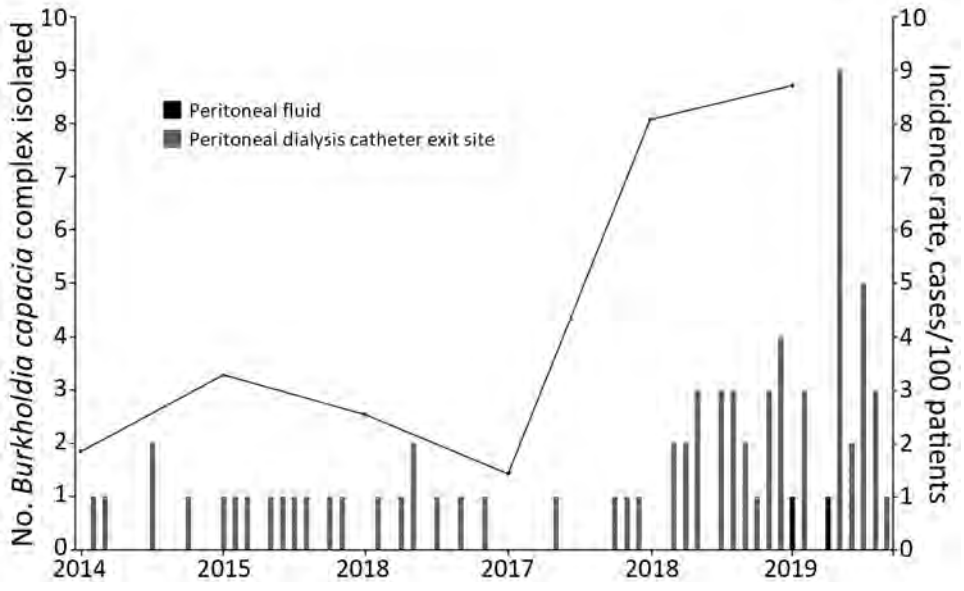

Figure 1. Epidemic curve and incidence rate of *Burkholderia cepacia* complex isolated from peritoneal dialysis patients, Hong Kong, China, January 2014–September 2019.

Table 2. Environmental specimens collected and tested for investigation of *Burkholderia cepacia* complex outbreak in peritoneal dialysis unit, Hong Kong, China, March 13, 2018–September 6, 2019*

Characteristic	No. specimens	Culture result (mean, median, range), CFU/mL
Peritoneal dialysis unit		
Environment		
Air samples	2	Negative for BCC
Swab specimens from sink and faucet	12	
Water samples from sink in ward	10	
Soaps from dispensers next to patient sinks	4	
Swab specimens from wound dressing trolleys	3	
Blood pressure cuffs, gloves, and tissue paper	6 (2 each)	
Connection shield SysIIK with povidone–iodine solution†	3	
Exit site care agents		
In-use povidone–iodine	10	Negative for BCC
Single-use prepackaged saline and sterile water	10 (5 each)	
White wine vinegar	3	
Aqueous chlorhexidine		
Brand A (outside hospital)	51	43 with BCC only (3.6×10^3, 1.9×10^2, $2.7–7.6 \times 10^4$); 4 with *Ralstonia* species only (77, 85, 46–93); 4 with BCC and *Ralstonia* species (120, 120, 94–130)
Brand B (outside hospital)	45	45 with BCC (5.9×10^4, 4.6×10^4, $2.9 \times 10^4–1.2 \times 10^5$)
Brand C (outside hospital)	4	4 with BCC (8.3×10^3, 6.8×10^3, $8 \times 10^2–1.9 \times 10^4$)
Brand D (outside hospital)	2	2 with BCC (2.8×10^5, 2.8×10^5, $2.4–3.2 \times 10^5$)
Brand E (outside hospital)	1	1 with BCC (1.5×10^5)
Brand F (outside hospital)	1	Negative for BCC
Brand G (from hospital)	47	Negative for BCC
Brand H (from hospital)	30	Negative for BCC
Brand B manufacturing site		
Environment		
Air samples	2	Negative for BCC
Plastic packaging	1	Negative for BCC
Plastic container in preparation room	1	Negative for BCC
Surface of fan in preparation room	1	Negative for BCC
Surface of air conditioner in preparation room	1	Negative for BCC
Specimens collected during dilution and packaging process		
5% chlorhexidine from original bottle	1	Negative for BCC
Chlorhexidine in measuring beaker	1	Negative for BCC
Distilled water	1	Negative for BCC
Diluted chlorhexidine in mixing compartment of semiautomated packaging machine ([I] in Figure 2), before mixing with stirring rod	1	BCC from enriched culture method with overnight incubation in neutralization broth
Stirring rod surface swab specimen, before mixing diluted chlorhexidine solution	1	Negative for BCC
Stirring rod surface swab specimen, after mixing diluted chlorhexidine solution	1	BCC from enriched culture method with overnight incubation in neutralization broth
Diluted chlorhexidine in mixing bowl of packaging machine, after mixing with stirring rod	1	BCC from enriched culture method with overnight incubation in neutralization broth
Newly packed 25 mL 0.05% aqueous chlorhexidine	16	16‡ with BCC 1.2×10^5, 1.2×10^5, $3.6 \times 10^4–2.4 \times 10^5$); 3 with concurrent *Achromobacter* species

*BCC, *Burkholderia cepacia* complex.
†Baxter Healthcare SA, https://www.baxter.com.
‡Three specimens had concurrent *Achromobacter* species found in culture.

type (ST) 1547, and all BCC isolated from brand B aqCHX and its manufacturing site were *B. cepacia* that had a novel ST (ST1693). The 2 BCC isolates from brand C were *B. cenocepacia* that had another novel sequence (ST1694).

The phylogenetic tree based on core SNPs was consistent with the MLST results showing 2 predominant clusters with highly related strains within each cluster (Figure 3). Strains from clusters A corresponded to brand A (and D and E) aqCHX and cluster B corresponded to brand B aqCHX, except that 1 brand A isolate (BCAP168) was different from cluster A strains. Both strains in cluster C corresponded to brand C aqCHX produced by a different company. A total of 47/52 patient isolates were indistinguishable or closely related to those in cluster A. Forty of these

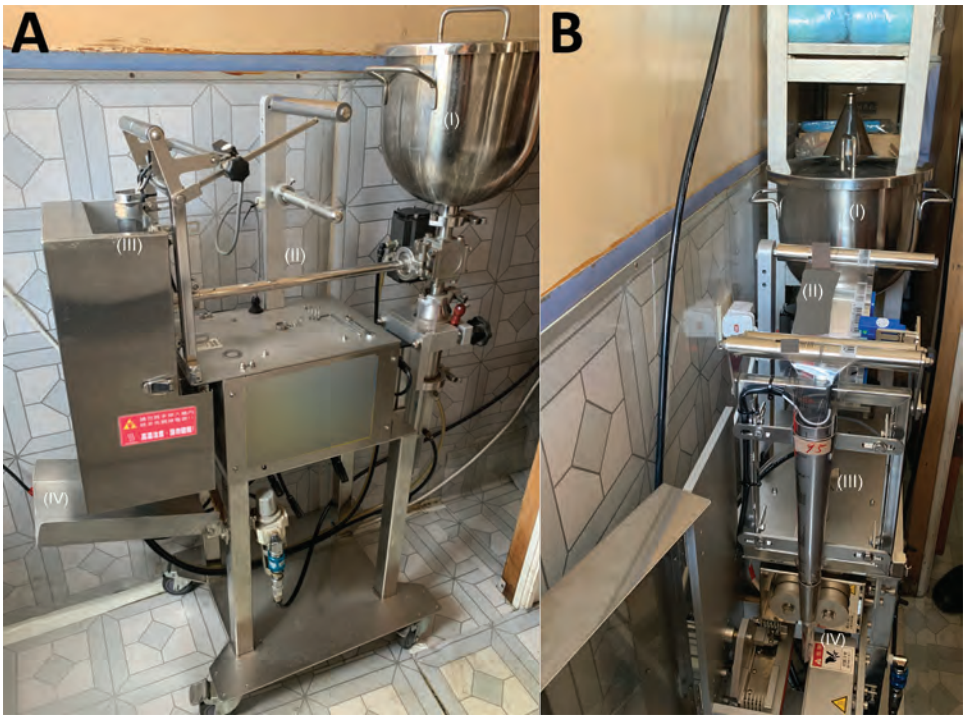

Figure 2. Semiautomated packing machine for aqueous chlorhexidine in brand B manufacturing site, Hong Kong, China, A) Mixing compartment (I), transfer tube from mixing compartment to dispensing end (II), area in which unused plastic packages are threaded (III), collection tray of newly packed 25 mL 0.05% aqueous chlorhexidine (IV). B) mixing compartment (I), unused plastic package (II), unused plastic package funneled to dispensing end (III), heat seal of 0.05% aqueous chlorhexidine into 25-mL packages (IV).

patients recalled using brand A for exit site care, 4 could not recall the brand used, and 3 reported using brand B. Of the 5 patients with isolates closely related to those in cluster B, 2 reported using brand B for exit site care, 2 reported using brand A, and 1 could not recall the brand used. The number of SNP differences in pairwise comparison of environment and patient isolates within cluster A was 0–165 and within cluster B was 0–32.

Outbreak Control

Upon reasonable suspicion of BCC contamination affecting prepacked aqCHX purchased in the community, the renal unit called all patients to stop such a practice and arranged alternative means of exit site disinfection. On September 17, 2019, the Hospital Authority and Centre for Health Protection (CHP), Department of Health, Hong Kong, were notified of the finding of BCC in prepackaged aqCHX. Further investigation by CHP identified 183 affected patients in public and private hospitals in Hong Kong (*35*). Several additional affected brands of aqCHX were identified and voluntarily recalled by the corresponding companies (*36*). We performed snapshot ESI surveillance between centers with routine and nonroutine chlorhexidine use by using data provided by the Hospital Authority; no major difference were found between the 2 practices (Table 3). Thus, sterile saline was recommended for routine exit site care in peritoneal dialysis patients instead of aqCHX.

On October 8, 2019, the Guidance Notes on Classification of Products as Pharmaceutical Product under the Pharmacy and Poisons Ordinance (Cap. 138) related to chlorhexidine was revised. Skin antiseptic products containing chlorhexidine are now classified as pharmaceutical products unless otherwise stated or under certain exceptions. This guidance took effect on July 8, 2020 (*37*).

Discussion

We report a polyclonal outbreak of BCC among peritoneal dialysis patients in our hospital that was caused by several contaminated brands of prepackaged aqCHX, which led to a territory-wide contact tracing that identified additional affected patients in other hospitals. Some observations can be made from this and previous BCC outbreaks. First, BCC outbreaks involving nonsterile sites were usually more prolonged; the mean outbreak duration was 85.4 days (median 66 days) when ≥50% of outbreak strains were isolated from sterile sites, compared with a mean of 245.9 days and a median of 199 days when ≥50% of BCC were isolated from nonsterile sites ($p = 0.001$) (Appendix Tables 3, 4). This finding might have occurred because BCC isolated from nonsterile sites might go unnoticed or were dismissed as sporadic, especially for patients with known risk factors, such as peritoneal dialysis catheters.

Also, the number of patients involved in an outbreak correlated with geographic distribution of the

contaminated source(s). For example, 2 recent, large BCC outbreaks involving 162 and 138 patients were caused by intrinsically contaminated intravenous saline and liquid docusate (*17*,*21*,*22*); both items were distributed to multiple states in the United States. From these and previous experiences (*38*), opportunistic environmental pathogens, such as BCC and nonanthrax *Bacillus*, might be used as indicator organisms for environmental contamination and be included as part of routine surveillance.

The use of whole-genome sequencing (WGS) provided high-resolution information for further analysis of this outbreak. First, it enabled accurate identification of BCC to species level and preliminary typing of bacterial strains through MLST. Phenotypic tests and MALDI-TOF mass spectrometry are inaccurate in speciation within BCC, and unlike previous BCC outbreaks, in which identical antibiogram profiles were found among outbreak-related BCC (*4*,*39*), the antibiogram profiles among isolates from our patients were variable.

Although WGS is becoming increasingly used for outbreak investigations, the technology is not readily available in usual clinical microbiology laboratories and can be costly. Thus, alternative molecular typing methods, such as MLST or restriction fragment length polymorphism, remains the first choice for nosocomial outbreak investigations because they often provide sufficient information for evaluation of smaller scale, more focused outbreaks. In addition, these methods are also helpful for preliminary evaluation of larger outbreaks. Nevertheless, we opted for WGS in our investigation because of anticipated large-scale involvement, and the need for high-resolution data for analysis to enable rapid enforcement of corrective measures at a regional level.

Phylogenetic analysis of the WGS data based on SNP differences unambiguously differentiated the outbreak BCC isolates into distinct clusters. Combined with epidemiologic findings and field investigation at brand B manufacturing site, we believe that the contamination of aqCHX most likely occurred at their corresponding manufacturing sites. First, brand A aqCHX was manufactured outside Hong Kong and had no direct geographic linkage with the brand B manufacturing site. Second, the 5% chlorhexidine from the unopened bottle at the brand B manufacturing site did not show any growth of BCC, and presence of BCC was only detected in samples taken from the semiautomated machine, implying that the

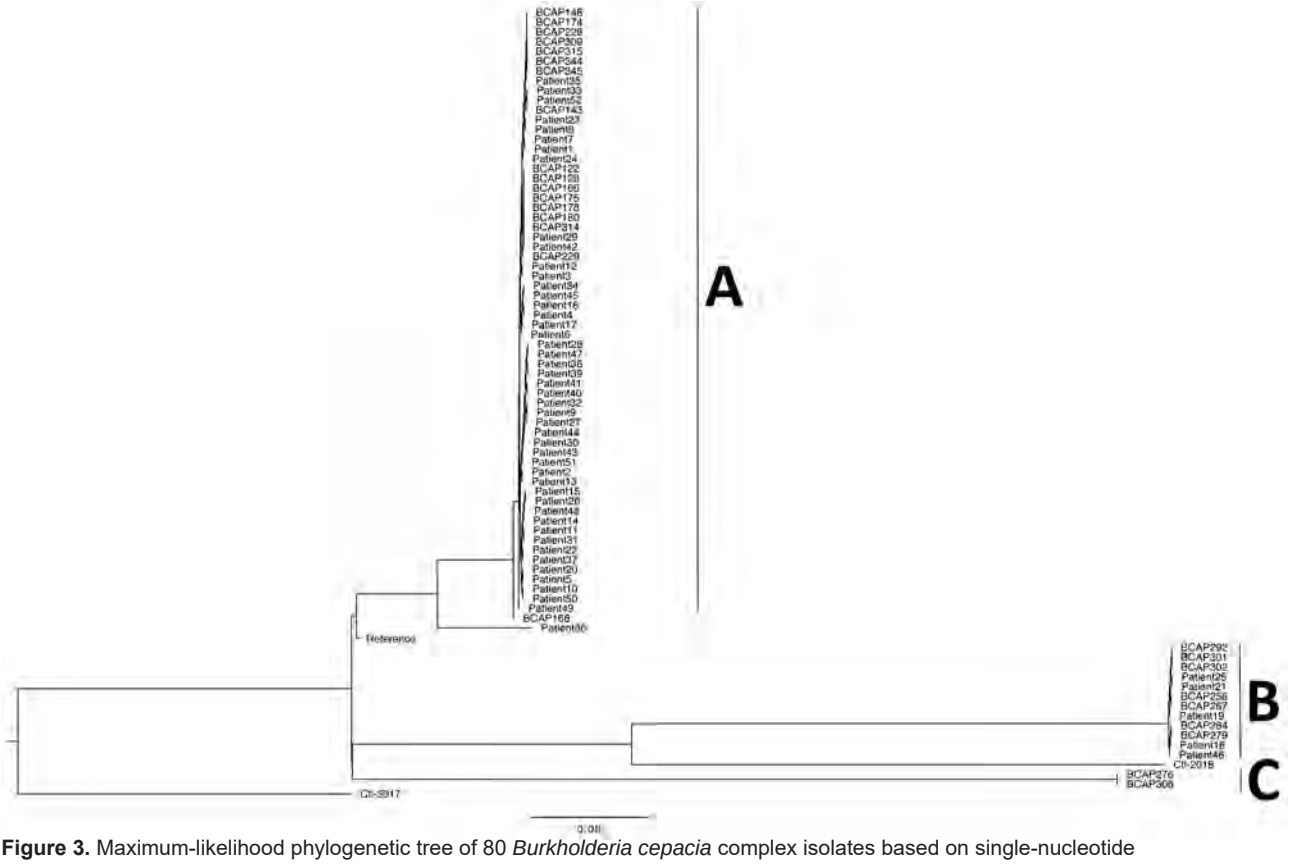

Figure 3. Maximum-likelihood phylogenetic tree of 80 *Burkholderia cepacia* complex isolates based on single-nucleotide polymorphisms, Hong Kong, China. A, B, and C indicate clusters. Scale bar indicates nucleotide substitutions per site.

Table 3. Exit site infection rate of various microorganisms for patients in peritoneal dialysis centers in public hospitals, Hong Kong, China*

Microorganisms causing peritoneal dialysis catheter exit site infections	No. infections/1,000 patient-years		p value
	Centers with routine CHX use, n = 2,530 patients	Centers without routine CHX use, n = 2,030 patients	
Coagulase-negative staphylococci	95.25	72.41	0.0096†
Diphtheroid bacilli	19.37	31.53	0.0128
Streptococcus species	74.70	65.02	0.2424
Methicillin-resistant *Staphylococcus aureus*	49.41	57.64	0.2570
Methicillin-sensitive *S. aureus*	62.45	70.44	0.3241
Enterobacterales‡	95.65	86.70	0.3457
Candida species§	21.34	25.62	0.3990

*Values are pooled data from centers with and without routine CHX use for exit site care (deduplication done per center). CHX use included 0.05% aqueous CHX and 2% and 4% CHX body wash. CHX, chlorhexidine.
†Not statistically significant after Holm-Bonferroni sequential correction (0.05/7 = 0.007).
‡Included *Citrobacter freundii*, *Enterobacter aerogenes*, *Escherichia coli*, *Klebsiella species*, *Morganella* species, *Providencia alcalifaciens*, *P. rettgeri*, *P. stuartii*, *Proteus species*, *Raoultella ornithinolytica*, *R. planticola*, and *R. terrigena*.
§Included *C. holmii*, *C. valida*, *Candida* species, and *Pichia* species.

contamination had occurred during processing at the manufacturing site, rather than in the raw material. Third, the WGS analysis of clusters A and B, corresponding to brands A and B, were genetically distant. Although we cannot be certain of the exact time and duration of contamination, the retrospective case finding of *B. cepacia* isolated among our peritoneal dialysis patients during 2014–2019 showed a substantial increase only since March 2018, suggestive of a relatively recent event. We suspect that lapses in good manufacturing practices (GMPs) at various sites of chlorhexidine dilution led to bacterial contamination from the environment into the production line. BCC are ubiquitous in the environment and strains that have a MIC (>100 mg/L chlorhexidine) have been described, in which the minimum bactericidal concentration can be 3 times higher than the MIC (*40*).

The relative chlorhexidine resistance of BCC was believed to be caused by chromosomally encoded, resistant–nodulation–division efflux pumps, which up-regulate in the presence of sublethal concentrations of chlorhexidine (*41*). Thus, chlorhexidine led to the selection of a predominant BCC strain exhibiting high levels of resistance to chlorhexidine specific to each manufacturing site. In comparison, chlorhexidine has better antibacterial activities against staphylococci and Enterobacterales; thus, contamination of chlorhexidine by these organisms is rare, even at low chlorhexidine concentrations (Appendix Figure) (*42*).

The peritoneal dialysis catheter exit site care practice was revisited during this outbreak. Our local guideline stated that sterile saline and antiseptics, such as aqCHX, are acceptable (*43*), and the International Society for Peritoneal Dialysis 2017 guidelines stated that there is no evidence to suggest any antiseptics being superior in lowering the ESI rate (*44*). Some peritoneal dialysis centers have adopted routine use of chlorhexidine for ES care but a local snapshot audit on ESI rate supported the use of either sterile saline or aqCHX for exit site care.

Before the described outbreak, prepackaged aqCHX products were not considered to be pharmaceutical products in our locality because they were not labeled for use on broken skin nor had medicinal claims, and as such, these products were not registered with the Pharmacy and Poisons Board. The updated CHP guidance issued in response to this outbreak compels all chlorhexidine-containing skin antiseptic for human and animal use to be classified as pharmaceutical products unless otherwise stated, or except that these products are clearly labeled in English and Chinese for washing hands only (or equivalent); or chlorhexidine is used as a preservative or antimicrobial agent in cosmetic products, and necessitates that GMPs be observed, together with additional regulatory measures (*45*). Because terminal sterilization might inactivate or compromise the antimicrobial activity of particular antiseptics including, chlorhexidine, GMPs are relied upon to ensure the quality of the chlorhexidine produced, coupled with microbial testing of products to demonstrate their compliance with the limit laid out by the authorities (*27*,*28*,*46*). We believe that antiseptics that are potentially used on wounds, compromised mucosal surfaces, exit sites or in immunocompromised patients should be subjected to regulations as pharmaceutical products to avoid future similar outbreaks.

This study had several limitations. First, the outbreak that we described was restricted to peritoneal dialysis patients. Non–peritoneal dialysis–related infections associated with contaminated aqCHX would not have been readily identified during initial case finding. Subsequent case finding based on exposure to contaminated aqCHX identified other affected groups of patients (e.g., persons with left ventricular–

assisted devices). Also, BCC isolated from peritoneal dialysis patients before September 6, 2019, and older lots of aqCHX were not available. Thus, only BCC strains identified from active patient surveillance and recent lots of prepackaged aqCHX were included for WGS. Therefore, phylogenetic analysis of the environmental and clinical strains might only reflect recent transmissions. Nevertheless, isolates subjected to WGS were from 12 patients who were among the 53 patients identified by the initial retrospective case finding. All of these isolates were highly related to strains within cluster A. Finally, investigation of brand C was not performed because there were no patient isolates within cluster C and none of the peritoneal dialysis patients used this brand. Other affected brands of aqCHX were imported from outside Hong Kong. Therefore, field investigation at the manufacturing sites for these brands was also not possible. Nevertheless, all affected brands were recalled and will be subject to the new regulatory measures.

In conclusion, our investigations identified a polyclonal outbreak of BCC caused by contamination of multiple brands of commercial aqCHX. The findings illustrated that genome sequencing enabled high-resolution and accurate analysis of the outbreak strains, which facilitated identification of the probable cause or point of contamination. Timely actions and coordination between renal units, the Microbiology and Infection Control Services, Hospital Authority, and Department of Health ensured prompt control of the outbreak and amendment of peritoneal dialysis catheter exit site care practice guidelines, voluntary territory-wide recall of the contaminated aqCHX, and tightening of regulatory control of chlorhexidine-containing skin antiseptics to prevent additional cases. Surveillance of environmental opportunistic pathogens, such as BCC, might enable these indicator organisms to be used to monitor environmental contamination for early detection of similar outbreaks.

Acknowledgments

We thank the Center for Health Protection, Department of Health, and S.K. Chuang for providing assistance in the investigation of the outbreak and comments that improved the manuscript; laboratory staff in the Department of Microbiology, Queen Mary Hospital, for providing additional effort in laboratory support during the outbreak investigation; and Herman Tse for providing advice on statistical analyses.

This study was supported in part by the Consultancy Service for Enhancing Laboratory Surveillance of Emerging Infectious Diseases of the Department of Health, Hong Kong; and the Collaborative Innovation Center for Diagnosis and Treatment of Infectious Diseases, the Ministry of Education of China.

About the Author

Dr. Sally C.Y. Wong is an honorary assistant professor in the Department of Microbiology, The University of Hong Kong, Hong, Hong, China. Her research interests include *Corynebacterium kroppenstedtii*, multidrug-resistant organisms, and infection control and prevention.

References

1. Burkholder WH. Sour skin, a bacterial rot of onion bulbs. Phytopathology. 1950;40:115–7.
2. Devanga Ragupathi NK, Veeraraghavan B. Accurate identification and epidemiological characterization of *Burkholderia cepacia* complex: an update. Ann Clin Microbiol Antimicrob. 2019;18:7. https://doi.org/10.1186/s12941-019-0306-0
3. Jones AM, Dodd ME, Govan JR, Barcus V, Doherty CJ, Morris J, et al. *Burkholderia cenocepacia* and *Burkholderia multivorans*: influence on survival in cystic fibrosis. Thorax. 2004;59:948–51. https://doi.org/10.1136/thx.2003.017210
4. Ko S, An HS, Bang JH, Park SW. An outbreak of *Burkholderia cepacia* complex pseudobacteremia associated with intrinsically contaminated commercial 0.5% chlorhexidine solution. Am J Infect Control. 2015;43:266–8. https://doi.org/10.1016/j.ajic.2014.11.010
5. Song JE, Kwak YG, Um TH, Cho CR, Kim S, Park IS, et al. Outbreak of *Burkholderia cepacia* pseudobacteraemia caused by intrinsically contaminated commercial 0.5% chlorhexidine solution in neonatal intensive care units. J Hosp Infect. 2018;98:295–9. https://doi.org/10.1016/j.jhin.2017.09.012
6. Gleeson S, Mulroy E, Bryce E, Fox S, Taylor SL, Talreja H. *Burkholderia cepacia*: an outbreak in the peritoneal dialysis unit. Perit Dial Int. 2019;39:92–5. https://doi.org/10.3747/pdi.2018.00095
7. Heo ST, Kim SJ, Jeong YG, Bae IG, Jin JS, Lee JC. Hospital outbreak of *Burkholderia stabilis* bacteraemia related to contaminated chlorhexidine in haematological malignancy patients with indwelling catheters. J Hosp Infect. 2008;70:241–5. https://doi.org/10.1016/j.jhin.2008.07.019
8. Romero-Gómez MP, Quiles-Melero MI, Peña García P, Gutiérrez Altes A, García de Miguel MA, Jiménez C, et al. Outbreak of *Burkholderia cepacia* bacteremia caused by contaminated chlorhexidine in a hemodialysis unit. Infect Control Hosp Epidemiol. 2008;29:377–8. https://doi.org/10.1086/529032
9. Lee S, Han SW, Kim G, Song DY, Lee JC, Kwon KT. An outbreak of *Burkholderia cenocepacia* associated with contaminated chlorhexidine solutions prepared in the hospital. Am J Infect Control. 2013;41:e93–6. https://doi.org/10.1016/j.ajic.2013.01.024
10. Montaño-Remacha C, Márquez-Cruz MD, Hidalgo-Guzmán P, Sánchez-Porto A, Téllez-Pérez FP. An outbreak of *Burkholderia cepacia* bacteremia in a hemodialysis unit, Cadiz, 2014 [in Spanish]. Enferm Infecc Microbiol Clin. 2015; 33:646–50. https://doi.org/10.1016/j.eimc.2015.02.013
11. Leong LE, Lagana D, Carter GP, Wang Q, Smith K, Stinear TP, et al. *Burkholderia lata* Infections from intrinsically contaminated chlorhexidine mouthwash, Australia, 2016.

Emerg Infect Dis. 2018;24:2109–11. https://doi.org/10.3201/eid2411.171929
12. Berkelman RL, Lewin S, Allen JR, Anderson RL, Budnick LD, Shapiro S, et al. Pseudobacteremia attributed to contamination of povidone–iodine with *Pseudomonas cepacia*. Ann Intern Med. 1981;95:32–6. https://doi.org/10.7326/0003-4819-95-1-32
13. Panlilio AL, Beck-Sague CM, Siegel JD, Anderson RL, Yetts SY, Clark NC, et al. Infections and pseudoinfections due to povidone–iodine solution contaminated with *Pseudomonas cepacia*. Clin Infect Dis. 1992;14:1078–83. https://doi.org/10.1093/clinids/14.5.1078
14. Frank MJ, Schaffner W. Contaminated aqueous benzalkonium chloride. An unnecessary hospital infection hazard. JAMA. 1976;236:2418–9. https://doi.org/10.1001/jama.1976.03270220038032
15. Lee CS, Lee HB, Cho YG, Park JH, Lee HS. Hospital-acquired *Burkholderia cepacia* infection related to contaminated benzalkonium chloride. J Hosp Infect. 2008;68:280–2. https://doi.org/10.1016/j.jhin.2008.01.002
16. Serikawa T, Kobayashi S, Tamura T, Uchiyama M, Tsukada H, Takakuwa K, et al. Pseudo outbreak of *Burkholderia cepacia* in vaginal cultures and intervention by hospital infection control team. J Hosp Infect. 2010;75:242–3. https://doi.org/10.1016/j.jhin.2009.11.013
17. Brooks RB, Mitchell PK, Miller JR, Vasquez AM, Havlicek J, Lee H, et al.; Burkholderia cepacia Workgroup. Multistate outbreak of *Burkholderia cepacia* complex bloodstream infections after exposure to contaminated saline Flush syringes: United States, 2016–2017. Clin Infect Dis. 2019;69:445–9. https://doi.org/10.1093/cid/ciy910
18. Moreira BM, Leobons MB, Pellegrino FL, Santos M, Teixeira LM, de Andrade Marques E, et al. *Ralstonia pickettii* and *Burkholderia cepacia* complex bloodstream infections related to infusion of contaminated water for injection. J Hosp Infect. 2005;60:51–5. https://doi.org/10.1016/j.jhin.2004.09.036
19. Moehring RW, Lewis SS, Isaacs PJ, Schell WA, Thomann WR, Althaus MM, et al. Outbreak of bacteremia due to *Burkholderia contaminans* linked to intravenous fentanyl from an institutional compounding pharmacy. JAMA Intern Med. 2014;174:606–12. https://doi.org/10.1001/jamainternmed.2013.13768
20. Pegues DA, Carson LA, Anderson RL, Norgard MJ, Argent TA, Jarvis WR, et al. Outbreak of *Pseudomonas cepacia* bacteremia in oncology patients. Clin Infect Dis. 1993;16:407–11. https://doi.org/10.1093/clind/16.3.407
21. Marquez L, Jones KN, Whaley EM, Koy TH, Revell PA, Taylor RS, et al. An outbreak of *Burkholderia cepacia* complex infections associated with contaminated liquid docusate. Infect Control Hosp Epidemiol. 2017;38:567–73. https://doi.org/10.1017/ice.2017.11
22. Glowicz J, Crist M, Gould C, Moulton-Meissner H, Noble-Wang J, de Man TJ, et al.; B. cepacia Investigation Workgroup. A multistate investigation of health care–associated *Burkholderia cepacia* complex infections related to liquid docusate sodium contamination, January–October 2016. Am J Infect Control. 2018;46:649–55. https://doi.org/10.1016/j.ajic.2017.11.018
23. Lalitha P, Das M, Purva PS, Karpagam R, Geetha M, Lakshmi Priya J, et al. Postoperative endophthalmitis due to *Burkholderia cepacia* complex from contaminated anaesthetic eye drops. Br J Ophthalmol. 2014;98:1498–502. https://doi.org/10.1136/bjophthalmol-2013-304129
24. Memish ZA, Stephens G, Balkhy HH, Cunningham G, Francis C, Poff G; Saudi National Guard Infection Prevention and Control Group. Outbreak of *Burkholderia cepacia* bacteremia in immunocompetent children caused by contaminated nebulized sulbutamol in Saudi Arabia. Am J Infect Control. 2009;37:431–2. https://doi.org/10.1016/j.ajic.2006.10.002
25. Ghazal SS, Al-Mudaimeegh K, Al Fakihi EM, Asery AT. Outbreak of *Burkholderia cepacia* bacteremia in immunocompetent children caused by contaminated nebulized sulbutamol in Saudi Arabia. Am J Infect Control. 2006;34:394–8. https://doi.org/10.1016/j.ajic.2006.03.003
26. Balkhy HH, Cunningham G, Francis C, Almuneef MA, Stevens G, Akkad N, et al. A national guard outbreak of *Burkholderia cepacia* infection and colonization secondary to intrinsic contamination of albuterol nebulization solution. Am J Infect Control. 2005;33:182–8. https://doi.org/10.1016/j.ajic.2005.01.001
27. Council of Europe. European pharmacopoeia. 9th ed. Strasbourg (France): The Council; 2016.
28. United States Pharmacopeial Convention. United States Pharmacopeia US. USP <60> microbiological examination of nonsterile roduct. Tests for *Burkholderia cepacia* complex. North Bethesda, Maryland, December 1, 2019 [cited 2020 May10]. https://www.pharmawebinars.com/usp-60-tests-for-burkholderia-cepacia-complex
29. Scott S. What is an "objectionable organism"? American Pharmaceutical Review, October 12, 2012 [cited 2019 Nov 16]. https://www.americanpharmaceuticalreview.com/Featured-Articles/122201-What-is-an-Objectionable-Organism-Objectionable-Organisms-The-Shifting-Perspective/
30. Elder D. Objectionable organisms in non-sterile medicinal products. European Pharmaceutical Review, January 4, 2018 [cited 2019 Nov 16] https://www.europeanpharmaceutical review.com/article/71150/objectionable-organisms-non-sterile-medicinal-products/
31. Cheng VC, Chen JH, Wong S, Leung SS, So SY, Lung DC, et al. Hospital outbreak of pulmonary and cutaneous zygomycosis due to contaminated linen items from substandard laundry. Clin Infect Dis. 2016;62:714–21. https://doi.org/10.1093/cid/civ1006
32. Cheng VC, Chan JF, Ngan AH, To KK, Leung SY, Tsoi HW, et al. Outbreak of intestinal infection due to *Rhizopus microsporus*. J Clin Microbiol. 2009;47:2834–43. https://doi.org/10.1128/JCM.00908-09
33. Jolley KA, Bray JE, Maiden MC. Open-access bacterial population genomics: BIGSdb software, the PubMLST.org website and their applications. Wellcome Open Res. 2018;3:124. https://doi.org/10.12688/wellcomeopenres.14826.1
34. Kaas RS, Leekitcharoenphon P, Aarestrup FM, Lund O. Solving the problem of comparing whole bacterial genomes across different sequencing platforms. PLoS One. 2014;9:e104984. https://doi.org/10.1371/journal.pone.0104984
35. Centre for Health Protection. Update on *Burkholderia cepacia* complex infection (with photos). Department of Health, Hong Kong Special Administrative Region, October 4, 2019 [cited 2019 Nov 27]. https://www.info.gov.hk/gia/general/201910/04/P2019100400763.htm
36. Centre for Health Protection. Further recall of antiseptic products (with photos). Department of Health, Hong Kong Special Administrative Region, September 30, 2019 [cited 2019 Nov 23]. https://www.info.gov.hk/gia/general/201909/30/P2019093000732.htm
37. Department of Health, Drug Office, Drug Evaluation and Registration and Import/Export Control Division, Drug office. Guidance notes on classification of products as

pharmaceutical products under the Pharmacy and Poisons Ordinance (Cap. 138). Department of Health, Hong Kong Special Administrative Region, October 8, 2019 [cited 2019 Nov 23]. https://www.drugoffice.gov.hk/eps/do/en/doc/guidelines_forms/Guide_on_PRClass.pdf
38. Cheng VC, Chen JH, Leung SS, So SY, Wong S, Wong SC, et al. Seasonal outbreak of *Bacillus* bacteremia associated with contaminated linen in Hong Kong. Clin Infect Dis. 2017;64(suppl 2):S91–S7.
39. Paul LM, Hegde A, Pai T, Shetty S, Baliga S, Shenoy S. An outbreak of *Burkholderia cepacia* bacteremia in a neonatal intensive care unit. Indian J Pediatr. 2016;83:285–8. https://doi.org/10.1007/s12098-015-1855-7
40. Rose H, Baldwin A, Dowson CG, Mahenthiralingam E. Biocide susceptibility of the *Burkholderia cepacia* complex. J Antimicrob Chemother. 2009;63:502–10. https://doi.org/10.1093/jac/dkn540
41. Coenye T, Van Acker H, Peeters E, Sass A, Buroni S, Riccardi G, et al. Molecular mechanisms of chlorhexidine tolerance in *Burkholderia cenocepac*ia biofilms. Antimicrob Agents Chemother. 2011;55:1912–9. https://doi.org/10.1128/AAC.01571-10
42. Al-Adham I, Haddadin R, Collier P. Types of microbicidal and microstatic agents. In: Fraise AP, Maillard J-Y, Sattar SA, editors. Russell, Hugo and Ayliffe's: principles and practice of disinfection, preservation and sterilization, 5th ed. New York: Wiley-Blackwell Publishing; 2012. p. 18–20.
43. Infection Control Branch, Center for Health Protection and Central Renal Committee. Infection control guidelines on nephrology services in Hong Kong. Department of Health and Hospital Authority, Hong Kong Special Administrative Region, 3rd ed (version 3.1), 2018 [cited 2019 Sep 30]. https://www.chp.gov.hk/files/pdf/ic_gu_nephrology_services_in_hk.pdf
44. Szeto CC, Li PK, Johnson DW, Bernardini J, Dong J, Figueiredo AE, et al. ISPD Catheter-related infection recommendations: 2017 update. Perit Dial Int. 2017;37:141–54. https://doi.org/10.3747/pdi.2016.00120
45. Cap. 138 Pharmacy and Poisons Ordinance. 1970 Jan 1, L.N. 186 of 1969, amended 2015 [cited 2019 Sep 30]. https://www.elegislation.gov.hk/hk/cap138
46. Medical Solution Division. White paper: quality of 3M Canada skin antiseptic drug products. 3M Canada, June 2018 [cited 2019 Sep 30]. https://multimedia.3m.com/mws/media/1455409O/white-paper-quality-of-3m-canada-drug-products.pdf

Address for correspondence: Vincent C.C. Cheng, Department of Microbiology, Queen Mary Hospital, Hong Kong, China; email: vcccheng@hku.hk

Severe Acute Respiratory Syndrome Coronavirus 2 Prevalence, Seroprevalence, and Exposure among Evacuees from Wuhan, China, 2020

Benjamin D. Hallowell,[1] Christina M. Carlson, Jesica R. Jacobs, Mary Pomeroy, Jonathan Steinberg, Mark W. Tenforde, Emily McDonald, Loretta Foster, Leora R. Feldstein, Melissa A. Rolfes, Amber Haynes, Glen R. Abedi, George S. Odongo, Kim Saruwatari, Errin C. Rider, Gina Douville, Neenaben Bhakta, Panagiotis Maniatis, Stephen Lindstrom, Natalie J. Thornburg, Xiaoyan Lu, Brett L. Whitaker, Shifaq Kamili, Senthilkumar K. Sakthivel, Lijuan Wang, Lakshmi Malapati, Janna R. Murray, Brian Lynch, Martin Cetron, Clive Brown, Shahrokh Roohi, Lisa Rotz, Denise Borntrager, Kenta Ishii, Kathleen Moser, Mohammad Rasheed, Brandi Freeman, Sandra Lester, Kizzmekia S. Corbett, Olubukola M. Abiona, Geoffrey B. Hutchinson, Barney S. Graham, Nicki Pesik, Barbara Mahon, Christopher Braden, Casey Barton Behravesh, Rebekah Stewart, Nancy Knight, Aron J. Hall, Marie E. Killerby

To determine prevalence of, seroprevalence of, and potential exposure to severe acute respiratory syndrome coronavirus 2 (SARS-CoV-2) among a cohort of evacuees returning to the United States from Wuhan, China, in January 2020, we conducted a cross-sectional study of quarantined evacuees from 1 repatriation flight. Overall, 193 of 195 evacuees completed exposure surveys and submitted upper respiratory or serum specimens or both at arrival in the United States. Nearly all evacuees had taken preventive measures to limit potential exposure while in Wuhan, and none had detectable SARS-CoV-2 in upper respiratory tract specimens, suggesting the absence of asymptomatic respiratory shedding among this group at the time of testing. Evidence of antibodies to SARS-CoV-2 was detected in 1 evacuee, who reported experiencing no symptoms or high-risk exposures in the previous 2 months. These findings demonstrated that this group of evacuees posed a low risk of introducing SARS-CoV-2 to the United States.

On December 31, 2019, a cluster of severe pneumonia cases in Wuhan, Hubei Province, China, was reported (*1*). On January 7, 2020, a novel coronavirus, severe acute respiratory syndrome coronavirus 2 (SARS-CoV-2), was isolated from samples associated with the cluster (*2*,*3*). As of May 1, 2020, a total of 3,175,207 coronavirus disease (COVID-19) cases had been confirmed and 224,172 persons had died worldwide; 84,385 cases and 4,643 deaths were in China (*4*). Also as of May 1, 2020, the US Centers for Disease Control and Prevention (CDC) was reporting ongoing worldwide transmission (*5*).

On January 20, 2020, a case of coronavirus disease (COVID-19) was confirmed in a US patient who had recently traveled to Wuhan (*6*). To slow the spread of the epidemic, on January 23, the government of China enacted a travel ban restricting all travel into and out of Wuhan, including air and rail travel, and

Author affiliations: Centers for Disease Control and Prevention, Atlanta, Georgia, USA (B.D. Hallowell, C.M. Carlson, J.R. Jacobs, M. Pomeroy, J. Steinberg, M.W. Tenforde, E. McDonald, L. Foster, L.R. Feldstein, M.A. Rolfes, A. Haynes, G.R. Abedi, G.S. Odongo, P. Maniatis, S. Lindstrom, N.J. Thornburg, X. Lu, B.L. Whitaker, S. Kamili, S.K. Sakthivel, L. Wang, L. Malapati, J.R. Murray, B. Lynch, M. Cetron, C. Brown, S. Roohi, L. Rotz, D. Borntrager, K. Ishii, K. Moser, B. Freeman, N. Pesik, B. Mahon, C. Braden, C. Barton Behravesh, R. Stewart, N. Knight, A.J. Hall, M.E. Killerby); Riverside University Health System-Public Health, Riverside, California, USA (K. Saruwatari, E.C. Rider, G. Douville, N. Bhakta); Synergy America Inc., Duluth, Georgia, USA (M. Rasheed, S. Lester); National Institutes of Health, Bethesda, Maryland, USA (K.S. Corbett, O.M. Abiona, G.B. Hutchinson, B.S. Graham)

DOI: https://doi.org/10.3201/eid2609.201590

[1]Current affiliation: Department of Health, Providence, Rhode Island, USA

suspending operation of buses, subways, and ferries within the city (*7*). As of January 23, a total of 571 confirmed COVID-19 cases had been reported in China (*8*).

After China enacted the travel ban, the US Department of State planned evacuation flights for US citizens and other third country nationals in Wuhan. We describe the demographic and clinical characteristics, potential exposures to SARS-CoV-2, personal protective measures implemented, and SARS-CoV-2 real-time reverse transcription PCR (rRT-PCR) and serologic test results for evacuees from 1 repatriation flight from Wuhan. These data can be used to better determine SARS-CoV-2 epidemiology, including assessing the point prevalence of past and current SARS-CoV-2 infections in this cohort and identifying factors associated with infection in this cohort. These findings can also be used to help estimate the initial risk for transmission to contacts in the United States posed by evacuees from Wuhan and are relevant to current and future implementation of public health control measures, such as isolation and quarantine.

Methods

We investigated quarantined evacuees from a January 28, 2020, repatriation flight from Wuhan to the United States. Before the flight departed Wuhan, evacuees were evaluated to ensure that they had no fever or respiratory signs/symptoms. At arrival in the United States and again at the quarantine facility, evacuees were asked to complete a US Traveler's Health Declaration form disclosing any symptoms; they were also screened for illness and fever, asked about symptoms in the past 72 hours, and asked about any high-risk exposures (including working in or visiting healthcare settings; caring for or visiting persons with fever, respiratory illness, or a confirmed COVID-19 diagnosis; or visiting any live animal markets) in Wuhan in the past 14 days. Those who reported symptoms or high-risk exposures were evaluated by a CDC Quarantine Medical Officer, who determined if they required further evaluation and isolation from the quarantined cohort.

Nasopharyngeal and oropharyngeal swab samples and serum specimens were obtained from participating evacuees when they arrived at the quarantine station in the United States. As part of quarantine procedures, evacuees were actively monitored for fever and respiratory signs/symptoms for 14 days after departure from Wuhan; any evacuee in whom either fever or respiratory signs/symptoms developed during this time was evaluated for COVID-19 (*9*), and additional nasopharyngeal and oropharyngeal specimens were collected (*10*,*11*). All specimens were collected, processed, and shipped to CDC for testing (*10*,*11*). Presence of SARS-CoV-2 in nasopharyngeal and oropharyngeal swab samples was confirmed by rRT-PCR detection of viral RNA in respiratory specimens (*12*). Serum specimens were initially tested for SARS-CoV-2 antibodies by SARS-CoV-2 ELISA (Appendix 1, https://wwwnc.cdc.gov/EID/article/26/9/20-1590-App1.pdf).

We asked evacuees to complete a detailed, self-administered survey during the flight from Wuhan (Appendix 2, https://wwwnc.cdc.gov/EID/article/26/9/20-1590-App2.pdf). The survey captured information on demographics, clinical signs/symptoms, travel outside of Hubei Province, face mask use, limitation of time spent in public, and past high-risk exposures (including contact with confirmed COVID-19 case-patients; persons with fever, acute respiratory illness, or both; healthcare and laboratory facilities; and animals and live animal markets). We assessed high-risk exposures over the past 2 weeks and the past 2 months. We compared high-risk exposures over the past 2 weeks with rRT-PCR results for persons who provided an upper respiratory specimen (because 14 days was the upper end of the estimated incubation period for COVID-19 [*13*,*14*]). We also compared high-risk exposures over the past 2 months with the serologic test results for evacuees who provided a serum sample (because SARS-CoV-2 had probably been circulating for the 2 months before their departure [*15*]).

We entered survey responses into REDCap electronic data capture tools hosted at CDC (*16*), and all entries were verified by a second reviewer for accuracy and completeness. Data were analyzed by using SAS software version 9.4 (SAS Institute, Inc., https://www.sas.com).

CDC determined that this investigation was public health surveillance (US Department of Health and Human Services, Title 45 Code of Federal Regulations 46, Protection of Human Subjects). Evacuees' participation in the collection of biological specimens and the survey was voluntary.

Results

At the time of arrival in the United States, no evacuee had a measured fever or reported any signs or symptoms that required further evaluation. Of the 195 evacuees, 193 completed surveys; 99% (191/193) of respondents provided a nasopharyngeal sample, an oropharyngeal sample, or 1 of each for SARS-CoV-2 rRT-PCR testing, and 96% (186/193) provided a serum sample for testing. The median age of all 193 evacuees was 42 (range 0–74) years, and 53% (100/189) were

male (Table 1). Most were either Asian (49%, 94/192) or White (35%, 68/192).

One evacuee reported having had close contact with a person with laboratory-confirmed COVID-19 in the previous 2 weeks. Specifically, reported exposures included direct physical contact, being within 6 feet of the person while that person was coughing or sneezing, taking an object handed from or handled by the person, and traveling in the same vehicle as the person (Table 2). No other evacuees reported exposure to a person with laboratory-confirmed COVID-19 in the previous 2 months. However, 6% (12/191) reported having had close contact with a person with fever, acute respiratory illness, or both in the previous 2 weeks and 16% (30/186) in the previous 2 months (Table 2). One evacuee had visited a live animal market in the previous 2 weeks and 5% (9/186) in the previous 2 months. Three percent (6/191) of evacuees had visited settings with nondomesticated live animals in the previous 2 weeks and 5% (10/186) in the previous 2 months. One percent (2/191) of evacuees had had direct physical contact with a nondomesticated live animal (both instances with stray dogs) in the previous 2 weeks. No additional evacuees had had direct physical contact with a nondomesticated live animal in the previous 2 months.

Table 1. Demographic characteristics of 193 evacuees on a repatriation flight from Wuhan, China, to the United States, January 2020

Characteristic	No./total no. (%)*
Age group, y	
<18	32/193 (17)
18–44	68/193 (35)
45–64	83/193 (43)
≥65	10/193 (5)
Sex	
M	100/189 (53)
F	89/189 (47)
Race/ethnicity	
White	68/192 (35)
Black	6/192 (3)
Asian	94/192 (49)
Multiracial	13/192 (7)
Hispanic	11/192 (6)
Underlying medical condition	
Chronic lung disease	1/191 (1)
Asthma/reactive airway disease	7/191 (4)
Diabetes mellitus type 1	2/187 (1)
Diabetes mellitus type 2	4/191 (2)
Hypertension	14/192 (7)
Chronic heart or cardiovascular disease	0/191 (0)
Chronic kidney disease	1/191 (1)
Liver disease	1/191 (1)
Noncancer immunosuppressive condition	1/189 (1)
Neurologic/neurodevelopmental disorder	1/191 (1)
Other chronic disease	11/191 (6)
Specimen submitted	
Nasopharyngeal and/or oropharyngeal swab sample	191/193 (99)
Serum	186/193 (96)

*Data for persons for whom responses were missing were excluded from the numerator and denominator.

During the previous month, after hearing about COVID-19 cases in Wuhan, 95% (178/188) of evacuees reported having limited their time in public in Wuhan, including avoiding public gatherings (87%), public transportation (84%), and all public settings (e.g., grocery stores or restaurants; 70%) (Table 3). In addition, in the previous month, after hearing about COVID-19 cases in Wuhan, 76% of evacuees reported having worn a face mask while in public spaces. This finding represented a significant increase from the 34% of evacuees who reported having worn a face mask while in public spaces in the previous 2 months (McNemar test statistic 74.05; $p<0.0001$).

Five percent (9/193) of evacuees reported having experienced signs or symptoms associated with COVID-19 (measured or subjective fever, cough, shortness of breath) in the previous 2 weeks, and 12% (24/193) reported signs/symptoms associated with COVID-19 in the previous 2 months. One evacuee who reported signs/symptoms associated with COVID-19 in the previous 2 weeks sought medical care, and no evacuee required hospitalization while in Wuhan (Table 4).

SARS-CoV-2 was not detected by rRT-PCR in any of the 190 nasopharyngeal or 190 oropharyngeal swab specimens collected from 191 unique evacuees (189 provided nasopharyngeal and oropharyngeal samples, 1 nasopharyngeal sample only, and 1 oropharyngeal sample only). During the 14-day quarantine period, fever developed in 2 evacuees; additional nasopharyngeal and oropharyngeal swab specimens were collected and tested, and SARS-CoV-2 was not detected in either specimen type.

One evacuee showed serologic evidence of a past SARS-CoV-2 infection. Serum from that person had antibodies against SARS-CoV-2 at titers of 400 determined by ELISA and 320 determined by microneutralization test. This person was male, was in the 19-44–year age group, was traveling without any family members, and reported no signs/symptoms associated with COVID-19 in the past 2 months. He reported no high-risk exposures (including exposure to or contact with live animals, live animal markets, persons known to be ill with COVID-19, or persons with fever or acute respiratory signs/symptoms). He reported that since early January he had spent limited time out in public, including avoiding public transport, avoiding public gatherings, and not attending

Table 2. Potential exposures to severe acute respiratory syndrome coronavirus 2 by 193 evacuees returning from Wuhan, China, to the United States, January 2020*

Exposure risk factors	No./total no. (%)†
Relevant exposures for serology results‡	
Animal contact	
Visited the Huanan Seafood Market in past 2 mo	1/186 (1)
Visited any live animal market in past 2 mo	9/186 (5)
Visited any settings with domesticated animals in past 2 mo	39/186 (21)
Visited any settings with nondomesticated animals in past 2 mo	8/186 (4)
Had direct contact with any animals in past 2 mo	52/186 (28)
Human contact	
Had close contact with laboratory-confirmed COVID-19 case-patient in past 2 mo	1/186 (1)
Had close contact with person with fever and/or acute respiratory illness in past 2 mo	30/186 (16)
High-risk settings	
Visited a healthcare setting (not in United States) in past *2* mo	8/186 (4)
Worked in a healthcare setting in Wuhan in past *2* mo	0/186 (0)
Worked in a laboratory setting in Wuhan in past *2* mo	0/186 (0)
Travel	
Did not travel outside of Hubei Province, China, in past *2* mo	62/186 (33)
Relevant exposures for PCR results§	
Animal contact	
Visited any live animal market in past 2 wk	1/191 (1)
Visited any settings with domesticated animals in past 2 wk	15/191 (8)
Visited any settings with nondomesticated animals in past 2 wk	6/191 (3)
Had direct physical contact with live domestic animals in past 2 wk	36/191 (19)
Had direct physical contact with live nondomestic animals in past 2 wk	2/191 (1)
Human contact	
Had close contact with laboratory-confirmed COVID-19 case-patient in past 2 wk	1/191 (1)
Had close contact with person with fever and/or acute respiratory illness in past 2 wk	12/191 (6)
High-risk settings	
Visited a healthcare setting (not in United States) in past 2 wk	7/191 (4)

*COVID-19, coronavirus disease.
†Data for persons for whom responses were missing were excluded from the denominator.
‡Limited to exposures within the past 2 mo and to persons who submitted serum sample.
§Limited to exposures within the past 2 wk and to persons who submitted a nasopharyngeal and/or oropharyngeal swab specimen.

school/university. ELISA results for the remaining 185 serum specimens measured SARS-CoV-2 antibody titers at <400, and the samples were therefore considered seronegative.

Discussion

Our report on SARS-CoV-2 prevalence, seroprevalence, and potential exposures among evacuees returning from Wuhan is part of the public health response enacted to slow transmission of SARS-CoV-2 in the United States. Although this population of evacuees is probably not representative of all Wuhan residents in terms of risk of acquiring SARS-CoV-2 infection, our results indicate limited exposure to SARS-CoV-2 among this group of early evacuees from Wuhan.

Compared with previously reported COVID-19 case-patients in Wuhan, our population was younger (median 42 vs. 59 years of age) and their reported frequency of potential SARS-CoV-2 exposures was lower, including exposure to persons with respiratory signs/symptoms, work-associated healthcare exposures, and exposure to live animal markets (*15*). Of note, although our questionnaire covered exposure to animals and animal markets, most transmission within Wuhan during the evacuees' relevant exposure period before the repatriation flight to the United States was probably human-to-human (*15,17*). Our study population, which consisted predominantly of US expatriates, probably had other factors that reduced their risk for exposure and were not documented as part of our investigation. For example, it is possible that the expatriates' households in Wuhan were smaller than other households in Wuhan, which has been associated with a lower risk for transmission (*18*–*21*); however, because we did not document household size in our investigation, we cannot show such an association. Nearly all evacuees took preventive measures to limit potential exposure to SARS-CoV-2 while in Wuhan. However, 16% of evacuees did have direct contact with persons who had fever or acute respiratory illness.

Previous investigations among evacuees traveling from Wuhan to Germany and Japan detected SARS-CoV-2 RNA in 7 asymptomatic persons (*22,23*), suggesting that symptom-based screening alone may not be effective for detecting SARS-CoV-2 infection. Evacuees in our study underwent intensive screening such that no evacuee had signs/symptoms at the time of evacuation and none had detectable SARS-CoV-2

in upper respiratory tract specimens, suggesting the absence of asymptomatic respiratory shedding among this group at the time of testing. In addition, no SARS-CoV-2 was detected in respiratory specimens from the 2 evacuees in whom fever developed during quarantine. The lack of SARS-CoV-2 detection in asymptomatic travelers at the time of testing and in the 2 travelers in whom fever developed could result from a lower risk for exposure among this group compared with Wuhan residents or other reported evacuees (*22*,*23*).

The ELISA and microneutralization tests used in this investigation have produced robust responses to serum from confirmed SARS-CoV-2 patients (B. Freeman et al., unpub data, https://www.biorxiv.org/content/10.1101/2020.04.24.057323v2 28). Although 24 evacuees reported signs/symptoms associated with COVID-19 (subjective fever, cough, or shortness of breath) in the previous 2 months, none were seropositive for SARS-CoV-2. In contrast, an antibody response was detected in 1 person who did not report illness in the previous 2 months, indicating past SARS-CoV-2 infection, suggestive of past asymptomatic or mildly symptomatic infection. The overall seroprevalence of 1% suggests a low level of exposure to SARS-CoV-2 over the preceding 2 months in Wuhan. However, a lack of antibody response may not mean an absence of past infection; serologic responses were not always found in persons with mild Middle East respiratory syndrome coronavirus illness and positive rRT-PCR results for that virus (*24*). Future serologic testing among COVID-19 case-patients may be useful for determining whether persons with asymptomatic or mild COVID-19 disease become seropositive.

Efforts by this cohort to limit their exposure by limiting their time in public may have helped prevent infection, even in a city with extensive ongoing community transmission. Because SARS-CoV-2 seems to be transmitted primarily through respiratory droplets, limiting time in public may have helped prevent infection because proximity to infected persons is needed for virus transmission (*25*). Before the evacuees in our study departed Wuhan, China was implementing measures to control SARS-CoV-2 by suspending public transport and vehicle traffic and canceling Lunar New Year gatherings (*7*). CDC currently recommends that all persons wear cloth face coverings in public; the purpose is to help protect others from potential droplet exposure, not to protect the persons wearing the face coverings (*26*). Thus, although 76% of evacuees reported mask use after hearing about COVID-19 in Wuhan, individual mask use probably had minimal effect on their individual risk of acquiring infection.

Information about virus prevalence, seroprevalence, and possible SARS-CoV-2 exposures in this population of evacuees has the potential to inform current and future quarantine and isolation policies. In this population, who underwent intensive screening and monitoring, we detected no evidence of current infection with SARS-CoV-2 and very limited evidence of past infection. Other than the 193 evacuees included in our study, 3 cases of COVID-19 were detected in the United States during quarantine of later cohorts of evacuees after signs/symptoms developed and the evacuees underwent testing, demonstrating the value of quarantine and active monitoring of evacuees to detect COVID-19 cases (*27*).

Table 3. Precautions taken to prevent infection with severe acute respiratory syndrome coronavirus 2 by 193 evacuees while in Wuhan, China*

Precaution	No./total no. (%)†		
	Total, n = 193	Submitted NP or OP sample,‡ n = 191	Submitted serum sample,§ n = 186
Face mask use			
Usually wore a face mask in past *2* mo while in public	63/185 (34)	63/184 (34)	63/178 (35)
Usually wore a face mask in past 1 mo while in public after hearing about COVID-19	143/188 (76)	143/187 (76)	138/181 (76)
Limited time in public			
In past 1 mo after hearing about COVID-19	178/188 (95)	176/186 (95)	171/181 (94)
By taking the following precautions			
Avoided public transport	150/178 (84)	148/176 (84)	144/171 (84)
Avoided public gatherings	154/178 (87)	153/176 (87)	148/171 (87)
Did not attend work¶	53/123 (43)	53/121 (44)	53/123 (43)
Did not attend school/university#	19/30 (63)	19/30 (63)	15/25 (60)
Avoided all public settings (e.g., grocery stores, restaurants)	125/178 (70)	124/176 (70)	119/171 (70)

*COVID-19, coronavirus disease; NP, nasopharyngeal swab; OP, oropharyngeal swab.
†Data for persons for whom responses were missing were excluded from the denominator.
‡Limited to persons who submitted an NP and/or OP specimen.
§Limited to persons who submitted serum specimen.
¶Limited to persons who reported an occupation (other than student, stay-at-home parent, or retired).
#Limited to persons 2–18 years of age and those reporting student as occupation.

Table 4. Signs/symptoms, clinical course, and past medical history for evacuees reporting illness who were on a repatriation flight from Wuhan, China, to the United States in early 2020*

Characteristic	No./total no. (%)†	
	Self-reported illness in past 2 mo, n = 39	Self-reported illness in past 2 wk, n = 13
Sign/symptom		
Measured fever	5/36 (14)	3/12 (25)
Subjective fever	16/37 (43)	2/13 (15)
Cough	15/36 (42)	6/12 (50)
Sore throat	21/38 (55)	9/13 (69)
Muscle aches	10/37 (27)	2/11 (18)
Headache	12/37 (32)	1/12 (8)
Shortness of breath	2/34 (6)	1/12 (8)
Vomiting	3/33 (9)	1/11 (9)
Diarrhea	7/36 (19)	1/12 (8)
Fatigue	16/37 (43)	3/12 (25)
Other	10/30 (33)	6/10 (60)
Any coronavirus sign/symptom‡	24/39 (62)	9/13 (69)
Identified as a person under investigation for COVID-19 signs/symptoms§	10/39 (26)	2/13 (15)
Sought medical care for illness in past 2 wk	1/39 (3)	0/13 (0)

*All persons who self-reported illness submitted serum and a nasopharyngeal or oropharyngeal swab specimen. COVID-19, coronavirus disease.
†Persons for whom responses were missing were excluded from the numerator and denominator.
‡Measured fever OR subjective fever, cough, or shortness of breath.
§Measured or subjective fever AND shortness of breath or cough.

Our investigation has limitations. First, the survey was self-administered and based on self-report; therefore, questions were open to interpretation and subject to reporting bias. Because respiratory specimens from asymptomatic persons were collected at a single point in time, we are unable to show whether asymptomatic shedding might have occurred later during quarantine. Also, rRT-PCR assays and serologic tests are inherently limited by their individual sensitivity and specificity; however, we believe that the limitations of test specificity and sensitivity across this population of evacuees were minimal. In addition, because only 1 serum specimen was taken at the time of US arrival, we were unable to detect antibodies that may have developed later.

As of May 1, a total of 1,062,446 COVID-19 cases had been confirmed in the United States, including 39 in repatriated persons (3 cases in 808 returned evacuees across 5 flights from Hubei Province and 36 cases from the Diamond Princess cruise ship) (*28*). Initial efforts to slow introduction of SARS-CoV-2 to the United States began in January 2020 and included quarantine of persons with high-risk exposures, screening of travelers at airports, and isolation and contact tracing of confirmed case-patients (*28*). Our investigation demonstrated that this group of evacuees posed a low risk of introducing SARS-CoV-2 to the United States, and their exposure to SARS-CoV-2 in Wuhan was probably limited. These results should help inform public health guidance on quarantine and isolation measures for travelers arriving from high-risk areas and further characterize the epidemiology of this emerging virus.

Acknowledgments

We thank the following members of the Riverside University System: Josephine Cortez, Anthony Martinez, Brianna Anderson, Hanh Nguyen, Kim Clifton, Vanessa Arreola, Jarrett Herbst, Jide Adeyeye, Stephanie Loe, Geoffrey Leung, Mike Mesisca, Gregory Harriman. We also thank the CDC COVID-19 Patient Under Investigation Team.

About the Author

At the time of the study, Dr. Hallowell was an Epidemic Intelligence Service Officer in the Division of Viral Diseases, National Center for Immunization and Respiratory Diseases, CDC. His research interests include epidemiology of infectious diseases, vaccines, and public health.

References

1. World Health Organization. Pneumonia of unknown cause—China [cited 2020 Feb 20]. https://www.who.int/csr/don/05-january-2020-pneumonia-of-unkown-cause-china
2. World Health Organization. Novel coronavirus (2019-nCoV) situation report–1: 21 January 2020 [cited 2020 Feb 20]. https://www.who.int/docs/default-source/coronaviruse/situation-reports/20200121-sitrep-1-2019-ncov.pdf
3. Gorbalenya AE, Baker SC, Baric RS, de Groot RJ, Drosten C, Gulyaeva AA, et al.; Coronaviridae Study Group of the International Committee on Taxonomy of Viruses. The species *Severe acute respiratory syndrome-related coronavirus*: classifying 2019-nCoV and naming it SARS-CoV-2. Nat Microbiol. 2020;5:536–44. https://doi.org/10.1038/s41564-020-0695-z
4. World Health Organization. Novel coronavirus (2019-nCoV) situation report–102 [cited 2020 May 1]. https://www.who.int/docs/default-source/coronaviruse/situation-reports/20200501-covid-19-sitrep.pdf

5. Centers for Disease Control and Prevention. Coronavirus disease 2019 [cited 2020 May 1]. https://www.cdc.gov/coronavirus/2019-ncov/travelers/index.html
6. Holshue ML, DeBolt C, Lindquist S, Lofy KH, Wiesman J, Bruce H, et al.; Washington State 2019-nCoV Case Investigation Team. First case of 2019 novel coronavirus in the United States. N Engl J Med. 2020;382:929–36. https://doi.org/10.1056/NEJMoa2001191
7. Chinazzi M, Davis JT, Ajelli M, Gioannini C, Litvinova M, Merler S, et al. The effect of travel restrictions on the spread of the 2019 novel coronavirus (COVID-19) outbreak. Science. 2020; 368:395-400. https://doi.org/10.1126/science.aba9757
8. World Health Organization. Novel coronavirus (2019-nCoV) situation report–3: 23 January 2020 [cited 2020 Mar 27]. https://www.who.int/docs/default-source/coronaviruse/situation-reports/20200123-sitrep-3-2019-ncov.pdf
9. Centers for Disease Control and Prevention. Evaluating and testing persons for coronavirus disease 2019 (COVID-19) [cited 2020 Mar 27]. https://www.cdc.gov/coronavirus/2019-nCoV/hcp/clinical-criteria.html
10. Centers for Disease Control and Prevention. Interim guidelines for collecting, handling, and testing clinical specimens from persons under investigation (PUIs) for 2019 novel coronavirus (2019-nCoV) [cited 2020 Feb 12]. https://www.cdc.gov/coronavirus/2019-nCoV/lab/guidelines-clinical-specimens.html
11. Centers for Disease Control and Prevention. Interim laboratory biosafety guidelines for handling and processing specimens associated with 2019 novel coronavirus (2019-nCoV) [cited 2020 Feb 12]. https://www.cdc.gov/coronavirus/2019-nCoV/lab/lab-biosafety-guidelines.html
12. Centers for Disease Control and Prevention. Real-time RT-PCR panel for detection 2019-novel coronavirus [cited 2020 May 18]. https://www.cdc.gov/coronavirus/2019-ncov/lab/guidelines-clinical-speciments.html
13. Patel A, Jernigan DB; 2019-nCoV CDC Response Team. Initial public health response and interim clinical guidance for the 2019 novel coronavirus outbreak—United States, December 31, 2019–February 4, 2020. MMWR Morb Mortal Wkly Rep. 2020;69:140–6. https://doi.org/10.15585/mmwr.mm6905e1
14. Backer JA, Klinkenberg D, Wallinga J. Incubation period of 2019 novel coronavirus (2019-nCoV) infections among travellers from Wuhan, China, 20-28 January 2020. Euro Surveill. 2020;25:2000062. https://doi.org/10.2807/1560-7917.ES.2020.25.5.2000062
15. Li Q, Guan X, Wu P, Wang X, Zhou L, Tong Y, et al. Early transmission dynamics in Wuhan, China, of novel coronavirus–infected pneumonia. N Engl J Med. 2020;382:1199–207. https://doi.org/10.1056/NEJMoa2001316
16. Harris PA, Taylor R, Thielke R, Payne J, Gonzalez N, Conde JG. Research electronic data capture (REDCap)—a metadata-driven methodology and workflow process for providing translational research informatics support. J Biomed Inform. 2009;42:377–81. https://doi.org/10.1016/j.jbi.2008.08.010
17. Hui DSI, I Azhar E, Madani TA, Ntoumi F, Kock R, Dar O, et al. The continuing 2019-nCoV epidemic threat of novel coronaviruses to global health—the latest 2019 novel coronavirus outbreak in Wuhan, China. Int J Infect Dis. 2020;91:264–6. https://doi.org/10.1016/j.ijid.2020.01.009
18. Sjödin H, Wilder-Smith A, Osman S, Farooq Z, Rocklöv J. Only strict quarantine measures can curb the coronavirus disease (COVID-19) outbreak in Italy, 2020. Euro Surveill. 2020;25:2000280. https://doi.org/10.2807/1560-7917.ES.2020.25.13.2000280
19. Sun K, Viboud C. Impact of contact tracing on SARS-CoV-2 transmission. Lancet Infect Dis. 2020;S1473-3099(20)30357-1.
20. Li W, Zhang B, Lu J, Liu S, Chang Z, Cao P, et al. The characteristics of household transmission of COVID-19. Clin Infect Dis. 2020 Apr 17 [Epub ahead of print]. https://doi.org/10.1093/cid/ciaa450
21. Bi Q, Wu Y, Mei S, Ye C, Zou X, Zhang Z, et al. Epidemiology and transmission of COVID-19 in 391 cases and 1286 of their close contacts in Shenzhen, China: a retrospective cohort study. Lancet Infect Dis. 2020; S1473-3099(20)30287-5. https://doi.org/10.1016/S1473-3099(20)30287-5
22. Hoehl S, Rabenau H, Berger A, Kortenbusch M, Cinatl J, Bojkova D, et al. Evidence of SARS-CoV-2 infection in returning travelers from Wuhan, China. N Engl J Med. 2020;382:1278–80. https://doi.org/10.1056/NEJMc2001899
23. Nishiura H, Kobayashi T, Yang Y, Hayashi K, Miyama T, Kinoshita R, et al. The rate of underascertainment of novel coronavirus (2019-nCoV) infection: estimation using Japanese passengers data on evacuation flights. J Clin Med. 2020;9:419. https://doi.org/10.3390/jcm9020419
24. Alanazi KH, Killerby ME, Biggs HM, Abedi GR, Jokhdar H, Alsharef AA, et al. Scope and extent of healthcare-associated Middle East respiratory syndrome coronavirus transmission during two contemporaneous outbreaks in Riyadh, Saudi Arabia, 2017. Infect Control Hosp Epidemiol. 2019;40:79–88. https://doi.org/10.1017/ice.2018.290
25. Wilder-Smith A, Freedman DO. Isolation, quarantine, social distancing and community containment: pivotal role for old-style public health measures in the novel coronavirus (2019-nCoV) outbreak. J Travel Med, 2020;27(2), taaa020. https://doi.org/10.1093/jtm/taaa020
26. Centers for Disease Control and Prevention. How to protect yourself & others [cited 2020 Apr 14]. https://www.cdc.gov/coronavirus/2019-ncov/prevent-getting-sick/prevention.html
27. Centers for Disease Control and Prevention. Coronavirus disease 2019 (COVID-19): cases in the U.S. [cited 2020 May 1]. https://www.cdc.gov/coronavirus/2019-ncov/cases-in-us.html
28. Jernigan DB; CDC COVID-19 Response Team. Update: public health response to the coronavirus disease 2019 outbreak—United States, February 24, 2020. MMWR Morb Mortal Wkly Rep. 2020;69:216–9. https://doi.org/10.15585/mmwr.mm6908e1

Address for correspondence: Marie E. Killerby, Centers for Disease Control and Prevention, 2500 Century Ctr, MailstopV25-1, Atlanta, GA 30345, USA; email: lxo9@cdc.gov

Pathology and Pathogenesis of SARS-CoV-2 Associated with Fatal Coronavirus Disease, United States

Roosecelis B. Martines,[1] Jana M. Ritter,[1] Eduard Matkovic, Joy Gary, Brigid C. Bollweg, Hannah Bullock, Cynthia S. Goldsmith, Luciana Silva-Flannery, Josilene N. Seixas, Sarah Reagan-Steiner, Timothy Uyeki, Amy Denison, Julu Bhatnagar, Wun-Ju Shieh, Sherif R. Zaki; COVID-19 Pathology Working Group[2]

An ongoing pandemic of coronavirus disease (COVID-19) is caused by infection with severe acute respiratory syndrome coronavirus 2 (SARS-CoV-2). Characterization of the histopathology and cellular localization of SARS-CoV-2 in the tissues of patients with fatal COVID-19 is critical to further understand its pathogenesis and transmission and for public health prevention measures. We report clinicopathologic, immunohistochemical, and electron microscopic findings in tissues from 8 fatal laboratory-confirmed cases of SARS-CoV-2 infection in the United States. All cases except 1 were in residents of long-term care facilities. In these patients, SARS-CoV-2 infected epithelium of the upper and lower airways with diffuse alveolar damage as the predominant pulmonary pathology. SARS-CoV-2 was detectable by immunohistochemistry and electron microscopy in conducting airways, pneumocytes, alveolar macrophages, and a hilar lymph node but was not identified in other extrapulmonary tissues. Respiratory viral co-infections were identified in 3 cases; 3 cases had evidence of bacterial co-infection.

The ongoing global pandemic of coronavirus disease (COVID-19), caused by severe acute respiratory syndrome coronavirus 2 (SARS-CoV-2), was identified in Wuhan, Hubei Province, China, and has spread rapidly around the world (*1*,*2*). As of May 18, 2020, World Health Organization official data reported 4,628,903 confirmed cases and 312,009 deaths (*2*). On January 20, 2020, the Centers for Disease Control and Prevention (CDC) confirmed a case in the United States; since then, all 50 US states, District of Columbia, Guam, Puerto Rico, Northern Mariana Islands, and US Virgin Islands have confirmed cases of COVID-19 (*2*–*4*).

Coronaviruses are enveloped, positive-stranded RNA viruses that infect many animals; human-adapted viruses likely are introduced through zoonotic transmission from animal reservoirs (*5*,*6*). Most known human coronaviruses are associated with mild upper respiratory illness. SARS-CoV-2 belongs to the group of betacoronaviruses that includes severe acute respiratory syndrome coronavirus (SARS-CoV) and Middle East respiratory syndrome coronavirus (MERS-CoV), which can infect the lower respiratory tract and cause a severe and fatal respiratory syndrome in humans (*7*). SARS-CoV-2 has ≥79.6% similarity in genetic sequence to SARS-CoV (*5*).

SARS-CoV-2 is highly transmissible among humans; fatality rates for COVID-19 vary and are higher among the elderly and persons with underlying conditions or immunosuppression (*8*,*9*). The current knowledge about COVID-19 pathogenesis and pathology in fatalities is based on a small number of described cases and extrapolations from what is known about other similar coronaviruses, such as SARS-CoV and MERS-CoV (*10*–*18*). Pathologic evaluation and determination of virus distribution and cellular localization within tissues is crucial to elucidating the pathogenesis of these fatal infections and can help guide development of therapeutic and preventive countermeasures. We report on the histopathologic features and detection of virus in tissues by immunohistochemistry (IHC) and electron microscopy (EM) from 8 confirmed fatal cases of COVID-19 in the United States.

Author affiliations: Centers for Disease Control and Prevention, Atlanta, Georgia, USA (R.B. Martines, J.M. Ritter, E. Matkovic, J. Gary, B.C. Bollweg, C.S. Goldsmith, L. Silva-Flannery, J.N. Seixas, S. Reagan-Steiner, T. Uyeki, A. Denison, J. Bhatnagar, W.-J. Shieh, S.R. Zaki); Synergy America Inc., Atlanta (H. Bullock).

DOI: https://doi.org/10.3201/eid2609.202095

[1]These authors contributed equally to this article.

[2]Members of the COVID-19 Pathology Working Group: Rhonda Cole, Amanda Lewis, Pamela Fair, Lindsey Estetter.

Materials and Methods

Study Patients and Data Collection

As part of the public health response to COVID-19, the CDC Infectious Diseases Pathology Branch (Division of High-Consequence Pathogens and Pathology, National Center for Emerging and Zoonotic Infectious Diseases) was consulted on autopsies of 8 patients with laboratory evidence of SARS-CoV-2 by reverse transcription PCR (RT-PCR) on respiratory swab specimens collected either before or after death. We reviewed available medical records and preliminary autopsy reports for information regarding demographics, symptom history, underlying conditions, infectious disease testing, imaging study findings, treatment and advanced supportive care received, and date of death. This investigation was reviewed in accordance with CDC's human subjects review procedures and was determined to not meet the definition of research.

Histopathology and Immunohistochemistry

We performed routine hematoxylin–eosin stains for histopathologic evaluation. We conducted an IHC assay for SARS-CoV-2 using a rabbit polyclonal antibody raised against SARS-CoV nucleocapsid (Novus Biologicals, https://www.novusbio.com) (*19*) at 1:100 dilution and a Mach 4 Universal AP Polymer Kit (Biocare Medical, https://biocare.net) with Permanent Red Chromogen (Cell Marque/Millipore Sigma, https://www.cellmarque.com). We pretreated the slides with heat-induced epitope retrieval with a citrate-based buffer (Biocare Medical). We ran appropriate negative controls in parallel, using normal rabbit serum in place of the primary antibody. We validated cross reactivity of the anti–SARS-CoV antibody with SARS-CoV-2 by testing controls created from SARS-CoV-2–infected Vero cells embedded with normal human tissues; we used this control as the positive control for subsequent IHC assays. The SARS-CoV nucleocapsid antibody did not cross-react with influenza A(H1N1) virus, influenza B virus, respiratory syncytial virus, parainfluenza virus type 3, human coronavirus (HCoV) 229E, or MERS-CoV in PCR-confirmed tissue samples. For cases with bronchopneumonia, we performed IHC testing for bacterial agents using a mouse monoclonal antibody raised against *Streptococcus pneumoniae* but known to also detect other *Streptococcus* spp. and a rabbit polyclonal anti-*Klebsiella pneumoniae* antibody (both from Thermo Fisher, https://www.thermofisher.com) known to also detect other gram-negative bacteria (*Escherichia coli*, *Haemophilus influenzae*, and *Pseudomonas* spp.).

For double-stained assays, we used Envision G/2 Double Stain System, Rabbit/Mouse (DAB Permanent Red) from Agilent Technologies (https://www.agilent.com). We used antibodies against CD163 (Leica Biosystems, https://www.leicabiosystems.com) or surfactant apoprotein A (Dako, https://www.agilent.com), followed by the anti–SARS-CoV nucleocapsid antibody (Novus Biologicals). We performed all assays according to the manufacturer's guidelines. We used SARS-CoV-2–infected Vero cells as a positive control and used non–COVID-19 cases and normal rabbit serum in place of primary antibody as negative controls.

Electron Microscopy

We obtained upper airway and lung tissue specimens from formalin-fixed samples, cut them into cubes, rinsed them with 0.1 mmol/L phosphate buffer, post-fixed them with 2.5% glutaraldehyde, and rinsed them in phosphate buffer. In addition, we removed tissue samples from areas corresponding to positive SARS-CoV-2 immunostaining from paraffin blocks with a 2-mm punch or from 4-μm sections on glass slides; we deparaffinized the samples in xylene and rehydrated. We processed tissues for transmission EM as described previously (*20*). We immersed the sections embedded in epoxy resin in boiling water, removed them from the slides with a razor blade, and cut out the areas of interest and glued them onto a blank EM block. We stained EM sections with uranyl acetate and lead citrate and examined them on a Thermo Fisher/FEI Tecnai Spirit or Tecnai BioTwin electron microscope.

RT-PCR

We extracted nucleic acids from formalin-fixed paraffin-embedded (FFPE) tissues and assessed them by a conventional RT-PCR specifically targeting the nucleocapsid gene of SARS-CoV-2 (J. Bhatnagar, unpub. data) and real-time RT-PCR/PCR targeting other respiratory pathogens, including influenza viruses, respiratory syncytial virus, human parainfluenza viruses, and *Streptococcus pneumoniae*, as described previously (*21*,*22*). The SARS-CoV-2 nucleocapsid assay detects SARS-CoV-2 and SARS-CoV but does not amplify MERS-CoV and other common human coronaviruses, including alphacoronavirus (HCoV-NL63) and betacoronavirus (HCoV-HKU1).

Results

Clinical Data

Of the 8 case-patients, 7 were residents of a long-term care facility (LTCF) in Washington state (Table

1) (23,24). Seven (87.5%) were White, non-Hispanic. The median age of the 8 case-patients was 73.5 years; 2 were <65 years of age. The median number of days from illness onset until death was 12.5 (range 6–15). Common signs and symptoms reported included fever (75%), cough (62.5%), and shortness of breath (62.5%). All patients had abnormal findings on chest radiographs. Case-patients were all hospitalized for a median of 3.5 days. Six (75%) patients received mechanical ventilation; 2 received comfort care. Underlying medical conditions were identified in all case-patients; hypertension (75%), chronic kidney disease (75%), cardiovascular disease (75%), obesity (62.5%), and diabetes (50%) were the most frequent conditions reported.

Histopathology, Immunohistochemistry, and Electron Microscopy

Histopathologic findings and results of testing performed on FFPE tissues showed mild to moderate tracheobronchitis was consistently present and characterized by mononuclear inflammation, with epithelial denudation and submucosal congestion (Table 2; Figure 1, panels A, B). The predominant lung pathology was diffuse alveolar damage (DAD); acute phases, organizing phases, or both were present in 7 (87.5%) of 8 patients. Desquamation of pneumocytes and the presence of hyaline membranes, alveolar edema and fibrin deposits, type II pneumocyte hyperplasia, and alveolar infiltrates, including increased alveolar macrophages, were seen (Figure 1, panels C, D). Squamous metaplasia and atypical pneumocytes were present in 3 case-patients, and rare multinucleated cells were present in 1 case-patient (patient no. 1) (Figure 1, panel E); no definitive viral inclusions were seen. One case-patient without DAD (patient no. 7) had diffuse bronchopneumonia with filling of alveolar spaces by mixed inflammation with abundant neutrophils (Figure 1, panel F). Three additional case-patients had focal bronchopneumonia and increased pulmonary intravascular leukocytes. Hemosiderin-laden macrophages (4/8), hemorrhage (4/8), mucus aspiration (3/8), emphysema (2/8), and microthrombi (1/8) were seen (Figure 2). Anthracosis, common in elderly persons as a result of chronic carbon accumulation, was present in the lungs and pulmonary hilar lymph nodes in all cases. In 6 cases, lymph nodes also showed sinus histiocytosis and hemophagocytosis in subcapsular sinuses. Notable pathologic findings in extrapulmonary tissues included evidence of chronic renal disease (5/8), acute renal tubular injury (3/8), hepatic steatosis (4/8) and cirrhosis (1/8), and focal myocardial fibrosis (3/8) (Figure 2). No myocarditis or myocardial necrosis and no notable histopathologic changes in the intestine were seen in any case. Brain tissues were not available for histopathologic evaluation or testing.

We detected SARS-CoV-2 by IHC in the upper airways in 4/8 (50%) case-patients and in the lungs in 7/8 (92%) case-patients. We observed immunostaining of viral antigens in upper airway and bronchiolar epithelium, submucosal gland epithelium, and in type I and type II pneumocytes, alveolar macrophages, and hyaline membranes in the lung (Figure 3, panels A–C, F). Upper airways and lung tissues

Table 1. Selected demographic and clinical characteristics of 8 case-patients with fatal severe acute respiratory syndrome coronavirus 2 infection

Characteristic	No. (%)
Sex	
M	4 (50)
F	4 (50)
Age group, y	
<65	2 (25)
≥65	6 (25)
Race/ethnicity	
White, non-Hispanic	7 (87.5)
Hispanic	1 (12.5)
Clinical symptoms	
Fever	6 (75)
Cough	5 (62.5)
Shortness of breath	5 (62.5)
Malaise	2 (25)
Myalgias	1 (12.5)
Diarrhea	1 (12.5)
Underlying health conditions	
≥1 condition	8 (100)
Hypertension	6 (75)
Chronic kidney disease*	6 (75)
Cardiovascular disease†	6 (75)
Obesity‡	5 (62.5)
Diabetes mellitus	4 (50)
Chronic lung disease§	2 (25)
Immunocompromised condition¶	3 (37.5)
Neurologic disorders	1 (12.5)
Other chronic diseases#	6 (75)
Radiographic findings	
Bilateral interstitial infiltrate or opacities	8 (100)
Pleural effusion	2 (25)
Clinical course	
Median days from illness onset to death (range)	12.5 (6–15)
Median days of hospitalization (range)	3.5 (1–8)
Mechanical ventilation**	6 (75)

*Chronic kidney disease requiring treatment with hemodialysis was reported in 2 case-patients.
†Number of cases includes patients with history of coronary artery disease, congestive heart failure, valvular heart disease, and/or cerebrovascular accident.
‡Obesity includes reported BMI >30 or mention of obesity or morbid obesity in the submitted medical records. Two patients had morbid obesity listed in the submitted medical records.
§Chronic obstructive pulmonary disease was the only reported underlying condition with chronic lung disease.
¶This includes persons immunosuppressed by solid organ transplant, corticosteroid therapy, or immunosuppressive medication.
#Includes any of the following: hyperlipidemia, thyroid disease, rheumatologic disorder, and obstructive sleep apnea.
**Two patients were transitioned to comfort care and were not intubated.

Table 2. Histopathologic features and severe acute respiratory syndrome coronavirus 2 detection in respiratory tissues from 8 coronavirus disease fatalities*

Patient no.	1	2	3	4	5	6	7	8
Minimum symptom duration, d	13	10	5	13	16	11	12	7
Tracheobronchitis	++	+	+	+	+	+	++	+
DAD, acute	+	+	++	++	–	–	–	+++
DAD, organizing	+++	+	++	++	+	+	–	+++
Squamous metaplasia	+	–	–	+	–	–	–	+
Atypical pneumocytes	+++	–	–	+	–	–	–	+
Interstitial pneumonitis	+	–	–	+	–	++	–	+
Bronchopneumonia	–	–	+	+	+	–	+++	–
Intravascular leukocytosis	–	–	+	+	+	–	–	–
Anthracosis	+	+	+	++	++	++	+	++
Other lung pathology	–	HLM	Hemorrhage, emphysema, MA	HLM, MA	HLM, MA	Hemorrhage, corpora amylacea	Hemorrhage, HLM, microthrombi	Hemorrhage, emphysema
SARS-CoV-2 IHC, upper airway	–	–	–	–	**	**	*	*
SARS-CoV-2 IHC, lung	–	+	+++	+++	+++	+	++	++
Electron microscopy, viral particles	NA	NA	+	+	+	+	NA	NA
Other agents detected	Influenza B	–	–	*Streptococcus* spp.	PI-3	*Streptococcus* spp.	PI-3	*Streptococcus* spp.

*DAD, diffuse alveolar damage; HLM, hemosiderin-laden macrophages; IHC, immunohistochemistry; MA, mucus aspiration; NA, not available; PI, parainfluenza; – , not present or negative; +, mild; ++, moderate; +++, extensive.

from all 8 case-patients were positive by SARS-CoV-2 RT-PCR. Double staining with surfactant showed colocalization of SARS-CoV-2 antigen with type II pneumocytes (Figure 3, panel D); double staining with CD-163 showed viral antigen colocalization with macrophages (Figure 3, panel E). We also found viral immunostaining in scattered macrophages in the hilar lymph node from 1 severely immunosuppressed patient with a history of solid-organ transplant (Figure 3, panel G). We did not detect SARS-CoV-2 by IHC in heart, liver, kidney, spleen, or intestine from any patient.

Six (75%) of 8 case-patients had either viral or bacterial co-infections, but not both, identified by IHC, PCR, or both in addition to SARS-CoV-2. Respiratory viral PCR testing detected parainfluenza virus type 3 coinfection in upper airway and lung tissue in 2/8 (25%) case-patients and influenza B virus coinfection in upper airway in 1 case-patient. Three (75%) of the 4 case-patients with SARS-CoV-2 and bronchopneumonia had immunostaining for *Streptococcus* spp. Two of these patients had nonpneumococcal *Streptococcus* spp. confirmed by PCR testing.

EM examination of respiratory tissues showed virions with prominent surface projections (spikes) characteristic of the family *Coronaviridae*. In the lung, extracellular virions free in the alveolar space were, on average, 105 nm in diameter, including surface projections (Figure 4, panel A). In upper airways, virions were seen extracellularly among the cilia and within the cytoplasm of respiratory epithelial cells (Figure 4, panel B; Figure 5). Intracellular virions in type II pneumocytes (Figure 4, panels C, D) and in cytoplasmic vesicles or phagosomes of alveolar macrophages (Figure 4, panel E) were, on average, 75 nm in diameter and lacked prominent spikes. Viral particles were also found associated with fibrin or hyaline membranes within alveolar spaces (Figure 4, panel F).

Discussion

The clinical distinction between SARS-CoV-2 and other respiratory viral infections is difficult because there are overlapping clinical features characterized by febrile illness with cough that lasts for several days before progressing to acute pneumonia. In addition, persons with SARS-CoV-2 and other respiratory viral infections may have atypical or minimal symptoms (*25*–*27*). Besides respiratory failure, particularly in patients with severe disease, fatigue, myalgia or arthralgia, chills, hepatic and renal dysfunction, lymphocytopenia, leukopenia, thrombocytopenia, and elevated inflammatory biomarkers have been described (*5*,*28*,*29*).

Histopathologic lesions attributed directly to the virus in these cases were limited to respiratory tissues; the predominant finding was DAD, with various levels of progression and severity. We saw no clear correlation of the pathologic phase of DAD to known symptom duration, which could be the result of underrecognition of early symptoms in elderly residents of LTCFs and underestimation of illness duration. Together, the histopathologic, IHC, and

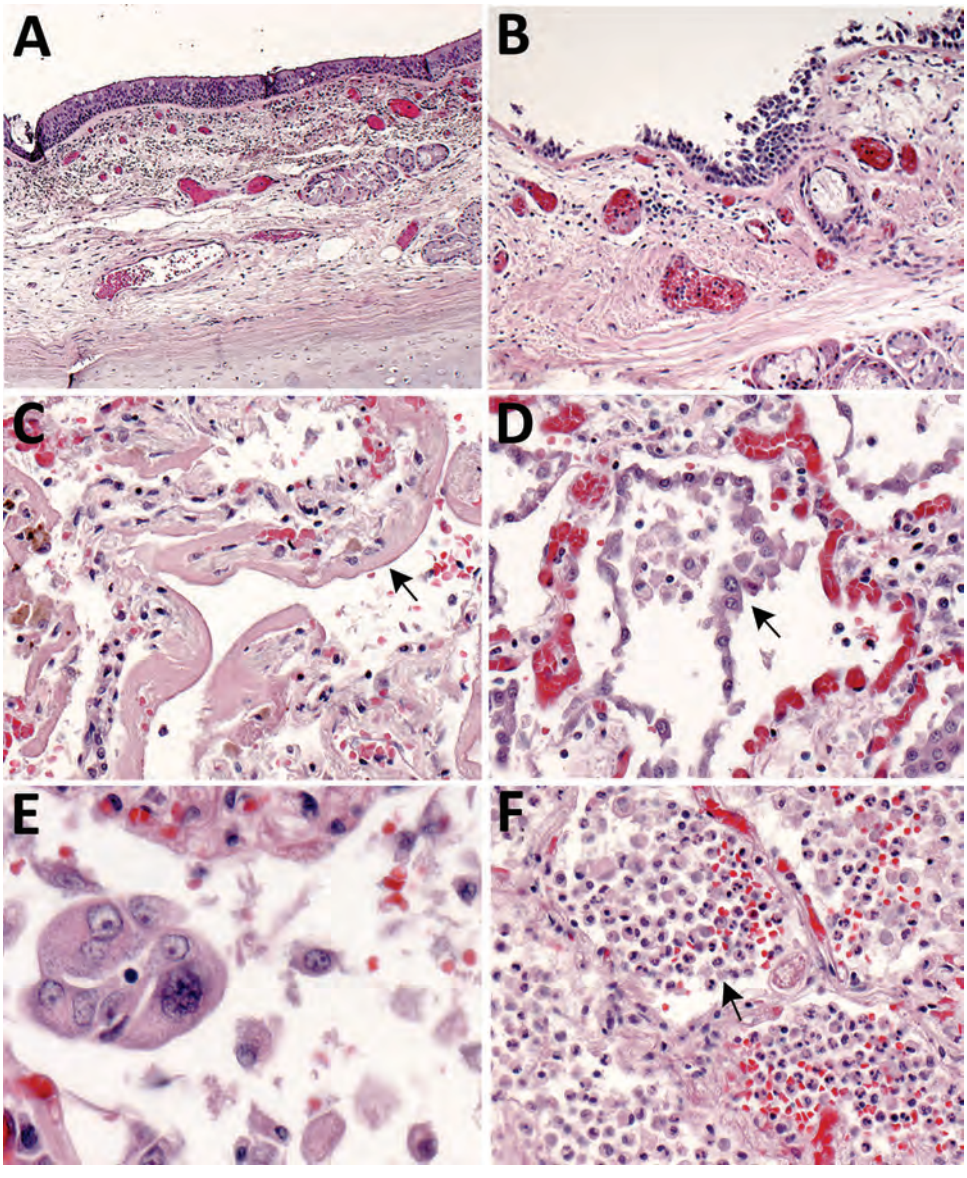

Figure 1. Pulmonary histopathology in fatal coronavirus disease cases caused by severe acute respiratory syndrome coronavirus 2 infection. A) Patient no. 5: tracheitis characterized by moderate mononuclear inflammation within the submucosa (original magnification ×10). B) Patient no. 3: extensive denudation of tracheal epithelium; submucosal congestion, mild edema, and mononuclear inflammation (original magnification ×10). C) Patient no. 4: exudative phase of diffuse alveolar damage characterized by abundant hyaline membranes lining alveolar spaces (arrow) (original magnification ×20). D) Patient no. 8: proliferative phase of diffuse alveolar damage characterized by proliferation of type II pneumocytes (arrow) (original magnification ×20). E) Patient no. 1: atypical pneumocytes with enlarged and multiple nuclei, and expanded cytoplasm in a case with proliferative DAD (original magnification ×40). F) Patient no. 7: bronchopneumonia with filling of alveolar spaces by neutrophils and patchy hemorrhage (arrow) (original magnification ×10).

EM findings in this report provide insight into SARS-CoV-2 pathogenesis. IHC testing, including double staining with surfactant, and EM confirmed viral tropism for pulmonary II pneumocytes. The ultrastructural observations are consistent with previous reports of SARS-CoV infection, with the exception that neither double-membrane vesicles nor nucleocapsid inclusions were detected (*15*,*20*). Viral antigen was also seen in respiratory epithelium of conducting airways (trachea, bronchi, and bronchioles) and occasionally in alveolar macrophages; infection of these cell types may be key in viral replication and trafficking. The respiratory epithelium is one of the first cell types encountered by inhaled virus; SARS-CoV-2 antigens were detected by IHC in ciliated epithelial cells from 50% of these case-patients and up to 16 days after known symptom onset. Ultrastructural analysis showed numerous extracellular viral particles along the ciliated surface and within ciliated columnar epithelial cells. These findings corroborate reports of high viral loads in the upper respiratory tract and support the potential for persons infected with SARS-CoV-2 to readily transmit the virus, with prolonged and continued viral shedding in severe cases (*30*,*31*).

Overall pathologic features in these 8 COVID-19 deaths were similar to those seen in SARS-CoV and MERS-CoV infections, and in available COVID-19 reports (*10*–*15*,*18*,*20*,*32*). However, the amount of viral antigen detected by IHC in lung tissue from these cases is more than what we have seen in SARS and MERS (*16*,*18*) cases submitted to our laboratory, and its extensive detection in epithelial cells of

the upper respiratory tract is unique among these highly pathogenic coronaviruses (*33*). In addition to direct viral effects on tissues, the immune response to viral infection likely plays a major role in determining clinical outcome, and acute decline in COVID-19 patients has been linked to an immune-mediated cytokine storm (*34*). Preliminary evaluation of immune cell populations in the respiratory tissues from these 8 cases revealed abundant T lymphocytes in the upper airways and lung parenchyma, with B lymphocytes in smaller numbers and predominating in areas of lymphoid aggregates (data not shown). Further investigation into the roles of these cell populations in COVID-19 is needed. In 6 of the 8 case-patients, sinus histiocytosis and hemophagocytosis were seen in hilar lymph nodes. However, SARS-CoV-2 antigens were detected by IHC in hilar lymph node macrophages from only 1 immunosuppressed patient. Lymph nodes are key sites for immune recognition and elimination of respiratory pathogens. Elucidating the immune response to, and the effects of immunosuppression on, SARS-CoV-2 infection is therefore of fundamental importance.

SARS-CoV-2 uses the angiotensin-converting enzyme 2 (ACE2) receptor to facilitate viral entry into target cells. ACE2 is expressed in multiple tissues throughout the body, including type II pneumocytes, myocardial cells, cholangiocytes, enterocytes, and oral mucosal epithelium (*5*,*35*,*36*). However, among these patients, SARS-CoV-2 antigens were not detected in extrapulmonary tissues besides hilar lymph node, and pathologic findings in other tissues were

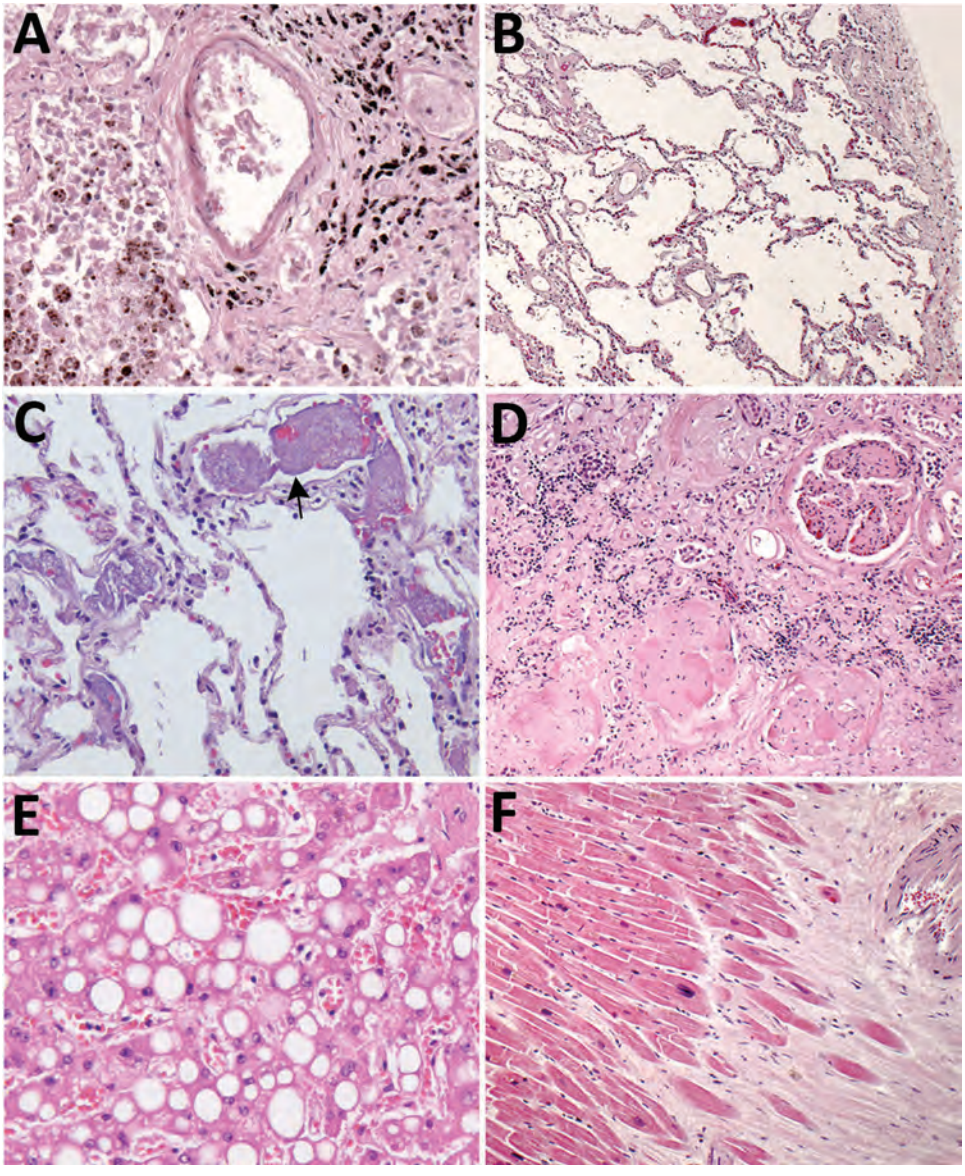

Figure 2. Histopathologic findings associated with underlying conditions in fatal coronavirus disease. A) Patient no. 2: lung, hemosiderin-laden macrophages (brown pigment, bottom left), and anthracosis (black pigment, top right) in a patient with congestive heart failure (original magnification ×20). B) Patient no. 3: lung, emphysema in a patient with chronic obstructive pulmonary disease (original magnification ×5). C) Patient no. 7: lung, pulmonary microthrombosis (arrow) (original magnification ×20). D) Patient no. 2: kidney, extensive glomerulosclerosis in a patient with renal disease (original magnification ×10). E) Patient no. 3: liver, steatosis in a patient with morbid obesity (original magnification ×20). F) Patient no. 2: heart, myocardial fibrosis and mild cardiomyocyte hypertrophy in a patient with cardiomegaly (original magnification ×5).

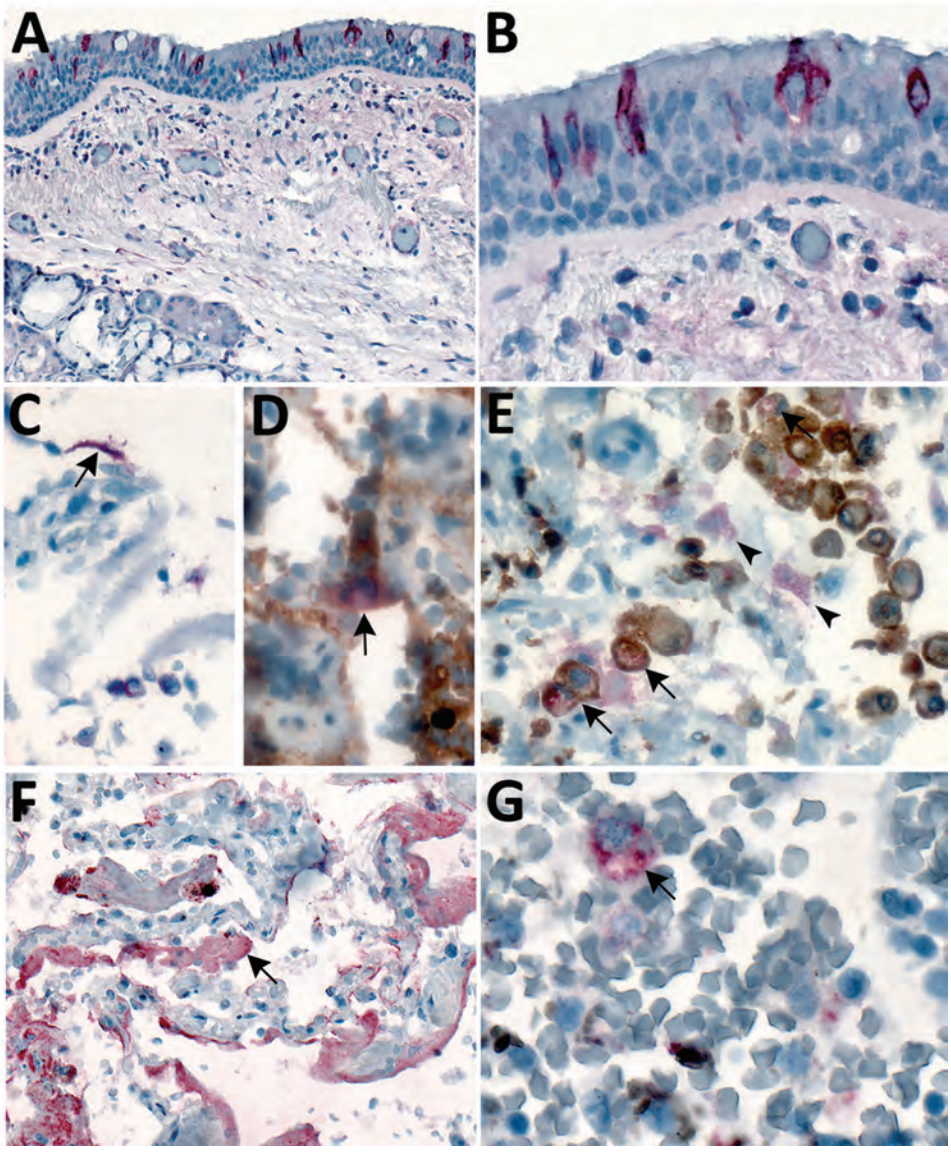

Figure 3. Immunostaining of severe acute respiratory syndrome coronavirus 2 in pulmonary tissues from fatal coronavirus disease cases. A) Patient no. 5: scattered immunostaining of tracheal epithelial cells (original magnification ×40). B) Patient no. 5: higher magnification shows immunostaining of ciliated cells (original magnification ×63). C) Patient no. 8: immunostaining of desquamated type I pneumocyte in an alveolar lumen (original magnification ×63). D) Patient no. 4: colocalization of SARS-CoV-2 viral antigen (red) with type II pneumocyte stained by surfactant (brown; arrow) (original magnification ×63). E) Patient no. 4: colocalization of SARS-CoV-2 viral antigen (red) with macrophages stained by CD163 (brown; arrows); virus immunostaining within type II pneumocytes is also seen (arrowheads) (original magnification ×40). F) Patient no. 4: extensive immunostaining of hyaline membranes in a region of exudative DAD (original magnification ×20). G) Patient no. 3: scattered immunostaining within macrophage in hilar lymph node; anthracosis is also present (original magnification ×63).

attributable to other underlying concurrent conditions. Some of the underlying conditions in these case-patients (e.g., hypertension, COPD) are associated with upregulation of ACE2 receptors; possible correlation of these conditions with COVID-19 severity warrants further exploration (*5*,*28*,*37*). COVID-19 cardiomyopathy and acute cardiac death during clinical resolution of pulmonary disease have been described (*24*,*38*). However, we did not observe any evidence of myocarditis or myocardial necrosis in the tissues of the 8 case-patients we examined. Reports have been made of coagulation abnormalities and pulmonary vascular perfusion issues without DAD in some COVID-19 patients (*39*,*40*), and we saw microthrombi in the lung from 1 case-patient who lacked DAD but had severe bacterial bronchopneumonia. These various and potentially severe cardiovascular complications of COVID-19 warrant further investigation into the specific mechanisms of SARS-CoV-2–induced cardiovascular injury, homeostatic derangement, or both.

Clinical studies have reported elevated liver enzymes in patients with COVID-19 (*28*,*29*). The lack of viral detection by IHC in the liver in this investigation suggests that for these case-patients, abnormal biomarkers of hepatic injury may not be the result of direct viral infection of hepatocytes. Gastrointestinal symptoms are not typically a prominent feature of COVID-19 but have been reported, and SARS-CoV-2 has been detected in fecal samples (*41*–*43*). However, no histopathologic findings or SARS-CoV-2 antigens were detected in gastrointestinal tissues, and diarrhea was reported for only 1 of these case-patients.

We identified viral co-infections in upper respiratory tract tissues from 3 case-patients, including 2 with parainfluenza virus 3 and 1 with influenza B virus, but the contribution of these co-infections to pulmonary disease and fatal outcomes is unknown. Although we identified streptococcal lower respiratory infections in 3 case-patients, none were caused by *Streptococcus pneumoniae*, and there was no strict correlation of these infections with mechanical ventilation among these case-patients. Because 7 of 8 case-patients discussed in this report were residents of a LTCF, their exposures and risks for viral and bacterial co-infections may be different from those for other patients. Few community-acquired bacterial

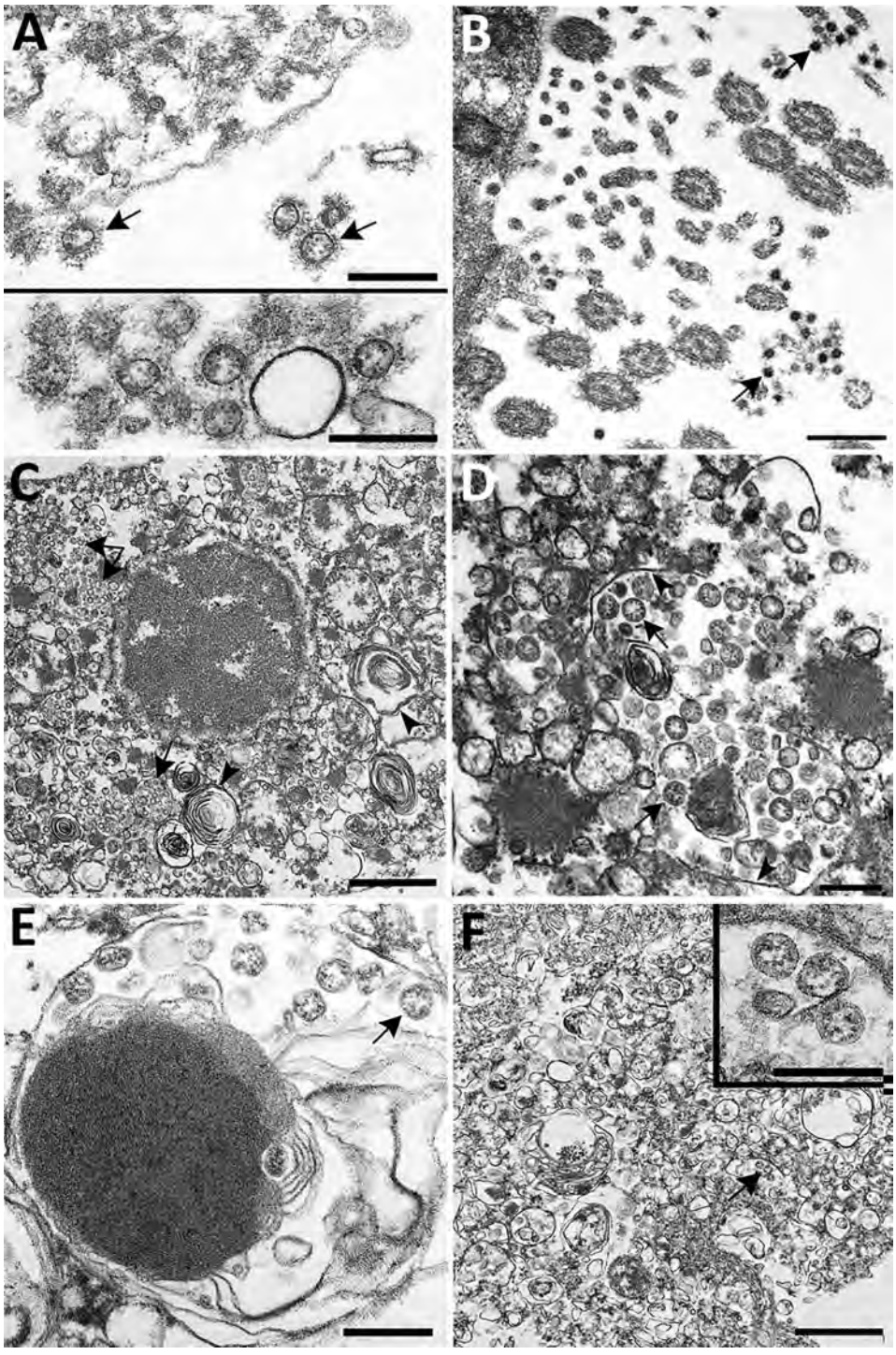

Figure 4. Ultrastructural features of severe acute respiratory syndrome coronavirus 2 lung infection in fatal coronavirus disease. A) Top: alveolar space containing extracellular virions (arrows) with prominent surface projections. Bottom: cluster of virions in the alveolar space. Scale bars indicate 200 nm. B) Extracellular virions (arrow) associated with ciliated cells of the upper airway. Scale bar indicates 200 nm. C) Membrane-bound vacuoles (arrows) containing viral particles within the cytoplasm of an infected type II pneumocyte; surfactant (lamellated material) indicted by arrowheads. Scale bar indicates 1 μm. D) Membrane-bound vacuole (double-headed arrow in panel C) containing virus particles (arrows) with the characteristic black dots that are cross-sections through the viral nucleocapsid. Arrowheads indicate vacuolar membrane. Scale bar indicates 200 nm. E) Viral particles (arrow) within a phagosome of an alveolar macrophage. Scale bar: 200 nm. F) Viral particles within a portion of a hyaline membrane. Scale bar indicates 800 nm. Inset: Higher magnification of virus particles indicated by arrow; scale bar indicates 200 nm.

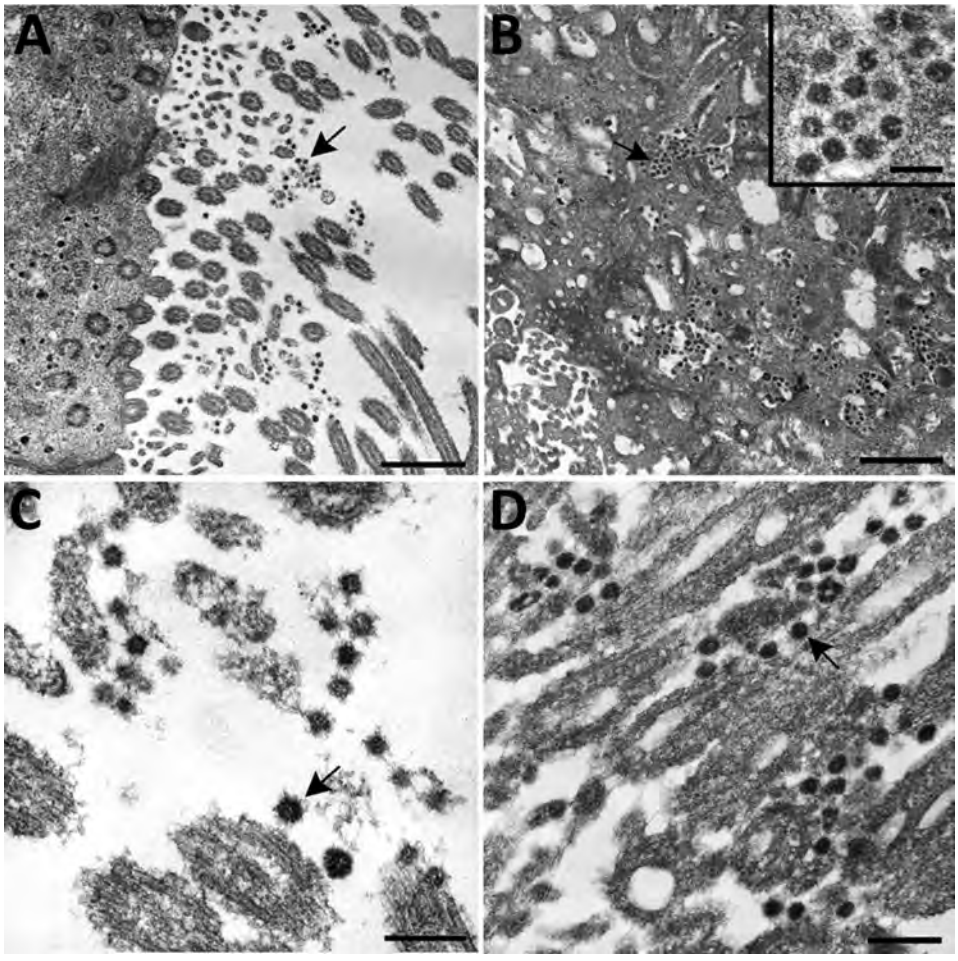

Figure 5. Ultrastructural features of severe acute respiratory syndrome coronavirus 2 infection within the upper airway of a fatal coronavirus disease case from formalin-fixed paraffin-embedded (FFPE) tissue. Viral particles associated with the cilia of ciliated cells (A, C, and D) and the cytoplasm of respiratory epithelial cells (B) in the upper airway are indicted by arrows. Images in panels A and C were obtained from FFPE tissue removed from a paraffin block using a 2-mm biopsy punch. Images in panels B and D were collected from a 3 μm section of FFPE tissue affixed to a glass slide. Viral particles visualized in FFPE samples were smaller than those observed from fresh tissue; extracellular viral particles in fresh tissue samples were 105 nm in diameter and those from FFPE tissues were 75 nm in diameter. Scale bars indicate 1 μm (panel A), 800 nm (panel B), and 200 nm (panels C and D).

infections have been reported in critically ill patients with COVID-19, but co-infections are not frequently reported with SARS and MERS (*17*,*32*,*44*). Co-infections may play a key role in increasing susceptibility to, and illness from, SARS-CoV-2 infection in a LTCF setting. Further investigation into this association, and characterization of the etiologic agents most commonly involved, is warranted and may contribute to improved overall management of COVID-19 disease.

This report describes the specific cellular and extracellular localization of SARS-CoV-2 in respiratory tissues, without any IHC evidence of the virus in other tissues. Although detection of SARS-CoV-2 RNA in blood or serum has been reported (*34*,*41*), we did not find evidence of systemic virus dissemination in these case-patients. Our findings highlight the importance of underlying conditions and pulmonary co-infections in COVID-19; these factors may potentially delay or confound diagnosis and contribute to adverse outcomes.

A limitation of this study is that 7 of 8 cases were from a single skilled nursing facility; findings may therefore not be representative of community-acquired SARS-CoV-2 infections. However, nosocomial transmission of viruses often parallels community outbreaks, and understanding disease transmission in healthcare settings is crucial (*25*,*45*). None of these case-patients had diagnoses of acute cardiac injury, myocarditis, or cardiomyopathy, so understanding the pathogenesis of cardiac injury with SARS-CoV-2 infection requires additional investigations in fatal cases with evidence of cardiac injury.

No clinical or histopathologic features are specific to SARS-CoV-2 infection. Demonstrating SARS-CoV-2 directly in lung tissue, when taken in context with any other pathology present, is critical to assessing its contribution to mortality. Herein, we establish the utility of IHC as a diagnostic modality for SARS-CoV-2 in FFPE tissues by localizing viral antigens in respiratory tissues from RT-PCR confirmed cases. This diagnostic method is particularly valuable for FFPE specimens from cases in which antemortem or postmortem respiratory swab testing for SARS-CoV-2 was not performed. We also

demonstrate virus identification in tissues by EM using various tissue sources (formalin-fixed wet tissue, FFPE blocks, and stained slides). Identification of SARS-CoV-2 cellular tropisms in the respiratory tract represents a crucial step forward in understanding the pathogenesis of SARS-CoV-2 infection and provides some insights relevant to the development of targeted therapeutic and preventive measures to combat COVID-19.

Acknowledgments

We thank Mitesh Patel and Monica Peabody for accessioning the cases, Natalie Thornburg and Azaibi Tamin for providing SARS-CoV-2 Vero cells culture, and Dominique Rollin for the preparation of SARS-CoV-2 culture control blocks. We also thank Nicole Yarid and Micheline Lublin for specimen collection; Agam Rao; Kaitlyn Sykes and Jessica Ferro for facilitating data collection and coordination efforts; and staff from the King County Medical Examiner's Office for their commitment in the context of this pandemic disease.

About the Authors

Dr. Martines is a pathologist with the Division of High-Consequence Pathogens and Pathology, National Center for Emerging and Zoonotic Infectious Diseases, CDC, Atlanta, Georgia, USA. Her primary research interest is in the pathology and pathogenesis of emerging infectious diseases, with particular interest in viral hemorrhagic fevers. Dr. Ritter is a pathologist with the Division of High-Consequence Pathogens and Pathology, National Center for Emerging and Zoonotic Infectious Diseases, CDC, Atlanta. Her primary research interest is the development of animal models for zoonotic and human infectious diseases.

References

1. Zhu N, Zhang D, Wang W, Li X, Yang B, Song J, et al.; China Novel Coronavirus Investigating and Research Team. A novel coronavirus from patients with pneumonia in China, 2019. N Engl J Med. 2020;382:727–33. https://doi.org/10.1056/NEJMoa2001017
2. World Health Organization. Coronavirus disease (COVID-19) pandemic. 2020 May 4 [cited 2020 May 5]. https://www.who.int/emergencies/diseases/novel-coronavirus-2019
3. Holshue ML, DeBolt C, Lindquist S, Lofy KH, Wiesman J, Bruce H, et al.; Washington State 2019-nCoV Case Investigation Team. First case of 2019 novel coronavirus in the United States. N Engl J Med. 2020;382:929–36. https://doi.org/10.1056/NEJMoa2001191
4. Harcourt J, Tamin A, Lu X, Kamili S, Sakthivel SK, Murray J, et al. Severe acute respiratory syndrome coronavirus 2 from patient with 2019 novel coronavirus disease, United States. Emerg Infect Dis. 2020;26:26. https://doi.org/10.3201/eid2606.200516
5. Zhou P, Yang XL, Wang XG, Hu B, Zhang L, Zhang W, et al. A pneumonia outbreak associated with a new coronavirus of probable bat origin. Nature. 2020;579:270–3. https://doi.org/10.1038/s41586-020-2012-7
6. Andersen KG, Rambaut A, Lipkin WI, Holmes EC, Garry RF. The proximal origin of SARS-CoV-2. Nat Med. 2020;26:450–2. https://doi.org/10.1038/s41591-020-0820-9
7. Chen Y, Liu Q, Guo D. Emerging coronaviruses: genome structure, replication, and pathogenesis. J Med Virol. 2020;92:418–23. https://doi.org/10.1002/jmv.25681
8. Bialek S, Boundy E, Bowen V, Chow N, Cohn A, Dowling N, et al.; CDC COVID-19 Response Team. Severe outcomes among patients with coronavirus disease 2019 (COVID-19)—United States, February 12–March 16, 2020. MMWR Morb Mortal Wkly Rep. 2020;69:343–6. https://doi.org/10.15585/mmwr.mm6912e2
9. Wu Z, McGoogan JM. Characteristics of and important lessons from the coronavirus disease 2019 (COVID-19) outbreak in China: summary of a report of 72,314 cases from the Chinese Center for Disease Control and Prevention. JAMA. 2020;323:1239–42. https://doi.org/10.1001/jama.2020.2648
10. Xu Z, Shi L, Wang Y, Zhang J, Huang L, Zhang C, et al. Pathological findings of COVID-19 associated with acute respiratory distress syndrome. Lancet Respir Med. 2020;8:420–2. https://doi.org/10.1016/S2213-2600(20)30076-X
11. Tian S, Hu W, Niu L, Liu H, Xu H, Xiao SY. Pulmonary pathology of early-phase 2019 novel coronavirus (COVID-19) pneumonia in two patients with lung cancer. J Thorac Oncol. 2020;15:700–4. https://doi.org/10.1016/j.jtho.2020.02.010
12. Barton LM, Duval EJ, Stroberg E, Ghosh S, Mukhopadhyay S. COVID-19 autopsies, Oklahoma, USA. Am J Clin Pathol. 2020;153:725–33. https://doi.org/10.1093/ajcp/aqaa062
13. Menter T, Haslbauer JD, Nienhold R, Savic S, Hopfer H, Deigendesch N, et al. Post-mortem examination of COVID19 patients reveals diffuse alveolar damage with severe capillary congestion and variegated findings of lungs and other organs suggesting vascular dysfunction. Histopathology. 2020 May 4 [Epub ahead of print]. https://doi.org/10.1111/his.14134
14. Wichmann D, Sperhake JP, Lütgehetmann M, Steurer S, Edler C, Heinemann A, et al. Autopsy findings and venous thromboembolism in patients with COVID-19: a prospective cohort study. Ann Intern Med. 2020 May 6 [Epub ahead of print]. https://doi.org/10.7326/M20-2003
15. Ksiazek TG, Erdman D, Goldsmith CS, Zaki SR, Peret T, Emery S, et al.; SARS Working Group. A novel coronavirus associated with severe acute respiratory syndrome. N Engl J Med. 2003;348:1953–66. https://doi.org/10.1056/NEJMoa030781
16. Shieh WJ, Hsiao CH, Paddock CD, Guarner J, Goldsmith CS, Tatti K, et al. Immunohistochemical, in situ hybridization, and ultrastructural localization of SARS-associated coronavirus in lung of a fatal case of severe acute respiratory syndrome in Taiwan. Hum Pathol. 2005;36:303–9. https://doi.org/10.1016/j.humpath.2004.11.006
17. Gu J, Korteweg C. Pathology and pathogenesis of severe acute respiratory syndrome. Am J Pathol. 2007;170:1136–47. https://doi.org/10.2353/ajpath.2007.061088
18. Ng DL, Al Hosani F, Keating MK, Gerber SI, Jones TL, Metcalfe MG, et al. Clinicopathologic, immunohistochemical, and ultrastructural findings of a fatal case of Middle East respiratory syndrome coronavirus infection in the United Arab Emirates, April 2014. Am J Pathol. 2016;186:652–8. https://doi.org/10.1016/j.ajpath.2015.10.024

19. Tseng CT, Huang C, Newman P, Wang N, Narayanan K, Watts DM, et al. Severe acute respiratory syndrome coronavirus infection of mice transgenic for the human angiotensin-converting enzyme 2 virus receptor. J Virol. 2007;81:1162–73. https://doi.org/10.1128/JVI.01702-06
20. Goldsmith CS, Tatti KM, Ksiazek TG, Rollin PE, Comer JA, Lee WW, et al. Ultrastructural characterization of SARS coronavirus. Emerg Infect Dis. 2004;10:320–6. https://doi.org/10.3201/eid1002.030913
21. Shieh WJ, Blau DM, Denison AM, Deleon-Carnes M, Adem P, Bhatnagar J, et al. 2009 Pandemic influenza A (H1N1): pathology and pathogenesis of 100 fatal cases in the United States. Am J Pathol. 2010;177:166–75. https://doi.org/10.2353/ajpath.2010.100115
22. Trzciński K, Bogaert D, Wyllie A, Chu ML, van der Ende A, Bruin JP, et al. Superiority of trans-oral over trans-nasal sampling in detecting *Streptococcus pneumoniae* colonization in adults. PLoS One. 2013;8:e60520. https://doi.org/10.1371/journal.pone.0060520
23. McMichael TM, Clark S, Pogosjans S, Kay M, Lewis J, Baer A, et al.; Public Health—Seattle and King County, Evergreen-Health, and CDC COVID-19 Investigation Team. COVID-19 in a long-term care facility—King County, Washington, February 27–March 9, 2020. MMWR Morb Mortal Wkly Rep. 2020;69:339–42. https://doi.org/10.15585/mmwr.mm6912e1
24. Arentz M, Yim E, Klaff L, Lokhandwala S, Riedo FX, Chong M, et al. Characteristics and outcomes of 21 critically ill patients with COVID-19 in Washington state. JAMA. 2020;141:428.
25. Kimball A, Hatfield KM, Arons M, James A, Taylor J, Spicer K, et al.; Public Health—Seattle and King County; CDC COVID-19 Investigation Team. Asymptomatic and presymptomatic SARS-CoV-2 infections in residents of a long-term care skilled nursing facility—King County, Washington, March 2020. MMWR Morb Mortal Wkly Rep. 2020;69:377–81. https://doi.org/10.15585/mmwr.mm6913e1
26. Arons MM, Hatfield KM, Reddy SC, Kimball A, James A, Jacobs JR, et al. Presymptomatic SARS-CoV-2 infections and transmission in a skilled nursing facility. N Engl J Med. 2020 Apr 24 [Epub ahead of print]. https://doi.org/10.1056/NEJMoa2008457
27. Luo Y, Trevathan E, Qian Z, Li Y, Li J, Xiao W, et al. Asymptomatic SARS-CoV-2 infection in household contacts of a healthcare provider, Wuhan, China. Emerg Infect Dis. 2020 Apr 24 [Epub ahead of print]. https://doi.org/10.3201/eid2608.201016
28. Guan WJ, Ni ZY, Hu Y, Liang WH, Ou CQ, He JX, et al.; China Medical Treatment Expert Group for Covid-19. Clinical characteristics of coronavirus disease 2019 in China. N Engl J Med. 2020;382:1708–20. https://doi.org/10.1056/NEJMoa2002032
29. Zhang C, Shi L, Wang FS. Liver injury in COVID-19: management and challenges. Lancet Gastroenterol Hepatol. 2020;5:428–30. https://doi.org/10.1016/S2468-1253(20)30057-1
30. Zhou F, Yu T, Du R, Fan G, Liu Y, Liu Z, et al. Clinical course and risk factors for mortality of adult inpatients with COVID-19 in Wuhan, China: a retrospective cohort study. Lancet. 2020;395:1054–62. https://doi.org/10.1016/S0140-6736(20)30566-3
31. Zou L, Ruan F, Huang M, Liang L, Huang H, Hong Z, et al. SARS-CoV-2 viral load in upper respiratory specimens of infected patients. N Engl J Med. 2020;382:1177–9. https://doi.org/10.1056/NEJMc2001737
32. Franks TJ, Chong PY, Chui P, Galvin JR, Lourens RM, Reid AH, et al. Lung pathology of severe acute respiratory syndrome (SARS): a study of 8 autopsy cases from Singapore. [Erratum in: Hum Pathol. 2004;35:138.] Hum Pathol. 2003;34:743–8. https://doi.org/10.1016/S0046-8177(03)00367-8
33. Zaki SR, Paddock CD. Viral infections of the lung. In: Tomashefski JF, Cagle PT, Farver CF, Fraire AE, editors. Dail and Hammar's pulmonary pathology. New York: Springer; 2008. p. 426–75.
34. Huang C, Wang Y, Li X, Ren L, Zhao J, Hu Y, et al. Clinical features of patients infected with 2019 novel coronavirus in Wuhan, China. Lancet. 2020;395:497–506. https://doi.org/10.1016/S0140-6736(20)30183-5
35. Wrapp D, Wang N, Corbett KS, Goldsmith JA, Hsieh C-L, Abiona O, et al. Cryo-EM structure of 2019-nCoV-2 spike in the prefusion conformation. Science. 2020;367:1260–3. https://doi.org/10.1126/science.abb2507
36. Xu H, Zhong L, Deng J, Peng J, Dan H, Zeng X, et al. High expression of ACE2 receptor of 2019-nCoV on the epithelial cells of oral mucosa. Int J Oral Sci. 2020;12:8. https://doi.org/10.1038/s41368-020-0074-x
37. Wang Y, Wang Y, Chen Y, Qin Q. Unique epidemiological and clinical features of the emerging 2019 novel coronavirus pneumonia (COVID-19) implicate special control measures. J Med Virol. 2020;92:568–76. https://doi.org/10.1002/jmv.25748
38. Zheng YY, Ma YT, Zhang JY, Xie X. COVID-19 and the cardiovascular system. Nat Rev Cardiol. 2020;17:259–60. https://doi.org/10.1038/s41569-020-0360-5
39. Terpos E, Ntanasis-Stathopoulos I, Elalamy I, Kastritis E, Sergentanis TN, Politou M, et al. Hematological findings and complications of COVID-19. Am J Hematol. 2020; Apr 13 [Epub ahead of print]. https://doi.org/10.1002/ajh.25829
40. Tan CW, Low JGH, Wong WH, Chua YY, Goh SL, Ng HJ. Critically ill COVID-19 infected patients exhibit increased clot waveform analysis parameters consistent with hypercoagulability. Am J Hematol. 2020 Apr 8 [Epub ahead of print]. https://doi.org/10.1002/ajh.25822
41. Wang W, Xu Y, Gao R, Lu R, Han K, Wu G, et al. Detection of SARS-CoV-2 in different types of clinical specimens. JAMA. 2020 Mar 11 [Epub ahead of print]. http://dx.doi.org/10.1001/jama.2020.3786
42. Xiao F, Tang M, Zheng X, Liu Y, Li X, Shan H. Evidence for gastrointestinal infection of SARS-CoV-2. Gastroenterology. 2020 Mar 3 [Epub ahead of print]. https://doi.org/10.1053/j.gastro.2020.02.055
43. Bhatraju PK, Ghassemieh BJ, Nichols M, Kim R, Jerome KR, Nalla AK, et al. Covid-19 in critically ill patients in the Seattle region—case series. N Engl J Med. 2020 Mar 30 [Epub ahead of print]. https://doi.org/10.1056/NEJMoa2004500
44. Zumla A, Hui DS, Perlman S. Middle East respiratory syndrome. Lancet. 2015;386:995–1007. https://doi.org/10.1016/S0140-6736(15)60454-8
45. Yang X, Yu Y, Xu J, Shu H, Xia J, Liu H, et al. Clinical course and outcomes of critically ill patients with SARS-CoV-2 pneumonia in Wuhan, China: a single-centered, retrospective, observational study. Lancet Respir Med. 2020;8:475–81. https://doi.org/10.1016/S2213-2600(20)30079-5

Address for correspondence: Roosecelis Brasil Martines, Centers for Disease Control and Prevention, 1600 Clifton Rd NE, Mailstop H18-SB, Atlanta, GA 30329-4027, USA; email: Roosecelis.BrasilMartines@cdc.hhs.gov

Encephalopathy and Encephalitis Associated with Cerebrospinal Fluid Cytokine Alterations and Coronavirus Disease, Atlanta, Georgia, USA, 2020

Karima Benameur,[1] Ankita Agarwal,[1] Sara C. Auld, Matthew P. Butters, Andrew S. Webster, Tugba Ozturk, J. Christina Howell, Leda C. Bassit, Alvaro Velasquez, Raymond F. Schinazi, Mark E. Mullins, William T. Hu

There are few detailed investigations of neurologic complications in severe acute respiratory syndrome coronavirus 2 infection. We describe 3 patients with laboratory-confirmed coronavirus disease who had encephalopathy and encephalitis develop. Neuroimaging showed nonenhancing unilateral, bilateral, and midline changes not readily attributable to vascular causes. All 3 patients had increased cerebrospinal fluid (CSF) levels of anti-S1 IgM. One patient who died also had increased levels of anti-envelope protein IgM. CSF analysis also showed markedly increased levels of interleukin (IL)-6, IL-8, and IL-10, but severe acute respiratory syndrome coronavirus 2 was not identified in any CSF sample. These changes provide evidence of CSF periinfectious/postinfectious inflammatory changes during coronavirus disease with neurologic complications.

The pandemic caused by severe acute respiratory syndrome coronavirus 2 (SARS-CoV-2) has led to >1.5 million infections in the United States (30% of global cases) and >90,000 deaths as of May 20, 2020 (*1*). Coronavirus disease (COVID-19, the clinical syndrome associated with SARS-Cov-2) is most commonly characterized by respiratory illness and viral pneumonia with fever, cough, and shortness of breath, and progression to acute respiratory distress syndrome in severe cases (*2*).

Although neurologic complications have been noted in previous human coronavirus infections (*3*–*5*), there are few in-depth investigations for neurologic syndromes associated with SARS-CoV-2 infection (*6*). This deficiency can result from the need to reduce unnecessary staff exposure and difficulties in establishing preillness neurologic status without regular family visitors. It is known that neurons and glia express the putative SARS-CoV-2 receptor angiotensin converting enzyme 2 (*7*), and that the related coronavirus SARS-CoV (responsible for the 2003 SARS outbreak) can inoculate the mouse olfactory bulb (*8*). If SARS-CoV-2 can enter the central nervous system (CNS) directly or through hematogenous spread, cerebrospinal fluid (CSF) changes, including viral RNA, IgM, or cytokine levels, might support CNS infection as a cause for neurologic symptoms. We report clinical, blood, neuroimaging, and CSF findings for 3 patients with laboratory-confirmed COVID-19 and a range of neurologic outcomes (neuro-COVID). We also show the presence of SARS-CoV-2 antibodies in the blood and CSF of these patients, consistent with CNS penetration of disease.

Methods

We describe the clinical, laboratory and radiologic findings for 3 patients with respiratory failure and neurologic complications caused by COVID-19. This case series was reviewed and exempted from Emory Institutional Review Board approval. Medical records were reviewed by 4 of the coauthors (K.B., A.A., M.E.M., and W.T.H.).

CSF Serologic Analysis, Cytokines, and Molecular Testing

We assessed CSF IgM by using an in-house ELISA against SARS-CoV-2 S1 or envelope (E) protein. This ELISA was modified from an in-house blood-based

Author affiliation: Emory University School of Medicine, Atlanta, Georgia, USA

DOI: https://doi.org/10.3201/eid2609.202122

[1]These authors contributed equally to this article.

ELISA with 90% sensitivity and 89% specificity for confirmed COVID-19 against 78 pre-2020 controls. CSF was serially diluted from 1:2 to 1:16, and CSF from 1 case-patient who had HIV infection (hospitalized during March 2020) and from 3 pre-2020 healthy subjects (*9*) were included for comparison. We measured levels of plasma IgG against the receptor-binding domain of S1 by using a commercial ELISA (GenScript, https://www.genscript.com) at a 1:16 dilution.

We analyzed CSF inflammatory proteins (MilliporeSigma, https://www.emdmillipore.com) by using a Luminex-200 platform and a modified manufacturer's protocol as described (*9*). These proteins include interleukin (IL)-1α, IL-1β, IL-2, IL-4, IL-6, IL-7, IL-8, IL-9, IL-10, IL12-p40, IL12-p70, interferon-gamma–induced protein 10 (IP-10), monocyte chemoattractant protein 1 (MCP-1/CCL2), macrophage-derived chemokine (MDC/CCL22), fractalkine (CX3CL1), and tumor necrosis factor α (TNF-α).

We performed molecular testing for SARS-CoV-2 by using real-time quantitative reverse transcription PCR (qRT-PCR). We extracted total nucleic acid from 120 μL of CSF from each person by using the EZ1 Virus Mini Kit version 2.0 and the EZ1 Advanced XL Instrument (QIAGEN, https://www.qiagen.com) after lysis with AVL lysis buffer (QIAGEN). We performed a 1-step qRT-PCR by using 2019-nCoV_N1 or 2019-nCoV_N2 combined Primer/Probe Mix (Integrated DNA Technologies, Inc., https://www.idtdna.com) in a Roche LightCycler 480 II (https://lifescience.roche.com), an endogenous control, and an in vitro transcribed full-length RNA of known titer (Integrated DNA Technologies, Inc.) as a positive control. We followed the same procedure for influenza A virus except using a primer/probe mixture (*10*) and a mitochondrial cytochrome oxidase subunit 2 DNA endogenous control (*11*). We tested all samples in duplicate.

Results

Clinical, Radiologic, and Laboratory Assessment

Patient 1, a 31-year-old African-American woman who had sickle cell disease (SCD) and was receiving dabigatran for a recent pulmonary embolus, came to a community hospital after 5 days of progressive dyspnea. An initial chest radiograph showed a right lower lobe infiltrate, and she was given a blood transfusion and antimicrobial drugs for presumed SCD crisis and pneumonia. Her breathing became more labored, and a repeat chest radiograph showed worsening bilateral infiltrates. A nasopharyngeal swab specimen was positive for SARS-CoV-2 and influenza A virus (negative for influenza B virus). She was empirically given hydroxychloroquine (400 mg daily) and peramivir (100 mg daily), but acute kidney injury and progressive hypoxemic respiratory failure developed. She was intubated and transferred to our institution on day 11. Her paralysis and sedation were discontinued on day 13 after improved oxygenation, but she remained comatose with absent brainstem reflexes on day 15.

Brain magnetic resonance imaging (MRI) showed nonenhancing cerebral edema and diffusion weighted imaging abnormalities predominantly involving the right cerebral hemisphere, as well as brain herniation (Figure 1). An occlusive thrombus was identified in the right internal carotid artery, and edema was also identified in the cervical spinal cord. The overall appearance was most consistent with encephalitis and myelitis, with superimposed hypoxic ischemic changes. CSF showed high opening pressure of 30 cm of water, 115 nucleated cells/mL, 7,374 erythrocytes/mL, an increased protein level (>200 mg/dL), and a glucose level within a standard range (Table). Her nucleated cell count remained strongly increased even after correction for the traumatic tap (≈1 nucleated cell/700 erythrocytes). Given a grave prognosis, the family withdrew life-sustaining care and the patient died on day 16.

Patient 2, a 34-year-old African-American man who had hypertension, showed development of fever, shortness of breath, and cough. Computed tomography of the chest showed bilateral, diffuse ground glass infiltrates. A nasopharyngeal swab specimen obtained on day 1 showed SARS-CoV-2. He was given a 6-day course of hydroxychloroquine, but hypoxic respiratory failure developed, which required intubation, followed by encephalopathy with myoclonus on day 9. His neurologic examination showed profound encephalopathy, absent corneal and gag reflexes, multifocal myoclonus involving both arms, and absent withdrawal to painful stimuli. Electroencephalography showed diffuse slowing with a suggestion that the myoclonus was seizure-related. Brain MRI on day 15 showed a nonenhancing hyperintense lesion within the splenium of the corpus callosum on fluid-attenuated inversion recovery and diffusion weighted imaging sequences (Figure 1). CSF showed high opening pressure of 48 cm H_2O, no pleocytosis, 27 erythrocytes/mL, a mildly increased protein level, and glucose level within the reference range.

Patient 3, a 64-year-old African-American man who had hypertension, showed development of cough, dyspnea, and fever with multifocal, patchy, ground glass opacities on chest computed tomography and a nasopharyngeal swab specimen positive for SARS-CoV-2. His symptoms progressed to hypoxic respiratory failure requiring intubation, and his multifocal

myoclonus began soon after starting to take hydroxychloroquine. His neurologic examination showed profound encephalopathy, absent oculocephalic reflex, multifocal myoclonus affecting bilateral arms and legs, absent withdrawal to pain, and diminished deep tendon reflexes. The resolution of his myoclonus coincided with fentanyl cessation, but it is not clear that the 2 symptoms were related. A motion-degraded brain MRI showed an equivocal nonenhancing area of fluid-attenuated inversion recovery abnormality in the right temporal lobe. CSF obtained on hospital day 11 showed a normal opening pressure; levels of nucleated cells, erythrocytes, and protein within reference ranges; and an increased glucose level (Table). His mentation began to improve on day 13, and he was subsequently discharged without major neurologic sequelae.

Serologic Analysis of Plasma and CSF

Plasma anti-S1 receptor-binding domain IgG levels were increased for all 3 patients, consistent with severe COVID-19 (T. Ozturk et al., unpub. data). An indirect ELISA for plasma showed an increased level of anti-S1 IgM for patients 1 (1:512) and 2 (1:256), a highly increased level of anti-S1 IgM for patient 3 (1:2,048); an increased level of anti-E IgM for patients 1 and 2 (1:128), and a standard level of anti-E IgM for patient 3.

An indirect ELISA for CSF showed markedly increased levels of IgM for SARS-CoV-2 S1 (Figure 2, panel A) and E (Figure 2, panel B) proteins for the most severely ill patient 1, and mildly elevated levels of IgM for S1 only for patients 2 and 3. The number of CSF erythrocytes in patient 1 suggested plasma contamination at an approximate dilution of 1:1,000, which still

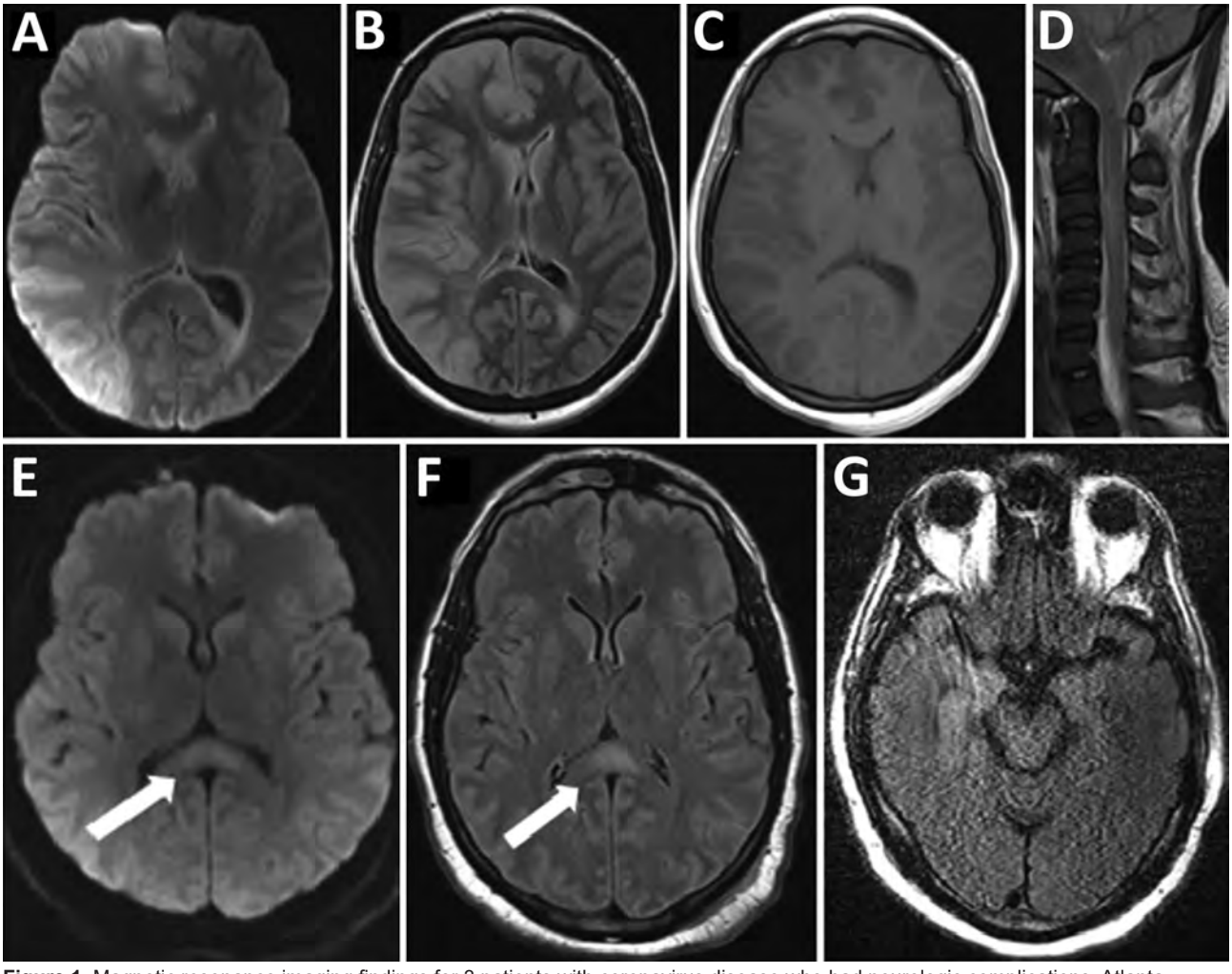

Figure 1. Magnetic resonance imaging findings for 3 patients with coronavirus disease who had neurologic complications, Atlanta, Georgia, USA, 2020. A–D) Patient 1 had right cerebral hemispheric restricted diffusion (diffusion weighted imaging in panel A) and cerebral edema (fluid-attenuated inversion recovery [FLAIR] in panel B) affecting gray matter and deep gray nuclei, without enhancement (panel C), and spinal edema (panel D). E, F) Patient 2 had a splenium lesion (diffusion weighted imaging in panel E and FLAIR recovery in panel F that was nonenhancing). Arrows indicate lesions in the splenium. G) Patient 3 had an equivocal fluid-attenuated inversion recovery FLAIR abnormality in the right temporal lobe.

Table. Characteristics of 3 patients with coronavirus disease and neurologic complications, Atlanta, Georgia, USA, 2020*

Characteristic	Patient 1	Patient 2	Patient 3
Neurologic findings			
Encephalopathy	Coma	Moderate	Mild
Brainstem reflexes affected	All	Corneal gag	Oculocephalic
Myoclonus	None	Arms	All limbs
Withdrawal to pain	Absent	Absent	Absent
CSF findings, reference value			
Appearance, clear	Cloudy	Clear	Clear
Opening pressure, 10–20 cm H_2O	30	48	12
Nucleated cells			
Total, 0–5/μL	115	1	0
% Neutrophils, 0%–6%	51	75	0
% Lymphocytes, 40%–80%	10	25	0
% Macrophages 15%–45%	39	0	0
Erythrocytes, 0/μL	3,426	29	7
Glucose, 40–70, mg/dL	40	111	88
Protein, 15–45, mg/dL	>200	37	21

*CSF, cerebrospinal fluid.

placed these CSF IgM levels higher than those for patients 2 and 3.

Inflammatory Protein Analysis for CSF

CSF from patients 1 and 3 underwent detailed inflammatory protein profiling as described (*9*,*12*,*13*). When we compared historical and present control subjects who had normal cognition (no viral illness) (*13*), we found that patients with COVID-19 and neurologic symptoms had increased CSF levels of IL-6, IL-8, IL-10, IP-10, and TNF-α (Figure 2, panel C). Levels of IL-8, IL-10, IP-10, and TNF-α were also available for subjects who had HIV-associated neurocognitive disorders (*12*). Increased levels of IL-8 and IL-10 appeared to be unique for neurologic complications of SARS-CoV-2, and increased levels of IP-10 and TNF-α were common features between neurologic complications of SARS-CoV-2 and HIV.

Viral Analysis of CSF

We used a real-time RT-PCR to test for SARS-CoV-2 and influenza A virus (tested because patient 1 showed a co-infection). Results were negative for all patients.

Discussion

We report 3 patients who had severe COVID-19 and showed development of various neurologic symptoms and findings in a US hospital. All patients had more severe symptoms affecting cortical and brainstem functions at the peak of their neurologic illnesses than a recent series of 7 case-patients with milder illness in France (*6*). All 3 patients were also co-incidentally given a short course of empiric hydroxychloroquine, although there was no temporal correlation between the medication and their neurologic manifestation. Similar to the case-series in France, we did not isolate SARS-CoV-2 RNA from CSF, although such viral RNA has been inconsistently identified in other cases (*14*). However, increased levels of CSF anti-S1 IgM and altered levels of CSF cytokines are consistent with direct CNS involvement by SARS-CoV-2. Because MRI changes seen in these patients could be caused by hypercoagulability (*15*) or metabolic encephalopathy (*16*), we propose that CSF investigation can improve the distinction between neurologic involvement of SARS-CoV-2 (or neuro-COVID) and neurologic symptoms caused by other COVID-related causes.

In health and many noninflammatory neurologic disorders, the intact blood–brain barrier prevents major central translocation by plasma immunoglobulins or cells that secrete them (*17*). Increased levels of CSF antibodies can thus result from disrupted blood–brain barrier, regulated migration of peripheral antibody-secreting cells into the CNS, or de novo antibody synthesis within the CNS. The relatively normal protein levels in patients 2 and 3 would argue against an unequivocal blood–brain barrier disruption. The lack of clear correlation between plasma and CSF titers provides some support for an active CNS process. The failure to detect CSF SARS-CoV-2 RNA does not diminish the likelihood of direct CNS infection because it is only recovered from blood in 1% of the actively infected cases (*18*), and increased levels CSF IgM are also more commonly found as evidence for CNS infection than viral recovery in other encephalitides, including those for infection with Japanese encephalitis virus (*19*), dengue virus (*20*), human parvovirus 4 (*21*), and rabies virus (*22*). At the same time, undetectable CSF RNA raises the possibility that mechanisms other than direct brain infection might account for the observed MRI and clinical changes. These changes include peri-infectious inflammation (mediated by antibodies, complement, or both) (*5*,*23*), vasculopathy,

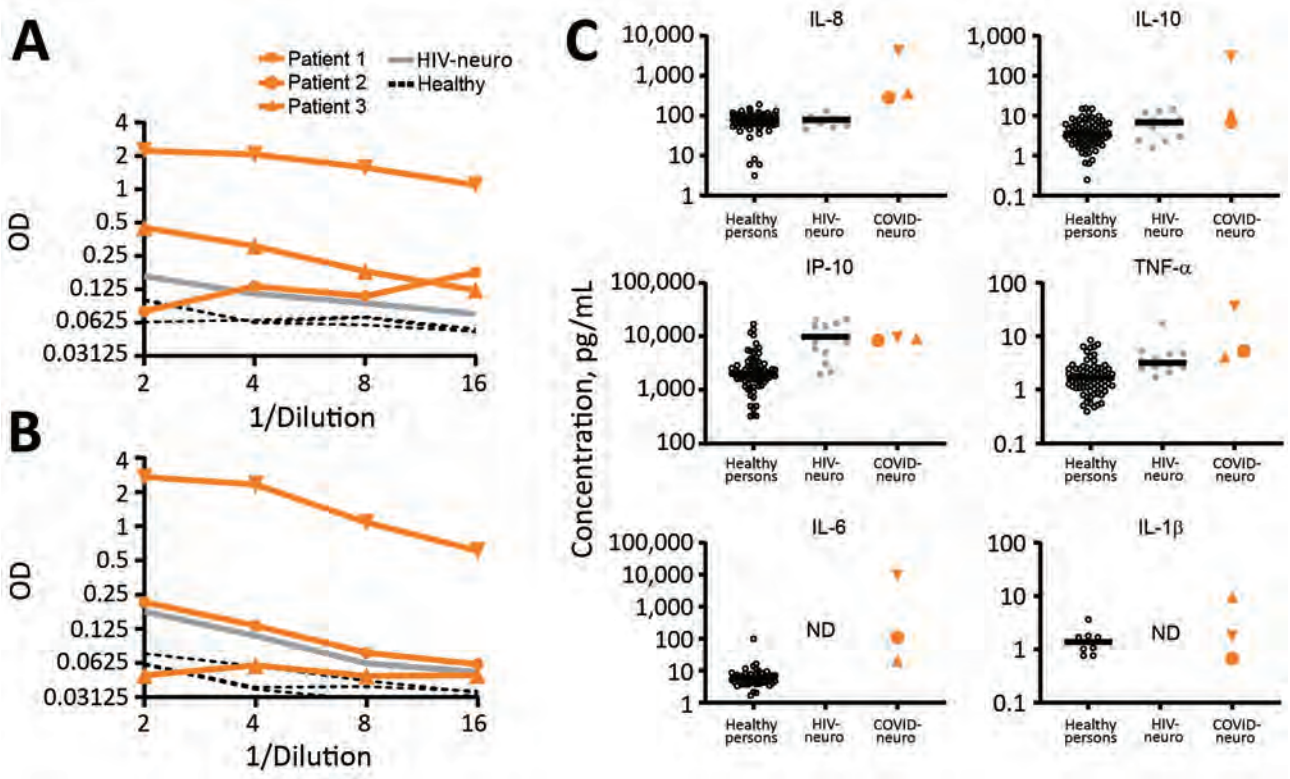

Figure 2. Cerebrospinal fluid (A and B) and inflammatory protein (C) analyses for patients with coronavirus disease and neurologic complications, Atlanta, Georgia, USA, 2020. Compared with healthy controls and patients who had HIV-associated neurocognitive disorder, CSF levels of anti-S1 IgM were high in patient 1, and moderately high in patients 2 and 3. In contrast, levels of CSF anti-E IgM were high only for patient 1 and within references ranges for patients 2 and 3. CSF inflammatory analysis showed increased levels of IL-8 and IL-10 more unique to neuro-COVID, and increased levels of IP-10 and TNF-α in neuro-COVID and HIV-neuro. Circles indicate patients whose interleukin levels were tested and used as controls (healthy, HIV). Horizontal bars indicate average values. COVID-neuro, coronavirus disease–associated neurologic complications; HIV-neuro, HIV-associated neurocognitive disorder; IL, interleukin; IP, interferon-γ–induced protein; OD, optical density, ND, not determined; neuro-COVID, neurologic complications associated with coronavirus disease; TNF, tumor necrosis factor.

and altered neurotransmission. Until definitive neuropathologic studies or effective antiviral therapies are possible, infectious and peri-infectious etiologies need to be examined for neuro-COVID.

Increased levels of CSF multiple cytokines in these neuro-COVID patients are consistent with earlier reports of cytokine analysis of blood (*24*; M. Woodruff et al., unpub. data). We additionally identified changes shared (and not shared) by SARS-CoV-2 and HIV. Factors associated with increased levels of CSF IL-10 in patients infected with HIV should be investigated in future neuro-COVID studies, and increased levels of CSF IL-8 might uniquely provide useful information on the pathophysiology of CNS. We did not include plasma cytokine levels because their levels are much more influenced by demographic factors than their CSF counterparts (W.T. Hu et al., unpub. data). A larger cohort is necessary to better distinguish between CSF and plasma cytokine alterations, and including patients without confounding disease (e.g., SCD in patient 1) or standard MRI results can also determine the relative roles of noninfectious/inflammatory causes of encephalopathy, including hypoxia or hypercoagulability (*25*,*26*). Nevertheless, we demonstrated in these case-patients that SARS-CoV-2 antibodies are detectable in the CSF for patients with neurologic complications and are associated with selective CSF cytokine alterations. Future investigations should align neurologic outcomes with CSF infectious and immunologic profiles, such that an evidence-based treatment algorithm can be determined for preventing and treating neuro-COVID-19.

R.F.S. is supported in part by the Emory Center for AIDS Research (National Institutes of Health [NIH] grant P30AI050409 and NIH grant R01MH116695); W.T.H. is supported by NIH grants R01AG054046, R01AG054991, and R01AG066203; and S.C.A. is supported in part by NIH/National Institute of Allergy and Infectious Diseases grant K23 AI34182.

About the Author

Dr. Benameur is an neurologist and associate professor in the Department of Neurology at Emory University School of Medicine, Atlanta, GA. Her primary research interest is in neuroinflammatory changes related to COVID-19

References

1. An P, Song P, Wang Y, Liu B. Asymptomatic patients with novel coronavirus disease (COVID-19). Balkan Med J. 2020; Jun 1 [Epub ahead of print]. https://doi.org/10.4274/balkanmedj.galenos.2020.2020.4.20
2. Chen T, Wu D, Chen H, Yan W, Yang D, Chen G, et al. Clinical characteristics of 113 deceased patients with coronavirus disease 2019: retrospective study. BMJ. 2020; 368:m1091. https://doi.org/10.1136/bmj.m1091
3. Lau KK, Yu WC, Chu CM, Lau ST, Sheng B, Yuen KY. Possible central nervous system infection by SARS coronavirus. Emerg Infect Dis. 2004;10:342–4. https://doi.org/10.3201/eid1002.030638
4. Arabi YM, Harthi A, Hussein J, Bouchama A, Johani S, Hajeer AH, et al. Severe neurologic syndrome associated with Middle East respiratory syndrome corona virus (MERS-CoV). Infection. 2015;43:495–501. https://doi.org/10.1007/s15010-015-0720-y
5. Wu Y, Xu X, Chen Z, Duan J, Hashimoto K, Yang L, et al. Nervous system involvement after infection with COVID-19 and other coronaviruses. Brain Behav Immun. 2020;Mar 30 [Epub ahead of print]. https://doi.org/10.1016/j.bbi.2020.03.031
6. Helms J, Kremer S, Merdji H, Clere-Jehl R, Schenck M, Kummerlen C, et al. Neurologic features in severe SARS-CoV-2 infection. N Engl J Med. N Engl J Med. 2020;Apr 15 [Epub ahead of print]. https://doi.org/10.1056/NEJMc2008597
7. Baig AM, Khaleeq A, Ali U, Syeda H. Evidence of the COVID-19 virus targeting the CNS: tissue distribution, host-virus interaction, and proposed neurotropic mechanisms. ACS Chem Neurosci. 2020;11:995–8. https://doi.org/ 10.1021/acschemneuro.0c00122
8. Netland J, Meyerholz DK, Moore S, Cassell M, Perlman S. Severe acute respiratory syndrome coronavirus infection causes neuronal death in the absence of encephalitis in mice transgenic for human ACE2. J Virol. 2008;82:7264–75. https://doi.org/10.1128/JVI.00737-08
9. Wharton W, Kollhoff AL, Gangishetti U, Verble DD, Upadhya S, Zetterberg H, et al. Interleukin 9 alterations linked to Alzheimer disease in African Americans. Ann Neurol. 2019;86:407–18. https://doi.org/10.1002/ana.25543
10. Puig-Barberà J, Natividad-Sancho A, Trushakova S, Sominina A, Pisareva M, Ciblak MA, et al.; Global Influenza Hospital Surveillance Study Group (GIHSN). Epidemiology of hospital admissions with influenza during the 2013/2014 Northern Hemisphere influenza season: results from the Global Influenza Hospital Surveillance Network. PLoS One. 2016;11:e0154970. https://doi.org/10.1371/journal.pone.0154970
11. Stuyver LJ, Lostia S, Adams M, Mathew JS, Pai BS, Grier J, et al. Antiviral activities and cellular toxicities of modified 2′,3′-dideoxy-2′,3′-didehydrocytidine analogues. Antimicrob Agents Chemother. 2002;46:3854–60. https://doi.org/10.1128/AAC.46.12.3854-3860.2002
12. Ozturk T, Kollhoff A, Anderson AM, Christina Howell J, Loring DW, Waldrop-Valverde D, et al. Linked CSF reduction of phosphorylated tau and IL-8 in HIV associated neurocognitive disorder. Sci Rep. 2019;9:8733. https://doi.org/10.1038/s41598-019-45418-2
13. Hu WT, Howell JC, Ozturk T, Gangishetti U, Kollhoff AL, Hatcher-Martin JM, et al. CSF cytokines in aging, multiple sclerosis, and dementia. Front Immunol. 2019;10:480. https://doi.org/10.3389/fimmu.2019.00480
14. Moriguchi T, Harii N, Goto J, Harada D, Sugawara H, Takamino J, et al. A first case of meningitis/encephalitis associated with SARS-coronavirus-2. Int J Infect Dis. 2020;94:55–8. https://doi.org/10.1016/j.ijid.2020.03.062
15. Terpos E, Ntanasis-Stathopoulos I, Elalamy I, Kastritis E, Sergentanis TN, Politou M, et al. Hematological findings and complications of COVID-19. Am J Hematol. 2020 Apr 15 [Epub ahead of print]. https://doi.org/10.1002/ajh.25829
16. Sharma P, Eesa M, Scott JN. Toxic and acquired metabolic encephalopathies: MRI appearance. AJR Am J Roentgenol. 2009;193:879–86. https://doi.org/10.2214/AJR.08.2257
17. Iwasaki A. Immune regulation of antibody access to neuronal tissues. Trends Mol Med. 2017;23:227–45. https://doi.org/10.1016/j.molmed.2017.01.004
18. Wang W, Xu Y, Gao R, Lu R, Han K, Wu G, et al. Detection of SARS-CoV-2 in different types of clinical specimens. JAMA. 2020 Mar 11 [Epub ahead of print]. https://doi.org/10.1001/jama.2020.3786
19. Dubot-Pérès A, Sengvilaipaseuth O, Chanthongthip A, Newton PN, de Lamballerie X. How many patients with anti-JEV IgM in cerebrospinal fluid really have Japanese encephalitis? Lancet Infect Dis. 2015;15:1376–7. https://doi.org/10.1016/S1473-3099(15)00405-3
20. Bastos MS, Martins VDCA, Silva NLD, Jezine S, Pinto S, Aprigio V, et al. Importance of cerebrospinal fluid investigation during dengue infection in Brazilian Amazonia region. Mem Inst Oswaldo Cruz. 2018;114:e180450. https://doi.org/10.1590/0074-02760180450
21. Arankalle VA, Srivastava N, Kushwaha KP, Sen A, Ramdasi AY, Patel PA, et al. Detection of human parvovirus 4 DNA in the patients with acute encephalitis syndrome during seasonal outbreaks of the disease in Gorakhpur, India. Emerg Microbes Infect. 2019;8:130–8. https://doi.org/10.1080/22221751.2018.1563455
22. Hu WT, Willoughby RE Jr, Dhonau H, Mack KJ. Long-term follow-up after treatment of rabies by induction of coma. N Engl J Med. 2007;357:945–6. https://doi.org/10.1056/NEJMc062479
23. Desforges M, Le Coupanec A, Dubeau P, Bourgouin A, Lajoie L, Dubé M, et al. Human coronaviruses and other respiratory viruses: underestimated opportunistic pathogens of the central nervous system? Viruses. 2019;12:14. https://doi.org/10.3390/v12010014
24. Huang C, Wang Y, Li X, Ren L, Zhao J, Hu Y, et al. Clinical features of patients infected with 2019 novel coronavirus in Wuhan, China. Lancet. 2020;395:497–506. https://doi.org/10.1016/S0140-6736(20)30183-5
25. Yin S, Huang M, Li D, Tang N. Difference of coagulation features between severe pneumonia induced by SARS-CoV2 and non-SARS-CoV2. J Thromb Thrombolysis. 2020 Apr 3 [Epub ahead of print]. https://doi.org/10.1007/s11239-020-02105-8
26. Nur E, Gaartman AE, van Tuijn CFJ, Tang MW, Biemond BJ. Vaso-occlusive crisis and acute chest syndrome in sickle cell disease due to 2019 novel coronavirus disease (COVID-19). Am J Hematol. 2020;95:725–6. https://doi.org/10.1002/ajh.25821

Address for correspondence: Karima Benameur, Department of Neurology, Emory University School of Medicine, 550 Peachtree St, Davis Fischer Bldg, Rm 3343, Atlanta, GA 30306, USA; email: kbename@emory.edu

Invasive Infections with *Nannizziopsis obscura* Species Complex in 9 Patients from West Africa, France, 2004–2020[1]

Dea Garcia-Hermoso, Samia Hamane, Arnaud Fekkar, Arnaud Jabet, Blandine Denis, Martin Siguier, Guy Galeazzi, Elie Haddad, Sophie Brun, Valérie Vidal, Gilles Nevez, Rozenn Le Berre, Maud Gits-Muselli, Fanny Lanternier, Stéphane Bretagne

Medscape EDUCATION ACTIVITY

In support of improving patient care, this activity has been planned and implemented by Medscape, LLC and Emerging Infectious Diseases. Medscape, LLC is jointly accredited by the Accreditation Council for Continuing Medical Education (ACCME), the Accreditation Council for Pharmacy Education (ACPE), and the American Nurses Credentialing Center (ANCC), to provide continuing education for the healthcare team.

Medscape, LLC designates this Journal-based CME activity for a maximum of 1.00 ***AMA PRA Category 1 Credit(s)***™. Physicians should claim only the credit commensurate with the extent of their participation in the activity.

Successful completion of this CME activity, which includes participation in the evaluation component, enables the participant to earn up to 1.0 MOC points in the American Board of Internal Medicine's (ABIM) Maintenance of Certification (MOC) program. Participants will earn MOC points equivalent to the amount of CME credits claimed for the activity. It is the CME activity provider's responsibility to submit participant completion information to ACCME for the purpose of granting ABIM MOC credit.

All other clinicians completing this activity will be issued a certificate of participation. To participate in this journal CME activity: (1) review the learning objectives and author disclosures; (2) study the education content; (3) take the post-test with a 75% minimum passing score and complete the evaluation at http://www.medscape.org/journal/eid; and (4) view/print certificate. For CME questions, see page 2307.

Release date: August 14, 2020; Expiration date: August 14, 2021

Learning Objectives

Upon completion of this activity, participants will be able to:

- Assess the clinical features of invasive fungal infection with *N. obscura* species complex, based on a series of 9 new confirmed human cases from 2004 to 2020
- Evaluate the microbiological features of invasive fungal infection with *N. obscura* species complex, based on a series of 9 new confirmed human cases from 2004 to 2020
- Determine the clinical implications of features of invasive fungal infection with *N. obscura* species complex, based on a series of 9 new confirmed human cases from 2004 to 2020

CME Editor

Jude Rutledge, BA, Technical Writer/Editor, Emerging Infectious Diseases. *Disclosure: Jude Rutledge has disclosed no relevant financial relationships.*

CME Author

Laurie Barclay, MD, freelance writer and reviewer, Medscape, LLC. *Disclosure: Laurie Barclay, MD, has disclosed no relevant financial relationships.*

Authors

Disclosures: ***Dea Garcia-Hermoso, PhD; Samia Hamane, MD; Arnaud Jabet, MS; Blandine Denis, MD, PhD; Guy Galeazzi, MD; Elie Haddad, MD; Sophie Brun, MD, PhD; Valérie Vidal, MD; Gilles Nevez, MD, PhD; Rozenn Le Berre, MD, PhD; Maud Gits-Muselli, MD; Fanny Lanternier, MD, PhD;*** *and* ***Stéphane Bretagne, MD, PhD,*** *have disclosed no relevant financial relationships.* ***Arnaud Fekkar, PharmD, PhD,*** *has disclosed the following relevant financial relationships: served as a speaker or a member of a speakers bureau for Gilead; received grants for clinical research from Janssen.* ***Martin Siguier, MD,*** *has disclosed the following relevant financial relationships: served as an advisor or consultant for Viiv Healthcare; other (travel expenses reimbursement) from Gilead.*

Nine new human invasive infections caused by the keratinophilic fungi *Nannizziopsis obscura* have been reported in France since 2004. The patients had variable clinical manifestations, had frequent dissemination, were mainly T-cell immunocompromised, and all originated from sub-Saharan West Africa. Before collection of the isolates, the etiologies of these infections were often misidentified, underscoring the extent of microscopic and cultural polymorphisms. All isolates but 1 had low MICs for the 8 antifungal drugs tested. When treated, patients received mainly azole therapy. Two of 7 patients with a known outcome died. We performed multilocus sequence analysis of *N. obscura* clinical strains and several strains of *Nannizziopsis* spp. isolated from reptiles. The human strains were clearly differentiated from the animal strains. *N. obscura* might be endemic to West Africa and responsible for undetected infections, which might become reactivated when immunosuppression occurs. *N. obscura* infection is probably underestimated because only sequencing enables proper identification.

Nannizziopsis spp. are described as keratinophilic ascomycetous fungi that cause dermal infections with frequently fatal outcomes in various reptiles (e.g., lizards, geckos, chameleons, iguanas, snakes, and crocodiles), mainly in captivity (*1*,*2*). *Nannizziopsis* spp. belong to the order of *Onygenales* and the recently described family of *Nannizziopsidaceae* (*1*). In humans, invasive *Nannizziopsis* spp. infection seems rare; only 5 cases have been reported to date (*1*,*3*–*7*). Such an observation suggests an actual rarity, a recent emergence because of modification in the ecoepidemiology (e.g., new populations at risk [*8*]), or previous underdiagnoses or misdiagnoses because of a lack of definite identification.

We describe 9 human cases of invasive fungal infection with *N. obscura* species complex identified in France during 2004–2020 (Table 1, https://wwwnc.cdc.gov/EID/article/26/9/20-0276-T1.htm), along with the initial identification from the 5 reporting hospitals. Isolates were sent to France's National Reference Center for Invasive Mycoses and Antifungals, where a polyphasic identification combining phenotypic features and molecular data was performed. Seven of the 9 cases were diagnosed after 2016.

The Patients

Patient 1 was 49-year-old HIV-positive man from Mali who was hospitalized for a liver abscess discovered in August 2004 during a stay in Mali. He was afebrile but had advanced AIDS (zero CD4 cell/mm^3). A liver needle aspiration showed hyphae with arthroconidia. The first identified colonies were *Trichosporon* spp., based on a positive urease test and presence of arthroconidia. The patient was given liposomal amphotericin B and metronidazole. After 15 days, the patient returned to Mali for personal reasons; no follow-up was possible. At that time, the organism had been identified as *Chrysosporium* spp.

Patient 2 was a 50-year-old man who came from Mali to undergo heart transplantation in January 2009 after 9 months of hospitalization for cardiac insufficiency. After transplantation, the patient had cytomegalovirus reactivation and multivisceral failure. One month later, he had onset of bacterial mediastinitis. He was surgically treated and received wide-spectrum antibiotics but no antifungals. The immunosuppressive therapy consisted of prednisone (15 mg/d) and ciclosporine. A serum sample was negative for *Aspergillus* galactomannan. Two months later (just 2 days before the death of the patient), a blood culture was positive, and the isolate was identified as *Geotrichum* spp. or *Chrysosporium* spp.

Patient 3 was a 58-year-old woman with diabetes who was from Mali but had been living in France for 30 years. In 2017, she reported a 2-week history of asthenia and chest pain without fever. She had renal transplantation in 2016 and was receiving tacrolimus, mycophenolate, and prednisone (5 mg/d). A computed tomography (CT) scan revealed an irregular lung nodule (14 mm in diameter). She received amoxicillin/clavulanic acid. Three months later, she had an abscess of the left thigh and multiple nodular skin lesions on both legs. A new CT scan showed an enlargement of the pulmonary nodule. Direct examination of the skin

Author affiliations: Institut Pasteur, Paris, France (D. Garcia-Hermoso, F. Lanternier, S. Bretagne); Hôpitaux Lariboisière–Saint-Louis-Fernand Widal, Assistance Publique–Hôpitaux de Paris, Paris (S. Hamane, A. Jabet, B. Denis, M. Siguier, M. Gits-Muselli, S. Bretagne); Groupe Hospitalier Pitié–Salpêtrière, Assistance Publique–Hôpitaux de Paris, Sorbonne Université, Paris (A. Fekkar); Hôpital Max Fourestier, Nanterre, France (G. Galeazzi); Centre Hospitalier Universitaire Hôtel-Dieu de France, Université de Saint-Joseph, Beirut, Lebanon (E. Haddad); Hôpital Avicenne, Assistance Publique–Hôpitaux de Paris, Bobigny, France (S. Brun, V. Vidal); Hôpital La Cavale Blanche, Centre Hospitalier Universitaire de Brest, Brest, France (G. Nevez, R. Le Berre); Université Paris 13, Paris (S. Brun); Université de Paris, Paris (M. Gits-Muselli, F. Lanternier, S. Bretagne)

DOI: https://doi.org/10.3201/eid2609.200276

[1]Preliminary results of this study were presented at the International Society for Human and Animal Mycology, June 30–July 4, 2018, Amsterdam, the Netherlands (poster 174, Medical Mycology 56, Supplement 2).

and lung biopsies revealed septate and vesiculous hyphae, and the culture resembled *Trichophyton* spp., which was eventually confirmed as *N. obscura* upon sequencing. Serum β-D-glucan was strongly positive (>500 pg/mL, positivity threshold ≥80 pg/ml), and serum *Aspergillus* galactomannan antigen was repeatedly negative. A whole-body positron emission tomography (PET)–CT scan showed multiple clinically latent hypermetabolic lesions (in the nasal septum, left breast, and mediastinal nodes). Voriconazole was initiated, then switched to posaconazole after *N. obscura* identification. The dose of tacrolimus was reduced, and mycophenolate mofetil was replaced by azathioprine. At 6 months, a new PET-CT scan showed a residual hypermetabolic pulmonary lesion. Posaconazole was stopped after 8 months. No relapse had occurred as of 1 year later.

Patient 4 was a 62-year-old man from Guinea who had been living in France for 12 years (recent trip to Guinea occurred ≈1 year before). He was hospitalized in July 2017 for several suppurated lesions on the right fibula (Figure 1, panel A) that were unresponsive to amoxicillin/clavulanic acid treatment. He had undergone renal transplantation in 2009 for hypertensive nephropathy and received mycophenolate mofetil, tacrolimus, and prednisone (5 mg/d). A CT scan confirmed tissue infiltration with small abscesses but showed no sign of bone involvement. Large-scale debridement was performed, and direct examination of infected tissues showed regular septate hyphae and arthroconidia (Figure 1, panel B). Yeast-like fungi appeared on Sabouraud–chloramphenicol–gentamycin slants. Microscopic examination showed arthroconidia, and the urease test was positive, suggesting the presence of *Trichosporon* spp. A whole-body PET-CT scan revealed asymptomatic hypermetabolic lesions in the contralateral leg and lung micronodules. Voriconazole was started when trichosporonosis was suspected and switched to posaconazole with the identification of *N. obscura*. Serum β-D-glucan was strongly positive (>500 pg/mL), whereas *Aspergillus* galactomannan antigen detection was negative. At 6 months, a PET-CT scan showed residual hypermetabolism around the right ankle. Onychomycosis of the right toe was noted, and a specimen was taken. Direct examination showed hyphae, but the culture was negative. Posaconazole was maintained for 2 years, with tacrolimus and prednisone (5 mg/d). A new PET-CT scan showed no hypermetabolic lesion.

Patient 5 was a 69-year-old woman from Guinea-Bissau who had been living in France for 10 years (her most recent trip to Guinea-Bissau occurred in 2016).

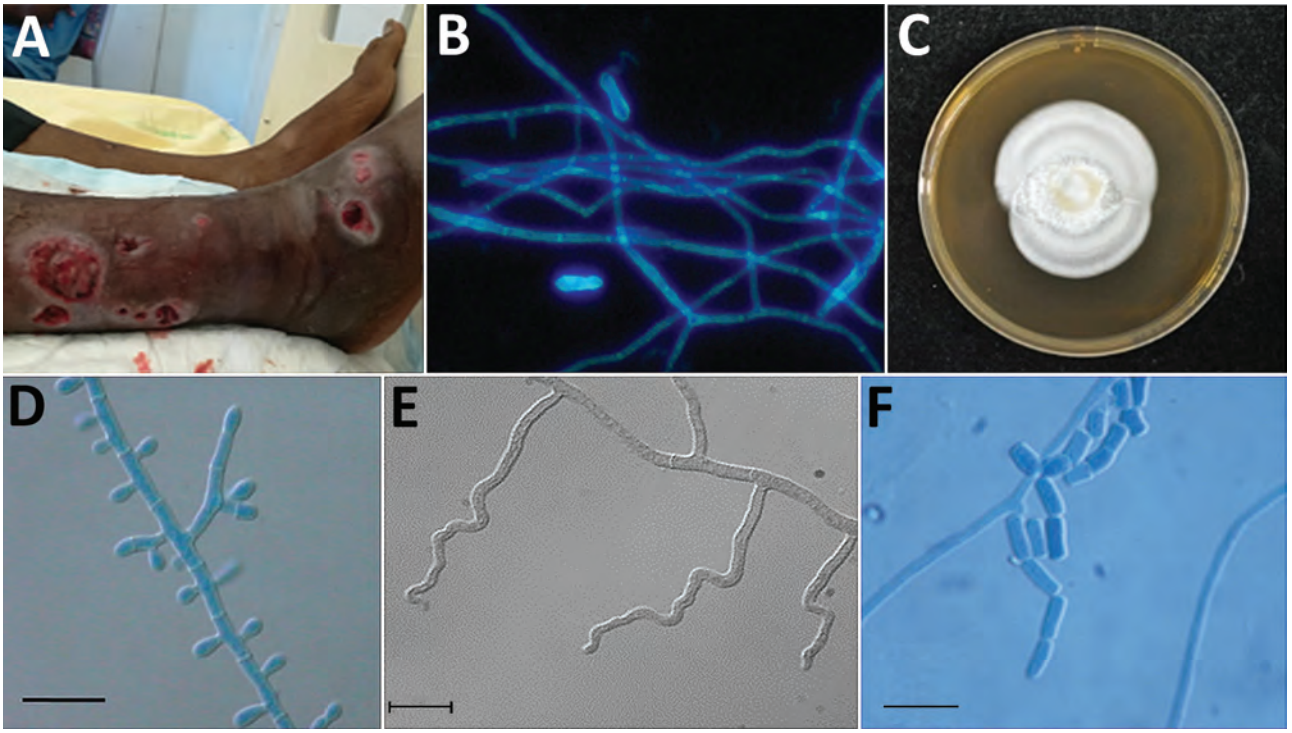

Figure 1. Features of *Nannizziopsis obscura* infections in patients from West Africa, France 2004–2020. A) Ulcerative lesions. B) Septate hyphae and arthroconidia on a calcofluor white direct examination (original magnification ×200). C) Macroscopic aspect on Sabouraud dextrose agar at 7 days. D) Septate conidiophore bearing clavate and sessile conidia. E) Undulate hyphae. F) Barrel-shaped arthroconidia. Scale bars indicate 10 μm.

She was admitted for the investigation of lung lesions. She had been treated for advanced mantle cell lymphoma in 2017, resulting in complete remission. In June 2018, a thoracic CT scan showed lymphadenopathy, lung nodules, and condensations treated with intravenous antibiotics and rituximab. In September 2018, disseminated nodular hyperchromic skin lesions appeared, and skin biopsies showed large septate hyphae with arthroconidia. A combination of voriconazole and liposomal amphotericin B was started for probable invasive mold infection. White mold colonies were observed after 5 days culture, and a presumptive identification of *Trichophyton* spp. was made. Terbinafine was added but was exchanged for voriconazole and liposomal amphotericin B when *N. obscura* was identified. Thirty days after admission, magnetic resonance imaging of the central nervous system showed diffuse, embolic-looking ischemia. Viral PCRs were negative in cerebrospinal fluid. Serum β-D-glucan was strongly positive (>500 pg/mL), and serum galactomannan was negative. Liver biopsy confirmed adult T-cell lymphoma or leukemia associated with human T-cell lymphotropic virus type 1 positivity. The patient died 3 weeks after admission despite intensive care and antifungal treatment.

Patient 6 was a 27-year-old woman from Guinea who was breast-feeding. She had been living in France since September 2017 and was seen at a tuberculosis control center in October 2018. A chest radiograph showed a mediastinal mass, which was confirmed by a chest CT scan. The mass (7 × 5 × 5 cm) invaded the left upper lobe, and thickening of the anterior arch of the second left rib was observed. She had no notable medical history. Pathologic examination of the surgically resected mediastinal mass showed hyphae inside an inflammatory and fibrous reaction invading the thymus, the brachiocephalic veins, the left upper lobe, and the chest wall. Serum β-D-glucan was positive (306 pg/mL). A first presumptive identification on culture was of *Trichophyton* spp. Posaconazole was started, then switched with voriconazole when *N. obscura* was identified. A reduction in mass size (from 71 × 39 mm to 62 × 36 mm) was observed on a CT scan after 7 months of treatment. The investigations of Card9 and Stat1 mutations, 2 genes known to be responsible for higher susceptibility to invasive fungal infections (*9*), showed wild type genotypes. Follow-up after that point was not possible.

Patient 7 was a 38-year-old man from Mali who was hospitalized for visual disturbance, retroorbital pain, and vomiting in September 2018. He had been living in France since 1990, making regular visits to relatives in Mali. He had undergone a renal transplant in 2015 and was receiving mycophenolate mofetil, tacrolimus, and prednisone (5 mg/d). He had experienced an acute rejection in March 2018, which was treated by high-dose methylprednisone. A brain CT scan showed hypodense lesions with mass effect. Results of magnetic resonance imaging without injection supported the diagnosis of glioblastoma. A cerebral biopsy showed numerous branched hyphae. *Candida* spp. infection was suspected, and liposomal amphotericin B (5 mg/d) was started in combination with fluconazole IV (200 mg/d). The treatment resulted in an improvement of the visual disturbance, and a new magnetic resonance imaging result confirmed the reduction of the mass effect. Culture results were positive, and the final identification made was *Nannizziopsis* spp. Serum β-D-glucan was strongly positive (>500 pg/mL), and serum galactomannan was negative. On October 9, fluconazole was switched for voriconazole, and the liposomal amphotericin B was maintained. Meanwhile, the patient experienced a chronic rejection of the graft, and hemodialysis was restarted on November 23. He was alive as of 12 months later.

Patient 8 was a 79-year-old man from Mali who had been living in France since 1963 (his most recent trip to Mali occurred in 2016). In August 2019, he sought care for an ulcerative lesion of the fifth right finger that had been evolving for several months. He had undergone a renal transplant in 2014 and was receiving mycophenolate mofetil, tacrolimus, and prednisone (5 mg/d). A pulmonary nodule was observed in 2017 and was only surveyed. Because of a recent increase in size (from 9 to 13 cm in diameter), a PET-CT scan was performed in April 2019 and showed multiple hypermetabolic pulmonary, abdominal, and muscular (left thigh) nodules. The pulmonary nodule was surgically removed in June 2019, and a necrotic abscess with hyphae was observed by the pathologist (no culture was performed). The evolution was indolent, although the patient had lost 10 kg in 6 months. In August 2019, a skin biopsy showed hyphae, and the culture was identified as *N. obscura* upon sequencing. Serum β-D-glucan was positive (255 pg/mL), and serum galactomannan was negative. Itraconazole was started in August 2019. The patient had been seen in July 2018 because of the same ulcerative lesion of his right hand. A swab specimen yielded a mold colony identified as *Trichophyton rubrum*, which was considered not clinically relevant. The identification of the stored isolate yielded *N. obscura*, which confirmed that the infection had been ongoing for ≥1 year. The patient was well as of 4 months after starting azole therapy.

Patient 9 was a 65-year-old man from Mali who had been living in France for >20 years. In December 2019, he sought care for a mass in front of the left clavicle that had appeared 6 months earlier during a stay in Bamako, Mali. The patient had undergone a renal transplant in 2018 and was receiving cyclosporine, tacrolimus, and prednisone (5 mg/d). A CT scan showed bone lysis of the clavicle with a subcutaneous abscess. A biopsy was performed, and the pathologist reported inflammation with hyphae. Spontaneous fistula occurred, yielding pus. *Nannizziopsis* sp. was identified in the culture. A PET-CT showed hypermetabolism of the left clavicle, and the presternal region extended to the manubrium along with hypermetabolism of a pulmonary nodule of the lingula. Serum β-D-glucan results were positive (>520 pg/mL). Treatment with voriconazole was started and a reappraisal scheduled after 12 weeks.

Materials and Methods

Morphologic Identification and Antifungal-Susceptibility Testing

Ten clinical isolates (2 isolates for patient 8) were checked for purity and subsequently subcultured on potato dextrose agar (PDA) (BD Diagnostic Systems, https://www.bd.com) and malt extract agar (MEA) 2% (Oxoid, http://www.oxoid.com) for 15 days at 30°C, 37°C, and 40°C to study fungal growth and sporulation. The type strain of *N. obscura* (isolate no. UAMH5875) was analyzed in parallel. Microscopic characteristics were examined on 5- to 7-day-old MEA slide cultures incubated at 30°C. Antifungal-susceptibility profiles were screened according to a slightly modified European Committee on Antimicrobial Susceptibility Testing procedure (*10*). All antifungal drugs were purchased from Alsachim (https://www.alsachim.com).

Molecular Characterization and Phylogenetic Analysis

We performed DNA extraction and amplified fragments of the internal transcribed region (ITS), the D1–D2 region of the large subunit (LSU) ribosomal DNA, and the actin gene (*11*) (Appendix, https://wwwnc.cdc.gov/EID/article/26/9/20-0276-App1.pdf). We conducted a preliminary similarity searching using BLASTn (https://blast.ncbi.nlm.nih.gov) against curated fungal reference databases. We conducted multiple sequence alignments and single-gene phylogenies in MEGA7 (*12*). In addition to the clinical isolates and the type strain of *N. obscura*, we incorporated the corresponding sequences of *N. draconii*, *N. chlamydospora*, *N. guarroi*, *N. vriesii*, and *N. arthrosporioides* that are published in GenBank (Appendix). *N. hominis* was not included because of the lack of LSU and actin sequences in the public databases. Phylogenetic analysis was done with a neighbor-joining method by using MEGA7 and with the maximum-likelihood method by using PhyML 3.0 (*13*) subjected to smart model selection at the NGPhylogeny integrative web service (https://ngphylogeny.fr) (*14*).

Ethics Considerations

We obtained approval from the Commission Nationale de l'Informatique et des Libertés, the national data-protection agency in France (approval no. 903395). This step ensured that the patients' data were kept anonymous according to national regulations.

Results

Morphology

All clinical strains and the type strain grew well on PDA at 30°C and 37°C. No growth was observed at 40°C. Cultures on PDA and MEA at 30°C were white with low aerial mycelium and a velvety to powdery texture, rarely zonate, or heaped and with a yellowish coloring on the reverse (Figure 1, panel C). In general, microscopic observations showed the typical, although nonspecific, features of the genus *Nannizziopsis* (e.g., hyaline, septate, smooth-walled hyphae). All isolates produced sessile conidia and arthroconidia, and some produced short hyphal branches in a wavelike motion (undulate hyphae) (Figure 1, panels D–F) (*5*).

Antifungal Susceptibility Testing

The MICs or minimal effective concentrations (MECs) of all 8 antifungals were low except for 1 strain. Median MICs were 0.25 mg/L (range 0.06–1 mg/L) for amphotericin B, 0.125 mg/L (range 0.014–4 mg/L) for itraconazole, 0.06 mg/L (range 0.03–2 mg/L) for voriconazole, 0.06 mg/L (range 0.014–2 mg/L) for posaconazole, 0.125 mg/L (range 0.06–2 mg/L) for isavuconazole, and 0.06 mg/L (range 0.014–0.5 mg/L) for terbinafine. Median MEC was 0.5 mg/L (range 0.25–1 mg/L) for caspofungin and 0.015 mg/L (range 0.015–0.06 mg/L) for micafungin.

Molecular Characterization and Phylogenetic Analyses

Similarity comparisons in public databases showed that all isolates belong to the genus *Nannizziopsis* and had percentage identity ranges of 96.0%–99.8% (475 bp length) for LSU, 88.0%–99.0% (>700 bp length) for ITS, and 85.0%–98.7% (>500 bp length) for actin genes. *N. guarroi* (GenBank accession no. MH874904) had the highest number of hits for LSU, whereas *N. vriesii*

(accession no. HF547893) had the highest number of hits for the actin gene. For ITS, the highest-scoring hits corresponded to a *Nannizziopsiaceae* strain (GenBank accession no. MF688808; 99%), followed by *Nannizziopsis* spp. (GenBank accession no. KY771169; 98.7%).

Multiple alignments for ITS2, LSU, and actin regions consisted of 283, 476, and 572 positions, of which 33 (11.6%), 31 (6.5%), and 128 (22.4%) were variable, respectively. The topologies observed on individual gene trees were very similar to those observed on a combined tree. The combined LSU-actin-ITS2 dataset of 1,331 positions had 192 (14.4%) of variable nucleotides.

The multilocus phylogenetic analysis revealed 2 main well-supported clades: 1 grouping all the clinical isolates, including the type strain of *N. obscura* and the named *N. obscura* species complex clade, and an additional clade assembling the 3 reptile *Nannizziopsis* species isolated from *Iguana iguana* (*N. guarroi*) and from bearded dragons, *Pogona vitticeps* (*N. draconii*, *N. chlamydospora*). *N. vriesii* and *N. arthrosporioides* were separated from the rest of the isolates and from each another (Figure 2).

Discussion

We describe 9 new cases of proven invasive infection with the *N. obscura* species complex in France. The most frequent clinical localizations were subcutaneous tissues (6 patients) and lung nodules (6 patients) (Table 1). Eight of the 9 patients had T-cell immunosuppression associated mainly with the prevention of solid organ rejection. The constant feature was the sub-Saharan origin of all patients. The infecting agent was initially misidentified as *Geotrichum* spp., *Trichosporon* spp., and *Trichophyton* spp. in the 5 different participating hospitals (Table 1). Confusion of *Nannizziopsis* spp. with *Geotrichum* spp. (*3*,*5*), *Trichosporon* spp., or *Trichophyton* spp (*5*) are also common in the literature (Table 2, https://wwwnc.cdc.gov/EID/article/26/9/20-0276-T2.htm). The most common finding upon direct examination at the microbiologic laboratories was the presence of nonspecific hyphae. On culture, *Nannizziopsis* spp. do not exhibit specific features (yeast-like or woolly aspect). Some characteristics of *Nannizziopsis* spp. are even shared with dermatophytes (e.g., cycloheximide tolerance and aleurioconidia). Dermatophytes can be involved in aggressive skin diseases, especially after renal transplantation (*15*). Moreover, empiric azole treatment might control the infection without a definite diagnosis. Because multilocus sequencing of the pathogen is often restricted to unusual localizations or therapeutic failures, a clear knowledge of the spectrum of *Nannizziopsis* spp. infections is lacking, which can explain, at least in part, the rarity of the cases reported.

The initial diagnosis also can be confused by the considerable diversity of the clinical manifestations. Some infections appeared as subacute; others were relatively indolent during periods of months or years. Records for these 9 patient show that the underlying diseases are also diverse, although dominated by HIV infection before 2006 (3 patients) and solid organ

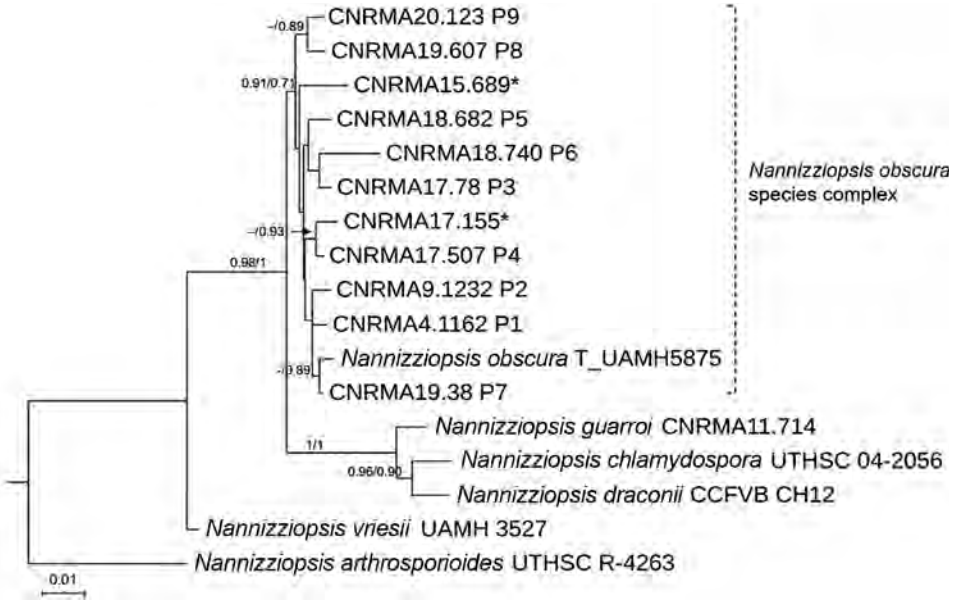

Figure 2. Maximum-likelihood tree obtained from combined large subunit ribosomal DNA, actin, and internal transcribed spacer 2 sequence data obtained from genomic analysis of *Nannizziopsis obscura* isolates from 9 patients from West Africa, France, 2004–2020, and reference sequences. Neighbor-joining bootstrap values or maximum-likelihood values are indicated on the branches. Support branch values <70% are not shown. Culture collection numbers appear next to sequences retrieved from GenBank, and type strains are indicated by a "T" after the species name. Patients from whom clinical isolates analyzed in this study were obtained are shown as P1–P9. The 2 isolates from patient 8 were morphologically and molecularly identical. Sequences marked with asterisks (*) refer to strains published by Nourrisson et al. (*6*). Scale bar indicates nucleotide substitutions per character.

transplantation (8 patients) after 2006; the most frequent clinical localizations were subcutaneous tissues (8 patients) and lung (7 patients) (Tables 1, 2). For some patients, the infection manifested as disseminated disease with brain abscess, lung nodules, or positive blood culture (Tables 1, 2). The association of serum β-D-glucan positivity and galactomannan negativity (7 and 6 patients tested in the 9-patient series, respectively) seems a useful adjunct, albeit unspecific. As a consequence, the suspicion of *Nannizziopsis* spp. infection cannot rely on a specific clinical manifestation and requires a tissue biopsy.

Our molecular study places all 10 *N. obscura* isolates (including 2 recovered from patient 8) into a well-supported phylogenetic lineage, separate from reptile isolates (Figure 2). Recent taxonomic revisions for the former *Chrysosporium* anamorph of *N. vriesii* complex resulted in the assignment of several species within the genus *Nannizziopsis* or within the 2 new genera of *Paranannizziopsis* and *Ophiodiomyces* (*1*,*5*). So far, only 2 species (*N. obscura* and *N. hominis*) have been definitely implicated in human pathology (*3*,*5*). The species *N. infrequens* was determined not to be responsible for an invasive infection and was disregarded by clinicians (*16*). Thus, *N. hominis* was reported in 3 patients before 2000, and *N. obscura* was reported in 4 patients after 2005 (*5*) and in 9 cases since then. *N. infrequens* and *N. hominis* exhibit good growth at 35°C, in contrast to the *Nannizziopsis* species implicated in reptile infections (*5*). Although our study clearly differentiates the human *N. obscura* isolates from our case series from the reptile isolates, the modest branch support value for the *N. obscura* clade (0.71 by maximum-likelihood method) suggests the possibility of potential new species. More taxa and additional gene sequences should be studied to investigate this hypothesis.

The issue of the portal of entry remains unclear. Subcutaneous nodules, ulcerative skin lesions, or both are frequently noted (e.g., in patients 2, 3, 4, 5,

Figure 3. Geographic distribution of 13 patients infected by *Nannizziopsis obscura* in West Africa. The different colors represent the number of cases in each country: red for 7 cases, orange for 2 cases, and green for only 1 reported case. The diameter of the circle indicated for each country is proportional to the number of cases reported.

8, and 9) (Table 1) and could have been the initial site of infection. Skin can be suspected because *Nannizziopsis* species are keratinophilic and cause extensive dermatitis with erosions and subsequent invasion of the subcutaneous structures in reptiles (*1*,*2*). When specifically investigated in this case series (i.e., patients 3 and 4) (Table 1), no *Nannizziopsis* organisms were recovered from skin or nail samples, even when patients had dermatomycoses or onyxis. On the other hand, the frequency of dissemination suggests inhalation as a possible route, with subcutaneous nodules as tissue localizations other than lung as a consequence of blood dissemination. Therefore, the infection scenario described for reptiles might not apply to humans.

We cannot provide firm recommendations for antifungal treatment because of the low number of patients in our study. The MICs show no intrinsic antifungal resistance. Azole therapy appears to be the first option, but the choice between posaconazole or voriconazole depends on the pharmacokinetics of each drug and its interactions with other medications. Decrease of immunosuppressive therapy might also contribute to improvement, and surgery can be a major part of treatment for some abscesses. However, as for many invasive fungal diseases, the final prognosis depends on that of the underlying disease.

The main epidemiologic observation is the geographic origin of the patients. All came from sub-Saharan West Africa or Africa when national origin was reported (Tables 1, 2; Figure 3). The preferred migration routes explained by historical reasons—The Gambia to England route (*7*) and Mali, Senegal, and Guinea to France route—observed in our case-series and in the literature (*6*), might have introduced bias. However, France and England also have immigrants from other parts of Africa, and *Nannizziopsis* spp. infections are described only in patients from semiarid countries. For the previously reported patients from Nigeria (*4*,*5*), the exact origin was not reported, but Nigeria also covers semiarid tropical zones. In patients for whom the information was known, the delay between the last trip to Africa and the onset of symptoms varied between 2 months and 3 years (Table 1). Patients could carry latent forms of the fungus and have onset of an opportunistic infection when their immunity fails, as described for other fungi, such as *Cryptococcus neoformans* (*17*) and *Histoplasma* spp. or other endemic mycoses (*18*).

These 9 new cases and the previously reported cases (*1*,*3*–*7*) highlight the difficulties in identifying the *N. obscura* species complex. These fungal infections are likely underdiagnosed because of features shared with more common species, such as *Trichophyton* spp. or *Trichosporon* spp. Matrix-assisted laser desorption/ionization time-of-flight mass spectrometry should accelerate the process of identifying organisms and updating public databases, such as the online mass spectrometry platform (https://msi.happy-dev.fr), which now includes a *N. obscura* profile. Up to now, these deep infections seemed to involve T-cell immunosuppressed patients with frequent dissemination or multifocus localizations. These molds are probably endemic in sub-Saharan Africa, but their precise geographic repartition and natural ecology remain to be established. Environmental studies would be necessary to further investigate the natural ecology of these molds, as has been done recently for the emerging *Emergomyces africanus* (*19*).

Acknowledgments

The authors thank all the clinicians who cared for the patients, especially Aude Barnier in the case of patient 6. We thank Mohammad Akhoundi for his ITS2 sequencing; Cécile Gautier for technical assistance regarding culture of strains, MIC determinations, and PCR tests; and Eurofins Genomics France for strain sequencing. We are also deeply thankful to Françoise Dromer, who commented on the manuscript.

The National Reference Center for Invasive Mycoses and Antifungals is supported by the French Center for Diseases Control (Santé Publique France) and Institut Pasteur in Paris. The funders had no role in the study design, data collection, or analysis or interpretation of data.

About the Author

Dr. Garcia-Hermoso is a research engineer at the Centre National de Référence Mycoses Invasives et Antifongiques. Her main research focuses on the polyphasic identification of filamentous fungi causing invasive mycosis in humans and the phylogenetic relationship among different groups of fungal species.

References

1. Stchigel AM, Sutton DA, Cano-Lira JF, Cabañes FJ, Abarca L, Tintelnot K, et al. Phylogeny of chrysosporia infecting reptiles: proposal of the new family *Nannizziopsiaceae* and five new species. Persoonia. 2013;31:86–100. https://doi.org/10.3767/003158513X669698
2. Cabañes FJ, Sutton DA, Guarro J. *Chrysosporium*-related fungi and reptiles: a fatal attraction. PLoS Pathog. 2014;10:e1004367.
3. Stillwell WT, Rubin BD, Axelrod JL. *Chrysosporium*, a new causative agent in osteomyelitis. A case report. Clin Orthop Relat Res. 1984;184:190–2.

4. Steininger C, van Lunzen J, Sobottka I, Rohde H, Horstkotte MA, Stellbrink H-J. Mycotic brain abscess caused by opportunistic reptile pathogen. Emerg Infect Dis. 2005;11:349–50. https://doi.org/10.3201/eid1102.040915
5. Sigler L, Hambleton S, Paré JA. Molecular characterization of reptile pathogens currently known as members of the chrysosporium anamorph of *Nannizziopsis vriesii* complex and relationship with some human-associated isolates. J Clin Microbiol. 2013;51:3338–57. https://doi.org/10.1128/JCM.01465-13
6. Nourrisson C, Vidal-Roux M, Cayot S, Jacomet C, Bothorel C, Ledoux-Pilon A, et al. Invasive infections caused by *Nannizziopsis* spp. molds in immunocompromised patients. Emerg Infect Dis. 2018;24:549–52. https://doi.org/10.3201/eid2403.170772
7. Baggott A, McGann H, Barton R, Ratner J. Disseminated *Nannizziopsis obscura* infection in a renal transplant patient—the first reported case. Med Mycol Case Rep. 2017;17:20–4. https://doi.org/10.1016/j.mmcr.2017.06.002
8. Fisher MC, Henk DA, Briggs CJ, Brownstein JS, Madoff LC, McCraw SL, et al. Emerging fungal threats to animal, plant and ecosystem health. Nature. 2012;484:186–94. https://doi.org/10.1038/nature10947
9. Lanternier F, Cypowyj S, Picard C, Bustamante J, Lortholary O, Casanova J-L, et al. Primary immunodeficiencies underlying fungal infections. Curr Opin Pediatr. 2013;25:736–47. https://doi.org/10.1097/MOP.0000000000000031
10. Guégan S, Garcia-Hermoso D, Sitbon K, Ahmed S, Moguelet P, Dromer F, et al.; French Mycosis Study Group. Ten-year experience of cutaneous and/or subcutaneous infections due to coelomycetes in France. Open Forum Infect Dis. 2016;3:ofw106. https://doi.org/10.1093/ofid/ofw106
11. Garcia-Hermoso D, Hoinard D, Gantier J-C, Grenouillet F, Dromer F, Dannaoui E. Molecular and phenotypic evaluation of *Lichtheimia corymbifera* (formerly *Absidia corymbifera*) complex isolates associated with human mucormycosis: rehabilitation of *L. ramosa*. J Clin Microbiol. 2009;47:3862–70. https://doi.org/10.1128/JCM.02094-08
12. Kumar S, Stecher G, Tamura K. MEGA7: Molecular Evolutionary Genetics Analysis version 7.0 for bigger datasets. Mol Biol Evol. 2016;33:1870–4. https://doi.org/10.1093/molbev/msw054
13. Guindon S, Dufayard J-F, Lefort V, Anisimova M, Hordijk W, Gascuel O. New algorithms and methods to estimate maximum-likelihood phylogenies: assessing the performance of PhyML 3.0. Syst Biol. 2010;59:307–21. https://doi.org/10.1093/sysbio/syq010
14. Lemoine F, Correia D, Lefort V, Doppelt-Azeroual O, Mareuil F, Cohen-Boulakia S, et al. NGPhylogeny.fr: new generation phylogenetic services for non-specialists. Nucleic Acids Res. 2019;47(W1):W260–5. https://doi.org/10.1093/nar/gkz303
15. Rouzaud C, Chosidow O, Brocard A, Fraitag S, Scemla A, Anglicheau D, et al.; French Mycoses Study Group. Severe dermatophytosis in solid organ transplant recipients: a French retrospective series and literature review. Transpl Infect Dis. 2018;20:e12799. https://doi.org/10.1111/tid.12799
16. Brandt ME, Gaunt D, Iqbal N, McClinton S, Hambleton S, Sigler L. False-positive *Histoplasma capsulatum* Gen-Probe chemiluminescent test result caused by a *Chrysosporium* species. J Clin Microbiol. 2005;43:1456–8. https://doi.org/10.1128/JCM.43.3.1456-1458.2005
17. Garcia-Hermoso D, Janbon G, Dromer F. Epidemiological evidence for dormant *Cryptococcus neoformans* infection. J Clin Microbiol. 1999;37:3204–9. https://doi.org/10.1128/JCM.37.10.3204-3209.1999
18. Brunet K, Alanio A, Lortholary O, Rammaert B. Reactivation of dormant/latent fungal infection. J Infect. 2018;77:463–8. https://doi.org/10.1016/j.jinf.2018.06.016
19. Schwartz IS, Lerm B, Hoving JC, Kenyon C, Horsnell WG, Basson WJ, et al. *Emergomyces africanus* in soil, South Africa. Emerg Infect Dis. 2018;24:377–80. https://doi.org/10.3201/eid2402.171351

Address for correspondence: Dea Garcia-Hermoso, Institut Pasteur, Centre National de la Recherche Scientifique, Centre National de Référence Mycoses Invasives et Antifongiques, Unité de Mycologie Moléculaire, UMR2000, 28 rue du Dr. Roux, 75015 Paris, France; email: dea.garcia-hermoso@pasteur.fr

Saprochaete clavata Outbreak Infecting Cancer Center through Dishwasher

Estelle Menu, Alexis Criscuolo, Marie Desnos-Ollivier, Carole Cassagne, Evelyne D'Incan, Sabine Furst, Stéphane Ranque, Pierre Berger, Françoise Dromer

Saprochaete clavata is a pathogenic yeast responsible for rare outbreaks involving immunocompromised patients, especially those with hematologic malignancies. During February 2016–December 2017, we diagnosed *S. clavata* infections in 9 patients (8 with fungemia), including 3 within 1 month, at a cancer center in Marseille, France. The patients (median age 58 years), 4 of 9 of whom had acute myeloid leukemia, were hospitalized in 3 different wards. Ten environmental samples, including from 2 dishwashers and 4 pitchers, grew *S. clavata*, but no contaminated food was discovered. The outbreak ended after contaminated utensils and appliances were discarded. Whole-genome sequencing analysis demonstrated that all clinical and environmental isolates belonged to the same phylogenetic clade, which was unrelated to clades from previous *S. clavata* outbreaks in France. We identified a dishwasher with a deficient heating system as the vector of contamination.

Saprochaete clavata (previously *Geotrichum clavatum*) is a rare emerging pathogen, an ascomycetous yeast-producing arthroconidia that causes invasive fungal infections in immunocompromised patients. The species has mainly been reported in Europe, often associated with sporadic cases or small outbreaks (*1*,*2*). Unlike *Magnusiomyces capitatus* (*3*,*4*), which has been associated with dairy products, *S. clavata* has rarely been isolated from environmental samples (*5*,*6*). Patients most at risk for infections from *Geotrichum* spp. have hematologic diseases with severe neutropenia (*7*) and are undergoing chemotherapy, mainly with cytarabine (*1*) or caspofungin (*8*). They often have central venous catheters (*9*).

In recent years, *S. clavata* fungemia outbreaks associated with high mortality rates in vulnerable patients with malignancies have been described throughout Europe, mainly in France (*1*), Italy (*2*,*10*), Czechia (*11*), and Spain (*12*). No source of contamination was identified in any of these outbreaks despite thorough investigation.

During February 2016–December 2017, the Paoli-Calmettes Institute, a cancer center in Marseille, France, was faced with an outbreak of *S. clavata* infections involving 9 patients hospitalized in 3 different wards, suggesting a common source of contamination. We describe the findings of an outbreak investigation that recovered *S. clavata* in different environmental samples, including from a dishwasher in the central kitchen and another, available to patients and their families, in the stem-cell transplant ward. Whole-genome sequencing (WGS) confirmed that the environmental and clinical isolates from patients belonged to the same phylogenetic clade. Handwashing, avoiding direct skin contact, checking air quality, and sterilizing food are routine practice to prevent contamination in hematology wards; however, examining dishwashers for contamination and operability may not be done routinely. Our findings should prompt adding dishwasher inspections to guidelines for preventing infection.

Materials and Methods

Case Definition Criteria

We defined *S. clavata* infection by obtaining ≥1 positive results for *S. clavata* blood culture from a usually sterile body site or from a bronchoalveolar lavage or tracheal aspirate of the respiratory tract. Infection was also confirmed by observing pleural fluid in a patient with pleural effusion or lung infection.

Author affiliations: Institut Hospitalo-Universitaire, Méditerranée Infection, Marseille, France (E. Menu, C. Cassagne, S. Ranque); Institut Pasteur, Paris, France (A. Criscuolo, M. Desnos-Ollivier, F. Dromer); Centre de Lutte Contre le Cancer, Institut Paoli-Calmettes, Fédération Unicancer, Marseille (E. D'Incan, S. Furst, P. Berger)

DOI: https://doi.org/10.3201/eid2609.200341

Mycologic Investigation

We collected a rectal swab specimen from all patients hospitalized in the stem-cell transplant unit during December 20–30, 2017. In addition, during December 22, 2017–January 19, 2018, we collected 95 environmental samples from food (powdered milk, a pea-sized amount from each package of cheese); tap water in 2 patients' room and water used for the coffee machine in 1 kitchen (500 μL); air filters; food-contact surfaces; non–food-contact surfaces in the rooms of infected patients; various kitchenware (vacuum flasks, cutlery); tables and chairs in the ward's kitchen; and microwaves, refrigerators, and dishwashers, including the dishwasher in the ward's central kitchen. For the dishwashers, we sampled inner surfaces, door seals, and the water outlet.

We used Sigma Transwab MW176S MWE medical wire sterile dry cotton swabs (Sigma Transwab, https://www.mwe.co.uk) for sampling as wide an area as possible. We discharged swabs in liquid Amies medium, then streak-plated the samples on Sabouraud dextrose agar plates supplemented with gentamicin and chloramphenicol (Bio-Rad, https://www.bio-rad.com) and BBL CHROMagar Candida plate (BD, https://www.bd.com). We identified species using Bruker Biotyper version MBT 3.1 matrix-assisted laser desorption/ionization time-of-flight (MALDI-TOF) mass spectrometry (Bruker, https://www.bruker.com) and nucleotide sequence analysis of the internal transcribed spacer (ITS) regions of the rRNA gene, as described elsewhere (*13*). The ITS sequences of the isolates were compared to those of the *S. clavata* type strain CBS425.71 (GenBank accession no. KF984489) isolated in Baltimore, Maryland, USA, in 1971.

All the strains we recovered from environmental and clinical samples and identified as *S. clavata* were stored at –20°C in cryotubes with bead tune Cryosystème Protect (Dutscher, https://www.dutscher.com). After subculturing all of the samples on Sabouraud agar slant (Bio-Rad), we sent them to the French National Reference Center for Invasive Mycoses and Antifungals (Institut Pasteur, Paris, France) for further characterization and comparison with selected clinical isolates collected through the nationwide surveillance program (Appendix Table, https://wwwnc.cdc.gov/EID/article/26/9/20-0341-App1.pdf).

WGS

After checking purity on chromogenic medium, we extracted DNA using a NucleoMag Plant kit (Macherey-Nagel, https://www.mn-net.com) in a KingFisher Flex system (Thermo Fisher Scientific, https://www.thermofisher.com). We sequenced whole genomes from each selected isolate (17 clinical and 10 environmental isolates) at the Mutualized Platform for Microbiology (Institut Pasteur, Paris, France) using a NextSeq 500 sequencer (Illumina, https://www.illumina.com). We constructed libraries using Nextera XT technology (Illumina) and sequenced genomes using a 2 × 150 nt paired-end run strategy. We preprocessed all reads with AlienTrimmer version 0.4.0 (https://bioweb.pasteur.fr/packages/pack@AlienTrimmer@0.4.0) to remove exogenous or low-quality bases, leading to a mean of 8.47M paired-end reads per sample (≈140 × sequencing depth, mean). We deposited FASTQ files for all isolates from Marseille at the European Nucleotide Archive BioProject (accession no. PRJEB36345).

Phylogenetic Analysis

For phylogenetic comparison, we used WGS data from 10 isolates studied during an outbreak described by Vaux et al. (BioProject accession no. ERP003645) (*1*); all reads from the BioProject ERP003645 isolates were preprocessed as described in previous sections. (The patients from whom the cultures were isolated correspond to patients 11–20 in the Appendix Table.) These reads included 5 isolates from epidemic clade A (CNRMA12.494, CNRMA12.559, CNRMA12.637, CNRMA12.667, CNRMA12.647) and 5 from epidemic clade B (CNRMA8.1167, CNRMA11.1183, CNRMA12.304, CNRMA12.615, CNRMA12.634). Overall, we studied a total of 38 isolates: 10 from BioProject ERP003645; 26 clinical and environmental isolates recovered in Marseille during the outbreak or its investigation, plus 1 clinical isolate, CNRMA15.181, recovered in 2015 in the same hospital in Marseille; and the *S. clavata* strain (CBS425.71).

For each preprocessed read sample, we performed short read mapping against the genome sequence of *S. clavata* clade A isolate CNRMA12.647 (GenBank accession no. CBXB000000000.1) using minimap2 version 2.17-r941 (*14*). We then inferred a pseudogenome following 4 rules: 1) we considered only aligned reads and sequenced bases associated with a Phred score >20; 2) we replaced each position with the character states observed in >80% of the aligned residues at that position; 3) we replaced every position covered by <10 aligned reads with the unknown character state "?"; and 4) we replaced all polymorphic positions located within strand-biased (set as <5 aligned reads on ≥1 strand) or over-covered regions (set as >200×) with the character state "X." Finally, after pooling all pseudogenome sequences into a unique matrix of aligned nucleotide

characters, we discarded each position containing >10% undefined character states (?, –, X, or N), resulting in 12,053,164 characters (including 261 variable characters), which we used to infer a maximum likelihood phylogenetic tree using IQ-TREE (http://www.iqtree.org) (*15*). To approximate the number of single-nucleotide polymorphisms (SNPs) shared by each branch of the phylogenetic tree, each branch length was multiplied by the total number of analyzed characters (i.e., 12,053,164) and the result was rounded to the closest integer.

Growth Temperature Testing

We analyzed the ability of 3 isolates of *S. clavata* (CBS425.71 type strain, CNRMA15.100, CNRMA14.292) and 3 isolates of *M. capitatus* (CBS162.80 type strain, CNRMA17.803, CNRMA17.775) to grow at high temperatures after 48 and 72 h of incubation. We subcultured isolates on Sabouraud agar medium at 30°C for 48h, then plated suspensions containing 10^3, 10^2, 10, and 1 colony-forming units in 5 μL of sterile distilled water on Sabouraud agar plates and incubated samples of each concentration at 30°C, 35°C, 37°C, 40°C, 45°C, and 48°C.

Results

Characteristics of the Patients

In December 2017, *S. clavata* infections were diagnosed in 3 patients (numbers 7–9 in the Table) within 3 weeks of admission to the Paoli-Calmettes Institute. This timing suggested a common source of contamination, even though the patients were hospitalized in 2 different wards, the stem-cell transplant

Table. Characteristics of patients with a culture positive for *Saprochaete clavata* in Marseille, France, February 2016–December 2017*

Characteristic	Patient no. 1	2	3	4	5	6	7	8	9
Age, y	58	38	45	66	57	68	65	56	68
Sex	M	F	M	F	M	M	F	M	M
Hospitalization ward	H	H	T	ICU	T	H	T	T	H
Immune status									
Underlying disease	Lymphoma	AML	MDS	Lymphoma	CLL	AML	ALL	AML	AML
Lymphocyte count, G/L	<0.1	0.1	5.6	0.2	0.1	0.1	0.8	0.1	0.1
Severe neutropenia, <500 /mm^3	Yes	Yes	No	Yes	Yes	Yes	Yes	Yes	Yes
Duration of neutropenia at time of positive culture, d	6	51	0	4	36	27	0	21	21
BMT	Yes	No BMT	Yes	No BMT	Yes	No BMT	Yes	Yes	Yes
Days from BMT to first positive culture	9		90		75		61	3	>90
Clinical signs at the time of positive culture									
Fever, temperature >38°C	Yes	Yes	Yes	Yes	NA	Yes	NA	Yes	Yes
Digestive symptoms	Yes	Yes	NA	NA	NA	NA	Yes	Yes	Yes
Diarrhea	Yes		NA	NA	NA	NA	Yes	Yes	
Constipation	NA	Yes	NA	NA	NA	NA		NA	Yes
Pulmonary symptoms	NA	Yes	Yes	NA	NA	NA	Yes	NA	Yes
Skin lesions	NA	NA	NA	Yes	Yes	NA	Yes	NA	NA
Positive culture results									
Date of first positive culture	2016 Feb 3	2017 Jan 16	2017 Jan 18	2017 Feb 26	2017 Apr 17	2017 Jun 29	2017 Dec 5	2017 Dec 10	2017 Dec 29
Days after admission	16	51	6	14	80	27	68	20	21
No. positive samples	1	1	2	7	5	9	1	10	5
Blood	1	1	None	5	4	9	1	9	5
Respiratory tract	None	None	2	2	1	None	None	None	None
Stool, rectal swab	None	None	None	None	None	None	None	1	None
Outcome									
Death within 90 d	No	Yes	Yes	Yes	No	Yes	Yes	No	No
Days after first positive culture	DNA	12	57	7	DNA	4	6	DNA	DNA
Treatment									
Venous access	Yes	Yes	Yes	Yes	Yes	Yes	Yes	Yes	Yes
Echinocandins	Micafungin	NP	NP	NP	NP	NP	Caspo	NP	NP
Azoles	NP	PCZ	NP	NP	VCZ	PCZ	VCZ	VCZ	VCZ, PCZ
Cytarabine	Yes	Yes	NP	NP		Yes	Yes	Yes	Yes
Ibrutinib	NP		NP	NP	Yes				
Apheresis platelet concentrates	NP	Yes	NP	NP	Yes	Yes	Yes	Yes	Yes

*ALL, acute lymphoblastic leukemia; ANL, acute myeloid leukemia; BMT, bone marrow transplant; Caspo, caspofungin; CLL, chronic lymphocytic leukemia; DNA, does not apply; H, hematology; ICU, intensive care unit; MDS, myelodysplastic syndromes; NA, not available; NP, not prescribed; PCZ, posaconazole; T, stem-cell transplant; VCZ, voriconazole.
†Bronchoalveolar lavage, tracheal aspirate.

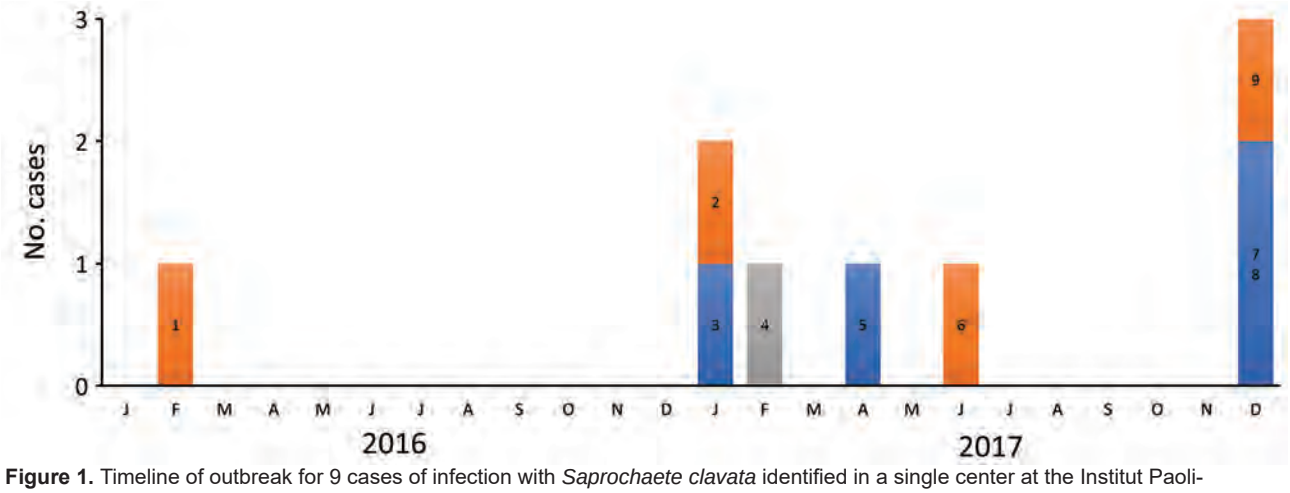

Figure 1. Timeline of outbreak for 9 cases of infection with *Saprochaete clavata* identified in a single center at the Institut Paoli-Calmettes, Marseille, France, February 2016–December 2017. The patients were hospitalized in 3 wards: the hematology unit (orange bar sections), the stem cell transplant unit (blue bar sections), and the intensive care unit (gray bar sections). Numbers 1–9 correspond to patient numbers in the Table.

and hematology units. A retrospective review of laboratory files revealed that *S. clavata* infection had been diagnosed in 6 additional patients during February 2016–July 2017 (Table; Figure 1), bringing the total identified to 9 patients. The 6 patients found retrospectively had been hospitalized in 3 different wards, the stem-cell transplant, hematology, and intensive care units. The median age of the 9 patients was 58 years (range 38–68 years); 6 (67%) were male. All of the patients had central venous catheters; 4 (44%) were treated for acute myeloid leukemia and 6 (67%) had cytarabine chemotherapy. Of the 41 samples testing positive for *S. clavata*, 35 (85%) were blood cultures; fungemia was detected in 8 (89%) of 9 patients on the basis of a mean of 4 (range 1–9) blood samples positive for *S. clavata*. In 5 patients, results were positive only for the blood samples. Results from rectal swab cultures were positive only for patient 8 (Table). Of note, 5 patients had digestive symptoms. The 90-day case fatality rate was 55% (5/9); median survival time for those 5 patients was 7 days after the first positive culture.

Mycological and Environmental Investigation

Among the 95 environmental samples, 75 were sterile, and 10 tested positive for fungi other than *S. clavata* (*Penicillium rubens*, *Lecytophora* sp., *Aspergillus creber*, *Alternaria citri*, *Trichoderma viride*, *Exophiala dermatidis*, *Alternaria alternata*, *Candida lusitaniae*, *Candida parapsilosis*, *Scopulariopsis cinerea*, and *Geotrichum capitatum*). Of the 10 *S. clavata*–positive samples, we collected 6 from the kitchen in the stem-cell transplant ward: 4 samples from the dishwasher (water outlet, interior surfaces, and door seal) and 2 samples from vacuum flasks, 1 each used for coffee and milk. Two of those samples had additional fungi species: milk recovered in 2015 in a patient pitcher lid in the hematologic ward contaminated with *C. lusitaniae* and a coffee pitcher lid from the stem cell transplant ward contaminated with *C. lusitaniae* and *C. parapsilosis*. In the stem cell transplant ward, only a sample from a table surface in patient 8's room tested positive for *S. clavata*. In the hematology ward, we collected *S. clavata*–positive samples from the coffee and milk pitcher lids but found no contamination of the dishwasher. In the central kitchen dishwasher, samples from the prewash area (Figure 2), where water is sprayed to loosen food particles on the dishes, tested positive for *S. clavata*. Finally, samples from 2 different cheeses, proposed as possible vectors at the time of the outbreak, tested negative.

Study of Growth Temperature

The isolates of *S. clavata* and *M. capitatus* tested exhibited similar growth at various temperatures. No growth was detected at ≥48°C.

WGS

Bioinformatic analysis of the WGS data yielded a robust phylogenetic classification for 38 isolates (Figure 3). The 5 isolates belonging to clade A and the 5 isolates from clade B (isolation years 2008–2012) clustered in 2 distinct clades, as described elsewhere (*1*). All of the isolates collected in Marseille after February 2016 clustered into a third new monophyletic clade, referred to as clade C, and had an estimated <10 SNP difference. Multiple isolates recovered from patients

2, 5, 8, and 9 exhibited ≤1 SNP mean difference. Isolates from both environmental and clinical samples clustered in clade C, suggesting a clonal outbreak with a probable common source. The CNRMA15.181 isolate, which was recovered at the same center in January 2015, clustered in neither clade C nor in any other previously identified clade.

Interventions and Control Measures

We discarded and replaced all *S. clavata*–contaminated fomites and the ward's dishwasher as soon as contamination was determined. Even if the water temperature could have achieved >60°C, the dishwasher was discarded because of incomplete drain cycles, seals in poor condition, and overall aging. We discarded the old vacuum flasks and replaced them with simpler models in which the entire device is accessible to washing (Figure 4). In addition, we instituted mandatory guidelines for thorough cleaning and washing after each use.

Discussion

Small outbreaks and sporadic cases of invasive infections due to *Geotrichum* spp. have been reported mostly, but not exclusively, in Europe. As in this outbreak, patients infected by *M. capitatus* and *S. clavata* often share a common clinical background of severe hematologic malignancy and neutropenia. *M. capitatus* (previously known as *G. capitatum*) is the most common reported involving patients in hematology wards (*4*,*16*); *S. clavata* infections are less often reported but occur as sporadic cases or small outbreaks that are usually (*2*,*10*,*11*), but not always (*1*), monocentric.

No study of *S. clavata* outbreaks has so far succeeded in identifying the contamination source (*10*). Contaminated milk jugs have been identified as the source of outbreaks from *M. capitatus* (*17*), and several reports have noted the role of food as a potential source of outbreaks of *Geotrichum* spp. (*17*,*18*). However, because of the lack of accurate databases, earlier reports relied on the association of arthroconidia with lack of urease activity to identify *Geotrichum* spp., and others misidentified *S. clavata* as *M. capitatus* (*19*). Therefore, it is possible that cheese and milk that were reported in the literature (*5*,*17*) to be positive with *Geotrichum* spp. could actually have been contaminated by *S. clavata*. However, to our knowledge, no report has associated *S. clavata* with cheese production (*20*).

Previously, we discovered that some yeast strains recovered from dishwashers were *S. clavata* and not *M. capitatus* as initially reported (*1*,*6*), which might reinforce ingestion as a possible route of *S. clavata* infection. This finding influenced our decision to sample dishwashers and the jugs and vacuum flasks used to deliver food to patients in the hematology and stem cell transplant wards at the cancer center. Recovering *S. clavata* from the dishwashers and jugs was the first step in explaining this monocentric outbreak, because the contaminated utensils from the hematology ward had been washed in those dishwashers. Another possible factor in the dishwasher's involvement in spreading infection might have been the nonremovable lids on the jugs, which could have prevented the dishwasher from completely removing food residues. In a laboratory setting,

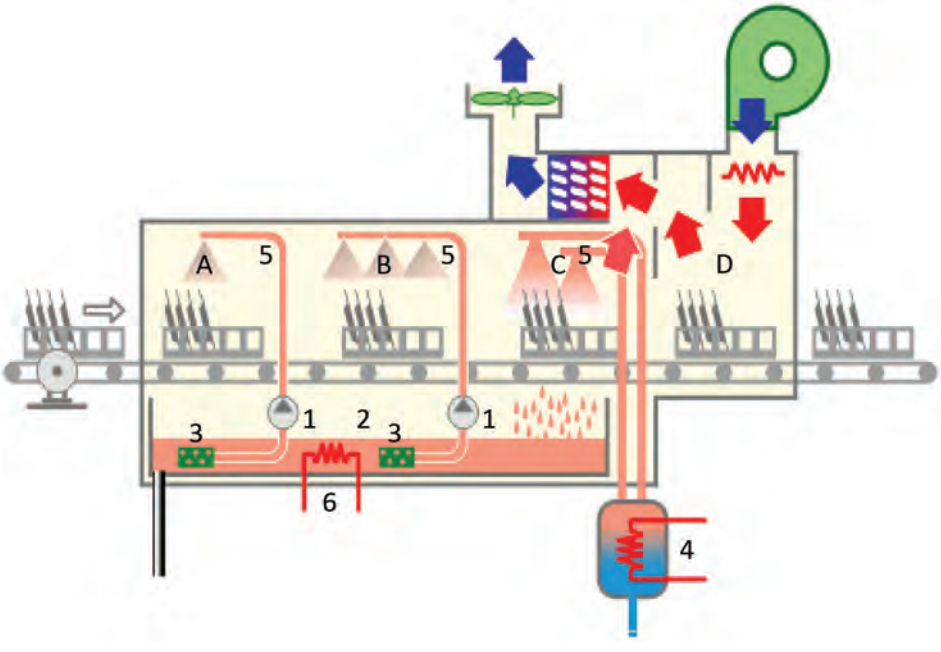

Figure 2. Schematic of dishwasher implicated in outbreak of *Saprochaete clavata* at the Institut Paoli-Calmettes, Marseille, France, February 2016–December 2017. A) Prewash area; B) wash area; C) rinse area; D) drying area. 1, pump; 2, prewash and wash trays; 3, filters; 4, rinse water heater; 5, wash arm; 6, wash heat resistor. Blue arrows indicate cool air flow; red arrows indicate hot air flow. (Figure modified from https://energieplus-lesite.be/techniques/cuisine-collective6/laverie-vaisselle/lave-vaisselle-description [cited 2020 May 20].)

S. clavata has been shown to not survive temperatures >48°C or contact with fungicidal sprays (M. Desnos-Ollivier, unpub. data). Therefore, it is possible that the temperature cycle of the dishwasher, normally capable of reaching temperatures >60°C, may have been dysregulated or the procedure or the detergent used to decontaminate dishes and utensils may have been insufficient. We did not assess these possibilities, but discarding the contaminated fomites and the old dishwasher seemed to control the outbreak. The dishwasher in the central kitchen was also contaminated, but only in the prewash area, ruling out its involvement in the spread of the fungus. Nevertheless, it was decontaminated as a precaution. Finally, we did not uncover any food source for the *S. clavata* infection, possibly because the initial contamination had occurred almost 2 years earlier or because we did not test the correct food samples.

The temporal association of *S. clavata* in the environment with the outbreak offered only a potential link; genetic relatedness needed to be demonstrated. WGS is being used increasingly to investigate outbreaks, especially when genotyping methods are not readily available, such as for rare species. In 2012, following the discovery of a clade, A, as the source of a multicenter outbreak of *S. clavata* infections in France, we designed a real-time PCR so we could rapidly distinguish isolates belonging to clade A or to another clade, B (NRCMA, unpub. data). Since the isolates recovered in Marseille belonged to neither of those clades, we used WGS to study strain relatedness. All of the isolates recovered in Marseille after early 2016,

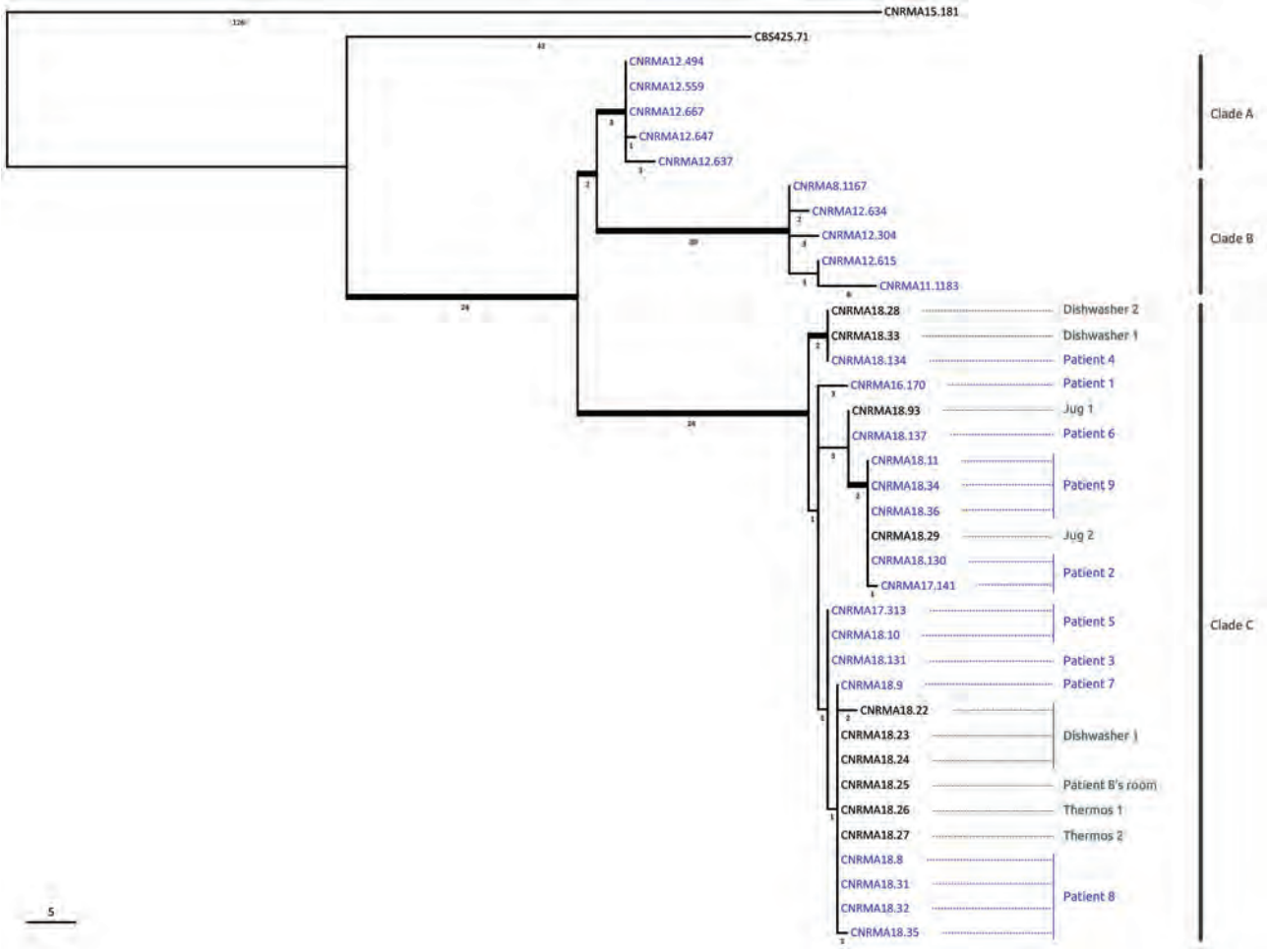

Figure 3. Phylogenetic tree of 38 *Saprochaete clavata* isolates, including isolates from outbreak of *Saprochaete clavata* at the Institut Paoli-Calmettes, Marseille, France, February 2016–December 2017. The unrooted maximum-likelihood tree was inferred from 12,053,164 nt characters with evolutionary model HKY (Hasegawa, Kishino, and Yano, 1985) + FO (base frequencies optimized by ML) + I (proportion of invariable sites optimized by ML). Thick branches are supported by >70% bootstrap supports (500 replicates). The approximated number of single-nucleotide polymorphisms is indicated below each branch. Blue indicates clinical isolates; gray indicates nonclinical isolates. Patient numbers correspond to those in the Table; clades A, B, and C are indicated at the right. Scale bar indicates single-nucleotide polymorphisms.

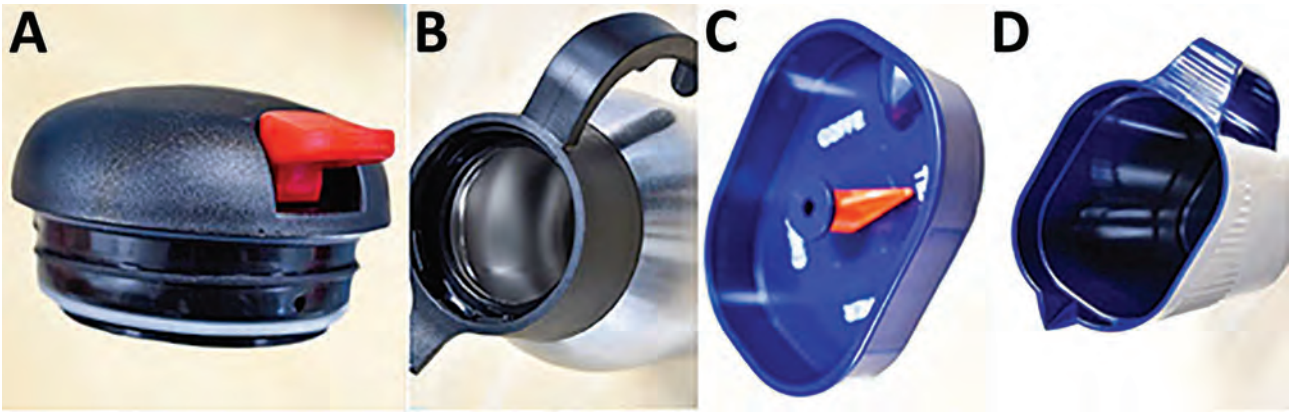

Figure 4. Vacuum flask styles used before and after outbreak of *Saprochaete clavata* at the Institut Paoli-Calmettes, Marseille, France, February 2016–December 2017. A) Old seal; B) old vacuum flask; C) new seal; D) new vacuum flask. The newer model is fully accessible to washing.

including environmental isolates, clustered together into a novel clade, C, different from the previously identified clades. Identifying a unique clade suggested a common source for the contamination, which was restricted to this cancer center in Marseille. Of note, a single case diagnosed in the cancer center in 2015 did not belong to clades A, B, or C and was thus considered a sporadic case.

Our investigation found that a dishwasher made available to patients in the kitchen of the stem cell transplant ward had been the vector of contamination. The fact that patient 4 had been hospitalized in neither the stem cell transplant ward nor the hematology ward before being infected leaves open the hypothesis that contaminated food, of an unknown source, could have contaminated utensils and then the dishwashers, which became vectors of *S. clavata* for other patients. This transmission scheme is supportable using our findings: the contaminated milk or coffee pitchers were used in both hematology and stem cell transplant units; environmental and clinical isolates clustered within the same clade; and the outbreak ended after we removed the pitchers, replaced the contaminated and potentially dysfunctional dishwasher in the stem cell transplant ward, and disinfected the dishwasher in the central kitchen.

Our findings suggest that food-related household appliances, such as dishwashers, can be anthropophilic ecologic niches for *S. clavata* and other life-threatening fungi. Combined with the trend toward providing patients a low-bacterial diet rather than a sterile diet (*21*), this possibility increases the potential for contaminated food. Therefore, routine procedures to protect severely ill patients from airborne or contact contamination should include regular microbiologic sampling, dishwasher testing and maintenance, and controlling the supply and distribution of food. In general, these findings stress the need for continuous extensive vigilance in hospital settings.

Acknowledgments

We thank the Mutualized Platform of Microbiology (P2M) of Institut Pasteur for whole-genome sequencing.

This work used the computational and storage services (TARS cluster) provided by the IT department at Institut Pasteur, Paris. This work was supported by Institut Pasteur and Santé Publique France.

About the Author

Dr. Menu is a researcher and practitioner at the University Hospital Institute Méditerranée Infection, Marseille, France, in the fields of parasitology and mycology. Her research interests include epidemiology and the development of new diagnostic methods for infectious parasitic and mycologic diseases.

References

1. Vaux S, Criscuolo A, Desnos-Ollivier M, Diancourt L, Tarnaud C, Vandenbogaert M, et al.; Geotrichum Investigation Group. Multicenter outbreak of infections by *Saprochaete clavata*, an unrecognized opportunistic fungal pathogen. mBio. 2014;5: e02309–14. https://doi.org/10.1128/mBio.02309-14
2. Del Principe MI, Sarmati L, Cefalo M, Fontana C, De Santis G, Buccisano F, et al. A cluster of *Geotrichum clavatum* (*Saprochaete clavata*) infection in haematological patients: a first Italian report and review of literature. Mycoses. 2016;59:594–601. https://doi.org/10.1111/myc.12508
3. Bouza E, Muñoz P. Invasive infections caused by *Blastoschizomyces capitatus* and *Scedosporium* spp. Clin Microbiol Infect. 2004;10(Suppl 1):76–85. https://doi.org/10.1111/j.1470-9465.2004.00842.x
4. García-Ruiz JC, López-Soria L, Olazábal I, Amutio E, Arrieta-Aguirre I, Velasco-Benito V, et al. Invasive infections

caused by *Saprochaete capitata* in patients with haematological malignancies: report of five cases and review of the antifungal therapy. Rev Iberoam Micol. 2013;30:248–55. https://doi.org/10.1016/j.riam.2013.02.004
5. Bouakline A, Lacroix C, Roux N, Gangneux JP, Derouin F. Fungal contamination of food in hematology units. J Clin Microbiol. 2000;38:4272–3. https://doi.org/10.1128/JCM.38.11.4272-4273.2000
6. Zalar P, Novak M, de Hoog GS, Gunde-Cimerman N. Dishwashers—a man-made ecological niche accommodating human opportunistic fungal pathogens. Fungal Biol. 2011;115:997–1007. https://doi.org/10.1016/j.funbio.2011.04.007
7. Girmenia C, Pagano L, Martino B, D'Antonio D, Fanci R, Specchia G, et al.; GIMEMA Infection Program. Invasive infections caused by *Trichosporon* species and *Geotrichum* capitatum in patients with hematological malignancies: a retrospective multicenter study from Italy and review of the literature. J Clin Microbiol. 2005;43:1818–28. https://doi.org/10.1128/JCM.43.4.1818-1828.2005
8. Bretagne S, Renaudat C, Desnos-Ollivier M, Sitbon K, Lortholary O, Dromer F; French Mycosis Study Group. Predisposing factors and outcome of uncommon yeast species-related fungaemia based on an exhaustive surveillance programme (2002–14). J Antimicrob Chemother. 2017;72:1784–93. https://doi.org/10.1093/jac/dkx045
9. Arendrup MC, Boekhout T, Akova M, Meis JF, Cornely OA, Lortholary O; European Society of Clinical Microbiology and Infectious Diseases Fungal Infection Study Group; European Confederation of Medical Mycology. ESCMID and ECMM joint clinical guidelines for the diagnosis and management of rare invasive yeast infections. Clin Microbiol Infect. 2014;20(Suppl 3):76–98. https://doi.org/10.1111/1469-0691.12360
10. Stanzani M, Cricca M, Sassi C, Sutto E, De Cicco G, Bonifazi F, et al. *Saprochaete clavata* infections in patients undergoing treatment for haematological malignancies: a report of a monocentric outbreak and review of the literature. Mycoses. 2019;62:1100–7. https://doi.org/ 10.1111/myc.12978
11. Buchta V, Bolehovská R, Hovorková E, Cornely OA, Seidel D, Žák P. *Saprochaete clavata* invasive infections – a new threat to hematological-oncological patients. Front Microbiol. 2019;10:2196. https://doi.org/10.3389/fmicb.2019.02196
12. Durán Graeff L, Seidel D, Vehreschild MJGT, Hamprecht A, Kindo A, Racil Z, et al.; FungiScope Group. Invasive infections due to *Saprochaete* and *Geotrichum* species: report of 23 cases from the FungiScope Registry. Mycoses. 2017;60:273–9. https://doi.org/10.1111/myc.12595
13. Cassagne C, Normand A-C, Bonzon L, L'Ollivier C, Gautier M, Jeddi F, et al. Routine identification and mixed species detection in 6,192 clinical yeast isolates. Med Mycol. 2016;54:256–65. https://doi.org/10.1093/mmy/myv095
14. Li H. Minimap2: pairwise alignment for nucleotide sequences. Bioinformatics. 2018;34:3094–100. https://doi.org/10.1093/bioinformatics/bty191
15. Nguyen L-T, Schmidt HA, von Haeseler A, Minh BQ. IQ-TREE: a fast and effective stochastic algorithm for estimating maximum-likelihood phylogenies. Mol Biol Evol. 2015;32:268–74. https://doi.org/10.1093/molbev/msu300
16. Trabelsi H, Néji S, Gargouri L, Sellami H, Guidara R, Cheikhrouhou F, et al. *Geotrichum capitatum* septicemia: case report and review of the literature. Mycopathologia. 2015;179:465–9. https://doi.org/10.1007/s11046-015-9869-2
17. Gurgui M, Sanchez F, March F, Lopez-Contreras J, Martino R, Cotura A, et al. Nosocomial outbreak of *Blastoschizomyces capitatus* associated with contaminated milk in a haematological unit. J Hosp Infect. 2011;78:274–8. https://doi.org/10.1016/j.jhin.2011.01.027
18. Benedict K, Chiller TM, Mody RK. Invasive fungal infections acquired from contaminated food or nutritional supplements: a review of the literature. Foodborne Pathog Dis. 2016;13:343–9. https://doi.org/10.1089/fpd.2015.2108
19. Desnos-Ollivier M, Blanc C, Garcia-Hermoso D, Hoinard D, Alanio A, Dromer F. Misidentification of *Saprochaete clavata* as *Magnusiomyces capitatus* in clinical isolates: utility of internal transcribed spacer sequencing and matrix-assisted laser desorption ionization–time of flight mass spectrometry and importance of reliable databases. J Clin Microbiol. 2014;52:2196–8. https://doi.org/10.1128/JCM.00039-14
20. Fröhlich-Wyder M-T, Arias-Roth E, Jakob E. Cheese yeasts. Yeast. 2019;36:129–41. https://doi.org/10.1002/yea.3368
21. van Dalen EC, Mank A, Leclercq E, Mulder RL, Davies M, Kersten MJ, et al. Low bacterial diet versus control diet to prevent infection in cancer patients treated with chemotherapy causing episodes of neutropenia. Cochrane Database Syst Rev. 2016;4:CD006247. https://doi.org/10.1002/14651858.CD006247.pub3

Address for correspondence: Françoise Dromer, Institut Pasteur, Molecular Mycology Unit, 28 rue du Docteur Roux, 75015 Paris, France; email : dromer@pasteur.fr

Q Fever Osteoarticular Infection in Children

Halima Dabaja-Younis, Michal Meir, Anat Ilivizki, Daniela Militianu, Mark Eidelman, Imad Kassis,[1] Yael Shachor-Meyouhas[1]

Medscape EDUCATION ACTIVITY

In support of improving patient care, this activity has been planned and implemented by Medscape, LLC and Emerging Infectious Diseases. Medscape, LLC is jointly accredited by the Accreditation Council for Continuing Medical Education (ACCME), the Accreditation Council for Pharmacy Education (ACPE), and the American Nurses Credentialing Center (ANCC), to provide continuing education for the healthcare team.

Medscape, LLC designates this Journal-based CME activity for a maximum of 1.00 ***AMA PRA Category 1 Credit(s)™***. Physicians should claim only the credit commensurate with the extent of their participation in the activity.

Successful completion of this CME activity, which includes participation in the evaluation component, enables the participant to earn up to 1.0 MOC points in the American Board of Internal Medicine's (ABIM) Maintenance of Certification (MOC) program. Participants will earn MOC points equivalent to the amount of CME credits claimed for the activity. It is the CME activity provider's responsibility to submit participant completion information to ACCME for the purpose of granting ABIM MOC credit.

All other clinicians completing this activity will be issued a certificate of participation. To participate in this journal CME activity: (1) review the learning objectives and author disclosures; (2) study the education content; (3) take the post-test with a 75% minimum passing score and complete the evaluation at http://www.medscape.org/journal/eid; and (4) view/print certificate. For CME questions, see page 2308.

Release date: August 18, 2020; Expiration date: August 18, 2021

Learning Objectives

Upon completion of this activity, participants will be able to:

- Examine the laboratory evaluation of suspected Q fever osteoarticular infection among children
- Analyze diagnostic criteria for Q fever osteoarticular infection among children
- Distinguish joints affected by Q fever osteoarticular infection in the current study
- Assess the management of Q fever osteoarticular infection among children

CME Editor

Dana C. Dolan, BS, Copyeditor, Emerging Infectious Diseases. *Disclosure: Dana C. Dolan, BS, has disclosed no relevant financial relationships.*

CME Author

Charles P. Vega, MD, Health Sciences Clinical Professor of Family Medicine, University of California, Irvine School of Medicine, Irvine, California. *Charles P. Vega, MD, has disclosed the following relevant financial relationships: served as an advisor or consultant for Johnson & Johnson Pharmaceutical Research & Development, LLC; GlaxoSmithKline; served as a speaker or a member of a speakers bureau for Genentech; GlaxoSmithKline.*

Authors

Disclosures: ***Halima Dabaja-Younis, MD; Michal Meir, MD; Anat Ilivizki, MD; Daniela Militianu, MD; Mark Eidelman, MD; Imad Kassis, MD;*** *and* ***Yael Shachor-Meyouhas, MD,*** *have disclosed no relevant financial relationships.*

Q fever osteoarticular infection in children is an underestimated disease. We report 3 cases of Q fever osteomyelitis in children and review all cases reported in the literature through March 2018. A high index of suspicion is encouraged in cases of an unusual manifestation, prolonged course, relapsing symptoms, nonresolving or slowly resolving osteomyelitis, culture-negative osteomyelitis, or bone histopathology demonstrating granulomatous changes. Urban residence or lack of direct exposure to animals does not rule out infection. Diagnosis usually requires use of newer diagnostic modalities. Optimal antimicrobial therapy has not been well established; some case-patients may improve spontaneously or during treatment with a β-lactam. The etiology of treatment failure and relapse is not well understood, and tools for follow-up are lacking. Clinicians should be aware of these infections in children to guide optimal treatment, including choice of antimicrobial drugs, duration of therapy, and methods of monitoring response to treatment.

Author affiliation: Ruth Rappaport Children's Hospital and Bruce Rappaport Faculty of Medicine, Haifa, Israel

DOI: https://doi.org/10.3201/eid2609.191360

[1]These authors contributed equally to the study and article.

Q fever is a zoonotic disease caused by the intracellular bacterium *Coxiella burnetii*. Persistent focalized Q fever infection in adults mainly manifests as endocarditis or as an endovascular infection. Cases of osteoarticular infection (OAI) have been scantly reported in the literature, rarely in children (*1*,*2*). Disease severity varies, similar to the clinical variations reported in adult patients (*1*).

C. burnetii infections are endemic to Israel. Because diagnosis requires a high level of suspicion, an increase in diagnoses over time may be partly related to physician awareness of the disease rather than true higher incidence (*3*). An observational study of 2,434 cases of *C. burnetii* infection in France (*4*) reported 58 pediatric cases, among which 22 (38%) were OAIs. This large study described the clinical characteristics of Q fever, the less common manifestations of Q fever such as lymphadenitis and lymphoma, and identified risk factors and screening tools predicting complications and death.

Because *C. burnetii* bacteria do not grow in standard laboratory cultures, serology is the first-line diagnostic method for *C. burnetii* infection. Phase II antibodies are predominant during primary infection and Phase I antibodies in persistent infection. Cutoffs of titers considered positive are debated and vary in different countries (*5*,*6*). Immunofluorescence assay (IFA) remains the preferred serology test because of its simplicity and accuracy. Complement fixation test (CFT) is more widely used despite its lower sensitivity (*1*,*2*,*5*). Immunohistochemistry and quantitative PCR of *C. burnetii*–infected tissues are also available (*5*,*6*).

Diagnosis may be aided by clinical criteria. One definite criterion, 2 major criteria, or 1 major and 3 minor criteria are needed for definitive diagnosis of persistent Q fever. Definite criteria include a positive result on culture, PCR, or immunochemistry of bone, synovial biopsy, or joint aspirate. Major criteria include positive blood culture or PCR, phase I IgG antibodies ≥800, evidence of bone or joint involvement by computed tomography scan, ultrasonography, magnetic resonance imaging (MRI), or abnormal positron emission tomography scan or indium leukocyte scan. Minor criteria include phase I IgG titer of 400–800 mg/dL, temperature ≥38°C, and mono- or polyarthralgia. These last diagnostic criteria have been proposed to enable diagnosis of *C. burnetii* persistent infection in cases in which titers are below the serologic cutoff (*5*). Other studies use a higher serology cutoff of phase I IgG ≥1,024 (*6*).

Optimal antimicrobial treatment for chronic Q fever OAI has not been well established. Pediatric treatment recommendations in Q fever OAI are based on treatment of Q fever endocarditis in adults (*7*). We describe 3 cases of Q fever osteomyelitis in children in Israel and a review of the related literature.

Case 1

A previously healthy 3-year-old boy was admitted for care with a limp of his right leg and swelling of his right ankle that began 3 weeks before admission. He had no history of trauma and had no fever or other systemic signs of infection. Results of complete blood count (CBC), C-reactive protein (CRP), and radiographic studies at admission were normal. MRI was performed and showed a lytic lesion in the talus bone, suspected to be a malignant space-occupying lesion (Figure 1). Open-bone biopsy was thus performed. Pathology revealed an acute inflammatory process with neutrophil and lymphocyte predominance, giant cells, and an epithelioid granuloma without necrosis, suggesting an infectious process (Figure 1). A swab sample from the tissue was found to be sterile despite the lack of previous antimicrobial therapy. Fungal and mycobacterial PCR results from the paraffin-embedded specimen were negative. Repeated physical examinations revealed signs of cellulitis around the surgical wound with no other systemic manifestations. The patient was treated with a first-generation cephalosporin for 6 weeks, and his clinical signs and symptoms were resolved completely.

Six months after his discharge, the child experienced swelling and mild cellulitis around his right ankle with no other symptoms. Synovial fluid from the ankle was sampled; bacterial, fungal, and mycobacterial cultures were all negative. The patient then recovered without any treatment. At 1 year after his initial admission, the patient experienced cellulitis at the same site. He was in good general health with no

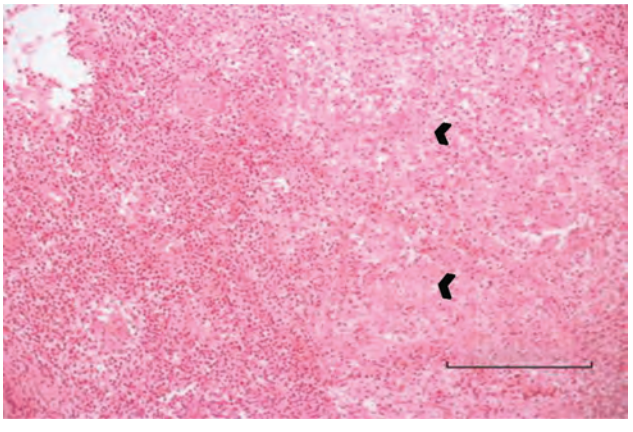

Figure 1. Bone biopsy specimen for a 3-year-old boy (case 1) with Q fever osteoarticular infection, Israel. Hematoxylin and eosin stain shows an acute inflammatory process with neutrophil and lymphocyte predominance. Small arrows indicate giant cells and epithelioid granuloma without necrosis. Bar indicates the diameter of a giant granuloma.

systemic signs of infection. Fluid aspirated from the right ankle, identified as pus, was cultured and analyzed using 16SrRNA PCR. Antimicrobial therapy with a first-generation cephalosporin was reinitiated, with good clinical response. Later in the treatment period, PCR results were found to be positive for C. burnetii; a positive PCR result is a definite criterion (5,8). IFA confirmed the diagnosis with high titer for phase I IgG, 1:6,400. Transthoracic echocardiography performed 1 month after diagnosis showed no valve involvement.

In light of clinical and radiological evidence of chronic osteomyelitis along with laboratory evidence (positive 16Sr RNA PCR and positive serologic results for *C. burnetii*), the patient was treated for persistent focalized Q fever. Treatment regimen included ciprofloxacin and rifampin for 12 months; full clinical and complete radiological resolution resulted.

Six years after his first infection, after being asymptomatic for 4 years, the patient again experienced pain and tenderness of the contralateral (left) foot and ankle without fever or systemic signs. Results of laboratory studies were unremarkable, but MRI of the ankle showed a Brodie's abscess of the distal tibia and sonography of the ankle showed a small amount of fluid. Results of testing for 16SrRNA from synovial fluid was negative. IFA revealed high titers for phase I IgG, 1:3,200. On the basis of the patient's history, clinical signs, and serology, treatment was begun with doxycycline, hydroxychloroquine, and rifampin. Shortly after treatment was started, the patient reported a new elbow pain. MRI study of the right elbow showed synovitis of the elbow and Brodie's abscess of the distal humerus. Based on the presumed diagnosis of Q fever multifocal recurrent osteomyelitis, triple antibiotic treatment was continued, and substantial improvement was seen by 4 months later. MRI study at the end of treatment revealed complete resolution of all pathological findings. Nearly 12 months after completing his treatment, the patient was asymptomatic.

Case 2

A previously healthy 2-year-old boy experienced limping for >3 weeks and had a recurrent low-grade fever in the week before admission. He had no history of trauma, exposure to animals, or ingestion of unpasteurized dairy products. At the time of admission, a physical examination noted obvious limping on his left leg but no localized tenderness or focal inflammatory signs. Results of CBC, CRP, and radiographic imaging of his lower limbs were unremarkable. Nuclear imaging (Technetium bone scan) demonstrated an increased signal in the talus of his left ankle (Figure 2, panel A). MRI study of the left ankle showed an intramedullary lesion of the talus compatible with an abscess (Figure 2, panels B, C, D). Empiric treatment with intravenous first-generation cephalosporin was initiated. After 2 weeks of therapy, the patient was only mildly improved. Bone biopsy was not performed because the location of the lesion was unreachable; serology for *C. burnetii* was performed, considering the prolonged symptoms and suboptimal response to therapy. After 6 weeks of antimicrobial therapy, although the patient no longer had symptoms or signs of infection, the *C. burnetii* serology result was unexpectedly positive: phase I IFA IgG titer was 1:200.

Confirmatory serology performed 2 weeks later showed a phase I IFA IgG titer of 1:800. At that time, the patient remained asymptomatic. A repeated MRI of the ankle showed the same lesion with no major changes. Results of a transthoracic echocardiogram, performed 3 months after initial care because of concern for possible endocarditis, were unremarkable. Considering the chronic course of Q fever OAI and the risk for relapse or progression to other manifestations, combined therapy of rifampin and trimethoprim/sulfamethoxazole (TMP/SMX) was initiated. The patient completed 1 year of treatment, throughout which he continued to be asymptomatic. MRI 12 months after treatment showed complete resolution of the primary talar lesion. Phase I IFA IgG titer at the end of treatment was 1:200.

Case 3

A previously healthy 3-year-old boy experienced swelling and tenderness over his left foot and calcaneus for 6 months before his admission. His body temperature was normal over that period, and he had no systemic signs of infection. Two falls and mild bruises of the same leg were reported around the time his symptoms began. The patient lived in a rural area and was exposed to livestock. Results of CBC, CRP, erythrocyte sedimentation rate (ESR), and radiographic studies conducted at the time of admission were unremarkable. MRI demonstrated synovitis of the small joints of the midfoot (Figure 3). The patient underwent fine-needle aspiration of the ankle, which was technically difficult. Synovial fluid from this aspiration was sterile despite no previous antimicrobial therapy; results of 16SrRNA and specific PCR for *C. burnetii* were negative.

Serology for Q fever was positive with high titer of phase I IgG, 1:1600, and of phase II, 1:1600, in IFA. Transthoracic echocardiography performed 1 month later showed no cardiac valve involvement. On the basis of the suggestive clinical signs, potential exposure

Figure 2. Imaging of the left ankle for a 2-year-old boy (case 2) with Q fever osteoarticular infection, Israel. A) A nuclear bone scan showing uptake in the talus (arrow). B–D) Magnetic resonance imaging sagittal T1 (B), sagittal T1 fat saturation + contrast (C), and sagittal short-TI inversion recovery (D) showing a lesion (white arrows) in the posterior aspect of the talus, noted to be an intramedullary Brodie's abscess in evolution, surrounded by intramedullary edema and accompanied by fluid in the joint.

to farm animals, and positive serology for *C. burnetii*, the patient was treated with rifampin and TMP/SMX for Q fever OAI. Repeated serology showed increasing titers: IgG phase II up to 6,400, and IgG phase I up to 3,200. Despite 8 months of antimicrobial treatment, the patient remained symptomatic with debilitating pain. MRI performed at that time revealed synovitis and osteomyelitis with intramedullary abscesses in the small bones of the midfoot, not amenable for drainage. Twelve months into his antimicrobial therapy, his health had improved overall, with decreasing pain and decreasing IgG phase I titers.

Literature Review

A review of the literature revealed 8 articles describing 29 pediatric cases of OAI caused by *C. burnetii* (*9*–*16*) (Appendix Table, https://wwwnc.cdc.gov/EID/article/26/9/19-1360-App1.xlsx). One of the 3 cases we describe was also described briefly in a published case series (*16*). Of the 31 total patients described, 24 (77.41%) were male; 29 (93.54%) were <10 years of age. All were previously healthy except for 1 patient who had acute lymphoblastic leukemia. Exposure to livestock or household animals was reported in most cases. Only 5 of 10 patients in Israel, including 2 of our 3 case-patients, led urban lifestyles (*9*–*16*).

Clinical manifestations were subtle or occult for 20 (65%) patients. In cases in which laboratory tests were reported, CBC and CRP results were mostly within reference ranges. ESR values, considered superior to other acute-phase reactants for assessment of chronic infections, were not reported for most cases of Q fever OAI.

In cases in which biopsies were performed, histology was consistent with inflammation and noncaseating granulomas. Results of bone or synovial biopsy and joint aspirate cultures were always negative; results for 16-S rRNA gene PCR for *C. burnetii* were positive in most of the joint aspirate cultures. In 16 (52%) cases, bone lesions were surgically debrided.

Most patients received combined therapy for 6–36 months. One case-patient was treated for a limited duration of 6 weeks with good initial response, but no data regarding long-term recovery were available. Three patients received no antimicrobial therapy, but they all underwent surgical debridement. Evidence of relapse was noted in 1 of those patients; data were unavailable for the other 2 patients because the follow-up period for those was brief.

In 18/31 cases (58%), the disease was multifocal, and in most cases a relapsing-remitting course was observed regardless of appropriate antimicrobial treatment. Eleven (35%) of 31 children had ≥1 recurrence; others had no reported recurrence. The observation of no recurrence may be biased; some cases were published shortly after completion of the patients' course of antimicrobial treatment, which precluded a substantial follow-up period (*9*–*16*). In cases in which serology was monitored during and after treatment, serology remained unchanged or even increased during follow-up, which can be explained by the unreliable role of serology as a test of cure in this disease (*9*–*16*).

Discussion

We describe 3 cases of definite *C. burnetii* OAI in children and provide a review of the literature for these cases. Diagnosis for these 3 patients was defined by the prolonged clinical symptoms associated with microbiological evidence. Major criteria including clinical evidence of OAI, bone or joint involvement visible on MRI, and diagnostic serologic titer were found in all 3 cases. The first case also had a positive *C. burnetii* PCR as a definite criterion (*5*,*8*).

Our review of the published cases with chronic Q fever OAI sheds additional light on this often underdiagnosed and easily missed infectious disease. A high index of suspicion is encouraged in cases of an unusual case manifestation, a chronic or subacute course, relapsing symptoms and signs, nonresolving or slowly resolving osteomyelitis, culture-negative osteomyelitis, exposure history to farm animals, or bone histology demonstrating granulomatous changes (*7*). Some cases improve spontaneously or during treatment with a β-lactam, which is not active against *C. burnetii*, and have no obvious rural contact, making diagnosis more challenging. Optimal antimicrobial therapy for chronic Q fever OAI has not been well established.

Current treatment recommendations are based on case series, retrospective cohort studies, and in vitro data. In the 3 cases we describe, the choice of treatment was based on recent literature and the safety and availability of the suggested drugs for the specific patient. The patient in case 1 was treated with ciprofloxacin and rifampin. Doxycycline therapy is considered ill-advised in children <8 years of age because of its side effects of teeth staining and weakening of enamel, especially in prolonged treatment. Of note, the US Centers for Disease Control and Prevention (CDC) in 2013 recommended the of use of doxycycline at a dose of 2.2 mg/kg twice per day for 2 weeks in children <8 years of age for the treatment of acute and chronic Q fever in United States (*17*). However, Q fever OAI requires a much longer treatment period with doxycycline, with a higher likelihood and potential for long-term adverse effects. Doxycycline is not approved in Israel for chronic use in children <8 years of age. Hydroxycholoroquine was not available in a liquid form and required special pharmacy preparation which could interfere with treatment continuity.

We diagnosed OAI in the other 2 case-patients shortly after the recurrence of osteomyelitis in case-patient 1. Considering the recurrence occurred while this patient was under treatment with ciprofloxacin and rifampin, we considered treatment failure using this regimen and therefore chose rifampin and TMP/SMX for the other 2 patients. TMP/SMX has been used in combination with doxycycline, ciprofloxacin, or rifampin according to reports available at that time (*11*,*12*).

The standard treatment of Q fever–persistent focalized infection in adult patients is hydroxychloroquine and doxycycline; this regimen leads to fewer recurrences. Minimal treatment duration in persistent infections is 18 months; we have no evidence to determine the duration of doxycycline and hydroxychloroquine therapy (*8*,*18*,*19*). The effectiveness of this therapy is likely to result from the alkalizing effect of chloroquine and its derivative, the hydroxyl, on lysosomal compartments, thus enabling improved doxycycline activity (*20*).

For children <8 years old, treatment with TMP/SMX or rifampin is preferred because of the risk for dental staining with prolonged tetracycline therapy (*7*). In vitro studies showed complete susceptibility to rifampin, TMP/SMX, and tetracyclines; heterogenous

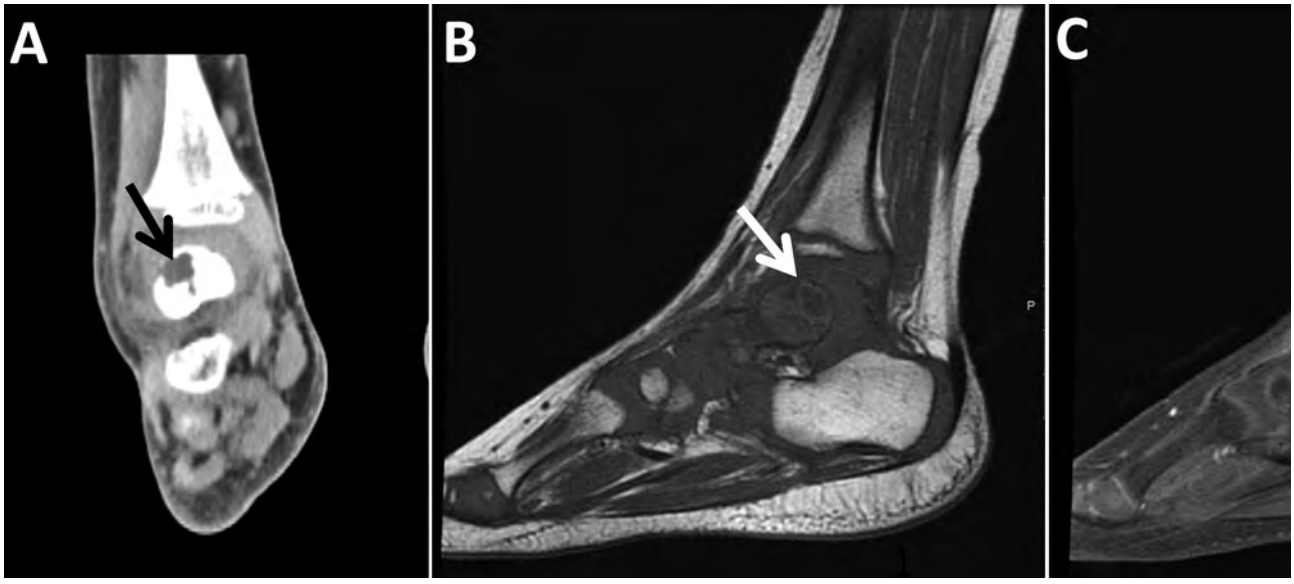

Figure 3. Imaging of the left ankle for a 3-year-old boy (case 3) with Q fever osteoarticular infection, Israel. A) Computed tomography imaging, coronal view, shows a lytic lesion in the talus (black arrow). B, C) Magnetic resonance imaging sagittal T1 (B) and sagittal T1 fat saturation + contrast (C) demonstrate a lesion in the posterior aspect of the talus (white arrows), determined to be an intramedullary abscess (Brodie's abscess) surrounded by edema.

susceptibility to fluoroquinolones and erythromycin; and a little inhibitory growth effect of β-lactam antimicrobial drugs (*21*). Studies show no consensus regarding optimal treatment duration of Q fever OAI in children. Minimum treatment duration was 6 months in most of the cases reviewed. Appropriate drug therapy did not necessarily prevent recurrences; in 16 (53%) cases, patients required surgical intervention despite adequate antimicrobial therapy (*9*–*16*). In addition to antimicrobial and surgical treatment, immunomodulatory agents including interferon gamma were found to be effective in vitro and in some case reports of chronic Q fever (*10*,*22*).

The etiology of treatment failure and relapse in Q fever OAI is not well understood. We were not able to conclude which treatment regimen was associated with the lowest recurrence rate; the same treatment regimens led to cure in some cases and treatment failure or relapse in others. We observed clinical recurrence and increasing antibody titers despite extended combined antimicrobial drug therapy (*23*).

Whether recurrence is related to reduced drug levels is unknown. In most cases, drug levels in blood or hair samples was not considered. In our institution, these tests were not routinely available. Doxycycline hair level assay testing to determine long-term compliance was deemed unnecessary because most of our patients were too young for treatment with doxycycline. No documentation of compliance was described; however, in our 3 cases, parents reported orange-stained urine during follow-up visits, indicating good compliance for rifampin. Our physicians had also evaluated parents administering medications as caring, dedicated, and reliable. Another factor that may explain the nonnegligible rate of recurrence is the dormancy of the intracellular bacterium. These dormant infectious particles turn to metabolically active in response to acidification of the endosome and are associated with the development of the parasitephorous vacuoles that allow the organism to replicate repeatedly (*24*,*25*).

Tools for follow-up are lacking. Acute-phase reactants were absent or only mildly elevated in in 17/20 (85%) cases, in which laboratory data were documented. Radiographic resolution is not expected over a period of several weeks. Serology may not change throughout the first years following clinical cure (*2*,*5*,*7*). We did not user newer imaging tools such as the 18F FDG-PET/CT described in recent studies (*4*,*5*,*26*) for follow-up in our cases.

In summary, pediatric OAI with prolonged course or inadequate response to empiric treatment should raise the suspicion of unusual pathogens such as *C. burnetii*. Further studies are needed to guide optimal treatment of Q fever OAI, including choice of antimicrobial drugs, duration of therapy, and methods of monitoring response to treatment. Diagnosis of Q fever OAI requires increased awareness and use of newer diagnostic modalities, and urban residence or lack of direct exposure to animals does not rule out infection, especially in countries in which Q fever is endemic.

About the Author

Dr. Dabaja-Younis is a pediatrician and infectious diseases consultant at Rambam Health Care Campus in Haifa, Israel, where she serves as infection control unit director in charge. Her main research areas are epidemiology and infection control.

References

1. Maltezou HC, Raoult D. Q fever in children. Lancet Infect Dis. 2002;2:686–91. https://doi.org/10.1016/S1473-3099(02)00440-1
2. Raoult D, Tissot-Dupont H, Foucault C, Gouvernet J, Fournier PE, Bernit E, et al. Q fever 1985–1998: clinical and epidemiologic features of 1,383 infections. Medicine (Baltimore). 2000;79:109–23. https://doi.org/10.1097/00005792-200003000-00005
3. Bishara J, Pitlik S, Yagupsky P, Hershkovitz D. Comparative incidence of acute Q fever in two ethnic groups in Israel. Eur J Clin Microbiol Infect Dis. 2004;23:224–5. https://doi.org/10.1007/s10096-003-1095-z
4. Melenotte C, Protopopescu C, Million M, Edouard S, Carrieri MP, Eldin C, et al. Clinical features and complications of *Coxiella burnetii* infections from the French National Reference Center for Q fever. JAMA Netw Open. 2018;1:e181580. https://doi.org/10.1001/jamanetworkopen.2018.1580
5. Eldin C, Mélenotte C, Mediannikov O, Ghigo E, Million M, Edouard S, et al. From Q fever to *Coxiella burnetii* infection: a paradigm change. Clin Microbiol Rev. 2017;30:115–90. https://doi.org/10.1128/CMR.00045-16
6. Anderson A, Bijlmer H, Fournier PE, Graves S, Hartzell J, Kersh GJ, et al. Diagnosis and management of Q fever—United States, 2013: recommendations from CDC and the Q Fever Working Group. MMWR Recomm Rep. 2013;62(RR-03):1–30.
7. Howard-Jones AR, Isaacs D. Systematic review of duration and choice of systemic antibiotic therapy for acute haematogenous bacterial osteomyelitis in children. J Paediatr Child Health. 2013;49:760–8. https://doi.org/10.1111/jpc.12251
8. Melenotte C, Million M, Raoult D. New insights in *Coxiella burnetii* infection: diagnosis and therapeutic update. Expert Rev Anti Infect Ther. 2020;18:75–86. https://doi.org/10.1080/14787210.2020.1699055
9. Britton PN, Macartney K, Arbuckle S, Little D, Kesson A. A rare case of Q fever osteomyelitis in a child from regional Australia. J Pediatric Infect Dis Soc. 2015;4:e28–31. https://doi.org/10.1093/jpids/piu095
10. Neth OW, Falcon D, Peromingo E, Soledad Camacho M, Rodríguez-Gallego C, Obando I. Successful management

of chronic multifocal Q fever osteomyelitis with adjuvant interferon-gamma therapy. Pediatr Infect Dis J. 2011;30:810–2. https://doi.org/10.1097/INF.0b013e31821487f5
11. Nourse C, Allworth A, Jones A, Horvath R, McCormack J, Bartlett J, et al. Three cases of Q fever osteomyelitis in children and a review of the literature. Clin Infect Dis. 2004;39:e61–6. https://doi.org/10.1086/424014
12. Cottalorda J, Jouve JL, Bollini G, Touzet P, Poujol A, Kelberine F, et al. Osteoarticular infection due to *Coxiella burnetii* in children. J Pediatr Orthop B. 1995;4:219–21. https://doi.org/10.1097/01202412-199504020-00018
13. Francis JR, Robson J, Wong D, Walsh M, Astori I, Gill D, et al. Chronic recurrent multifocal Q fever osteomyelitis in children. Pediatr Infect Dis J. 2016;35:972–6. https://doi.org/10.1097/INF.0000000000001211
14. Costa B, Morais A, Santos AS, Tavares D, Seves G, Gouveia C. Q fever chronic osteomyelitis in two children. Pediatr Infect Dis J. 2015;34:1269–71. https://doi.org/10.1097/INF.0000000000000861
15. Khatami A, Sparks RT, Marais BJ. A case of pediatric Q fever osteomyelitis managed without antibiotics. Pediatrics. 2015;136:e1629–31. https://doi.org/10.1542/peds.2015-0024
16. Sachs N, Atiya-Nasagi Y, Beth-Din A, Levy I, Ben-Shimol S, Tasher D et al. Chronic Q fever infections in Israeli children—a 25-year nationwide study. Pediatr Infect Dis J. 2018; 37:3:212-217. https://doi.org/10.1097/INF.0000000000001790
17. Gaillard T, Briolant S, Madamet M, Pradines B. The end of a dogma: the safety of doxycycline use in young children for malaria treatment. Malar J. 2017;16:148. https://doi.org/10.1186/s12936-017-1797-9
18. Million M, Thuny F, Richet H, Raoult D. Long-term outcome of Q fever endocarditis: a 26-year personal survey. Lancet Infect Dis. 2010;10:527–35. https://doi.org/10.1016/S1473-3099(10)70135-3
19. Angelakis E, Edouard S, Lafranchi M-A, Pham T, Lafforgue P, Raoult D. Emergence of Q fever arthritis in France. J Clin Microbiol. 2014;52:1064–7. https://doi.org/10.1128/JCM.03371-13
20. Maurin M, Benoliel AM, Bongrand P, Raoult D. Phagolysosomal alkalinization and the bactericidal effect of antibiotics: the *Coxiella burnetii* paradigm. J Infect Dis. 1992;166:1097–102. https://doi.org/10.1093/infdis/166.5.1097
21. Raoult D, Torres H, Drancourt M. Shell-vial assay: evaluation of a new technique for determining antibiotic susceptibility, tested in 13 isolates of *Coxiella burnetii*. Antimicrob Agents Chemother. 1991;35:2070–7. https://doi.org/10.1128/AAC.35.10.2070
22. Dellacasagrande J, Capo C, Raoult D, Mege JL. IFN-gamma-mediated control of *Coxiella burnetii* survival in monocytes: the role of cell apoptosis and TNF. J Immunol. 1999;162:2259–65.
23. Levy PY, Drancourt M, Etienne J, Auvergnat JC, Beytout J, Sainty JM, et al. Comparison of different antibiotic regimens for therapy of 32 cases of Q fever endocarditis. Antimicrob Agents Chemother. 1991;35:533–7. https://doi.org/10.1128/AAC.35.3.533
24. Marmion BP, Storm PA, Ayres JG, Semendric L, Mathews L, Winslow W, et al. Long-term persistence of *Coxiella burnetii* after acute primary Q fever. QJM. 2005;98:7–20. https://doi.org/10.1093/qjmed/hci009
25. Voth DE, Heinzen RA. Lounging in a lysosome: the intracellular lifestyle of *Coxiella burnetii*. Cell Microbiol. 2007;9:829–40. https://doi.org/10.1111/j.1462-5822.2007.00901.x
26. Eldin C, Melenotte C, Million M, Cammilleri S, Sotto A, Elsendoorn A, et al. ^{18}F-FDG PET/CT as a central tool in the shift from chronic Q fever to *Coxiella burnetii* persistent focalized infection. Medicine (Baltimore). 2016;95:e4287. https://doi.org/10.1097/MD.0000000000004287

Address for correspondence: Halima Dabaja-Younis, Pediatric Infectious Diseases Unit, Ruth Rappaport Children's Hospital, Rambam Health Care Campus, PO Box 9602, Haifa 31096, Israel; email: h_dabaja@rambam.health.gov.il

Web-Based Interactive Tool to Identify Facilities at Risk of Receiving Patients with Multidrug-Resistant Organisms

Rany Octaria, Allison Chan, Hannah Wolford, Rose Devasia, Troy D. Moon, Yuwei Zhu, Rachel B. Slayton, Marion A. Kainer

To identify facilities at risk of receiving patients colonized or infected with multidrug-resistant organisms (MDROs), we developed an interactive web-based interface for visualization of patient-sharing networks among healthcare facilities in Tennessee, USA. Using hospital discharge data and the Centers for Medicare and Medicaid Services' claims and Minimum Data Set, we constructed networks among hospitals and skilled nursing facilities. Networks included direct and indirect transfers, which accounted for ≤365 days in the community outside of facility admissions. Authorized users can visualize a facility of interest and tailor visualizations by year, network dataset, length of time in the community, and minimum number of transfers. The interface visualizes the facility of interest with its connected facilities that receive or send patients, the number of interfacility transfers, and facilities at risk of receiving transfers from the facility of interest. This tool will help other health departments enhance their MDRO outbreak responses.

Antimicrobial resistance (AMR) is an urgent public health threat causing an estimated 2,868,700 infections and 35,900 deaths each year in the United States (*1*). Multidrug-resistant organisms (MDROs), including carbapenem-resistant *Enterobacteriaceae* (CRE), methicillin-resistant *Staphylococcus aureus* (MRSA), and organisms related to antimicrobial drug use and resistance, such as *Clostridioides difficile*, often are the causative agents in healthcare-associated infections (*1*,*2*). Studies show that these pathogens can colonize patients for extended periods of time (*3*). One study found that 38% of patients colonized with CRE were still colonized even a year after discharge from a facility (*4*); such patients can serve as reservoirs for MDROs in the community or in healthcare facilities.

Previous healthcare exposure is a known risk factor for MDRO infections (*5*,*6*). Older adults, patients with underlying medical conditions, and residents of long-term care facilities (LTCFs) are more likely to have multiple healthcare exposures, making them more likely to develop infections (*7*). Movement of patients across healthcare facilities can serve as a means of spreading MDROs across a community and introducing new pathogens into a region. Interfacility patient sharing has been associated with higher incidence of both CRE and *C. difficile* infections (*5*,*8*).

A mathematical modeling study found that facility-level infection prevention measures alone are insufficient to prevent transmissions (*9*). A coordinated approach to contain MDROs among interconnected healthcare facilities and public health reduced acquisition by 74% in a small network model over 5 years and 55% in a large network over 15 years (*9*). Beginning in 2017, the Centers for Disease Control and Prevention (CDC) issued guidance for state and local health departments and healthcare facilities to contain novel MDROs (*10*). The guidance classifies organisms into 3 tiers based on public health threat and outlines the recommended containment approach, which includes a coordinated approach among healthcare facilities, public health, and laboratories (*10*).

Despite numerous research publications on the role patient-sharing networks play in elucidating MDRO transmission, few address the application of these networks in public health practice. We used

Author affiliations: Vanderbilt University Graduate School, Nashville, Tennessee, USA (R. Octaria); Healthcare Associated Infections and Antimicrobial Resistance Program, Tennessee Department of Health, Nashville (R. Octaria, A. Chan, R. Devasia, M.A. Kainer); Centers for Disease Control and Prevention, Atlanta, Georgia, USA (H. Wolford, R.B. Slayton); Vanderbilt University Medical Center, Nashville (T.D. Moon, Y. Zhu, M.A. Kainer)

DOI: https://doi.org/10.3201/eid2609.191691

patient-sharing networks to design tailored strategies to help public health contain the spread of MDROs. We developed an interactive tool to visualize networks of patient sharing among hospitals and skilled nursing facilities (SNFs) in the state of Tennessee. Our tool enabled the Tennessee Department of Health (TDH) to identify facilities at risk of receiving patients suspected to be colonized with AMR pathogens.

Methods

Patient Matching

We constructed interfacility patient-sharing networks from the Tennessee Hospital Discharge Data System (HDDS) inpatient admissions, and Centers for Medicare and Medicaid Services (CMS) claims and Minimum Data Set (MDS; https://www.cms.gov). The HDDS dataset included all inpatient admissions to Tennessee acute-care hospitals (ACHs) licensed by TDH; admission to LTCFs and Department of Veterans Affairs hospitals were not captured in this dataset. We used HDDS data to summarize patient-sharing data among Tennessee facilities, including ACHs critical access hospitals (CAH), long-term acute-care hospitals (LTACH), and inpatient rehabilitation facilities (IRFs) from January 2014–December 2017.

We linked admissions of each patient in the HDDS dataset with a multilevel matching process by using patient identifiers. First, we linked consecutive admissions for ≤365 days by matching the combination of date of birth, sex, and Social Security number (SSN). In this step, we considered admissions of the same person to be those that matched for date of birth, sex, and first and last name, even if the SSN was missing or had a 1-digit difference. Subsequently, we linked admissions that did not generate matches in the first step by matching the combination of date of birth, sex, and full name, even with ≥2-digit differences in the SSN. To protect patient privacy, patient-level admission data used for matching were saved in secured hard-drives that were connected to the computer only when generating facility-level data.

The CMS dataset included claims data and data from the MDS, which captured all inpatient admissions of CMS fee-for-service beneficiaries to Tennessee hospitals and SNFs. We used MDS admission and discharge assessments to identify all visits of Medicare beneficiaries to SNFs, a type of LTCF that is not as intensive as hospital but offers more intensive medical and nursing services, such as subacute care (*11*). We combined MDS visits with CMS claims data that included admissions in all types of hospitals in the HDDS to create a more complete dataset of visits for Medicare beneficiaries. We linked admissions in MDS to patients by matching the CMS beneficiary identification number. We aggregated facilities by using the facilities' CMS certification number, which is different than facility aggregation in the HDDS dataset. The CDC modeling unit conducted aggregation by using the secure environment of the CMS Virtual Research Data Center before sharing the facility-level aggregate data to TDH.

Network Construction

Because of differences in aggregation, we constructed the CMS and HDDS networks separately. The CMS dataset aggregated facilities based on their CMS certification number, but HDDS aggregated based on the assigned Tennessee state licensing registration.

From each data source, we constructed 2 types of networks that connected healthcare facilities through uninterrupted patient sharing (UPS) and total patient sharing (TPS) (*12*). UPS, or direct transfers, connect a pair of facilities when a patient is discharged from 1 facility and admitted directly to another facility within 1 day. We accounted for patients who spent time in the community between healthcare admissions through the TPS network, which connects a pair of facilities through direct and indirect transfers. An indirect transfer occurs when a patient is discharged from 1 facility and readmitted to another facility within 2–365 days. The number of days between consecutive admissions was calculated by subtracting the next admission date and the current discharge date. We constructed subnetworks from the overall TPS network for 30 and 365 days in the community.

In our visualizations, each healthcare facility is represented by a node. A pair of nodes is connected by a line, also known as an edge in network analysis, weighted by the number of 1-way patient shares between pairs of facilities. For example, a patient discharged from a facility on September 30, 2015 and admitted to another on September 29, 2016, represents 1 indirect transfer. A patient can be represented by multiple edges in the same network. For example, if hospital A discharged Mr. X on January 30 and hospital B admitted Mr. X 2 weeks later, the TPS network graph would represent this connection as an edge with a weight of 1 going from node A to node B. If Mr. X is then admitted to SNF C 2 months later, this indirect transfer will be represented only as another edge from node B to C, but not A to C.

Network Analysis

We used an ego network design for the tool; this type of social network consists of a focal node (ego) and the

nodes to which it is connected, directly or indirectly. In our tool, the facility of interest in each web session acts as the ego facility. We defined the following centrality measures for each ego facility by calendar year and by type of network: in-degree, out-degree, weighted in-degree, and weighted out-degree. We defined in-degree as the total number of facilities that sent transfers to a given facility and out-degree as the total number of facilities that received transfers from a given facility (*12*). We defined weighted in-degree as the total number of patient transfers sent to a given facility and weighted out-degree as the total number of patient transfers sent from a given facility (*8*). We used the Fruchterman-Reingold force-directed graph drawing algorithm to assign the relative positions of each facility in the network graph (*13*). We accounted for several characteristics of the healthcare facility, including the type of facility and the Emergency Medical Services (EMS) region in which the facility is located (Figure 1). Tennessee EMS regions represent the referral patterns of the EMS services and hospitals, and the coordinating areas for emergency preparedness activities, which TDH uses to aggregate MDRO surveillance data.

At-risk facilities targeted in public health containment efforts can vary based on the circumstances of each outbreak. For our purposes, we defined at-risk facilities as downstream facilities that historically were identified to have received patients from the ego facility. At-risk facilities also were classified as the facilities receiving the most historical transfers from the ego facility if there were >10 downstream facilities. To evaluate the long-term stability of these identified at-risk facilities in the HDDS network, we evaluated the top downstream facilities of 5 randomly selected ego facilities across different EMS regions from 2014–2017. For each ego facility, we compared the 5 downstream facilities receiving the most transfers between pairs of consecutive years to quantify the aggregate percent change in the top 5 downstream facilities.

Web-Based Application

We developed a password-protected web-based application using Shiny (R Studio Inc., https://www.rstudio.com) to enable public health personnel to access network visualizations and transfer statistics easily. Approved usernames and passwords are managed internally by TDH Healthcare Associated Infections and Antimicrobial Resistance (HAI/AR) program. Authorized users can access the Shiny web application to visualize the network of a facility of interest (ego) through a user-friendly interface at the website, https://tnhealthhai.shinyapps.io/patient-sharing (Figure 2). The ego facility is the facility of interest that serves as the center of the visualized network for the current online session. Users can select from menus to tailor the displayed plot based on the data source, HDDS or MDS; year; length of interim time in the community; and the ego facility.

In the network plot, the node color represents Tennessee EMS regions, node size represents number of beds, and node shape represents facility type. The thickness of the edge is weighted on the number of 1-way transfers, including multiple transfers of 1 patient, between a facility pair. When users place the cursor over a node, the tooltip function displays the facility name, facility type, and number of beds. A slider widget enables users to set the lower threshold of 1-way transfers between each pair of facilities displayed for the session (Figure 2).

The Shiny application has 2 display tabs, plot and transfer statistics. The plot tab displays a visualization of the ego-network and all facilities that shared patients with the ego facility (Figure 3). When users hover the cursor over an edge, the application displays the number of 1-way transfers. Users can interact by applying filters for region or facility of interest, and by dragging the position of different nodes.

The transfer statistics tab displays facility-level characteristics and facilities most at risk to

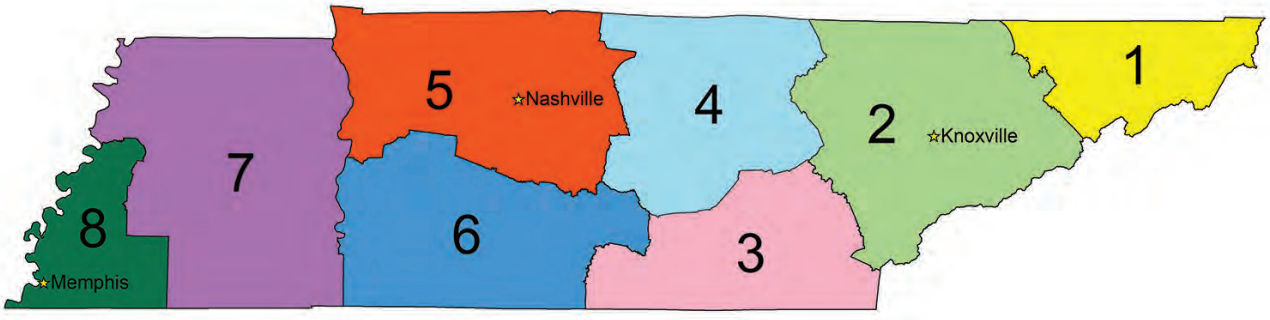

Figure 1. Emergency Medical Services (EMS) regions in Tennessee, USA: 1) Northeast; 2) East; 3) Southeast; 4) Upper Cumberland; 5) Mid-Cumberland; 6) South Central; 7) West; and 8) Memphis-Delta. The 8 EMS regions represent the referral patterns for EMS services and hospitals and for coordination for emergency preparedness activities. The Tennessee Department of Health uses EMS regions to aggregate multidrug-resistant organisms surveillance data. Stars indicate metropolitan areas within EMS regions.

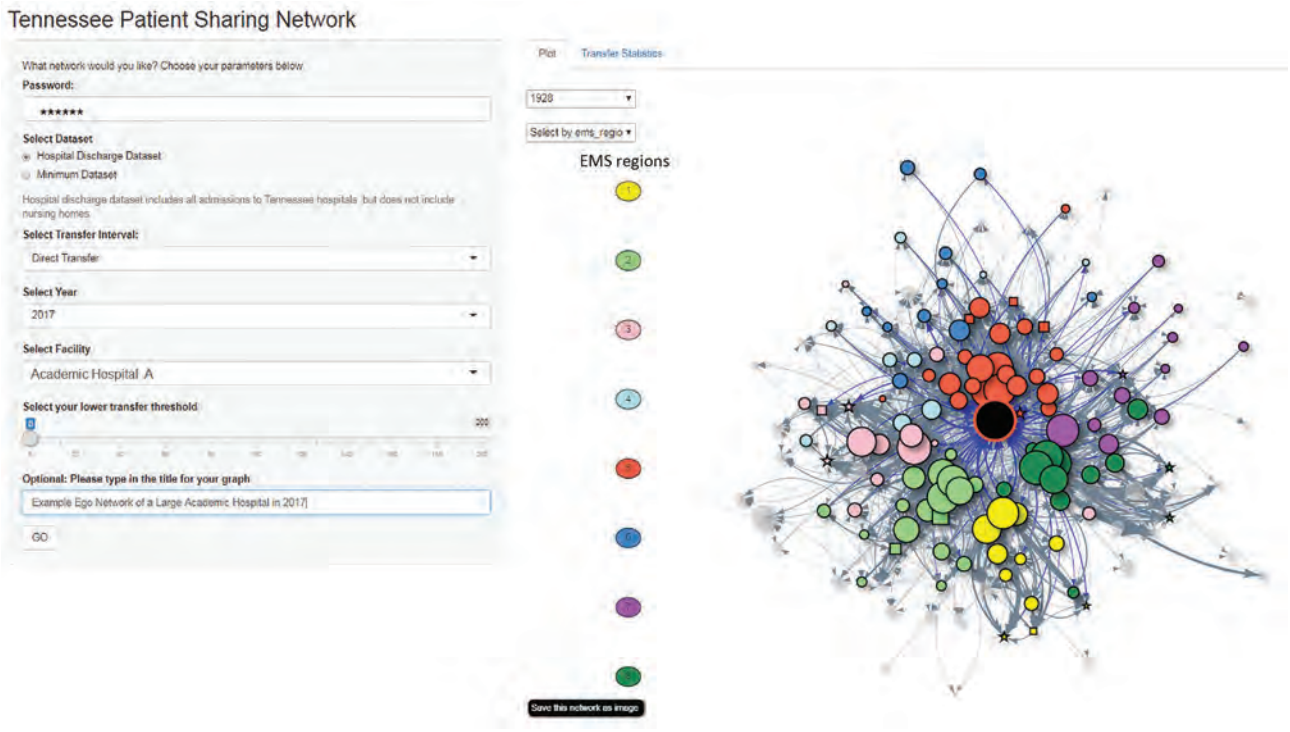

Figure 2. Screenshot of the initial user interface and network graph visualization tab of the web-based application developed to identify healthcare facilities at risk of receiving patients with multidrug-resistant organisms. The application was designed using Shiny (R Studio Inc., https://www.rstudio.com). The network graph is visualized by using a force-directed layout. Black node in the center indicates the facility of interest (ego facility). Tennessee EMS regions are represented by the node color for connected facilities and is represented by the color of the node border for the ego facility. Users can change visualizations interactively during real-time use. EMS, Emergency Medical Services.

receive transfers from the ego facility (Figure 4). It also lists the ego facility's type, city, EMS region, number of licensed beds, and centrality measures and displays a table of facilities at risk to receive transfers from the ego facility. The list defaults to a descending order of facilities by the number transfers from the ego facility. Users can filter or sort the table display based on facility name, facility type, number of beds, county, and EMS region. A download button allows users to import the table as comma-separated values, or as Microsoft Excel (https://www.microsoft.com) or portable document format (PDF) files.

Software

Data cleaning and person-matching were completed in SAS 9.4 (SAS Institute, Cary, NC, USA). We conducted network analyses by using the Statnet and network visualization by using visNetwork packages, both in Rstudio version 3.5.2 (R Studio Inc.) (*14*,*15*). As described previously, we developed the interactive web-based network visualization application by using Shiny. We uploaded de-identified facility-level datasets to the shinyapps.io server hosted on Amazon Web Services (Amazon, https://aws.amazon.com) infrastructure in the United States. These datasets had facility-level patient transfer statistics and characteristics, including licensed facility names, number of beds, facility type, and city and county of address.

Ethics Considerations

The patient-sharing network project was exempted from the institutional review boards (IRBs) at CDC (IRB no. 032416JO), TDH (IRB no. 923990-1), and Vanderbilt University (IRB no. 161676). This work was conducted under a data use agreement between CDC and CMS. CDC's Human Research Protection Office determined this project was exempt from regulations governing the protection of human subjects in research under 45 CFR 46.101(b).

Results

The Shiny web application includes facility-level patient sharing data from the 2014–2017 HDDS dataset and Medicare datasets from 2014 and 2016. Both data sources had 3 networks for each transfer interval: direct, 30, and 365 days. The 2017 HDDS network included a total of 146 hospitals of 4 types; 116 ACH, 13

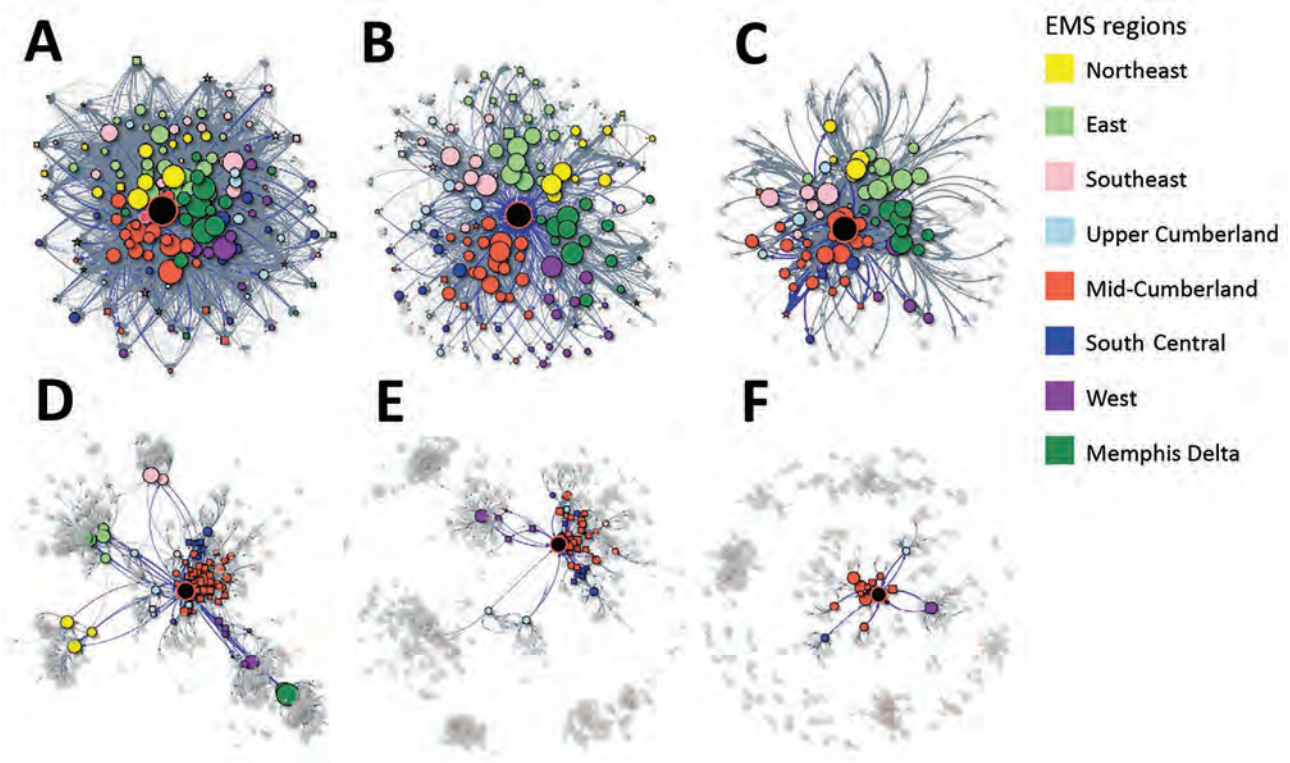

Figure 3. Varying user-tailored ego network visualizations in the web-based interactive tool to identify facilities at risk of receiving patients with multidrug-resistant organisms. Panels demonstrate options for visualizations for a large academic hospital from the HDDS and Centers for Medicare and Medicaid claims and MDS. Real-time use of the application enables users to tailor visualizations by facility, patient transfer threshold, and type of network. Black node in the center indicates the facility of interest (ego facility). The EMS region is represented by the node color for connected facilities and is represented by the color of the node border for the ego facility. Displays shown use the HDDS dataset (A–C) and MDS dataset (D–F). Panels A and D demonstrate a total patient sharing network; B and E demonstrate an uninterrupted patient sharing network; C and F are examples of alterations in patient threshold transfers and displays facilities that have >50 patient transfers to or with the ego facility. EMS, Emergency Medical Services; MDS, minimum dataset; HDDS, Tennessee Hospital Discharge Data System.

CAH, 9 IRF, and 8 LTACH. In 2017, the HDDS dataset recorded 886,277 inpatient hospitalizations representing 494,153 patients. Among patients discharged from Tennessee hospitals in 2017, a total of 29.5% (145,953) were readmitted to another Tennessee hospital within 365 days. The median interval of time in the community was 46 (IQR 11–109) days; 13.8% of patients who were readmitted to a different hospital were directly transferred.

The 2016 CMS dataset reported 381,627 stays to 465 Tennessee facilities representing 196,528 unique patients. These 465 facilities included 91 ACHs, 16 CAH, 10 LTACHs, 10 IRFs, 322 SNFs, 1 children's hospital, and 15 psychiatric hospitals, as classified by the CMS certification numbers. Among all admissions to a Tennessee facility, 82.9% (316,368) of patients had a previous healthcare admission within 365 days; 29.9% of those readmissions were a direct transfer from a healthcare facility. The median interval of time in the community was 11 (IQR 0–108) days. Our downstream facility analysis showed that among the 5 randomly selected facilities, 84% (range 80%–88%) of the facilities in the top 5 from the prior year were in the top 5 again in the succeeding year (Appendix, https://wwwnc.cdc.gov/EID/article/26/9/19-1691-App1.xlsx).

Discussion

TDH has used this interactive tool to improve statewide awareness of the importance of interfacility connectedness, particularly during outbreaks and for containment responses of novel MDROs. We designed the tool as a web-based application for real-time, easy access with internet browsers from computer desktops or handheld devices. This flexibility ensures public health staff can access the application to identify at-risk facilities in a variety of settings, such as when in the field performing point prevalence surveys or during routine office work. The application has helped epidemiologists and infection

preventionists prioritize communication during public health containment responses.

We have demonstrated that a facility's ego network can accurately predict the facilities patients visit after discharge from the index facility during an outbreak (*6*). The TDH HAI/AR team used the application during a particular multifacility outbreak that had evidence of MDRO interfacility and intrafacility transmission. The tool allowed us to identify facilities that frequently received patients from the 2 ego facilities involved in the outbreak. TDH alerted these downstream facilities, which led them to consider admission screening for incoming patients from the 2 ego facilities. TDH plans to continue to use this tool during similar outbreaks. Facility transmission warrants public health action to alert downstream facilities to consider admission screening or enhanced contact precautions for patients admitted from the ego facility.

In addition, the TDH HAI/AR team introduced and demonstrated the use of this application to infection preventionists at hospitals and nursing homes through a variety of webinars and in-person presentations across the state. TDH received requests from facility infection preventionists for line lists of downstream facilities because they were planning containment efforts and wanted to understand which facilities receive the most patients from their facilities. TDH did not provide hospital infection preventionists access to the application but fulfilled requests by emailing exported line lists as Excel documents. Information on downstream facilities can help inform which facilities to target for relationship development and likely will assist with communication during patient transfers.

The TDH HAI/AR team performs targeted infection control assessments as part of a MDRO prevention strategy. These assessments, conducted by TDH infection preventionists, are nonregulatory, consultative, on-site healthcare facility visits to identify gaps in infection prevention specific to a targeted pathogen or area of concern. Our web-based Shiny application was and will continue to be used to identify highly connected facilities in each EMS region and across the

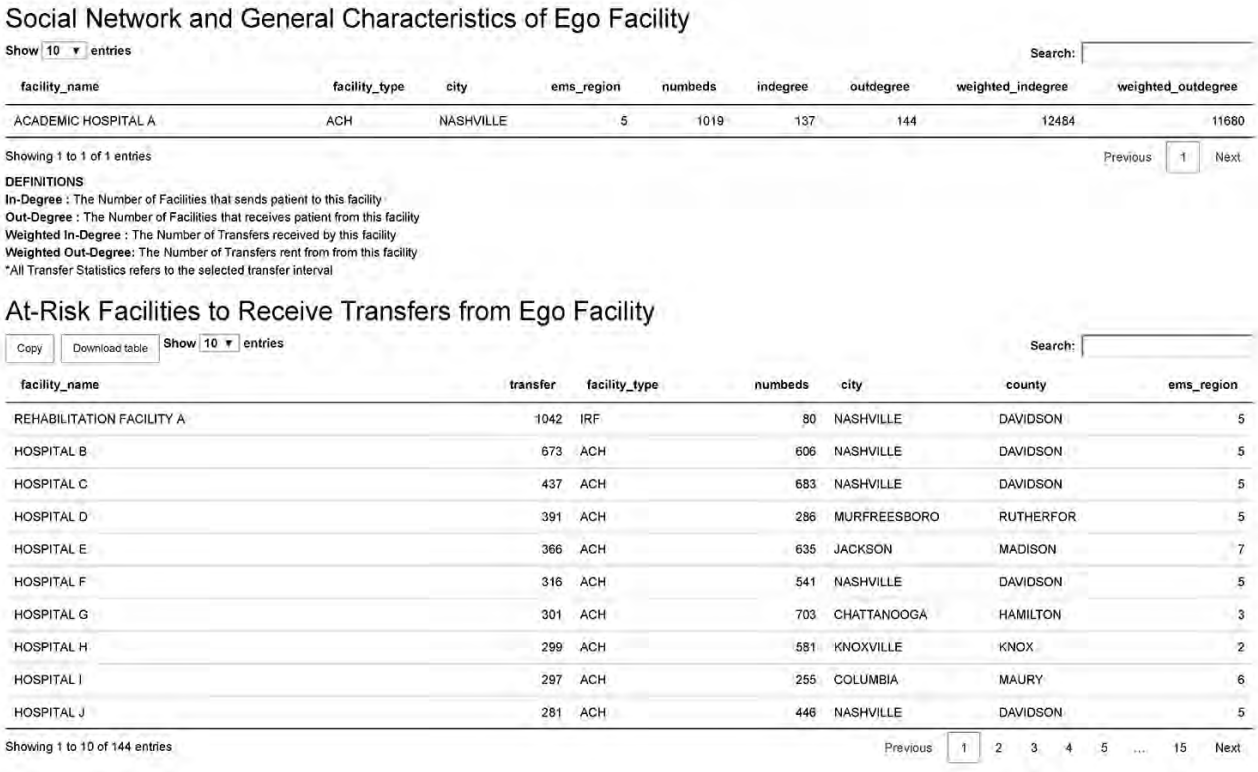

Social Network and General Characteristics of Ego Facility

Show 10 entries Search:

facility_name	facility_type	city	ems_region	numbeds	indegree	outdegree	weighted_indegree	weighted_outdegree
ACADEMIC HOSPITAL A	ACH	NASHVILLE	5	1019	137	144	12484	11680

Showing 1 to 1 of 1 entries Previous 1 Next

DEFINITIONS
In-Degree : The Number of Facilities that sends patient to this facility
Out-Degree : The Number of Facilities that receives patient from this facility
Weighted In-Degree : The Number of Transfers received by this facility
Weighted Out-Degree: The Number of Transfers rent from from this facility
*All Transfer Statistics refers to the selected transfer interval

At-Risk Facilities to Receive Transfers from Ego Facility

Copy Download table Show 10 entries Search:

facility_name	transfer	facility_type	numbeds	city	county	ems_region
REHABILITATION FACILITY A	1042	IRF	80	NASHVILLE	DAVIDSON	5
HOSPITAL B	673	ACH	606	NASHVILLE	DAVIDSON	5
HOSPITAL C	437	ACH	683	NASHVILLE	DAVIDSON	5
HOSPITAL D	391	ACH	286	MURFREESBORO	RUTHERFOR	5
HOSPITAL E	366	ACH	635	JACKSON	MADISON	7
HOSPITAL F	316	ACH	541	NASHVILLE	DAVIDSON	5
HOSPITAL G	301	ACH	703	CHATTANOOGA	HAMILTON	3
HOSPITAL H	299	ACH	581	KNOXVILLE	KNOX	2
HOSPITAL I	297	ACH	255	COLUMBIA	MAURY	6
HOSPITAL J	281	ACH	446	NASHVILLE	DAVIDSON	5

Showing 1 to 10 of 144 entries Previous 1 2 3 4 5 … 15 Next

Figure 4. Screenshot of the transfer statistics tab of the web-based interactive tool to identify facilities at risk of receiving patients with multidrug-resistant organisms. This function displays facility characteristics and downstream facilities that are most likely to receive transfers from the ego facility. The second tab of the application's user interface includes 2 tables. The top table displays detailed social network and facility characteristics for the ego facility. The bottom table displays the facilities at highest risk to receive patients from the ego facility, which are downstream facilities. The table defaults to sort the number of patient transfers in descending order. Users can interactively choose a column to sort and filter this table, which can be used to identify facilities at risk during outbreaks or regional detection of a novel organism. Hospital names have been de-identified for privacy.

state. Prior studies found a correlation between the incidence of MDROs in a healthcare facility and the facility level of connectedness, measured by weighted in-degree and out-degree (*6*,*8*). Identification of highly connected facilities is valuable because it enables us to perform preemptive targeted infection control assessments before the introduction and spread of MDROs. Public health staff can assist by ensuring adequate infection prevention practices are in place at highly connected facilities where a potential for catalyzing interfacility transmission exists.

Our patient-sharing network has several strengths. Access to the hospital discharge data and granular patient identifiers enabled us to conduct person matching with high-level identifiers. We were able to use a robust method to match patients from populations with any insurance coverage for statewide data in HDDS. Moreover, the use of 2 complementary datasets established a highly inclusive picture of a facility's ego network. With both the HDDS and CMS datasets, ACHs, CAHs, IRFs, LTACHs, and SNFs could be included in our analyses each time an ego facility is evaluated. Previously published patient-sharing network analyses were constructed by using partial data that included only direct patient transfers; a subset of patient population, such as CMS beneficiaries; hospitals; or county-level data (*6*,*8*,*12*,*16*).

The inclusion of SNFs was critical for analysis because LTCFs are a key component to a hospital's patient sharing network (*17*). Although not all types of LTCFs were included our network, the inclusion of SNFs represent the facilities carrying a considerable burden of MDRO infections. Point prevalence analysis of MDS data found that MDRO infections were found in 4.2% of nursing home residents in the United States (*18*). Colonization with MDROs were found to be more common among nursing home residents (*19*,*20*). Smaller cohort studies showed gram-negative bacteria was found in 39% of nursing home residents and MRSA was found in 42% (*19*,*21*). Thus, communication with LTCFs is crucial for outbreak management and prevention activities.

An additional strength of the application is its built-in flexibility, which allows the user to tailor the colonization period for specific organisms. The inclusion of 365 days as the longest transfer period for indirect transfers reflects the documented colonization period of CRE in the community (*22*), but users can change this parameter to account for MDROs with shorter colonization periods. The application also can display facilities connected only through direct transfers or through 30-day indirect transfers, which might reflect the colonization period of different MDROs more closely.

One limitation is the construction of 2 separate networks with the HDDS and CMS datasets. Ideally, the tool would include 1 large network with all facilities, but the construction of separate HDDS and CMS networks was required because of the differences in facility aggregation. Although both networks include ACHs, the unique number varies in each because of the difference in aggregation. Aggregating facility-level transfer data together might result in loss of information about some granular patient-sharing patterns in HDDS. One CMS certification number from the datasets can represent a group of tertiary hospitals within the same organization, creating a challenge to merge these data with the HDDS database. More recent CMS datasets include ZIP code information and the CMS certification number. We hope to use this additional datapoint in future analyses while exploring facility aggregation and standardization strategies for our databases.

We will continue to develop and improve the application with the addition of upstream facilities. We will update the network data and facility characteristics for the application annually with the most recent HDDS and CMS data. We also plan to develop models to outline the risk for transmissions based on their relative position in the network. We are working to merge the HDDS and CMS network data by standardizing facility identifications for a unified patient sharing network that provides a more complete picture of the patient population. Finally, we plan to expand the availability of this web-based platform to other public health departments by developing a feature to allow for external data uploads so health department staff can visualize their regional patient transfer networks. Access to information on patient-sharing networks would assist public health departments in mitigating MDRO transmission in their jurisdictions.

The findings and conclusions in this report are those of the authors and do not necessarily represent the official position of the Centers for Disease Control and Prevention or the Tennessee Department of Health.

R.O. reports nonfinancial support and other support from the Tennessee Department of Health during the conduct of the study and grants from federal funding from the Centers for Disease Control and Prevention (CDC) outside the submitted work. M.A.K. reports grants and nonfinancial support from CDC during the conduct of the study; nonfinancial support from Council of State and Territorial Epidemiologists (CSTE); non-financial support from the Society for Healthcare Epidemiology of America;

personal fees and nonfinancial support from Infectious Disease Consulting Corporation (IDCC); personal fees and nonfinancial support from WebMD; nonfinancial support from the Association for Professionals in Infection Control and Epidemiology (APIC); nonfinancial support from the American Society for Microbiology; and personal fees and nonfinancial support from Pfizer outside the submitted work. All other authors had nothing to disclose.

About the Author

Dr. Octaria is an epidemiology doctoral student at Vanderbilt University who is embedded with the Tennessee Department of Health. Her research interest is epidemiology of antimicrobial resistance organisms and network epidemiology.

References

1. US Centers for Disease Control and Prevention. Antibiotic resistance threats in the United States 2013 [cited 2018 Oct 28]. https://www.cdc.gov/drugresistance/threat-report-2013/pdf/ar-threats-2013-508.pdf
2. Jacob JT, Klein E, Laxminarayan R, Beldavs Z, Lynfield R, Kallen AJ, et al. Vital signs: carbapenem-resistant Enterobacteriaceae. MMWR Morb Mortal Wkly Rep. 2013;62:165–70. PubMed
3. Zimmerman FS, Assous MV, Bdolah-Abram T, Lachish T, Yinnon AM, Wiener-Well Y. Duration of carriage of carbapenem-resistant Enterobacteriaceae following hospital discharge. Am J Infect Control. 2013;41:190–4. https://doi.org/10.1016/j.ajic.2012.09.020
4. Guh AY, Bulens SN, Mu Y, Jacob JT, Reno J, Scott J, et al. Epidemiology of carbapenem-resistant Enterobacteriaceae in 7 US communities, 2012–2013. JAMA. 2015;314:1479–87. https://doi.org/10.1001/jama.2015.12480
5. Ray MJ, Lin MY, Weinstein RA, Trick WE. Spread of carbapenem-resistant Enterobacteriaceae among Illinois healthcare facilities: the role of patient sharing. Clin Infect Dis. 2016;63:889–93. https://doi.org/10.1093/cid/ciw461
6. Ray MJ, Lin MY, Tang AS, Arwady MA, Lavin MA, Runningdeer E, et al. Regional spread of an outbreak of carbapenem-resistant Enterobacteriaceae through an ego network of healthcare facilities. Clin Infect Dis. 2018;67:407–10. https://doi.org/10.1093/cid/ciy084
7. Logan LK, Weinstein RA. The epidemiology of carbapenem-resistant Enterobacteriaceae: the impact and evolution of a global menace. J Infect Dis. 2017;215(suppl_1):S28–36. https://doi.org/10.1093/infdis/jiw282
8. Simmering JE, Polgreen LA, Campbell DR, Cavanaugh JE, Polgreen PM. Hospital transfer network structure as a risk factor for *Clostridium difficile* infection. Infect Control Hosp Epidemiol. 2015;36:1031–7. https://doi.org/10.1017/ice.2015.130
9. Slayton RB, Toth D, Lee BY, Tanner W, Bartsch SM, Khader K, et al. Vital Signs: estimated effects of a coordinated approach for action to reduce antibiotic-resistant infections in health care facilities—United States. MMWR Morb Mortal Wkly Rep. 2015;64:826–31. https://doi.org/10.15585/mmwr.mm6430a4
10. US Centers for Disease Control and Prevention. Interim guidance for a public health response to contain novel or targeted multidrug-resistant organisms (MDROs) 2019 [cited 2019 Jul 29]. https://www.cdc.gov/hai/containment/guidelines.html
11. US Department of Health and Human Services, US Department of Defense, US Department of Veteran Affairs. National action plan to prevent health care-associated infections: road map to elimination 2013 [cited 2019 Sep 29]. https://health.gov/our-work/health-care-quality/health-care-associated-infections/national-hai-action-plan
12. Lee BY, McGlone SM, Song Y, Avery TR, Eubank S, Chang C-C, et al. Social network analysis of patient sharing among hospitals in Orange County, California. Am J Public Health. 2011;101:707–13. https://doi.org/10.2105/AJPH.2010.202754
13. Fruchterman TMJ, Reingold EM. Graph drawing by force-directed placement. Softw-Pract Exp. 1991;21:1129–64.
14. Thieurmel B, Robert T. visNetwork: an R package for network visualization. 2016 [cited 2020 Jul 14]. http://datastorm-open.github.io/visNetwork
15. Handcock MS, Hunter DR, Butts CT, Goodreau SM. Statnet: software tools for the statistical modeling of network data 2003 [cited 2020 Jul 14]. http://statnetproject.org
16. Landon BE, Keating NL, Barnett ML, Onnela J-P, Paul S, O'Malley AJ, et al. Variation in patient-sharing networks of physicians across the United States. JAMA. 2012;308:265–73. https://doi.org/10.1001/jama.2012.7615
17. Lee BY, Song Y, Bartsch SM, Kim DS, Singh A, Avery TR, et al. Long-term care facilities: important participants of the acute care facility social network? PLoS One. 2011;6:e29342. https://doi.org/10.1371/journal.pone.0029342
18. Dumyati G, Stone ND, Nace DA, Crnich CJ, Jump RLP. Challenges and strategies for prevention of multidrug-resistant organism transmission in nursing homes. Curr Infect Dis Rep. 2017;19:18. https://doi.org/10.1007/s11908-017-0576-7
19. O'Fallon E, Kandel R, Schreiber R, D'Agata EMC. Acquisition of multidrug-resistant gram-negative bacteria: incidence and risk factors within a long-term care population. Infect Control Hosp Epidemiol. 2010;31:1148–53. https://doi.org/10.1086/656590
20. Kahvecioglu D, Ramiah K, McMaughan D, Garfinkel S, McSorley VE, Nguyen QN, et al. Multidrug-resistant organism infections in US nursing homes: a national study of prevalence, onset, and transmission across care settings, October 1, 2010–December 31, 2011. Infect Control Hosp Epidemiol. 2014;35(S3):S48–55. https://doi.org/10.1086/ 677835
21. O'Fallon E, Pop-Vicas A, D'Agata E. The emerging threat of multidrug-resistant gram-negative organisms in long-term care facilities. J Gerontol A Biol Sci Med Sci. 2009;64:138–41. https://doi.org/10.1093/gerona/gln020
22. Haverkate MR, Weiner S, Lolans K, Moore NM, Weinstein RA, Bonten MJM, et al. Duration of colonization with *Klebsiella pneumoniae* carbapenemase-producing bacteria at long-term acute care hospitals in Chicago, Illinois. Open Forum Infect Dis. 2016;3:ofw178. https://doi.org/10.1093/ofid/ofw178

Address for correspondence: Rany Octaria, Tennessee Department of Health, Communicable and Environmental Diseases and Emergency Preparedness, 710 James Robertson Pkwy, Nashville, TN 37243, USA; email: Rany.Octaria@tn.gov

Isolation, Sequence, Infectivity, and Replication Kinetics of Severe Acute Respiratory Syndrome Coronavirus 2

Arinjay Banerjee, Jalees A. Nasir,[1] Patrick Budylowski,[1] Lily Yip, Patryk Aftanas, Natasha Christie, Ayoob Ghalami, Kaushal Baid, Amogelang R. Raphenya, Jeremy A. Hirota, Matthew S. Miller, Allison J. McGeer, Mario Ostrowski, Robert A. Kozak, Andrew G. McArthur, Karen Mossman, Samira Mubareka

Since its emergence in Wuhan, China, in December 2019, severe acute respiratory syndrome coronavirus 2 (SARS-CoV-2) has infected ≈6 million persons worldwide. As SARS-CoV-2 spreads across the planet, we explored the range of human cells that can be infected by this virus. We isolated SARS-CoV-2 from 2 infected patients in Toronto, Canada; determined the genomic sequences; and identified single-nucleotide changes in representative populations of our virus stocks. We also tested a wide range of human immune cells for productive infection with SARS-CoV-2. We confirm that human primary peripheral blood mononuclear cells are not permissive for SARS-CoV-2. As SARS-CoV-2 continues to spread globally, it is essential to monitor single-nucleotide polymorphisms in the virus and to continue to isolate circulating viruses to determine viral genotype and phenotype by using in vitro and in vivo infection models.

Severe acute respiratory syndrome coronavirus 2 (SARS-CoV-2) emerged in December 2019 in Wuhan, China (*1*). SARS-CoV-2 has since spread to ≈185 countries and infected ≈6 million persons, among whom ≈380,000 have died (*2*). On January 23, 2020, a case of coronavirus disease (COVID-19) was detected in Toronto, Canada (*3*); since then, multiple cases have been identified across Canada. As SARS-CoV-2 spreads globally, the virus is likely to adapt and evolve. It is critical to isolate SARS-CoV-2 viruses to characterize their ability to infect and replicate in multiple human cell types and to determine if the virus is evolving in its ability to infect human cells and cause severe disease. Isolating the virus also provides the opportunity to share the virus with other researchers for development and testing of diagnostics, drugs, and vaccines.

We isolated SARS-CoV-2 from 2 patients with COVID-19 and determined the genomic sequence of each isolate (SARS-CoV-2/SB2 and SARS-CoV-2/SB3-TYAGNC). In addition, we studied the replication kinetics of SARS-CoV-2/SB3-TYAGNC in human fibroblast, epithelial, and immune cells.

Methods

Cells

We maintained Vero E6 cells (African green monkey cells; American Type Culture Collection [ATCC], https://www.atcc.org) in Dulbecco's modified Eagle medium (DMEM) supplemented with 10% fetal bovine serum (FBS) (Sigma-Aldrich, https://www.sigmaaldrich.com) and 1× L-glutamine and penicillin/streptomycin (Pen/Strep; Corning, https://ca.vwr.com). Calu-3 cells (human lung adenocarcinoma derived; ATCC) were cultured as previously mentioned (*4*), as were THF cells (human telomerase life-extended cells) (*5*). THP-1 cells (monocytes; ATCC) were cultured in RPMI medium (Gibco Laboratories, https://www.thermofisher.com) supplemented with 10% FBS, 2mM L-glutamine, 1× penicillin/

Author affiliations: McMaster University, Hamilton, Ontario, Canada (A. Banerjee, J.A. Nasir, K. Baid, A.R. Raphenya, J.A. Hirota, M.S. Miller, A.G. McArthur, K. Mossman); University of Toronto, Toronto, Ontario, Canada (P. Budylowski, N. Christie, A. Ghalami, A.J. McGeer, M. Ostrowski, R.A. Kozak, S. Mubareka); Sunnybrook Research Institute, Toronto (L. Yip, P. Aftanas, R.A. Kozak, S. Mubareka); Mount Sinai Hospital, Toronto (A.J. McGeer)

DOI: https://doi.org/10.3201/eid2609.201495

[1]These authors contributed equally to this article.

streptomycin, and 0.05 mM β-mercaptoethanol. THP-1 cells (monocytes and differentiated macrophages and dendritic cells) were differentiated into macrophages by using 50 ng/mL lymphocyte/granulocyte/macrophage–colony stimulating factor (LGM-CSF; R&D Systems, https://www.rndsystems.com) plus 50 ng/mL macrophage–colony stimulating factor (R&D Systems) and into dendritic cells by using 50 ng/mL granulocyte/macrophage-colony stimulating factor (GM-CSF; R&D Systems) plus 500 U/mL interleukin-4 (BioLegend, https://www.biolegend.com). We purified peripheral blood mononuclear cells (PBMCs) from 2 healthy donors (OM8066 and OM8067) into CD4+, CD8+, CD19+, monocytes, and other cells (CD4–, CD8–, CD19–) by using a CD4+ selection kit that uses immunomagnetic negative selection, a CD8+ selection kit, a phycoerythrin-positive selection kit, and a monocyte-negative selection kit, all by STEMCELL Technologies (https://www.stemcell.com; Appendix Figure 1, https://wwwnc.cdc.gov/EID/article/26/9/20-1495-App1.pdf). We resuspended CD4+, CD8+, CD19+ and CD4–, CD8–, CD19– cells in R-10 media (RPMI + 2 mM L-glutamine + 10% FBS + penicillin/streptomycin) plus 20 U/mL interleukin-2. Primary monocytes were resuspended in R-10 media. This work was approved by the Sunnybrook Research Institute Research Ethics Board (149–1994) and the Research Ethics Boards of St. Michael's Hospital and the University of Toronto (REB 20–044; for PBMCs).

Isolation and Quantification

We seeded Vero E6 cells at a concentration of 3×10^5 cells/well in a 6-well plate. The next day, we collected 200 μL of mid-turbinate swab samples from 2 COVID-19 patients, mixed it with 200 μL of DMEM containing 16 μg/mL TPCK-treated trypsin and inoculated the cells. After 1 h, the inoculum was replaced with DMEM containing 2% FBS and 6 μg/mL TPCK-treated trypsin. We observed the cells daily under a light microscope. Supernatant from the cells was used to determine virus titers (50% tissue culture infectious dose [$TCID_{50}$]/mL) according to the Spearman and Karber method (*6*,*7*) as outlined previously (*8*).

Quantitative Real-Time PCR

To detect SARS-CoV-2 in cell culture supernatant, we removed 140 μL of supernatant and performed detection of viral nucleic acids by reverse transcription PCR (RT-PCR), following an adaptation of the Corman et al. protocol (*9*). In brief, we extracted viral RNA from infected cells by using a QIAamp viral RNA kit (QIAGEN, https://www.qiagen.com) according to the manufacturer's instructions. The RT-PCR reactions were conducted by using Luna Universal qPCR Master Mix (New England Biolabs, https://www.neb.ca) according to the manufacturer's instructions. Two separate gene targets were used for detection, the 5′ untranslated region (UTR) and the envelope (E) gene. Primers and probes used were 5′ UTR forward GTTGCAGCCGATCATCAGC, 5′ UTR reverse GACAAGGCTCTCCATCTTACC, and 5′ UTR probe FAM-CGGTCACACCCGGAC-GAAACCTAG-BHQ-1; and E-gene forward CAG-GTACGTTAATAGTTAATAGCGT, E-gene reverse ATATTGCAGCAGTACGCACACA, and E-gene probe CAL Fluor Orange 560-ACACTAGCCATCCT-TACTGCGCTTCG-BHQ-1. The cycling conditions were 1 cycle of denaturation at 60°C for 10 min, then 95°C for 2 min, followed by 44 amplification cycles at 95°C for 10 s and 60°C for 15 s. Analysis was performed by using Rotor-Gene Q software (QIAGEN) to determine cycle threshold (C_t).

Electron Microscopy

Samples were fixed in 10% neutral buffered formalin (Sigma-Aldrich), for 1 h. Pellets were washed with 0.1 M phosphate buffer (pH 7.0) and postfixed with 1% osmium tetroxide in 0.1 M phosphate buffer (pH 7.0) for 1 h. Pellets were washed with distilled water and en-bloc stained with 2% uranyl acetate in distilled water for 2 h. Pellets were washed with distilled water and dehydrated in a series of ethanol concentrations. Pellets were infiltrated with Araldite Embed 812 resin (VWR, https://us.vwr.com) and cured at 65°C for 48 h. Resin blocks were trimmed, polished, and 9 nm thin sections were ultramicrotomed (Leica Reichert Ultracut E, https://www.leica-microsystems.com) and mounted on transmission electron microscopy grids. Thin sections were stained with 5% uranyl acetate and 5% lead citrate. Sections were imaged by using transmission electron microscopy (Talos L120C; ThermoFisher Scientific, https://www.thermofisher.com) and an LaB6 (lanthanum hexaboride) filament at 120 kV. We scanned 10 fields per cell type, each at a different magnification level: 2,600×, 8,500×, 17,500×, and 36,000×.

Immunofluorescence

To detect SARS-CoV-2 proteins in Vero E6 and CD4+ T lymphocytes, we infected cells with SARS-CoV-2 at a 0.1 multiplicity of infection (MOI) for 24 h. After 24 h, we fixed the cells in 10% neutral buffered formalin (Sigma-Aldrich). After fixation, cells were permeabilized and blocked as previously described (*10*). Cells were stained in suspension by using a

previously described protocol (*10*). For primary antibody staining, we used a combination of 6.6 μg/mL rabbit anti-SARS-CoV-2 N (BioVision, https://www.biovision.com) plus 10 μg/mL recombinant human anti-SARS-CoV-2 spike S1 (GenScript, https://www.genscript.com) and 1:100 diluted serum from a recovered COVID-19 patient (OM8073) (Figure 1, panels A, B). To confirm SARS-CoV-2 staining in CD4+ T cells, we used 10 μg/mL recombinant human SARS-CoV-2 spike S1 antibody as primary staining antibody (GenScript) alone (Figure 1, panel C). For secondary antibodies, we used 1 μg/mL mouse anti-human FITC (BioLegend) and 4 μg/mL goat anti-rabbit Alexa Fluor 488 (abcam, https://www.abcam.com). After staining, cells were spun at 500 × *g* for 5 min in a 96-well plate. The cells were observed under an EVOS FL digital microscope (VWR).

Flow Cytometry

To prepare cells for flow cytometry, we washed 100 μL (400,000 cells) of primary CD4+, CD8+, and CD19+ cells and monocytes with 1 mL of phosphate-buffered saline (PBS) and spun the cells at 500 *g* for 5 min. The cells were resuspended in 100 μL of Live/Dead

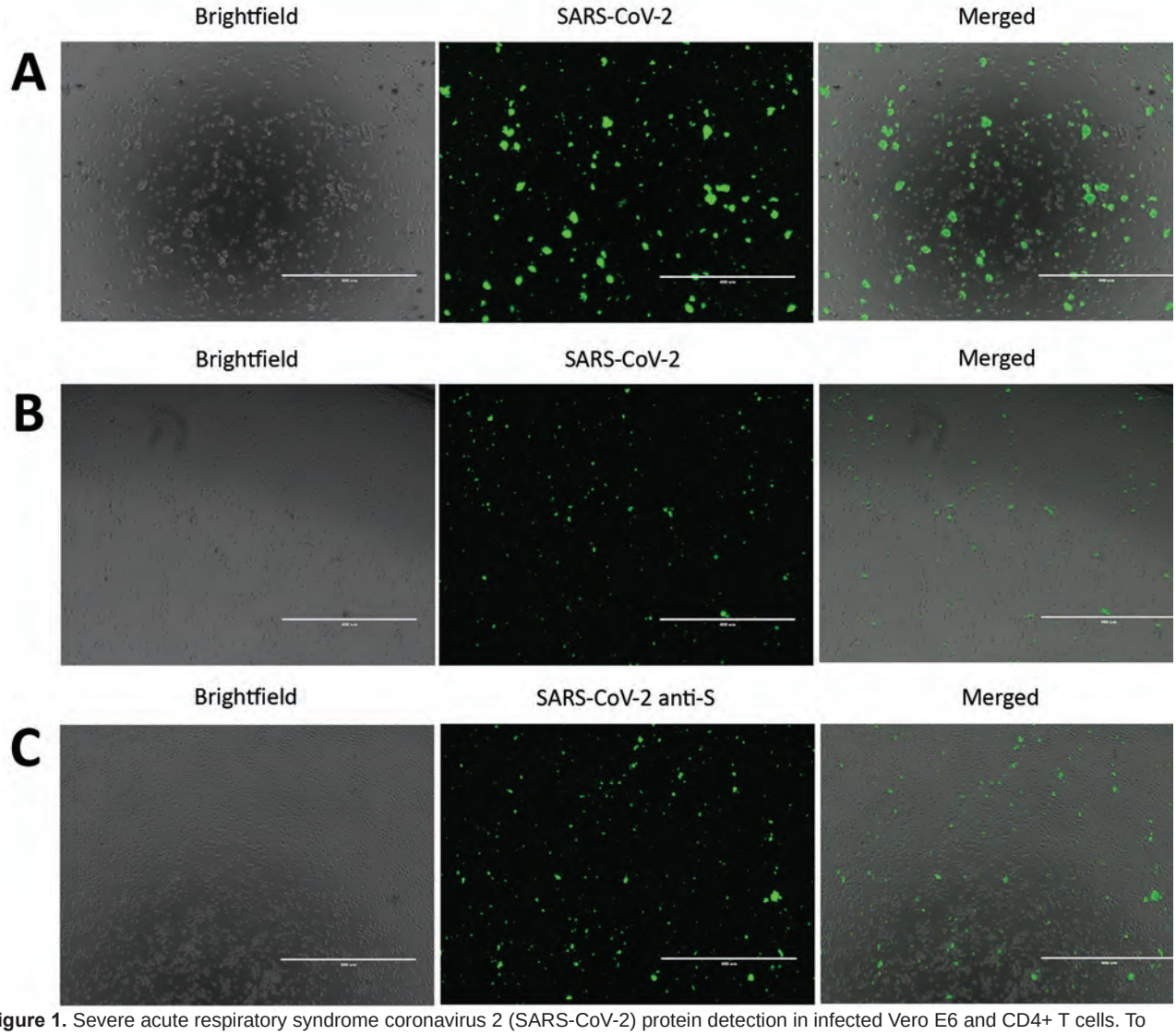

Figure 1. Severe acute respiratory syndrome coronavirus 2 (SARS-CoV-2) protein detection in infected Vero E6 and CD4+ T cells. To detect SARS-CoV-2 protein expression, we infected Vero E6 and CD4+ T cells with SARS-CoV-2 at a multiplicity of infection of 0.1 for 24 h. We immunostained these cells and observed them by using fluorescent microscopy. A) SARS-CoV-2–infected and immunostained Vero E6 cells. B) SARS-CoV-2–infected and immunostained CD4+ T cells. For panels A and B, cells were stained by using an antibody cocktail consisting of SARS-CoV-2 S1 antibody, SARS-CoV-2 N antibody, and diluted serum from a recovered coronavirus disease patient. C) SARS-CoV-2 infected CD4+ T cells immunostained with SARS-CoV-2 S1 antibody (anti-S). Scale bars indicate 400 μm; original magnification ×10.

Violet stain (ThermoFisher Scientific) according to the manufacturer's recommendation and diluted 1:1,000 in PBS. Cells were incubated at 4°C for 30 min. Next, cells were washed with 1 mL of fluorescence-activated cell sorting buffer (in-house reagent) and spun at 500 × *g* for 5 min. Cells were then stained with 100 µL of their respective stains (αCD4-FITC, αCD8-FITC, αCD19-FITC, αCD14-APC; BioLegend) at a concentration of 1 µg/mL for 30 min at 4°C. After staining, the cells were washed with 1 mL of fluorescence-activated cell sorting buffer and spun at 500 × *g* for 5 min. Extra aliquots of cells were left unstained and also spun at 500 × *g* for 5 min. The pellets were resuspended in 100 µL of 1% paraformaldehyde (ThermoFisher Scientific) and analyzed. Samples were run on the BD LSRFortessa X-20 (BD, https://www.bdbiosciences.com). To exclude debris and dead cells, we stained the cells with Live/Dead Violet stain, which stains dead cells brightly. Cells were then analyzed on a flow cytometer, and brightly stained cells were excluded. The remaining cells were then analyzed for the expression of their respective cell surface markers to assess purity.

Sequencing and Phylogenetic Relationship

RNA was extracted from the supernatant of Vero E6 cells after 1 passage by using the QIAamp Viral RNA Mini kit (QIAGEN) without addition of carrier RNA. We synthesized double-stranded DNA for sequencing library preparation by using the Liverpool SARS-CoV-2 amplification protocol (*11*). Two 100-µM primer pools were prepared by combining primer pairs in an alternating fashion to prevent amplification of overlapping regions in a single reaction. In a PCR tube, we added 1 µL Random Primer Mix (ProtoScript II First Strand cDNA Synthesis Kit; New England Biolabs) to 7 µL extracted RNA and denatured it on a SimpliAmp Thermal Cycler (ThermoFisher Scientific) at 65°C for 5 min and then incubated it on ice. We then added 10 µL 2X ProtoScript II Reaction Mix and 2 µL 10X ProtoScript II Enzyme Mix to the denatured sample and performed cDNA synthesis under the following conditions: 25°C for 5 min, 48°C for 15 min, and 80°C for 5 min. After cDNA synthesis, in a new PCR tube we combined 2.5 µL cDNA with 12.5 µL Q5 High-Fidelity 2X Master Mix (New England Biolabs), 8.8 µL nuclease-free water (ThermoFisher Scientific), and 1.125 µL of 100 µM primer pool 1 or 2. PCR cycling was then performed as follows: 98°C for 30 s, followed by 40 cycles of 98°C for 15 s and 65°C for 5 min.

All PCRs were purified by using RNAClean XP (Beckman Coulter, https://www.beckmancoulter.com) at a 1.8× bead-to-amplicon ratio and eluted in 30 µL of RNase-free water (AmericanBio, https://www.americanbio.com). We quantified 2 µL of amplified material by using a Qubit 1X dsDNA assay (ThermoFisher Scientific) according to the manufacturer's instructions. Illumina sequencing libraries were prepared by using a Nextera DNA Flex Library Prep Kit and Nextera DNA CD Indexes (Illumina, https://www.illumina.com) according to the manufacturer's instructions. Paired-end 150-bp sequencing was performed for each library on a MiniSeq with a 300-cycle mid-output reagent kit (Illumina), multiplexed with targeted sampling of ≈40,000 clusters per library. Sequencing reads from pools 1 and 2 were combined (as R1 and R2), amplification primer sequences were removed by using Cutadapt version 1.18 (*12*), and Illumina adaptor sequences were removed and low-quality sequences trimmed or removed by using Trimmomatic (version 0.36) (*13*). Final sequence quality and confirmation of adaptor/primer trimming were confirmed by using FASTQC version 0.11.5 (*14*). SARS-CoV-2 genome sequences were assembled by using UniCycler version 0.4.8 (default settings, except for conservative mode) (*15*) and assembly statistics were generated by QUAST (version 5.0.2) (*16*). Sequencing depth and completeness of coverage of the assembled genomes was additionally assessed by using Bowtie2 version 2.3.4.1 (*17*) alignment of the sequencing reads against the assembled contigs, and statistics were generated by ngsCAT (version 0.1) (*18*). Sequence variation in the assembled genomes was assessed by comparing sequences in BLASTN (http://blast.ncbi.nlm.nih.gov//Blast.cgi) with SARS-CoV-2 genomes available in GenBank as well as BreSeq version 0.35.0 (*19*) analysis relative to GenBank entry MN908947.3 (first genome sequence reported from the original outbreak in Wuhan). We constructed a phylogenetic tree (Appendix Figure 2) by using maximum-likelihood based on a multiple sequence alignment and RAxML-HPC BlackBox with the general time-reversible plus gamma plus invariate sites model for among-site rate variation (*20*).

Results

For virus isolation, we inoculated Vero E6 cells with aliquots of mid-turbinate swab samples and monitored the cells for cytopathic effects (CPE) daily. Relative to mock-inoculated cells, cells inoculated with both samples (SARS-CoV-2/SB2 and SARS-CoV-2/SB3-TYAGNC) displayed extensive CPE 72 h after infection (Figure 2, panel A). We collected 200 µL of cell culture supernatant and re-infected a fresh layer of Vero E6 cells. After 24 hours, both wells containing

cells that were reinoculated displayed extensive CPE (Figure 2, panel B). We extracted viral RNA from the supernatant and confirmed the presence of SARS-CoV-2 by using a diagnostic quantitative real-time PCR (Figure 2, panel C). We also confirmed the presence of coronavirus-like particles in infected Vero E6 cells by electron microscopy (Figure 2, panel D).

Next, we performed genome sequencing of both isolates, generating genome sequences with 7,500-8,000–fold coverage and ≈94% completeness, with only ≈260 bp and ≈200 bp at the 5′ and 3′ termini undetermined (Table; Appendix Figure 2). SARS-CoV-2/SB2 and SARS-CoV-2/SB3-TYAGNC shared synonymous and nonsynonymous substitutions with those

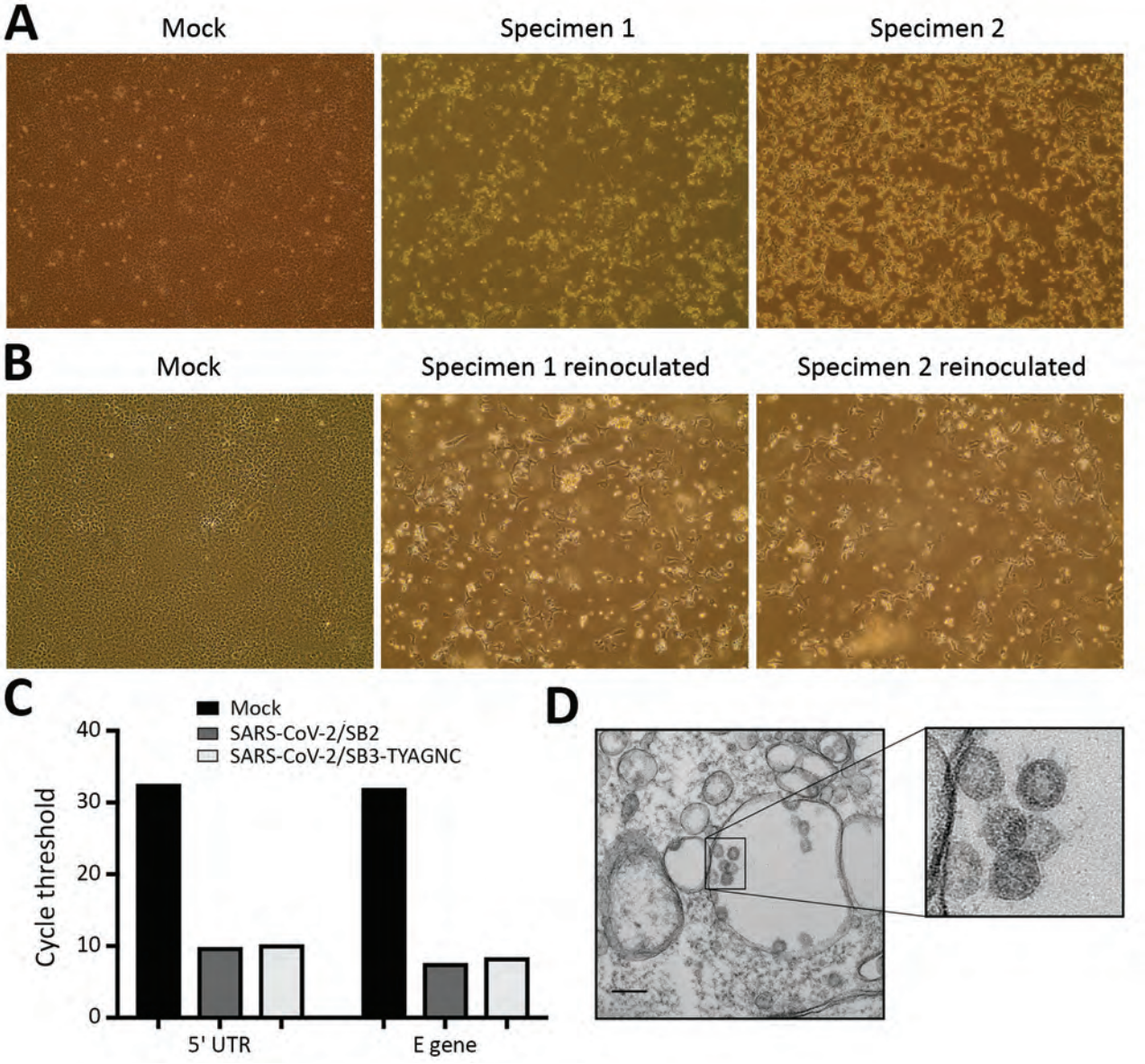

Figure 2. Isolating severe acute respiratory syndrome coronavirus 2 (SARS-CoV-2) from patients with coronavirus disease (COVID-19). A) Vero E6 cells were mock inoculated or inoculated with midturbinate clinical specimens from COVID-19 patients. Cells were incubated for 72 h and observed for cytopathic effect (CPE) under a light microscope. Original magnification ×10. B) To determine if supernatant from Vero E6 cells that were mock inoculated or inoculated with clinical specimens contained replication competent virus, we reinoculated a fresh monolayer of Vero E6 cells and observed cells under a light microscope for CPE after 24 h. Original magnification ×10. C) Quantitative real-time PCR was used to detect SARS-CoV-2 5′-UTR and E gene in RNA extracted from supernatant that was collected from Vero E6 cells that were mock infected or infected with clinical specimens from COVID-19 patients for 72 h. D) Electron micrograph of Vero E6 cells that were reinfected for 48 h with supernatant that was collected from Vero E6 cells infected with clinical specimens. Original magnification ×36,000. Inset, zoomed and cropped from the original electron micrograph, shows coronavirus-like particles. M, mock specimen; specimen 1, SARS-CoV-2/SB2; specimen 2, SARS-CoV-2/SB3-TYAGNC. E, envelope; UTR, untranslated region.

Table. Sequencing read and genome assembly statistics used in study of isolation, sequence, infectivity, and replication kinetics of SARS-CoV-2*

Metric or mutation	SARS-CoV-2/SB2	SARS-CoV-2/SB3_TYAGNC
Number of paired reads	730,137 bp	690,167 bp
Reads from SARS-CoV-2	94.0%	94.4%
Number of assembly contigs	1	1
Assembly N50	29,494 bp	29,369 bp
Average depth of coverage of reads	7940.0-fold	7550.1-fold
Total assembly length	29,494 bp	29,369 bp
SARS-CoV-2 assembly completeness	98.6%	98.2%
Unresolved 5′ sequence	262 bp	272 bp
Unresolved 3′ sequence	200 bp	205 bp
Pos. 884 (orf1ab polyprotein)		**R207C (CGT→TGT)**
Pos. 1397 (orf1ab polyprotein)	**V378I (GTA→ATA)**	**V378I (GTA→ATA)**
Pos. 2832 (orf1ab polyprotein)	K856R (AAG→AGG)	
Pos. 3040 (orf1ab polyprotein)		Y925Y (TAC→TAT)
Pos. 8327 (or1ab polyprotein)	18.1% of reads suggest L2688F (CTT→TTT)	
Pos. 8653 (orf1ab polyprotein)		**M2796I (ATG→ATT)**
Pos. 10353 (orf1ab polyprotein)	5.6% of reads suggest K3363T (AAG→ACG)	
Pos. 11074 (orf1ab polyprotein)	10.2% of reads suggest +TTT and a deletion between positions 10809 and 13203	
Pos. 11083 (orf1ab polyprotein)	**L3606F (TTG→TTT)**	**L3606F (TTG→TTT)**
Pos. 25413 (orf3a protein)		36.7% of reads suggest I7I (ATC→ATT)
Pos. 28688 (nucleocapsid phosphoprotein)	**L139L (TTG→CTG)**	**L139L (TTG→CTG)**

*Predicted mutations are relative to the MN908947.3 SARS-CoV-2 genome (29,903 bp). Mutations within codons are underlined. All mutations were predicted by 100% of sequencing reads mapping to that position, unless otherwise noted. None of the mutations with support from <100% of sequencing reads appeared in the final assembled genome consensus sequences. Substitutions in boldface have been observed in direct sequencing of patient isolates (S. Mubareka, A.G.McArthur, unpub. data). orf1ab, open reading frame 1ab; pos., position; SARS-CoV-2, severe acute respiratory syndrome coronavirus 2.

independently observed in direct sequencing of clinical isolates (Table; S. Mubareka and A.G. McArthur, unpub. data). SARS-CoV-2/SB2 also contained a nonsynonymous substitution at position 2832 (K856R in open reading frame [ORF] 1ab polyprotein) and 3 regions with mutations or a deletion supported by a minority of sequencing reads, but SARS-CoV-2/SB3-TYAGNC had only an additional synonymous substitution in ORF1ab polyprotein (Y925Y) plus a minority of sequencing reads supporting another synonymous substitution in the ORF3a protein (Table). Furthermore, maximum-likelihood phylogenetic analysis including >1,900 SARS-CoV-2 isolates from GISAID (https://www.gisaid.org) placed both SARS-CoV-2/SB2 and SARS-CoV-2/SB3-TYAGNC within a clade of isolates from patients around the globe but with evidence of travel history associated with the COVID-19 outbreak in Iran (Appendix Figure 2). As such, SARS-CoV-2/SB3-TYAGNC was used for subsequent studies as the best representative of a clinical viral isolate. Raw sequencing reads for each isolate are available in the National Center for Biotechnology Information under BioProject PRJNA624792. Only sequencing reads that aligned by Bowtie2 to the MN908947.3 SARS-CoV-2 genome were included in the deposited sequence files.

To determine the replication kinetics of SARS-CoV-2 in human structural and immune cells, we infected Calu-3 cells, THF cells, Vero E6 cells (African green monkey kidney epithelial), THP-1 cells, and primary PBMCs from healthy human donors (CD4+, CD8+, CD19+, monocytes, and other PBMCs; Appendix Figure 1) with an MOI of 0.01. We monitored virus replication in the cell lines for 72 h (Figure 3). We also determined virus replication in PBMCs from healthy donors for 48 h (Figure 3). SARS-CoV-2 propagated to high titers in Vero E6 and Calu-3 cells (Figure 3). SARS-CoV-2 did not replicate efficiently in THF cells (Figure 3). Of note, human immune cell lines and primary PBMCs from healthy donors did not support SARS-CoV-2 replication (Figure 3).

To further support virus replication data, we imaged infected human epithelial, fibroblast, and immune cells by using electron microscopy after 48 h of infection with SARS-CoV-2 at an MOI of 0.01 (Figure 4). We scanned 10 different fields per cell type, each using 4 different magnifications—2,600×, 8,500×, 17,500×, and 36,000×—to determine if the cell populations contained virus-like particles. Virus-like particles were detected in 7/10 fields in Vero E6 cells and 8/10 fields in Calu-3 cells (Figure 4, panels A, B). We also detected virus-like particles in 2/10 fields in primary CD4+ T cells (Figure 4, panel C). We did not observe any virus-like particles in other human immune cells that were experimentally infected with

SARS-CoV-2 (Figure 4, panels D–J). To determine if virus-like particles can be detected in Vero E6 cells and PBMCs at earlier time points, we infected these cell populations with SARS-CoV-2 at an MOI of 0.01 and imaged the cells with electron microscopy at 6 h and 12 h after infection (Appendix Figures 3, 4). We observed virus-like particles in 9/10 fields at 6 h after infection and 10/10 fields at 12 h after infection in Vero E6 cells (Appendix Figure 3, panel A, Figure 4, panel A). We also observed virus-like particles in 1/10 fields at 6 h and 1/10 fields at 12 h after infection in CD4+ T cells (Appendix Figure 3, panel B, and Figure 4, panel B). None of the other infected PBMC populations contained detectable virus-like particles (Appendix Figure 3, panels C–F, and Figure 4, panels C–F).

To confirm SARS-CoV-2 infection and protein expression in CD4+ T cells, we infected Vero E6 and CD4+ T cells with SARS-CoV-2 at an MOI of 0.1 for 24 h. We immunostained these cells and observed them by using fluorescent microscopy. To enhance our ability to detect SARS-CoV-2 proteins in these cells, we immunostained the cells by using a cocktail of antibodies that included SARS-CoV-2 S1 antibody, SARS-CoV-2 N antibody, and diluted serum from a recovered COVID-19 patient (Figure 1, panels A and B). We were able to detect SARS-CoV-2 infected Vero E6 and CD4+ T cells by using this antibody cocktail (Figure 1, panels A, B). Furthermore, to confirm SARS-CoV-2 infection of CD4+ T cells by using a single antibody, we immunostained infected CD4+ T cells with anti-SARS-CoV-2 S1 antibody and were able to detect infected cells in the population (Figure 1, panel C).

Discussion

We report the isolation of 2 replication competent SARS-CoV-2 virus samples from COVID-19 patients in Canada. We used TPCK-treated trypsin to facilitate virus isolation from clinical specimens (Figure 2, panel A). Exogenous trypsin activates SARS-CoV spike proteins more efficiently and facilitates cellular entry (*21*). Exogenous trypsin treatment also enhances infectivity of other zoonotic batborne coronaviruses (*22*). Furthermore, TPCK-treated trypsin has been used to successfully isolate SARS-CoV-2 in China (*1*). In our study, subsequent infection and virus replication did not require any additional TPCK-treated trypsin (Figure 2, panel B). The presence of CPE alone does not indicate successful isolation of a coronavirus. Mid-turbinate samples from adults with acute respiratory distress may often contain other microbes, including viruses (*23*). Thus, to identify our cell culture isolates, we sequenced them to confirm that they were reflective of the SARS-CoV-2 infecting patients worldwide, selecting SARS-CoV-2/SB3-TYAGNC for experimental

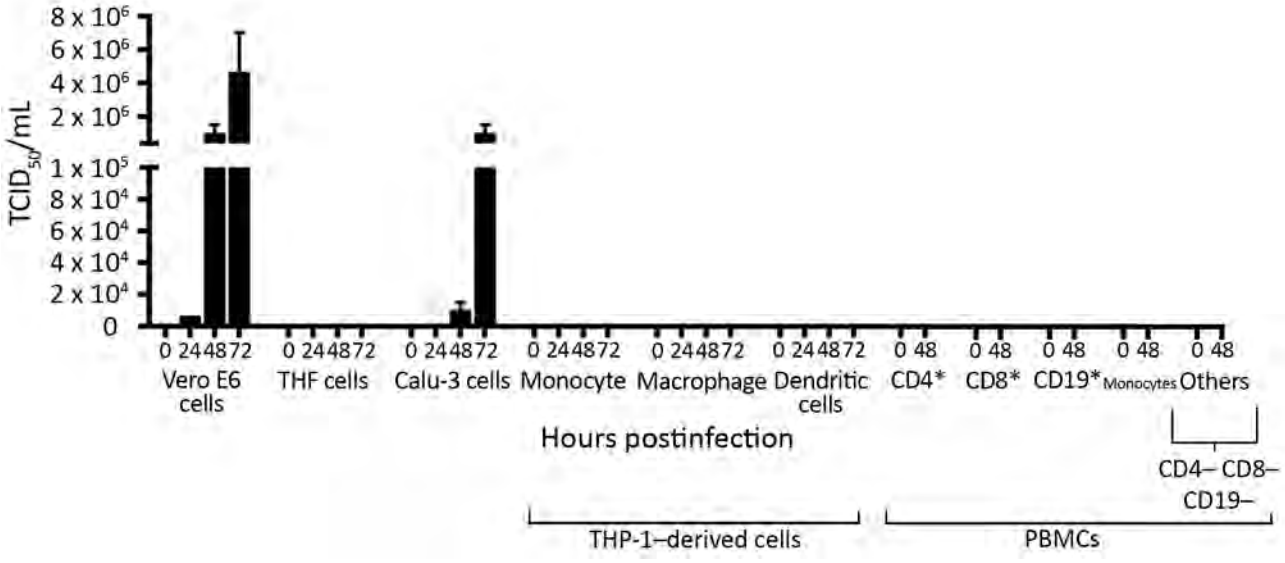

Figure 3. Replication of severe acute respiratory syndrome coronavirus 2 (SARS-CoV-2) in human structural and immune cells. To identify human cells that support SARS-CoV-2 replication, we infected human cell lines and primary cells at a multiplicity of infection of 0.01 (n = 2 independent experiments; supernatant from each experiment was titrated in triplicate). We infected Vero E6 cells as a control. THF (human telomerase life-extended cells) and Calu-3 cells (human lung adenocarcinoma–derived) cells represent human structural cells. THP-1 is a monocyte cell line that was used to derive macrophages and dendritic cells. PBMCs from 2 healthy human donors were used to generate CD4+, CD8+, CD19+, monocytes, and other (CD4–, CD8–, CD19–) cell populations. Supernatant from infected cells was collected at various times and titrated on Vero E6 cells to determine virus titers ($TCID_{50}$). PBMC, peripheral blood mononuclear cell; $TCID_{50}$, 50% tissue culture infectious dose.

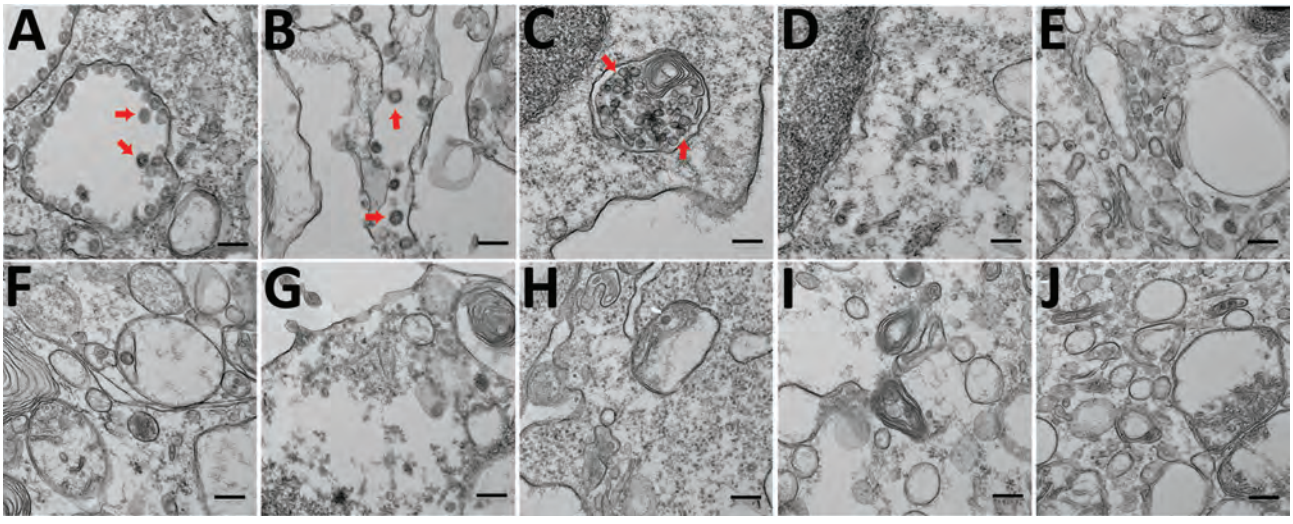

Figure 4. Electron micrographs of severe acute respiratory syndrome coronavirus 2 (SARS-CoV-2)–infected cells. To detect coronavirus-like particles in experimentally infected human structural and immune cells, we infected a range of cells with SARS-CoV-2 at a multiplicity of infection of 0.01 for 48 h. The cells were fixed, processed, and imaged by using a transmission electron microscope (10 fields/cell type). A representative image of each cell type is shown. Virus-like particles are indicated by red arrows. A) Vero E6 cells. B) Calu-3 cells. C) CD4+ PBMCs. D) CD8+ PBMCs. E) CD19+ PBMCs. F) Monocytes from PBMCs. G) Other cells from PBMCs (CD4–, CD8–, CD19– cell populations). H) THP-1 monocyte. I) THP-1-derived macrophage. J) THP-1-derived dendritic cell. PBMC, peripheral blood mononuclear cell. Scale bars indicate 200 nm.

investigation because this isolate produced fewer minority sequencing reads (Table).

SARS-CoV caused the 2003–2004 outbreak of severe acute respiratory syndrome. SARS-CoV can infect structural (*24*) and immune cell lines (*25*) from humans in vitro. To identify cell types that can support productive infection of SARS-CoV-2, we infected a range of human cell populations with SARS-CoV-2/SB3-TYAGNC. Both Vero E6 and Calu-3 cells supported SARS-CoV-2 replication to high titers (Figure 3), as reported in other recent studies (*26*,*27*). Previously, SARS-CoV was also shown to replicate efficiently in Vero E6 cells (*24*). Vero E6 cells are immunodeficient, with deficiencies in innate antiviral interferon signaling, which makes them ideal candidates for virus isolation (*28*). However, to enable studies on SARS-CoV-2–host interactions, it is important to identify human lung epithelial cells with intact immune responses that can support SARS-CoV-2 replication. We and others have previously shown that SARS-CoV and Middle East respiratory syndrome coronavirus (MERS-CoV) replicate efficiently in Calu-3 cells (*8*,*29*,*30*). In addition, SARS-CoV–induced and MERS-CoV–induced immune responses have been studied in Calu-3 cells (*30*,*31*). The ability to infect Calu-3 cells with SARS-CoV-2 (Figure 3) will facilitate in vitro studies of virus–host interactions using SARS-CoV-2. Other commonly used human lung cells, such as A549, do not support efficient replication of SARS-CoV-2 (*26*). Furthermore, hTERT (human telomerase reverse transcriptase) THF cells also did not support virus replication (Figure 3).

Previous studies have shown that human immune cells, such as THP-1 cells, are susceptible to SARS-CoV infection (*25*). In our study, human immune cell populations, including THP-1–derived cell lines and primary cells (PBMCs) did not support productive SARS-CoV-2 replication (Figure 3). Although primary CD4+ T cells did not support productive virus replication, we observed virus-like particles in these cells by electron microscopy (Figure 4, panel C). We also detected SARS-CoV-2 proteins in infected CD4+ T cells by using fluorescent microscopy (Figure 1, panels B, C). This finding is consistent with that recently reported by Wang et al. when they demonstrated that SARS-CoV-2 and pseudotyped viruses could enter human T-cell lines (MT-2) (*32*). Those authors also noted that SARS-CoV-2 replication was abortive in MT-2 cells. SARS-CoV-2 transcript levels in infected MT-2 cells increased at 6 h after infection but remained steady at later time points, indicating a lack of virus replication in these cells (*32*). This finding is similar to abortive replication observed in MERS-CoV–infected T lymphocytes (*33*). However, the study by Wang et al. did not quantify virus titers in the supernatant from infected cells. In our study, we could not detect any replication-competent virus in the supernatant that was collected from SARS-CoV-2–infected CD4+ T cells (Figure 3). Human

immune cells lack expression of angiotensin-converting enzyme 2 (*34*) (https://www.proteinatlas.org), the functional receptor of SARS-CoV-2 (*1*,*35*). Emerging data indicate that there could be other receptors, such as CD147, that may facilitate cellular entry of SARS-CoV-2 (K. Wang et al., unpub. data, https://www.biorxiv.org/content/10.1101/2020.03.14.988345v1). Additional studies are needed to determine the full breadth of cellular receptors and coreceptors that may facilitate entry of SARS-CoV-2. Thus, although it is intriguing that CD4+ T cells may be susceptible to SARS-CoV-2, our data show that these cells are not permissive to SARS-CoV-2 replication in vitro. More studies are required to fully identify the effects of SARS-CoV-2 entry in CD4+ T lymphocytes.

In conclusion, we report that although a human lung cell line supported replication of SARS-CoV-2, the virus did not propagate in any of the tested immune cell lines or primary human immune cells. Although we did not observe a productive infection in CD4+ primary T lymphocytes, we observed virus-like particles in these cells by electron microscopy. Thus, SARS-CoV-2 can enter CD4+ primary T lymphocytes but is unable to replicate efficiently. Our data shed light on a wider range of human cells that may or may not be permissive for SARS-CoV-2 replication, and our study strongly suggests that the human immune cells tested do not support a productive infection with SARS-CoV-2.

Acknowledgments

We acknowledge Lindsey Fiddes' help with electron microscopy. SARS-CoV-2 Liverpool protocol genome amplification primer sequences were generously shared by Public Health England.

This study was supported by a Canadian Institutes of Health Research (CIHR) COVID-19 rapid response grant to principal applicant K.M. and co-applicants A.B., A.G.M., M.S.M., and S.M. A.B. was funded by the Natural Sciences and Engineering Research Council of Canada. J.A.N. was supported by funds from the Comprehensive Antibiotic Resistance Database. B.P.A. and A.R.R. were supported by CIHR funding (PJT-156214 to A.G.M.). Computer resources were supplied by the McMaster Service Lab and Repository computing cluster, funded in part by grants to A.G.M. from the Canadian Foundation for Innovation. Additional cloud computing needs were funded by the Comprehensive Antibiotic Resistance Database. J.A.H. is supported by the Canada Research Chairs Program and an Ontario Early Career Researcher Award. M.S.M. is supported by a CIHR COVID-19 rapid response grant, a CIHR New Investigator Award, and an Ontario Early Researcher Award.

About the Author

Dr. Banerjee is a postdoctoral research fellow at McMaster University, Hamilton. His research interests include coronavirus–host interactions in humans and bats as well as the evolution of antiviral immune responses in bats.

References

1. Zhou P, Yang XL, Wang XG, Hu B, Zhang L, Zhang W, et al. A pneumonia outbreak associated with a new coronavirus of probable bat origin. Nature. 2020;579:270–3. https://doi.org/10.1038/s41586-020-2012-7
2. Dong E, Du H, Gardner L. An interactive web-based dashboard to track COVID-19 in real time. Lancet Infect Dis. 2020;20:533–4. https://doi.org/10.1016/S1473-3099(20)30120-1
3. Marchand-Senécal X, Kozak R, Mubareka S, Salt N, Gubbay JB, Eshaghi A, et al. Diagnosis and management of first case of COVID-19 in Canada: lessons applied from SARS. Clin Infect Dis. 2020;ciaa227. https://doi.org/10.1093/cid/ciaa227
4. Aguiar JA, Huff RD, Tse W, Stämpfli MR, McConkey BJ, Doxey AC, et al. Transcriptomic and barrier responses of human airway epithelial cells exposed to cannabis smoke. Physiol Rep. 2019;7:e14249. https://doi.org/10.14814/phy2.14249
5. Banerjee A, Zhang X, Yip A, Schulz KS, Irving AT, Bowdish D, et al. Positive selection of a serine residue in bat IRF3 confers enhanced antiviral protection. iScience. 2020;23:100958. https://pubmed.ncbi.nlm.nih.gov/32179480/https://doi.org/10.1016/j.isci.2020.100958
6. Hamilton MA, Russo RC, Thurston RV. Trimmed Spearman-Karber method for estimating median lethal concentrations in toxicity bioassays. Environ Sci Technol. 1977;11:714–9. https://doi.org/10.1021/es60130a004
7. Spearman C. The method of "right and wrong cases" (constant stimuli) without Gauss's formulae. Br J Psychol. 1908;2:227–42. https://doi.org/10.1111/j.2044-8295.1908.tb00176.x
8. Banerjee A, Falzarano D, Rapin N, Lew J, Misra V. Interferon regulatory factor 3-mediated signaling limits Middle East respiratory syndrome (MERS) coronavirus propagation in cells from an insectivorous bat. Viruses. 2019;11:E152. https://doi.org/10.3390/v11020152
9. Corman VM, Landt O, Kaiser M, Molenkamp R, Meijer A, Chu DKW, et al. Detection of 2019 novel coronavirus (2019-nCoV) by real-time RT-PCR. Euro Surveill. 2020;25. https://doi.org/10.2807/1560-7917.ES.2020.25.3.2000045
10. Banerjee A, Falzarano D, Misra V. Caution: choice of fixative can influence the visualization of the location of a transcription factor in mammalian cells. Biotechniques. 2018;65:65–9. https://doi.org/10.2144/btn-2018-0060
11. Quick J, Grubaugh ND, Pullan ST, Claro IM, Smith AD, Gangavarapu K, et al. Multiplex PCR method for MinION and Illumina sequencing of Zika and other virus genomes directly from clinical samples. Nat Protoc. 2017;12:1261–76. https://doi.org/10.1038/nprot.2017.066
12. Martin M. Cutadapt removes adapter sequences from high-throughput sequencing reads [cited 2020 Jun 2]. https://journal.embnet.org/index.php/embnetjournal/article/view/200
13. Bolger AM, Lohse M, Usadel B. Trimmomatic: a flexible trimmer for Illumina sequence data. Bioinformatics.

2014;30:2114–20. https://doi.org/10.1093/bioinformatics/btu170
14. Andrew S. FastQC: A quality control tool for high throughput sequence data [cited 2020 Apr 9]. http://www.bioinformatics.babraham.ac.uk/projects/fastqc/
15. Wick RR, Judd LM, Gorrie CL, Holt KE. Unicycler: resolving bacterial genome assemblies from short and long sequencing reads. PLOS Comput Biol. 2017;13:e1005595. https://doi.org/10.1371/journal.pcbi.1005595
16. Gurevich A, Saveliev V, Vyahhi N, Tesler G. QUAST: quality assessment tool for genome assemblies. Bioinformatics. 2013;29:1072–5. https://doi.org/10.1093/bioinformatics/btt086
17. Langmead B, Salzberg SL. Fast gapped-read alignment with Bowtie 2. Nat Methods. 2012;9:357–9. https://doi.org/10.1038/nmeth.1923
18. López-Domingo FJ, Florido JP, Rueda A, Dopazo J, Santoyo-Lopez J. ngsCAT: a tool to assess the efficiency of targeted enrichment sequencing. Bioinformatics. 2014;30:1767–8. https://doi.org/10.1093/bioinformatics/btu108
19. Deatherage DE, Barrick JE. Identification of mutations in laboratory-evolved microbes from next-generation sequencing data using *breseq*. Methods Mol Biol. 2014;1151:165–88. https://doi.org/10.1007/978-1-4939-0554-6_12
20. Kozlov AM, Darriba D, Flouri T, Morel B, Stamatakis A. RAxML-NG: a fast, scalable and user-friendly tool for maximum likelihood phylogenetic inference. Bioinformatics. 2019;35:4453–5. https://doi.org/10.1093/bioinformatics/btz305
21. Simmons G, Bertram S, Glowacka I, Steffen I, Chaipan C, Agudelo J, et al. Different host cell proteases activate the SARS-coronavirus spike-protein for cell-cell and virus-cell fusion. Virology. 2011;413:265–74. https://doi.org/10.1016/j.virol.2011.02.020
22. Menachery VD, Dinnon KH III, Yount BL Jr, McAnarney ET, Gralinski LE, Hale A, et al. Trypsin treatment unlocks barrier for zoonotic bat coronaviruses infection. J Virol. 2019;94:e01774-19. https://doi.org/10.1128/JVI.01774-19
23. Larios OE, Coleman BL, Drews SJ, Mazzulli T, Borgundvaag B, Green K, et al.; STOP-Flu Study Group. Self-collected mid-turbinate swabs for the detection of respiratory viruses in adults with acute respiratory illnesses. PLoS One. 2011;6:e21335. https://doi.org/10.1371/journal.pone.0021335
24. Kaye M, Druce J, Tran T, Kostecki R, Chibo D, Morris J, et al. SARS-associated coronavirus replication in cell lines. Emerg Infect Dis. 2006;12:128–33. https://doi.org/10.3201/eid1201.050496
25. Yen YT, Liao F, Hsiao CH, Kao CL, Chen YC, Wu-Hsieh BA. Modeling the early events of severe acute respiratory syndrome coronavirus infection in vitro. J Virol. 2006;80:2684–93. https://doi.org/10.1128/JVI.80.6.2684-2693.2006
26. Harcourt J, Tamin A, Lu X, Kamili S, Sakthivel SK, Murray J, et al. Severe acute respiratory syndrome coronavirus 2 from patient with coronavirus disease, United States. Emerg Infect Dis. 2020;26:1266–73. https://doi.org/10.3201/eid2606.200516
27. Matsuyama S, Nao N, Shirato K, Kawase M, Saito S, Takayama I, et al. Enhanced isolation of SARS-CoV-2 by TMPRSS2-expressing cells. Proc Natl Acad Sci U S A. 2020;117:7001–3. https://doi.org/10.1073/pnas.2002589117
28. Emeny JM, Morgan MJ. Regulation of the interferon system: evidence that Vero cells have a genetic defect in interferon production. J Gen Virol. 1979;43:247–52. https://doi.org/10.1099/0022-1317-43-1-247
29. Tseng CT, Tseng J, Perrone L, Worthy M, Popov V, Peters CJ. Apical entry and release of severe acute respiratory syndrome-associated coronavirus in polarized Calu-3 lung epithelial cells. J Virol. 2005;79:9470–9. https://doi.org/10.1128/JVI.79.15.9470-9479.2005
30. Lau SKP, Lau CCY, Chan KH, Li CPY, Chen H, Jin DY, et al. Delayed induction of proinflammatory cytokines and suppression of innate antiviral response by the novel Middle East respiratory syndrome coronavirus: implications for pathogenesis and treatment. J Gen Virol. 2013;94:2679–90. https://doi.org/10.1099/vir.0.055533-0
31. Yoshikawa T, Hill TE, Yoshikawa N, Popov VL, Galindo CL, Garner HR, et al. Dynamic innate immune responses of human bronchial epithelial cells to severe acute respiratory syndrome-associated coronavirus infection. PLoS One. 2010;5:e8729. https://doi.org/10.1371/journal.pone.0008729
32. Wang X, Xu W, Hu G, Xia S, Sun Z, Liu Z, et al. SARS-CoV-2 infects T lymphocytes through its spike protein-mediated membrane fusion. Cell Mol Immunol. 2020. https://doi.org/10.1038/s41423-020-0424-9
33. Chu H, Zhou J, Wong BH, Li C, Chan JF, Cheng ZS, et al. Middle East respiratory syndrome coronavirus efficiently infects human primary T lymphocytes and activates the extrinsic and intrinsic apoptosis pathways. J Infect Dis. 2016;213:904–14. https://doi.org/10.1093/infdis/jiv380
34. Uhlén M, Fagerberg L, Hallström BM, Lindskog C, Oksvold P, Mardinoglu A, et al. Proteomics. Tissue-based map of the human proteome. Science. 2015;347:1260419. https://doi.org/10.1126/science.1260419
35. Hoffmann M, Kleine-Weber H, Schroeder S, Krüger N, Herrler T, Erichsen S, et al. SARS-CoV-2 cell entry depends on ACE2 and TMPRSS2 and is blocked by a clinically proven protease inhibitor. Cell. 2020;181:271–280.e8. https://doi.org/10.1016/j.cell.2020.02.052

Address for correspondence: Karen Mossman, McMaster University, 1280 Main St W, Hamilton, Ontario L8S 4L8, Canada; email: mossk@mcmaster.ca

Evaluation of World Health Organization–Recommended Hand Hygiene Formulations

Miranda Suchomel, Maren Eggers, Steffen Maier, Axel Kramer, Stephanie J. Dancer, Didier Pittet

As a result of the coronavirus disease pandemic, commercial hand hygiene products have become scarce and World Health Organization (WHO) alcohol-based hand rub formulations containing ethanol or isopropanol are being produced for hospitals worldwide. Neither WHO formulation meets European Norm 12791, the basis for approval as a surgical hand preparation, nor satisfies European Norm 1500, the basis for approval as a hygienic hand rub. We evaluated the efficacy of modified formulations with alcohol concentrations in mass instead of volume percentage and glycerol concentrations of 0.5% instead of 1.45%. Both modified formulations met standard requirements for a 3-minute surgical hand preparation, the usual duration of surgical hand treatment in most hospitals in Europe. Contrary to the originally proposed WHO hand rub formulations, both modified formulations are appropriate for surgical hand preparation after 3 minutes when alcohol concentrations of 80% wt/wt ethanol or 75% wt/wt isopropanol along with reduced glycerol concentration (0.5%) are used.

Because commercial products are hardly or no longer available due to the coronavirus disease (COVID-19) pandemic, alcohol-based hand rub formulations for hygienic and surgical hand treatment published by the World Health Organization (WHO) in 2009 (*1*) for local production in developing countries are now being produced for use in hospitals worldwide. As shown previously (*2*), neither the formulation based on ethanol 80% vol/vol (WHO I) nor that based on isopropanol 75% vol/vol (WHO II), meets the efficacy requirements of the European Norm (EN) 12791 (*3*), which must be fulfilled to obtain approval as a surgical hand preparation in Europe. Each WHO-recommended formulation is also insufficient for hygienic hand antisepsis when 3 mL is applied for 30 seconds (*4*) according to the test method described in EN 1500 (*5*). The requirements can be met only if the volume is doubled (6 mL) and exposure is extended to 60 seconds (*4*). But sufficient efficacy has been achieved by using modified WHO formulations with an increased alcohol concentration of 80% wt/wt ethanol or 75% wt/wt isopropanol at 3 mL for 30 seconds (*4*).

On the basis of those results, we modified both WHO formulations by increasing their alcohol concentrations through changing their volume percentages into weight percentages and by prolonging the duration of application from 3 to 5 minutes. These modifications have been shown to render the immediate effects of both formulations noninferior to the reference of EN 12791, but this improvement was not observed for the so-called 3-hour effect (i.e., 3 hours after hand antisepsis) (*6*). Because the high glycerol concentration (1.45% vol/vol) of the original formulations has been shown to exert a negative influence on the 3-hour efficacy of alcohols (*7*), we performed further studies by reducing the glycerol content of the WHO formulations by 50%. By increasing the alcohol concentration by ≈5% and reducing glycerol concentrations to 0.725%, both modified WHO formulations meet the efficacy requirements of EN 12791 when used for 5 minutes (*8*). Although both new formulations were successfully tested for a 5-minute application, our suggestions for improving efficacy were not accepted by the WHO because the common duration for surgical hand preparation in most hospitals is 3 minutes. Furthermore, no information on dermal

Author affiliations: Medical University, Vienna, Austria (M. Suchomel, S. Maier); Laboratory Prof. Gisela Enders & Colleagues MVZ and Institute of Virology, Infectiology and Epidemiology e.V., Stuttgart, Germany (M. Eggers); University of Medicine, Greifswald, Germany (A. Kramer); Hairmyres Hospital, National Health Service, Lanarkshire, Scotland, UK (S.J. Dancer); Edinburgh Napier University, Edinburgh, Scotland, UK (S.J. Dancer); World Health Organization, Geneva, Switzerland (D. Pittet); University of Geneva Hospitals and Faculty of Medicine, Geneva (D. Pittet)

DOI: https://doi.org/10.3201/eid2609.201761

tolerability and healthcare workers' acceptance of these modified formulations was available.

In 2019, Menegueti et al (*9*) showed that a modified WHO I formulation containing only 0.5% glycerol led to better ratings of skin tolerance than the original WHO formulation containing 1.45% or a modification containing 0.75% glycerol. Because all such alternative formulations require testing for not only dermal tolerability but also for bactericidal performance, we investigated the efficacy of these modified WHO formulations (mass instead of volume percentage ethanol or isopropanol and 0.5% instead of 1.45% glycerol) according to EN 12791 (*3*), with an application duration of 3 minutes, as commonly used in surgical theaters in Europe.

Materials and Methods

We used 2 formulations in this study. WHO I modified comprised ethanol (for analysis; Merck KGaA, https://www.emdgroup.com) 80% wt/wt, hydrogen peroxide (for analysis; Merck) 0.125% vol/vol, and glycerol (for analysis; Merck) 0.5% vol/vol. WHO II modified comprised isopropanol (for analysis; Merck) 75% wt/wt, hydrogen peroxide 0.125% vol/vol, and glycerol 0.5% vol/vol. For the reference alcohol of EN 12791, we used N-propanol (for analysis; Merck) 60% (vol/vol) without additions (*3*).

We recruited 24 volunteers from the Institute for Hygiene and Applied Immunology, Medical University of Vienna (Vienna, Austria), to participate in the study. Exclusion criteria were age <18 years and skin breaks on hands (e.g., cuts, abrasions or other skin disorders). Nails were short and clean and volunteers agreed to not use any antibacterial soap or other antibacterial substance during the trial, starting from 1 week before testing. Volunteers were also asked to not use any hand rub or hand cream on trial days. All volunteers provided written informed consent. The study protocol was approved by the institutional ethics committee of the Medical University of Vienna (ethical vote no. 2092/2019).

Culture media were as described in EN 12791 (*3*). For sampling and dilution fluids, we used tryptic soy broth (CASO broth; Merck). For counting plates, we used tryptic soy agar (CASO agar; Merck). Neutralizing agents were not necessary for any of the tested modified WHO formulations because even dilution in pure broth without supplement in previous validation tests has been shown to neutralize any antimicrobial effect (*4*).

We compared the efficacy of the modified WHO formulations with that of the standardized reference surgical hand treatment described in EN 12791. We used a Latin-square design with 3 groups, each with 8 randomly allocated volunteers, and as many experimental runs as there were formulations, including the reference. In every run, we tested all hand treatment procedures concurrently. At the end of the third test run, every volunteer had used each formulation once. We spaced test runs apart by 1 week to allow reversion of normal skin flora.

We used the test method described in EN 12791 (*3*). In brief, after a preparatory hand wash for 1 minute with 5 mL of 20% nonmedicated soap applied onto wet hands to remove transient bacterial flora and any other soil, participants rinsed their hands under running tap water and dried them with soft paper towels. Pretreatment values were established by rubbing and kneading the fingertips, including the thumbs, of both hands for 1 minute at the base of a petri dish (diameter 9 cm) containing 10 mL of sampling fluid, one for each hand. Subsequently, surgical hand antisepsis was performed according to the standardized hand rub procedure of EN 12791 by applying and rubbing as many 3-mL portions of the study formulations (i.e., WHO I modified, WHO II modified, or reference) onto both hands up to the wrists as necessary to keep the hands wet for 3 minutes.

According to EN 12791, the efficacy of a preoperative hand procedure is determined immediately and 3 hours after hand antisepsis. Thus, to assess the posttreatment values of a formulation, we sampled one randomly selected hand as described for the pretreatment values immediately after hand antisepsis (immediate effect). The other hand was gloved and sampled 3 hours later to assess the 3-hour effect. We performed quantitative surface cultures from all sampling fluids and dilutions on tryptic soy agar, incubated counting plates for a total of 48 hours at 36°C ± 1°, and counted colony-forming units.

For statistical analyses, we expressed all colony counts per mL of sampling fluid as decadic logarithms. From the intra-individual differences between $\log_{10}$ pretreatment minus $\log_{10}$ posttreatment values, we calculated individual $\log_{10}$ reduction factors separately for immediate and 3-hour effects. We tested pretreatment values of study formulations and the reference formulation for significant differences by means of the Friedman analysis of variance with an agreed significance level of $p = 0.05$. Subsequently, we tested the differences between the $\log_{10}$ reduction factors from each study formulation and the appropriate values of the reference for significance by a nonparametric noninferiority test according to Hodges-Lehmann. We rejected inferiority of a study formulation and assumed noninferiority if the Hodges-Lehmann

upper 97.5% confidence limits for the differences in $\log_{10}$ bacterial reductions between study formulations and reference treatment were smaller than the agreed inferiority margin of 0.75 $\log_{10}$ (immediate effect) or 0.85 $\log_{10}$ (3-hour effect). We set the level of significance at p = 0.025 (1-sided). Furthermore, we used the Wilcoxon matched-pairs, signed-ranks test to test for a suspected sustained effect at p = 0.01 (1-sided) if—as concluded from a higher mean $\log_{10}$ reduction—a study formulation was suspected to be more efficacious than the reference antisepsis procedure 3 hours after antisepsis.

Results

We observed no significant differences between the means of the $\log_{10}$ pretreatment bacterial counts for the immediate and 3-hour efficacy tests. Hence, the baseline for each study formulation can be considered equivalent.

Overall, immediate effects were comparable to that of the reference alcohol of EN 12791; typical magnitude was mean $\log_{10}$ reductions of >2.00 (Table). Each modified formulation was even more effective than the reference alcohol immediately after hand antisepsis. Each modified formulation also met the 3-hour efficacy requirements of EN 12791. The mean $\log_{10}$ bacterial reduction of the formulation based on isopropanol was greater by 0.15 $\log_{10}$ than that of the reference alcohol, but this difference was not significant (p = 0.01 by Wilcoxon matched-pairs signed-ranks test), so sustained efficacy cannot be confirmed.

Discussion

The COVID-19 pandemic has led to scarcity of commercial hand antisepsis agents, and healthcare institutions worldwide are seeking alternatives. Since the end of February 2020, pharmacies in Europe have been producing the WHO-recommended formulations either for sale or as donations for personal use by the general population or use in healthcare settings. Use of hygienic hand preparations made with the original WHO-recommended formulations might be justifiable to prevent infection or transmission of pathogens outside patient care. However, to be approved in Europe, preparations for hygienic hand antisepsis used in healthcare facilities must meet the bactericidal efficacy requirements of EN 1500 (*5*) under practical use conditions. Both WHO-recommended formulations failed the EN 1500 requirements with use of 3 mL for 30 seconds, the common duration of application in hospitals in Europe (*4*). Sufficient bactericidal efficacy could be achieved with the original WHO-recommended formulation with 6 mL in 60 seconds or with 3 mL in 30 seconds when modified formulations with increased alcohol concentrations of 80% wt/wt ethanol or 75% wt/wt isopropanol were used (*4*). In general, a shortening of the necessary exposure time may help medical personnel comply with hand hygiene standards. A recent study (A. Kratzel et al., unpub. data, https://www.biorxiv.org/content/10.1101/2020.03.10.986711v1) showed that severe acute respiratory coronavirus 2 can be inactivated within 30 seconds by both WHO-recommended formulations but also by modifications as proposed by us in 2013 (*8*) or used by Allegranzi et al. (*10*) in a before–after intervention cohort study.

The use of WHO-recommended formulations in hospitals, including for surgical hand preparation, is paramount despite the lack of commercial agents. In Europe, before a product is allowed to be used for surgical hand preparation, its efficacy must be evaluated in the laboratory on the hands of volunteers according to EN 12791 (*3*), the most stringent available in vivo test method for efficacy testing. This testing ensures that results are generated under controlled conditions but also under as near as possible practical in vivo conditions. The bacterial reduction is measured directly after hand antisepsis on one hand (immediate effect) and after 3 hours on the other (gloved) hand (3-hour effect). According to the requirements of the norm, a formulation shall not be significantly less efficacious than a reference procedure at both times (i.e., immediately and 3 hours after application). The 2009 WHO guideline reported that WHO I did not pass EN 12791 under 2 laboratory testing conditions and WHO II under 1 of 2 laboratory testing conditions (*1*). Even

Table. Immediate and 3-hour effects after 3-minute application of modified WHO formulations compared with 3-minute applications of reference surgical hand antiseptic treatment according to European Norm 12791

	Immediate effect		3-hour effect	
Formulation	Mean $\log_{10}$ reduction	Hodges-Lehmann upper 97.5% confidence limit†	Mean $\log_{10}$ reduction	Hodges-Lehmann upper 97.5% confidence limit‡
WHO I modified with ethanol	2.99 ± 1.03	0.03 n.i.	1.95 ± 0.97	0.55 n.i.
WHO II modified with isopropanol	2.95 ± 1.03	0.23 n.i.	2.17 ± 1·48	0.47 n.i.
Reference	2.64 ± 0.93	Not applicable	2.02 ± 1.06	Not applicable

*n = 24 study participants. n.i., noninferior versus reference; WHO, World Health Organization.
†With an agreed inferiority margin of 0.75 $\log_{10}$.
‡With an agreed inferiority margin of 0.85 $\log_{10}$.

prolonging the duration of application to 5 minutes, the longest duration allowed by EN 12791, did not achieve a favorable outcome for the original WHO formulations (*2*,*6*). Increasing the alcohol concentration of both formulations by ≈5% (by changing to weight percentage concentrations) rendered the immediate effect of the 2 formulations noninferior to the reference; unfortunately, the 3-hour effect was still significantly less effective than the reference alcohol (*6*). The reason for these results was attributed to the high concentration of glycerol (1.45% vol/vol). Although the 3-hour effects of each formulation with reduced glycerol content (0.725%) were rendered noninferior to the reference, glycerol-free preparations were even more effective than reference EN 12791. We have been able to show how the WHO formulations can be improved to meet the European standards; however, our proposals have not yet been endorsed. One of the arguments given was the lack of data on acceptance and tolerability for the modified formulations. Another argument was the necessary application duration of 5 minutes for surgical hand preparation, which does not correspond with common practice.

Frequent use of alcohol-based hand rubs can cause skin dryness unless emollients or humectants such as glycerol are added to the formulation. A recent study (*9*) evaluated the skin tolerability of healthcare workers to the original WHO formulation containing 1.45% glycerol against 3 other concentrations (0%, 0.5%, and 0.75%) of glycerol in a tropical climate healthcare setting. Dermal application of glycerol, a trihydroxy alcohol, increases the endogenous delivery of glycerol with improvement of stratum corneum hydration, skin barrier function, and mechanical properties. It also inhibits stratum corneum lipid phase transition, protection against irritating stimuli, and enhancement of desmosomal degradation (*11*). A modified WHO formulation containing only 0.5% glycerol leads to better ratings of skin tolerance than the original formulation and may therefore offer the best balance between skin tolerance and antimicrobial efficacy. In addition, it is useful to have the same alcohol-based hand rub formulation in the surgical setting and in other medical settings, especially if products are scarce. Because glycerol availability is also critical during the current pandemic, lowering the glycerol concentration might improve availability of these alcohol-based formulations in areas with limited supplies, such as developing countries.

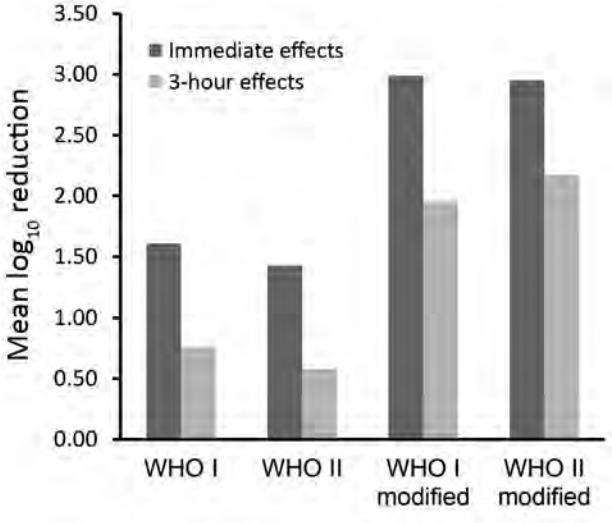

Figure. Comparison of the immediate and 3-hour effects of the WHO-recommended (WHO I and WHO II) and modified (WHO I modified and WHO II modified) formulations among 24 volunteers after a 3-minute surgical hand preparation according to European Norm 12791 (*3*). WHO I: ethanol 80% vol/vol + glycerol 1.45% vol/vol + hydrogen peroxide 0.125% vol/vol. WHO II: isopropanol 75% vol/vol + glycerol 1.45% vol/vol + hydrogen peroxide 0.125% vol/vol. WHO I modified: ethanol 80% wt/wt + glycerol 0.5% vol/vol + hydrogen peroxide 0.125% vol/vol. WHO II modified: isopropanol 75% wt/wt + glycerol 0.5% vol/vol + hydrogen peroxide 0.125% vol/vol. WHO, World Health Organization.

In this study, we were able to show, once again, that the effect on the resident skin flora of the original WHO formulations can be improved if the concentration of the alcohols is increased by using weight instead of volume percentage. In addition, by further reducing the glycerol content from 1.45% to 0.725% or to 0.50%, the 3-hour effects of each formulation can be improved to such an extent that the requirement of the European test standard is already ensured after 3 minutes of application. Although the criteria for use as a product regulated by the US Food and Drug Administration differ from the EN requirements, these results could also be of interest to US healthcare providers. Reductions achieved with the modified formulations were >1 $\log_{10}$ step higher than those achieved with the original WHO-recommended formulations when applied for 3 minutes for both immediate and 3-hour effects (Figure).

On the basis of these results and considering the current situation, we believe that the original WHO formulations should be urgently reconsidered. We therefore recommend a modification of the WHO I formulation with 80% wt/wt ethanol, 0.125% vol/vol hydrogen peroxide, and 0.50% vol/vol glycerol and a modification of the WHO II formulation with 75% wt/wt isopropanol, 0.125% vol/vol hydrogen peroxide, and 0.50% vol/vol glycerol.

Acknowledgments

We thank Martina Weinlich for her excellent technical help.

About the Author

Dr. Suchomel works as a scientist at the Institute of Hygiene and Applied Immunology, Medical University of Vienna. Her primary research interest is infection prevention, especially hand hygiene.

References

1. World Health Organization. WHO guidelines on hand hygiene in health care. Geneva: The Organization; 2009.
2. Kampf G, Ostermeyer C. World Health Organization–recommended hand-rub formulations do not meet European efficacy requirements for surgical hand disinfection in five minutes. J Hosp Infect. 2011;78:123–7. https://doi.org/10.1016/j.jhin.2011.02.005
3. European Committee for Standardization. European Norm (EN) 12791. Chemical disinfectants and antiseptics. Surgical hand disinfection—test method and requirement (phase 2/step 2). Brussels: The Committee; 2018.
4. Suchomel M, Kundi M, Pittet D, Weinlich M, Rotter ML. Testing of the World Health Organization recommended formulations in their application as hygienic hand rubs and proposals for increased efficacy. Am J Infect Control. 2012;40:328–31. https://doi.org/10.1016/j.ajic.2011.06.012
5. European Committee for Standardization. European Norm (EN) 1500. Chemical disinfectants and antiseptics—hygienic hand disinfection—test method and requirement (phase 2/step 2). Brussels: The Committee; 2018.
6. Suchomel M, Kundi M, Allegranzi B, Pittet D, Rotter ML. Testing of the World Health Organization-recommended formulations for surgical hand preparation and proposals for increased efficacy. J Hosp Infect. 2011;79:115–8. https://doi.org/10.1016/j.jhin.2011.05.005
7. Suchomel M, Rotter M, Weinlich M, Kundi M. Glycerol significantly decreases the three hour efficacy of alcohol-based surgical hand rubs. J Hosp Infect. 2013;83:284–7. https://doi.org/10.1016/j.jhin.2012.11.030
8. Suchomel M, Kundi M, Pittet D, Rotter ML. Modified World Health Organization hand rub formulations comply with European efficacy requirements for preoperative surgical hand preparations. Infect Control Hosp Epidemiol. 2013;34:245–50. https://doi.org/10.1086/669528
9. Menegueti MG, Laus AM, Ciol MA, Auxiliadora-Martins M, Basile-Filho A, Gir E, et al. Glycerol content within the WHO ethanol-based handrub formulation: balancing tolerability with antimicrobial efficacy. Antimicrob Resist Infect Control. 2019;8:109. https://doi.org/10.1186/s13756-019-0553-z
10. Allegranzi B, Aiken AM, Zeynep Kubilay N, Nthumba P, Barasa J, Okumu G, et al. A multimodal infection control and patient safety intervention to reduce surgical site infections in Africa: a multicentre, before-after, cohort study. Lancet Infect Dis. 2018;18:507–15. https://doi.org/10.1016/S1473-3099(18)30107-5
11. Fluhr JW, Darlenski R, Surber C. Glycerol and the skin: holistic approach to its origin and functions. Br J Dermatol. 2008;159:23–34. https://doi.org/10.1111/j.1365-2133.2008.08643.x

Address for correspondence: Miranda Suchomel, Institute of Hygiene and Applied Immunology, Medical University of Vienna, Kinderspitalgasse 15, 1090 Vienna, Austria; email: miranda.suchomel@meduniwien.ac.at

Retrospective Description of Pregnant Women Infected with Severe Acute Respiratory Syndrome Coronavirus 2, France

Alexandre J. Vivanti, Jérémie Mattern, Christelle Vauloup-Fellous, Jacques Jani, Luc Rigonnot, Larissa El Hachem, Agnès Le Gouez, Céline Desconclois, Imane Ben M'Barek, Jeanne Sibiude, Alexandra Benachi, Olivier Picone, Anne-Gaël Cordier

Few data are available on the management of pregnant women infected with severe acute respiratory syndrome coronavirus 2 (SARS-CoV-2). We conducted a retrospective study of 100 pregnant women with SARS-CoV-2 infection in 4 obstetric units in the Paris metropolitan area of France during March 12–April 13, 2020. Among patients, 52 (52%) were hospitalized, 10 (10%) in intensive care units (ICUs). Women with higher body mass indexes (BMIs; median 30.7 kg/m^2) were more likely to be hospitalized in ICUs than other women (median BMI 26.2 kg/m^2). Women hospitalized in ICUs had lower lymphocyte count at diagnosis (median 0.77 × 10^9 cells/L) than women not hospitalized in ICUs (median lymphocyte count 1.15 × 10^9 cells/L). All women requiring oxygen >5 L/min were intubated. Clinical and laboratory evaluation of SARS-CoV-2–positive pregnant women at the time of diagnosis can identify patients at risk for ICU hospitalization.

Recent literature from China, Italy, and the United States suggests that pregnant women are not at higher risk for severe forms of coronavirus disease (COVID-19) from infection with severe acute respiratory syndrome (SARS) coronavirus 2 (SARS-CoV-2), contrary to what has been reported with SARS and MERS (*1*–*3*). Nevertheless, 3%–35% of infected pregnant women were hospitalized in intensive care units (ICUs) (*2*,*4*–*7*) and respiratory and hematology anomalies were described, just as in the nonpregnant infected population (*8*). In the third trimester, and especially after 37 weeks' gestation, the fetal prognosis is driven by maternal clinical tolerance and by whether a cesarean delivery is required. Few cases of vertical transmission have been published (*6*–*9*), and no data are available on the risk factors for such transmission. However, between 24 and 32 weeks' gestation, the risk for premature birth and the need to reduce its effects on neonatal outcome by giving steroids and magnesium sulfate to the mother complicate decision-making. Little published data are available on the management of SARS-CoV-2-infected pregnant women (*10*). We describe the experience of 4 tertiary referral obstetric units in managing such cases in the Paris metropolitan area of France.

Author affiliations: Antoine Béclère Hospital, Paris Saclay University, Clamart, France (A.J. Vivanti, J. Mattern, A. Le Gouez, C. Desconclois, A. Benachi); Paul Brousse Hospital, Paris Saclay University, Villejuif, France (C. Vauloup-Fellous); University Hospital Brugmann, Université Libre de Bruxelles, Brussels, Belgium (J. Jani); Centre Hospitalier Sud-Francilien, Corbeil-Essonnes, France (L. Rigonnot, L. El Hachem); Bicêtre Hospital, Paris Saclay University, Le Kremlin-Bicêtre, France (I. Ben M'Barek, A.-G. Cordier); Louis Mourier Hospital, Paris University, Colombes, France (J. Sibiude, O. Picone)

DOI: https://doi.org/10.3201/eid2609.202144

Materials and Methods

Study Design and Population

We conducted a retrospective multicenter review of the medical records of all pregnant women with SARS-CoV-2 from March 12–April 13, 2020, in 4 tertiary referral obstetric units in the Paris metropolitan area. Hospitals included in the study were Antoine Béclère, Clamart; Bicêtre Hospital, Le Kremlin Bicêtre; Louis-Mourier, Colombes; and Centre Hospitalier Sud Francilien, Evry. All women in the second and third trimester of pregnancy (≥14 weeks' gestation) had real-time reverse transcription PCR (RT-PCR) testing of respiratory tract samples to detect

SARS-CoV-2. Gestational age was calculated according to crown–rump length measurement at the first-trimester scan. Because of the moderate sensitivity of RT-PCR (*11*–*13*), patients with negative results also had computed tomography imaging of the chest, which was considered positive when meeting conventional criteria for SARS-CoV-2 infection (*14*). Patients were considered cured ≥10 days after the positive diagnosis and without clinical signs for 48 h, or 14 days from the beginning of the disease with only benign signs without hospitalization.

We retrospectively allocated women to subgroups according to location for further care after first assessment. The outpatient follow-up group was defined as infected pregnant women who could return home after assessment in the emergency department. Close outpatient follow-up was undertaken and included a daily call from an obstetrician/gynecologist. In the case of suspected worsening, such as fever, dyspnea, or tachycardia, or obstetric concern, women were asked to return to the hospital for further assessment and hospitalized, if needed. The conventional hospitalization group was defined as women immediately hospitalized after SARS-CoV-2 diagnosis because close medical supervision or noninvasive oxygen therapy with flow rates <3 L/min, was needed. The ICU hospitalization group was defined as women hospitalized in ICUs because of clinical worsening, including respiratory distress or increased

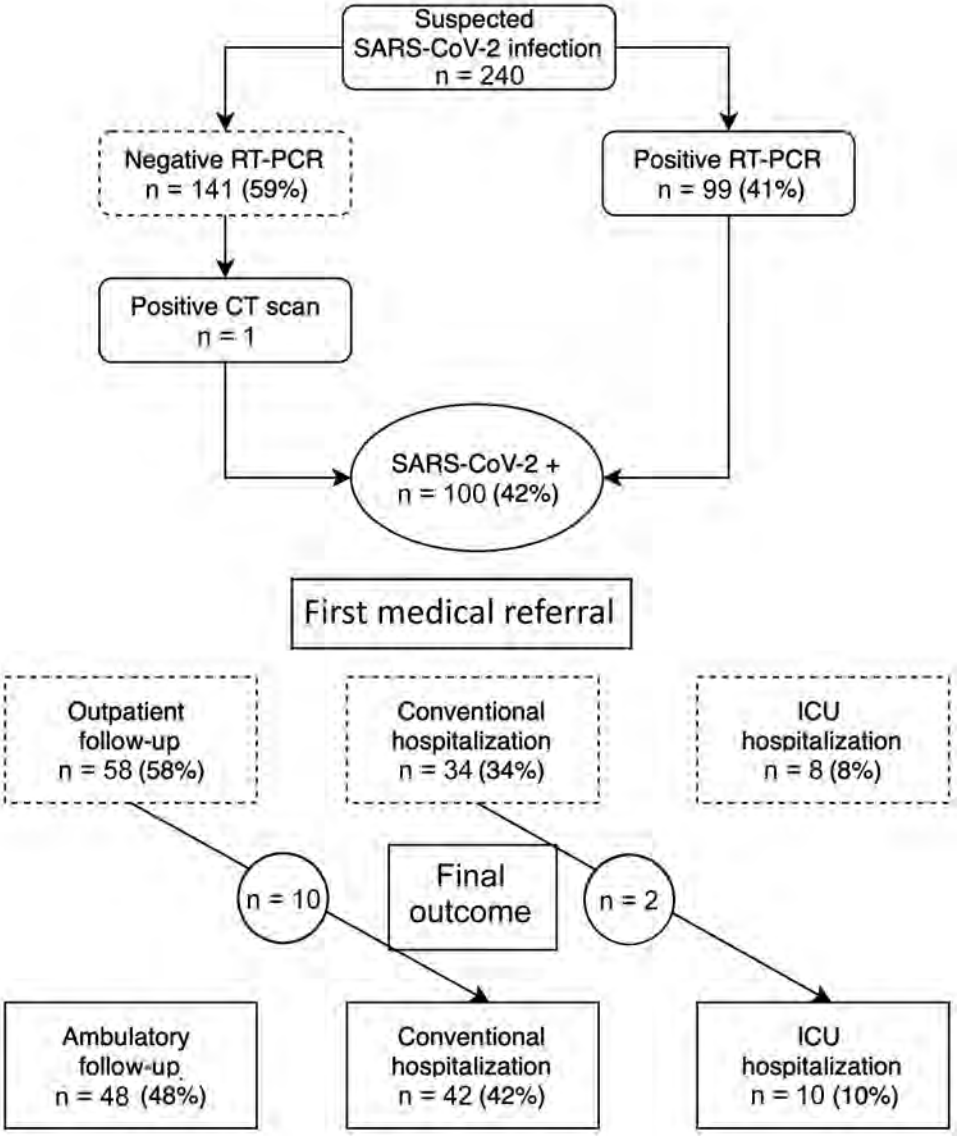

Figure. Flowchart of study data showing status and medical referral in a cohort of pregnant women with SARS-CoV-2 infection, France. CT, computed tomography; RT-PCR, reverse transcription PCR; SARS-CoV-2, severe acute respiratory syndrome coronavirus 2.

oxygen requirement, and the need for continuous medical supervision, noninvasive high-flow oxygen delivery, or invasive mechanical ventilation.

Sample Collection

Laboratory samples were obtained for RT-PCR and prepared as follows. Nasopharyngeal swabs were obtained following US Centers for Disease Control and Prevention guidelines (*15*). Swabs were placed in Virocult viral transport media (Sigma, https://www.sigmaaldrich.com). All specimens were kept at 4°C and tested within 24 hours.

RT-PCR

Viral RNA was extracted from 200 µL of clinical samples with the NucliSENS easyMag kit (BioMérieux, https://www.biomerieux.com) and eluted in 100 µL. The RealStar SARS-CoV-2 RT-PCR Kit 1.0 (Altona Diagnostics GmbH, https://www.altona-diagnostics.com) targeting the E gene, specific for lineage B-betacoronavirus, and the S gene, specific for SARS-CoV-2, was used, according to the manufacturer's recommendations. The assay includes a heterologous amplification system as an internal positive control to identify possible RT-PCR inhibition and to confirm the integrity of the reagents of the kit. Thermal cycling was performed at 55°C for 20 min for reverse transcription, followed by 95°C for 2 min, and then 45 cycles of 95°C for 15 s, 55°C for 45 s, and 72°C for 15 s with an Applied Biosystems ViiA7 instrument (ThermoFisher Scientific, https://www.thermofisher.com). A cycle threshold <40 was considered positive for SARS-CoV-2 RNA.

Table 1. Baseline characteristics at diagnosis for pregnant women infected with sever acute respiratory syndrome 2, France*

Maternal and obstetric characteristics	Value
Total patients	100
Median age, y (IQR)	33.7 (29–36.7)
Median gravidity (IQR)	3 (1.8–4)
Median parity (IQR)	1 (0–3)
Median BMI, kg/m^2 (IQR)	27.0 (23.5–30.6)
Preexisting conditions	
Diabetes mellitus	7 (7)
Chronic high blood pressure	6 (6)
Tobacco use	2 (2)
Asthma	9 (9)
Median gestational age at diagnosis, wk (IQR)	31.3 (25.6–35.6)
14–24	18 (18)
25–32	41 (41)
33–37	20 (20)
>37	20 (20)
Early postpartum	1 (1)
Signs and symptoms	
Fever	62 (62)
Cough	80 (80)
Dyspnea	30 (30)
Myalgia	26 (26)
Anosmia	16 (16)
Sore throat	9 (9)
Diarrhea or vomiting	10 (10)
Rash	0
Other signs	13 (13)

*Values are no. (%) except as indicated. BMI, body mass index; IQR, interquartile range.

Data Collection and Statistical Analysis

We retrospectively collected clinical, laboratory, and imaging data on mothers and newborns from medical records. We performed statistical analyses by using GraphPad Prism version 8.0.0 (GraphPad Software, https://www.graphpad.com). We used a 2-tailed Mann-Whitney U test for statistical analysis of continuous variables and Fisher exact test for statistical analysis of categorical variables. We expressed continuous variables as median with interquartile range (IQR) and categorical variables as number (percentage). We considered $p<0.05$ statistically significant.

This study was approved by the institutional review board of the French College of Obstetricians and Gynecologists (approval no. CEROG OBS-2020–0402). All data were de-identified to ensure patient privacy and confidentiality.

Results

Maternal Characteristics and Signs and Symptoms at Diagnosis

During March 12–April 13, 2020, a total of 240 women were tested for SARS-CoV-2 infection during pregnancy or the early postpartum period because of relevant symptoms (Figure). Among them, 100 (42%) were considered infected; 99 (41%) had a positive RT-PCR, and 1 woman with a negative RT-PCR test was considered positive because computed tomography imaging of the chest was compatible with SARS-CoV-2 infection. The median age of the infected women was 33.7 years (range 29–36.7 years); 81 (81%) were tested after 24 weeks' gestation, and 18 (18%) were tested between 14 and 24 weeks' gestation. One asymptomatic patient was tested 2 days postpartum because of an isolated increase in activated partial thromboplastin time (aPPT; ratio 1.40), but signs of primary coagulopathy or consumption were not noted, and the patient's platelet count was 154 × 10^9/L, prothrombin time ratio was 100%, and fibrinogen activity was 5.5 g/L.

A few patients had underlying conditions, including 9 (9%) with asthma, 7 (7%) with diabetes mellitus, and 6 (6%) with chronic high blood pressure. Median body mass index (BMI) was 27.0 kg/m^2

Table 2. Maternal and obstetric characteristics according to medical referral for pregnant women with severe acute respiratory syndrome 2 infection, France*

Characteristics	Non-ICU hospitalization, n = 90	ICU hospitalization, n = 10	p value
Median age, y (IQR)	33.2 (29.1–36.7)	33.6 (28.3–34.3)	0.89
Median BMI, kg/m^2 (IQR)	26.2 (23–29.7)	30.7 (29.8–33.1)	0.003
Underlying conditions, no. (%)			
Diabetes mellitus	7 (8)	0	1
Chronic high blood pressure	5 (6)	1 (10)	0.48
Tobacco use	2 (2)	0	1
Asthma	7 (8)	2 (20)	0.22
Median gestational age at diagnosis, wks (IQR)	31.3 (25–35.6)	28.5 (26.9–34.2)	0.78

*ICU, intensive care unit; IQR, interquartile range

(IQR 23.5–30.6 kg/m^2). At diagnosis, all but 1 woman experienced symptoms compatible with SARS-CoV-2 infection; 80 (80%) had cough, 62 (62%) had fever, 30 (30%) had dyspnea, 26 (26%) had myalgia, 16 (16%) had anosmia, and 10 (10%) had gastrointestinal symptoms. None reported rash (Table 1).

After a first evaluation, 58 (58%) of the infected women were eligible for close outpatient follow-up; 10 (17%) were hospitalized during later follow-up. Forty-two (42%) women were immediately hospitalized, 8 (19%) in ICUs and 34 (80.9%) in conventional wards. Later, 2 women were switched from conventional hospitalization to the ICU because of increased respiratory symptoms. Among all patients, 32 (32%) required oxygen therapy. At the end of the study period, 48 (48%) patients received outpatient follow-up only, and 52 (52%) were hospitalized, 42 in conventional wards and 10 in ICUs.

We found that women with a high BMI (30.7 kg/m^2 [IQR 29.8–33.1 kg/m^2]) were more likely to be hospitalized in ICUs than women with lower BMIs (26.2 kg/m^2 [IQR 23–29.7 kg/m^2]; p = 0.003). We noted no statistically significant difference in maternal age, gravidity, parity, gestational age at diagnosis, or preexisting medical conditions among patients admitted to ICUs (Table 2). We performed a similar comparison between women with outpatient follow-up (BMI 26.2 kg/m^2 [IQR 22.9–29.9 kg/m^2]) and women who required hospitalization (BMI 30.7 kg/m^2 [IQR 24.5–30.9 kg/m^2]). We noted BMI also was the only maternal baseline characteristic with a statistically significant difference (p = 0.003) between the 2 groups (Appendix Table 1, https://wwnc.cdc.gov/EID/article/26/9/20-2144-App1.pdf). No maternal thromboembolic event was noted during the study period.

Laboratory Parameters at SARS-CoV-2 Diagnosis

We analyzed laboratory parameters at diagnosis for maternal medical care (Table 3). Lymphocyte count at diagnosis was lower in women hospitalized in ICUs (0.77 × 10^9 cells/L [IQR 0.7–1× 10^9 cells/L]) than in women in the conventional hospitalization or outpatient follow-up groups (1.15 × 10^9 cells/L [IQR 0.9–1.6 × 10^9 cells/L]; p = 0.01). Moreover, the proportion of women with lymphocytopenia at diagnosis also was much higher in the ICU group (89%) than in the rest of the cohort (36%; p = 0.008). Hemoglobin count at diagnosis was lower in women who needed hospitalization in ICUs (9.8 g/dL [IQR 9.3–11.3 g/dL]) than in the rest of the cohort (11.4 g/

Table 3. Laboratory parameters at diagnosis according to medical referral for pregnant women with severe acute respiratory syndrome 2 infection, France*

	Non-ICU hospitalization, n = 90		ICU hospitalization, n = 10		
Laboratory findings	Median (IQR)	No. (%)	Median (IQR)	No. (%)	p value
Hemoglobin, g/dL	11.4 (10.5–12.2)	64 (66.7)	9.8 (9.3–11.3)	9 (90)	0.02
Platelet count, × 10^9/L	230 (162–273)	63 (70.0)	205 (164–271)	9 (90)	0.98
Leukocyte count, × 10^9 cells/L	7.2 (5.4–8.9)	63 (70.0)	6.6 (6.1–7.2)	9 (90)	0.68
Lymphocyte count, × 10^9 cells/L	1.15 (0.9–1.6)	58 (64.4)	0.77 (0.7–1)	9 (90)	0.01
Lymphocytopenia, <1.00 × 10^9 cells/L	NA	21/58 (36.2)†	NA	8/9 (88.9)†	0.008
Prothrombin time, %	100 (99–100)	53 (58.9)	100 (100–100)	7 (70)	0.61
aPPT, ratio	1.06 (1–1.2)	52 (57.8)	1.12 (1–1.4)	7 (70)	0.16
Prolonged aPPT ratio (≥1.20)	NA	13/53 (24.5)†	NA	3/7 (43)†	0.38
Fibrinogen activity, g/L	4.8 (4–5.8)	45 (50.0)	5.1 (4.5–5.5)	6 (60)	0.73
AST, U/L	25 (20–35)	48 (53.3)	30 (22–59)	8 (80)	0.38
ALT, U/L	17 (11–32)	49 (54.4)	19 (12–48)	8 (80)	0.46
C-reactive protein, mg/L	23 (9–42)	53 (58.9)	27 (22–108)	8 (80)	0.15
Creatinine, μmol/L	47 (41–57)	45 (50.0)	50 (38–55)	7 (70)	0.94

*ALT, alanine aminotransferase; aPPT, activated partial thromboplastin time; AST, aspartate aminotransferase; ICU, intensive care unit; IQR, interquartile range; NA, not applicable.
†Per available results.

dL [IQR 10.5–12.2 g/dL]; p = 0.02). We did not detect any statistically significant differences between the 3 groups for white cell count, prothrombin time, aPPT, fibrinogen activity, alanine aminotransferase, aspartate aminotransferase, C-reactive protein, or creatinine. We performed a similar comparison between women with outpatient follow-up and women who required hospitalization and found no statistically significant between-group differences in any laboratory parameter (Appendix Table 2). We assessed laboratory parameters at diagnosis and oxygen therapy requirements and noted that women with lymphocytopenia and prolonged aPPT at diagnosis were more likely to need an oxygen therapy (Appendix Table 3). Similarly, we noted lower lymphocyte counts, increased aPPT ratios, and increased C-reactive protein levels for women who required oxygen therapy than for the others.

Table 4. Obstetric and neonatal outcomes for 100 pregnant women with severe acute respiratory syndrome 2 infection, France*

Obstetric outcomes	Value
Ongoing pregnancies	67 (67.0)
Stillbirths or miscarriages	0
Deliveries	33 (33.0)
Median days between SARS-CoV-2 diagnosis and delivery (IQR)	3 (1–9)
Delivery mode	
Vaginal	17 (51.5)
Spontaneous labor	9 (52.9)
Induced labor, reason	8 (47.1)
Respiratory degradation	4 (50.0)
Preeclampsia	1 (12.5)
Intrahepatic cholestasis	1 (12.5)
Reduced fetal movements	1 (12.5)
Premature rupture of membranes	1 (12.5)
Caesarean delivery, reason	16 (48.5)
Respiratory distress	12 (36.4)
Major coagulopathy	1 (6.3)
Severe preeclampsia	1 (6.3)
Non-reassuring fetal heart rate	1 (6.3)
Definitive cervicoisthmic cerclage	1 (6.3)
Gestational age at birth, wk, median (IQR)	37.9 (35–40.1)
≥37	20 (60.6)
32–36	13 (39.4)
24–31	7 (21.2)
Twin pregnancies	3 (3.0)
Neonates†	36
Birthweight z-score, g, median (IQR)	0.15 (–0.75 to 0.64)
<10th percentile	1 (3)
Apgar score <7	
1 min	8 (22)
5 min	4 (11)
10 min	1 (3)
Umbilical arterial pH, median (IQR)	7.26 (7.24–7.29)
Neonatal intubation	6 (17)
NICU hospitalization	10 (28)
Neonatal death	0
Neonate SARS-CoV-2–positive	1 (3)

*Values are no. (%) except where indicated. IQR, interquartile range; SARS-CoV-2, severe acute respiratory syndrome coronavirus 2.
†33 women gave birth, including 3 sets of twins.

Obstetric and Neonatal Outcomes

At the end of the study period, 33 women (33%) had delivered 36 neonates, including 3 twin deliveries. Median gestational age of neonates was 37.9 weeks (IQR 35–40.1 weeks) (Table 4). Deliveries in SARS-CoV-2-infected women represented 2.4% of the 1,362 deliveries in the 4 hospitals. Preterm births, those at <37 weeks' gestation, represented 39% of the whole cohort; the median interval between SARS-CoV-2 diagnosis and delivery was 3 days (IQR 1–9 days). No stillbirths or miscarriages occurred among the study population. Among deliveries, 16 (48%) were cesarean deliveries, 13 (36%) of which were because of SARS-CoV-2 infection, 12 because of maternal respiratory distress, and 1 because of major coagulopathy. All women who delivered before 32 weeks' gestation were given antenatal magnesium sulfate therapy. All but 1 of the women who delivered before 34 weeks' gestation were given antenatal corticosteroid therapy (2 doses of betamethasone 12 mg given intramuscularly 24 hours apart).

Only 1 neonate had a birthweight below the 10th percentile; 10 were hospitalized in the neonatal ICU (NICU) because of prematurity. No neonatal acidosis was noted; median umbilical arterial pH was 7.26 (IQR 7.24–7.29), even for most severe maternal cases.

All the neonates were tested for SARS-CoV-2 infection. Only 1 neonate tested positive for SARS-CoV-2; his mother had no severe clinical symptoms but experienced cough and fever at 35 weeks' gestation. At admission, her laboratory workup showed mild thrombocytopenia and prolonged aPPT. Her symptoms improved rapidly during early postpartum. The infant did not require oxygen, but results of RT-PCR testing on nasopharyngeal secretions were positive. He did not show signs of respiratory illness.

Among 3 twin pregnancies, the mother's SARS-CoV-2 diagnosis was made between 31.4 and 35.4 weeks' gestation; 1 of the mothers was severely obese (BMI 49 kg/m^2). At the time of diagnosis, 1 patient had severe lymphocytopenia (0.35 × 10^9 cells/L) and another had prolonged aPTT (ratio 1.22). Two women were hospitalized because of dyspnea; both had cesarean deliveries, at 31.7 and 35.4 weeks' gestation, due to increased respiratory complications, but neither was admitted to the ICU. The third had a vaginal delivery at 37 weeks' gestation. One pair of twins was hospitalized in the NICU because of prematurity. Neonatal acidosis was not observed in any cases.

Pregnant Women in ICUs

At the end of the study period, 10 (10%) patients had been admitted to ICUs: 7 during prenatal period

Table 5. Maternal outcomes of 10 pregnant women admitted to the intensive unit with severe acute respiratory syndrome coronavirus 2, France*

ID	Age, y	BMI, kg/m^2	Underlying conditions	GA, wk, d		Time, h		Intubation, d	ICU stay, d	Drug regimens	Complications
				At diagnosis	At intubation	From O_2 >5 L/min to intubation	From intubation to delivery				
1	30.9†	35.8	NA	28, 5	29, 0	15.5	0	10	12	Lopinavir	NA
2	26.5†	29.9	NA	38, 1	POD 2	7	NA	15	16	Hydroxy	Surgical site infection
3	24.9†	25.7	Asthma	28, 5	30, 1	10	0	11	13	Lopinavir	Iatrogenic pancreatitis
4	32.6†	41.8	Hyper-tension	26, 0	26, 1	10.5	7	36	38	Lopinavir	Refractory hypoxemia
5	33.6	30.8	NA	26, 6	27, 6	5.5	0	2	3	NA	NA
6	39.4	31.3	Hashimoto thyroiditis	40, 5	POD 8	25	NA	4	5	NA	NA
7	33.1†	30.5	NA	23, 5	23, 5	1	Ongoing pregnancy	13	14	Hydroxy	Iatrogenic transient hepatitis
8	33.4	29.7	NA	28, 2	NA	NA	NA	NA	3	NA	NA
9	26.1	33.7	Asthma	36, 0	POD 1	24	NA	1	2	NA	NA
10	42.1†	29.3	NA	26, 6	27, 2	160	0	13	14	NA	NA

*BMI, body mass index; GA, gestational age; Hydroxy, hydroxychloroquine; ID, patient identification; NA, not applicable; POD, postoperative day.
†Patients who experienced acute respiratory distress syndrome before intubation.

(median gestational age at admission 27.9 weeks [IQR 27.2–28.8 weeks]) and 3 during early postpartum, ≤3 days postpartum (Table 5). Among patients admitted to ICUs, 9 (90%) required intubation after oxygen requirements reached >5 L/min; the mean interval between increased oxygen need and intubation was 28.7 hours (SD ± 49.9 h). Six patients had acute respiratory distress syndrome (ARDS); 5 were treated with drug regimen, 3 with lopinavir, and 2 with hydroxychloroquine; 1 was placed in the prone position for ARDS. The average length of stay in the ICU was 9.1 ± 5.7 days.

Among women hospitalized in ICUs, 8 had cesarean deliveries because of rapid respiratory worsening: 5 before 32 weeks' gestation, 1 between 32 and 37 weeks' gestation, and 2 after 37 weeks' gestation (Table 6). During their ICU stays, 3 women had complications: 1 had surgical site infection after cesarean delivery, 1 had iatrogenic pancreatitis attributed to lopinavir with Balthazar grade C, and 1 had iatrogenic and transient hepatitis attributed to hydroxychloroquine. No maternal deaths were noted. Among neonates delivered in this group, no acidosis or birthweight below the 10th percentile were noted. Five neonates were hospitalized in NICUs because of prematurity; 1 died at 7 days of age because of prematurity and bacterial sepsis (Tables 5, 6). Two women left the ICU with ongoing pregnancies.

Discussion

We report detailed experience managing 100 patients infected with SARS-CoV-2 in tertiary referral

Table 6. Obstetric and neonatal outcomes for pregnant women admitted to an intensive care unit with severe acute respiratory syndrome coronavirus 2, France*

ID	Prenatal corticosteroid, GA, wk, d†	Prenatal magnesium sulfate, GA, wk, d†	Time from diagnosis to delivery, d	Mode of delivery	GA at birth, wk, d	Birthweight, g (z-score)	5-min Apgar score	Umbilical arterial pH	Neonatal intubation	NICU
1	NA	29	2	Cesarean	29	1,400 (1.10)	7	7.26	Y	Y
2	NA	NA	8	Cesarean	39, 1	3,290 (0.06)	10	7.21	N	N
3	30, 1	30+1	11	Cesarean	30, 2	1,500 (0.75)	8	7.25	Y	Y
4	26, 4	26+4	7	Cesarean	27, 1	1,010 (0.82)	1	7.28	Y	Y
5	26, 1	26, 4	7	Cesarean	27, 6	890 (–0.83)	3	7.24	Y	Y
6	NA	NA	1	Cesarean	40, 6	3,570 (0.18)	3	ND	N	N
7	NA	23, 5	Ongoing pregnancy	NA	NA	NA	NA	NA	NA	NA
8	NA	29, 4	Ongoing pregnancy	NA	NA	NA	NA	NA	NA	NA
9	NA	NA	1	Cesarean	36, 1	2,940 (0.49)	10	ND	N	N
10	26, 6	27, 1	3	Cesarean	27, 2	1,065 (1.12)	10	7.27	Y	Y

*All neonates tested negative for SARS-CoV-2. GA, gestational age; NA, not applicable; ND, not done; SARS-CoV-2, severe acute respiratory syndrome coronavirus 2.
†At time of drug administration.

obstetric units during the COVID-19 pandemic in France. Nearly half (48/100) received close outpatient follow-up without any clinically significant events. The other 52 were hospitalized for monitoring or oxygen therapy, including 10 (10%) who had critical infections and required hospitalization in ICUs. Lymphocytopenia, anemia, and need for oxygen flow >5 L/min at the time of diagnosis seem to be associated with a critical infection.

The management of pregnant women with SARS-CoV-2 is a particularly critical issue in tertiary referral obstetric units. In our cohort, 52% of patients were hospitalized and 9% required invasive ventilation. The rate of severe and critical forms of COVID-19 reported among this group is higher than previously reported (*5*,*6*,*17*–*21*), which can be explained by the general admissions to tertiary referral obstetric units. Tertiary obstetric units accept women with high-risk pregnancies and referrals from other maternity hospitals that lack technical platforms needed to support them. The 4 centers in our study offer adult and neonatal resuscitation, enabling optimal maternal management. Clinicians must weigh the continuation of the pregnancy against all the risks associated with premature birth that can lead to neonatal death. Having an adult ICU in the same facility as the maternity ward makes it possible to continue the pregnancy under conditions that seem acceptable.

Maternal and fetal clinical assessment at the time of diagnosis is essential for appropriate medical referral. Systematic laboratory tests, including hemoglobin level, blood count, hemostasis, and inflammatory evaluation, at the time of SARS-CoV-2 diagnosis in pregnant women could help to determine the level of risk for progression to an unfavorable form. Lymphocytopenia, increased C-reactive protein, and increased aPPT have an unfavorable prognostic value that could lead to an increased risk for severe COVID-19 forms in nonpregnant adults (*22*–*25*). Our study underlines the need to consider the lymphocyte count in the choice of medical approach; when counts are acceptable, outpatient management can be safely considered. However, close telemonitoring is required. In our cohort, 17% of patients followed up on an outpatient basis subsequently required hospitalization.

During early pregnancy (<32 weeks' gestation), clinicians tried to continue the pregnancy because of the neonatal risks associated with premature birth. ICU hospitalization alone was not a criterion for delivery. However, analysis of our cohort data shows that in all pregnant women, a need for increasing oxygen flow rate to >5 L/min was a signal for invasive ventilation. All but 1 patient on invasive ventilation required cesarean delivery due to ventilatory instability. Antenatal corticosteroid therapy before 34 weeks' gestation and a neuroprotective course of magnesium sulfate before 32 weeks' gestation appears to be safe and appropriate when oxygen requirements increase. An average interval of ≥24 hours between the increase in oxygen flow rate to >5 L/min and invasive ventilation enables the administration of ≥1 of 2 recommended doses of corticosteroids and a complete course of magnesium sulfate.

Our study reports clinical and laboratory data at the time of diagnosis used to identify prognostic factors associated with an adverse outcome in pregnant women infected with SARS-CoV-2. Our findings can help clinicians around the world combat the pandemic.

Our study has several limitations. First, although we wanted to identify prognostic factors associated with adverse outcomes, our sample size of patients admitted to the ICU was too small to perform a robust multivariate analysis; our results are purely descriptive and not predictive. Second, our study used clinical and laboratory data only at the time of diagnosis, and we did not evaluate the effect of subsequent laboratory and clinical features. Finally, our study was retrospective and had missing data values.

Among our cohort, preterm births (<37 weeks' gestation) accounted for 39% of all deliveries and the cesarean delivery rate was 48%. However, the preterm birth and cesarean delivery rates we report could be lower once all the women with SARS-CoV-2 infections have given birth and full information becomes available.

Specific information on pregnant women receiving care for COVID-19 is still lacking, and literature from China reports low infection rates in this population. Tertiary referral obstetric units with a maternal ICU play a major role in the management of symptomatic pregnant women. In addition to maternal respiratory symptoms, neonatal conditions related to spontaneous or induced prematurity in relation to SARS-CoV-2 infection must be considered. In our study, careful clinical and laboratory evaluation at the time of diagnosis enabled safe outpatient monitoring for almost half of the pregnant women. Further investigations are required to assess the true risks associated with SARS-CoV-2 infection during pregnancy.

About the Author

Dr. Vivanti is a senior lecturer in obstetrics and gynecology at Antoine Béclère Hospital, University Paris Saclay, Clamart, France. His research interests include fetal medicine and surgery, high risk pregnancy, genetics, and neurodevelopment.

References

1. Rasmussen SA, Smulian JC, Lednicky JA, Wen TS, Jamieson DJ. Coronavirus disease 2019 (COVID-19) and pregnancy: what obstetricians need to know. Am J Obstet Gynecol. 2020;222:415–26. https://doi.org/10.1016/j.ajog.2020.02.017
2. Breslin N, Baptiste C, Gyamfi-Bannerman C, Miller R, Martinez R, Bernstein K, et al. Coronavirus disease 2019 infection among asymptomatic and symptomatic pregnant women: two weeks of confirmed presentations to an affiliated pair of New York City hospitals. Am J Obstet Gynecol MFM. 2020;2:100118. https://doi.org/10.1016/j.ajogmf.2020.100118
3. Zaigham M, Andersson O. Maternal and perinatal outcomes with COVID-19: A systematic review of 108 pregnancies. Acta Obstet Gynecol Scand. 2020;99:823–829. https://doi.org/10.1111/aogs.13867
4. Ferrazzi EM, Frigerio L, Cetin I, Vergani P, Spinillo A, Prefumo F, et al. COVID-19 Obstetrics Task Force, Lombardy, Italy: executive management summary and short report of outcome. Int J Gynaecol Obstet. 2020;149:377–8. https://doi.org/10.1002/ijgo.13162
5. Liu Y, Chen H, Tang K, Guo Y. Clinical manifestations and outcome of SARS-CoV-2 infection during pregnancy. J Infect. 2020 Mar 4 [Epub ahead of print]. https://doi.org/10.1016/j.jinf.2020.02.028
6. Chen H, Guo J, Wang C, Luo F, Yu X, Zhang W, et al. Clinical characteristics and intrauterine vertical transmission potential of COVID-19 infection in nine pregnant women: a retrospective review of medical records. Lancet. 2020; 395:809–15. https://doi.org/10.1016/S0140-6736(20)30360-3
7. Yu N, Li W, Kang Q, Xiong Z, Wang S, Lin X, et al. Clinical features and obstetric and neonatal outcomes of pregnant patients with COVID-19 in Wuhan, China: a retrospective, single-centre, descriptive study. Lancet Infect Dis. 2020; 20:559–64. https://doi.org/10.1016/S1473-3099(20)30176-6
8. Vlachodimitropoulou Koumoutsea E, Vivanti AJ, Shehata N, Benachi A, Le Gouez A, Desconclois C, et al. COVID19 and acute coagulopathy in pregnancy. J Thromb Haemost. 2020. 2020 Apr 17 [Epub ahead of print]. https://doi.org/10.1111/jth.14856
9. Dong L, Tian J, He S, Zhu C, Wang J, Liu C, et al. Possible vertical transmission of SARS-CoV-2 from an infected mother to her newborn. JAMA. 2020;323:1846–48. https://doi.org/10.1001/jama.2020.4621
10. Della Gatta AN, Rizzo R, Pilu G, Simonazzi G. Coronavirus disease 2019 during pregnancy: a systematic review of reported cases. Am J Obstet Gynecol. 2020;223:36–41. https://doi.org/10.1016/j.ajog.2020.04.013
11. Corman VM, Landt O, Kaiser M, Molenkamp R, Meijer A, Chu, DK, et al. Detection of 2019 novel coronavirus (2019-nCoV) by real-time RT-PCR. Euro Surveil. 2020;25:2000045. https://doi.org/10.2807/1560-7917.ES.2020.25.3.2000045
12. Zhang W, Du R-H, Li B, Zheng XS, Yang XL, Hu B, et al. Molecular and serological investigation of 2019-nCoV infected patients: implication of multiple shedding routes. Emerg Microbes Infect. 2020;9:386–9. https://doi.org/10.1080/22221751.2020.1729071
13. Wang W, Xu Y, Gao R, Lu R, Han K, Wu G, et al. Detection of SARS-CoV-2 in different types of clinical specimens. JAMA. 2020 Mar 11 [Epub ahead of print]. https://doi.org/10.1001/jama.2020.3786
14. Ai T, Yang Z, Hou H, Zhan C, Chen C, Lv W, et al. Correlation of chest CT and RT-PCR testing in coronavirus disease 2019 (COVID-19) in China: a report of 1014 cases. Radiology. 2020 Feb 26 [Epub ahead of print]. https://doi.org/10.1148/radiol.2020200642
15. US Centers for Disease Control and Prevention. Coronavirus disease 2019 (COVID-19) [cited 2020 Apr 29]. https://www.cdc.gov/coronavirus/2019-ncov/index.html
16. US Centers for Disease Control and Prevention. Considerations for inpatient obstetric healthcare settings [cited 2020 Apr 29]. https://www.cdc.gov/coronavirus/2019-ncov/hcp/inpatient-obstetric-healthcare-guidance.html
17. Di Mascio D, Khalil A, Saccone G, Rizzo G, Buca D, Liberati M, et al. Outcome of coronavirus spectrum infections (SARS, MERS, COVID 1 –19) during pregnancy: a systematic review and meta-analysis. Am J Obstet Gynecol MFM. 2020 Mar 25 [Epub ahead of print]. https://doi.org/10.1016/j.ajogmf.2020.100107
18. Ferrazzi E, Frigerio L, Savasi V, Vergani P, Prefumo F, Barresi S, et al. Vaginal delivery in SARS-CoV-2-infected pregnant women in Northern Italy: a retrospective analysis. BJOG. 2020 Apr 27 [Epub ahead of print]. https://doi.org/10.1111/1471-0528.16278
19. Schwartz DA. An analysis of 38 pregnant women with COVID-19, their newborn infants, and maternal-fetal transmission of SARS-CoV-2: maternal coronavirus infections and pregnancy outcomes. Arch Pathol Lab Med. 2020 Mar 17 [Epub ahead of print]. https://doi.org/10.5858/arpa.2020-0901-SA
20. Wang S-S, Zhou X, Lin X-G, Liu Y-Y, Wu J-L, Mwamaka Sharifu L, et al. Experience of clinical management for pregnant women and newborns with novel coronavirus pneumonia in Tongji Hospital, China. Curr Med Sci. 2020;40:285–289. https://doi.org/10.1007/s11596-020-2174-4
21. Yan J, Guo J, Fan C, Juan J, Yu X, Li J, et al. Coronavirus disease 2019 in pregnant women: a report based on 116 cases. Am J Obstet Gynecol. 2020;223:111.e1–14 https://doi.org/10.1016/j.ajog.2020.04.014
22. Henry BM, de Oliveira MHS, Benoit S, Plebani M, Lippi G. Hematologic, biochemical and immune biomarker abnormalities associated with severe illness and mortality in coronavirus disease 2019 (COVID-19): a meta-analysis. Clin Chem Lab Med. 2020;58:1021–8. https://doi.org/10.1515/cclm-2020-0369
23. Lippi G, Plebani M, Henry BM. Thrombocytopenia is associated with severe coronavirus disease 2019 (COVID-19) infections: a meta-analysis. Clin Chim Acta. 2020;506:145–8. https://doi.org/10.1016/j.cca.2020.03.022
24. Liu Y, Yang Y, Zhang C, Huang F, Wang F, Yuan J, et al. Clinical and biochemical indexes from 2019-nCoV infected patients linked to viral loads and lung injury. Sci China Life Sci. 2020;63:364–74. https://doi.org/10.1007/s11427-020-1643-8
25. Ruan Q, Yang K, Wang W, Jiang L, Song J. Clinical predictors of mortality due to COVID-19 based on an analysis of data of 150 patients from Wuhan, China. Intensive Care Med. 2020;46:846–848. https://doi.org/10.1007/s00134-020-05991-x

Address for correspondence: Alexandre J. Vivanti, Service de Gynécologie-Obstétrique, Hôpital A. Béclère, GHU Paris Saclay, APHP, 157 rue de la Porte de Trivaux, 92140 Clamart, France; email: alexandre.vivanti@aphp.fr

Heterogeneity of Dengue Illness in Community-Based Prospective Study, Iquitos, Peru

William H. Elson, Robert C. Reiner, Crystyan Siles, Isabel Bazan, Stalin Vilcarromero, Amy R. Riley-Powell, Ania B. Kawiecki, Helvio Astete, Robert D. Hontz, Chris M. Barker, Gonzalo M. Vazquez-Prokopec, Amy C. Morrison, Thomas W. Scott, John P. Elder, Alan L. Rothman, Valerie A. Paz-Soldan

Measuring heterogeneity of dengue illness is necessary to define suitable endpoints in dengue vaccine and therapeutic trials and will help clarify behavioral responses to illness. To quantify heterogeneity in dengue illness, including milder cases, we developed the Dengue Illness Perceptions Response (IPR) survey, which captured detailed symptom data, including intensity, duration, and character, and change in routine activities caused by illness. During 2016–2019, we collected IPR data daily during the acute phase of illness for 79 persons with a positive reverse transcription PCR result for dengue virus RNA. Most participants had mild ambulatory disease. However, we measured substantial heterogeneity in illness experience, symptom duration, and maximum reported intensity of individual symptoms. Symptom intensity was a more valuable predicter of major activity change during dengue illness than symptom presence or absence alone. These data suggest that the IPR measures clinically useful heterogeneity in dengue illness experience and its relation to altered human behavior.

Dengue classically presents as an acute febrile illness lasting ≈5 days and accompanied by headache, musculoskeletal pain, and rash (*1*). A minority of infected persons show development of plasma leakage syndrome, intravascular volume loss, or major bleeding, which can lead to shock and death (*2*). There are 4 serotypes of dengue (DENV), and persons show development of long-lasting immunity to the specific serotype after infection. Cross-reactive immunity provides short-term protection against other serotypes. However, under some circumstances, previous infection with a different serotype increases the risk for severe disease (*3*). The World Health Organization (WHO) classification of dengue focuses on distinguishing between mild cases (classic dengue) and persons with or at risk for major adverse outcomes or death (severe disease) (*4*–*6*). Moreover, most literature describing the clinical manifestations of dengue evaluates the health-care-seeking population whose symptoms are likely to be more severe. DENV infections associated with milder illness have not been subjected to similar systematic analysis or characterization.

Although the focus on severe disease is an obvious priority, there is value to characterizing the subjective illness experience in persons who have milder disease. As dengue vaccine development evolves, one of the challenges will be to accurately measure the effect of vaccination on the severity of illness. Measuring the rates of severe disease in vaccine trials is an insensitive approach and addresses only the small fraction of cases meeting these criteria, leaving open the possibility that vaccinated persons not meeting the criteria for severe disease had a meaningfully different disease experience than unvaccinated persons. Behavioral responses and reactions to illness depend on the illness experience of a person and will determine whether they attend work or school, self-medicate, seek medical attention, and move around their neighborhood, potentially infecting mosquitoes at other sites (*7*). Quantifying these relationships will help identify the human factors essential for virus

Author affiliations: University of California Davis, Davis, California, USA (W.H. Elson, A.B. Kawiecki, C.M. Barker, A.C. Morrison, T.W. Scott); University of Washington School of Medicine, Seattle, Washington, USA (R.C. Reiner); US Naval Medical Research Unit No. 6, Lima and Iquitos, Peru (C. Siles, I. Bazan, S. Vilcarromero, H. Astete, R.D. Hontz, A.C. Morrison); University of Sussex, Brighton, UK (A.R. Riley-Powell); Tulane School of Public Health and Tropical Medicine, New Orleans, Louisiana, USA (A.R. Riley-Powell, V.A. Paz-Soldan); Emory University, Atlanta, Georgia, USA (G.M. Vazquez-Prokopec); San Diego State University, San Diego, California, USA (J.P. Elder); University of Rhode Island, Providence, Rhode Island, USA (A.L. Rothman)

DOI: https://doi.org/10.3201/eid2609.191472

transmission, guide the design of improved control strategies, assist policy makers in assessing the burden of dengue illness and healthcare needs, and guide allocation of resources.

As part of a larger epidemiologic study we developed the dengue Illness Perceptions Response (IPR) survey to gather data to characterize the dengue illness experience of a person, including the range and intensity of symptoms, and to measure the response of a person to their illness. We outline the development and application of the IPR, and to illustrate its potential value, we describe and quantify the heterogeneity of dengue illness and its associations with behavior changes.

Methods

Ethics

The study protocol was approved by the Naval Medical Research Unit No. 6 (NAMRU-6) Institutional Review Board (IRB) (protocol #NAMRU6.2014.0028) in compliance with all applicable federal regulations governing the protection of human subjects. IRB relying agreements were established between NAMRU-6, the University of California Davis, Tulane University, Emory University, and the University of California, San Diego. The protocol was reviewed and approved by the Loreto Regional Health Department, which oversees health research in Iquitos.

Field Site

We conducted the study in an established research unit in the Amazonian city of Iquitos, Peru (*7*–*9*). Based in the department of Loreto, Iquitos has a population of ≈400,000 and mostly relies on tourism and extractive industries (*8*,*10*). More than half of the population of Loreto depend on government health insurance, which is available for persons living in poverty (*11*). Dengue is endemic to Iquitos, and 1 serotype typically dominates at any one time; all 4 DENV serotypes have circulated in Iquitos over the past 3 decades (*8*). The force of infection for DENV in Iquitos was calculated to vary from 0 to 0.33 infections/susceptible person/year during 1999–2010 (*12*). In March 2016, Zika virus was detected in Iquitos, and its transmission dominated for ≈1.5 years (*13*). Since 2017, the Asian-American strain of DENV-2 has been the dominant circulating serotype (A.C. Morrison, unpub. data).

Development of IPR Survey

On the basis of the experience of our team in collecting dengue symptom data and the available literature, we developed a focus group guide used to facilitate 6 mixed-sex focus groups to assess how persons who had recently had dengue illness (or an adult family member of a child who was infected) described the experience, including the range, duration, and precise location of symptoms; ways to describe the severity of the symptoms; and word choices related to the symptoms. Focus group participants (n = 52) were persons who had laboratory-confirmed dengue (positive result on DENV reverse transcription PCR [RT-PCR]) during the previous 3 months and who were recruited by ongoing community or clinic-based febrile illness surveillance. Using the range of symptoms and descriptions elicited through the focus groups, the research team developed a first version of the IPR, which was reviewed by collaborating experts and 3 local clinicians experienced in managing dengue to ensure its medical relevance. These data informed the IPR development, helping to define the symptoms to be included and descriptive terms used for symptoms and determine how to measure symptom intensity (there was almost unanimous support for scales using facial expressions to grade intensity).

The IPR survey that was implemented collected data on 36 symptoms; depending on the specific symptom, these data included presence, duration, intensity, character, frequency and location of symptoms (Appendix Table 1, https://wwwnc.cdc.gov/EID/article/26/9/19-1472-App1.pdf). We learned about descriptive terms for various symptoms: musculoskeletal pain was most commonly described as "beaten up," affecting the whole body. Headaches were most commonly described as a "generalized pressure." Abdominal pain was most commonly described as "cramping" and most frequently located in the epigastrium. The survey also asked to what extent symptoms had affected daily activities: no change, minor change, or major change. The IPR was then piloted on 54 persons: 7 children <10 years of age, 10 persons 10–20 years of age, and 37 persons >20 years of age. Feedback from this pilot testing was used to guide final modifications of the survey; data from these persons are not included in the main analyses.

Study Design

The study followed a contact-cluster design. Persons positive for serum DENV RNA by RT-PCR (index case-participants) were identified through community- or clinic-based febrile illness surveillance (*7*,*14*). At the time of blood collection, we administered a retrospective movement survey to the index case-participants

to identify locations visited in the previous 15 days. As soon as the initial PCR result was available, usually the next weekday, persons (contacts) from the home of the index case-participants and any residential locations visited by the index case-participants were then invited to provide a blood sample, regardless of the presence of symptoms; we tested consenting persons for serum DENV RNA by using RT-PCR. The protocol enabled requesting follow-up samples from PCR-negative contacts at intervals of no less than 2 days; we tested a median of 2 (interquartile range 2–3) blood samples from contacts by using PCR.

Index case-participants and any contacts with positive RT-PCR results (*15*) for DENV RNA were invited to respond to a series of surveys relating to symptoms (IPR), movements throughout the city, health related qualify of life, and illness-related expenditures. The IPR survey was applied daily (where possible), starting from the day of the positive RT-PCR result until there were no reported symptoms for 2 days, and then again 30 days later. Inclusion criteria for the study were an age ≥5 years, DENV viremia documented by RT-PCR, and willingness to provide informed consent or assent for persons 5–17 years of age.

Data Analysis and Statement

We used CommCare (https://www.dimagi.com), an open-source software platform, to develop a digital version of the IPR, which we administered by using handheld tablets (*16*). Survey data were uploaded to CommCare secure server where it could be reviewed by senior project members for discrepancies and corrected if necessary. We forwarded data to a PostgreSQL database (https://www.postgresql.org) and directly accessed this database and analyzed the data by using R version 3.5.1 (*17*). We categorized symptoms into the following clinically defined groups: constitutional, fever, headache, musculoskeletal, abdominal, cutaneous, respiratory, bleeding, and other (Appendix Table 2). The final dataset included the first 14 days of illness for each participant, indicating for these days symptom intensities from 0 (absence) to 10 (most intense). The survey solicited the maximum symptom intensity experienced between the day of collection and either the day the symptom started (in the first IPR) or the previous survey (in subsequent IPRs). Intensities recorded in the first IPR were assigned to the first date that the specific symptom was reported and any gaps in intensity data were imputed with linear interpolation. For days after the final survey, intensities and frequencies of symptoms were assumed to be 0. From this dataset we calculated the duration of illness and of specific symptoms, and the proportion of symptoms that were reported on each day of illness. Suspected dengue was defined following the 2009 WHO guidelines as fever and ≥2 of the following symptoms: headache, retroorbital pain, nausea/vomiting, muscle/joint pains, and rash (*4*).

We performed a correlation analysis of symptom intensities, excluding imputed intensity values, by using the cor function in the stats package in R with use argument as pairwise.complete.observations and method argument as spearman to generate a correlation matrix and then plotted a heatmap and dendrogram derived from the correlation matrix by using the pheatmap function in the pheatmap package (*18*). To compare index and contact cases, we first compared the mean number of reported symptoms by using a 2-sided Student *t*-test, and then compared the proportions of persons reporting specific symptoms by using the Fisher exact test. Because there were 36 comparisons, we applied a Bonferroni correction to the α value.

To explore the relationship between major activity change and individual symptom intensity, we performed logistic regression by using the glm function in the stats package in R, designating major activity change (present or absent) as the dependent variable and symptom intensity, age, and sex as independent variables. To evaluate the benefit of collecting intensity data versus only symptom presence and absence, we performed 2 logistic regression models for each symptom by using major activity change as the response variable and either symptom intensity or binary symptom presence as the explanatory variable. We used the difference in the model Akaike Information Criteria (Δ-AIC) as a means to compare the 2 models, with a positive AIC favoring the use of intensity over presence or absence. All data and R code used for this analysis are available (https://github.com/hammoire/dengue_ipr).

Results

We enrolled 79 persons who completed a total of 429 IPR surveys (median 5 surveys/person) (Table 1). A total of 55 persons were enrolled through febrile illness surveillance (index case-participants), 42 through community-based surveillance, and 13 through clinic-based surveillance. The remaining 24 persons were enrolled through cluster investigations (contact case-participants); these case-participants were identified from the total of 408 contacts tested (72% of the 567 eligible contacts). Index and contact case-participants were similar in age and sex. The first survey was completed a median of 3 days after the onset of symptoms (range

Table 1. Baseline characteristics of participants tested for heterogeneity of dengue illness in community-based prospective study, Iquitos, Peru*

Characteristic	Total	Index	Contact
No. participants	79	55	24
No. surveys	429	309	120
Sex, no. (%)			
M	38 (48)	27 (49)	11 (46)
F	41 (52)	28 (51)	13 (54)
Median age, y (IQR)	17 (12–27.5)	17 (14–26)	14.5 (9.5–31)
Day at diagnosis (IQR)	3 (2–4)	4 (3–5)	2 (1–3)
Serotype, %			
DENV-2	76 (96)	53 (96)	23 (96)
DENV-3	3 (4)	2 (4)	1 (4)
WHO suspected dengue† (%)	67 (85)	51 (93)	16 (67)
Warning signs, no. (%)	20 (25)	18 (33)	2 (8)
Hospitalized, no. (%)	7 (9)	6 (11)	1 (4)

*DENV, dengue virus; IQR, interquartile range; WHO, World Health Organization.
†Persons who met the 2009 WHO criteria for suspected dengue (see Methods).

–1 to 8 days). A total of 75% of participants completed the follow-up survey at a median of 36 days after the onset of symptoms (range 21–82 days). Seven (9%) participants were hospitalized during the course of their acute infection (Table 1).

Frequency and Duration of Symptoms

We summarized the overall frequency (Appendix Figure 1) and duration (Appendix Figure 2) of symptoms. The frequency of individual symptoms did not differ by sex or age group (younger vs. older than 18 years of age). All symptoms occurred more frequently in index case-participants than in contact case-participants, with the exception of vaginal bleeding. These differences were only significant for bad taste and chills ($p<0.01$ with Bonferroni correction) (Appendix Table 3).

Participants reported a mean symptom duration of 7.37 days. One person (a contact case-participant) experienced no symptoms. A total of 5 persons experienced ≥1 symptoms between the follow-up visit and the last form in the acute phase of illness, including nausea (2), malaise (2), headache (1), congestion (1), itching (1), and fainting (1).

Timing and Characterization of Symptoms

We report the timing of each of 13 symptoms for which duration data were collected (Figure 1). Malaise preceded other symptoms by 1 day in a substantial fraction of cases and was still reported by >30% of

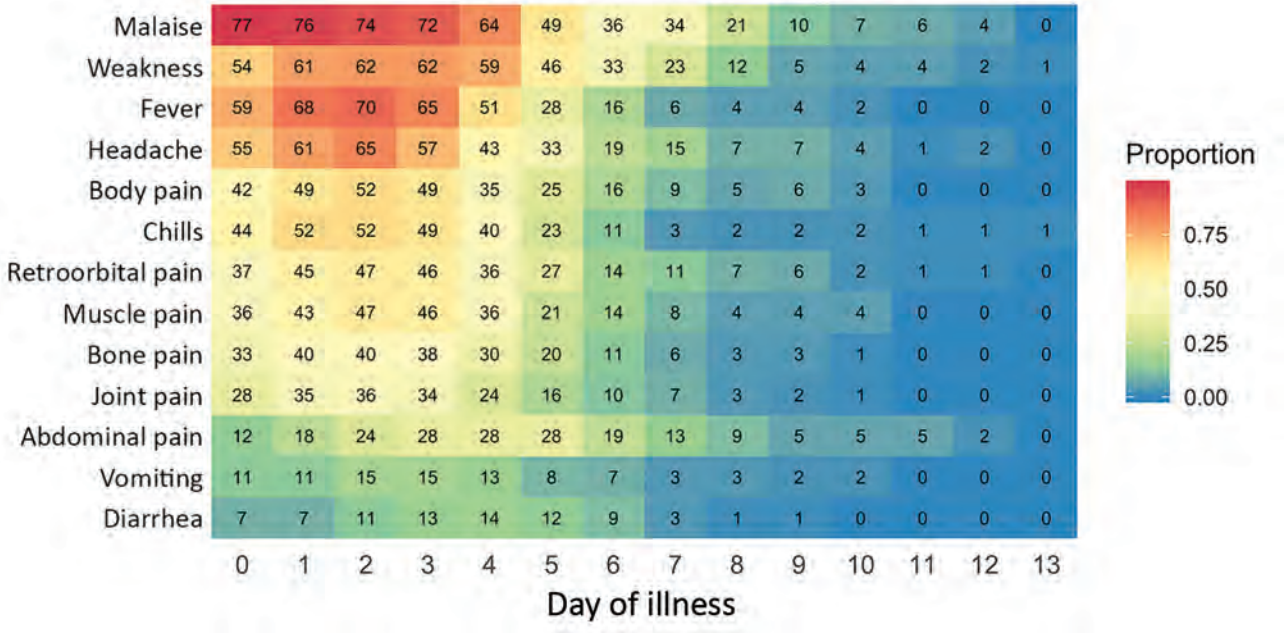

Figure 1. Timing of 13 key dengue symptoms for participants tested for heterogeneity of dengue illness in community-based prospective study, Iquitos, Peru. The x-axis represents day of illness and y-axis individual symptoms. Numbers in tiles indicate total number of persons with a symptom on that day. A total of 79 persons infected with dengue virus participated in surveys.

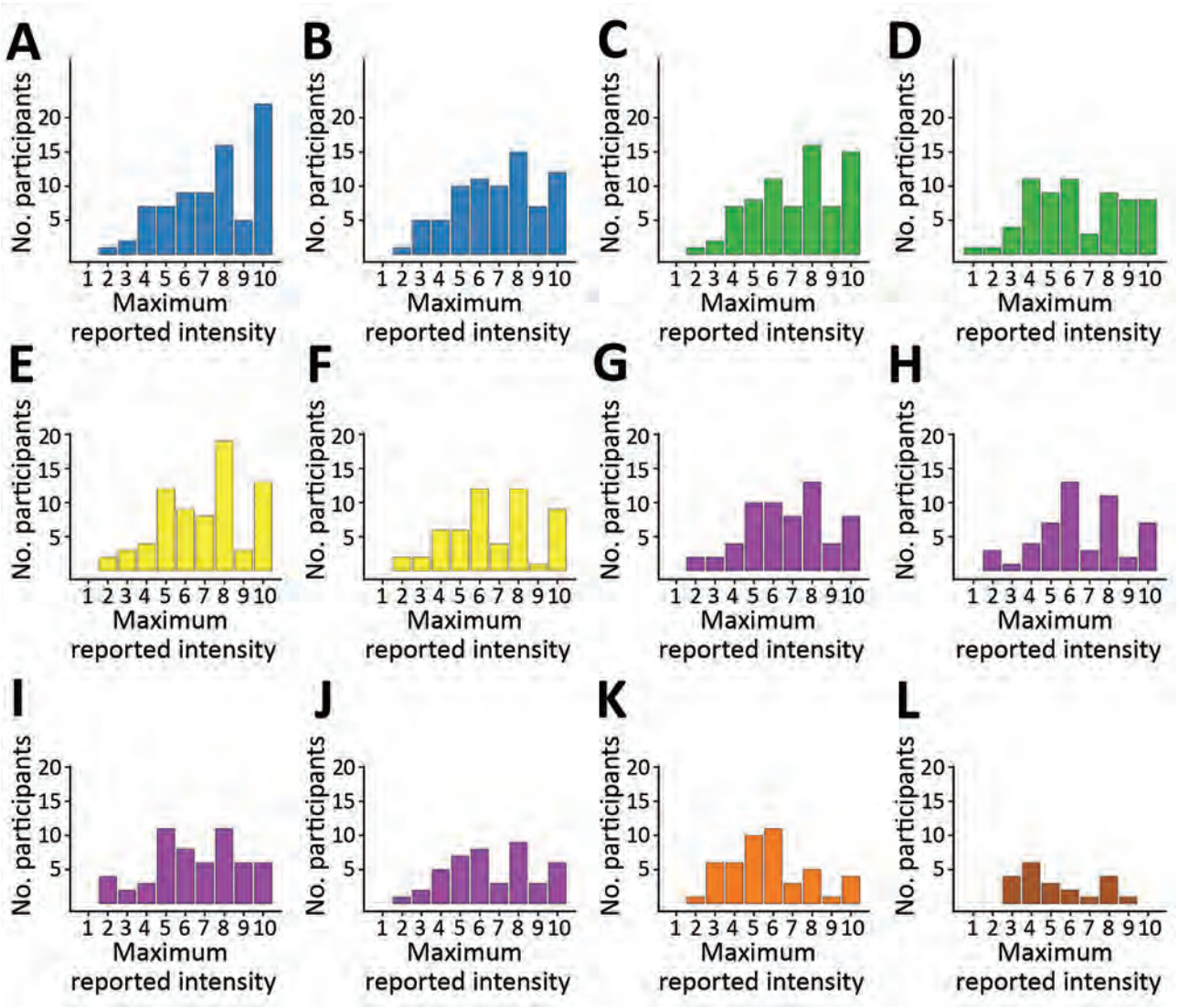

Figure 2. Histograms of maximum reported symptom intensities for participants tested for heterogeneity of dengue illness in community-based prospective study, Iquitos, Peru. Persons who did not report symptoms were excluded. Colors in histograms correspond to symptom groups defined in Appendix Figure 1 https://wwwnc.cdc.gov/eid/article/26/9/19-1472-App1.pdf. Values for each panel are no. (%) of participants who reported the specific symptom at any time during their illness. A) malaise, 78 (98.7); B) weakness, 76 (96.2); C) fever, 74 (93.7); D) chills, 65 (82.3); E) headache, 72 (91.1); F) retroorbital pain, 54 (68.4); G) body pain, 61 (77.2); H) bone pain, 51 (64.6); I) muscle pain, 57 (72.2); J) joint pain, 45 (57.0); K) abdominal pain, 47 (59.5); L) sore throat, 21 (26.6).

persons at day 7. Fever, headache, and pain (body/muscle/bone/joint) were most frequently reported on days 1–3, whereas abdominal pain was most frequently reported on days 3–5 (Figure 1).

We found substantial heterogeneity in reported maximum intensity per symptom by participants. We compiled the distribution of the maximum intensity reported by each person during the illness period for 12 key symptoms on a 10-point scale (Figure 2). Symptoms with the highest median values for maximum intensity (excluding those that did not report the symptom at all) were malaise and fever (*8*), body pain, headache, muscle pain, and weakness (*7*) (Figure 2).

We report the trajectories of symptom intensity over the course of the illness for 6 symptoms (Figure 3); if the symptom was absent, an intensity of 0 was assigned. For the study population as a whole, the intensity of individual symptoms followed a similar timing as the presence or absence of each symptom. However, there was substantial variation in the trajectories of symptom intensity by participant (Figure 3).

We report correlations between the intensities of individual symptoms and the hierarchical clustering

dendrogram of symptom intensities (Figure 4). Pairwise correlations ranged from 0.12 (sore throat vs. weakness) to 0.81 (body pain vs. muscle pain). Symptom intensity scores clustered into distinct groups (i.e., constitutional [malaise and weakness], fever/chills, headache/retroorbital pain, and musculoskeletal [body, muscle, bone, and joint pains]). Abdominal pain and sore throat did not cluster with other symptoms in this analysis.

Symptom Intensity and Activity Change

A total of 48 (61%) participants reported a major change in their daily activities on ≥1 days, 25 participants (32%) reported a minor change in daily activities, and only 6 participants (8%) reported no change in daily activities during their illness. On the basis of logistic regression models analyzing major activity change as a function of individual symptom intensities, corrected for age and sex, weakness had the strongest association with major activity change (odds ratio 1.48, 95% CI 1.36–1.63), followed by malaise (odds ratio 1.36, 95% CI 1.25–1.48) (Table 2).

To assess the added value of measuring symptom intensity versus only symptom absence or presence, we compared logistic regression models that used major activity change as the dependent variable (compared with minor or no activity change as reference) and either the presence of a symptom or the symptom intensity as the independent variable. The difference in the model (Δ-AIC) was used to compare the 2 models, in which a positive Δ-AIC would favor the use of symptom intensity over presence/absence alone. Symptoms with the greatest positive Δ-AIC were malaise (Δ-AIC 42.1), weakness (Δ-AIC 35.8), and fever (Δ-AIC 20.8) (Table 2). These data indicate that symptom intensity is more valuable than symptom presence or absence alone as a predictor of major activity change during DENV infection.

Discussion

Symptoms reported most frequently by study participants were consistent with classical descriptions of dengue illness, other cohort studies, and WHO guidelines, as well as the key symptoms reported by participants in our focus groups (*19*–*22*), although a large fraction of participants reported less typical gastrointestinal or respiratory symptoms. Participants enrolled as contact case-participants reported

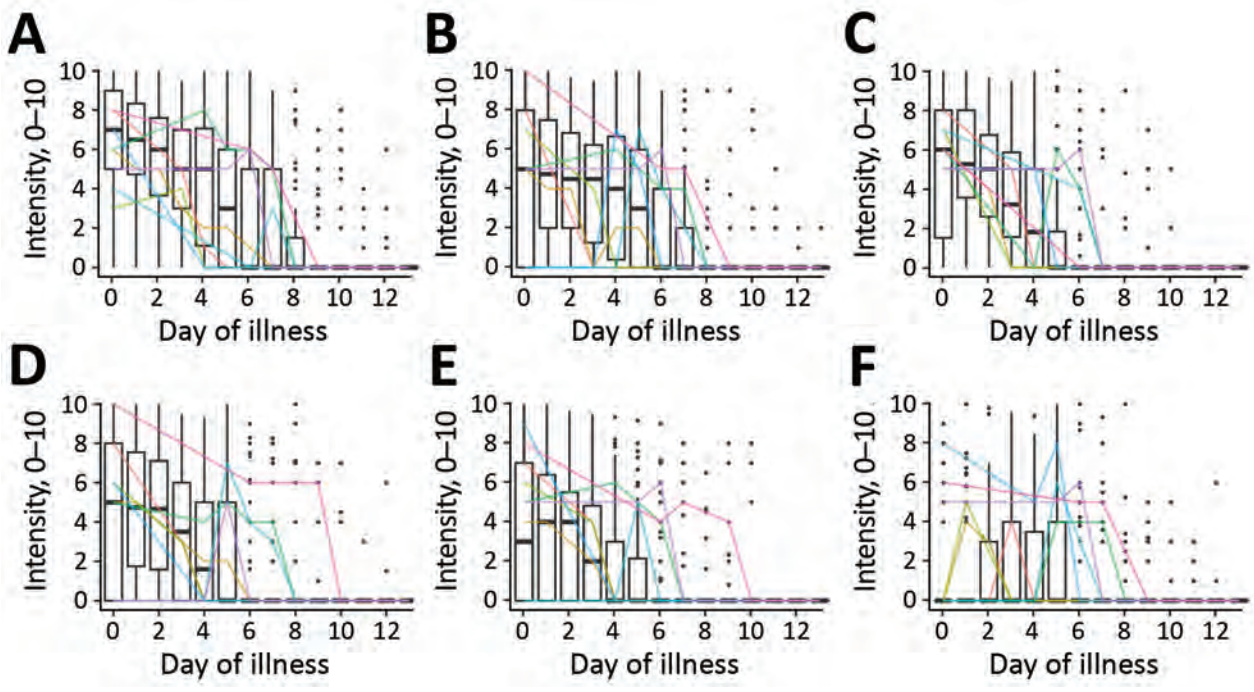

Figure 3. Symptom intensities (scale 0–10) for 6 symptoms over the first 14 days of illness (0–13) for participants tested for heterogeneity of dengue illness in community-based prospective study, Iquitos, Peru. A) Malaise; B) weakness; C) fever; D) headache; E) body pain; F) abdominal pain. Box plots indicate trends for the study population as a whole. Dark horizontal lines indicate median, upper limit of box indicates 75th percentile, lower limit of box indicates 25th percentile, upper whisker extends to the largest value ≤1.5 times the interquartile range; and lower whisker extends to the smallest value ≥1.5 times the interquartile range. Black dots indicate individual scores. Colored lines indicate trajectories for a random sample of 10 individual participants.

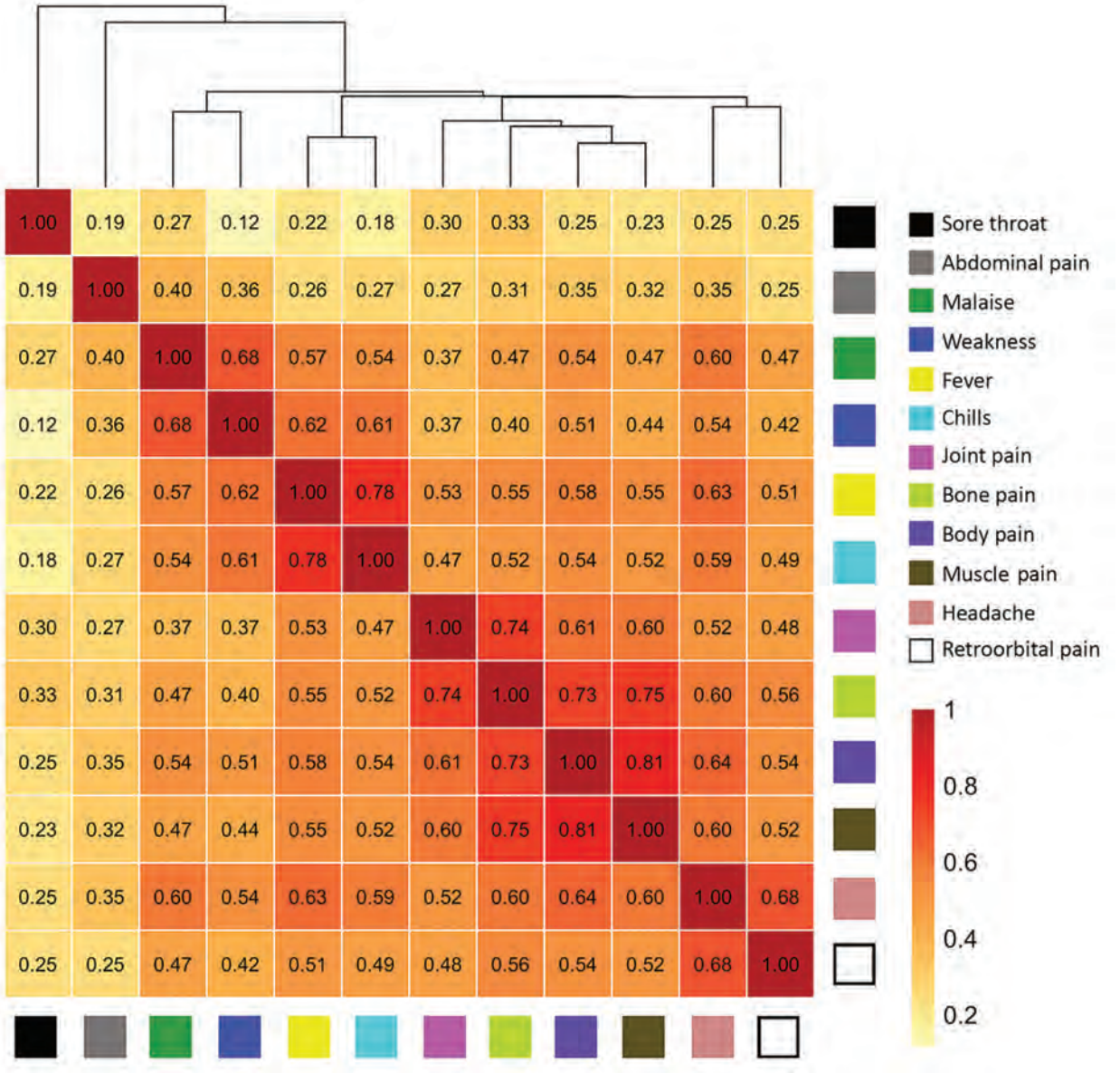

Figure 4. Correlations of intensities of individual symptoms (379 surveys, 79 participants) and hierarchical clustering for participants tested for heterogeneity of dengue illness in community-based prospective study, Iquitos, Peru. Tile colors indicate strength of correlations. The height at which symptoms are linked in the dendrogram indicates how strongly they are related (lower height indicates a closer link).

fewer symptoms, similar to the findings in cluster investigations performed in Thailand (*23*). Some of these persons might otherwise not have sought medical attention. Only 1 (contact case-participant) person reported no symptoms. This finding conflicts with evidence suggesting that only 12%–25% of DENV infections are apparent (*24*,*25*). However, it is likely that administering the IPR survey encouraged reporting of symptoms that would not have been recalled in the context of a retrospective questionnaire, possibly explaining the relatively high symptomatic to asymptomatic ratio in our sample. We only collected data for persons who had a positive RT-PCR result (persons with only immunologic evidence of seroconversion to DENV were not included). This limitation has been associated with a higher frequency of symptoms (*23*).

Although most persons had mild dengue illness, our data demonstrate a range of intensity levels for individual symptoms. The IPR survey also enabled us to identify symptom groups within which daily intensities were highly correlated

(r >0.70): constitutional (malaise and weakness), fever (fever and chills), headache (headache and retroorbital pain), and musculoskeletal pain (body, muscle, bone, and joint pain).

Abdominal pain was reported by 59% of participants, but only 13% reported severe abdominal pain (intensity >6). Abdominal pain followed a somewhat different time course from and showed substantially lower correlation with the symptom groups listed above. This finding is consistent with a distinct physiologic mechanism for abdominal pain. It also supports guidelines classifying severe abdominal pain as a warning sign, although few of our participants had evidence of plasma leakage or severe bleeding.

Although our study population consisted primarily of persons with mild dengue illness, participants still reported a substantial impact of illness on daily activities. Use of intensity scores for the major symptoms substantially improved the assessment of the effects of illness on daily activities when compared with use of symptom presence/absence alone. Therefore, the ability of the IPR survey to capture this aspect of heterogeneity in nonhospitalized persons with dengue could help improve assessment of either beneficial or detrimental effects of interventions, as proposed by Thomas et al. (*26*). Moreover, the causes of specific symptoms in dengue remain poorly defined (*19*); instruments such as the IPR survey could potentially be used to explore these underlying mechanisms.

Recently, a group of experts proposed a data collection tool to capture the overall experience of a person with dengue based on how their symptoms affect general wellness and functionality (*26*). The Dengue Illness Index (DII) records the presence or absence of symptoms daily. Our IPR survey has similarities to the DII, but a major difference is that the IPR solicited the assessment of the intensity of key symptoms of a participant. Our data suggest that persons are able to provide such an assessment and that intensity data add information relevant to the overall assessment of illness impact.

Thomas et al. (*26*) proposed a strategy for tabulating the DII to yield a single illness score. We did not assign weights a priori for the different symptom intensities. Our data showing high correlations within symptom groups suggests that each symptom should not be given equal weight. We are exploring approaches to express the symptom severity data to a single or small number of the most informative parameters (e.g., principal component analysis). Regardless of the specific approach used to score dengue symptom severity, it will be essential to define the relationships of severity score to other external measures of illness impact. In addition to data on change in daily activities, described here, persons also provided data on movement (*14*) and on a health-related quality of life survey, which we are incorporating into future analyses.

Our findings should be interpreted in light of several additional limitations. The IPR survey was administered to participants by research staff using a tablet-based application. Some choices in the design of the tablet-based survey addressed operational needs or preferences of the research team. These considerations created some unanticipated challenges and required minor modifications to the tool during the course of our study. For example, as a result of delays in receiving RT-PCR results or missed follow-up assessments, it was difficult to accurately assign a start and end date of some symptoms for some persons. Imputation of missing data introduces error into our dataset that is difficult to quantify. Our sample size is relatively small and homogenous in host and viral populations. Our study was focused on evaluation of persons with acute DENV infection and did not include participants with nondengue febrile illnesses for comparison. Persons who participated in the focus groups or the main study are not representative of the overall population of Iquitos (e.g., greater time availability or willingness to engage with medical personnel). That said, the instrument development process, which engaged participants recently given a diagnosis of DENV infection and clinical experts who reviewed the literature, resulted in a tool that assessed a wide range of symptoms and potential behavioral responses, which we believe could be applied in other settings, although

Table 2. Effect of symptom intensity on reporting of major activity change for participants tested for heterogeneity of dengue illness in community-based prospective study, Iquitos, Peru

Symptom	Odds ratio (95% CI)*	Δ-AIC†
Malaise	1.36 (1.25–1.48)	42.1
Weakness	1.48 (1.36–1.63)	35.8
Fever	1.28 (1.19–1.38)	20.8
Abdominal	1.34 (1.22–1.48)	9.9
Body pain	1.32 (1.22–1.43)	9.1
Headache	1.27 (1.17–1.37)	9.0
Chills	1.31 (1.21–1.43)	3.3
Muscle pain	1.25 (1.15–1.35)	2.7
Joint pain	1.23 (1.13–1.34)	−0.0
Retroorbital pain	1.11 (1.03–1.2)	−0.1
Sore throat	1.02 (0.87–1.18)	−0.5
Bone pain	1.24 (1.15–1.36)	−1.4

*Shown is the increase in odds of reporting a major activity change when symptom intensity is increased by 1 point for each of the 12 symptoms. †Δ-AIC, difference in Akaike Information Criteria between models by using binary symptom presence versus symptom intensity (0–10) as a predictor of major activity change. A positive Δ-AIC favors the use of intensity over presence of symptom alone.

piloting the tool before use elsewhere is advisable. Febrile illness surveillance was limited to selected neighborhoods, and contacts were identified on the basis of social proximity. Given the long-standing interactions of the research team with the local population and the demographics of study participants, we do not expect these considerations to have introduced major bias in our results.

Our data support the feasibility and rationale of efforts to quantify dengue illness in future natural history and intervention studies. Our experience should be useful to guide development of reliable and validated tools for this purpose. We anticipate that the IPR survey could be adapted to other formats, including self-administration by research subjects, and to other languages, but these efforts would require modifications and further validation. Further studies are needed to test our results across other populations, to assign appropriate weights to individual symptom scores, and to correlate with other biologic and epidemiologic measures of disease impact.

Acknowledgments

We thank the residents of Iquitos for participating in this study; Loreto Regional Health Department, including Hugo Rodriguez-Ferruci, Christian Carey, Carlos Alvarez, Hernan Silva, and Wilma Casanova Rojas, for providing support and facilitating our work in Iquitos; the leadership of the NAMRU-6 Virology and Emerging Infections Department for providing institutional support, IRB guidance, and supervising field staff; the NAMRU-6 IRB and Research Administration Program for providing commentary and advice; the NAMRU-6 Virology and Emerging Infections Department field teams for providing daily support and without whom the capture of acute-phase dengue cases would not have been possible; the Movement team (Alfonso Vizcarra, Jhonny C. López, Lorena Q. Flores, and Esther J. Ríos) for providing assistance during data collection; and Gabriela Vasquez de la Torre for providing administrative support.

This study was supported by the US National Institutes of Health/National Institute of Allergy and Infectious Diseases (award no. P01AI098670 to T.W.S.), the Military Infectious Disease Research Program (award no. S0520_15_Li), and the US Department of Defense Global Emerging Infections Systems Research Program (work unit no. 847705.82000.25GB.B0016. A.R.R.-P. was supported by the Wellcome Trust (#212712/Z/18/Z).

About the Author

Dr. Elson is a physician and research consultant working for the University of California Davis, Davis, CA. His research interests include clinical and epidemiologic aspects of arboviral diseases, including dengue and Zika, and vectorborne disease control.

References

1. World Health Organization. Dengue: guidelines for diagnosis, treatment, prevention and control, 2009. Geneva: The Organization [cited 2019 Mar 14]. http://www.ncbi.nlm.nih.gov/books/NBK143157
2. Simmons CP, Farrar JJ, Nguyen V, Wills B. Dengue. N Engl J Med. 2012;366:1423–32. https://doi.org/10.1056/NEJMra1110265
3. Martínez-Vega RA, Carrasquila G, Luna E, Ramos-Castañeda J. ADE and dengue vaccination. Vaccine. 2017;35:3910–2. https://doi.org/10.1016/j.vaccine.2017.06.004
4. World Health Organization Special Programme for Research and Training in Tropical Diseases. Dengue: guidelines for diagnosis, treatment, prevention, and control, 2009 [cited 2020 Jun 3]. https://apps.who.int/iris/handle/10665/44188
5. World Health Organization. Dengue haemorrhagic fever: diagnosis, treatment, prevention, and control. 2nd ed. Geneva: The Organization; 1997.
6. Srikiatkhachorn A, Rothman AL, Gibbons RV, Sittisombut N, Malasit P, Ennis FA, et al. Dengue: how best to classify it. Clin Infect Dis. 2011;53:563–7. https://doi.org/10.1093/cid/cir451
7. Stoddard ST, Forshey BM, Morrison AC, Paz-Soldan VA, Vazquez-Prokopec GM, Astete H, et al. House-to-house human movement drives dengue virus transmission. Proc Natl Acad Sci U S A. 2013;110:994–9. https://doi.org/10.1073/pnas.1213349110
8. Morrison AC, Minnick SL, Rocha C, Forshey BM, Stoddard ST, Getis A, et al. Epidemiology of dengue virus in Iquitos, Peru 1999 to 2005: interepidemic and epidemic patterns of transmission. PLoS Negl Trop Dis. 2010;4:e670. https://doi.org/10.1371/journal.pntd.0000670
9. Morrison AC, Gray K, Getis A, Astete H, Sihuincha M, Focks D, et al. Temporal and geographic patterns of *Aedes aegypti* (Diptera: Culicidae) production in Iquitos, Peru. J Med Entomol. 2004;41:1123–42. https://doi.org/10.1603/0022-2585-41.6.1123
10. Peru National Institute of Statistics and Informatics INEI [in Spanish] [cited 2019 Mar 15]. https://www.inei.gob.pe/estadisticas/indice-tematico/poblacion-y-vivienda
11. Ministry of Health Peru. Comprehensive Health Insurance [in Spanish] [cited 2019 Mar 15]. http://www.sis.gob.pe/portal/estadisticas/resumen.html
12. Reiner RC Jr, Stoddard ST, Forshey BM, King AA, Ellis AM, Lloyd AL, et al. Time-varying, serotype-specific force of infection of dengue virus. Proc Natl Acad Sci

U S A. 2014;111:E2694–702. https://doi.org/10.1073/pnas.1314933111
13. Ministry of Health Peru. Situation for the health situation analysis, 2019, week 19 [in Spanish]. [cited 2019 Jun 6]. https://www.dge.gob.pe/portal/index.php?option=com_content&view=article&id=664
14. Schaber KL, Paz-Soldan VA, Morrison AC, Elson WHD, Rothman AL, Mores CN, et al. Dengue illness impacts daily human mobility patterns in Iquitos, Peru. PLoS Negl Trop Dis. 2019;13:e0007756. https://doi.org/10.1371/journal.pntd.0007756
15. Sadon N, Delers A, Jarman RG, Klungthong C, Nisalak A, Gibbons RV, et al. A new quantitative RT-PCR method for sensitive detection of dengue virus in serum samples. J Virol Methods. 2008;153:1–6. https://doi.org/10.1016/j.jviromet.2008.06.023
16. CommCare by Dimagi. Data collection app [cited 2019 Apr 5]. https://www.dimagi.com/commcare
17. R Core Team. R: a language and environment for statistical computing. Vienna: R Foundation for Statistical Computing, 2013 [cited 2020 Jun 3]. http://www.R-project.org
18. Kolde R. pheatmap: pretty heatmaps, 2019. R package version 1.0.12 [cited 2020 Jun 3]. https://CRAN.R-project.org
19. Wilder-Smith A, Ooi E-E, Horstick O, Wills B. Dengue. Lancet. 2019;393:350–63. https://doi.org/10.1016/S0140-6736(18)32560-1
20. Potts JA, Rothman AL. Clinical and laboratory features that distinguish dengue from other febrile illnesses in endemic populations. Trop Med Int Health. 2008;13:1328–40. https://doi.org/10.1111/j.1365-3156.2008.02151.x
21. Cobra C, Rigau-Pérez JG, Kuno G, Vorndam V. Symptoms of dengue fever in relation to host immunologic response and virus serotype, Puerto Rico, 1990–1991. Am J Epidemiol. 1995;142:1204–11. https://doi.org/10.1093/oxfordjournals.aje.a117579
22. Halsey ES, Baldeviano GC, Edgel KA, Vilcarromero S, Sihuincha M, Lescano AG. Symptoms and immune markers in *Plasmodium*/dengue virus co-infection compared with mono-infection with ether in Peru. PLoS Negl Trop Dis. 2016;10:e0004646. https://doi.org/10.1371/journal.pntd.0004646
23. Yoon I-K, Srikiatkhachorn A, Hermann L, Buddhari D, Scott TW, Jarman RG, et al. Characteristics of mild dengue virus infection in Thai children. Am J Trop Med Hyg. 2013;89:1081–7. https://doi.org/10.4269/ajtmh.13-0424
24. Bhatt S, Gething PW, Brady OJ, Messina JP, Farlow AW, Moyes CL, et al. The global distribution and burden of dengue. Nature. 2013;496:504–7. https://doi.org/10.1038/nature12060
25. Stanaway JD, Shepard DS, Undurraga EA, Halasa YA, Coffeng LE, Brady OJ, et al. The global burden of dengue: an analysis from the Global Burden of Disease Study 2013. Lancet Infect Dis. 2016;16:712–23. https://doi.org/10.1016/S1473-3099(16)00026-8
26. Thomas SJ, Agulto L, Hendrickx K, Erpicum M, Tomashek KM, Cassetti MC, et al. Dengue illness index: a tool to characterize the subjective dengue illness experience. PLoS Negl Trop Dis. 2018;12:e0006593. https://doi.org/10.1371/journal.pntd.0006593

Address for correspondence: Valerie A. Paz-Soldán, Global Community Health and Behavioral Sciences Department, Tulane University School of Public Health and Tropical Medicine, 1440 Canal St, Ste 2200, New Orleans, LA 70112, USA; email: vpazsold@tulane.edu

Association of Biosecurity and Hygiene Practices with Environmental Contamination with Influenza A Viruses in Live Bird Markets, Bangladesh

Sukanta Chowdhury, Eduardo Azziz-Baumgartner, James C. Kile, Md. A. Hoque, Mohammed Z. Rahman, Md. E. Hossain, Probir K. Ghosh, Syed S.U. Ahmed, Erin D. Kennedy, Katharine Sturm-Ramirez, Emily S. Gurley

In Bangladesh, live bird market environments are frequently contaminated with avian influenza viruses. Shop-level biosecurity practices might increase risk for environmental contamination. We sought to determine which shop-level biosecurity practices were associated with environmental contamination. We surveyed 800 poultry shops to describe biosecurity practices and collect environmental samples. Samples from 205 (26%) shops were positive for influenza A viral RNA, 108 (14%) for H9, and 60 (8%) for H5. Shops that slaughtered poultry, kept poultry overnight, remained open without rest days, had uneven muddy floors, held poultry on the floor, and housed sick and healthy poultry together were more frequently positive for influenza A viruses. Reported monthly cleaning seemed protective, but disinfection practices were not otherwise associated with influenza A virus detection. Slaughtering, keeping poultry overnight, weekly rest days, infrastructure, and disinfection practices could be targets for interventions to reduce environmental contamination.

Highly pathogenic avian influenza A(H5N1) virus causes outbreaks in poultry and sporadic infections in humans globally (*1*,*2*). H5N1 virus is endemic to poultry in several countries in Southeast Asia, including Bangladesh, and causes major economic loss, as well as human illness and death (*1*,*3*–*5*). During 2007–2018, Bangladesh reported >550 highly pathogenic avian influenza outbreaks in poultry, 90% of which were reported from commercial poultry farms (*2*). Since 2008, eight human H5N1 cases, including 1 death, have been reported in Bangladesh; 3 of these cases were in live bird market (LBM) workers presumably exposed to infected poultry in the LBM (*1*). Vietnam, Thailand, Indonesia, Hong Kong, China, and Cambodia have also reported human cases of H5N1 infection with a history of poultry exposure in LBMs, suggesting that LBMs can facilitate spread of H5N1 infection among poultry and from poultry to humans (*6*,*7*).

Bangladesh has a large number of LBMs in urban areas in which multiple poultry species from backyard and commercial farms are housed together for sale; several studies detected highly pathogenic and low pathogenicity avian influenza viruses (AIVs) in LBM poultry and the environment (*8*–*13*). An LBM-based surveillance detected AIVs in waterfowl (4%) and environmental samples from poultry markets (29%). During 2007–2012, many subtypes, including H5N1, H5N2, H7N9, and H9N2, were identified in waterfowl and environmental samples (*14*). In 1 study, 9 (2%) of 450 LBM workers from 12 LBMs across Bangladesh had antibodies against H5N1 virus (*15*). Such findings suggest that environmental contamination with AIVs occurs in Bangladesh and that poultry workers are at risk for contracting AIVs from infected poultry in LBMs and their contaminated environment.

Affected countries have introduced interventions to reduce the spread of AIVs in LBMs, including

Author affiliations: icddr,b, Dhaka, Bangladesh (S. Chowdhury, M.Z. Rahman, M.E. Hossain, P.K. Ghosh, S.S.U. Ahmed, K. Sturm-Ramirez, E.S. Gurley); Chattogram Veterinary and Animal Sciences University, Chattogram, Bangladesh (S. Chowdhury, M.A. Hoque); Centers for Disease Control and Prevention, Atlanta, Georgia, USA (E. Azziz-Baumgartner, J.C. Kile, E.D. Kennedy, K. Sturm-Ramirez); Johns Hopkins Bloomberg School of Public Health, Baltimore, Maryland, USA (E.S. Gurley)

DOI: https://doi.org/10.3201/eid2609.191029

temporary or permanent LBM closure, banning overnight poultry storage, and mandatory rest day(s), as well as daily cleaning of surfaces to reduce environmental contamination (*16*–*22*). Temporary, weekly 1-day closures at live poultry markets in Guangzhou, China, was implemented for effective disinfection in response to the H7N9 outbreaks during 2013–2014 (*23*). However, market-level interventions have not been effective in reducing environmental contamination in Bangladesh. The infrastructure and daily activities of individual poultry shops within markets are heterogeneous (*9*). Because individual poultry shops have their own infrastructure and biosecurity controls, shop-level analyses might be useful in developing and designing effective interventions. Our study aimed to assess the shop-level prevalence of influenza A virus contamination among LBM shops across Bangladesh and to identify biosecurity and hygiene practices that are associated with risk for and protection from influenza A virus contamination.

Methods

Bangladesh has 10 metropolitan areas where large numbers of LBMs are located. We conducted a cross-sectional study in all 10 areas (Figure 1).

Selection of LBMs and Poultry Shops

We determined that we needed 800 poultry shops to detect ≥1% prevalence of AIV with 95% confidence and 0.7% precision. Initially, the field team visited each metropolitan area to identify all LBMs and count the number of individually owned poultry shops in each market. After visiting all the cities, we prepared a list of LBMs with ≥10 poultry shops for each

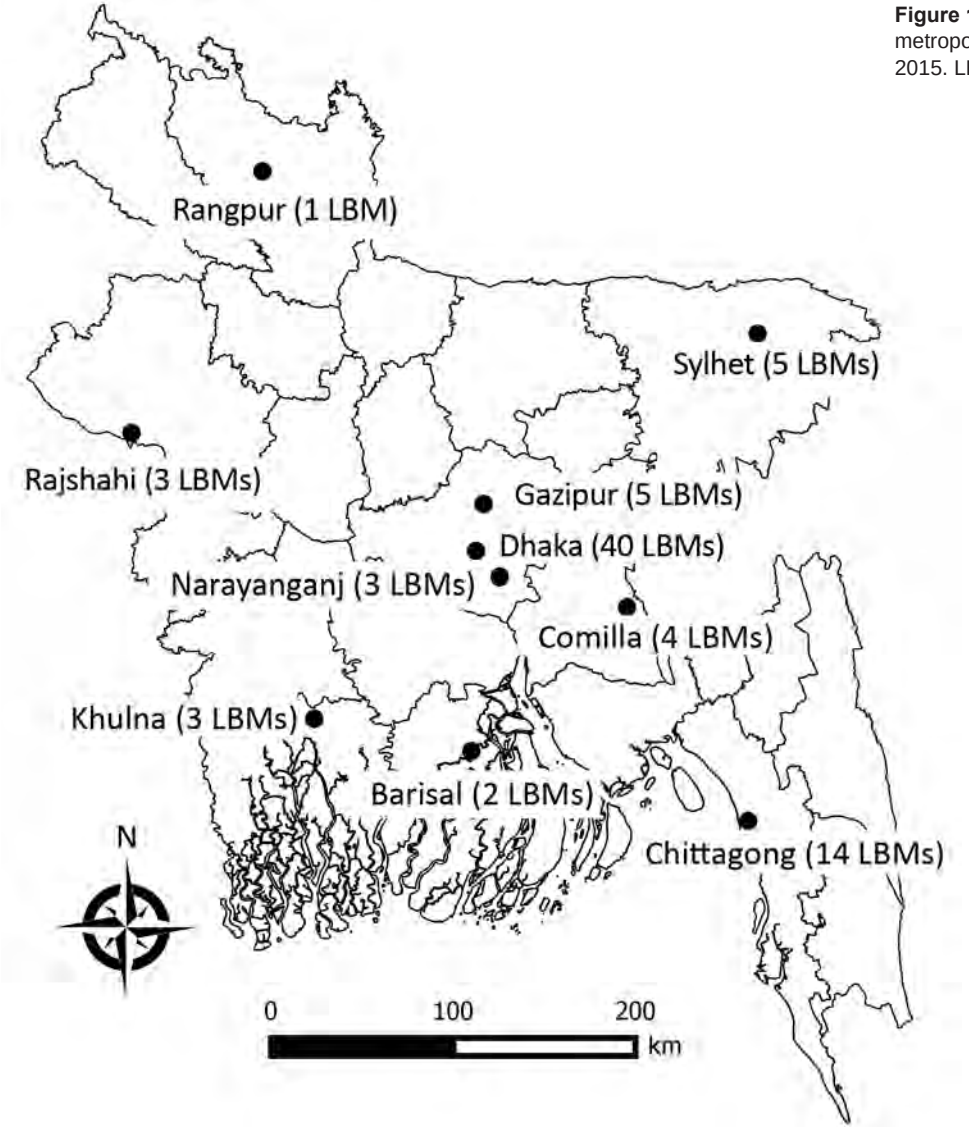

Figure 1. Locations of LBMs, 10 metropolitan areas, Bangladesh, March 2015. LBM, live bird market.

metropolitan area. We then selected 80 LBMs from 10 metropolitan areas by using a proportionate random sampling technique. Finally, we enrolled 10 shops in each LBM by using a random number generator.

Biosecurity Measures and Other Practices

During March 2015, the field team visited each selected shop to interview poultry shop owners or workers and collect information about shop characteristics, poultry transactions, and biosecurity and hygiene practices. On the basis of previously identified risk factors and recommended biosecurity and hygiene practices, we hypothesized that cleaning, disinfection, overnight poultry storage, a weekly rest day, practice of poultry slaughtering within shops, type of floor, poultry holding areas, presence of waterfowl, poultry density, number of poultry species, source of poultry, and the separation of sick poultry from healthy poultry could be associated with the detection of AIV in the poultry shop environment (Appendix 1, https://wwwnc.cdc.gov/EID/article/26/9/19-1029-App1.pdf) (*11*,*17*,*19*,*21*,*22*,*24*–*28*). In a questionnaire (Appendix 2, https://wwwnc.cdc.gov/EID/article/26/9/19-1029-App2.pdf), we defined cleaning as "cleaning of poultry holding areas with water and/or broom," and we defined disinfection as "cleaning of poultry holding areas with a disinfectant." We asked owners whether they cleaned poultry holding areas daily, weekly, monthly, or did not clean within the past month. We asked whether they disinfected poultry holding areas weekly, monthly, or did not disinfect within the last month. The field team also collected some market-level information by interviewing members of the market committee.

Sample Collection

From each selected shop, we collected 8–10 swab specimens of poultry droppings, cages, feed, drinking water, slaughtering surfaces and utensils, slaughtering by-products, offal, shop floors, or waste bins. We pooled the 8–10 samples from each shop and tested them as a single sample. Some shops had no slaughtering facilities within their premises. From these shops, we collected swab specimens from other sources, including poultry droppings, cages, feed, and drinking water. We collected 1 pooled sample from each of 800 selected shops during March 2015 because highly pathogenic avian influenza (H5N1) activity typically peaks during January–March (*29*).

Laboratory Testing

We used a real-time reverse transcription PCR detection kit for typing and subtyping influenza viruses and fluorescent TaqMan probes at the icddr,b (*30*). Primers and probes specific for the matrix gene were used to detect influenza A viruses. To identify H5, H7, and H9 subtypes in influenza A virus–positive samples, we used H5, H7, and H9 hemagglutinin gene–specific primers and probes (*30*).

Observations

On the basis of laboratory testing results, we identified all influenza A/H5–positive shops and an equal number of influenza A virus–negative shops by using a random number generator and a list of influenza A virus–negative shops. Field staff observed each selected shop for a 3-hour period during April 2015. Staff observed cleaning and disinfection activities of selected poultry shops during surprise visits at times when cleaning activities were scheduled. Field staffs were blinded to the laboratory test results of selected shops.

Statistical Analysis

We summarized characteristics of poultry shops, including infrastructure and biosecurity and hygiene measures, by using descriptive analyses. We estimated the presence of environmental contamination with influenza A viruses in shops and 95% CIs. Initially, we constructed a conceptual framework to identify causal association and confounders as described (*31*) (Figure 2). We then performed univariate analyses to estimate odds ratios (ORs). Exposure variables associated with outcomes with $p \leq 0.2$ in univariate analysis and confounder variables from the conceptual framework were selected for multivariate analyses. We used backward stepwise selection of variables with a significance level of 0.05 to construct models. We then used mixed-effect logistic regression multivariate models, accounting for clustering by metropolitan area and market, to estimate adjusted ORs (aORs). We assessed collinearity by calculating the variance inflation factor for independent variables used in the regression models (*32*). Weekly cleaning was highly correlated with daily cleaning practices; therefore, we removed weekly cleaning from the model during multivariate analyses. We calculated model χ^2 and R^2 (the coefficient of determination) to measure goodness-of-fit for multivariate regression model. We performed all statistical analyses by using Stata version 13 software (StataCorp LLC, https://www.stata.com).

Ethics

Field staff obtained written consent from shop owners or poultry workers for data and sample collection from their shops. The icddr,b Research Review Committee

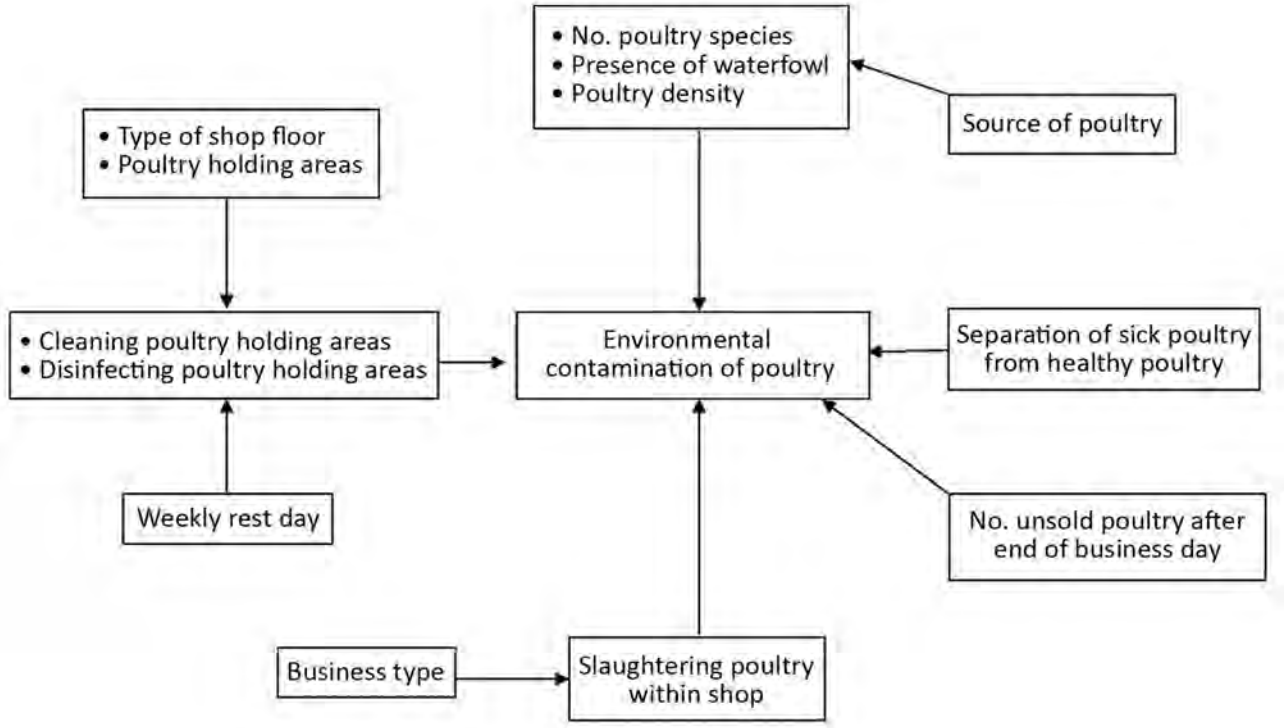

Figure 2. Conceptual framework for shop-level environmental contamination with avian influenza viruses in live bird markets, Bangladesh, March 2015.

and Ethical Review Committee reviewed and approved the study protocol (protocol no. PR-15012).

Results

We identified 104 LBMs that had ≥10 poultry shops. Among these LBMs, we selected 800 shops in 80 LBMs for sample and data collection (Table 1). The average number of poultry shops in each market was 20 (SD 10.5, range 10–55). Most (77%) poultry shops were retail and sold live poultry directly to consumers. The average size of each poultry shop was 9 m^2, and the average duration of trade per day was 14 hours. Chickens were the predominant poultry species sold at LBMs, and 91% of shops had a >1 poultry species the day of our visit (Table 2). A total of 6% of shops sold waterfowl only, and 4% sold chickens and ducks.

Poultry shopkeepers housed poultry in different types of settings, including wire cages, bamboo cages, and on the floor. Most (80%) poultry shops had uneven floor surfaces, partially made with tiles/concrete and mud. Poultry shop owners collected poultry from different sources, including wholesale markets, intermediaries, and directly from poultry farms. Most (86%) poultry shops slaughtered poultry on premises. Cleaning and disinfecting practices varied among poultry shops: 468 shops (59%) reported cleaning poultry holding areas daily, 185 (23%) reported using a disinfectant once a week, 592 (74%) reported frequently working throughout the week (i.e., not following the recommended weekly day of rest), and 654 shops (82%) reported keeping unsold poultry after the end of each business day.

Laboratory Results for Environmental Specimens

Environmental specimens from 205 (26%, 95% CI 23%–29%) shops were positive for influenza A viral RNA; 108 (14%, 95% CI 11%–16%) were positive for the H9 subtype and 60 (8%, 95% CI 6%–9%) were positive for the H5 subtype (Table 1). An additional 37 (5%, 95% CI 3%–6%) influenza A–positive shops had samples that were not subtypeable with H5, H7, and H9 primers. Samples from 29 (4%) shops were confirmed for both H5 and H9 subtypes. No samples were positive for H7 (95% CI 0%–0.5%). Shops in all 10 cities had at ≥1 sample positive for influenza A viral RNA, and 7 cities (70%) had shops positive for the H5 subtype. Among the 80 LBMs, ≥1 shop from 74 markets (93%) was positive for influenza A viral RNA, and ≥1 shop from 35 markets (44%) was positive for influenza A/H5 RNA. Environmental samples from 6 LBMs (3 from Chittagong, 1 from Dhaka, 1 from Khulna, and 1 from Comilla) were negative for influenza A viral RNA.

Table 1. Influenza A and avian influenza virus contamination of live bird market shops, by metropolitan area, Bangladesh, March 2015

Metropolitan cities	No. live bird markets investigated	Total no. shops tested	No. (%) shops positive for influenza A	No. (%) shops positive for influenza A/H5	No. (%) shops positive for influenza A/H9
Dhaka	40	400	116 (29)	46 (12)	52 (13)
Chittagong	14	140	15 (12)	3(2)	7 (5)
Gazipur	5	50	14 (28)	1 (2)	9 (18)
Sylhet	5	50	25 (50)	2 (4)	21 (42)
Comilla	4	40	5 (13)	0	3 (8)
Rajshahi	3	30	7 (23)	1 (3)	4 (13)
Khulna	3	30	3 (10)	0	2 (7)
Narayanganj	3	30	10 (33)	4 (13)	5 (17)
Barisal	2	20	5 (25)	0	3 (15)
Rangpur	1	10	5 (50)	3 (30)	2 (20)
Total	80	800	205 (26)	60 (8)	108 (14)

Observational Findings

We conducted observations in 60 influenza A/H5 virus–positive and 60 influenza A virus–negative shops. We did not find any major differences in cleaning and disinfection practices between influenza A/H5 virus–positive and influenza A virus–negative shops. Surveyors observed cleanings in 85% of influenza A/H5 virus–positive shops and 86% of influenza A virus–negative shops. Among these shops, only 2% of influenza A/H5 virus–positive shops performed disinfection by using washing powder or another recognized disinfectant, whereas 3% of influenza A virus–negative shops performed disinfection during our period of observation.

Associations between Shop-Level Biosecurity, Hygiene, and AIV Environmental Surface Contamination with Influenza A Viruses

We showed by using univariate analyses that poultry shops that kept poultry on the floor (OR 3.86, 95% C: 1–15.07; p = 0.05), slaughtered poultry within the shop (OR 1.7, 95% CI 1.08–2.67; p = 0.02), had unsold poultry after the end of the business day (OR 2.29, 95% CI 1.44–3.63; p<0.01), did not rest 1 day a week (OR 1.34, 95% CI 1.14–1.58; p = 0.01), kept sick and healthy appearing poultry together (OR 1.25, 95% CI 1–1.58; p = 0.05), and had uneven floor surfaces (partly made with tiles/concrete and mud) (OR 4.01, 95% CI 2.53–6.36; p<0.01) were more likely to be positive for influenza A viral RNA in environmental samples compared with shops that did not have these characteristics (Table 3). Poultry shops that reportedly cleaned poultry holding areas either daily (OR 0.41, 95% CI 0.27–0.62; p<0.01), weekly (OR 0.37, 95% CI 0.18–0.73; p<0.01), or monthly (OR 0.2, 95% CI 0.08–0.49; p<0.01), and had weekly disinfection (OR 0.81, 95% CI 0.61–1.07; p = 0.14) seemed less likely to be positive for influenza A viral RNA compared with shops that did not.

In the final multivariate analysis model, we showed that poultry shops that slaughtered poultry within the shop (aOR 1.87, 95% CI 1.11–3.14; p = 0.01), had unsold poultry after the end of the business day (aOR 2.35, 95% CI 1.4–3.93; p<0.01), did not rest 1 day a week (aOR 1.35, 95% CI 1.12–1.63; p<0.01), had uneven floor surfaces (partly made with tiles/concrete and mud) (aOR 3.64, 95% CI 2.32–5.71; p<0.01), held poultry on the floor (aOR 3.95, 95% CI 1.27–12.23; p = 0.01), and kept sick and healthy appearing poultry together (aOR 1.31, 95% CI 1.06–1.62; p = 0.01) were significantly more likely to be positive for influenza A viruses compared with shops that did not report these characteristics (Table 3). Reported monthly cleaning was protective (aOR 0.47, 95% CI 0.28–0.8; p<0.01), but disinfecting practices of poultry holding areas was still not significantly associated with influenza A virus detection in the multivariate model (p = 0.85). The final model selected seemed to fit data well (χ^2 76.29, df 11, p<0.001, and R^2 0.596). No market-level factors, including central cleaning and disinfection practices, were significantly associated with influenza A virus detection in the multivariate model (Appendix 1).

Table 2. Daily poultry trade at 800 live bird market shops selected for the study, by poultry species, Bangladesh, March 2015

Poultry sold	No. (%) shops	Mean no. poultry/day (range)		
		Stocked/day	Sold/day	Leftover/day
Only chicken	722 (90)	210 (20–3,760)	159 (10–3,760)	52 (0–1,650)
Only waterfowl	3 (1)	130 (50–290)	108 (32–252)	22 (10–38)
Only pigeon	5 (1)	90 (50–150)	41 (5–80)	49 (30–70)
Two poultry species	57 (7)	267 (20–1333)	185 (10–850)	83 (5–895)
More than 2 poultry species	13 (2)	522 (48–3,000)	296 (33–1,075)	227 (10–1,925)

Discussion

Evaluation of existing biosecurity and hygiene practices is necessary to develop and design interventions to reduce the spread of AIVs in LBMs. Our study provides a detailed depiction of the daily operation of poultry shops and current biosecurity and hygiene practices in selected LBMs of Bangladesh. We identified certain biosecurity and hygiene practices associated with environmental contamination with AIVs: slaughtering poultry within shops, having unsold poultry after the end of the business day, skipping rest days, uneven floor surfaces, holding poultry on the floor, and keeping sick and healthy appearing poultry together.

Our study determined that most shops did not implement biosecurity practices, which have reduced AIV in other countries. For example, biosecurity and hygiene practices, including weekly rest days, depopulation, and cleaning with disinfectant, reduced the risk for AIV detection in poultry and environmental specimens in China (*28*). The prevalence of H7N9 virus in environmental specimens

Table 3. Shop-level biosecurity practices and environmental contamination with 800 influenza A viruses in 10 metropolitan areas, Bangladesh, March 2015*

Variable	No. (%) shops	No. (%) shops positive for influenza A viruses, n = 205	OR (95% CI)	p value	Adjusted OR (95% CI)†	p value†
Poultry species						
Single	731 (91)	184 (25)	Referent	NA		
Multiple	69 (9)	21 (30)	1.45 (0.9–2.32)	0.12		
Presence of waterfowl						
No	752 (94)	190 (25)	Referent	NA		
Yes	48 (6)	15 (31)	1.68 (0.86–3.32)	0.13		
Poultry holding areas						
Only wire cage	281 (35)	55 (20)	Referent	NA	Referent	NA
Only bamboo cage	153 (19)	53 (35)	2.12 (0.85–5.28)	0.1	2.24 (0.87–5.77)	0.09
Only floor	24 (3)	9 (38)	3.86 (1–15.07)	0.05	3.95 (1.27–12.23)	0.01
Mixed	342 (43)	88 (26)	1.72 (0.96–3.09)	0.06	1.71 (0.96–3.04)	0.06
Cleaning poultry holding areas						
No cleaning in past month	26 (3)	12 (46)	Referent	NA	Referent	NA
Monthly	68 (9)	10 (14)	0.2 (0.08–0.49)	<0.01	0.47 (0.28–0.8)	<0.01
Weekly‡	238 (30)	57 (24)	0.37 (0.18–0.73)	<0.01	NA	NA
Daily	468 (59)	126 (27)	0.41 (0.27–0.62)	<0.01	1.09 (0.91–1.31)	0.31
Disinfecting poultry holding areas						
No disinfection in past month	577 (72)	150 (26)	Referent	NA		
Monthly	38 (5)	10 (26)	1.1 (0.53–2.25)	0.79		
Weekly	185 (23)	45 (24)	0.81 (0.61–1.07)	0.14		
Slaughtering poultry within shop						
No	115 (14)	18 (16)	Referent	NA	Referent	NA
Yes	685 (86)	187 (27)	1.7 (1.08–2.67)	0.02	1.87 (1.11–3.14)	0.01
Presence of unsold poultry after the end of business day						
No poultry left	146 (18)	19 (13)	Referent	NA	Referent	NA
Presence of unsold poultry	654 (82)	186 (28)	2.29 (1.44–3.63)	<0.01	2.35 (1.4–3.93)	<0.01
Weekly rest day						
Yes	208 (26)	51 (25)	Referent	NA	Referent	NA
No	592 (74)	154 (26)	1.34 (1.14–1.58)	<0.01	1.35 (1.12–1.63)	<0.01
Source of poultry						
Poultry farm	49 (6)	12 (24)	Referent	NA		
Intermediaries	54 (7)	10 (19)	0.85 (0.27–2.64)	0.78		
Wholesale market	525 (66)	143 (27)	1.05 (0.51–2.16)	0.88		
Multiple sources	172 (21)	40 (23)	0.94 (0.35–2.49)	0.9		
Separation of sick poultry from healthy flocks						
Yes	357 (45)	85 (24)	Referent	NA	Referent	NA
No	443 (55)	120 (27)	1.25 (1–1.58)	0.05	1.31 (1.06–1.62)	0.01
Type of shop floor						
Tiles/concrete	244 (31)	32 (13)	Referent	NA	Referent	NA
Dirt/mud	33 (4)	8 (24)	3.61 (1.7–7.67)	<0.01	3.2 (1.46–7.09)	<0.01
Mixed	523 (65)	165 (32)	4.01 (2.53–6.36)	<0.01	3.64 (2.32–5.71)	<0.01
Poultry density/mm^2						
≤32	568 (71)	147 (26)	Referent	NA		
≥33	232 (29)	58 (25)	0.89 (0.68–1.15)	0.39		

*Variables for geographic location of metropolitan areas and live bird markets were adjusted to account for clustering effects in univariate and multivariate analysis. NA, not applicable; OR, odds ratio.
†Only statistically significant relationships are shown for adjusted OR (95% CI) data and corresponding p values.
‡The weekly cleaning variable was removed from the multivariate model because of collinearity. Model fit: model χ^2 76.29, p<0.001, df 11; adjusted generalized R^2 0.596.

from LBMs in China decreased after the closure of live poultry markets (*33*). Daily waste removal was found to be protective in Indonesia (*17*). In the United States, environmental contamination decreased after implementing routine cleaning and disinfection (*19*,*22*). Although monthly cleaning was found to be protective in reducing environmental contamination with AIVs in this study, most shops in Bangladesh do not disinfect, and their current biosecurity practices do not seem to prevent environmental contamination. Moreover, most of the studied shops had rough dirt and mud floors that are less suitable for proper cleaning and disinfection, indicating poor market infrastructure.

Globally, countries reporting human cases of AIV also have LBMs contaminated with AIVs. AIV contamination of LBM environments increases the risk for infection and amplification of the virus in virus-free birds. In addition, if the AIV is zoonotic, as are H7N9, H5N1, and H5N6 viruses, increased viremia in birds increases the risk for human exposure and infection. For example, in Vietnam, AIVs were detected in 3.2% of poultry specimens collected from LBMs; in Egypt, H5N1 virus was detected in poultry in 12.4% of LBMs; in China, H7N9 virus was detected in 10% of environmental specimens from LBMs; in Indonesia, AIVs were detected in 47% of environmental specimens from LBMs; in Thailand, H5N1 virus was detected in 3.1% of market poultry; and in Bangladesh, AIVs were detected in 23% of poultry specimens (*10*,*17*,*33*–*35*). In our study, >90% of the LBMs were positive for influenza A viruses, and 44% were specifically positive for AIV H5 RNA. Detection of AIV RNA in environmental samples indicates that market poultry were infected with AIVs near the time of sample collection and might excrete, secrete, or contaminate surfaces and humans through their carcasses, feathers, and offal. Our study findings also confirmed the presence of 2 subtypes (H5 and H9) of AIV, which might lead to genetic reassortment and evolution of new AIV strains in poultry of public health concern (*29*).

Epidemiologic studies have described the effectiveness of weekly or monthly rest days in reducing environmental contamination of LBMs with AIV (*21*,*24*). The number of human cases of infection with H7N9 virus has been observed to be reduced after permanent or temporary closure of LBMs and the culling of poultry (*24*,*25*,*33*,*36*). The government of Bangladesh imposed an order in 2012 to practice weekly rest days for cleaning and disinfecting LBMs within Dhaka (*37*). Nevertheless, 1 study found 74% of poultry shop owners did not practice weekly rest days, which might increase the risk for environmental contamination. A weekly rest day should be enforced by the government to decrease the risk for AIV circulation in LBMs.

Unsold poultry can play a major role in maintaining virus circulation in markets (*25*). Unsold infected poultry can infect incoming poultry, promoting further transmission of influenza viruses in susceptible birds. Banning overnight poultry storage in China reduced H9N2 virus isolation in chickens (84%) (*24*). In our study, most (82%) poultry shops reported that they stored poultry overnight in their shops to sell the next day. A previous study from Bangladesh also found that 73% of poultry shops kept poultry in their stalls for >1 day (*38*).

Slaughtering by-products, such as blood and offal, of AIV-infected poultry provide the most likely opportunity for environmental contamination and subsequent human exposure to high loads of virus. In Indonesia, slaughtering poultry within market premises was a risk factor for environmental contamination (*17*,*26*). H7N9 virus was detected in swab samples collected from surfaces of chopping boards in China (*33*). Persons from China and Bangladesh prefer to purchase live chickens that are slaughtered in the market at the time of purchase (*9*,*36*). A study suggested introducing central slaughtering of all live poultry in the LBM to control the risk posed of AIVs (*39*). In Bangladesh, most poultry shops, including those in this study, sold and slaughtered poultry within their shop (*9*). This practice might increase the risk for AIV contamination and perpetuate the exposure of poultry to AIV in LBMs. Although our study did not assess AIV transmission within LBMs, we cannot rule out the risk for AIV transmission to humans through slaughtering of infected poultry. We recommend introducing centralized slaughter facilities in LBMs to decrease the spread of AIV.

LBMs in Bangladesh are larger (ranging from 10 to 55 poultry shops) than those in Hong Kong, where the number of poultry shops in each LBM was 3–24 (*21*). Maintaining effective biosecurity and hygiene measures might be more difficult in larger LBMs that had poor infrastructure. The infrastructures of LBMs in city areas were quite similar. However, the prevalence of H5 and H9 subtypes varied between cities and might naturally differ in virus ecology by farm or geographic site. The infrastructure of our studied poultry shops within LBMs was often rudimentary: most were fully enclosed by walls, but most had rough muddy floors, unsystematic poultry holding areas, poor waste disposal systems, and unconfined slaughtering facilities. Urban markets have more

poultry shops than rural markets. Urban LBMs usually are open every day, whereas rural LBMs are open once or twice per week. Bangladesh should consider investing in poultry shop infrastructure improvements and biosecurity practices, particularly in city areas, to better control environmental contamination with AIVs.

In China, poultry trading networks linked with LBMs were strongly associated with a higher prevalence of H7N9 virus among poultry and risk for H7N9 transmission to humans (*36*). Movement of infected poultry between markets has a major role in the spread of AIVs from 1 market to another (*17*,*40*). Poultry market supply chains in urban areas of Bangladesh are complex, collecting poultry from different sources, including directly from farms, intermediaries, or wholesale markets. These complex networks might promote a high number of contacts between infected and susceptible marketed birds and, therefore, increase AIV transmission potential within the trade networks.

This cross-sectional study design might have limited interpretation of some of the results. Although AIV circulation and amplification at LBMs are continuous processes influenced by time-dependent parameters, such as time to last cleaning before sampling and time to last poultry introduction/mixing before sampling, we only examined environmental contamination for AIVs at 1 point in time and did not explore time from last cleaning or disinfection. No additional laboratory tests were performed to characterize viral load and viability of AIVs detected because of limited funding. Therefore, it is unclear if the AIVs detected during the study were infectious to humans. The information we collected from poultry shop owners and workers about biosecurity might have been affected by social desirability bias, which might have underestimated the prevalence of practices that place shop at risk for contamination with AIVs.

In conclusion, our study identified risky practices, hygiene, and infrastructure in Bangladesh LBMs associated with an increased likelihood of shop contamination with AIVs. Improvement of these biosecurity practices, such as removing poultry at the end of the day, observing weekly rest days, introducing centralized slaughter facilities, and regular cleaning and disinfection, might help to prevent AIV contamination. LBM infrastructure, including floors, poultry holding areas, waste disposal systems, and slaughtering facilities, also need improvement. Potential valuable shop-level interventions to address these deficiencies in biosecurity practices might include training for poultry shop owners and poultry workers about effective biosecurity practices to reduce AIV contamination and the risk AIV poses to humans in Bangladesh.

Acknowledgments

We thank Susan C. Trock and Nord Zeidner for providing scientific input during protocol development, Gladys Leterme for proofreading and editing the manuscript, and field staff for their efforts during sample and data collection. The icddr,b is also grateful to the governments of Bangladesh, Canada, Sweden, and the United Kingdom for providing core/unrestricted support and acknowledge with gratitude the commitment of the Centers for Disease Control and Prevention to its research efforts.

This study was supported by the Centers for Disease Control and Prevention (cooperative agreement no. 1U01GH001207-01).

About the Author

Dr. Chowdhury is a veterinary epidemiologist at the icddr,b, Dhaka, Bangladesh. His primary research interests are epidemiology, infectious diseases surveillance, antimicrobial drug resistance, food safety, public health advocacy, and One Health issues.

References

1. World Health Organization. Cumulative number of confirmed human cases of avian influenza A(H5N1) reported to WHO, 2019 [cited 2020 May 18]. https://www.who.int/influenza/human_animal_interface/2019_02_12_tableH5N1.pdf
2. World Organisation for Animal Health. Update on avian influenza in animals (types H5 and H7), 2018 [cited 2020 May 18]. http://www.oie.int/en/animal-health-in-the-world/update-on-avian-influenza/2018
3. Rushton J, Viscarra R, Bleich EG, McLeod A. Impact of avian influenza outbreaks in the poultry sectors of five South East Asian countries (Cambodia, Indonesia, Lao PDR, Thailand, Viet Nam) outbreak costs, responses and potential long term control. World's Poultry Science Journal. 2005;61:491–514. https://doi.org/10.1079/WPS200570
4. Smith GJ, Naipospos TS, Nguyen TD, de Jong MD, Vijaykrishna D, Usman TB, et al. Evolution and adaptation of H5N1 influenza virus in avian and human hosts in Indonesia and Vietnam. Virology. 2006;350:258–68. https://doi.org/10.1016/j.virol.2006.03.048
5. Chowdhury S, Hossain ME, Ghosh PK, Ghosh S, Hossain MB, Beard C, et al. The pattern of highly pathogenic avian influenza H5N1 outbreaks in south Asia. Trop Med Infect Dis. 2019;4:138. https://doi.org/10.3390/tropicalmed4040138
6. Wan X-F, Dong L, Lan Y, Long L-P, Xu C, Zou S, et al. Indications that live poultry markets are a major source of human H5N1 influenza virus infection in China. J Virol. 2011;85:13432–8. https://doi.org/10.1128/JVI.05266-11
7. Webster RG. Wet markets—a continuing source of severe acute respiratory syndrome and influenza? Lancet. 2004;363:234–6. https://doi.org/10.1016/S0140-6736(03)15329-9

8. Nakamura S, Maeda N, Miron IM, Yoh M, Izutsu K, Kataoka C, et al. Metagenomic diagnosis of bacterial infections. Emerg Infect Dis. 2008;14:1784–6. https://doi.org/10.3201/eid1411.080589
9. Biswas P, Giasuddin M, Nath B, Islam M, Debnath N, Yamage M. Biosecurity and circulation of influenza A (H5N1) virus in live bird markets in Bangladesh, 2012. Transbound Emerg Dis. 2015; 64:883–91.
10. Negovetich NJ, Feeroz MM, Jones-Engel L, Walker D, Alam SM, Hasan K, et al. Live bird markets of Bangladesh: H9N2 viruses and the near absence of highly pathogenic H5N1 influenza. PLoS One. 2011;6:e19311. https://doi.org/10.1371/journal.pone.0019311
11. Sayeed MA, Smallwood C, Imam T, Mahmud R, Hasan RB, Hasan M, et al. Assessment of hygienic conditions of live bird markets on avian influenza in Chittagong metro, Bangladesh. Prev Vet Med. 2017;142:7–15. https://doi.org/10.1016/j.prevetmed.2017.04.009
12. Turner JC, Feeroz MM, Hasan MK, Akhtar S, Walker D, Seiler P, et al. Insight into live bird markets of Bangladesh: an overview of the dynamics of transmission of H5N1 and H9N2 avian influenza viruses. Emerg Microbes Infect. 2017;6:e12. https://doi.org/10.1038/emi.2016.142
13. Kim Y, Biswas PK, Giasuddin M, Hasan M, Mahmud R, Chang Y-M, et al. Prevalence of avian influenza A(H5) and A(H9) viruses in live bird markets, Bangladesh. Emerg Infect Dis. 2018;24:2309–16. https://doi.org/10.3201/eid2412.180879
14. Khan SU, Gurley ES, Gerloff N, Rahman MZ, Simpson N, Rahman M, et al. Avian influenza surveillance in domestic waterfowl and environment of live bird markets in Bangladesh, 2007–2012. Sci Rep. 2018;8:9396. https://doi.org/10.1038/s41598-018-27515-w
15. Nasreen S, Khan SU, Luby SP, Gurley ES, Abedin J, Zaman RU, et al. Highly pathogenic avian influenza A(H5N1) virus infection among workers at live bird markets, Bangladesh, 2009–2010. Emerg Infect Dis. 2015;21:629–37. https://doi.org/ 10.3201/eid2104.141281
16. Kung NY, Guan Y, Perkins NR, Bissett L, Ellis T, Sims L, et al. The impact of a monthly rest day on avian influenza virus isolation rates in retail live poultry markets in Hong Kong. Avian Dis. 2003;47(Suppl):1037–41. https://doi.org/10.1637/0005-2086-47.s3.1037
17. Indriani R, Samaan G, Gultom A, Loth L, Irianti S, Adjid R, et al. Environmental sampling for avian influenza virus A (H5N1) in live-bird markets, Indonesia. Emerg Infect Dis. 2010;16:1889–95. https://doi.org/10.3201/eid1612.100402
18. Murhekar M, Arima Y, Horby P, Vandemaele KA, Vong S, Zijian F, et al.; World Health Organization Regional Office for the Western Pacific Event Management Team. Avian influenza A(H7N9) and the closure of live bird markets. Western Pac Surveill Response J. 2013;4:4–7. https://doi.org/10.5365/wpsar.2013.4.2.008
19. Trock SC, Gaeta M, Gonzalez A, Pederson JC, Senne DA. Evaluation of routine depopulation, cleaning, and disinfection procedures in the live bird markets, New York. Avian Dis. 2008;52:160–2. https://doi.org/10.1637/7980-040607-Reg
20. Fournié G, Guitian J, Desvaux S, Cuong VC, Dung H, Pfeiffer DU, et al. Interventions for avian influenza A (H5N1) risk management in live bird market networks. Proc Natl Acad Sci U S A. 2013;110:9177–82. https://doi.org/10.1073/pnas.1220815110
21. Lau EH, Leung YH, Zhang LJ, Cowling BJ, Mak SP, Guan Y, et al. Effect of interventions on influenza A (H9N2) isolation in Hong Kong's live poultry markets, 1999–2005. Emerg Infect Dis. 2007;13:1340–7. https://doi.org/10.3201/eid1309.061549
22. Bulaga LL, Garber L, Senne DA, Myers TJ, Good R, Wainwright S, et al. Epidemiologic and surveillance studies on avian influenza in live-bird markets in New York and New Jersey, 2001. Avian Dis. 2003;47(Suppl):996–1001. https://doi.org/10.1637/0005-2086-47.s3.996
23. Yuan J, Tang X, Yang Z, Wang M, Zheng B. Enhanced disinfection and regular closure of wet markets reduced the risk of avian influenza A virus transmission. Clin Infect Dis. 2014;58:1037–8. https://doi.org/10.1093/cid/cit951
24. Leung YH, Lau EH, Zhang LJ, Guan Y, Cowling BJ, Peiris JS. Avian influenza and ban on overnight poultry storage in live poultry markets, Hong Kong. Emerg Infect Dis. 2012;18:1339–41. https://doi.org/10.3201/eid1808.111879
25. Offeddu V, Cowling BJ, Malik Peiris JS. Interventions in live poultry markets for the control of avian influenza: a systematic review. One Health. 2016;2:55–64. https://doi.org/10.1016/j.onehlt.2016.03.002
26. Samaan G, Gultom A, Indriani R, Lokuge K, Kelly PM. Critical control points for avian influenza A H5N1 in live bird markets in low resource settings. Prev Vet Med. 2011;100:71–8. https://doi.org/10.1016/j.prevetmed.2011.03.003
27. Yuan J, Lau EH, Li K, Leung YH, Yang Z, Xie C, et al. Effect of live poultry market closure on avian influenza A(H7N9) virus activity in Guangzhou, China, 2014. Emerg Infect Dis. 2015;21:1784–93. https://doi.org/10.3201/eid2110.150623
28. Yuan J, Tang X, Yang Z, Wang M, Zheng B. Enhanced disinfection and regular closure of wet markets reduced the risk of avian influenza A virus transmission. Clin Infect Dis. 2014;58:1037–8. https://doi.org/10.1093/cid/cit951
29. Durand LO, Glew P, Gross D, Kasper M, Trock S, Kim IK, et al. Timing of influenza A(H5N1) in poultry and humans and seasonal influenza activity worldwide, 2004–2013. Emerg Infect Dis. 2015;21:202–8. https://doi.org/10.3201/eid2102.140877
30. Centers for Disease Control and Prevention. Laboratory support for influenza surveillance (CLSIS). Atlanta: The Centers; 2013.
31. Greenland S, Pearl J, Robins JM. Causal diagrams for epidemiologic research. Epidemiology. 1999;10:37–48. https://doi.org/10.1097/00001648-199901000-00008
32. Dormann CF, Elith J, Bacher S, Buchmann C, Carl G, Carré G, et al. Collinearity: a review of methods to deal with it and a simulation study evaluating their performance. Ecography. 2013;36:27–46. https://doi.org/10.1111/j.1600-0587.2012.07348.x
33. Wang X, Liu S, Mao H, Yu Z, Chen E, Chai C. Surveillance of avian H7N9 virus in various environments of Zhejiang Province, China before and after live poultry markets were closed in 2013–2014. PLoS One. 2015;10:e0135718. https://doi.org/10.1371/journal.pone.0135718
34. Nguyen DT, Bryant JE, Davis CT, Nguyen LV, Pham LT, Loth L, et al. Prevalence and distribution of avian influenza A(H5N1) virus clade variants in live bird markets of Vietnam, 2011–2013. Avian Dis. 2014;58:599–608. https://doi.org/10.1637/10814-030814-Reg
35. Abdelwhab EM, Selim AA, Arafa A, Galal S, Kilany WH, Hassan MK, et al. Circulation of avian influenza H5N1 in live bird markets in Egypt. Avian Dis. 2010;54:911–4. https://doi.org/10.1637/9099-100809-RESNOTE.1
36. Zhou X, Li Y, Wang Y, Edwards J, Guo F, Clements AC, et al. The role of live poultry movement and live bird market

biosecurity in the epidemiology of influenza A (H7N9): a cross-sectional observational study in four eastern China provinces. J Infect. 2015;71:470–9. https://doi.org/10.1016/j.jinf.2015.06.012
37. Biswas PK, Giasuddin M, Nath BK, Islam MZ, Debnath NC, Yamage M. Biosecurity and circulation of influenza A (H5N1) virus in live bird markets in Bangladesh, 2012. Transbound Emerg Dis. 2017;64:883–91. https://doi.org/10.1111/tbed.12454
38. Sarker S, Talukder S, Chowdhury E, Das P. Knowledge, attitudes and practices on biosecurity of workers in live bird markets at Mymensingh, Bangladesh. Journal of Agricultural and Biological Science. 2011;6:12–7.
39. Yu H, Wu JT, Cowling BJ, Liao Q, Fang VJ, Zhou S, et al. Effect of closure of live poultry markets on poultry-to-person transmission of avian influenza A H7N9 virus: an ecological study. Lancet. 2014;383:541–8. https://doi.org/10.1016/S0140-6736(13)61904-2
40. Van Kerkhove MD, Vong S, Guitian J, Holl D, Mangtani P, San S, et al. Poultry movement networks in Cambodia: implications for surveillance and control of highly pathogenic avian influenza (HPAI/H5N1). Vaccine. 2009; 27:6345–52. https://doi.org/10.1016/j.vaccine.2009.05.004

Address for correspondence: Sukanta Chowdhury, Programme for Emerging Infections, International Centre for Diarrheal Diseases Research, Mohakhali 1212, Bangladesh; email: sukanta@icddrb.org or sukanta.icddrb@yahoo.com

Costs Associated with Nontuberculous Mycobacteria Infection, Ontario, Canada, 2001–2012

Lauren C. Ramsay, Emily Shing, John Wang, Theodore K. Marras, Jeffrey C. Kwong, Sarah K. Brode, Frances B. Jamieson, Beate Sander

To determine incidence-based healthcare costs attributable to nontuberculous mycobacterial (NTM) pulmonary disease (PD) and NTM pulmonary isolation (PI), from the healthcare payer perspective, we conducted a population-based matched cohort study in Ontario, Canada. We established cohorts of patients with incident NTM-PD and NTM-PI during 2001–2012 by using individually linked laboratory data and health administrative data, matched to unexposed persons from the general population. To estimate attributable costs for acute and long-term illness, we used a phase-of-care approach. Costs were stratified by age, sex, and healthcare resource, and reported in 2018 Canadian dollars (CAD) and US dollars (USD), standardized to 10 days. Costs were highest during the before-death phase (NTM-PD CAD $1,352 [USD $1,044]; NTM-PI CAD $731 [USD $565]). The cumulative mean attributable 1-year costs were CAD $14,953 (USD $11,541) for NTM-PD and CAD $8,729 (USD $6,737) for NTM-PI. Costs for patients with NTM-PD and NTM-PI were higher than those for unexposed persons.

Pulmonary disease (PD) caused by nontuberculous mycobacteria (NTM) is an emerging public health threat (*1*). As identification of persons with NTM-PD increases (*2*,*3*), information about the economic burden of NTM-PD can help decision makers set funding priorities. NTM-PD accounts for most NTM infections and poses particular challenges (*4*). One challenge is that NTM-PD often occurs in patients with preexisting conditions such as cystic fibrosis, lung cancer, and chronic obstructive pulmonary disease (*5*,*6*); these conditions affect the spectrum and severity of signs and symptoms (*7*). Treatment of NTM-PD is complex, typically involving use of ≥3 antimicrobial agents for ≥18 months (*5*). Eradication of the organism is challenging; a recent meta-analysis demonstrated a success rate of 60% for eradication of *Mycobacterium avium* complex PD (MAC-PD) (*8*). Furthermore, recurrence after completed treatment for MAC-PD is extremely common; recurrence rates are 30% at 14 months (*9*) and ≈50% at 4 years (*10*). During 1998–2010, the prevalence of NTM-PD in Ontario, Canada, increased; the 5-year prevalence increased from 29.3 (1998–2002) to 41.3 (2003–2007) cases/100,000 persons (*2*).

The costs of NTM-PD in Canada are not well established; to the best of our knowledge, no studies have used population-based data to estimate associated costs. One study conducted in a tertiary care center in Toronto, Ontario, estimated the median monthly cost per NTM-PD patient to be approximately CAD $500; most of the costs were associated with medications (*11*). Although informative, that study considered only 1 clinic and did not account for potential long-term costs. Our objective with this study was to determine the costs associated with NTM-PD and with pulmonary isolation of NTM from patients without disease (NTM-PI), from the healthcare payer perspective, in Ontario, Canada, during 2001–2012.

Methods

Study Design and Participants

We conducted a population-based matched cohort study to examine attributable costs of NTM-PD and

Author affiliations: University Health Network, Toronto, Ontario, Canada (L.C. Ramsay, T.K. Marras, J.C. Kwong, S.K. Brode, B. Sander); University of Toronto, Toronto (L.C. Ramsay, T.K. Marras, J.C. Kwong, S.K. Brode, F.B. Jamieson, B. Sander); Public Health Ontario, Toronto (E. Shing, J. Wang, J.C. Kwong, F.B. Jamieson, B. Sander); ICES, Toronto (J. Wang, J.C. Kwong, S.K. Brode, B. Sander); West Park Healthcare Centre, Toronto (S.K. Brode)

DOI: https://doi.org/10.3201/eid2609.190524

NTM-PI from the healthcare payer perspective (Ontario Ministry of Health and Long-Term Care, Toronto, ON, Canada). Costs were identified by using provincial health administration data, including physician services, emergency department data, hospitalizations, prescription medications (for those ≥65 years of age), population data (e.g., census information and death records), and special collections (e.g., specific disease registries) (*12*). These data can be individually linked by using unique encoded identifiers at ICES (formerly the Institute for Clinical Evaluative Sciences), an independent, nonprofit research institute in Ontario, whose legal status under Ontario health information privacy law allows it to collect and analyze healthcare and demographic data without consent for health system evaluation and improvement (*12*). Descriptions of key ICES databases are described in more detail elsewhere (*13*–*15*). Our study was approved by the ethics review boards of Public Health Ontario and the University Health Network. All data analyses were conducted by using SAS version 9.4 (SAS Institute, https://www.sas.com).

We identified incident cases of NTM by using laboratory data from Public Health Ontario (https://www.publichealthontario.ca) for 2001–2012. NTM-PD was defined by the microbiological criteria of the American Thoracic Society/Infectious Diseases Society of America (ATS/IDSA) diagnostic guidelines: NTM isolation from >2 sputum samples (isolation of the same species within 2 years) or >1 positive sample from bronchoalveolar lavage or pleural fluid (5). NTM-PI was defined by NTM isolation from only 1 sputum sample. Persons were excluded if age, sex, or birth date data were not available; if they did not live in Ontario on the index date; if they were >100 years of age on the index date (i.e., the beginning of healthcare resource utilization related to NTM); if laboratory-confirmed M. gordonae had been isolated from them; or if laboratory-confirmed NTM had been isolated from them in the 3 years before the accrual period (January 1, 1998–December 31, 2000).

Because dates of disease onset were unknown, we adjusted index dates by using joinpoint (https://surveillance.cancer.gov/joinpoint) analysis on the cost curve (where a change in costs indicates change in healthcare use) and clinical judgement to estimate an onset of 30 days before laboratory confirmation of NTM. In the 30 days before laboratory confirmation, clinical judgement reconciled the increasing costs with the expectation of physician visits, possible hospitalizations, and a large number of clinical investigations.

Matched unexposed persons (who never had NTM-PD or NTM-PI) were drawn from the general population in the Registered Persons Database (https://datadictionary.ices.on.ca/Applications/DataDictionary/Library.aspx?Library=RPDB). We matched unexposed and exposed persons at a ratio of 3:1 by using a combination of hard-matching and propensity score matching without replacement (Tables 1, 2). We used a logistic regression model that regressed exposure status to calculate the propensity score based on the following covariates: rurality (using the Rurality Index of Ontario [*16*]), neighborhood income quintile, and underlying conditions 2 years before index date (using the Johns Hopkins Adjusted Clinical Groups System [*17*]). Persons were hard-matched by age, sex, and index date as well as within 0.2 SDs of the logit of the propensity score (*18*). To examine the effect of NTM-PD and NTM-PI on costs before death, we rematched each exposed person who died during the observation period (2001–2012) with 3 unexposed persons from the general population who also died during the same period, by using covariates assessed 180 days before death (Table 1).

Outcomes

We evaluated deaths (10-day, 30-day, 90-day, 1-year), acute hospital admissions (within 5 and 30 days of index date), and hospital lengths of stay. We calculated costs by using person-level costing methods established by ICES (*14*). This method uses administrative data to calculate long-term costs of incident cases from an index date to a defined point in time (death or the end of an observation window). In this method, costs are inflated by using the healthcare-specific Consumer Price Index reported by Statistics Canada (*14*). The publicly funded healthcare service categories included were acute inpatient hospitalizations, emergency visits, same-day surgeries and other ambulatory treatments, inpatient rehabilitation, complex continuing care, long-term care, inpatient mental health, physician services, home care, eligible prescription medications, and devices (*14*).

Cost Analyses

We calculated all costs in 2015 Canadian dollars (CAD) and present results in 2018 CAD and US dollars (USD). Costs were inflated from 2015 CAD by using the healthcare-specific Consumer Price Index (*19*) and converted to 2018 USD (1 CAD = 0.77 USD) (*20*). Using phase-of-care methods, we estimated NTM-PD– and NTM-PI–attributable healthcare costs for acute and long-term illness. We defined 3 phases (acute, continuing, and subsequent) by using joinpoint analysis (*21*) and clinical judgment. Clinical judgment supported the results of joinpoint analysis

Table 1. Variables used for matching persons exposed to nontuberculous mycobacteria to unexposed persons in study of costs associated with nontuberculous mycobacteria infection, Ontario, Canada, 2001–2012*

Variable	Index date	Death date
Baseline covariates–hard-matching		
Index date	± 30 d	NA
Death date	NA	± 90 d
Age	± 1 y	± 5 y
Sex	Exact	Exact
Propensity score variable		
Rurality Index of Ontario†	At index date	180 d before death
Neighborhood income quintile	At index date	180 d before death
Collapsed aggregated diagnosis groups‡	2 y before index date	

*Persons were hard-matched with regard to age, sex, and index date as well as within 0.2 SDs of the logit of the propensity score. To examine the effect of nontuberculous mycobacteria on costs before death, exposed persons who died during the observation period were rematched with 3 unexposed persons from the general population who also died during the same period, by use of covariates assessed 180 days before. NA, not applicable.
†The Rurality Index of Ontario is a weighted function of community population/density, travel time to nearest basic referral center, and travel time to nearest advanced referral center (https://content.oma.org//wp-content/uploads/2008rio-fulltechnicalpaper.pdf).
‡The Johns Hopkins ACG system (https://www.hopkinsacg.org) groups comorbid diagnoses into clinical groups considering illness recurrence, severity, and resource use intensity.

with consideration of typical patterns of physician visits, clinical investigations, treatment initiation, and illness duration. We divided the acute care (phase 1) into 2 parts: initial and subsequent. The remaining phases were continuing care (phase 2) and before death (phase 3). Phase 1 was estimated to last 150 days from the index date; the first 60 days were defined as initial care and the remaining 90 days as subsequent care. Phase 2 started 70 days before death. Observation time was divided into phases in order of final, initial, and subsequent care; the remaining observation time was allocated to continuing care. For example, if a

Table 2. Baseline characteristics of exposed and unexposed persons after matching for NTM-PD and NTM-PI cohorts in study of costs associated with nontuberculous mycobacteria infection, Ontario, Canada, 2001–2012*

Characteristic	Exposed persons	Unexposed persons	Standardized difference
NTM-PD			
No. persons	7,243	21,729	
Mean age, y	66.1	66.1	0
Mean propensity score	6.6	6.6	0.01
Mean CADG score	5.5	5.5	0.02
Sex			
M	49.3	49.3	0
F	50.7	50.7	0
Income quintile			
1	26.8	24.2	0.06
2	21.3	21.0	0.01
3	18.1	17.7	0.01
4	16.7	18.0	0.03
5	17.2	19.1	0.05
Rurality			
Not rural	96.2	94.6	0.08
Rural	3.8	5.4	0.08
NTM-PI			
No. persons	8,393	25,179	
Mean age, y	61.0	61.0	0
Mean propensity score	6.7	6.7	0.01
Mean CADG score	5.1	5.1	0.02
Sex			
M	51.1	51.1	0
F	48.9	48.9	0
Income quintile			
1	31.0	28.9	0.05
2	23.3	22.1	0.03
3	16.9	17.2	0.01
4	15.1	16.3	0.03
5	13.8	15.5	0.05
Rurality			
Not rural	97.2	95.8	0.07
Rural	2.9	4.2	0.07

*Data are percentages unless otherwise indicated. CADG, collapsed aggregated diagnosis groups; NTM-PD, nontuberculous mycobacteria pulmonary disease; NTM-PI, nontuberculous mycobacteria pulmonary isolation.

person was observed for 400 days, the last 70 days were assigned to the before-death phase and the first 150 days to initial (60 days) and subsequent (90 days) care, cumulatively representing phase 1; the remaining 180 days were allocated to the continuing care phase.

We calculated phase-specific attributable costs as the mean difference between matched pairs, and we used bootstrapping to calculate the 95% CI of the mean difference (22). Costs were measured as 10-day intervals throughout the observation period. We also considered attributable costs by persons' age category, sex, and healthcare spending category. We determined attributable mean 1-year costs by applying 10-day survival probabilities from the first year after diagnosis to the mean 10-day phase-specific costs, as we described.

Sensitivity Analysis

We conducted a sensitivity analysis by removing persons identified in the Ontario Cancer Registry (https://datadictionary.ices.on.ca/Applications/DataDictionary/Library.aspx?Library=OCR) and the Canadian Cystic Fibrosis Data Registry (https://datadictionary.ices.on.ca/Applications/DataDictionary/Library.aspx?Library=CFDR) as having any history of lung cancer or cystic fibrosis because of possible differences in expected complications and costs associated with these conditions. We performed cost analysis for the matched cohort without these persons and by using the same methods we described.

Results

Study Cohort

During 2001–2012, a total of 7,384 NTM-PD cases and 8,580 NTM-PI cases were identified and linked to administrative data (Table 3). The mean (± SD) age of NTM-PD patients was 66.1 (± 15.6) years and of NTM-PI patients was 61.1 (± 18.3) years. Of the NTM-PD patients, 3,732 (50.5%) were female, 316 (4.3%) lived in rural areas, and the mean collapsed aggregated diagnosis groups score was 5.5 (± 2.1). Of the NTM-PI patients, 4,158 (48.5%) were female, 285 (3.3%) lived in rural areas, and the mean collapsed aggregated diagnosis groups score was 5.1 (± 2.2).

Of the NTM-PD patients, 272 (3.7%) were admitted to a hospital within 5 days of the index date and 3,839 (52.0%) were admitted within 30 days. The mean (± SD) length of hospital stay was 11.1 (± 20.5) days for those admitted within 5 days and 10.7 (± 24.0) days for those admitted within 30 days. For these patients, the 90-day all-cause mortality rate was 6.0% (n = 444) and the 1-year rate was 13.9% (n = 1,024).

Of the NTM-PI patients, 241 (2.8%) were admitted to the hospital within 5 days and 2,294 (26.7%) within 30 days; mean (± SD) length of stay was 10.6

Table 3. Baseline characteristics of patients with confirmed nontuberculous mycobacterial pulmonary disease and pulmonary isolation of nontuberculous mycobacteria, Ontario, Canada, 2001–2012*

Characteristic	NTM-PD	NTM-PI
Infected persons	7,384 (100)	8,580 (100)
Age category at index, y		
<5	<6 (<0.1)	<6 (<0.1)
5–24	<123 (<1.7)	<296 (<3.4)
25–44	633 (8.6)	1,466 (17.1)
45–54	799 (10.8)	1,201 (14.0)
55–64	1,272 (17.2)	1,398 (16.3)
65–74	1,953 (26.5)	1,834 (21.4)
75–84	2,078 (28.1)	1,775 (20.7)
≥85	526 (7.1)	610 (7.1)
Sex		
F	3,732 (50.5)	4,158 (48.5)
M	3,652 (49.5)	4,422 (51.5)
Rural residence		
No	7,065 (95.7)	8,289 (96.7)
Yes	316 (4.3)	285 (3.3)
CADG distribution, score		
Mean ± SD	5.48 ± 2.1	5.08 ± 2.2
Median	6	5
Income quintile		
1 (lowest)	1,985 (27.0)	2,671 (31.3)
2	1,562 (21.2)	1,978 (23.2)
3	1,325 (18.0)	1,435 (16.8)
4	1,224 (16.6)	1,287 (15.1)
5 (highest)	1,260 (17.1)	1,165 (13.6)
Died	2,821 (38.2)	2,381 (27.8)

*Units are no. (%) unless otherwise indicated. CADG, collapsed aggregated diagnosis group.

(± 22.9) days for those admitted within 5 days and 14.0 (28.5) days for those admitted within 30 days. For these patients, the 90-day all-cause mortality rate was 3.4% (n = 294) and the 1-year rate was 8.6% (n = 738).

We matched 7,243 (98.1%) of NTM-PD and 8,393 (97.8%) of NTM-PI patients to unexposed persons. All standardized differences were <0.1, indicating good balance (Table 2). We matched 3,116 (98.8%) of NTM-PD and 2,616 (97.8%) of NTM-PI patients who died and found that standardized differences were <0.1 for both groups.

Cost Analysis

For NTM-PD and NTM-PI, the mean attributable costs over the first 3 phases declined to the lowest cost during the continuous care phase (CAD $236 [USD $182], 95% CI CAD $199–$272 [USD $154–$210] for NTM-PD; CAD $133 [USD $103], 95% CI CAD $111–$154 [USD $85–$119] for NTM-PI). Costs then increased to the highest costs in the before-death phase (CAD $1,352 [USD $1,044], 95% CI CAD $1,104–$1,601 [USD $852–$1,236] for NTM-PD; CAD $731 [USD $565], 95% CI $506–$958 [USD $390–$739] for NTM-PI) (Table 4). For NTM-PD and NTM-PI, hospitalizations accounted for the largest proportion of costs across all phases. In the initial infection phase, 67.9% (CAD $663 [USD $512]) of NTM-PD costs and 65.5% (CAD $415 [USD $320]) of NTM-PI costs were for hospitalization.

For NTM-PD and NTM-PI patients, mean attributable hospitalization costs were highest before death (NTM-PD CAD $1,265 [USD $976], 95% CI CAD $1,033–$1,498 [USD $797–$1,156]; NTM-PI CAD $737 [USD $569], 95% CI CAD $524–$949 [USD $404–$732]) and second highest during the initial infection phase (NTM-PD CAD $663 [USD $512], 95% CI CAD $603–$723 [USD $465–$558]; NTM-PI CAD $415 [USD $321], 95% CI CAD $382–$450 [USD $294–$347]). Physician service costs were greatest during the initial infection stage, costing an average of CAD $187 (USD $144), 95% CI CAD $177–$196 (USD $137–$151) more than uninfected persons for NTM-PD and CAD $119 (USD $92), 95% CI CAD $114–$125 (USD $88–$97) more than uninfected persons for NTM-PI.

For NTM-PD patients, costs were greatest during the before-death phase and the initial infection phase (Figure 1). The highest costs before death were found for patients in the <25 years age group (CAD $7,952 [USD $6,138], 95% CI CAD $3,840–$19,744 [USD –$2,963 to $15,238]; n= 7) and declined in each subsequent age group; the lowest costs before death were found for patients ≥85 years of age (CAD $762 [USD $588], 95% CI CAD $379–$1,145 [USD $293–$883]; n = 778). Similarly, the highest costs before death for NTM-PI patients were for those <25 years of age (CAD $16,303 [USD $12,583], 95% CI CAD $16,161–$16,446 [USD $12,473–$12,692], n<6); however, the lowest attributable costs were for those 25–44 years of age (CAD $261 [USD $202], 95% CI CAD –$2,519 to $3,041 [USD –$1,944 to $2,347]; n = 57), followed by declining costs in each of the subsequent age categories: 45–64 years (n = 351), 65–84 years (n = 1,440), and ≥85 years (n = 822) (Figure 2).

Overall, mean attributable costs were higher for male than for female NTM-PD patients in all phases except before death, when attributable costs were higher for female than male patients (Figure 3). In the before-death phase, NTM-PD female and male attributable costs were CAD $1,316 (USD $1,016), 95% CI CAD $925–$1,709 (USD $714–$1,319) for female patients and CAD $1,166 (USD $900), 95% CI CAD $826–$1,505 (USD $638–$1,162) for male patients. For NTM-PI patients during all phases, mean attributable costs were higher for male than for female patients (Figure 4). The mean attributable cumulative 1-year costs adjusted for survival were CAD $14,953 (USD $11,541) per NTM-PD patient and CAD $8,729 (USD $6,737) per NTM-PI patient.

Sensitivity Analysis

After removing from analysis persons with a history of lung cancer or cystic fibrosis, we matched 6,461 NTM-PD and 7,887 NTM-PI patients to unexposed persons. For NTM-PD, total mean attributable 10-day costs per patient were CAD $951 (USD $734), 95% CI CAD $875–$1,027 (USD $675–$792) for initial infection; CAD $428 (USD $330), 95% CI CAD $370–$485 (USD $286–$374) for subsequent care; CAD $190 (USD $146), 95% CI CAD $153–$227 (USD $118–$175) for continuous care; and CAD $1,479 (USD $1,141), 95% CI CAD $1,176–$1,780 (USD $908–$1,374) for before-death phases (Table 5). For the same phases, the total mean attributable costs for NTM-PI patients were CAD $614 (USD $474), 95% CI CAD $570–$659 (USD $440–$508); CAD $220 (USD $170), 95% CI CAD $189–$253 (USD $146–$195); CAD $108 (USD $83), 95% CI CAD $85–$130 (USD $66–$100); and CAD $850 (USD $656), 95% CI CAD $589–$1,110 (USD $455–$857). For NTM-PD patients, the attributable costs in the sensitivity analysis were significantly lower during the subsequent care and continuous care phases. For NTM-PI patients, the costs were significantly lower during the continuous care phase only.

Discussion

In this study, we found higher attributable healthcare costs to be associated with persons with NTM-PD or

NTM-PI compared with persons without NTM. The highest costs were associated with hospitalizations, particularly during the initial infection and before-death phases; overall costs were markedly lower during the subsequent care and continuous care phases. Hospital admissions within 30 days of index date were

Table 4. Ten-day mean attributable costs by phase for nontuberculous mycobacterial pulmonary disease and nontuberculous mycobacterial pulmonary isolation, Ontario, 2001–2012*

Spending category (no. patients)	Cost, CAD		
	Exposed persons	Unexposed persons	Attributable (95% CI)
Nontuberculous mycobacterial pulmonary disease			
Initial infection (6,906)			
Total	1,209	232	977 (905–1,048)
Hospitalization	724	61	663 (603–723)
Emergency department	35	6	29 (27–31)
Drugs	60	37	23 (19–26)
Physicians	232	45	187 (177–196)
Other	158	83	75 (62–88)
Subsequent care (6,906)			
Total	713	218	494 (438–549)
Hospitalization	360	55	305 (258–352)
Emergency department	12	6	6 (5–7)
Drugs	67	37	30 (26–34)
Physicians	114	41	73 (68–79)
Other	160	80	80 (65–95)
Continuous care (6,489)			
Total	530	294	236 (199–272)
Hospitalization	196	75	120 (92–149)
Emergency department	13	8	5 (4–6)
Drugs	73	43	29 (26–33)
Physicians	77	45	33 (30–36)
Other	171	123	48 (34–61)
Before-death (2,835)			
Total	5,300	3,947	1,352 (1,104–1,601)
Hospitalization	3,757	2,492	1,265 (1,032–1,497)
Emergency department	111	108	2 (−2 to 6)
Drugs	110	105	5 (−3 to 14)
Physicians	573	417	156 (130–182)
Other	749	825	−76 (−128 to −24)
Nontuberculous mycobacterial pulmonary isolation			
Initial infection (8,171)			
Total	822	189	633 (591–676)
Hospitalization	464	49	415 (381–449)
Emergency department	32	5	27 (25–29)
Drugs	48	30	18 (15–20)
Physicians	158	38	120 (114–125)
Other	121	67	54 (42–67)
Subsequent care (8,171)			
Total	436	183	253 (222–284)
Hospitalization	178	45	133 (109–156)
Emergency department	11	5	6 (5–7)
Drugs	51	30	21 (17–24)
Physicians	80	37	43 (40–47)
Other	117	67	50 (39–62)
Continuous care (7,860)			
Total	387	253	133 (111–154)
Hospitalization	122	64	57 (42–72)
Emergency department	11	7	4 (3–5)
Drugs	57	36	22 (19–25)
Physicians	60	40	20 (18–22)
Other	136	106	29 (19–40)
Before death (2,374)			
Total	4,532	3,800	731 (506–958)
Hospitalization	3,088	2,351	736 (524–949)
Emergency department	124	108	17 (12–22)
Drugs	108	101	7 (−1 to 15)
Physicians	474	412	62 (40–83)
Other	738	827	−90 (−146 to −34)

*Costs presented in 2018 Canadian dollars (CAD). In 2018, $1 CAD = $0.77 US dollars.

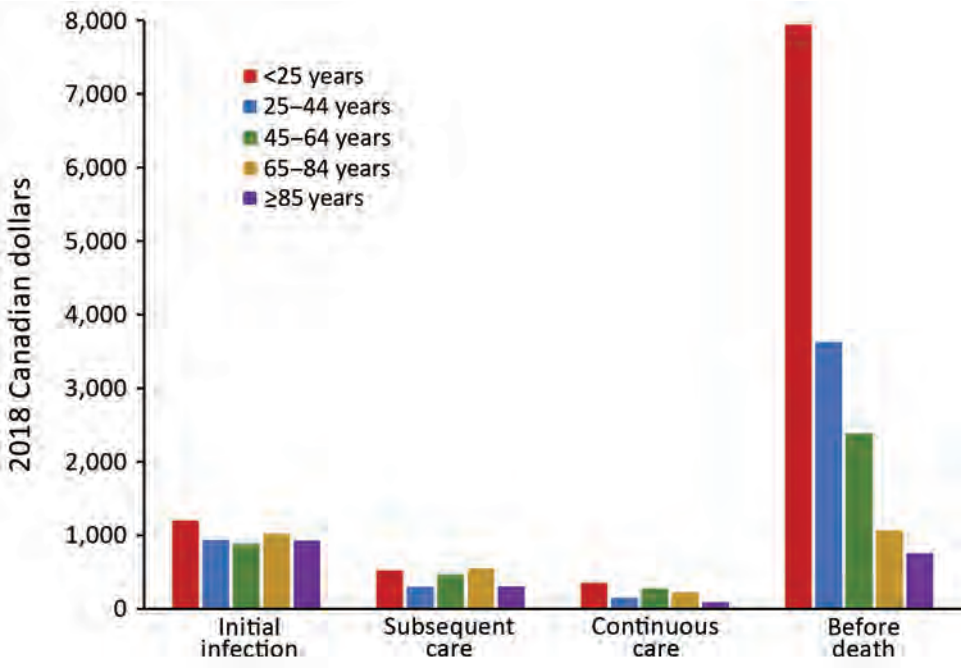

Figure 1. Ten-day mean attributable costs for nontuberculous mycobacterial pulmonary disease patients by phase, stratified by age, Ontario, Canada, 2001–2012. Number of patients per category: initial infection, 6,906; subsequent care, 6,906; continuous care, 6,489; before death, 2,835.

more common among NTM-PD (52%) than NTM-PI (27%) patients. Incident cases in Ontario during our observation period were an average of 225 cases of NTM-PD and 191 cases of NTM-PI. On the basis of the cumulative 1-year costs, this finding would translate into an estimated total annual healthcare cost of CAD $3,369,765 (USD $2,600,730) for NTM-PD and CAD $1,667,863 (USD $1,287,229) for NTM-PI.

For all phases, 10-day mean attributable costs were higher for patients with NTM-PD than for those with NTM-PI. However, healthcare costs were significantly higher for patients with NTM-PI than for persons without NTM infection. Although 1 positive sputum sample may be clinically insignificant for some persons, for others it might represent the single isolation of a chronically present organism. It is therefore possible that some persons with NTM-PI had true disease, which may explain the higher healthcare costs. Alternatively, the higher healthcare costs may relate to a non-NTM lung condition that prompted

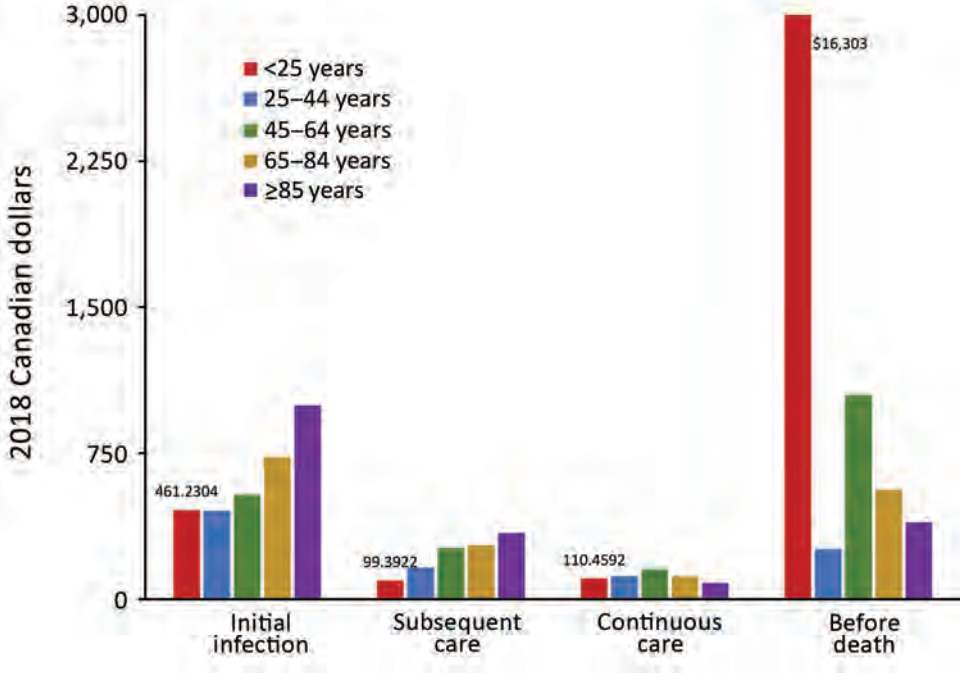

Figure 2. Ten-day mean attributable costs for nontuberculous mycobacterial pulmonary isolation patients by phase, stratified by age, Ontario, Canada, 2001–2012. Number of patients per category: initial infection, 8,171; subsequent care, 8,171; continuous care, 7,860; before death, 2,374.

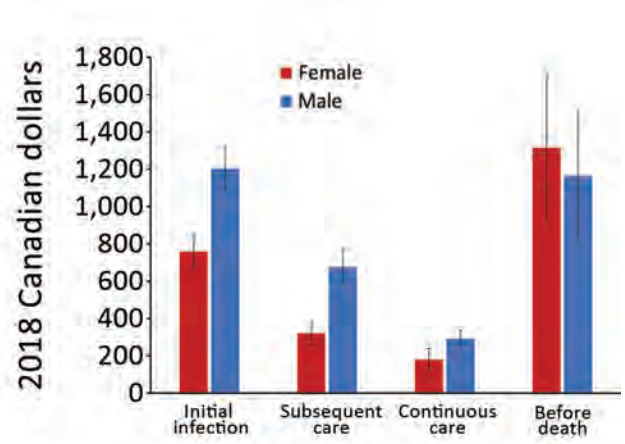

Figure 3. Ten-day mean attributable costs for nontuberculous mycobacterial pulmonary disease patients by phase, stratified by sex, Ontario, Canada, 2001–2012. Number of patients per category: initial infection, 6,906; subsequent care, 6,906; continuous care, 6,489; before death, 2,835. Error bars indicate 95% CIs.

specimen collection for culture, whereby the positive NTM culture was a nonsignificant bystander. Unfortunately, we do not have data on negative cultures to explore this further.

Overall, mean attributable costs for some phases were somewhat lower in the sensitivity analysis after we removed from analysis persons with a history of lung cancer or cystic fibrosis, which may result from expected increased costs for patients with related conditions. The lack of larger differences in attributable costs between these analyses may be explained by effective matching that used comorbidity scores that may have already accounted for these conditions in the cohort used for the primary analysis.

This study has limitations. Secondary use of health administrative data are prone to errors that could result in misclassification bias. Regarding the diagnosis of NTM-PD, we assumed that all patients who fulfilled the microbiological criteria of the ATS/IDSA guidelines truly had cases of NTM-PD. This assumption is highly accurate (positive predictive value 70%–100%), but some patients are invariably incorrectly classified as having NTM-PD (*23*–*26*). However, the finding that attributable healthcare costs for patients with NTM-PI were comparably high supports the finding of high costs associated with pulmonary NTM infection. In addition, the retrospective use of administrative data is limited by the variables that are available. Because this research was conducted from the healthcare payer perspective, the results capture only direct healthcare costs of NTM-PD and NTM-PI, not societal or indirect costs, which includes not capturing all medication costs associated with NTM because these costs are captured only for those with publicly funded medication coverage (i.e., adults ≥65 years of age and those receiving social assistance).

This study was strengthened by using both hard-matching and propensity score matching to reduce bias between unexposed and exposed persons. By matching on major covariates, we reduced the potential confounding by these covariates, allowing for a more robust estimate of NTM-PD and NTM-PI attributable costs. This study was further strengthened by using Ontario health administrative data, which contain extensive data on Ontario population healthcare use. Ontario is the most populous province in Canada (≈40% of the population) and is fairly representative of the population of Canada (*27*). In addition, the Public Health Ontario laboratory processes ≈95% of NTM isolates for the province (*28*), providing almost complete capture of microbiologically defined incident NTM-PD and NTM-PI cases in Ontario.

Previous studies have estimated the economic costs of NTM-PD in Canada and elsewhere. One group focused on the direct costs of NTM without assessing total healthcare costs. A retrospective study of 91 patients with NTM-PD treated at a clinic in Ontario reported that CAD $500/month was associated with NTM treatment, including costs of medications and their administration, physicians' fees, and diagnostic tests (*11*). That study, however, was unable to study all healthcare costs and was limited to 1 clinic, introducing substantial bias. One study in the United States estimated the cost of antibiotic treatment (but excluded costs of administration) for NTM-PD patients during 2004–2005 and found that among 27 eligible patients, the median monthly treatment cost was

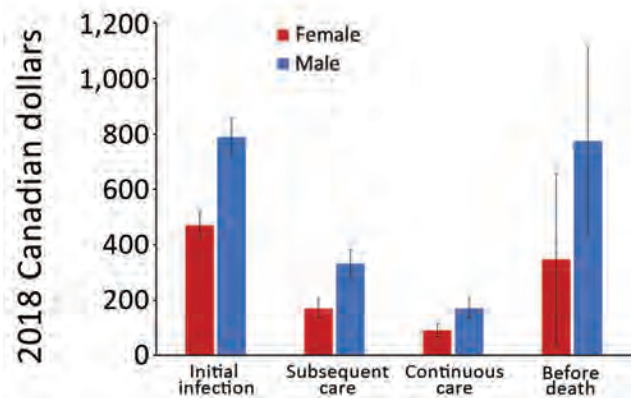

Figure 4. Ten-day mean attributable costs for nontuberculous mycobacterial pulmonary isolation patients by phase, stratified by sex, Ontario, Canada, 2001–2012. Number of patients per category: initial infection, 8,171; subsequent care, 8,171; continuous care, 7,860; before death, 2,374. Error bars indicate 95% CIs.

Table 5. Sensitivity analysis 10-day mean attributable costs by phase for nontuberculous mycobacterial pulmonary disease and nontuberculous mycobacterial pulmonary isolation, Ontario, Canada, 2001–2012*

Phase (no. patients)	Cost, CAD		
	Exposed persons	Unexposed persons	Attributable (95% CI)
Nontuberculous mycobacterial pulmonary disease			
Mean cost by phase			
Initial infection (6,187)	1,189	238	951 (875–1,027)
Subsequent care (6,187)	653	227	428 (370–485)
Continuous care (5,907)	493	304	190 (153–227)
Before death (2,204)	5,662	4,183	1,479 (1,176–1,781)
Nontuberculous mycobacterial pulmonary isolation			
Mean cost by phase			
Initial infection (7,693)	807	193	614 (570–659)
Subsequent care (7,693)	412	192	220 (189–253)
Continuous care (7,471)	370	261	108 (85–130)
Before death (1,963)	4,692	3,843	850 (589–1,110)

*Analysis excluded persons with a history of lung cancer or cystic fibrosis. CAD, 2018 Canadian dollars. In 2018, $1 CAD in 2018 = $0.77 US dollars.

USD $481 (*29*). Comparing the results of this study to the results from our analysis is difficult because not all medication costs are captured in Ontario's health administrative data and because of differences in costs associated with healthcare systems in Canada and the United States. Another study conducted in the United States, which sought to estimate the direct costs of investigating and managing NTM-PD, used Medicare beneficiary data and costs from the literature to determine that medication costs made up most of NTM direct healthcare costs (*30*). Another study of direct NTM costs focused on patients with refractory MAC-PD. That study used a physician survey method and found that in Canada, average annual direct medical costs were CAD $16,200 and also presented data for Germany, France, and the United Kingdom (costs 9,700–17,900 Euros) (*31*). Although clear that the costs associated with refractory MAC-PD were high, the biased population (refractory disease) makes comparison with our study results difficult. Furthermore, the above-mentioned studies ignored total healthcare costs, which are undoubtedly influenced by the effects of NTM-PD on other diseases.

A second group of studies included all healthcare costs associated with NTM-PD. In a study performed in a managed care population in the United States, total healthcare costs for NTM-PD patients exceeded those for controls by USD $44,070 in the first year after diagnosis and $19,124 in the second (index date) (*32*). Limitations of that study included the lack of phase-of-illness modeling and the use of hard-matching by age and sex and statistical adjustment for underlying conditions. The results of propensity score matched analyses led to attenuation of the differences, which were still substantial. The comparison between the sampling of a US population enrolled in certain managed care programs and a population-based Ontario sample is difficult, but both studies identified a substantial increase in cost among patients with pulmonary NTM. A study in Germany investigated total healthcare costs among patients with incident NTM-PD compared with controls matched by age, sex, and Charlson Comorbidity Index category, identifying patients from a large and likely representative national-level database (*33*). Studied costs were incurred within the 3 years after NTM diagnosis; mean total healthcare expenditures for NTM-PD patients were ≈4 times those of controls (39,599 vs. 10,006 Euros) (*33*). The comparison was limited by probable inadequate matching, in that Charlson Comorbidity Index category probably provides relatively coarse discrimination among patients with varying levels of illness severity.

The qualitative results of our study may be transferable to jurisdictions with similar healthcare systems (i.e., publicly funded) and with similar population health profiles, but the magnitude of cost associated with NTM undoubtedly varies according to system-specific costs. NTM-PD and NTM-PI are responsible for substantial economic burden in Ontario. These results can be used in future economic evaluations to inform policy making on prevention, screening, and treatment options.

This study was funded by Public Health Ontario through the Project Initiation Fund. This study was supported by ICES, which is funded by an annual grant from the Ontario Ministry of Health and Long-Term Care (MOHLTC). Parts of this material are based on data and information compiled and provided by: the MOHLTC, Canadian Institute for Health Information (CIHI), Cystic Fibrosis Canada, and by Cancer Care Ontario (CCO). The analyses, conclusions, opinions and statements expressed herein are solely those of the authors and do not reflect those of the funding or data sources; no endorsement is intended or should be inferred.

J.C.K. was supported by a Clinician Scientist Award from the University of Toronto Department of Family and Community Medicine. T.K.M. received grants and personal fees from Insmed, personal fees from Horizon, personal fees from RedHill, and personal fees from Astra-Zeneca, personal fees from Novartis, outside the submitted work. S.K.B. received funds paid to her institution from Insmed for a clinical trial relating to NTM disease and Boehringer Ingelheim for continuing medical education relating to NTM disease. All other authors have no conflicts to report.

About the Author

Ms. Ramsay is a PhD student at the University of Toronto and a Research Associate at the University Health Network in Toronto. Her primary research interests are population-based costing studies and public health.

References

1. Brode SK, Daley CL, Marras TK. The epidemiologic relationship between tuberculosis and non-tuberculous mycobacterial disease: a systematic review. Int J Tuberc Lung Dis. 2014;18:1370–7. https://doi.org/10.5588/ijtld.14.0120
2. Marras TK, Mendelson D, Marchand-Austin A, May K, Jamieson FB. Pulmonary nontuberculous mycobacterial disease, Ontario, Canada, 1998–2010. Emerg Infect Dis. 2013;19:1889–91. https://doi.org/10.3201/eid1911.130737
3. Henkle E, Hedberg K, Schafer S, Novosad S, Winthrop KL. Population-based incidence of pulmonary nontuberculous mycobacterial disease in Oregon 2007 to 2012. Ann Am Thorac Soc. 2015;12:642–7. https://doi.org/10.1513/AnnalsATS.201412-559OC
4. Brode SK, Marchand-Austin A, Jamieson FB, Marras TK. Pulmonary versus nonpulmonary nontuberculous mycobacteria, Ontario, Canada. Emerg Infect Dis. 2017;23:1898–901. https://doi.org/10.3201/eid2311.170959
5. Griffith DE, Aksamit T, Brown-Elliott BA, Catanzaro A, Daley C, Gordin F, et al.; ATS Mycobacterial Diseases Subcommittee; American Thoracic Society; Infectious Diseases Society of America. An official ATS/IDSA statement: diagnosis, treatment, and prevention of nontuberculous mycobacterial diseases. Am J Respir Crit Care Med. 2007;175:367–416. https://doi.org/10.1164/rccm.200604-571ST
6. Adjemian J, Olivier KN, Seitz AE, Holland SM, Prevots DR. Prevalence of nontuberculous mycobacterial lung disease in U.S. Medicare beneficiaries. Am J Respir Crit Care Med. 2012;185:881–6. https://doi.org/10.1164/rccm.201111-2016OC
7. Griffith DE, Fordham von Reyn C, Bloom A. Overview of nontuberculous mycobacterial infections in HIV-negative patients. UpToDate [cited 2020 Jan 2]. https://www-uptodate-com.myaccess.library.utoronto.ca/contents/overview-of-nontuberculous-mycobacterial-infections-in-hiv-negative-patients?search=nontuberculous%20mycobacterial%20infections&source=search_result&selectedTitle=1~150&usage_type=default&display_rank=1
8. Kwak N, Park J, Kim E, Lee C-H, Han SK, Yim J-J. Treatment outcomes of *Mycobacterium avium* complex lung disease: a systematic review and meta-analysis. Clin Infect Dis. 2017;65:1077–84. https://doi.org/10.1093/cid/cix517
9. Koh W-J, Moon SM, Kim S-Y, Woo M-A, Kim S, Jhun BW, et al. Outcomes of *Mycobacterium avium* complex lung disease based on clinical phenotype. Eur Respir J. 2017;50:1602503. https://doi.org/10.1183/13993003.02503-2016
10. Wallace RJ Jr, Brown-Elliott BA, McNulty S, Philley JV, Killingley J, Wilson RW, et al. Macrolide/azalide therapy for nodular/bronchiectatic *Mycobacterium avium* complex lung disease. Chest. 2014;146:276–82. https://doi.org/10.1378/chest.13-2538
11. Leber A, Marras TK. The cost of medical management of pulmonary nontuberculous mycobacterial disease in Ontario, Canada. Eur Respir J. 2011;37:1158–65. https://doi.org/10.1183/09031936.00055010
12. Institute for Clinical Evaluative Sciences. ICES data [cited 2018 Nov 12]. https://www.ices.on.ca/Data-and-Privacy/ICES-data
13. Cadarette SM, Wong L. An introduction to health care administrative data. Can J Hosp Pharm. 2015 May-Jun;68:232–7. https://doi.org/10.4212/cjhp.v68i3.1457
14. Wodchis WP, Bushmeneva K, Nikitovic M, Mckillop I. Guidelines on person-level costing using administrative databases in Ontario [cited 2018 Nov 12]. https://tspace.library.utoronto.ca/bitstream/1807/87373/1/Wodchis%20et%20al_2013_Guidelines%20on%20Person-Level%20Costing.pdf
15. Institute for Clinical Evaluative Sciences. ICES data dictionary [cited 2020 Jan 2]. https://datadictionary.ices.on.ca/Applications/DataDictionary/Default.aspx
16. Kralj B. Measuring "rurality" for purposes of health-care planning: an empirical measure for Ontario. Ont Med Rev. 2000;67:33–52.
17. The Johns Hopkins ACG® System [cited 2018 Jul 2]. https://www.hopkinsacg.org
18. Austin PC. Optimal caliper widths for propensity-score matching when estimating differences in means and differences in proportions in observational studies. Pharm Stat. 2011;10:150–61. https://doi.org/10.1002/pst.433
19. Statistics Canada. Consumer price index, annual average, not seasonally adjusted [cited 2020 Jan 2]. https://www150.statcan.gc.ca/t1/tbl1/en/tv.action?pid=1810000501
20. Bank of Canada. Annual exchange rates [cited 2020 Jan 2]. https://www.bankofcanada.ca/rates/exchange/annual-average-exchange-rates
21. Kim HJ, Fay MP, Feuer EJ, Midthune DN. Permutation tests for joinpoint regression with applications to cancer rates. Stat Med. 2000;19:335–51. https://doi.org/10.1002/(SICI)1097-0258(20000215)19:3<335::AID-SIM336>3.0.CO;2-Z
22. Austin PC, Small DS. The use of bootstrapping when using propensity-score matching without replacement: a simulation study. Stat Med. 2014;33:4306–19. https://doi.org/10.1002/sim.6276
23. Andréjak C, Thomsen VØ, Johansen IS, Riis A, Benfield TL, Duhaut P, et al. Nontuberculous pulmonary mycobacteriosis in Denmark: incidence and prognostic factors. Am J Respir Crit Care Med. 2010;181:514–21. https://doi.org/10.1164/rccm.200905-0778OC
24. Prevots DR, Shaw PA, Strickland D, Jackson LA, Raebel MA, Blosky MA, et al. Nontuberculous mycobacterial lung disease prevalence at four integrated health care delivery systems. Am J Respir Crit Care Med. 2010;182:970–6. https://doi.org/10.1164/rccm.201002-0310OC
25. Winthrop KL, Baxter R, Liu L, McFarland B, Austin D, Varley C, et al. The reliability of diagnostic coding and laboratory data to identify tuberculosis and nontuberculous mycobacterial disease among rheumatoid arthritis patients using anti-tumor necrosis factor therapy.

Pharmacoepidemiol Drug Saf. 2011;20:229–35. https://doi.org/10.1002/pds.2049
26. Marras TK, Mehta M, Chedore P, May K, Al Houqani M, Jamieson F. Nontuberculous mycobacterial lung infections in Ontario, Canada: clinical and microbiological characteristics. Lung. 2010;188:289–99. https://doi.org/10.1007/s00408-010-9241-8
27. Statistics Canada. Census profile, 2016 census [cited 2020 Jan 7]. https://www12.statcan.gc.ca/census-recensement/2016/dp-pd/prof/details/Page.cfm?Lang=E&Geo1=PR&Code1=35&Geo2=&Code2=&Data=Count&SearchText=Ontario&Sear
28. Al Houqani M, Jamieson F, Chedore P, Mehta M, May K, Marras TK. Isolation prevalence of pulmonary nontuberculous mycobacteria in Ontario in 2007. CAD Respir J. 2011;18:19–24. https://doi.org/10.1155/2011/ 865831
29. Ballarino GJ, Olivier KN, Claypool RJ, Holland SM, Prevots DR. Pulmonary nontuberculous mycobacterial infections: antibiotic treatment and associated costs. Respir Med. 2009;103:1448–55. https://doi.org/10.1016/j.rmed.2009.04.026
30. Strollo SE, Adjemian J, Adjemian MK, Prevots DR. The burden of pulmonary nontuberculous mycobacterial disease in the United States. Ann Am Thorac Soc. 2015;12:1458–64. https://doi.org/10.1513/AnnalsATS.201503-173OC
31. Goring SM, Wilson JB, Risebrough NR, Gallagher J, Carroll S, Heap KJ, et al. The cost of *Mycobacterium avium* complex lung disease in Canada, France, Germany, and the United Kingdom: a nationally representative observational study. BMC Health Serv Res. 2018;18:700. https://doi.org/10.1186/s12913-018-3489-8
32. Marras TK, Mirsaeidi M, Chou E, Eagle G, Zhang R, Leuchars M, et al. Health care utilization and expenditures following diagnosis of nontuberculous mycobacterial lung disease in the United States. J Manag Care Spec Pharm. 2018;24:964–74. https://doi.org/10.18553/jmcp.2018.18122
33. Diel R, Jacob J, Lampenius N, Loebinger M, Nienhaus A, Rabe KF, et al. Burden of non-tuberculous mycobacterial pulmonary disease in Germany. Eur Respir J. 2017;49:1602109. https://doi.org/10.1183/13993003.02109-2016

Address for correspondence: Lauren Ramsay, University Health Network, Toronto General Hospital, Eaton Building, 10th Fl, Rm 248, 200 Elizabeth St, Toronto, ON M5G 2C4, Canada; email: lauren.ramsay@theta.utoronto.ca

No Change in Risk for Antibiotic-Resistant Salmonellosis from Beef, United States, 2002–2010

Solenne Costard,[1] Jane G. Pouzou,[1] Keith E. Belk, Paul S. Morley, John W. Schmidt, Tommy L. Wheeler, Terrance M. Arthur, Francisco J. Zagmutt[1]

Restricting antibiotic use in food production animals is a target for reducing antimicrobial drug–resistant infections in humans. We used US surveillance data to estimate the probability of antibiotic-resistant nontyphoidal salmonellosis per meal made with beef during 2002–2010. Applying data for nontyphoidal *Salmonella* in raised-without-antibiotics cattle, we tested the effect of removing antibiotic use from all beef cattle production. We found an average of 1.2 (95% credible interval 0.6–4.2) antibiotic-resistant nontyphoidal salmonellosis cases per 1 million beef meals made with beef initially contaminated with antibiotic-resistant nontyphoidal *Salmonella* at slaughter or retail and 0.031 (95% credible interval 0.00018–0.14) cases per 1 million meals irrespective of beef contamination status. Neither outcome showed sustained change except for increases in 2003 and 2009 (>98% confidence) when larger or more outbreaks occurred. Switching all beef production to a raised-without-antibiotics system may not have a significant effect on antibiotic-resistant nontyphoidal salmonellosis (94.3% confidence).

Increased antimicrobial resistance (AMR), or antibiotic resistance, has resulted in initiatives to reduce the use of antibiotics in food production animals (*1*,*2*), but quantification of the public health effects of decreasing antibiotic use in livestock remains limited (*3*,*4*). Reduction of antibiotic use in livestock can lower resistance prevalence (i.e., proportion of pathogens with resistance) in animals (*4*), but some studies show that pathogen prevalence may be higher in livestock raised without antibiotics (*5*). Because transmission of foodborne pathogens is proportional to the prevalence of pathogens in the food source (*6*), quantifying the change in human antibiotic-resistant foodborne illnesses resulting from reduced antibiotic use in livestock is vital.

In the United States, the most common bacterial cause of foodborne illness is nontyphoidal *Salmonella* (NTS), which leads to >1 million foodborne illnesses and 20,000 hospitalizations per year (*7*). Antibiotic-resistant NTS is among the top 18 AMR threats in the United States (*8*), causing 100,000 infections annually. The Centers for Disease Control and Prevention National Antimicrobial Resistance Monitoring System (NARMS) tracks resistance to 25 antibiotics in patient samples positive for isolates such as NTS (*9*), including the clinically relevant antibiotics ciprofloxacin and ceftriaxone.

Multiple assessments of human AMR risk from meats have been performed (*10*–*14*). However, most focused on only 1 class of antibiotic (*10*,*11*), had limited or no longitudinal data (*14*), or were not based on nationwide surveillance at the animal source (*11*). Quantitative assessments of AMR risk with a more comprehensive resistance definition (*15*), such as resistance to any class, or to ≥3 classes, that use representative, longitudinal data, are critical to defining the risks and benefits from policy with regard to antibiotic use in livestock (*3*). Surveillance studies of antibiotic use and AMR in humans and livestock can be used to generate estimates of risk based on empirical data and can show the results of long-term conditions or systematic changes over time.

Our objective with this study was to use beef as a model to quantify trends in the longitudinal relationship between human NTS infections and antibiotic-resistant NTS in meats. We also used the estimates to predict change in antibiotic-resistant salmonellosis resulting from hypothetical scenarios of antibiotic restriction in beef cattle.

Methods

We developed a stochastic model to quantify the risk for antibiotic-resistant nontyphoidal salmonellosis

Author Affiliations: EpiX Analytics, Fort Collins, Colorado, USA (S. Costard, J.G. Pouzou, F.J. Zagmutt); Colorado State University, Fort Collins (K.E. Belk); Texas A&M University, Canyon, Texas, USA (P.S. Morley); US Department of Agriculture, Clay Center, Nebraska, USA (J.W. Schmidt, T.L. Wheeler, T.M. Arthur)

DOI: https://doi.org/10.3201/eid2609.190922

[1]These authors contributed equally to this article.

per meal made with beef during 2002–2010. Our model follows the method of previously published AMR risk assessments (*6*,*16*) but uniquely addresses temporal changes and relies solely on nationwide surveillance data (Appendix Table 1, https://wwwnc.cdc.gov/EID/article/26/9/19-0922-App1.pdf).We used this model for 3 objectives: 1) estimate the risk for antibiotic-resistant nontyphoidal salmonellosis per meal made with beef, using the yearly cases of illnesses (Ill_{res}) and the number of meals made with beef that year ($Meal_{res}$) (Figure 1); 2) evaluate change over time in all model outcomes; and 3) assess the effect that potential future restrictions on antibiotic use in beef cattle would have on antibiotic-resistant nontyphoidal salmonellosis disease burden (Appendix).

Risk for Antibiotic-Resistant Nontyphoidal Salmonellosis Attributable to Beef

Annual Incidence of Beef-Attributable Antibiotic-Resistant Nontyphoidal Salmonellosis (Ill_{res} Incidence) per 100,000 Persons

We obtained the annual total nontyphoidal salmonellosis cases in the United States for 1998–2015 from FoodNet (https://www.cdc.gov/foodnet), an active foodborne disease surveillance system, after adjusting for the proportion of the US population included in FoodNet surveillance sites. To correct for underdiagnosis and restrict case estimates to domestically acquired foodborne cases, we also included adjustment factors constant for the study period. By using annual food attribution estimates derived from the National Outbreak Reporting System (NORS; https://www.cdc.gov/nors/index.html), cases of nontyphoidal salmonellosis were further restricted to foodborne cases attributed to ground beef and intact beef. To ensure that the resistance fraction is specific to nontyphoidal salmonellosis attributed to consumption of beef, we estimated the fraction of beef-attributed nontyphoidal salmonellosis cases with AMR by matching cases in the Centers for Disease Control and Prevention data collected from clinical patient samples as part of NARMS (*17*) with beef-attributable outbreak data from NORS by using sample metadata, (Appendix Table 1). We calculated incidence of Ill_{res} by using the population of the United States in the relevant year.

Annual Meals Prepared with Beef Initially Contaminated with Antibiotic-Resistant NTS ($Meals_{res}$)

We calculated the number of beef meals consumed annually in the United States by using beef disappearance data from the US Department of Agriculture (USDA) (*18*) and the mean grams of beef consumed per beef meal from the National Health and Nutrition Examination Survey (*19*). We estimated the prevalence of NTS in beef by using USDA Food Safety and Inspection Service surveillance data, and we derived the fraction of isolates with AMR from USDA NARMS and US Food and Drug Administration NARMS data (*9*). $Meals_{res}$ were stratified by beef cut (ground beef data for 2002–2015 vs. intact beef for 1998–2010). By using $Meals_{res}$, we assumed that the beef used to prepare a meal was initially contaminated (as measured at the slaughter plant or retail) with the pathogen. This assumption does not necessarily mean that the actual meal consumed was contaminated because safe cooking and handling practices would reduce or completely inactivate the bacterial load.

Risk for Antibiotic-Resistant Nontyphoidal Salmonellosis per Beef Meal

Dividing Ill_{res} by $Meals_{res}$ resulted in the probability of antibiotic-resistant nontyphoidal salmonellosis per meal made with beef initially contaminated with antibiotic-resistant NTS (P_{ill}). Also, by using all meals in the denominator, we calculated the probability of antibiotic-resistant nontyphoidal salmonellosis per meal made with beef, regardless of contamination status (P_{meal}) (Figure 1). We report both risk outcomes per 1 million meals, on a per-year basis (P_{ill} and P_{meal}) and as the mean of each for all years combined ($P_{ill,overall}$ and $P_{meal,overall}$). We repeated the analyses for NTS with multidrug resistance (NTS_{MDR}) (i.e., resistance to ≥3 antimicrobial classes) and for clinically relevant resistance (NTS_{CRR}), also known as resistance of concern (i.e., resistance to ≥5 drugs or quinolones [ciprofloxacin] or third-generation cephalosporins [ceftriaxone]) (*8*).

Testing for Temporal Changes

To identify the confidence of a consistent increase (or decrease) in each outcome over the study period, we used Mann-Kendall trend test bootstrapping (*20*). In addition, we used numerical integration to compute the confidence in pairwise year-to-year Bayesian posterior differences (*21*) and the difference between the mean of each outcome in the last years of the study period versus the remaining previous years. Unlike the Mann-Kendall tests, the year-to-year test identified short-term changes, and the comparison of the first versus the last 5 years of the study period provided an assessment of nonlinear changes during the study period.

Scenario Analysis: Effects of Hypothetical Antibiotic Restriction in Beef Production

Relationship between Antibiotic Use and Antibiotic-Resistant NTS in Beef

To model the relationship between antibiotic use and antibiotic-resistant NTS, we used nationwide data (C.P. Fossler, USDA, pers. comm., 2018 Jul 16) from the National Animal Health Monitoring System feedlot survey (*22*). The feedlot survey is based on a nationwide representative sample of farms and thus captures the effect of long-term and current antibiotic practices on AMR. In the survey, individual fecal pats from raised-without-antibiotics cattle and conventionally raised cattle were collected to estimate the prevalence of NTS isolates and the fraction of these with AMR. These 2 parameters were combined to measure the overall prevalence of antibiotic-resistant NTS in raised-without-antibiotics cattle and conventionally raised cattle and to derive the relative risk (RR) of antibiotic-resistant NTS prevalence in raised-without-antibiotics versus conventionally raised cattle.

Prediction of Changes in Beef-Attributable Antibiotic-Resistant Nontyphoidal Salmonellosis

We constructed 2 scenarios to evaluate Ill_{res} changes from hypothetical antibiotic restriction in beef production. We assumed no changes in slaughtering, processing, consumer habits, and food preparation.

For scenario 1, we estimated the change in antibiotic-resistant nontyphoidal salmonellosis if all beef production were switched to raised-without-antibiotics by using the annual estimated Ill_{res} for 2002–2010 and the RR of antibiotic-resistant NTS prevalence in raised-without-antibiotics versus conventionally raised cattle. By doing so, we assumed that the animal-level prevalence of antibiotic-resistant NTS is proportional (but not equal to) its prevalence in meals prepared with beef and that RR has a direct linear effect on the change in Ill_{res}. This relationship is documented for food pathogens (*6*,*23*), including NTS (*24*), so here we assumed that it extends to antibiotic-resistant isolates.

To relax this assumption, for scenario 2, we empirically estimated the relationship between antibiotic-resistant NTS prevalence in beef and Ill_{res} via Poisson

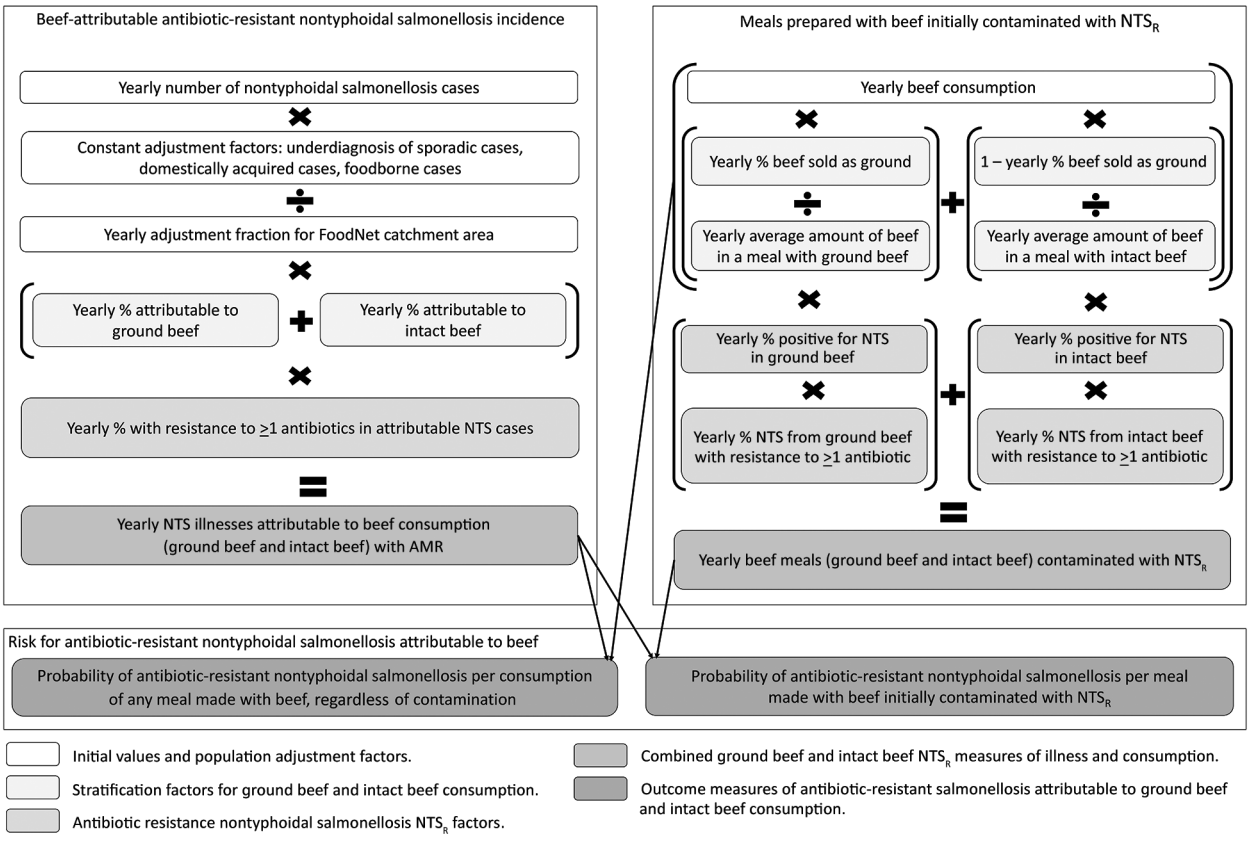

Figure 1. Conceptual model and data sources for calculation of risk for beef-attributable antibiotic-resistant nontyphoidal salmonellosis per 1 million beef meals (P_{ill}) for study of risk for antimicrobial-resistant salmonellosis from beef, United States, 2002–2010. NTS, nontyphoidal *Salmonella*; NTS$_R$, antibiotic-resistant NTS.

regression and used the Poisson regression to create an adjustment factor to the calculations done for scenario 1. For each scenario, we reported the posterior confidence in the change in Ill_{res} being <0 (i.e., reduction of antibiotic-resistant nontyphoidal salmonellosis) for each year of the study and for all years combined.

Model Implementation

We used R version 3.4.1 (https://www.R-project.org) to perform all analyses. We used Monte Carlo simulation to calculate the posterior uncertainty in all outcomes. Statistical significance was assessed at the 95% confidence level. We performed a sensitivity analysis of the key drivers of P_{ill} and $P_{ill,overall}$ by calculating the effect that extreme values of each input had on the output means (Appendix).

Results

Descriptive Statistics of Main Parameters and Risk Measures

During 2002–2010, approximately 554 billion beef meals were consumed, 59% as ground beef. Of these meals, 4% came from beef at slaughter or retail with NTS, half of which were antibiotic-resistant (11.23 billion, 95% CrI 9.08–13.54 billion). Approximately 93% of meals with beef initially contaminated with antibiotic-resistant NTS were made with ground beef (10.4 billion meals, 95% CrI 8.3–12.73 billion) (Figure 2), resulting from higher prevalence of both NTS and antibiotic-resistant NTS in ground than intact beef (Table 1). Yet, the attribution of nontyphoidal salmonellosis, regardless of antibiotic resistance, was relatively even between ground and intact beef (Figure 2). The total incidence of Ill_{res} was 0.64 (0.0036–2.75)/100,000 persons.

During 2002–2010, the mean risk for antibiotic-resistant nontyphoidal salmonellosis was 0.031 cases (95% CrI 0.00018–0.14)/1 million beef meals; intact and ground beef contributed equally to the rate (Table 1; Figure 2). The risk per million beef meals initially contaminated with NTS was 1.8 (95% CrI 0.007–8.5) overall, 1.16 (95% CrI 0.0015–5.2) for ground beef and 9.5 (95% CrI 0.03–50) for intact beef (Figure 2). The higher $P_{ill,overall}$ for intact beef possibly indicates a higher risk from consumption of intact beef carrying antibiotic-resistant NTS.

Tests for Temporal Changes in Main Parameters and Risk Measures

None of the tested parameters or outcomes based on a resistance definition of ≥1 antibiotic (i.e., $Meals_{res}$ or Ill_{res} per 100,000 population [Figure 2], or P_{ill} or P_{meal} [Figure 3]) showed a sustained change (Table 2). We also observed no change when we used multidrug resistance (MDR) and clinically relevant resistance (CRR) as the definition of resistance (Table 2; Appendix Figures 5–8), except that meals made with ground beef contaminated with NTS_{CRR} declined during 2002–2015. More differences based on the last 5 years of the study period were found. The risk for NTS_{MDR} per 1 million meals made with ground beef initially contaminated with NTS_{MDR} increased during 2010–2015, while the number of these meals made with NTS_{MDR}-contaminated ground

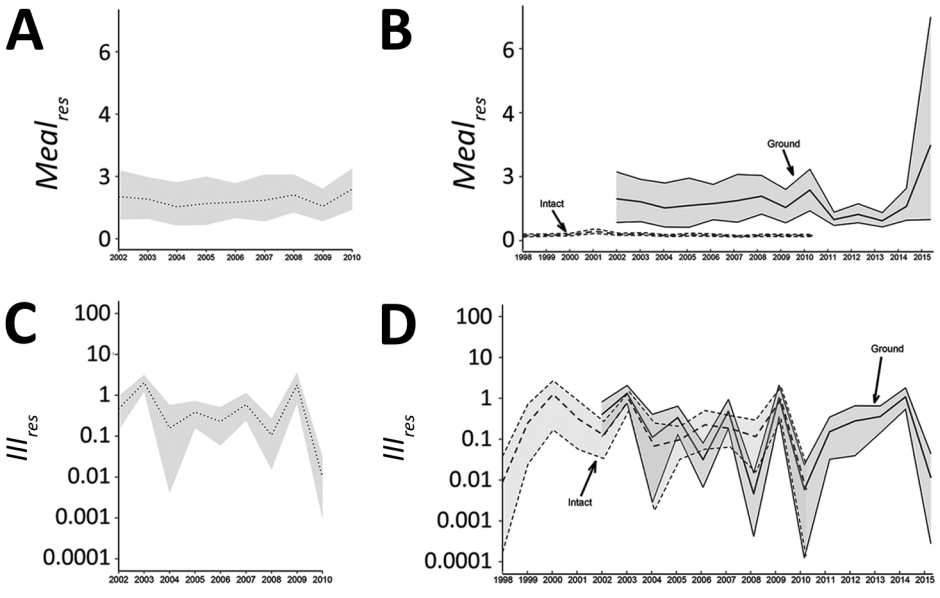

Figure 2. Estimates of the number of annual beef meals (in millions) prepared with beef initially contaminated with NTS resistant to >1 antibiotic ($Meal_{res}$) and of the incidence of salmonellosis with resistance to >1 antibiotic and attributable to beef (Ill_{res}) per 100,000 persons, United States, 2002–2010. A) $Meal_{res}$ for total beef, 2002–2010. B) $Meal_{res}$ stratified as ground (2002–2014) or intact (1998–2010) cuts. C) Ill_{res}, 2002–2010. D) Ill_{res} attributable to beef stratified as ground (2002–2014) or intact (1998–2010) cuts. Center lines represent means; gray shading represents 95% credible intervals; for panels B and D, light gray shading represents intact beef and dark gray shading indicates ground beef.

Table 1. Calculations of beef consumption, NTS, and risk for antimicrobial-resistant salmonellosis from beef, United States*

Input	Mean (95% CrI)	
	2002–2010†	Any years with data
Meals prepared with beef		
Total	554B (527B–581B)	554B (527B–581B)
Ground	326B (306B–345B)	497B (473B–521B)
Intact	228B (219B–238B)	329B (319B–339B)
Meals prepared with beef carrying NTS		
Total	24.9B (22.5B–27.0B)	24.9B (22.5B–27.0B)
Ground	22.5B (20.3B–24.9B)	36.3B (31.1B–42.7B)
Intact	2.4B (2.1B–2.7B)	4.2B (3.7B–4.6B)
Meals prepared with beef carrying NTS_R ($Meal_{res}$)		
Total	11.2B (9.08B–13.54B)	11.2B (9.08B–13.54B)
Ground	10.4B (8.3B–12.71B)	16.22B (12.69B–20.90B)
Intact	811M (708M–925M)	1.30B (1.16B–1.46B)
Nontyphoidal salmonellosis attributable to beef, no. cases/100,000 US population		
Total	15.10 (0.096–44.44)	15.10 (0.096–44.44)
Ground	8.27 (0.028–25.99)	8.99 (0.028–26.94)
Intact	6.83 (0.028–20.07)	6.75 (0.043–19.72)
Ill_{res}/100,000 US population		
Total	0.64 (0.0036,2.75)	0.64 (0.0036–2.75)
Ground	0.39 (0.0007,1.54)	0.36 (0.0008–1.46)
Intact	0.25 (0.001,1.25)	0.31 (0.00084–1.54)
Nontyphoidal salmonellosis attributable to beef/1 million beef meals		
Total	0.74 (0.0046–2.20)	0.74 (0.0046–2.20)
Ground	0.70 (0.0022–2.25)	0.78 (0.0024–2.35)
Intact	0.81 (0.0034–2.38)	0.78 (0.0051–2.29)
Nontyphoidal salmonellosis attributable to beef/1 million NTS beef meals		
Total	17.1 (11.4–24.0)	17.1 (11.4–24.0)
Ground	10.2 (6.73–14,4)	12.9 (8.6–18.2)
Intact	82.1 (53.8–118.1)	70.4 (46.7–100)
P_{meal}		
Total	0.031 (0.00018–0.14)	0.031 (0.00018–0.14)
Ground	0.031(0.000056–0.13)	0.031 (0.000067–0.13)
Intact	0.032 (0.0001–0.15)	0.036 (0.00013–0.18)
P_{ill}		
Total	1.78 (0.007–8.56)	1.78 (0.007–8.56)
Ground	1.15 (0.001–5.38)	1.25 (0.001–5.21)
Intact	9.10 (0.039–47.21)	9.48 (0.032–50.19)

*Years included are 2002–2015 for ground beef, 1998–2010 for intact beef, and 2002–2010 for total beef. Calculations include measures of exposure (meals prepared from beef with various states of microbiological contamination), disease incidence (no. illness cases/100,000 US population), and different measures of disease risk per meals consumed. B, billion; Ill_{res}, antibiotic-resistant nontyphoidal salmonellosis attributable to beef; M, million; NTS, nontyphoidal *Salmonella*; NTS_R, antibiotic-resistant NTS; P_{meal}, antibiotic-resistant nontyphoidal salmonellosis/1 million beef meals; P_{ill}, antibiotic-resistant nontyphoidal salmonellosis/1 million NTS_R beef meals.
†Years 2002–2010 summary statistics reflect the data used to create the combined totals.

beef decreased (Table 2). In contrast, for CRR, the beef-attributable risk for CRR nontyphoidal salmonellosis was significantly lower for all beef meals initially contaminated—and ground beef specifically—in the last 5 years of data, as were both the incidence of CRR nontyphoidal salmonellosis and its risk per 1 million beef meals, overall and for intact beef (Table 2).

We found some year-to-year variations in Ill_{res}, P_{ill}, and P_{meal} but generally no yearly changes in meals made with beef initially contaminated with antibiotic-resistant NTS ($Meal_{res}$). For all beef and for ground beef and intact beef individually, defining resistance as resistance to ≥1 antibiotic, Ill_{res}, P_{ill}, and P_{meal} were higher in 2003 and 2009 and a peak for ground beef also occurred in 2014. $Meals_{res}$ showed no significant year-to-year changes for all beef cuts combined. Intact beef $Meals_{res}$ had 1 peak in 2001 (100% confidence). When MDR and CRR were used as the resistance definition, only the peaks in 2003 and in 2014 remained significant. A peak in some intact beef risks and illnesses was also observed in 2000 (Table 2).

Scenario Analysis of Changes in Antibiotic-Resistant Nontyphoidal Salmonellosis Resulting from Antibiotic Restriction in Beef Production

In the first scenario analysis, we found no significant changes (≤94.3% confidence) in antibiotic-resistant salmonellosis for any year when switching from current antibiotic practices to hypothetical 100% raised-without-antibiotics production. The mean change in the number of antibiotic-resistant nontyphoidal salmonellosis cases across the study period was –5,218 (Figure 4), ranging from an additional 1,441 resistant

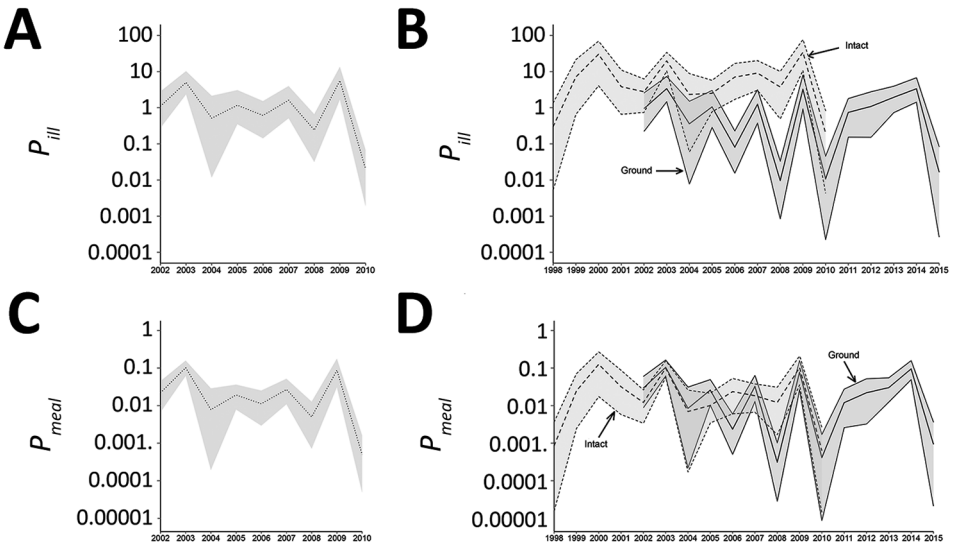

Figure 3. Estimates of the risk of antibiotic-resistant nontyphoidal salmonellosis per 1 million beef meals initially contaminated with antibiotic-resistant nontyphoidal Salmonella (P_{ill}) and per 1 million beef meals (P_{meal}) regardless of contamination status, United States, 2002–2010. Center lines represent means and gray shading represents the 95% credible intervals. A) P_{ill} for total beef, 2002–2010. B) P_{ill} stratified by intact (1998–2010) or ground beef (2002–2014). C) P_{meal} for total beef, 2002-2010. D) P_{meal} stratified by by intact (1998–2010) or ground beef (2002–2014). For panels B and D, light gray shading represents intact beef; dark gray shading indicates ground beef.

nontyphoidal salmonellosis cases to a reduction of 14,350 cases.

The second scenario (Figure 4), in which the direct linear assumption was relaxed, predicted significant decreases (>98% confidence) in cases for 2003 (–5,152) and 2009 (–4,763) and a significant increase of 1,098 cases (99.9% confidence) in 2010. However, switching to 100% raised-without-antibiotics production did not significantly change the number of antibiotic-resistant nontyphoidal salmonellosis cases over the full study period combining all 9 years (–8,588, 95% CrI –27,842 to 16,317, 60% confidence).

Discussion

Our risk analysis uses nationwide surveillance data on animal production and human illnesses to longitudinally estimate antibiotic-resistant nontyphoidal salmonellosis in the United States and assess how it might be affected by antibiotic restriction in livestock. Our approach is grounded in empirical data and minimizes assumptions while modeling parameter uncertainty and its effect on the results. Although farm-to-fork AMR risk analyses have been published (*10*), recent work has followed more parsimonious approaches like ours (*11*–*14*). However, direct comparison with other published risk analyses is difficult because most focus on the association between antibiotic use and AMR for a single drug and rarely include longitudinal data.

In our 2002–2010 analysis, the risks were stable over time; on average, a case of antibiotic-resistant salmonellosis occurred <1 time per 32 million meals made with beef or <1 time per 500,000 meals made with beef initially contaminated with antibiotic-resistant NTS. Likewise, prevalence of the antibiotic-resistant pathogen in beef available at retail in the United States and in the food production chain remained stable. Exceptions were 2 years in which more beef-attributable illnesses occurred than was typical for other years: 5 average-sized outbreaks (8% of attributable outbreaks) in 2003 and 2 *Salmonella* Montevideo outbreaks with high total case numbers in 2009.

The proportion of MDR and CRR was higher in NTS isolates from NARMS matched to outbreaks in 2003 and 2009 than in other years: 80% of matched samples in 2003 had CRR, and all 2009 *Salmonella* Montevideo matched samples to (71% of all matched 2009 cases) had MDR. This increase remained after we adjusted for exposure to infection in the form of meals prepared with beef with NTS and the fraction of these with AMR, which were stable. The association between MDR and CRR and larger/more frequent outbreaks may suggest a link between MDR/CRR and pathogenicity or infectivity, as described by Guillard et al. (*25*). Yet, in vitro phenotypic resistance does not fully capture actual clinical outcomes. Current foodborne surveillance programs do not record outcomes of AMR illnesses such as treatment failures and their consequences (e.g., extra hospitalizations). Estimating treatment failures resulting from resistant infections and the relative contribution of different sources of AMR—including antibiotic use in livestock—would better quantify the

societal cost benefit of curtailing resistant illnesses from livestock.

In our analysis, we had to estimate AMR specific to beef-attributable cases because the NARMS database contains salmonellosis cases of any source and yet resistance of salmonella varies by source (*9*). Lacking direct links between the NORS outbreak data used in source attribution and the outbreaks in NARMS, we used timing of the infection, state, and serotype to match cases. Although this method enabled us to approximate resistance in beef-attributable cases (5% vs. 22% AMR across human NARMS samples for NTS over the study period), use of this method probably resulted in some misclassification of the NARMS samples. This issue would be easily alleviated if a unique outbreak identifier were available in both datasets.

Of note, the per-portion risk for susceptible or resistant salmonellosis from beef initially contaminated was ≈8 times higher for intact cuts of beef than for ground beef. Because the prevalence of susceptible and resistant pathogens is greater for ground beef, the total illnesses are evenly split between types of beef, as are attributed illnesses, a result also noted by Laufer et al. (*26*). Intact cuts include some high-risk foods such as delicatessen

Table 2. Confidence in a significant monotonic trend in the data (bootstrapped Mann-Kendall test) and in the difference between posteriors estimates of the last 5 years versus the previous years for measures of beef consumption, NTS illnesses, and risk for antimicrobial resistant salmonellosis from beef, United States*

Variable	Monotonic (confidence trend exists), %	Last 5 vs. previous years (confidence difference exists), %	Years found significantly higher based on all pairwise comparisons†
$Meals_{res}$	38.2	68.7	None
Ground	66.6	44.7	None
Intact	88.0	93.8	None
$Meals_{res,MDR}$	87.0	86.3	None
Ground	94.5 (D)	85.8	None
Intact	53.0	98.4 (D)	2001
$Meals_{res,CRR}$	82.0	85.7	None
Ground	96.7 (D)	94.5	None
Intact	34.2	91.4	None
Ill_{res}	82.0	67.2	2003, 2009
Ground	66.8	55.3	2003, 2009, 2014
Intact	57.3	69.0	2003, 2009
$Ill_{res,MDR}$	86.6	87.2	2003
Ground	67.0	57.6	2003, 2014
Intact	61.9	84.5	2000, 2003
$Ill_{res,CRR}$	90.6	100 (D)	2003
Ground	70.1	54.7	2003
Intact	66.2	98.6 (D)	2000, 2003
P_{meal}	82.1	84.7	2003, 2009
Ground	62.9	54.7	2003, 2009, 2014
Intact	56.8	70.5	2003, 2009
$P_{meal, MDR}$	86.7	97.7 (D)	2003
Ground	66.9	50.8	2003, 2014
Intact	61.9	85.0	2000, 2003
$P_{meal, CRR}$	91.0	99.9 (D)	2003
Ground	67.2	49.9	2003
Intact	70.4	98.7(D)	2003
P_{ill}	87.3	84.1	2003, 2009
Ground	54.4	75.2	2003, 2009, 2014
Intact	42.6	49.9	2003, 2009
$P_{ill,MDR}$	82.2	86.0	2003
Ground	46.5	97.6 (I)	2003, 2014
Intact	53.2	66.1	2003
$P_{ill,CRR}$	87.0	99.6 (D)	2003
Ground	36.8	99.9 (D)	2003, 2014
Intact	70.5	91.7	2000, 2003

*D indicates that a significant decrease was found; I indicates that a significant increase was found, based on a 95% limit. CRR, clinically relevant resistance; Ill_{res}, human cases of beef-attributable antibiotic-resistant NTS; $Ill_{res,MDR}$, human cases of beef-attributable MDR NTS; $Ill_{res,CRR}$, human cases of beef-attributable CRR NTS; $Meals_{res}$, meals prepared with beef initially contaminated with antibiotic-resistant NTS resistant to ≥1 antibiotic; $Meals_{res,MDR}$, meals prepared with beef initially contaminated with NTS resistant to ≥2 antibiotics; $Meals_{res,CRR}$, meals prepared with beef initially contaminated with NTS with CRR; MDR, multidrug-resistant; NTS, nontyphoidal *Salmonella*; P_{meal}, probability of antibiotic-resistant NTS per meal made with beef of any kind; $P_{meal,MDR}$, probability of MDR NTS per meal made with beef of any kind; $P_{meal,CRR}$, probability of clinically relevant antibiotic-resistant NTS per meal made of beef of any kind; P_{ill}, probability of antibiotic-resistant NTS per meal made with beef initially contaminated with antibiotic-resistant NTS; $P_{ill,MDR}$, probability of MDR NTS per meal made with beef initially contaminated with MDR NTS; $P_{ill,CRR}$, probability of CRR NTS per meal made with beef initially contaminated with CRR NTS.
†Based on pairwise posterior comparisons between all years.

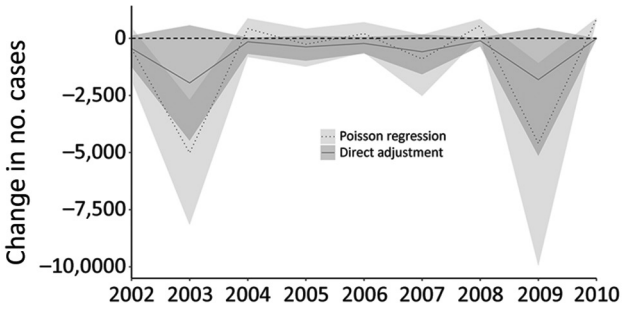

Figure 4. Predicted changes in each year's cases of antimicrobial-resistant salmonellosis from beef, United States, 2002–2010. Mean and 95% credible intervals of the predicted change are shown for the hypothetical scenario of 100% raised-without-antibiotics beef consumption, assuming a direct linear relationship between prevalence of antimicrobial-resistant *Salmonella* in beef and antimicrobial-resistant salmonellosis cases (solid line and dark grey shading), contrasted with the result from adjusting the relationship of beef resistance and prevalence with human cases based on the Poisson regression between the 2 variables (dotted line and light grey shading).

roast beef and ready-to-eat products (*27*). Doneness might also partly explain this finding. A survey found that 61% of US consumers preferred their steak medium or rarer (*28*), and another study found that 21% of restaurant customers requested medium or rarer hamburgers (*29*).

Using NTS in beef, beef-attributable salmonellosis cases, and resistance to ≥1 antibiotic provided a case definition that maximizes the chances of finding a statistical signal in this dataset, should a trend exist in the outcomes. Consequently, the lack of sustained change suggests that the modeled risks were indeed stable nationwide. Assuming that, as often described, antibiotic use in beef production is a key driver of AMR illnesses in humans, we consider 2 alternative explanations for this stability: either antibiotic use was stable during the study period or sustained use in beef resulted in a plateau in AMR salmonellosis so that changes in use can no longer affect the outcome. Although nationwide data on antibiotic use is unavailable for the study period, antibiotic use in beef is unlikely to have remained stable. For example, the fraction of beef cattle treated with tylosin in feed or water increased from 42.3% in 1999 to 71.2% in 2010 (*30*,*31*), whereas in Canada, where beef production practices are equivalent to those in the United States, overall use in beef decreased during 2008–2012 (*32*). A hypothetical resistance plateau cannot be empirically answered without detailed use data, but its implication is that changes such as the recent US Food and Drug Administration feed directive should eventually reduce beef-attributable antibiotic-resistant nontyphoidal salmonellosis. This hypothesis warrants a re-estimation of our model in the future.

An alternative hypothesis for the lack of change is that antibiotic use in beef does not significantly affect incidence of human AMR salmonellosis. This hypothesis does not necessarily imply a lack of risk but a risk that is too small or confounded to be measured. Empirical data for this effect are scarce because field studies typically link antibiotic use to AMR in animals or animal products, not in human illnesses. Benedict et al. (*33*) described how exposure to antibiotics in feedlot cattle did not affect AMR presence in non–type-specific *Escherichia coli*. Others have described a lower prevalence of resistance resulting from decreased use (*4*), although pathogen prevalence among raised-without-antibiotics livestock may be higher than that among conventionally raised animals (*5*). Although our study cannot confirm or refute this hypothesis, it provides new empirical evidence based on nationwide estimates and can be further updated as antibiotic practices in livestock are documented.

The scenarios with all raised-without-antibiotics beef cattle enabled us to model a hypothetical upper limit of the human health effect of antibiotic reduction and resulted in nonsignificant changes in resistant illnesses overall. This finding held true even under an unrealistic assumption of a direct decrease in resistant illnesses resulting from decreased pathogen prevalence and resistance after complete withdrawal of antibiotics. Being based solely on nationwide estimates—resistant illnesses based on surveillance data and the effect of antibiotic use on antibiotic-resistant NTS based on a nationwide survey (*22*)—these findings suggest that, according to collected surveillance data, reducing antibiotic use in cattle may not significantly reduce antibiotic-resistant nontyphoidal salmonellosis by a measurable level. Although external validation is not feasible because no other study, to our knowledge, has directly tested human and animal resistance at a national level, these results are consistent with those of recent studies of cecal contents of fed cattle (*5*) and ground beef (*34*) that found few AMR differences between raised-without-antibiotics and conventionally raised cattle production. Our findings also demonstrate that a direct relationship between prevalence of antibiotic-resistant NTS in beef and resulting AMR salmonellosis is not supported by current surveillance data.

This analysis suggests that the risk of contracting antibiotic-resistant nontyphoidal salmonellosis from beef consumption is <1 time/32 million beef meals and remained stable during 2002–2010. Despite

assessing salmonellosis only, our work highlights improvements needed to better quantify the effect that antibiotic use in livestock has on human health: monitoring of clinical outcomes in foodborne surveillance programs, better connection between surveillance for foodborne pathogen resistance and outbreak sourcing, and detailed studies exploring the effect of raised-without-antibiotics production practices on pathogen prevalence and resistance throughout the farm-to-fork production chain. Elucidating not only consumers' exposure to resistant pathogens but also how exposure translates into resistant illnesses and, ultimately, treatment failures, is required for the development of optimal AMR reduction strategies.

Acknowledgments

We thank Michael D. Apley for his constructive feedback on the model and interpretation of results.

K.E.B., P.S.M., J.W.S., T.L.W., T.M.A. contributed to the study design and manuscript review and editing.

This work was supported by a research contract from the Beef Checkoff. The funders had no role in the study design, data collection or analysis, manuscript preparation, nor the decision to publish this work.

USDA is an equal opportunity provider and employer. Names are necessary to report factually on available data; however, the USDA neither guarantees nor warrants the standard of product, and use of the name by the USDA implies no approval of the product to the exclusion of others that may also be suitable.

About the Author

Dr. Costard is an epidemiologist working as a senior consultant at EpiX Analytics in Fort Collins, CO, USA. Her research interests include risk analysis, simulation modeling, and quantitative decision-support tools in general, with special interests in health risk management strategies and food safety.

References

1. European Commission. Regulation (EC) no. 1831/2003 of the European Parliament and of the Council of 22 September 2003 on additives for the use in food and nutrition [cited 2019 Mar 4]. https://eur-lex.europa.eu/legal-content/EN/TXT/PDF/?uri=CELEX:32003R1831&from=EN
2. Office of Information and Regulatory Affairs. Veterinary feed directive [cited 2018 Oct 18]. https://www.reginfo.gov/public/do/eAgendaViewRule?pubId=201404&RIN=0910-AG95.
3. Landers TF, Cohen B, Wittum TE, Larson EL. A review of antibiotic use in food animals: perspective, policy, and potential. Public Health Rep. 2012;127:4–22. https://doi.org/10.1177/003335491212700103
4. Tang KL, Caffrey NP, Nóbrega DB, Cork SC, Ronksley PE, Barkema HW, et al. Restricting the use of antibiotics in food-producing animals and its associations with antibiotic resistance in food-producing animals and human beings: a systematic review and meta-analysis. Lancet Planet Health. 2017;1:e316–27. https://doi.org/10.1016/S2542-5196(17)30141-9
5. Vikram A, Rovira P, Agga GE, Arthur TM, Bosilevac JM, Wheeler TL, et al. Impact of "raised without antibiotics" beef cattle production practices on occurrences of antimicrobial resistance. Appl Environ Microbiol. 2017;83:e01682-17. https://doi.org/10.1128/AEM.01682-17
6. Williams MS, Ebel ED, Vose D. Framework for microbial food-safety risk assessments amenable to Bayesian modeling. Risk Anal. 2011;31:548–65. https://doi.org/10.1111/j.1539-6924.2010.01532.x
7. Scallan E, Hoekstra RM, Angulo FJ, Tauxe RV, Widdowson M-A, Roy SL, et al. Foodborne illness acquired in the United States—major pathogens. Emerg Infect Dis. 2011;17:7–15. https://doi.org/10.3201/eid1701.P11101
8. Centers for Disease Control and Prevention. Antibiotic resistance threats in the United States, 2013 [cited 2018 Dec 5]. https://www.cdc.gov/drugresistance/pdf/ar-threats-2013-508.pdf
9. Centers for Disease Control and Prevention. National Antimicrobial Resistance Monitoring System (NARMS): 2014 human isolates surveillance report [cited 2018 Jan 10]. https://www.cdc.gov/narms/pdf/2014-Annual-Report-narms-508c.pdf
10. Anderson SA, Yeaton Woo RW, Crawford LM. Risk assessment of the impact on human health of resistant *Campylobacter jejuni* from fluoroquinolone use in beef cattle. Food Control. 2001;12:13–25. https://doi.org/10.1016/S0956-7135(00)00014-1
11. Food and Drug Administration Center for Veterinary Medicine. The human health impact of fluoroquinolone resistant *Campylobacter* attributed to the consumption of chicken [cited 2018 Oct 16]. https://www.fda.gov/downloads/animalveterinary/safetyhealth/recallswithdrawals/ucm152308.pdf
12. European Food Safety Authority. ECDC/EFSA/EMA second joint report on the integrated analysis of the consumption of antimicrobial agents and occurrence of antimicrobial resistance in bacteria from humans and food-producing animals. EFSA J. 2017;15:4872.
13. Carmo LP, Nielsen LR, da Costa PM, Alban L. Exposure assessment of extended-spectrum beta-lactamases/AmpC beta-lactamases-producing *Escherichia coli* in meat in Denmark. Infect Ecol Epidemiol. 2014;4:1.
14. Collineau L, Backhans A, Dewulf J, Emanuelson U, Grosse Beilage E, Lehébel A, et al. Profile of pig farms combining high performance and low antimicrobial usage within four European countries. Vet Rec. 2017;181:657–657. https://doi.org/10.1136/vr.103988
15. Magiorakos A-P, Srinivasan A, Carey RB, Carmeli Y, Falagas ME, Giske CG, et al. Multidrug-resistant, extensively drug-resistant and pandrug-resistant bacteria: an international expert proposal for interim standard definitions for acquired resistance. Clin Microbiol Infect. 2012;18:268–81. https://doi.org/10.1111/j.1469-0691.2011.03570.x
16. Hald T, Wong DMALF, Aarestrup FM. The attribution of human infections with antimicrobial resistant *Salmonella* bacteria in Denmark to sources of animal origin. Foodborne Pathog Dis. 2007;4:313-26. https://doi.org/10.1089/fpd.2007.0002

17. Centers for Disease Control and Prevention. National Antimicrobial Resistance Monitoring System (NARMS): human data [cited 2018 Oct 18]. https://wwwn.cdc.gov/narmsnow
18. US Department of Agriculture. Livestock & meat domestic data. Annual historical red meat supply and disappearance and per capita disappearance data [cited 2018 Oct 18]. https://www.ers.usda.gov/data-products/livestock-meat-domestic-data/livestock-meat-domestic-data/#Beef
19. Centers for Disease Control and Prevention. National Health and Nutrition Examination Survey data [cited 2017 Feb 4]. http://wwwn.cdc.gov/nchs/nhanes/search/nhanes03_04.aspx
20. Yue S, Pilon P. A comparison of the power of the *t* test, Mann-Kendall and bootstrap tests for trend detection/Une comparaison de la puissance des tests *t* de Student, de Mann-Kendall et du bootstrap pour la détection de tendance. Hydrol Sci J. 2004;49:21–37. https://doi.org/10.1623/hysj.49.1.21.53996
21. Gelman A, Carlin J, Stern H, Dunson D, Vehtari A, Rubin D. Bayesian data analysis, 3rd ed. [cited 2017 Mar 7]. https://www.crcpress.com/Bayesian-Data-Analysis-Third-Edition/Gelman-Carlin-Stern-Dunson-Vehtari-Rubin/p/book/9781439840955
22. Dargatz DA, Kopral CA, Erdman MM, Fedorka-Cray PJ. Prevalence and antimicrobial resistance of *Salmonella* isolated from cattle feces in United States feedlots in 2011. Foodborne Pathog Dis. 2016;13:483–9. https://doi.org/10.1089/fpd.2016.2128
23. Williams MS, Ebel ED, Vose D. Methodology for determining the appropriateness of a linear dose-response function. Risk Anal. 2011;31:345–50. https://doi.org/10.1111/j.1539-6924.2010.01518.x
24. Williams MS, Ebel ED. Estimating changes in public health following implementation of hazard analysis and critical control point in the United States broiler slaughter industry. Foodborne Pathog Dis. 2012;9:59–67. https://doi.org/10.1089/fpd.2011.0951
25. Guillard T, Pons S, Roux D, Pier GB, Skurnik D. Antibiotic resistance and virulence: understanding the link and its consequences for prophylaxis and therapy. BioEssays. 2016;38:682–93. https://doi.org/10.1002/bies.201500180
26. Laufer AS, Grass J, Holt K, Whichard JM, Griffin PM, Gould LH. Outbreaks of *Salmonella* infections attributed to beef —United States, 1973–2011. Epidemiol Infect. 2015;143:2003–13. https://doi.org/10.1017/S0950268814003112
27. US Department of Agriculture Food Safety Inspection Service. Risk assessment of lethality standards for RTE meat and poultry [cited 2020 Feb 18]. https://www.fsis.usda.gov/wps/wcm/connect/ace90cc5-2be2-4fa3-9ed5-2b186cae976c/Salm_RTE_Risk_Assess_ExecSumm_Sep2005.pdf?MOD=AJPERES
28. Reicks AL, Brooks JC, Garmyn AJ, Thompson LD, Lyford CL, Miller MF. Demographics and beef preferences affect consumer motivation for purchasing fresh beef steaks and roasts. Meat Sci. 2011;87:403–11. https://doi.org/10.1016/j.meatsci.2010.11.018
29. Bogard AK, Fuller CC, Radke V, Selman CA, Smith KE. Ground beef handling and cooking practices in restaurants in eight states. J Food Prot. 2013;76:2132–40. https://doi.org/10.4315/0362-028X.JFP-13-126
30. US Department of Agriculture. Feedlot 2011. Part III: Trends in health and management practices on U.S. feedlots, 1994–2011 [cited 2016 Oct 31]. https://www.aphis.usda.gov/animal_health/nahms/feedlot/downloads/feedlot2011/Feed11_dr_Part%20III.pdf
31. US Department of Agriculture. Feedlot 2011. Part IV: Health and health management on U.S. feedlots with a capacity of 1,000 or more head [cited 2016 Oct 31]. https://www.aphis.usda.gov/animal_health/nahms/feedlot/downloads/feedlot2011/Feed11_dr_PartIV.pdf
32. Brault SA, Hannon SJ, Gow SP, Warr BN, Withell J, Song J, et al. Antimicrobial use on 36 beef feedlots in western Canada: 2008–2012. Front Vet Sci. 2019;6:329. https://doi.org/10.3389/fvets.2019.00329
33. Benedict KM, Gow SP, McAllister TA, Booker CW, Hannon SJ, Checkley SL, et al. Antimicrobial resistance in *Escherichia coli* recovered from feedlot cattle and associations with antimicrobial use. PLoS ONE. 2015;10:e0143995. https://doi.org/10.1371/journal.pone.0143995
34. Vikram A, Miller E, Arthur TM, Bosilevac JM, Wheeler TL, Schmidt JW. Similar levels of antimicrobial resistance in U.S. food service ground beef products with and without a "raised without antibiotics" claim. J Food Prot. 2018;81:2007–18. https://doi.org/10.4315/0362-028X.JFP-18-299

Address for correspondence: Francisco Zagmutt, EpiX Analytics, LLC, 375 E Horsetooth Ave, #2-100, Fort Collins, CO 80525, USA; email: fzagmutt@epixanalytics.com

Detection of H1 Swine Influenza A Virus Antibodies in Human Serum Samples by Age Group[1]

Elien Vandoorn, Isabel Leroux-Roels, Geert Leroux-Roels, Anna Parys, Amy Vincent, Kristien Van Reeth

Most H1 influenza A viruses (IAVs) of swine are derived from past human viruses. As human population immunity against these IAVs gradually decreases, the risk of reintroduction to humans increases. We examined 549 serum samples from persons 0–97 years of age collected in Belgium during 2017–2018 for hemagglutination inhibiting and virus neutralizing antibodies against 7 major H1 swine IAV (swIAV) clades and 3 human progenitor IAVs. Seroprevalence (titers ≥40) rates were ≥50% for classical swine and European human-like swIAVs, ≥24% for North American human-like δ1a and Asian avian-like swIAVs, and ≤10% for North American human-like δ1b and European avian-like swIAVs, but rates were age-dependent. Antibody titers against human-like swIAVs and supposed human precursor IAVs correlated with correlation coefficients of 0.30–0.86. Our serologic findings suggest that European avian-like, clade 1C.2.1, and North American human-like δ1b, clade 1B.2.2.2, H1 swIAVs pose the highest pandemic risk.

Humans and swine are susceptible to influenza A viruses (IAVs) of hemagglutinin (HA) subtypes H1 and H3, which are widespread in both species. Human IAVs frequently are transmitted to swine, after which the HA surface protein generally undergoes slower antigenic evolution (drift) in swine than in humans (*1*–*3*). Therefore, swine can be considered a reservoir for past human IAVs. Because antigenic drift variants of human IAVs replace each other over time, younger persons only have been exposed to more recent strains and human population immunity against older human IAVs gradually decreases (*4*). Consequently, human-origin swine IAVs (swIAVs) can be reintroduced into the human population after a certain period and cause a pandemic, as illustrated by the influenza A(H1N1)pdm09 virus (pH1N1) (*5*). The H1 of this swine-origin virus is related to the H1 of human seasonal H1N1 IAVs that circulated in 1918–1950. In 2009, only persons born before the 1950s had cross-reactive antibodies against pH1N1, so a pandemic was possible (*6*,*7*).

The evolution of swIAVs is different from and more complex than that of human IAVs because of multiple introductions of human IAVs into swine and geographic separation of swine populations (*8*). H1 swIAV colloquial names indicate their origin and region of circulation. An improved classification system subdivides H1 swIAVs into 3 lineages and 28 clades on the basis of H1 nucleotide sequence homology (*9*). The lineages are 1A, 1B, and 1C, with the number representing the subtype (H1) and the letter representing the lineage. Clades and subclades are indicated with 1–3 digits. Classical swine lineage 1A contains IAVs with the human 1918 pandemic H1N1 virus as a common ancestor. Most clades are restricted to America and Asia, but pH1N1 viruses (1A.3.3.2) circulate in swine and humans worldwide. Human seasonal lineage 1B contains swIAVs with an H1 derived from human seasonal IAVs. These human-like H1 swIAVs emerged in Europe in the late 1980s and in North America in the early 2000s. Eurasian avian lineage 1C contains swIAVs that originated from avian IAVs. These avian-like swIAVs emerged in Europe in 1979 and spread to Asia in 1993 (*10*–*13*). Apart from antigenic evolution in the HA, IAVs also can evolve via exchange of gene segments with other IAVs of different subtypes or clades infecting the same cell, called reassortment (*14*), which frequently occurs in pigs.

Author affiliations: Ghent University, Merelbeke, Belgium (E. Vandoorn, A. Parys, K. Van Reeth); Ghent University and Ghent University Hospital, Ghent, Belgium (I. Leroux-Roels, G. Leroux-Roels); National Animal Disease Center, Ames, Iowa, USA (A. Vincent)

DOI: https://doi.org/10.3201/eid2609.191796

[1]Preliminary results from this study were presented at the Fourth International Symposium on Neglected Influenza Viruses, April 18–20, 2018, Brighton, United Kingdom; at the BELVIR conference, December 20, 2018, Brussels, Belgium; and at the 1918 Pandemic Conference, February 7–8, 2019, Ypres, Belgium.

A reassortant IAV with an antigenically novel HA and the capacity to infect and spread in humans could cause a pandemic.

Since 2010, 35 zoonotic infections with H1 swIAVs were reported in North America and 10 in Europe (*15*–*17*; Parys et al., unpub. data). Human population immunity is a major factor determining the pandemic risk for swIAVs. Hemagglutination inhibiting (HI) and virus neutralizing (VN) antibodies in serum are accepted correlates of protection (*18*). Evaluating humans of different age groups for HI and VN antibody titers against a range of antigenically different swIAVs might help clarify the public health risk.

In a previous seroprevalence study for H3 swIAVs in humans from Luxembourg, we demonstrated a correlation with the nature of the swIAV and its relation to human IAVs on the one hand and the persons' birth year on the other (*19*). A large comparative seroprevalence study for H1 swIAVs is lacking. Previous studies examined limited numbers of H1 swIAVs or samples or did not evaluate the relation between birth year and antibody responses (*12*,*13*,*20*–*25*). In addition, most studies were conducted before or during the 2009 pandemic, but the circulation of pH1N1 viruses in humans likely changed the serologic profile against H1 swIAVs. We assessed prevalence and titers of protective antibodies against all major H1 swIAV clades in various age groups in Belgium in 2017. We also examined the relation between antibodies against human-like swIAVs and their presumed human seasonal ancestor IAV. The results will help assess the public health risk for different H1 swIAVs.

Materials and Methods

Sample Collection

During August 2017–January 2018, a total of 549 anonymized serum samples were collected from immunocompetent persons with unknown influenza vaccination or infection history born during 1920–2017 at Ghent University Hospital (Ghent, Belgium). Samples included ≈6 per birth year with ≈1:1 ratio between male and female patients. Exclusion criteria included active oncologic disease or hematologic malignancies, immunosuppressive treatment, organ transplantation, admission to intensive care, and end-stage renal disease on dialysis treatment. This study was approved by the Commission for Medical Ethics of the Ghent University Hospital (approval no. 2017/0834).

Viruses

Samples were evaluated for antibodies against 11 viruses representing 7 major H1 swIAV clades circulating in Europe, North America, and Asia; 2 human seasonal progenitor IAVs for European and North American human-like swIAVs; and 1 human seasonal IAV that circulated right before the pH1N1 virus (Table 1). We used epidemiologic data (*10*–*12*) and the H1 classification system (*9*) to select major H1 swIAV clades. We selected test viruses on the basis of amino acid homology and antigenic relatedness to currently circulating swIAVs of each clade. We selected the human progenitor IAVs based on the literature (*26*,*27*).

We downloaded nucleotide sequences of the viruses' HA1, the main target of neutralizing antibodies, from Genbank and translated these to amino acids. We used the MUSCLE algorithm for sequence alignment and the Jones-Taylor-Thornton model and nearest-neighbor-interchange heuristic method to construct maximum-likelihood trees in MEGA7 (*28*). We determined the percent of amino acid homology between test viruses and numbers of identical amino acids in presumed antigenic sites (*29*) with MEGA7 and R version 3.2.2 (*30*).

We obtained North American swIAVs and corresponding swine serum from the U.S. Department

Table 1. Swine and human H1 influenza A virus strains used in hemagglutination inhibition and virus neutralization assays of human serum samples, Belgium*

Virus strain	Abbreviation	Subtype	Colloquial name H1	H1 clade	H1 GenBank Accession no.
A/swine/Gent/28/2010	swG10	H1N1	European avian-like	1C.2.1	KP406525
A/swine/Hong Kong/2032/2011	swHK11	H1N1	Asian avian-like	1C.2.3	KM028543
A/Taiwan/1/86	TW86	H1N1	Human seasonal	1B.1-like	X17224
A/swine/Gent/26/2012	swG12	H1N2	European human-like	1B.1.2.1	KP406526
A/New Caledonia/20/99	NC99	H1N1	Human seasonal	1B.2-like	DQ508857
A/swine/Alabama/A01104091/2016	swAL16	H1N2	North American human-like δ1a	1B.2.2.1	KX247675
A/swine/Illinois/A01047020/2010	swIL10	H1N2	North American human-like δ1b	1B.2.2.2	JQ756323
A/swine/Oklahoma/A01290605/2013	swOK13	H1N1	North American human-like δ1b	1B.2.2.2	KF791395
A/Brisbane/59/2007	BR07	H1N1	Human seasonal	1B.2-like	CY058487
A/swine/Ohio/511445/2007	swOH07	H1N1	North American classical swine γ	1A.3.3.3	EU604689
A/California/04/2009	CA09	pH1N1	2009 pandemic	1A.3.3.2	FJ966082

*Viruses are ordered chronologically according to the year of circulation of the selected human test viruses TW86, NC99, BR07, and CA09; horizontal rules within table represent grouping of epidemiologically related human and swine influenza A viruses, with the oldest (ancestor) virus mentioned first.

of Agriculture-Agricultural Research Service. We obtained human seasonal IAVs and corresponding ferret serum from Francis Crick Institute (London, UK), and Asian swIAV from Hong Kong University (Hong Kong). We antigenically characterized test viruses in cross-HI and cross-VN assays with postvaccination swine serum for swIAVs or postinfection ferret serum for human seasonal IAVs. Because serum against A/Brisbane/59/2007 was not available, we used ferret serum against A/Egypt/10/2007 instead; the HA sequence is identical in both. We propagated viruses in MDCK cells; all passages were ≤6. We calculated antigenic distances from HI and VN titers as described previously (*31*) and converted these into antigenic dendrograms by using the neighbor-joining method in MEGA7. One antigenic unit represents a 2-fold difference in HI or VN titer.

Serologic Assays

We tested individual samples in HI assays and pooled samples per birth year in VN assays for antibodies against each test virus. Both assays were performed according to standard procedures (*32*,*33*). We expressed antibody titers for HI as the reciprocal of the highest serum dilution showing complete hemagglutination inhibition of 4 hemagglutinating units of virus or, for VN, 50% neutralization of 100 $TCID_{50}$ (50% tissue culture infective doses) of virus. The starting dilution was 1:20, and we considered a titer of ≥40 positive.

Statistical Analyses

We calculated geometric mean titers (GMTs) and 95% CIs for HI and VN antibody titers of samples from each birth decade against each test virus by using log_2-transformed data. Samples with a titer <20 were assigned a titer of 10. For non-stratified data, we calculated Spearman correlation coefficients (CCs) between HI titers or between VN titers against different viruses. We used Kruskal-Wallis and Mann-Whitney U tests to compare antibody titers between age groups for a certain virus or between viruses for a certain age group. We used Fisher exact test to compare proportions of positive samples. For all statistical tests, we applied Bonferroni adjustment of the p values and we considered corrected p values of <0.05 statistically significant. We performed all analyses by using R version 3.2.2.

Results

Genetic and Antigenic Relatedness Between Test Viruses

We tested samples for antibodies against 11 IAVs from the classical swine 1A, human seasonal 1B, or Eurasian avian 1C lineage. HA1 aa sequence homology between viruses of different lineages was <75% with 19–35/50 identical amino acids in presumed antigenic sites. Classical swine and avian-like IAVs were phylogenetically most closely related (Figure 1, panel A; Table 2). Within-lineage HA1 aa homology was 82%–97%, with 36–49 identical amino acids in

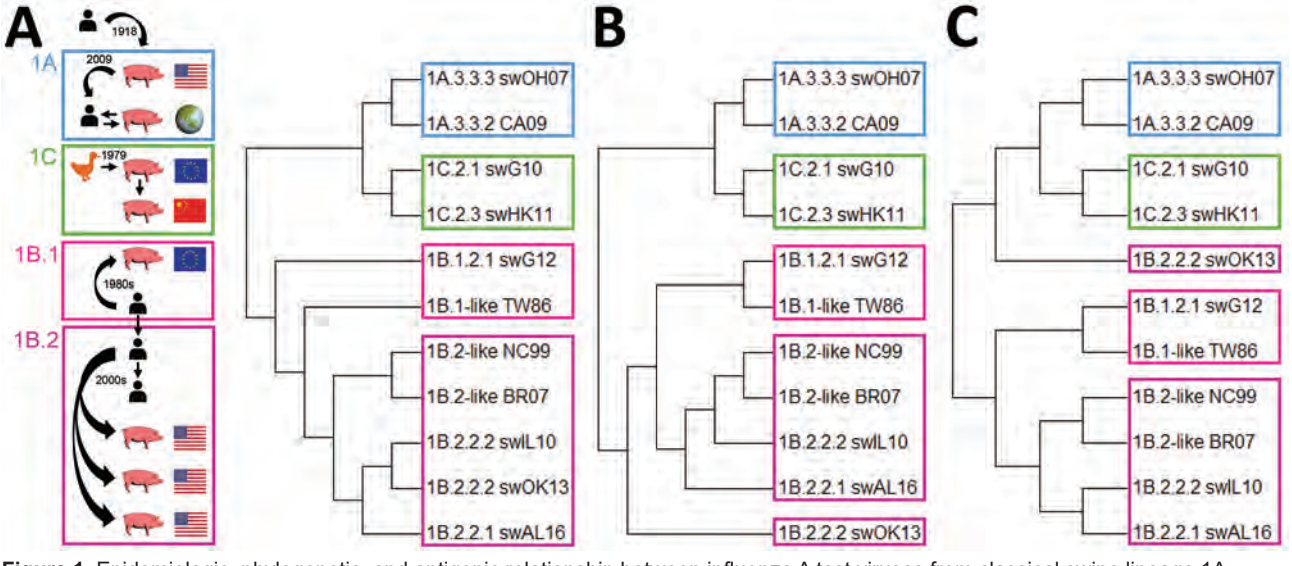

Figure 1. Epidemiologic, phylogenetic, and antigenic relationship between influenza A test viruses from classical swine lineage 1A, human seasonal lineage 1B, and Eurasian avian lineage 1C. A) Schematic representation of the H1 IAV epidemiology and maximum-likelihood neighbor-joining phylogenetic tree of the HA1 of representative test viruses. B) Antigenic dendrogram based on antigenic distances in cross-hemagglutination inhibition assays. C) Antigenic dendrogram based on antigenic distances in cross-virus neutralization assays. IAV, influenza A virus.

Table 2. Percentage amino acid homology (lower left) and number of identical amino acids out of 50 aa in presumed antigenic sites (upper right) (*28*) between hemagglutinin 1 of human and swine H1 influenza A viruses used as test viruses in hemagglutination inhibition and virus neutralization assays*

	Eurasian avian		Human seasonal							Classical swine	
	swG10	swHK11	TW86†	swG12	NC99†	swAL16	swIL10	swOK13	BR07†	swOH07	CA09
Virus strain	Europe 1C.2.1	Asia 1C.2.3	1B.1-like	Europe 1B.1.2.1	1B.2-like	N. Am. 1B.2.2.1	N. Am. 1B.2.2.2	N. Am. 1B.2.2.2	1B.2-like	N. Am. 1A.3.3.3	World 1A.3.3.2
swG10	–	49	22	19	23	24	23	23	23	32	34
swHK11	96.0	–	23	20	23	25	23	23	23	33	35
TW86	73.4	72.2	–	41	41	38	36	32	38	23	23
swG12	69.1	68.5	89.6	–	35	33	33	32	32	21	22
NC99	73.3	72.1	93.9	85.9	–	42	42	36	47	24	24
swAL16	71.5	71.2	89.3	81.6	91.4	–	45	40	40	23	27
swIL10	72.1	71.5	89.6	83.4	94.2	92.9	–	43	42	23	25
swOK13	72.0	72.0	86.8	81.8	90.2	89.2	94.8	–	36	20	24
BR07	72.7	71.5	90.8	83.7	96.9	89.9	92.3	88.6	–	24	24
swOH07	74.0	74.3	74.3	71.6	73.0	72.4	71.8	70.5	73.6	–	44
CA09	73.4	72.5	73.4	70.9	72.4	73.9	72.1	71.1	72.4	90.8	–

*Viruses are ordered chronologically according to the year of circulation of the selected human test viruses TW86, NC99, BR07, and CA09; horizontal rules within table represent grouping of epidemiologically related human and swine influenza A viruses, with the oldest (ancestor) virus mentioned first. Complete isolate names are provided in Table 1. IAV, influenza A virus; N. Am., North America; –, not applicable.
†Human IAV that no longer circulates; TW86 is the presumed human precursor for human-like H1 swine IAVs in Europe; NC99 is the presumed human precursor for human-like H1 swine IAVs in North America; BR07 is a human seasonal IAV that circulated right before the influenza A(H1N1)pdm09 virus; the influenza A(H1N1)pdm09 virus, represented by CA09, is circulating in both humans and swine worldwide.

antigenic sites. Human-like swIAVs and their presumed human seasonal progenitor IAV shared 90%–94% aa in the HA1 and 36–42 aa in antigenic sites.

Antigenic dendrograms based on cross-HI and cross-VN assays showed similar trends to the phylogenetic tree, except for swOK13 (Tables 3–5; Figure 1). This North American human-like δ1b swIAV (1B.2.2.2) clustered separately from other IAVs of its lineage, including its presumed human ancestor, NC99.

Seroreactivity against Human Seasonal IAVs

We tested human serum samples against human seasonal IAVs related to 1B swIAVs from 1986 (TW86), 1999 (NC99), and 2007 (BR07) to evaluate a person's potential exposure to or vaccination with these IAVs. Overall, 39% were seropositive for TW86, 31% for NC99, and 22% for BR07 in HI and 48% were seropositive for TW86, 51% for NC99, and 29% for BR07 in VN (Figures 2, 3). Seroprevalences and GMTs against TW86 were highest for persons born during 1977–1986 and lowest for the 2 youngest groups, those born during 1997–2017 (Tables 6, 7). For NC99 and BR07, HI responses were highest for those born during 1987–1996, and VN responses were highest for those born during 1937–1946 (NC99 only) and 1997–2006. Persons born during 2007–2017 had minimal responses. Antibody responses against human seasonal IAVs were related to birth year and the year of virus isolation, with peak responses in persons born right before the virus circulated and lowest responses in persons born afterwards.

Table 3. Cross-reactivity between human and swine H1 influenza A viruses in hemagglutination inhibition assay*

	Eurasian avian		Human seasonal							Classical swine	
	swG10	swHK11	TW86†	swG12	NC99†	swAL16	swIL10	swOK13	BR07†	swOH07	CA09
Virus strain	Europe 1C.2.1	Asia 1C.2.3	1B.1-like	Europe 1B.1.2.1	1B.2-like	N. Am. 1B.2.2.1	N. Am. 1B.2.2.2	N. Am. 1B.2.2.2	1B.2-like	N. Am. 1A.3.3.3	World 1A.3.3.2
swG10	**640**	40	<20	<20	<20	<20	<20	<20	<20	<20	20
swHK11	640	**640**	<20	<20	<20	<20	<20	<20	<20	40	40
TW86	<20	<20	**1,280**	160	20	<20	<20	<20	<20	<20	<20
swG12	20	<20	160	**1,280**	20	20	<20	<20	<20	<20	<20
NC99	<20	<20	<20	<20	**640**	<20	<20	<20	80	<20	<20
swAL16	<20	<20	<20	<20	160	**320**	20	<20	20	<20	<20
swIL10	<20	<20	<20	<20	40	40	**320**	<20	160	<20	<20
swOK13	<20	<20	<20	<20	<20	<20	<20	**640**	<20	<20	<20
BR07	<20	<20	<20	<20	40	<20	<20	<20	**1,280**	<20	<20
swOH07	20	40	<20	<20	<20	<20	<20	20	<20	**1,280**	640
CA09	20	20	<20	<20	<20	<20	<20	<20	<20	160	**1,280**

*Viruses are ordered chronologically according to the year of circulation of the selected human test viruses TW86, NC99, BR07, and CA09; horizontal rules within table represent grouping of epidemiologically related human and swine influenza A viruses, with the oldest (ancestor) virus mentioned first. Complete isolate names are provided in Table 1. Bold indicates HI titer against the homologous virus. IAV, influenza A virus; HI, hemagglutination inhibition; N. Am., North America.
†Human IAV that no longer circulates; TW86 is the presumed human precursor for human-like H1 swine IAVs in Europe; NC99 is the presumed human precursor for human-like H1 swine IAVs in North America; BR07 is a human seasonal IAV that circulated right before the influenza A(H1N1)pdm09 virus;

Table 4. Cross-reactivity between human and swine H1 IAVs in virus neutralization assay*

	Eurasian avian		Human seasonal							Classical swine	
	sG10	swHK11	TW86†	swG12	NC99†	swAL16	swIL10	swOK13	BR07†	swOH07	CA09
Virus strain	Europe 1C.2.1	Asia 1C.2.3	1B.1-like	Europe 1B.1.2.1	1B.2-like	N. Am. 1B.2.2.1	N. Am. 1B.2.2.2	N. Am. 1B.2.2.2	1B.2-like	N. Am. 1A.3.3.3	World 1A.3.3.2
swG10	**1,920**	40	<20	<20	<20	<20	<20	<20	<20	<20	20
swHK11	640	**640**	<20	<20	30	<20	<20	<20	40	60	80
TW86	<20	<20	**1,920**	320	40	<20	<20	<20	<20	<20	30
swG12	<20	<20	120	**3,840**	20	20	<20	<20	<20	<20	<20
NC99	<20	<20	<20	<20	**1,280**	30	80	<20	160	<20	<20
swAL16	<20	<20	<20	<20	640	**960**	80	<20	160	<20	<20
swIL10	<20	<20	<20	<20	120	160	**3,840**	<20	320	<20	<20
swOK13	<20	<20	<20	<20	<20	<20	20	**1,280**	<20	<20	20
BR07	<20	<20	<20	<20	240	<20	60	<20	**2,560**	<20	<20
swOH07	<20	60	<20	20	20	<20	<20	<20	120	**1,920**	960
CA09	<20	<20	<20	<20	<20	<20	<20	<20	<20	160	**3,840**

*Viruses are ordered chronologically according to the year of circulation of the selected human test viruses TW86, NC99, BR07, and CA09; horizontal rules within table represent grouping of epidemiologically related human and swine influenza A viruses, with the oldest (ancestor) virus mentioned first. Complete isolate names are provided in Table 1. Bold indicates VN titer against the homologous virus IAV, influenza A virus; VN, virus neutralization; N. Am., North America.
†Human IAV that no longer circulates; TW86 is the presumed human precursor for human-like H1 swine IAVs in Europe; NC99 is the presumed human precursor for human-like H1 swine IAVs in North America; BR07 is a human seasonal IAV that circulated right before the influenza A(H1N1)pdm09 virus; the influenza A(H1N1)pdm09 virus, represented by CA09, is circulating in both humans and swine worldwide.

Seroreactivity against swIAVs of the Eurasian Avian Lineage 1C

The major avian-origin swIAV clades are European avian-like 1C.2.1, represented by swG10, and Asian avian-like 1C.2.3, represented by swHK11. For swG10, 10% of all samples tested positive in HI and 7% in VN (Figures 2, 3). Seroprevalence was ≤20% and GMTs were ≤20 for all age groups except the oldest, those born during 1920–1926, with 40% seropositive in HI and GMTs for HI and VN of 24 (Tables 6, 7).

For swHK11, overall seroprevalence was 25% in HI and 34% in VN. As for swG10, responses against swHK11 were highest for those born during 1920–1926; 52% in HI, 72% in VN, and GMTs ≥38. Responses were minimal in both HI and VN for persons born during 1947–1956; 11% in HI, 10% in VN, and GMTs <20.

Seroreactivity against swIAVs of the Human Seasonal Lineage 1B

European human-like swIAV swG12 (1B.1.2.1) represents the human-like H1 swIAV clade circulating in Belgium, and TW86 was selected as its presumed human ancestor virus. At least half of all samples tested positive for swG12, 50% in HI and 59% in VN (Figures 2, 3). We noted statistically significant differences in seroprevalences and GMTs, which were higher (62% in HI and 74% in VN; GMTs ≥44) in persons born before 1996 than in persons born during 1997–2017 (5% in HI and in VN; GMTs <20; p<0.001) (Tables 6, 7). GMTs peaked (≥87) in HI in those born during 1977–1986 and in VN for those born during 1967–1976. Results for swG12 were similar to those for its presumed human ancestor virus, TW86.

Table 5. Antigenic distance in units between human and swine H1 IAVs in cross-hemagglutination inhibition assays (upper right) and cross-virus neutralization assays (lower left)*

	Eurasian avian		Human seasonal							Classical swine	
	swG10	swHK11	TW86†	swG12	NC99†	swAL16	swIL10	swOK13	BR07†	swOH07	CA09
Virus strain	Europe 1C.2.1	Asia 1C.2.3	1B.1-like	Europe 1B.1.2.1	1B.2-like	N. Am. 1B.2.2.1	N. Am. 1B.2.2.2	N. Am. 1B.2.2.2	1B.2-like	N. Am. 1A.3.3.3	World 1A.3.3.2
swG10	–	1.67	4.96	4.67	4.49	4.15	4.30	4.24	4.69	4.41	4.23
swHK11	1.93	–	5.20	5.03	4.77	4.53	4.69	4.50	4.92	3.75	3.82
TW86	4.84	4.98	–	2.12	4.77	4.54	4.79	4.80	5.14	5.63	5.54
swG12	4.87	5.09	2.31	–	4.77	4.33	4.74	4.77	5.14	5.65	5.53
NC99	4.65	4.37	4.72	4.85	–	2.62	3.04	4.35	2.74	5.19	5.08
swAL16	4.62	4.53	4.79	4.71	1.75	–	2.65	3.99	3.67	4.91	4.75
swIL10	4.95	4.93	5.27	5.19	2.50	2.29	–	4.11	2.75	5.09	4.92
swOK13	4.34	4.44	4.79	4.83	4.47	4.44	4.63	–	4.56	4.65	4.81
BR07	4.77	4.36	4.97	5.06	1.91	2.75	2.75	4.63	–	5.35	5.26
swOH07	4.65	3.48	5.07	5.21	4.71	4.80	5.12	4.73	4.44	–	1.43
CA09	4.59	3.91	4.89	5.28	5.09	5.01	5.33	4.53	5.17	2.06	–

*Viruses are ordered chronologically according to the year of circulation of the selected human test viruses TW86, NC99, BR07, and CA09; horizontal rules within table represent grouping of epidemiologically related human and swine influenza A viruses, with the oldest (ancestor) virus mentioned first. Complete isolate names are provided in Table 1. IAV, influenza A virus; N. Am., North America; – not applicable.
†Human IAV that no longer circulates; TW86 is the presumed human precursor for human-like H1 swine IAVs in Europe; NC99 is the presumed human precursor for human-like H1 swine IAVs in North America; BR07 is a human seasonal IAV that circulated right before the influenza A(H1N1)pdm09 virus; the influenza A(H1N1)pdm09 virus, represented by CA09, is circulating in both humans and swine worldwide.

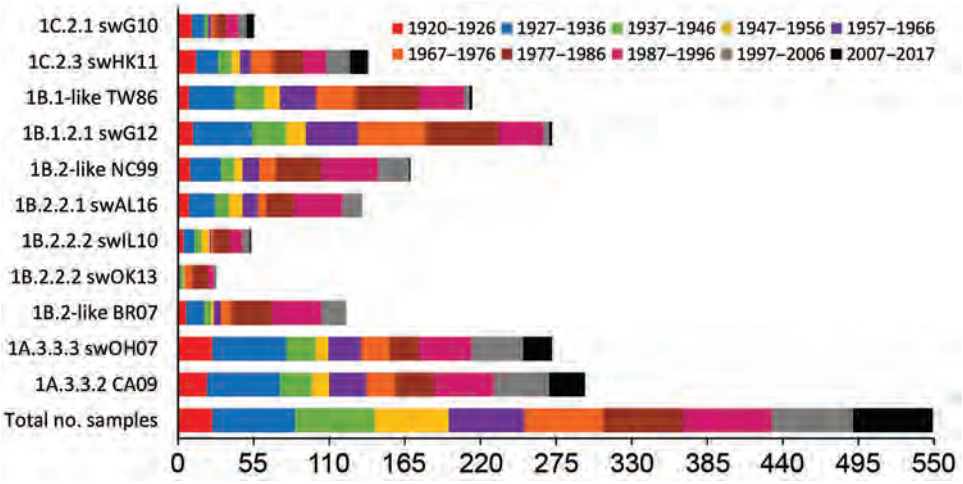

Figure 2. Number of positive human serum samples in the hemagglutination inhibition assay (titer ≥40) for each test virus compared with the total number of samples tested per birth cohort. Birth cohorts are represented as different colors. During August 2017–January 2018, a total of 549 serum samples were collected from immunocompetent persons in Belgium.

North American human-like δ H1 swIAVs (1B.2) result from the introduction of a human IAV in the early 2000s, and we selected NC99 as their presumed human ancestor. For the most prevalent δ1 clade (1B.2.2), swAL16 represents subclade δ1a (1B.2.2.1), whereas swIL10 and swOK13 represent subclade δ1b (1B.2.2.2).

Among samples, 24% tested positive for swAL16 in HI and 39% in VN (Figures 2, 3). Seroprevalences and GMTs were highest in those born during 1987–1996 in HI (55%; GMT 35) and in those born during 1947–1956 in VN (70%; GMT 59), but no antibodies against swAL16 were detected in the youngest group, those born during 2007–2017 (Tables 6, 7). Like for European human-like virus swG12 (1B.1.2.1), antibody responses against North American δ1a virus swAL16 (1B.2.2.1) resembled those against its presumed human ancestor virus, NC99.

For the δ1b swIAVs (1B.2.2.2), ≤10% were seropositive (swIL10, 10% in HI and VN; swOK13, 5% in HI and 4% in VN) (Figures 2, 3). We did not see statistically significant differences in seroprevalences between the 2 δ1b swIAVs or between age groups, with following exceptions. HI-seroprevalence of those born during 1927–1936 was statistically significantly higher for swIL10 (13%) than for swOK13 (2%; p<0.04). HI seroprevalence for swOK13 of those born during 1977–1986 was statistically significantly higher (21%) compared with groups born during 1927–1936 (2%), 1957–1966 (0), and 2007–2017 (0; p<0.04). GMTs were <20 in all age groups except those born during 1937–1956, who had VN GMTs of 22–30 against swIL10 (Tables 6, 7). Unlike the other 2 human-like swIAVs tested, responses against δ1b swIAVs (1B.2.2.2) did not concur with those against the presumed human ancestor virus NC99. Responses against swIL10 and swOK13 were generally statistically significantly lower than against NC99 (p<0.05).

Seroreactivity against swIAVs of the Classical Swine Lineage 1A

We used swOH07 as reference virus to evaluate antibody responses against classical swine virus clade γ

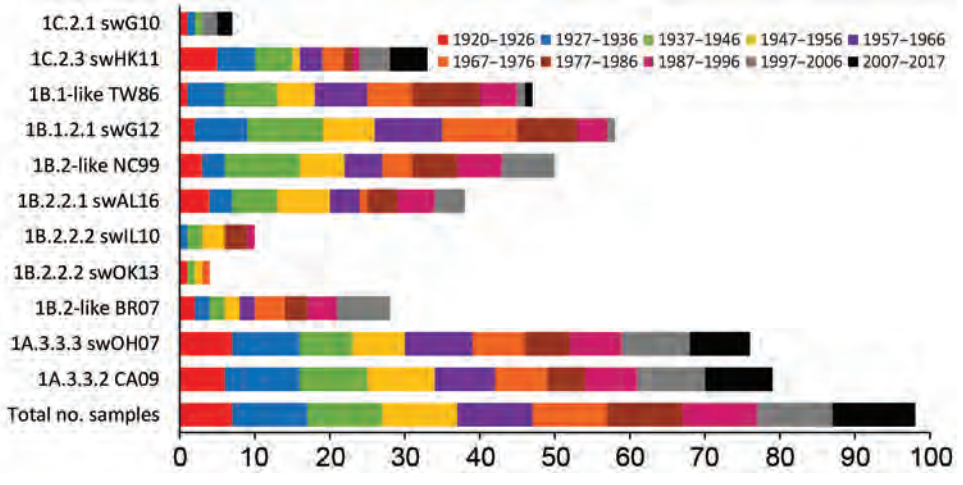

Figure 3. Number of positive human serum samples in the virus neutralization assay (titer ≥40) for each test virus compared with the total number of samples per birth cohort. Birth cohorts are represented as different colors. During August 2017–January 2018, a total of 549 serum samples were collected from immunocompetent persons in Belgium and pooled per year of birth (n = 98).

Table 6. Geometric mean of hemagglutination inhibition antibody reactivity against different H1 influenza A viruses of humans and swine in different age groups of the population, 2017–2018, Belgium*

Birth year range (age, y‡)	No.	Eurasian avian		Human seasonal							Classical swine	
		swG10 Eur. 1C.2.1	swHK11 Asia 1C.2.3	TW86† 1B.1-like	swG12 Eur. 1B.1.2.1	NC99† 1B.2-like	swAL16 N. Am. 1B.2.2.1	swIL10 N. Am. 1B.2.2.2	swOK13 N. Am. 1B.2.2.2	BR07† 1B.2-like	swOH07 N. Am. 1A.3.3.3	CA09 World 1A.3.3.2
1920–26 (91–97)	25	24 (16–38)	38 (24–60)	21 (15–31)	26 (18–39)	25 (18–35)	24 (17–35)	14 (11–17)	12 (10–16)	19 (14–28)	236 (147–379)	125 (70–222)
1927–36 (81–90)	60	15 (12–19	20 (16–26)	38 (29–51)	49 (39–61)	24 (20–28)	20 (17–24)	15 (13–18)	12 (11–13)	18 (15–20)	116 (87–155)	98 (73–132)
1937–46 (71–80)	58	12 (10–13)	15 (12–18)	26 (19–36)	30 (22–40)	16 (13–20)	14 (12–17)	12 (11–14)	12 (10–13)	12 (11–13)	23 (17–31)	28 (20–38)
1947–56 (61–70)	54	10 (10–11)	12 (11–14)	17 (13–23)	19 (15–25)	14 (12–17)	16 (13–20)	12 (11–14)	10 (10–11)	11 (10–13)	15 (12–19)	18 (14–23)
1957–66 (51–60)	55	11 (10–13)	14 (12–17)	31 (22–42)	55 (42–72)	17 (13–21)	16 (14–20)	11 (10–12)	11 (10–12)	13 (11–16)	25 (20–32)	32 (24–44)
1967–76 (41–50)	57	12 (11–14)	18 (14–23)	34 (26–44)	76 (60–97)	16 (13–20)	14 (12–16)	12 (10–13)	12 (11–14)	14 (12–17)	23 (18–29)	25 (19–33)
1977–86 (31–40)	58	14 (12–17)	25 (19–32)	97 (68–138)	87 (69–110)	42 (31–57)	22 (17–28)	17 (14–21)	18 (15–22)	29 (23–38)	27 (22–34)	39 (28–54)
1987–96 (21–30)	65	13 (11–16)	19 (16–23)	45 (32–65)	37 (28–50)	42 (32–54)	35 (28–44)	15 (12–17)	13 (12–15)	40 (31–52)	37 (28–48)	54 (39–74)
1997–2006 (11–20)	59	14 (12–17)	21 (17–27)	13 (11–15)	13 (11–15)	22 (18–28)	19 (15–23)	14 (12–16)	11 (10–12)	18 (15–23)	48 (35–66)	73 (49–109)
2007–17 (0–10)	58	13 (11–16)	18 (13–24)	11 (10–12)	11 (10–12)	10 (10–11)	10 (10–10)	11 (10–12)	10 (10–10)	10 (10–10)	24 (18–33)	35 (24–53)
All (0–97)	549	13 (13–14)	18 (17–20)	28 (25–31)	33 (30–36)	21 (19–23)	18 (17–19)	13 (13–14)	12 (12–12)	17 (16–18)	35 (31–38)	42 (37–47)

*Values expressed represent geometric mean hemagglutination inhibition titers (95% CI). Eur., Europe; N. Am., North America.
†Human IAV that no longer circulates; TW86 is the presumed human precursor for human-like H1 swine IAVs in Europe; NC99 is the presumed human precursor for human-like H1 swine IAVs in North America; BR07 is a human seasonal IAV that circulated right before the influenza A(H1N1)pdm09 virus; the influenza A(H1N1)pdm09 virus, represented by CA09, is circulating in both humans and swine worldwide.
‡Age at the end of 2017.

(1A.3.3.3) and CA09 as reference virus to evaluate classical swine virus clade pH1N1 (1A.3.3.2), which derived its HA from γ swIAVs. Overall, ≥50% of the samples tested positive for swOH07 (50% in HI; 78% in VN) and CA09 (54% in HI; 81% in VN), with high seroprevalences in all age groups (36%–100% in HI; 50%–100% in VN), except in those born during 1947–1956 in HI (swOH07, 17%; CA09, 24%) (Figures 2, 3). HI titers peaked in the 2 oldest groups, those born during 1920–1936; VN titers peaked in the 2 oldest groups and in those born during 1997–2006 (Tables 6, 7). No statistically significant difference was noted in responses against classical swine γ (1A.3.3.3) and pH1N1 (1A.3.3.2) IAVs.

Correlations Between Antibody Titers against Human Seasonal and Swine IAVs

Antibody titers against epidemiologically related human and swine IAVs were highly correlated for classical swine viruses swOH07 (1A.3.3.3) and CA09 (1A.3.3.2), European human-like swIAV swG12 (1B.1.2.1) and human ancestor IAV TW86, North American human-like δ1a swIAV swAL16 (1B.2.2.1) and human ancestor IAV NC99, and European and Asian avian-like swIAVs swG10 (1C.2.1) and swHK11 (1C.2.3) (CC = 0.68–0.86 in HI; CC = 0.63–0.77 in VN; Table 8). Of note, titers against avian-like and classical swine IAVs also were strongly correlated (CC = 0.55–0.68 in HI; CC = 0.49–0.67 in VN). In contrast, CCs were low between titers against North American human-like δ1b viruses swIL10 and swOK13 (1B.2.2.2) and human ancestor virus NC99 (0.42–0.43 in HI; 0.30–0.39 in VN [the first value of which is not statistically significant]).

Discussion

Our results show that serum antibody responses of immunocompetent persons in Belgium against

Table 7. Geometric mean of virus neutralization titers and antibody reactivity against different human and swine H1 influenza A viruses in different age groups of the population, 2017–2018, Belgium*

Birth year range (age, y‡)	Eurasian avian		Human seasonal							Classical swine	
	swG10 Europe 1C.2.1	swHK11 Asia 1C.2.3	TW86† 1B.1-like	swG12 Europe 1B.1.2.1	NC99† 1B.2-like	swAL16 N. Am. 1B.2.2.1	swIL10 N. Am. 1B.2.2.2	swOK13 N. Am. 1B.2.2.2	BR07† 1B.2-like	swOH07 N. Am. 1A.3.3.3	CA09 World 1A.3.3.2
1920–6 (91–97)	24 (8–68)	67 (24–187)	14 (8–25)	17 (9–33)	29 (13–65)	29 (13–62)	16 (9–28)	18 (11–32)	19 (10–37)	170 (54–533)	111 (49–254)
1927–36 (81–90)	13 (9–19)	34 (19–58)	38 (26–57)	57 (39–84)	27 (21–34)	26 (17–40)	14 (10–20)	19 (12–27)	20 (12–33)	93 (63–135)	101 (79–128)
1937–46 (71–80)	14 (8–23)	31 (18–54)	68 (39–118)	98 (64–149)	53 (41–68)	36 (23–55)	22 (13–35)	17 (11–26)	34 (23–50)	42 (25–69)	85 (55–133)
1947–56 (61–70)	11 (9–13)	19 (12–30)	29 (16–54)	59 (38–93)	36 (22–60)	59 (34–102)	30 (21–44)	18 (12–26)	19 (12–30)	47 (27–83)	73 (45–119)
1957–66 (51–60)	10 (10–10)	20 (13–32)	52 (37–72)	80 (51–124)	40 (28–58)	36 (25–53)	11 (9–13)	11 (9–13)	26 (14–47)	52 (40–67)	72 (45–116)
1967–76 (41–50)	11 (9–13)	23 (14–36)	41 (22–76)	109 (76–158)	27 (16–47)	16 (10–26)	11 (9–13)	13 (9–19)	24 (13–45)	40 (22–74)	38 (22–66)
1977–86 (31–40)	10 (10–10)	14 (9–21)	86 (55–137)	81 (47–138)	38 (22–65)	27 (15–48)	18 (11–30)	13 (10–17)	23 (14–37)	35 (19–65)	31 (16–60)
1987–96 (21–30)	10 (10–10)	15 (10–24)	41 (20–83)	34 (18–64)	46 (25–84)	43 (23–78)	13 (9–21)	11 (9–13)	35 (21–58)	46 (31–67)	47 (26–86)
1997–2006 (11–20)	15 (9–26)	31 (15–64	17 (10–27)	15 (10–22)	53 (29–99)	33 (20–55)	10 (10–10)	11 (9–14)	40 (23–70)	117 (54–256)	149 (58–379)
2007–17 (0–10)	18 (9–37)	37 (15–90)	11 (9–15)	12 (9–15)	11 (9–14)	10 (10–10)	10 (10–10)	10 (10–10)	10 (10–10)	70 (26–189)	88 (35–221)
All (0–97)	13 (11–14)	25 (21–31)	33 (28–40)	44 (36–54)	33 (28–39)	28 (24–33)	14 (13–16)	13 (12–15)	23 (20–27)	60 (50–73)	71 58–86)

*Values expressed represent geometric mean virus neutralization titers of pooled serum samples per birth year (95% CI).
N. Am., North America; Boldface indicates geometric mean VN titers of pooled serum samples per birth year.
†Human IAV that no longer circulates; TW86 is the presumed human precursor for human-like H1 swine IAVs in Europe; NC99 is the presumed human precursor for human-like H1 swine IAVs in North America; BR07 is a human seasonal IAV that circulated right before the influenza A(H1N1)pdm09 virus; the influenza A(H1N1)pdm09 virus, represented by CA09, is circulating in both humans and swine worldwide.
‡Age at the end of 2017.

major H1 swIAV clades depend on the swIAV tested and its relation to human seasonal IAVs and the person's birth year. Overall seroprevalences were high (≥50%) for classical swine (1A.3.3.2, 1A.3.3.3) and for European human-like (1B.1.2.1) swIAVs, intermediate (≥24%) for North American human-like δ1a (1B.2.2.1) and Asian avian-like (1C.2.3) swIAVs, and low (≤10%) for North American human-like δ1b (1B.2.2.2) and European avian-like (1C.2.1) swIAVs. Our results are consistent with previous studies that aimed to compare antibody responses in nonswine workers with those in persons with frequent swine contact (*7*,*20*–*25*), although those studies examined only a limited number of swIAV clades or samples. Overall, most previous studies showed lower seroprevalences for Asian avian-like (2%–10%) and European avian-like (0–5%) swIAVs in the general population or in nonswine workers (*13*,*20*,*22*–*24*). A 2010 study in the United Kingdom also found a lower seroprevalence of 11% for a European human-like (1B.1.2.1) swIAV (*24*). The major difference between our study and studies conducted before or during the 2009 pandemic is the lower seroprevalence of 3%–15% for classical swine IAVs in previous studies (*13*,*20*,*22*–*24*). The circulation of pH1N1 viruses (1A.3.3.2) likely contributes to increased seroprevalence rates against these related classical swine IAVs. In our study, the oldest group, those born during 1920–1926 who are 91–97 years of age, had the highest antibody responses against H1 swIAVs of classical swine (1A.3.3) and avian-like (1C.2) lineages, for which antibody titers were correlated (*13*,*20*,*21*). Responses against human seasonal IAVs and related European and North American δ1a human-like H1 swIAVs (1B) generally were highest in those born during 1977–1996, who are 21–40 years of age, and lowest in those born during 1996–2017, who are 0–20 years of age. Responses against North American δ1b human-like H1 swIAVs (1B.2.2.2) generally were low across all age cohorts.

Antibody responses against past human seasonal IAVs TW86, NC99, and BR07 generally peaked in persons born near the time during which the respective IAV or similar viruses circulated, whereas responses were low in most persons born after. Within an age group, responses generally were highest against an antigenic representative of the virus encountered first. These findings concur with the theory of antigenic seniority: humans are expected to

have antibodies against human seasonal IAVs that circulated after their birth, with highest responses against the virus encountered first. Antigenic seniority likely occurs because of periodic boosting of these antibodies by subsequent exposures to related human seasonal IAVs (*4*,*34*,*35*). Antibody titers against European human-like swIAV swG12 (1B.1.2.1) and North American human-like δ1a swIAV swAL16 (1B.2.2.1) concur with those against their respective human ancestor viruses TW86 and NC99 because of close antigenic relationship to their ancestor IAV. Overall high seroprevalences against pH1N1 virus CA09 (1A.3.3.2) and antigenically closely related classical swine γ virus swOH07 (1A.3.3.3) can be explained by recent exposure to currently circulating pH1N1 viruses. Because the oldest persons were born during 1920–1936, when human IAVs closely related to the 1918 pandemic virus, the ancestor of classical swine IAVs, circulated, they could have had cross-reactive antibodies against classical swine IAVs before 2009. These antibodies might have been boosted by later exposure to pH1N1 viruses, which might account for the high responses in this group (*6*,*7*). Consistent with results for serum samples collected after pH1N1 virus infection in a previous study (*21*), cross-reactivity was higher against the Asian than against the European avian-like H1 swIAV, which differ by only 1 aa in antigenic sites (Table 2). Whether this single amino acid mutation is the reason for the difference in seroprevalence is still unknown (*36*,*37*).

European human-like (1B.1.2.1) and North American human-like δ1a (1B.2.2.1) H1 swIAVs are antigenically more closely related to their human ancestor than North American human-like δ1b (1B.2.2.2) H1 swIAVs (Figure 1; Tables 3, 4). North American human-like δ H1 swIAVs (1B.2) have been shown to drift 4 times faster than European human-like H1 swIAVs (1B.1). Increased antigenic diversity of the former since 2008 has led to the emergence of swIAVs that are antigenically distinct from the human precursors, mainly within the δ1b subclade (*3*,*27*). This evolution can explain the recognition of selected European human-like and North American human-like δ1a but not North American human-like δ1b H1 swIAVs by human serum samples. Because the human ancestor IAVs no longer circulate in humans, swine can be considered a reservoir for old human IAVs. Seroprevalences for European human-like and North American human-like δ1a H1 swIAVs are expected to decrease over time because the youngest age groups were never exposed to these human IAVs. On the basis of our results, we estimate that it could take ≤80 years for the population to become fully susceptible.

Seroprevalences of immunocompetent persons in Belgium for swIAVs representing major H1 swIAV clades suggest that North American human-like δ1b (1B.2.2.2) and European avian-like (1C.2.1) H1 swIAVs currently pose the highest risk to public health. North American human-like δ1b (1B.2.2.2) swIAVs rapidly drifted away from its human ancestor, whereas European avian-like (1C.2.1) swIAVs never circulated in humans. Seroprevalences of ≤10% for these viruses are comparable to 2%–19% against the pH1N1 virus right before the pandemic (*7*). Our results suggest that the risk of reintroduction

Table 8. Spearman correlation coefficients between hemagglutination inhibition antibody titers against human and swine H1 influenza A viruses (upper right) and between virus neutralization antibody titers against human and swine H1 influenza A viruses (lower left)*

	Eurasian avian		Human seasonal							Classical swine	
	swG10	swHK11	TW86†	swG12	NC99†	swAL16	swIL10	swOK13	BR07†	swOH07	CA09
Virus strain	Europe 1C.2.1	Asia 1C.2.3	1B.1-like	Europe 1B.1.2.1	1B.2-like	N. Am. 1B.2.2.1	N. Am. 1B.2.2.2	N. Am. 1B.2.2.2	1B.2-like	N. Am. 1A.3.3.3	World 1A.3.3.2
swG10	–	0.68	NS	0.16	0.19	0.19	NS	0.26	0.18	0.56	0.55
swHK11	0.63	–	0.24	0.26	0.32	0.31	0.23	0.43	0.30	0.68	0.63
TW86	NS	NS	–	0.84	0.52	0.43	0.21	0.35	0.35	0.25	0.26
swG12	NS	NS	0.77	–	0.42	0.41	0.23	0.37	0.28	0.30	0.27
NC99	NS	NS	0.46	0.37	–	0.69	0.42	0.43	0.75	0.36	0.36
swAL16	NS	NS	NS	NS	0.71	–	0.53	0.38	0.58	0.43	0.39
swIL10	NS	NS	NS	0.37	0.39	0.52	–	0.37	0.45	0.30	0.26
swOK13	NS	NS	NS	NS	NS	NS	0.35	–	0.39	0.33	0.34
BR07	NS	NS	NS	NS	0.76	0.57	NS	NS	–	0.30	0.31
swOH07	0.55	0.67	NS	NS	NS	NS	NS	NS	NS	–	0.86
CA09	0.49	0.62	NS	NS	NS	NS	NS	NS	NS	0.74	–

*Viruses are ordered chronologically according to the year of circulation of the selected human test viruses TW86, NC99, BR07, and CA09; horizontal rules within table represent grouping of epidemiologically related human and swine influenza A viruses, with the oldest (ancestor) virus mentioned first. Complete isolate names are provided in Table 1. N. Am., North America; NS, not significant; –, not applicable.
†Human IAV that no longer circulates; TW86 is the presumed human precursor for human-like H1 swine IAVs in Europe; NC99 is the presumed human precursor for human-like H1 swine IAVs in North America; BR07 is a human seasonal IAV that circulated right before the influenza A(H1N1)pdm09 virus; the influenza A(H1N1)pdm09 virus, represented by CA09, is circulating in both humans and swine worldwide.

of these H1 swIAVs in the human population might be higher than for H3 swIAVs, given that ≥20% of persons 0–100 years of age from Luxembourg tested seropositive for representative European and North American cluster IV H3 swIAVs in 2010 (*19*). Seroprevalences against the other currently circulating human-like H1 swIAV clades were higher than against 1B.2.2.2 and 1C.2.1, but these viruses, along with H3 swIAVs, also keep evolving in swine. As they continue to drift away from their human ancestor and population immunity wanes with lack of exposure, these viruses might also pose a risk to public health soon.

We evaluated human population immunity against H1 swIAVs on the basis of serum HI and VN antibodies, which are directed against the highly variable head region of the HA. We did not measure antibodies or T-cell responses against the HA stalk, the neuraminidase, or internal viral proteins, such as the nucleoprotein. Although these immune mechanisms are much less potent than neutralizing anti-HA antibodies, their targets are more conserved between IAVs of humans and swine (*38*–*42*). Therefore, persons with minimal antibody titers in our study still might have some degree of immunity and protection against zoonotic infection with swIAVs. Furthermore, population immunity is only one aspect determining the pandemic potential of swIAVs (*18*). Another factor is their ability to spread in humans, which is difficult to investigate (*43*). Our results stress the need for continuous surveillance and characterization of circulating swIAVs and frequent monitoring of humans for antibodies against these swIAVs.

Acknowledgments

We thank Nele Dennequin, Melanie Bauwens, and Nathalie Vanderheijden for excellent technical assistance.

This study was financed by the project Evolution, Pathobiology and Pandemic Potential of Swine Influenza Viruses (EVAFLU) of the Belgian Federal Service for Public Health, Food Chain Safety and Environment (grant no. RF 16/6305).

About the Author

Ms. Vandoorn was a PhD student at the Laboratory of Virology, Faculty of Veterinary Medicine, Ghent University, during the study period. Her primary research interests are swine influenza A virus surveillance in Belgium and the Netherlands and broadly protective vaccination strategies for influenza A viruses.

References

1. de Jong JC, Smith DJ, Lapedes AS, Donatelli I, Campitelli L, Barigazzi G, et al. Antigenic and genetic evolution of swine influenza A (H3N2) viruses in Europe. J Virol. 2007;81:4315–22. https://doi.org/10.1128/JVI.02458-06
2. Furuse Y, Shimabukuro K, Odagiri T, Sawayama R, Okada T, Khandaker I, et al. Comparison of selection pressures on the HA gene of pandemic (2009) and seasonal human and swine influenza A H1 subtype viruses. Virology. 2010;405:314–21. https://doi.org/10.1016/j.virol.2010.06.018
3. Lewis NS, Russell CA, Langat P, Anderson TK, Berger K, Bielejec F, et al.; ESNIP3 consortium. The global antigenic diversity of swine influenza A viruses. eLife. 2016;5:e12217. https://doi.org/10.7554/eLife.12217
4. Fonville JM, Wilks SH, James SL, Fox A, Ventresca M, Aban M, et al. Antibody landscapes after influenza virus infection or vaccination. Science. 2014;346:996–1000. https://doi.org/10.1126/science.1256427
5. Smith GJD, Vijaykrishna D, Bahl J, Lycett SJ, Worobey M, Pybus OG, et al. Origins and evolutionary genomics of the 2009 swine-origin H1N1 influenza A epidemic. Nature. 2009;459:1122–5. https://doi.org/10.1038/nature08182
6. Skountzou I, Koutsonanos DG, Kim JH, Powers R, Satyabhama L, Masseoud F, et al. Immunity to pre-1950 H1N1 influenza viruses confers cross-protection against the pandemic swine-origin 2009 A (H1N1) influenza virus. J Immunol. 2010;185:1642–9. https://doi.org/10.4049/jimmunol.1000091
7. Broberg E, Nicoll A, Amato-Gauci A. Seroprevalence to influenza A(H1N1) 2009 virus—where are we? Clin Vaccine Immunol. 2011;18:1205–12. https://doi.org/10.1128/CVI.05072-11
8. Vincent A, Awada L, Brown I, Chen H, Claes F, Dauphin G, et al. Review of influenza A virus in swine worldwide: a call for increased surveillance and research. Zoonoses Public Health. 2014;61:4–17. https://doi.org/10.1111/zph.12049
9. Anderson TK, Macken CA, Lewis NS, Scheuermann RH, Van Reeth K, Brown IH, et al. A phylogeny-based global nomenclature system and automated annotation tool for H1 hemagglutinin genes from swine influenza A viruses. MSphere. 2016;1:e00275-16. https://doi.org/10.1128/mSphere.00275-16
10. Anderson TK, Campbell BA, Nelson MI, Lewis NS, Janas-Martindale A, Killian ML, et al. Characterization of co-circulating swine influenza A viruses in North America and the identification of a novel H1 genetic clade with antigenic significance. Virus Res. 2015;201:24–31. https://doi.org/10.1016/j.virusres.2015.02.009
11. Watson SJ, Langat P, Reid SM, Lam TT-Y, Cotten M, Kelly M, et al.; ESNIP3 Consortium. Molecular epidemiology and evolution of influenza viruses circulating within European swine between 2009 and 2013. J Virol. 2015;89:9920–31. https://doi.org/10.1128/JVI.00840-15
12. Yang H, Chen Y, Qiao C, He X, Zhou H, Sun Y, et al. Prevalence, genetics, and transmissibility in ferrets of Eurasian avian-like H1N1 swine influenza viruses. Proc Natl Acad Sci U S A. 2016;113:392–7. https://doi.org/10.1073/pnas.1522643113
13. Vijaykrishna D, Smith GJD, Pybus OG, Zhu H, Bhatt S, Poon LLM, et al. Long-term evolution and transmission dynamics of swine influenza A virus. Nature. 2011;473:519–22. https://doi.org/10.1038/nature10004
14. Khiabanian H, Trifonov V, Rabadan R. Reassortment patterns in swine influenza viruses. PLoS One. 2009;4:e7366. https://doi.org/10.1371/journal.pone.0007366

15. European Centre for Disease Prevention and Control. Risk assessment: Update—swine-origin triple reassortant influenza A(H3N2) variant viruses in North America, 17 August 2012. Stockholm: The Centre; 2012 [cited 2020 May 3] https://www.ecdc.europa.eu/sites/default/files/media/en/publications/publications/1208-ter-rapid-risk-assessment-influenza-ah3n2-us.pdf
16. US Centers for Disease Control and Prevention. Fluview [cited 2020 May 3]. https://gis.cdc.gov/grasp/fluview/Novel_Influenza.html
17. World Health Organization. Influenza monthly risk assessment summary [cited 2020 May 3]. https://www.who.int/influenza/human_animal_interface/HAI_Risk_Assessment
18. Trock SC, Burke SA, Cox NJ. Development of framework for assessing influenza virus pandemic risk. Emerg Infect Dis. 2015;21:1372–8. https://doi.org/10.3201/eid2108.141086
19. Qiu Y, Muller CP, Van Reeth K. Lower seroreactivity to European than to North American H3N2 swine influenza viruses in humans, Luxembourg, 2010. Euro Surveill. 2015;20:25–33. https://doi.org/10.2807/1560-7917.ES2015.20.13.21078
20. Gerloff NA, Kremer JR, Charpentier E, Sausy A, Olinger CM, Weicherding P, et al. Swine influenza virus antibodies in humans, western Europe, 2009. Emerg Infect Dis. 2011;17:403–11. https://doi.org/10.3201/eid1703.100851
21. Perera RAPM, Riley S, Ma SK, Zhu H-C, Guan Y, Peiris JSM. Seroconversion to pandemic (H1N1) 2009 virus and cross-reactive immunity to other swine influenza viruses. Emerg Infect Dis. 2011;17:1897–9. https://doi.org/10.3201/eid1710.110629
22. Hoschler K, Thompson C, Casas I, Ellis J, Galiano M, Andrews N, et al. Population susceptibility to North American and Eurasian swine influenza viruses in England, at three time points between 2004 and 2011. Euro Surveill. 2013;18:20578. https://doi.org/10.2807/1560-7917.ES2013.18.36.20578
23. Krumbholz A, Lange J, Dürrwald R, Walther M, Müller TH, Kühnel D, et al. Prevalence of antibodies to European porcine influenza viruses in humans living in high pig density areas of Germany. Med Microbiol Immunol (Berl). 2014;203:13–24. https://doi.org/10.1007/s00430-013-0309-y
24. Fragaszy E, Ishola DA, Brown IH, Enstone J, Nguyen-Van-Tam JS, Simons R, et al.; Flu Watch Group; Combating Swine Influenza (COSI) Consortium. Increased risk of A(H1N1)pdm09 influenza infection in UK pig industry workers compared to a general population cohort. Influenza Other Respir Viruses. 2016;10:291–300. https://doi.org/10.1111/irv.12364
25. Bravo-Vasquez N, Karlsson EA, Jimenez-Bluhm P, Meliopoulos V, Kaplan B, Marvin S, et al. Swine influenza virus (H1N2) characterization and transmission in ferrets, Chile. Emerg Infect Dis. 2017;23:241–51. https://doi.org/10.3201/eid2302.161374
26. Brown IH, Harris PA, McCauley JW, Alexander DJ. Multiple genetic reassortment of avian and human influenza A viruses in European pigs, resulting in the emergence of an H1N2 virus of novel genotype. J Gen Virol. 1998;79:2947–55. https://doi.org/10.1099/0022-1317-79-12-2947
27. Rajao DS, Anderson TK, Kitikoon P, Stratton J, Lewis NS, Vincent AL. Antigenic and genetic evolution of contemporary swine H1 influenza viruses in the United States. Virology. 2018;518:45–54. https://doi.org/10.1016/j.virol.2018.02.006
28. Kumar S, Stecher G, Tamura K. MEGA7: molecular evolutionary genetics analysis version 7.0 for bigger datasets. Mol Biol Evol. 2016;33:1870–4. https://doi.org/10.1093/molbev/msw054
29. Brownlee GG, Fodor E. The predicted antigenicity of the haemagglutinin of the 1918 Spanish influenza pandemic suggests an avian origin. Philos Trans R Soc Lond B Biol Sci. 2001;356:1871–6. https://doi.org/10.1098/rstb.2001.1001
30. R Core Team. R: a language and environment for statistical computing. Vienna: R Foundation for Statistical Computing; 2017 [cited 2019 Sep 7]. https://www.r-project.org
31. Peeters B, Reemers S, Dortmans J, de Vries E, de Jong M, van de Zande S, et al. Genetic versus antigenic differences among highly pathogenic H5N1 avian influenza A viruses: consequences for vaccine strain selection. Virology. 2017;503:83–93. https://doi.org/10.1016/j.virol.2017.01.012
32. World Health Organization. Manual for the laboratory diagnosis and virological surveillance of influenza. Geneva: The Organization;2011 [cited 2017 May 14]. https://apps.who.int/iris/bitstream/handle/10665/44518/9789241548090_eng.pdf
33. Van Reeth K, Gregory V, Hay A, Pensaert M. Protection against a European H1N2 swine influenza virus in pigs previously infected with H1N1 and/or H3N2 subtypes. Vaccine. 2003; 21:1375–81. https://doi.org/10.1016/S0264-410X(02)00688-6
34. Miller MS, Gardner TJ, Krammer F, Aguado LC, Tortorella D, Basler CF, et al. Neutralizing antibodies against previously encountered influenza virus strains increase over time: a longitudinal analysis. Sci Transl Med. 2013;5:198ra107. https://doi.org/10.1126/scitranslmed.3006637
35. Nachbagauer R, Choi A, Hirsh A, Margine I, Iida S, Barrera A, et al. Defining the antibody cross-reactome directed against the influenza virus surface glycoproteins. Nat Immunol. 2017;18:464–73. https://doi.org/10.1038/ni.3684
36. Koel BF, Burke DF, Bestebroer TM, van der Vliet S, Zondag GCM, Vervaet G, et al. Substitutions near the receptor binding site determine major antigenic change during influenza virus evolution. Science. 2013;342:976–9. https://doi.org/10.1126/science.1244730
37. Lewis NS, Anderson TK, Kitikoon P, Skepner E, Burke DF, Vincent AL. Substitutions near the hemagglutinin receptor-binding site determine the antigenic evolution of influenza A H3N2 viruses in U.S. swine. J Virol. 2014;88:4752–63. https://doi.org/10.1128/JVI.03805-13
38. Dormitzer PR, Galli G, Castellino F, Golding H, Khurana S, Del Giudice G, et al. Influenza vaccine immunology. Immunol Rev. 2011;239:167–77. https://doi.org/10.1111/j.1600-065X.2010.00974.x
39. Van Reeth K. The post-2009 influenza pandemic era: time to revisit antibody immunodominance. J Clin Invest. 2018;128:4751–4. https://doi.org/10.1172/JCI124151
40. Xing Z, Cardona CJ. Preexisting immunity to pandemic (H1N1) 2009. Emerg Infect Dis. 2009;15:1847–9. https://doi.org/10.3201/eid1511.090685
41. Krause JC, Crowe JE Jr. Committing the oldest sins in the newest kind of ways—antibodies targeting the influenza virus type A hemagglutinin globular head. Microbiol Spectr. 2014;2:AID-0021–2014. https://doi.org/10.1128/microbiolspec.AID-0021-2014
42. La Gruta NL, Turner SJ. T cell mediated immunity to influenza: mechanisms of viral control. Trends Immunol. 2014;35:396–402. https://doi.org/10.1016/j.it.2014.06.004
43. Reperant LA, Kuiken T, Osterhaus ADME. Adaptive pathways of zoonotic influenza viruses: from exposure to establishment in humans. Vaccine. 2012;30:4419–34. https://doi.org/10.1016/j.vaccine.2012.04.049

Address for correspondence: Kristien Van Reeth, Laboratory of Virology, Faculty of Veterinary Medicine, Ghent University, Salisburylaan 133, 9820 Merelbeke, Belgium; email: kristien.vanreeth@ugent.be

Incidence and Seroprevalence of Avian Influenza in a Cohort of Backyard Poultry Growers, Egypt, August 2015–March 2019

Mokhtar R. Gomaa,[1] Amira S. El Rifay,[1] Dina Abu Zeid, Mona A. Elabd, Eman Elabd, Ahmed Kandeil, Noura M. Abo Shama, Mina N. Kamel, Mohamed A. Marouf, Ahmed Barakat, Samir Refaey, Amal Naguib, Pamela P. McKenzie, Richard J. Webby, Mohamed A. Ali, Ghazi Kayali

Currently enzootic avian influenza H5N1, H9N2, and H5N8 viruses were introduced into poultry in Egypt in 2006, 2011, and 2016, respectively. Infections with H5N1 and H9N2 were reported among poultry-exposed humans. We followed 2,402 persons from households raising backyard poultry from 5 villages in Egypt during August 2015–March 2019. We collected demographic, exposure, and health condition data and annual serum samples from each participant and obtained swab samples from participants reporting influenza-like illness symptoms. We performed serologic and molecular analyses and detected 4 cases of infection with H5N1 and 3 cases with H9N2. We detected very low seroprevalence of H5N1 antibodies and no H5N8 antibodies among the cohort; up to 11% had H9 antibodies. None of the exposure, health status, or demographic variables were related to being seropositive. Our findings indicate that avian influenza remains a public health risk in Eqypt, but infections may go undetected because of their mild or asymptomatic nature.

For more than a decade, Egypt had endemic avian influenza viruses (AIVs) that infected humans and caused substantial economic losses in the poultry industry (*1*). Co-circulation of highly pathogenic avian influenza (HPAI) H5N1 and H5N8 viruses and low pathogenic avian influenza (LPAI) H9N2 viruses among poultry was observed (*2*). The widespread circulation of various AIV subtypes in domestic poultry resulted in evolutionary changes that affected several virus characteristics (*3*–*6*).

According to the World Health Organization, the number of confirmed human H5N1 cases in Egypt is 359, of which 120 were fatal (*7*). Those cases were detected by public health surveillance when the patients were admitted to hospitals with influenza-like illness (ILI) and had a history of poultry contact (*8*). However, this number is likely an underestimate because many patients might have mild symptoms or be asymptomatic and are less likely to seek medical care and therefore would not be tested or reported. Serologic testing might be a better tool in understanding the actual prevalence of disease because it can identify patients with mild or asymptomatic infections (*9*). A 3-year seroprevalence study showed that ≈2% of persons in Egypt exposed to poultry had been infected with H5N1 (*10*). This study demonstrated that the number of cases is underreported and that the case-fatality rate is consequently overestimated. Another study conducted in Beheira Governorate, located between the cities of Alexandria and Cairo and through which substantial transport between those 2 urban centers occurs, showed that the seroprevalence rate for H5 antibodies was 4% in poultry workers (*11*,*12*).

H9N2 viruses circulating in poultry in Egypt have human-like rather than avian-like receptor specificity (*6*). The clinical symptoms of H9N2 infection in humans are always mild, which complicates detection of human cases through hospital-based surveillance systems (*13*). Four laboratory-confirmed

Author affiliations: National Research Centre, Giza, Egypt (M.R. Gomaa, A.S. El Rifay, D. Abu Zeid, M.A. Elabd, E. Elabd, A. Kandeil, N.M. Abo Shama, M.N. Kamel, M.A. Marouf, M.A. Ali); Ain Shams University, Cairo, Egypt (A. Barakat); Ministry of Health and Population, Cairo (S. Refaey, A. Naguib); St. Jude Children's Research Hospital, Memphis, Tennessee, USA (P.P. McKenzie, R.J. Webby); Human Link, Hazmieh, Lebanon (G. Kayali); University of Texas Health Sciences Center at Houston, Houston, Texas, USA (G. Kayali)

DOI: https://doi.org/10.3201/eid2609.200266

[1]These authors contributed equally to this article.

human cases of H9N2 infection were reported to the World Health Organization from Egypt during March 2015–April 2016. Seroprevalence of H9N2 antibodies in persons in Egypt exposed to poultry were 5.6% and 7.5% during the first 2 years of introduction of H9N2 in Egypt (*10*).

Since 2017, several H5N8 outbreaks of clade 2.3.4.4 (group B) have been detected in domestic poultry in several governorates in Egypt (*2*,*14*). No human cases of H5N8 were reported in Egypt or elsewhere.

Serologic studies and hospital-based surveillance do not provide accurate estimates of incidence of avian influenza infections in exposed humans. Hence, we designed a household prospective cohort study to examine the incidence, human-to-human transmission, and prognosis of AIV infections among poultry-exposed growers in Egypt.

Methods

Study Design

Details of the study design and protocol were previously published (*15*). In brief, households raising backyard poultry were selected from 5 villages in 4 Nile Delta governorates (Sharkiya, Gharbiya, Kafr El Sheikh, and Qalyubiya) and Fayyoum Governorate starting in August 2015. Baseline enrollment was completed in March 2017. Follow-up period 1 occurred April 2017–March 2018, and follow-up period 2 occurred April 2018–March 2019. All persons within the household who were >2 years of age were invited to participate. Household data pertaining to raising poultry was collected. Individual demographic, poultry exposure, and health condition data were collected. At the baseline and follow-up period 1, a serum sample was collected from each participant.

As of April 2017, study staff were visiting enrolled households on a weekly basis to check whether any study participant was reporting ILI symptoms. ILI was defined as having fever of ≥38°C as well as cough, sore throat, or both. The frequency of household visits was increased to twice per week with the start of the influenza season, which typically occurs October–March in Egypt. When a study participant was verified to have ILI symptoms, a serum sample was collected, and nasal and an oropharyngeal swab specimens were obtained and tested by reverse transcription PCR (RT-PCR) for influenza A infection. If any of the samples tested positive for influenza A, the person was considered an index case-patient, and the study team obtained nasal and oropharyngeal swab specimens from the participant on days 3, 6, 9, and 14 after the first swab day and a serum sample on day 14. Furthermore, all previously enrolled participants residing with the index case-patient were swabbed according to the same sampling schedule.

Laboratory Methods

Reverse-genetics avian influenza viruses (rg A/chicken/Egypt/D10552B/2015 [clade 2.2.1.2 H5N1]) and (rgA/green-winged teal/Egypt/871/2016 [clade 2.3.4.4 H5N8] and A/chicken/Egypt/D10802C/2015 [G1-like H9N2]) were cultivated in 10 day-old, specific pathogen–free, embryonated chicken eggs and incubated for 48 h at 37°C, then chilled at 4°C for 4 h. The allantoic fluid was harvested, clarified, tested for the hemagglutinin (HA) gene and 50% tissue culture infective dose titer, and then frozen at -80°C until use.

Collected blood samples were kept on ice until they reached the laboratory on the same day. Serum was separated by centrifugation at 1,000 × *g*, aliquoted, and frozen at -20°C until use. Virus microneutralization assay was performed to test all collected serum samples for antibodies against the 3 AIVs (*16*). Chicken hyperimmune serum samples previously produced individually against the 3 viruses were used as positive controls and included in each assay. Neutralization capacity for each enrolled participant's serum sample of infected MDCK cells was tested for hemagglutination activity of viruses by using 0.5% chicken red blood cells (RBCs) in an HA gene assay. The absence of hemagglutination was considered a positive test result for antibodies to the virus. Virus microneutralization assay positivity was considered at an endpoint titer of ≥1:80. Seasonal influenza A/Brisbane/10/07(H3N2) and pandemic A/California/04/09(H1N1) viruses were used to determine seroprevalence antibodies against both viruses by a hemagglutination inhibition (HI) assay, using 0.5% turkey RBCs (17).

Molecular Detection

Nasal and oropharyngeal swabs were subjected to viral RNA extraction by using the QIAamp Viral RNA Mini Kit (QIAGEN, https://www.qiagen.com), followed by detection of influenza A infection by M gene RT-PCR (*17*). Influenza A–positive samples were subtyped with RT-PCR using subtype-specific primers for HA gene subtyping (*18*). As soon as a participant had a positive M gene RT-PCR result, they were informed and advised to seek medical care. Amplicons of the appropriate sizes of positive HA gene subtypes were subsequently gel-purified by using the QIAGEN Gel Extraction Kit and then delivered for sequencing at a sequencing facility in South Korea (Macrogen,

https://www.macrogen.com). Sequences were assembled by using SeqMan Lasergene 7 (DNASTAR, https://www.dnastar.com). Sequence alignments were performed by using BioEdit version 7.0 (https://www.biodeit.software.informer.com). The phylogenetic tree was constructed by using MEGA version 7 (https://www.megasoftware.net) by applying the neighbor-joining method with the Kimura 2-parameter substitution model and 1,000 bootstrap replicates.

Statistical Analyses

SPSS Stastistics 23 (IBM, https://www.ibm.com) was used for statistical analyses. Statistical differences between proportions were tested by using the Pearson's χ^2 test or Fisher exact test. The Student *t*-test was used to compare continuous variables. A p value $\leq$0.05 was considered statistically significant.

Ethical Considerations

This study was approved by the institutional review boards of Human Link and St. Jude Children's Research Hospital and by the Ethics Committee of the National Research Centre. Written informed consent was obtained from adults $\geq$18 years of age. Informed assent and parental approval were obtained for participants 14–17 years of age. Oral assent and parental approval were obtained for participants 7–13 years of age. Parental approval was obtained for participants 2–7 years of age.

Results

A total of 2,402 participants were enrolled from 390 households in the 5 study sites (Appendix Table, https://wwwnc.cdc.gov/EID/article/26/9/20-0266-App1.pdf). The median number of participants per household was 5 (range 1–20). Various domestic mammals and poultry were raised by the households, most frequently chickens and ducks. Approximately one third of the households raised pigeons and geese, whereas ≈12% raised turkeys (Table 1). Table 2 shows the distribution of poultry-raising practices followed by participants. Approximately 17% of households reported raising poultry within the household, whereas ≈53% kept the poultry on the roof and ≈30% in a barn. Dead poultry was disposed of by burying, discarding in a closed trash bag, or burning by 44% of the respondents, whereas 56% either dumped the carcasses in the open trash or in small water canals. Approximately 38% said that they would consult a veterinarian when they noticed ill poultry, and 14% said that they would isolate the ill birds from the rest of the flock. Approximately 33% of respondents said they would get rid of the sick bird while it was alive, whereas ≈12% said they would slaughter and eat it. One third of the respondents reported using avian influenza vaccines for their poultry, but only 1% of those were able to determine that the vaccine was used against H5N1 influenza virus, whereas the rest did not know what the vaccine was used against. Vaccination was mostly performed by a veterinarian (77%) or by a hired aid or a family member.

Table 1. Animals raised by enrolled households in a study of avian influenza among backyard poultry growers, Egypt, August 2015–March 2019

Animal	% Households	Median no. animals (range)
Chickens	91.3	15 (1–100)
Ducks	83.6	10 (1–700)
Pigeons	34.4	10 (1–100)
Geese	27	4 (1–20)
Donkeys	25.9	1 (1–3)
Buffaloes	25.6	2 (1–7)
Cows	24.6	1 (1–7)
Sheep	15.3	1 (1–30)
Goats	12.1	2 (1–30)
Turkeys	11.7	14 (1–15)
Dogs	8.2	2 (1–4)
Rabbits	7.8	5 (1–70)
Horses	5.8	1 (1–10)
Cats	2.5	7 (1–10)
Camels	0.01	1 (1–2)

Demographic and health data of the participants are summarized in Table 3. Respondents' age ranged from 2 to 102 years. The mean age was 25 years, and the median age was 21 years. The distribution of enrolled participants by sex, age (adults versus children), and marital status (single versus other) was almost the same. Most participants were uneducated

Table 2. Poultry-raising practices reported by participants in a study of avian influenza among backyard poultry growers, Egypt, August 2015–March 2019

Characteristic	No. (%)
Where do you keep the poultry?	
On the roof	1,267 (52.7)
In a barn	716 (29.8)
Inside the house	419 (17.4)
What do you do with poultry carcasses?	
Bury	255 (10.6)
Place in a closed bag and throw in the trash	728 (30.3)
Burn	83 (3.5)
Throw in the trash without a bag	652 (27.1)
Throw in a water stream without a bag	684 (28.5)
What do you do if you suspect sick poultry?	
Nothing	81 (3.4)
Set loose away from the house	791 (32.9)
Seek veterinary advice	909 (37.8)
Quarantine away from the rest of the flock	332 (13.8)
Slaughter and consume the meat	289 (12.0)
Do you vaccinate poultry against avian influenza?	
Yes	902 (37.6)
No	1,500 (62.4)
Who administers the vaccine?	
Family member	155 (17.1)
Veterinarian	698 (77.4)
Worker	49 (5.4)

or received only a primary education (68%), and 12% had a job as a skilled laborer or professional. Approximately 10% had chronic health problems, and ≈2% had long-term respiratory problems. Less than 10% reported currently using tobacco. Only 4 participants reported ever receiving the influenza vaccine.

The median number of days per week that the participants had direct contact with poultry was 6 days. The participants spent a median of 10 minutes per day in direct contact each time they came in direct exposure with the poultry. Table 4 summarizes the poultry exposure practices of the participants. More than 70% reported cleaning poultry cages or feeding poultry, whereas 30% reported not having any direct poultry exposure. Among those who had direct poultry exposure (cleaning or feeding), only 10% reported using a dedicated garment. Approximately one third of the participants reported slaughtering poultry. Slaughtered poultry were mostly kept in a dedicated barrel to bleed (80%), but 20% of respondents left that to occur in the open. Most of the respondents cleaned the used utensils after slaughtering, mostly by using soap and water. Slaughter waste was disposed in closed bags and thrown into the trash (46% of respondents), thrown in open trash (25%), or dumped into small canals (29%).

Table 3. Demographic and health data of participants in a study of avian influenza among backyard poultry growers, Egypt, August 2015–March 2019

Characteristic	No. (%)*
Age group, y	
2–6	381 (15.9)
7–14	552 (23.0)
15–17	142 (5.9)
≥18	1,322 (55.2)
Sex	
F	1,317 (54.9)
M	1,080 (45.1)
Educational level	
Not educated	822 (34.3)
Elementary	800 (33.4)
Intermediate	448 (18.7)
Vocational	35 (1.5)
Secondary	95 (4.0)
College	116 (4.8)
Graduate degree	78 (3.3)
Marital status	
Divorced	8 (0.3)
Married	1,048 (43.7)
Single, never married	1,232 (51.4)
Widowed	109 (4.5)
Occupation	
Toddler	339 (14.2)
Student	783 (32.8)
Housewife	698 (29.2)
Unskilled labor or unemployed	282 (11.8)
Skilled labor or professional	287 (12.0)
Chronic disease	
Yes	250 (10.4)
No	2,147 (89.6)
Long-term breathing problems	
Yes	45 (1.9)
No	2,340 (98.1)
Current tobacco user	
Yes	203 (8.6)
No	2,164 (90.3)
Ever received the influenza vaccine	
Yes	4 (0.2)
No	2,377 (99.8)

*Totals do not add up to 2,402 for all characteristics because of missing data.

Serologic findings at baseline and follow-up period 1 (2017–2018) are shown in Table 5. Serum samples were successfully collected from 2,397 persons at baseline and from 2,051 at follow-up period 1. Seroprevalence of H1N1 antibodies was ≈30% and of H3N2 antibodies was ≈50%. At baseline, 9 (0.4%) participants had H5N1 antibodies. Four participants had a titer of 1:80, and 5 had a titer of 1:160. Of the 9 participants, 7 came from 2 adjacent homes. At follow-up period 1, only 4 (0.2%) participants were seropositive for H5N1 antibodies, 3 with 1:80 titers and 1 with a 1:160 titer. None of the participants who were seropositive at baseline remained seropositive at follow-up period 1. At baseline, 266 (11%) participants had H9N2 antibodies. Of these, the 227 had 1:80 titers, 37 had 1:160 titers, and 2 had 1:320 titers. Household clusters of seropositive persons were observed for 223 participants, with cluster sizes ranging from 2 to 10 participants. At follow-up period 1, only 3 (0.1%) participants had H9N2 antibodies. All participants had a 1:80 titer and were from the same household, and only 1 of these participants was positive at baseline with the same titer. No participants had H5N8 antibodies at baseline or follow-up period 1.

During follow-up period 1, a total of 400 participants (16.7% of the cohort) were confirmed to have ILI symptoms. Of these, 113 were positive for influenza A by RT-PCR (28% of those with ILI and 4.7% of cohort overall). Four case-patients were subtyped as infected with H5N1 virus by RT-PCR and confirmed by sequencing. The incidence of H5N1 infection in this cohort of 2,402 persons was 17 cases/10,000 exposed persons. Phylogenetic analysis revealed that the viruses causing the infection were of clade 2.2.1.2, which are unique to and endemic in Egypt.

The first case was in a 5-year-old boy with exposure to poultry at the household and at a live bird market. Only the swabs obtained on day 1 of the illness were positive for H5N1. The serum sample titer obtained on day 1 was <1:10, whereas a titer of 1:40 was detected on day 14. The boy's symptoms included fever, cough, sore throat, myalgia, malaise, headache, runny nose, and diarrhea. Fever persisted for 4 days; cough and sore throat continued to occur throughout

the 14-day follow-up period. No household contacts showed symptoms, virus shedding, or seroconversion.

Case 2 was in an 11-year-old girl with direct contact with chickens and ducks. Only the swabs obtained on day 1 of the illness were positive for H5N1. The girl's serum sample titers were <1:10. Symptoms included fever, cough, sore throat, malaise, headache, and runny nose. Fever and sore throat persisted for 2 days; all other symptoms cleared by the fourth day. No household contacts showed symptoms, virus shedding, or seroconversion.

Case 3 was in a 5-year-old boy with direct contact with chickens and ducks. Swabs continued to be positive up to day 9 of sampling. The boy's serum sample titers were <1:10. Symptoms included fever, cough, sore throat, malaise, headache, diarrhea, myalgia, and runny nose. Fever and cough persisted until day 9; all other symptoms were clear by the fourth day. No household contacts showed symptoms, virus shedding, or seroconversion.

Case 4 was in a 27-year-old woman who had direct contact with chickens and ducks. Swabs continued to be positive up to day 9 of sampling. The woman's serum sample titers were <1:10. Symptoms included fever, cough, sore throat, malaise, headache, myalgia, and runny nose. Sore throat and cough persisted until day 12; all other symptoms were clear by the fourth day. No household contacts showed symptoms, virus shedding, or seroconversion.

During follow-up period 2, a total of 2,189 participants remained in the study, compared with 2,402 who participated in follow-up period 1. Of these, 740 (33.8%) participants were confirmed to have ILI symptoms, of whom 158 were positive for influenza A by RT-PCR (21% of those with ILI and 7.2% of the cohort overall). Four case-patients were infected with H9N2 and 1 with H5N1 virus according to RT-PCR results, which were confirmed by sequencing. The incidence of H9N2 infection was 18 cases/10,000 exposed persons. Incidence of H5N1 was 5 cases/10,000 exposed persons. Phylogenetic analysis revealed that the H9N2 viruses causing the infection were G1-like viruses (Appendix Figure 1), similar to viruses circulating in poultry in Egypt, whereas the H5N1 viruses were of clade 2.2.1.2 (Appendix Figure 2).

The H5N1 case was in a 10-year-old girl with direct contact with chickens and ducks. Swabs were

Table 4. Poultry exposure data of participants in a study of avian influenza among backyard poultry growers, Egypt, August 2015–March 2019

Characteristic	No. (%)*
What is the type of exposure you have with poultry?	
Cleaning area where poultry is kept	671 (28.0)
Feeding poultry	366 (15.3)
Only walk through area where poultry is kept	300 (12.5)
Play in area where poultry is kept	347 (14.5)
Do you usually slaughter poultry?	
Yes	694 (31.3)
No	1,526 (68.7)
Use of personal protective equipment while slaughtering poultry	
Yes (apron, boots, dedicated garment, face mask, gloves)	75 (10.8)
No	619 (89.2)
Where is slaughtered poultry kept to bleed?	
In a dedicated barrel	553 (79.6)
In a sink	45 (6.5)
On the floor inside the house	49 (7.1)
On the floor outside the house	47 (6.8)
Are tools cleaned after slaughtering?	
Yes	684 (98.6)
No	10 (1.4)
How are tools cleaned?	
Water only	103 (14.8)
Soap and water	539 (77.7)
Disinfectant	52 (7.5)
Use of personal protective equipment while defeathering poultry	
Yes (apron, boots, dedicated garment, face mask, gloves)	54 (7.8)
No	640 (92.2)
Method of disposing slaughtering waste	
Place in a closed bag and throw in the trash	299 (45.7)
Feed to other animals	1 (0.2)
Throw in the trash without a bag	163 (24.9)
Throw in a water stream without a bag	191 (29.2)

*Totals do not add up to 2,402 for all characteristics because of missing data or structure of the question.

Table 5. Seroprevalence of antibodies against influenza A virus subtypes H5N1, H5N8, H9N2, H1N1, and H3N2 in participants in a study of avian influenza among backyard poultry growers, Egypt, August 2015–March 2019

Period and influenza virus subtype	No. (%)
Baseline period, August 2015–March 2017	
H5N1 positive	9 (0.4)
H5N1 negative	2,388 (99.6)
H5N8 positive	0
H5N8 negative	2,397 (100.0)
H9N2 positive	266 (11.1)
H9N2 negative	2,131 (88.9)
H1N1 positive	656 (29.5)
H1N1 negative	1,569 (70.5)
H3N2 positive	1,115 (49.3)
H3N2 negative	1,148 (50.7)
Follow-up period 1, April 2017–March 2018	
H5N1 positive	4 (0.2)
H5N1 negative	2,046 (99.8)
H5N8 positive	0
H5N8 negative	2,046 (100.0)
H9N2 positive	3 (0.1)
H9N2 negative	2,043 (99.9)
H1N1 positive	612 (29.8)
H1N1 negative	1,439 (70.2)
H3N2 positive	1,034 (50.5)
H3N2 negative	1,015 (49.5)

*Totals do not add up to 2,402 at baseline period or 2,189 at follow-up period 1 because of missed serum sample collection or insufficient sample volume.

positive on day 1 only. The girl's serum sample titers were <1:10. Symptoms included fever, cough, sore throat, and myalgia. Sore throat and cough persisted until day 12; all other symptoms were clear by the fourth day. Two household contacts showed symptoms but were negative for H5, virus shedding, or seroconversion.

The first H9N2 case was in a 64-year-old woman with direct contact with chickens and ducks. Swabs were positive up to day 5 of sampling. The woman's serum sample titers were <1:10. Symptoms included fever, cough, sore throat, diarrhea, runny nose, and myalgia, all of which persisted up to 8 days. No household contacts showed symptoms, virus shedding, or seroconversion.

The second H9N2 case was in an 8-year-old girl with direct contact with chickens and ducks. Swabs were positive up to day 5 of sampling. The girl's serum sample titers were <1:10. Symptoms included fever, cough, sore throat, runny nose, and myalgia, all of which persisted up to 5 days except for coughing, which continued for 3 more days. No household contacts showed symptoms, virus shedding, or seroconversion.

The third H9N2 case was in a 15-year-old boy with direct contact with chickens and ducks. Swabs were positive up to day 5 of sampling. The boy's serum sample titers were <1:10. Symptoms included fever, cough, sore throat, runny nose, and myalgia, all of which persisted up to 10 days. No household contacts showed symptoms, virus shedding, or seroconversion.

The fourth H9N2 case was in a 13-year-old girl. This case was detected 3 days after follow-up of another H3N2-positive case-patient in her household. Of the 5 members in her household, 4 had low-grade fever. H9N2 was detected in nasal and oral swab specimens from the case-patient, and the remaining household contacts were either negative or had H3N2 infection. The case-patient had low-grade fever, sore throat, runny nose, malaise, and breathing difficulty up to 6 days after detection.

Discussion

We conducted a large prospective household cohort study of AIV infections among persons exposed to backyard poultry in Egypt. Our study design solved several problems that were noted by other similar studies (*19*,*20*). The larger sample size provided enough statistical power to detect the rare event of detecting active infection with AIVs. Following the households closely enabled us to detect those cases and document case-patients' shedding, symptoms, and seroconversion. This approach also enabled us to verify whether human-to-human transmission was occurring.

Our epidemiologic findings confirm that backyard poultry raising practices have low to no biosecurity measures; these practices included keeping poultry within the household, disposing dead poultry in the open trash or water streams, and letting ill poultry loose. Growers did not frequently use personal protective equipment while exposed to poultry. Few of them reported using dedicated garments while tending to poultry, even though this measure was a main recommendation of previous educational campaigns. Similarly, only 10% of participants who reported slaughtering poultry (the riskiest behavior because of the aerosols generated [*21*]) used any personal protective equipment. Reviewing, revising, and updating health education and awareness campaigns based on scientific evidence might assist in decreasing the incidence of infection with AIVs in Egypt (*21*).

Very low seroprevalence of H5N1 antibodies was detected, whereas up to 11% of the participants had H9 antibodies, possibly because during the study period H5N1 infection was rare in poultry but H9N2 infection was common (*2*). Another explanation for the low level of seroprevalence noted, especially against H5N1, is that some sampling was conducted over summer months, when avian influenza activity is low. Further explanation might include waning antibody titers or lack of seroconversion.

None of the participants had H5N8 antibodies, even though these viruses are not uncommon in poultry in Egypt. In the United States, humans who were exposed to birds infected with clade 2.3.4.4 H5 viruses did not show any acute respiratory symptoms (*22*). Viruses of this clade might not be transmitting efficiently from birds to humans because they have limited capacity for replication and transmission in mammals and mammalian cell lines (*23*).

None of the exposure, health status, or demographic variables we collected were associated with being seropositive. This finding might indicate that being seropositive is related to factors not collected in this study, such as host genetic factors or other behaviors.

Our study had enough power to detect active infection with AIVs. Human infections with H5N1 and H9N2 but not H5N8 were detected. Egypt had previously reported human cases of H5N1 and H9N2 infection; human infection with H5N8 has not been reported. Incidence of infection with any avian influenza virus was 5–18 cases/10,000 poultry-exposed persons, meaning that the number of reported cases is much lower than the number of infections that actually occur. This occurrence can be explained by the fact that none of the case-patients we detected died or required hospitalization, which would make them easily missed by hospital- or clinic-based surveillance. Although the number of reported cases might be underestimated, the reported case-fatality rates are overestimated because of the mild and asymptomatic cases that were missed.

The reported symptoms were similar to symptoms of infection with seasonal influenza viruses. All case-patients had fever, cough, sore throat, and myalgia. Malaise and diarrhea occurred in a few cases. Most case-patients used over-the-counter antipyretic or anti-inflammatory drugs to treat their symptoms. Shedding duration ranged from 1 to 9 days, but no human-to-human transmission was detected, meaning that exposure to viruses that infected the poultry remains the source of human infection. Because of delays in confirming avian influenza in study participants, we were not able to obtain samples from poultry at the time when the participant was ill. Sampling poultry at the same time of sampling humans would have provided better information on how poultry infections correlate with human infections. The exact routes of transmission from poultry to humans, whether direct contact or aerosol, remain to be determined. Observing or documenting behaviors through surveys does not pinpoint transmission routes; hence, future studies should consider measuring individual exposure by using virologic methods, such as determining presence of virus on surfaces or in the air to which humans are exposed, especially in household settings, similar to what has been done in live bird market settings (*24*–*28*).

Serologic and virologic findings were not correlated, especially for H9N2 infections. In follow-up period 1, no cases of H9N2 were detected, yet 11% of the participants had antibodies. In follow-up period 2, cases were detected, but seroprevalence was almost negligible. These findings indicate that relying on serologic tests alone to estimate disease incidence might be misleading, given that many case-patients do not seroconvert, as we found in this study.

In conclusion, backyard poultry growers in Egypt continue to be infected with AIVs that are enzootic in their poultry. To eliminate human cases, poultry infections should be controlled and growers' awareness increased to decrease the adverse effects of substandard poultry-raising practices.

This work was funded by the National Institute of Allergy and Infectious Diseases, National Institutes of Health, US Department of Health and Human Services (contract no. HHSN272201400006C), and supported by an internal fund from Human Link.

About the Author

Mr. Gomaa is a PhD student in microbiology and Dr. El Rifay is an assistant professor at the National Research Centre in Cairo. Their interests are studying the incidence and prevalence of avian influenza and other emerging zoonotic viruses. They are also interested in conducting surveillance for these viruses at the human–animal interface.

References

1. Aly MM, Arafa A, Hassan MK. Epidemiological findings of outbreaks of disease caused by highly pathogenic H5N1 avian influenza virus in poultry in Egypt during 2006. Avian Dis. 2008;52:269–77. https://doi.org/10.1637/8166-103007-Reg.1
2. Kandeil A, Hicks JT, Young SG, El Taweel AN, Kayed AS, Moatasim Y, et al. Active surveillance and genetic evolution of avian influenza viruses in Egypt, 2016–2018. Emerg Microbes Infect. 2019;8:1370–82. https://doi.org/10.1080/22221751.2019.1663712
3. Cattoli G, Milani A, Temperton N, Zecchin B, Buratin A, Molesti E, et al. Antigenic drift in H5N1 avian influenza virus in poultry is driven by mutations in major antigenic sites of the hemagglutinin molecule analogous to those for human influenza virus. J Virol. 2011;85:8718–24. https://doi.org/10.1128/JVI.02403-10
4. El-Shesheny R, Kandeil A, Bagato O, Maatouq AM, Moatasim Y, Rubrum A, et al. Molecular characterization of avian influenza H5N1 virus in Egypt and the emergence

of a novel endemic subclade. J Gen Virol. 2014;95:1444–63. https://doi.org/10.1099/vir.0.063495-0
5. Kandeil A, El-Shesheny R, Maatouq AM, Moatasim Y, Shehata MM, Bagato O, et al. Genetic and antigenic evolution of H9N2 avian influenza viruses circulating in Egypt between 2011 and 2013. Arch Virol. 2014;159:2861–76. https://doi.org/10.1007/s00705-014-2118-z
6. Kandeil A, El-Shesheny R, Maatouq A, Moatasim Y, Cai Z, McKenzie P, et al. Novel reassortant H9N2 viruses in pigeons and evidence for antigenic diversity of H9N2 viruses isolated from quails in Egypt. J Gen Virol. 2017;98:548–62. https://doi.org/10.1099/jgv.0.000657
7. World Health Organization. Cumulative number of confirmed human cases for avian influenza A(H5N1) reported to WHO, 2003–2019. 2019 [cited 2020 Feb 6]. https://www.who.int/influenza/human_animal_interface/2019_11_25_tableH5N1.pdf
8. Refaey S, Azziz-Baumgartner E, Amin MM, Fahim M, Roguski K, Elaziz HA, et al. Increased number of human cases of influenza virus A(H5N1) infection, Egypt, 2014–15. Emerg Infect Dis. 2015;21:2171–3. https://doi.org/10.3201/eid2112.150885
9. Zhang AJX, To KKW, Tse H, Chan K-H, Guo K-Y, Li C, et al. High incidence of severe influenza among individuals over 50 years of age. Clin Vaccine Immunol. 2011;18:1918–24. https://doi.org/10.1128/CVI.05357-11
10. Gomaa MR, Kayed AS, Elabd MA, Zeid DA, Zaki SA, El Rifay AS, et al. Avian influenza A(H5N1) and A(H9N2) seroprevalence and risk factors for infection among Egyptians: a prospective, controlled seroepidemiological study. J Infect Dis. 2015;211:1399–407. https://doi.org/10.1093/infdis/jiu529
11. Samaha H, Ibrahim MS, Ayoub M, Shaaban SI. Seroepidemiology of avian influenza viruses H5 and H9 in Beheira Governorate. Alex J Vet Sci. 2015;44:86–92. https://doi.org/10.5455/ajvs.161061
12. Young SG, Kitchen A, Kayali G, Carrel M. Unlocking pandemic potential: prevalence and spatial patterns of key substitutions in avian influenza H5N1 in Egyptian isolates. BMC Infect Dis. 2018;18:314. https://doi.org/10.1186/s12879-018-3222-6
13. Pusch EA, Suarez DL. The multifaceted zoonotic risk of H9N2 avian influenza. Vet Sci. 2018;5:E82. https://doi.org/10.3390/vetsci5040082
14. World Organization for Animal Health (OIE). Update on avian influenza in animals 2017 [cited 2020 Feb 6]. https://www.oie.int/en/animal-health-in-the-world/update-on-avian-influenza/2017
15. El Rifay AS, Elabd MA, Abu Zeid D, Gomaa MR, Tang L, McKenzie PP, et al. Household transmission of zoonotic influenza viruses in a cohort of Egyptian poultry growers. JMIR Res Protoc. 2015;4:e74. https://doi.org/10.2196/resprot.4331
16. World Health Organization. Serological diagnosis of influenza by microneutralization assay. 2010 [cited 2020 Feb 6]. https://www.who.int/influenza/gisrs_laboratory/2010_12_06_serological_diagnosis_of_influenza_by_microneutralization_assay.pdf
17. World Health Organization. WHO manual on animal influenza diagnosis and surveillance. 2002 [cited 2020 Feb 6]. https://www.who.int/csr/resources/publications/influenza/whocdscsrncs20025rev.pdf
18. Lee MS, Chang PC, Shien JH, Cheng MC, Shieh HK. Identification and subtyping of avian influenza viruses by reverse transcription-PCR. J Virol Methods. 2001;97:13–22. https://doi.org/10.1016/S0166-0934(01)00301-9
19. Khurelbaatar N, Krueger WS, Heil GL, Darmaa B, Ulziimaa D, Tserennorov D, et al. Little evidence of avian or equine influenza virus infection among a cohort of Mongolian adults with animal exposures, 2010–2011. PLoS One. 2014;9:e85616. https://doi.org/10.1371/journal.pone.0085616
20. Krueger WS, Khuntirat B, Yoon IK, Blair PJ, Chittagarnpitch M, Putnam SD, et al. Prospective study of avian influenza virus infections among rural Thai villagers. PLoS One. 2013;8:e72196. https://doi.org/10.1371/journal.pone.0072196
21. Bertran K, Clark A, Swayne DE. Mitigation strategies to reduce the generation and transmission of airborne highly pathogenic avian influenza virus particles during processing of infected poultry. Int J Hyg Environ Health. 2018;221:893–900. https://doi.org/10.1016/j.ijheh.2018.05.013
22. Arriola CS, Nelson DI, Deliberto TJ, Blanton L, Kniss K, Levine MZ, et al.; H5 Investigation Group. Infection risk for persons exposed to highly pathogenic avian influenza A H5 virus-infected birds, United States, December 2014–March 2015. Emerg Infect Dis. 2015;21:2135–40. https://doi.org/10.3201/eid2112.150904
23. Kaplan BS, Russier M, Jeevan T, Marathe B, Govorkova EA, Russell CJ, et al. Novel highly pathogenic avian A(H5N2) and A(H5N8) influenza viruses of clade 2.3.4.4 from North America have limited capacity for replication and transmission in mammals. MSphere. 2016;1:e00003–00016. https://doi.org/10.1128/mSphere.00003-16
24. Bertran K, Balzli C, Kwon Y-K, Tumpey TM, Clark A, Swayne DE. Airborne transmission of highly pathogenic influenza virus during processing of infected poultry. Emerg Infect Dis. 2017;23:1806–14. https://doi.org/10.3201/eid2311.170672
25. Indriani R, Samaan G, Gultom A, Loth L, Irianti S, Adjid R, et al. Environmental sampling for avian influenza virus A (H5N1) in live-bird markets, Indonesia. Emerg Infect Dis. 2010;16:1889–95. https://doi.org/10.3201/eid1612.100402
26. Kang M, He J, Song T, Rutherford S, Wu J, Lin J, et al. Environmental sampling for avian influenza A(H7N9) in live-poultry markets in Guangdong, China. PLoS One. 2015;10:e0126335. https://doi.org/10.1371/journal.pone.0126335
27. Zhou J, Wu J, Zeng X, Huang G, Zou L, Song Y, et al. Isolation of H5N6, H7N9 and H9N2 avian influenza A viruses from air sampled at live poultry markets in China, 2014 and 2015. Euro Surveill. 2016;21:30331. https://doi.org/10.2807/1560-7917.ES.2016.21.35.30331
28. Wu Y, Lin J, Yang S, Xie Y, Wang M, Chen X, et al. The molecular characteristics of avian influenza viruses (H9N2) derived from air samples in live poultry markets. Infect Genet Evol. 2018;60:191–6. https://doi.org/10.1016/j.meegid.2018.01.009

Address for correspondence: Ghazi Kayali, Camelia 2 Building, Said Freiha St, Hazmieh, Baabda, Lebanon; email: ghazi@human-link.org; Mohamed A. Ali, El Buhouth St, Dokki, Giza 12311, Egypt; email: mohamed.ali@human-link.org

Risk-Based Estimate of Human Fungal Disease Burden, China

Ling-Hong Zhou,[1] Ying-Kui Jiang,[1] Ruo-Yu Li, Li-Ping Huang, Ching-Wan Yip, David W. Denning,[2] Li-Ping Zhu[2]

We conducted a systematic literature review to obtain risk population–based fungal disease incidence or prevalence data from China. Data were categorized by risk factors and extrapolated by using most recent demographic figures. A total of 71,316,101 cases (5.0% of the population) were attributed to 12 risk factors and 17 fungal diseases. Excluding recurrent *Candida* vaginitis (4,057/100,000 women) and onychomycosis (2,600/100,000 persons), aspergillosis (317/100,000 persons) was the most common problem; prevalence exceeded that in most other countries. Cryptococcal meningitis, an opportunistic infection, occurs in immunocompetent persons almost twice as often as AIDS. The pattern of fungal infections also varies geographically; *Talaromyces marneffei* is distributed mainly in the Pearl River Basin, and the Yangtze River bears the greatest histoplasmosis burden. New host populations, new endemic patterns, and high fungal burdens in China, which caused a huge impact on public health, underscore the urgent need for building diagnostic and therapeutic capacity.

Fungal diseases constitute a growing problem worldwide, causing a large, but poorly quantified, impact on public health (*1*). The incidence of fungal infections varies according to geographic region, socioeconomic conditions, and the number of persons with underlying conditions. China is one of the largest countries in the world (largest population and third largest land area). It has almost every type of weather niche, from the Pacific coast in the south to the snowy mountains in the Qinghai–Tibet Plateau, and even tropical rain forest. Many endemic fungal infections are present in China, along with globally distributed fungal pathogens. Although China has become the world's second largest economy, it is still a developing country, with millions of impoverished citizens who are susceptible to fungal infections. Fungal keratitis, one of the major causes of avoidable blindness, has been relatively neglected (*2*). Moreover, old pathogens such as *Histoplasma* and *Talaromyces marneffei* (talaromycosis) have expanded (*3,4*); new hosts contributing to new therapies for malignant and autoimmune disease have increased (*5,6*); and new patterns, including aspergillosis in pulmonary tuberculosis (PTB) and chronic obstructive pulmonary disease (COPD), are emerging (*7,8*). In addition, the lack of effective drugs, shortages of well-trained medical care personnel, and unaffordable antifungal drugs result in severe outcomes. Therefore, an estimation of fungal disease burden is needed for China to increase public health awareness and facilitate effective interventions.

As in most other countries, fungal infections are not reportable in China, and the incidence and prevalence are difficult to calculate because of the lack of population-based surveillance data and few high quality epidemiology studies. The Chinese National Fungal Diseases Surveillance System (http://www.chifungi.cn) was established on May 18, 2019, but no data have been released yet. Even with this dearth of data, we have attempted to estimate the burden of fungal disease in China.

Materials and Methods

Study Procedures

We conducted a literature review for published epidemiology papers that discussed fungal infections in China. If no epidemiological data existed for a particular fungal disease, we estimated the burden based on fungal infection incidence or prevalence and the specific populations at risk (Figure 1; Appendix Table 1, https://wwwnc.cdc.gov/EID/article/26/9/20-0016-App1.pdf).

Author affiliations: Huashan Hospital, Shanghai, China; and Fudan University, Shanghai (L.-H. Zhou, Y.-K. Jiang, L.-P. Huang, C.-W. Yip, L.-P. Zhu); Peking University First Hospital, Beijing, China (R.-Y. Li); Peking University, Beijing (R.-Y. Li); National Clinical Research Center for Skin and Immune Diseases, Beijing (R.-Y. Li); Wythenshawe Hospital, Manchester, UK (D.W. Denning); University of Manchester, Manchester (D.W. Denning); Global Action Fund for Fungal Infections, Geneva, Switzerland (D.W. Denning)

DOI: https://doi.org/10.3201/eid2609.200016

[2]These authors contributed equally to this article.

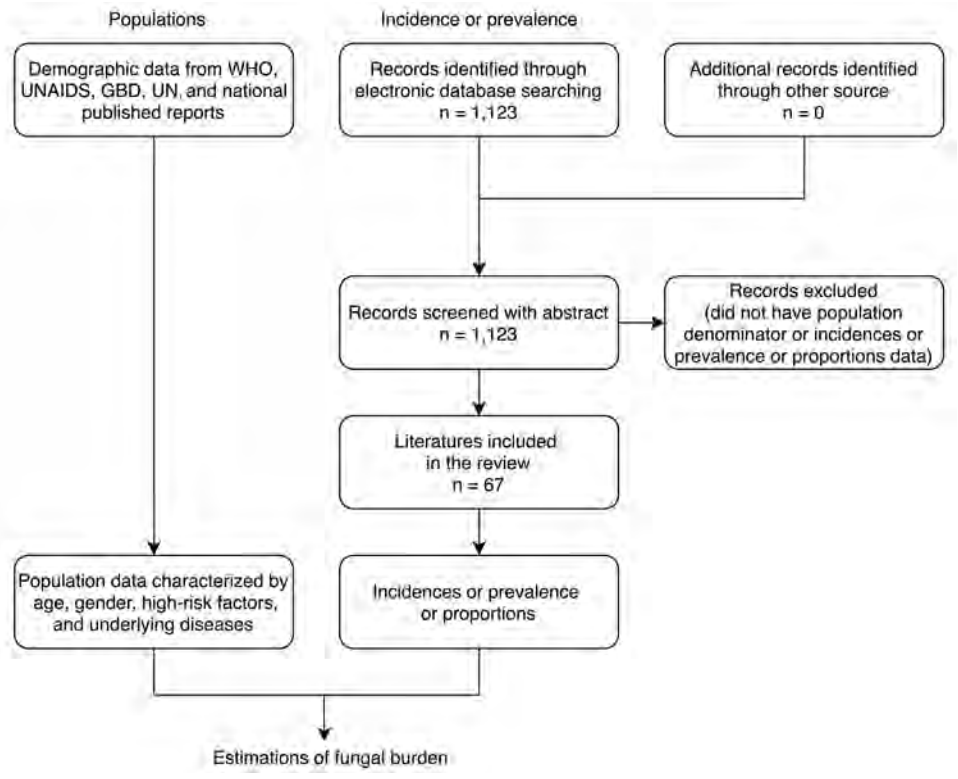

Figure 1. Flowchart of literature review for the human fungal disease burden in China. Reports published in English during January 1950–October 2019 were searched. GBD, Global Burden of Disease, Injuries, and Risk Factors Study; UNAIDS, the Joint Nations Program on HIV/AIDS; UN, United Nations Population Division; WHO, World Health Organization.

High-Risk Population Data

We obtained population statistics, including China's total, child, and female populations 14–49 years of age, from the United Nations Population Division (*9*). We derived data on HIV/AIDS in China from the Joint Nations Program on HIV/AIDS (UNAIDS) (*10*); we used the same source to calculate the proportion of HIV patients on antiretroviral therapy (ART). We consulted the World Health Organization (WHO) tuberculosis report to obtain data on tuberculosis patients; we assumed that 5.6% of these patients died (*11*). The numbers of lung cancer and hematological malignancy cases were derived from Global Cancer Observatory (GLOBOCAN) reports (*5*); data related to transplant recipients were derived from China Organ Transplantation Registration System (COTR) (*12*). For other high-risk populations, we extracted data from relevant published reports (Table 1).

Selection of Studies for Incidence or Prevalence Data

We conducted a systematic literature review and identified published epidemiology papers. We searched Web of Science, PubMed, and Embase databases for all the eligible studies published during January 1, 1950–October 7, 2019. Studies selected for this analysis were published in English; we included population-based incidence studies, population-based surveillance systems, and national investigation data. If no available incidence or prevalence data from China were found, we considered published global or international data. All search strings are listed in Appendix Table 2 and studies contributing to estimates for each fungal disease are listed in Appendix Table 3. All the assumptions and calculations for different fungal diseases are detailed in Table 2.

Analysis of Data

Candidiasis Burden Estimations

We estimated burdens of invasive candidiasis, *Candida* peritonitis, *Candida* peritonitis as a complication of chronic ambulatory peritoneal dialysis (CAPD), and recurrent vulvovaginal candidiasis (RVVC). To estimate invasive candidiasis, we first assessed candidemia incidence in intensive care units (ICUs). Because ≈20% of candidemia episodes in Asia occur in ICUs (*19*), we used these data to estimate annual incidence for all units. We then estimated *Candida* peritonitis by assuming that there were 2 episodes of candidemia per episode of intraabdominal candidiasis in the ICU, based on a large prospective study (*20*). In addition, we estimated *Candida* peritonitis in CAPD using data from the First Affiliated Teaching Hospital in Tianjin (*21*). For RVVC, when

Table 1. Population characteristics in China, by age, gender, high-risk factors, and underlying diseases*

Population characteristic	No., in thousands	Reference
Total population	1,433,784	UN, 2019 (*9*)
Population of children 0–14 y	254,930	UN, 2020 (*9*)
Female population, 15–49 y	403,377	UN, 2020 (*9*)
Population >40 y	688,074	UN, 2020 (*9*)
People living with HIV	810	UNAIDS, 2017 (*10*)
Proportion of HIV patients on ART	40%	UNAIDS, 2017 (*10*)
Adults living with HIV and CD4 <200 cells/μL	106	Assumes a 5-y decline in immunity
AIDS related deaths	26	UNAIDS, 2017 (*10*)
Annual cases of TB	856	WHO 2017 (*11*)
Annual cases of pulmonary TB who survive	844	WHO 2017 (*11*)
Adults with asthma (4.2%) population	49,512	Huang, 2019 (*13*)
Adults with COPD (7.2% of population)	102,377	Zhu, 2018 (*14*)
Adults with COPD admitted to hospital each year (20.1%)	29,382	Zhu, 2018 (*14*)
Lung cancer	774.3	GLOBOCAN, 2018 (*1*)
Liver transplants per year	4.73	COTR (*12*)
Renal transplants per year	10.8	COTR (*12*)
Lung transplants per year	0.3	COTR (*12*)
Heart transplants per year	0.56	COTR (*12*)
Allogeneic stem cell transplants per year	5.0	Xu, 2016 (*15*)
Acute myelogenous leukemia	41.2	40% of GLOBOCAN leukemia and multiple myeloma total, 2018 (*1*)
No. patients on peritoneal dialysis	73.9	Wilkie and Davies, 2017 (*16*)
Intensive care unit beds	86.0	Murthy, 2012 (*17*)
Intensive care admissions surviving >24 h	5,126	Du, 2013 (*18*)

*ART, antiretroviral therapy; COPD, chronic obstructive pulmonary disease; COTR, China Organ Transplantation Registration System; TB, tuberculosis; UN, United Nations Population Division; UNAIDS, the Joint Nations Program on HIV/AIDS; WHO, World Health Organization.

prevalence data were not available, we used the rate of women with RVVC from a recent global estimate (*22*). We assumed that esophageal candidiasis occurred in 20% of patients with HIV who were not on ART and 5% of those taking ART annually (*23*). Oral candidiasis was estimated only in patients with HIV; we assumed that it occurs in 45% of patients with AIDS annually (*24*).

Aspergillosis Burden Estimations

We calculated burdens of invasive aspergillosis (IA), chronic pulmonary aspergillosis (CPA), allergic bronchopulmonary aspergillosis (ABPA), and severe asthma with fungal sensitization (SAFS). We estimated the annual incidence of IA in hematological malignancy, solid and hematopoietic stem cell transplant (HSCT) recipients, lung cancer, COPD, and deaths from AIDS. We estimated that acute myeloid leukemia accounted for 40% of the annual incidence of all leukemias and multiple myeloma in 2018 (*5*). We took the rate of IA of 13% in hematological malignancy from a study from Taiwan (*25*), where mold-active prophylaxis was not given, and an equal number of cases were seen in all other leukemia and lymphoma cases. Among allogeneic HSCT recipients, we assumed an IA rate of 10% and rates in solid organ transplant recipients of 2% (renal), 6% (heart), 4% (liver), and 20% (lung) (*23*). For patients with lung cancer, we used a rate of 2.6% from a large study from China (*26*). To estimate the annual incidence of IA in patients with COPD, we used a recent study in Guangzhou Province, which found that the rate of IA in hospitalized patients with COPD was 3.9% (*27*). The annual hospitalization rate was a mean of 20.9%, and the number of patients with COPD came from a systematic review (*28*), from which we estimated the hospitalized patients with COPD. Although this information was not reported from China, we assumed a 4% autopsy incidence of IA in patients with AIDS (*29*).

We used the WHO 2017 figures for PTB to calculate CPA (*11*). We calculated CPA incidence after PTB based on our previous estimate, assuming that 22% of patients are left with a pulmonary cavity and that 22% of these patients develop CPA each year, as did 2% of those without a cavity (*30*). This calculation derives an annual incidence of CPA, which we converted to a 5-year period prevalence by assuming a 15% annual death or surgical resection rate. Given that PTB is one of several underlying causes of CPA, we conservatively assumed that PTB was primarily responsible for 33% of all CPA cases (*31*).

The reported rate of asthma in adults in China has increased from 1.42% in 2012 to 4.2% in 2019 (*13*). Ma et al. ascertained that 2.5% of these patients had ABPA (in secondary care) (*32*). Severe asthma proportion of adult asthmatics was estimated at 10%, as in other country estimates (*23*). We used a conservative fungal sensitization rate of 33% (as in other countries) to estimate the number of SAFS (*23*). No estimation

was made about cystic fibrosis in China because few patients currently survive to adulthood.

HIV-Related Infection Burden Estimation

We estimated burdens of cryptococcal meningitis (CM), *Pneumocystis* pneumonia (PCP), talaromycosis, and histoplasmosis. We ignored other HIV-related infections because of the lack of population-based data. We derived data for patients with AIDS from those who had a 5-year decline in CD4 counts to <200 cells/mL in the total population of HIV patients. We estimated the annual incidence of CM at 8% in patients with AIDS (CD4 count

Table 2. Assumptions and calculations for the estimations of fungal disease burden, China*

Fungal diseases†	Assumptions	Calculations
Candidemia	1. Candidemia episodes in ICU = (ICU beds × 365/median length of ICU stay) × (rate of candidemia in ICU/1,000 admissions) 2. 20% of candidemia episodes in Asia occur in ICU	Candidemia = Candidemia episodes in ICU/0.20
Candida peritonitis	Rate of *Candida* peritonitis is 50% of cases of candidemia in ICU	*Candida* peritonitis = candidemia in ICU × 50%
Candida peritonitis CAPD	1. 3.7% were *Candida* peritonitis in all episodes of infection 2. Overall infection incidence was 0.27 episodes/patient/year	*Candida* peritonitis CAPD = peritoneal dialysis × 0.27 × 3.7%
Oral candidiasis	Assumed to occur in 45% of AIDS cases annually	Oral candidiasis = AIDS × 45%
Esophageal candidiasis	Assumed to occur in 20% of HIV patients not on ART and 5% of patients taking ART annually	Esophageal candidiasis = (0.2 × HIV patients not on ART) + (0.05 × HIV patients on ART)
RVVC	Assumed to occur in 7.2% of the female population 15–49 years of age	RVVC = (female population 15–49) × 7.2%
IA	1. In hematologic malignancy, annual incidence of all leukemias and multiple myeloma × 40% × 13% a. Acute myeloid leukemia estimated at 40% of annual incidence of leukemias and multiple myeloma b. 13% of patients with acute myeloid leukemia developed IA 2. IA in solid and HSCT recipients: assumed 10% in a-HSCT recipients, 2% of renal transplants, 6% of heart transplants, 4% of liver transplants, 20% of lung transplants 3. IA in 2.6% of patients with lung cancer 4. IA in COPD: COPD patients × 20.9% × 3.9% a. Annual hospitalization rate for COPD = 20.9% b. 3.9% of hospitalized COPD patients developed IA 5. IA in 4% of HIV/AIDS patients	IA = IA in hematologic malignancy + IA in solid and HSCT recipients + IA in lung cancer patients + IA in COPD patients + IA in HIV/AIDS patients
CPA	1. TB-related CPA: assuming rate of 22% among patients with lung cavities, 2% of patients without cavities 2. 22% of patients with pulmonary TB have residual lung cavities 3. One third of underlying diseases of CPA are TB	Total CPA = TB-related CPA × 3
ABPA	1. 4.2% of adults in China have asthma 2. 2.5% of adults with asthma have ABPA	ABPA = adults with asthma × 2.5%
SAFS	1. Assume a conservative 33% rate of fungal sensitization in patients with severe asthma 2. 10% of adults with asthma have severe asthma	SAFS = adult population × 33% × 10%
CM	1. 7.1% of patients with HIV/AIDS 2. HIV-related CM is 21% of total CM 3. Annual incidence of 0.43/100,000 in children	CM = (7.1% × HIV/AIDS patients / 21%) + 0.43/100,000 × child population
PCP	1. 22.4% of HIV-positive patients during a 2y period 2. HIV-related PCP is 70.22% of total PCP	PCP = 22.4% × HIV/AIDS patients / 2 / 70.22%
Talaromycosis	Assume 20% of AIDS patients geographically exposed, attack rate 15%	Talaromycosis = HIV/AIDS patients × 20% × 15%
Histoplasmosis	Assume 67% of AIDS patients geographically exposed, attack rate 5%	Histoplasmosis = HIV/AIDS patients × 5% × 67%
Mucormycosis	Assume prevalence is 0.2/100,000 in total population	Mucormycosis = total population × 0.2/100,000
Fungal keratitis	0.007% of total population	Fungal keratitis = total population × 0.007%
Onychomycosis	2.6% of total population	Onychomycosis = total population × 2.6%

*ABPA, allergic bronchopulmonary aspergillosis; ART, antiretroviral therapy; CAPD, continuous ambulatory peritoneal dialysis; CM, cryptococcal meningitis; CPA, chronic pulmonary aspergillosis; HSCT, hematopoietic stem cell transplant: IA, invasive aspergillosis; ICU, intensive care unit; PCP, pneumocystis pneumonia; RVVC, recurrent *Candida* vaginitis; SAFS, severe asthma with fungal sensitization.

†Example for reading the table: burden of candidemia = candidemia episodes in ICU / 0.20 = (ICU beds × 365 / median length stay in ICU) × (rate of candidemia in ICU/1000 admissions) /0.20 = (86,027 × 365 / 6.126) × (3.2 / 1000) / 0.20 = 82,011.

<200 cells/mL) (*33*) and estimated the overall CM annual incidence based on the assumption that the proportion of HIV-positive patients with CM was 21% (*34*). In children, 23 cases of CM were diagnosed over a 5-year period (2007–2012) in Shijiazhuang, giving an annual incidence of 0.43/100,000 (*35*). We conservatively estimated the 2-year incidence of PCP at 22% of patients with AIDS (*36*), which comprises 70% of total cases (*37*). Only 20% of the HIV population was assumed to be geographically at risk for infection with *T. marneffei*; the attack rate was 15% in patients with AIDS (*3*). Disseminated histoplasmosis was assumed to occur in 5% of the geographically exposed population (estimated at 67%) of patients with AIDS (*4*).

Mucormycosis, Fungal Keratitis, and Onychomycosis Burden Estimation

Mucormycosis is a rare fungal infection; the prevalence rate is 0.2–140.0/1 million population (*38*). We used a global prevalence rate (2.0/1 million population) to estimate the burden. To estimate the burden of fungal keratitis, which is usually caused by *Fusarium* spp. and *Aspergillus* spp. in China, we used the overall prevalence of 0.007% according to a multicenter study (*2*). We used the global prevalence rate (2.6%) from 11 population-based studies to estimate the onychomycosis burden (*39*).

Epidemiology Maps

For talaromycosis and histoplasmosis, which showed new endemic trends, we prepared epidemiology maps according to the number of reported cases in China. We searched the PubMed database for articles published in China during January 1, 1950–October 7, 2019. Reports published in English were included. Search strings and references contributing to the talaromycosis map are listed in Appendix Table 4, and those contributing to the histoplasmosis map are listed in Appendix Table 5.

Prediction of HIV-Related Invasive Fungal Burden

We made a simple prediction model to estimate the HIV-related fungal burden by 2050. We derived the prediction data for total population in the next 50 years from UN data (*40*), and we collected data on HIV and AIDS cases during 2012–2017 to make a linear regression model to predict the number of HIV cases in 2050. If early testing and ART are at the current level, we estimate that 20.4% of HIV patients will develop advanced HIV disease over time (*10*). Based on our assumptions, we also predicted the burdens of invasive fungal diseases, including CM, PCP, and talaromycosis.

Results

Population Profiles

According to the UN data, the population of China was ≈1.4 billion in 2019, of whom 18% were children; 688 million adults were >40 years of age, of whom 403 million were women 15–49 years of age (*9*). The current total number of reported HIV infections in China is 810,000, and there were 26,000 AIDS-related deaths in 2017. Thus, 784,000 persons were living with HIV in China in 2019, of whom 60% were not receiving ART and 165,018 had AIDS (CD4 <200) (*10*). The detailed population characteristics and high-risk populations are described in Table 1.

Candidiasis Burden

The overall fungal burden in China, according to major risk factors, is summarized in Table 3. In 2012, there were an estimated 86,027 intensive care beds, in China and the rate of candidemia in ICU was documented at 3.2/1000 ICU admissions. The median length of stay in the ICU in China is 6.1 days. Thus, there are 16,402 candidemia episodes in the ICU, and we estimated a total of 82,011 episodes of candidemia per year in all units. Although *C. albicans* remains the most common species associated with candidiasis in ICU patients, other non–*albicans Candida* (NAC) is becoming increasingly common, and patients with NAC usually have longer antifungal therapy, longer ICU or hospital stay, and slightly higher death rates (*41*).

We also estimated 8,201 cases of postsurgical *Candida* peritonitis (intraabdominal candidiasis) by making the assumption that the rate of *Candida* peritonitis is 50% of cases of candidemia in the ICU. Given that there were 73,871 patients on CAPD in China in 2017, we estimated 738 peritonitis cases by using the *Candida* peritonitis episode rate of 0.01/patient-year.

Except for cutaneous disease, recurrent *Candida* vaginitis is the most common fungal disease, with aspergillosis, including IA, CPA, ABPA, and SAFS, next (Figure 2). We used the base case of RVVC prevalence in adult premenopausal women (15–49 years of age) previously published: 29,082,000 (range 21,812,000–36,353,000) affected women (*22*). In addition, 74,258 cases of oral candidiasis and 49,240 cases of esophageal candidiasis were expected annually in patients with HIV.

Aspergillosis Burden

We obtained an estimate of 1,178,747 cases of IA (82.1/100,000 population). We estimated 32,840 cases in immunocompromised patients and those

Table 3. Summary of fungal infection burden in China according to major risk factors*

Infection	No. infections per underlying disorder per year					Total no. cases	Rate/100,000 population
	None	HIV/AIDS	Respiratory	Cancer	ICU		
Candidemia	NE	NE	NE	65,609	16,402	82,011	5.72
Candida peritonitis							
ICU + surgery	NE	NE	NE	NE	8,939	8,939	0.62
CAPD	738	NE	NE	NE	NE	738	0.05
Oral candidiasis	NE	74,258	NE	NE	NE	74,258	5.18
Esophageal candidiasis	NE	49,204	NE	NE	NE	49,204	3.43
Recurrent *Candida* vaginitis	29,082,000	NE	NE	NE	NE	29,082,000	4,056.68†
IA	NE	1,040	1,145,908	31,800	NE	1,178,748	82.21
CPA	NE	NE	488,716	NE	NE	488,716	34.09
ABPA	NE	NE	1,237,797	NE	NE	1,237,797	86.33
SAFS	NE	NE	1,633,892	NE	NE	1,633,892	113.96
CM	26,249	13,086	NE	26,172	NE	65,607	4.57
PCP	NE	18,482	NE	9,241	NE	27,723	1.93
Talaromycosis	NE	4,951	NE	NE	NE	4,951	0.35
Mucormycosis	2,868	NE	NE	NE	NE	2,868	0.20
Fungal keratitis	100,365	NE	NE	NE	NE	100,365	7.00
Onychomycosis	37,278,384	NE	NE	NE	NE	37,278,384	2,600.00
Total burden	66,490,604	161,021	4,506,313	132,822	25,341	71,316,101	7,002.32

*ABPA, allergic bronchopulmonary aspergillosis; ART, antiretroviral therapy; CAPD, continuous ambulatory peritoneal dialysis; CM, cryptococcal meningitis; CPA, chronic pulmonary aspergillosis; IA, invasive aspergillosis; ICU, intensive care unit; NE, no estimation could be made because of the lack of data; PCP, pneumocystis pneumonia; SAFS, severe asthma with fungal sensitization.
†Female population only.

with cancer; of these, 20,000 were in patients with lung cancer and 1,040 in patients with AIDS. The remainder of IA cases in this immunocompromised group were in patients with hematologic malignancies, lymphoma, and transplants. We also calculated 1,145,908 IA cases derived from COPD.

In China, there were 844,500 survivors of tuberculosis in 2017 (*11*). We expect an annual incidence of 51,683 cases of tuberculosis-related CPA, and we estimated a 5-year period prevalence of 162,905 cases. Because tuberculosis probably comprises only one third of underlying CPA, the total period prevalence estimate is 488,716 cases (34/100,000 population).

Nearly 50 million adults with asthma live in China; of these, 10% have severe asthma. Regarding ABPA, the assumption is that 2.5% of adult asthmatics are affected, leading to a prevalence of 1,237,797 cases. Among patients with severe asthma, we estimate that 1.6 million have SAFS.

Burdens of HIV-Related Infections

CM occurs mainly in immunocompromised populations other than HIV patients in China, as well as in immunocompetent individuals. We thus obtained an estimate of adult CM: 13,086 in patients with AIDS and 26,172 each in immunocompromised and in immunocompetent persons. For CM in children, we estimated 77 cases annually, with an annual incidence of 0.43/100,000 population. We calculated a total of 65,507 CM cases.

We estimated the number of patients with PCP in China as 27,723 (18,482 with HIV and 9,241 with other immunocompromised conditions). This estimate implies an annual incidence of 1.93/100,000 population.

We estimated 4,951 talaromycosis cases in patients with AIDS in southern China. From the literature review, we identified 3,163 cases from 12 different provinces. The provinces with the highest prevalence are Guangxi and Guangdong, which each reported >1,000 cases (Figure 3, panel A). Both provinces are located in Pearl River Basin, possibly indicating an endemic trend.

We identified 380 histoplasmosis cases in China from the literature review (Figure 3, panel B). Most of the cases were reported in the region where the Yangtze River flows, also suggesting a new endemic pattern in China. Disseminated histoplasmosis in patients with AIDS was assumed to affect 5,528 persons annually, but we were unable to estimate the burden in non–HIV-infected persons or the burden of chronic pulmonary histoplasmosis. For the prediction of HIV-related invasive fungal burden by 2050, using annual data from 2012–2017 and extrapolating with our estimates, we expect 86,303 cases of PCP, 61,105 cases of CM, and 23,117 cases of *T. marneffei* infection (Figure 4).

Mucormycosis, Fungal Keratitis, and Onychomycosis Burden

We estimated mucormycosis using the global prevalence rate and calculated 2,868 cases. We estimated fungal keratitis based on the total population and estimated 100,365 cases of fungal keratitis annually in China. We estimated 37,278,384 cases of onychomycosis using the global data.

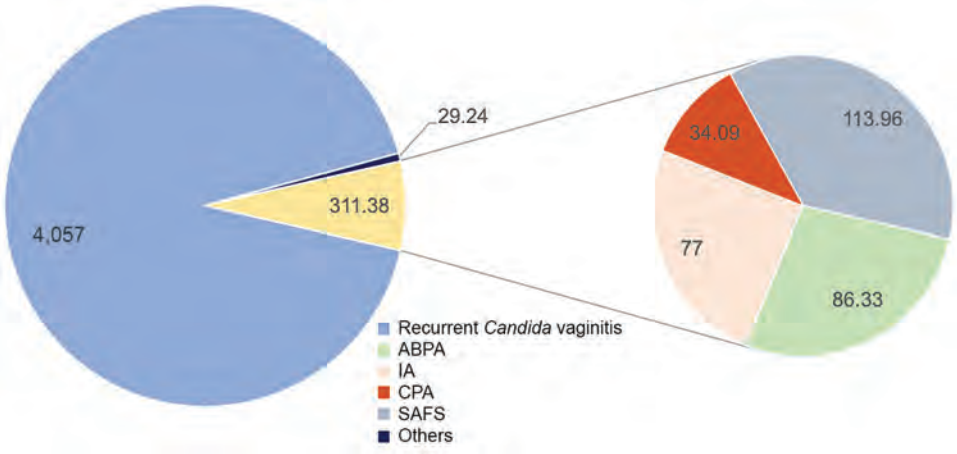

Figure 2. Estimated annual incidence (cases/100,000 population) of common fungal diseases in China. ABPA, allergic bronchopulmonary aspergillosis; CPA, chronic pulmonary aspergillosis; IA, invasive aspergillosis; SAFS, severe asthma with fungal sensitization.

Discussion

In this study, we estimated that 71 million persons suffer from a fungal disease in China. A total of 2.4% of the population is affected (excluding onychomycosis because it is superficial), similar to results in other reports from Senegal, Brazil, France, Korea and Germany; the prevalence range is 1.6%–3.6% (*1*). Multiple new host risk factors other than HIV/AIDS or hematologic malignancy, especially COPD, asthma, and lung cancer, are associated with fungal disease. We found that even immunocompetent children and women may develop fungal diseases. Chronic respiratory diseases, notably PTB and COPD, are risk factors for all manifestations of aspergillosis. Old pathogens, including *T. marneffei* and *Histoplasma capsulatum*, exhibit new endemic trends; the Pearl River Basin bears the greatest burden for *T. marneffei* and the Yangtze River for *H. capsulatum*. Our study contributes to the currently limited data on the burden of fungal disease in China and provides a basis for public health and research priorities.

The incidence of candidiasis has increased in recent years (*17*). Candidemia is probably underestimated, as we have used only ICU data to explore the total burden of all high-risk populations. Considering the wide use of broad-spectrum antimicrobial drugs and the demographic shift with a largely increasing elderly population, we expect infections to be on the rise.

We have estimated the oral and esophageal candidiasis burdens in HIV-positive patients; these are certainly underestimates of these infections, because many of the populations at risk could not be assessed, such as patients with cancer, those taking oral or inhaled corticosteroids, and newborns. Although the proportions of oral or esophageal candidiasis in this kind of population might be small, given the relatively large size compared to the rather small HIV population, these cases could multiply our estimates. In addition, oral and esophageal candidiasis and colonization are associated with mucosal malignancy and particularly associated with high alcohol consumption (*42*). If the high number of unsuspected cases of esophageal candidiasis based on data from South Korea is also true in China, this association could contribute to the high number of esophageal cancers seen annually in China (307,359 cases) (*43*), which could further increase the social and economic burden.

IA is usually severe and fatal, unless diagnosed early. Although profoundly immunocompromised patients are at higher risk, the enormous estimate for China is mostly driven by COPD (97%). Our estimate of IA prevalence in liver transplant recipients of 4% is higher than the report from China at 1.7% (*44*), but that study was based on histology or culture alone, which is much less sensitive than *Aspergillus* antigen detection. The same applies to renal transplant recipients (*45*). Other underlying conditions were newly recognized risk factors for IA, such as diabetes mellitus, systemic lupus erythematosus, and postoperative and burn infections related to contaminated air in hospitals; these were not included in our estimation because of the unavailable incidence rate. Nevertheless, the number of IA cases could also be overestimated because *Aspergilli* are common fungi in the environment, and a positive result from non–aseptic fluid culture does not always represent disease. On the other hand, we have not estimated IA in most medical ICU patients, and not included the potential for IA complicating annual influenza cases or an epidemic.

In contrast to other countries, where CM is often diagnosed in patients with HIV or immunocompromised patients, in China, a high proportion of cryptococcosis was reported in immunocompetent persons (*34*). Jiang et al. reported on 159 HIV-negative

patients with CM, of whom 85 were normal hosts; however, whether these persons were immunocompetent is unknown, because several genetic predisposition factors for CM have been found in the ethnic Chinese population (*46*). Most large-scale studies have been conducted in adults; few were dedicated to pediatric populations. Although children account for only 0.9%–2.0% of all cryptococcal cases, the death rate is high, up to 43% (*47*). In a 12-year retrospective study in Beijing, 53 pediatric case-patients were encountered, of whom 41 had no underlying conditions (*48*). However, the denominator was unavailable. Only an annual incidence of 0.43/100,000 HIV-negative children was reported from the Acute Meningitis-Encephalitis Syndrome Surveillance project (*35*). Because of the lack of surveillance networks in China, additional studies are required, especially for immunocompetent patients.

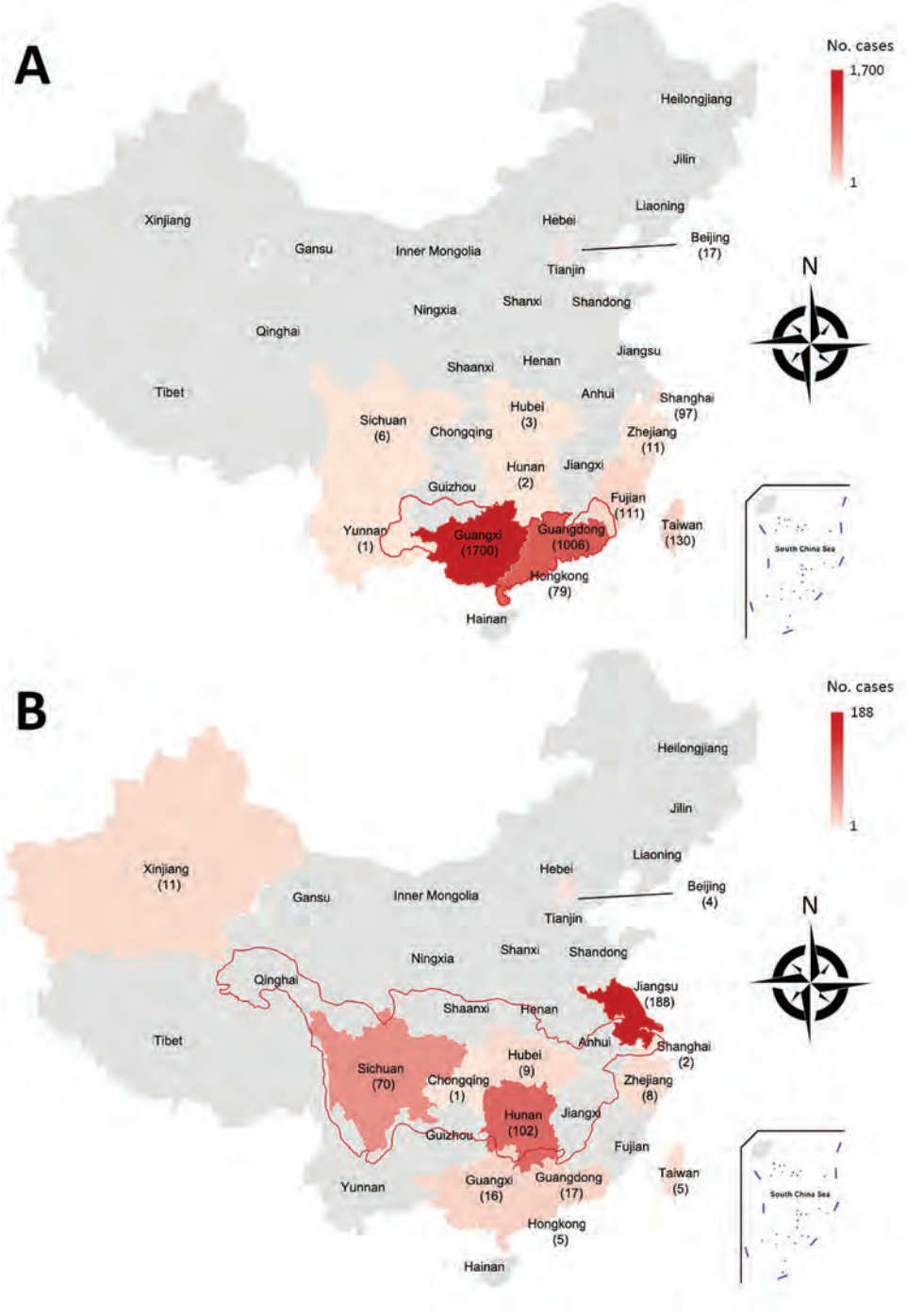

Figure 3. Epidemiology maps for talaromycosis and histoplasmosis, according to the number of reported cases, China. A) Map for talaromycosis. Red border indicates Pearl River basin. B) Map for histoplasmosis. Red border indicates Yangtze River region. Reports published in English during January 1950–October 2019 were searched.

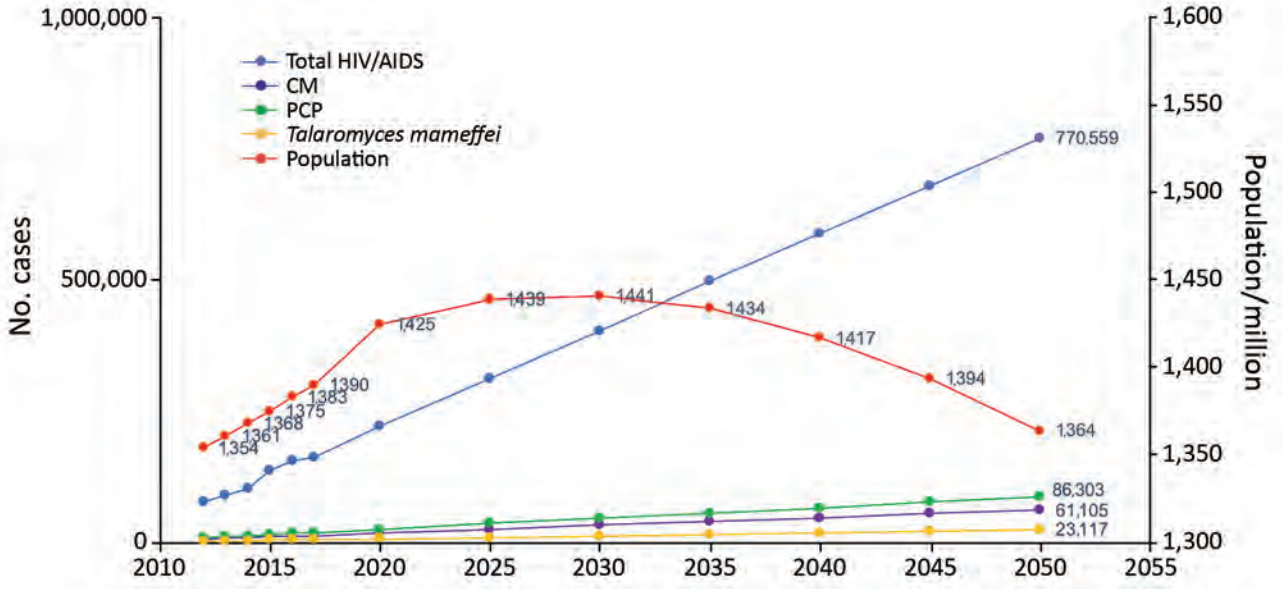

Figure 4. Prediction of HIV-related invasive fungal burden in China by 2050, based on ART and HIV-related disease incidence levels for 2012–2017. ART, antiretroviral therapy; CM, cryptococcal meningitis; PCP, pneumocystis pneumonia.

Although histoplasmosis is a common endemic mycosis in North America, several sporadic cases were reported in China, especially in the Yangtze River region, which was traditionally thought to be nonendemic for *Histoplasma capsulatum* (*3*). However, >300 histoplasmosis cases have been reported since 1990, and only 17 were identified as imported cases, indicating many authochthonous cases in China (*3*). *T. marneffei* infection, the other fatal endemic opportunistic fungal infection disease in Asia, was reported mostly in the southern part of China, possibly linked to an altered microeukaryotic community in subtropical rivers caused by global warming (*49*). Because this disease was associated mainly with HIV/AIDS, we estimated the incidence only in HIV-positive patients. In addition, given the low national reported statistics of HIV infection (*3*), the estimation of talaromycosis burden may be far underestimated. More large population-based studies are needed to better clarify the frequency of these fungal infections in these at-risk patients.

The government of China has worked to improve healthcare over the past 2 decades. However, HIV remains a major public health issue, showing the fastest growth among 45 infectious diseases during 2004–2013 with an annual percentage change of 16.3% (*50*). Therefore, we made a prediction of HIV-related opportunistic fungal infections. According to our data, it is likely that CM, PCP, and *T. marneffei* infection are major health burdens, which call for much more clinical training, financial support, and public policies.

Even though the incidence rate was low compared with those for bacterial and viral infections, our study represents a heavy fungal burden considering the immense population base and high mortality of nonsuperficial mycoses. The drawbacks of our study are the few studies conducted in the country for some infections; the prevalence or incidence are not available for those diseases, including sporotrichosis and some dermatophytosis. Epidemiologic studies are required and population-based surveillance data remain to be estimated, both nationally and regionally. Improved epidemiologic data are necessary for better awareness, better diagnostics, and better therapies.

Acknowledgments

We thank Xin-Hua Weng for his support and encouragement for the study.

This study was supported by the National Natural Science Foundation of China (grant no. 81971911 and grant no. 8151968 to L.P.Z.) and Major Infectious Diseases Such as AIDS and Viral Hepatitis Prevention and Control Technology Major Projects of China (grant no. 2018ZX10712-001 to R.Y.L.).

About the Author

Dr. Zhou is a PhD student at Huashan Hospital, Fudan University, Shanghai, China. Her primary research interests are invasive fungal disease diagnosis and treatment.

References

1. Global Action Fund for Fungal Infections. Publications: key recent contributions to the academic literature and individual country burdens [cited 2019 Oct 7]. http://www.gaffi.org/media/academic-papers
2. Song X, Xie L, Tan X, Wang Z, Yang Y, Yuan Y, et al. A multi-center, cross-sectional study on the burden of infectious keratitis in China. PLoS One. 2014;9:e113843. https://doi.org/10.1371/journal.pone.0113843
3. Hu Y, Zhang J, Li X, Yang Y, Zhang Y, Ma J, et al. *Penicillium marneffei* infection: an emerging disease in mainland China. Mycopathologia. 2013;175:57–67. https://doi.org/10.1007/s11046-012-9577-0
4. Pan B, Chen M, Pan W, Liao W. Histoplasmosis: a new endemic fungal infection in China? Review and analysis of cases. Mycoses. 2013;56:212–21. https://doi.org/10.1111/myc.12029
5. The Lancet. GLOBOCAN 2018: counting the toll of cancer. Lancet. 2018;392:985. https://doi.org/10.1016/S0140-6736(18)32252-9
6. Hung ML, Liao HT, Chen WS, Chen MH, Lai CC, Tsai CY, et al. Invasive aspergillosis in patients with systemic lupus erythematosus: a retrospective study on clinical characteristics and risk factors for mortality. Lupus. 2018;27:1944–52. https://doi.org/10.1177/0961203318796294
7. Chinese State Statistical Bureau. China Statistical Yearbook 2018 [cited 2019 Oct 7]. http://www.stats.gov.cn/tjsj/ndsj/2018/indexch.htm
8. Wang C, Xu J, Yang L, Xu Y, Zhang X, Bai C, et al.; China Pulmonary Health Study Group. Prevalence and risk factors of chronic obstructive pulmonary disease in China (the China Pulmonary Health [CPH] study): a national cross-sectional study. Lancet. 2018;391:1706–17. https://doi.org/10.1016/S0140-6736(18)30841-9
9. United Nations Population Division. World population prospects 2019 [cited 2019 Oct 7]. https://population.un.org/wpp/Download/Standard/Population
10. UNAIDS. AIDS info: people living with AIDS receiving ART [cited 2019 Oct 7]. http://www.unaids.org/en/dataanalysis/datatools/aidsinfo
11. World Health Organization. Tuberculosis country profiles [cited 2019 Oct 7]. http://www.who.int/tb/country/data/profiles/en/index.html
12. Chinese Ministry of Health. China Organ Transplantation Registration System [cited 2019 Oct 7]. http://www.cotr.cn
13. Huang K, Yang T, Xu J, Yang L, Zhao J, Zhang X, et al.; China Pulmonary Health (CPH) Study Group. Prevalence, risk factors, and management of asthma in China: a national cross-sectional study. Lancet. 2019;394:407–18. https://doi.org/10.1016/S0140-6736(19)31147-X
14. Zhu B, Wang Y, Ming J, Chen W, Zhang L. Disease burden of COPD in China: a systematic review. Int J Chron Obstruct Pulmon Dis. 2018;13:1353–64. https://doi.org/10.2147/COPD.S161555
15. Xu LP, Wu DP, Han MZ, Huang H, Liu QF, Liu DH, et al. A review of hematopoietic cell transplantation in China: data and trends during 2008–2016. Bone Marrow Transplant. 2017;52:1512–8. https://doi.org/10.1038/bmt.2017.59
16. Wilkie M, Davies S. Insights on peritoneal dialysis in China. Perit Dial Int. 2018;38(Suppl 2):S16–8. https://doi.org/10.3747/pdi.2018.00224
17. Murthy S, Wunsch H. Clinical review: international comparisons in critical care—lessons learned. Crit Care. 2012;16:218. https://doi.org/10.1186/cc11140
18. Du B, An Y, Kang Y, Yu X, Zhao M, Ma X, et al.; China Critical Care Clinical Trial Group. Characteristics of critically ill patients in ICUs in mainland China. Crit Care Med. 2013;41:84–92. https://doi.org/10.1097/CCM.0b013e31826a4082
19. Tan BH, Chakrabarti A, Li RY, Patel AK, Watcharananan SP, Liu Z, et al.; Asia Fungal Working Group (AFWG). Incidence and species distribution of candidaemia in Asia: a laboratory-based surveillance study. Clin Microbiol Infect. 2015;21:946–53. https://doi.org/10.1016/j.cmi.2015.06.010
20. Montravers P, Mira J-P, Gangneux J-P, Leroy O, Lortholary O; AmarCand study group. A multicentre study of a ntifungal strategies and outcome of *Candida* spp. peritonitis in intensive-care units. Clin Microbiol Infect. 2011;17:1061–7. https://doi.org/10.1111/j.1469-0691.2010.03360.x
21. Hu S, Tong R, Bo Y, Ming P, Yang H. Fungal peritonitis dialysis: 5-year review from a North China center. Infection. 2019;47:35–43. https://doi.org/10.1007/s15010-018-1204-7
22. Denning DW, Kneale M, Sobel JD, Rautemaa-Richardson R. Global burden of recurrent vulvovaginal candidiasis: a systematic review. Lancet Infect Dis. 2018;18:e339–47. https://doi.org/10.1016/S1473-3099(18)30103-8
23. Gamaletsou MN, Drogari-Apiranthitou M, Denning DW, Sipsas NV. An estimate of the burden of serious fungal diseases in Greece. Eur J Clin Microbiol Infect Dis. 2016;35:1115–20. https://doi.org/10.1007/s10096-016-2642-8
24. Matee MI, Scheutz F, Moshy J. Occurrence of oral lesions in relation to clinical and immunological status among HIV-infected adult Tanzanians. Oral Dis. 2000;6:106–11. https://doi.org/10.1111/j.1601-0825.2000.tb00110.x
25. Chen CY, Sheng WH, Tien FM, Lee PC, Huang SY, Tang JL, et al. Clinical characteristics and treatment outcomes of pulmonary invasive fungal infection among adult patients with hematological malignancy in a medical centre in Taiwan, 2008–2013. J Microbiol Immunol Infect. 2020;53:106–14. https://doi.org/10.1016/j.jmii.2018.01.002
26. Yan X, Li M, Jiang M, Zou LQ, Luo F, Jiang Y. Clinical characteristics of 45 patients with invasive pulmonary aspergillosis: retrospective analysis of 1711 lung cancer cases. Cancer. 2009;115:5018–25. https://doi.org/10.1002/cncr.24559
27. Xu H, Li L, Huang WJ, Wang LX, Li WF, Yuan WF. Invasive pulmonary aspergillosis in patients with chronic obstructive pulmonary disease: a case control study from China. Clin Microbiol Infect. 2012;18:403–8. https://doi.org/10.1111/j.1469-0691.2011.03503.x
28. Zhu B, Wang Y, Ming J, Chen W, Zhang L. Disease burden of COPD in China: a systematic review. Int J Chron Obstruct Pulmon Dis. 2018;13:1353–64. https://doi.org/10.2147/COPD.S161555
29. Khoo S, Denning DW. Invasive aspergillosis in patients with AIDS. Clin Infect Dis. 1994;19(suppl1):S41–8. https://doi.org/10.1093/clinids/19.supplement_1.s41
30. Denning DW, Pleuvry A, Cole DC. Global burden of chronic pulmonary aspergillosis as a sequel to pulmonary tuberculosis. Bull World Health Organ. 2011;89:864–72. https://doi.org/10.2471/BLT.11.089441
31. Smith NL, Denning DW. Underlying conditions in chronic pulmonary aspergillosis including simple aspergilloma. Eur Respir J. 2011;37:865–72. https://doi.org/10.1183/09031936.00054810
32. Ma YL, Zhang WB, Yu B, Chen YW, Mu S, Cui YL. Prevalence of allergic bronchopulmonary aspergillosis in Chinese patients with bronchial asthma [in Chinese]. Zhonghua Jie He He Hu Xi Za Zhi. 2011;34:909–13.
33. Chen J, Zhang R, Shen Y, Liu L, Qi T, Wang Z, et al. Serum cryptococcal antigen titre as a diagnostic tool and a predictor of mortality in HIV-infected patients with cryptococcal

meningitis. HIV Med. 2019;20:69–73. https://doi.org/10.1111/hiv.12679
34. Li Z, Liu Y, Cao H, Huang S, Long M. Epidemiology and clinical characteristics of cryptococcal meningitis in China (1981–2013): a review of the literature. Med Mycol: Open Access. 2017;3:1. https://doi.org/10.21767/2471-8521.100022
35. Guo J, Zhou J, Zhang S, Zhang X, Li J, Sun Y, et al. A case-control study of risk factors for HIV-negative children with cryptococcal meningitis in Shi Jiazhuang, China. BMC Infect Dis. 2012;12:376. https://doi.org/10.1186/1471-2334-12-376
36. Chan CK, Alvarez Bognar F, Wong KH, Leung CC, Tam CM, Chan KC, et al. The epidemiology and clinical manifestations of human immunodeficiency virus-associated tuberculosis in Hong Kong. Hong Kong Med J. 2010;16:192–8.
37. Guo F, Chen Y, Yang SL, Xia H, Li XW, Tong ZH. Pneumocystis pneumonia in HIV-infected and immunocompromised non-HIV infected patients: a retrospective study of two centers in China. PLoS One. 2014;9:e101943. https://doi.org/ 10.1371/journal.pone.0101943
38. Prakash H, Chakrabarti A. Global epidemiology of mucormycosis. J Fungi (Basel). 2019;5:26. https://doi.org/10.3390/jof5010026
39. Sigurgeirsson B, Baran R. The prevalence of onychomycosis in the global population: a literature study. J Eur Acad Dermatol Venereol. 2014;28:1480–91. https://doi.org/10.1111/jdv.12323
40. United Nations Population Division. Demographic components of future population growth [cited 2019 Oct 7]. https://www.un.org/en/development/desa/population/theme/trends/dem-comp-change.asp
41. Gong X, Luan T, Wu X, Li G, Qiu H, Kang Y, et al. Invasive candidiasis in intensive care units in China: risk factors and prognoses of *Candida albicans* and non-*albicans Candida* infections. Am J Infect Control. 2016;44:e59–63. https://doi.org/10.1016/j.ajic.2015.11.028
42. Alnuaimi AD, Wiesenfeld D, O'Brien-Simpson NM, Reynolds EC, McCullough MJ. Oral *Candida* colonization in oral cancer patients and its relationship with traditional risk factors of oral cancer: a matched case-control study. Oral Oncol. 2015;51:139–45. https://doi.org/10.1016/j.oraloncology.2014.11.008
43. Choi JH, Lee CG, Lim YJ, Kang HW, Lim CY, Choi JS. Prevalence and risk factors of esophageal candidiasis in healthy individuals: a single center experience in Korea. Yonsei Med J. 2013;54:160–5. https://doi.org/10.3349/ymj.2013.54.1.160
44. Yang CH, He XS, Chen J, Ouyang B, Zhu XF, Chen MY, et al. Fungal infection in patients after liver transplantation in years 2003 to 2012. Ann Transplant. 2012;17:59–63. https://doi.org/10.12659/AOT.883695
45. Zhang XD, Hu XP, Yin H, Wang W, Zhang X, Ma LL, et al. *Aspergillus* pneumonia in renal transplant recipients. Chin Med J (Engl). 2008;121:791–4. https://doi.org/10.1097/00029330-200805010-00007
46. Jiang YK, Wu JQ, Zhao HZ, Wang X, Wang RY, Zhou LH, et al. Genetic influence of Toll-like receptors on non-HIV cryptococcal meningitis: an observational cohort study. EBioMedicine. 2018;37:401–9. https://doi.org/10.1016/j.ebiom.2018.10.045
47. Gumbo T, Kadzirange G, Mielke J, Gangaidzo IT, Hakim JG. *Cryptococcus neoformans* meningoencephalitis in African children with acquired immunodeficiency syndrome. Pediatr Infect Dis J. 2002;21:54–6. https://doi.org/ 10.1097/00006454-200201000-00012
48. Liu L, Guo L, Liu Y, Chen T, Li S, Yang Y, et al. Clinical characteristics and prognosis of pediatric cryptococcosis in Beijing Children's Hospital, 2002–2014. Eur J Pediatr. 2017;176:1235–44. https://doi.org/10.1007/s00431-017-2974-0
49. Chen W, Ren K, Isabwe A, Chen H, Liu M, Yang J. Stochastic processes shape microeukaryotic community assembly in a subtropical river across wet and dry seasons. Microbiome. 2019;7:138. https://doi.org/10.1186/s40168-019-0749-8
50. Yang S, Wu J, Ding C, Cui Y, Zhou Y, Li Y, et al. Epidemiological features of and changes in incidence of infectious diseases in China in the first decade after the SARS outbreak: an observational trend study. Lancet Infect Dis. 2017;17:716–25. https://doi.org/10.1016/S1473-3099(17)30227-X

Address for correspondence: Li-Ping Zhu, Department of Infectious Diseases, Huashan Hospital, Fudan University, 12 Central Urumqi Road, Shanghai 200040, China; email: zhulp@fudan.edu.cn

Molecular Description of a Novel *Orientia* Species Causing Scrub Typhus in Chile

Katia Abarca, Constanza Martínez-Valdebenito,[1] Jenniffer Angulo,[1] Ju Jiang, Christina M. Farris, Allen L. Richards, Gerardo Acosta-Jamett, Thomas Weitzel

Scrub typhus is a potentially fatal rickettsiosis caused by *Orientia* species intracellular bacteria of the genus *Orientia*. Although considered to be restricted to the Asia Pacific region, scrub typhus has recently been discovered in southern Chile. We analyzed *Orientia* gene sequences of 16S rRNA (*rrs*) and 47-kDa (*htrA*) from 18 scrub typhus patients from Chile. Sequences were ≥99.7% identical among the samples for both amplified genes. Their diversity was 3.1%–3.5% for *rrs* and 11.2%–11.8% for *htrA* compared with *O. tsusugamushi* and 3.0% for *rrs* and 14.8% for *htrA* compared with *Candidatus* Orientia chuto. Phylogenetic analyses of both genes grouped the specimens from Chile in a different clade from other *Orientia* species. Our results indicate that *Orientia* isolates from Chile constitute a novel species, which, until they are cultivated and fully characterized, we propose to designate as *Candidatus* Orientia chiloensis, after the Chiloé Archipelago where the pathogen was identified.

Scrub typhus is a potentially fatal rickettsial infection transemitted by larval stage trombiculid mites called chiggers. Scrub typhus is caused by *Orientia tsutsugamushi*, a strictly intracellular bacterium with a remarkable genetic and antigenic diversity (*1*,*2*). Although this disease has been known since at least 313 CE and currently threatens >1 billion people in Asia and Australasia, it is widely underdiagnosed and underreported (*3*,*4*). Disinterest has been influenced by the perception that scrub typhus is a geographically limited disease, threatening rural populations within a certain region, known as the "tsutsugamushi triangle," and rarely affecting travelers (*5*,*6*).

This paradigm, however, has recently been brought into question with evidence of scrub typhus being found in the Middle East, Africa, and South America (*7*–*12*). Genomic information on *Orientia* strains from Chile has been insufficient and scrub typhus in the Middle East region is caused by a new *Orientia* species, *Candidatus* Orientia chuto (*6*), highlighting that our current knowledge on the spectrum of *Orientia* species is incomplete (*13*). Here, we discuss the molecular description and phylogenetic analysis of a potential third pathogenic *Orientia* species detected in 18 patients with scrub typhus in southern Chile.

Materials and Methods

Patients and Samples

The clinical samples described in this study were derived from 18 patients with confirmed scrub typhus diagnosed during February 2016–February 2019. All cases were acquired in southern Chile and diagnosed as part of an ongoing surveillance project of the Chilean Rickettsia and Zoonosis Research Group. The project was approved by the Comité Ético Científico, Pontificia Universidad Católica de Chile (Santiago, Chile; #12–170 and #160816007) and the Naval Medical Research Center (Silver Spring, MD, USA; PJT-16-24) (*9*,*14*,*15*).

We collected, stored, and extracted DNA from buffy coat preparations and eschar specimens as described elsewhere (*9*,*15*). Eschar samples consisted of swab specimens taken from the base or crust material of eschar, which we mechanically desegregated using sterile glass beads. DNA was automatically extracted from eschar and blood samples using MagNA Pure System (Roche Molecular Systems, https://diagnostics.roche.com), according to the manufacturer's instructions. All included DNA specimens derived from eschar samples,

Author affiliations: Escuela de Medicina, Pontificia Universidad Católica de Chile, Santiago, Chile (K. Abarca, C. Martínez-Valdebenito, J. Angulo); Naval Medical Research Center, Silver Spring, Maryland, USA (J. Jiang, C.M. Farris); Uniformed Services University of the Health Sciences, Bethesda, Maryland, USA (A.L. Richards); Facultad de Ciencias Veterinarias, Universidad Austral de Chile, Valdivia, Chile (G. Acosta-Jamett); Clínica Alemana de Santiago, Facultad de Medicina Clínica Alemana, Universidad del Desarrollo, Santiago (T. Weitzel)

DOI: https://doi.org/10.3201/eid2609.200918

[1]These authors contributed equally to this article.

except the BM2016-I sample, which was only from the buffy coat specimen.

PCR Assays and Sequencing

We initially assessed all extracted DNA samples by a newly designed genus-specific quantitative PCR (Orien16S qPCR assay), as described elsewhere (*15*,*16*). For further analysis, we performed seminested PCRs targeting the 16S rRNA gene (*rrs*), 47-kDa high-temperature requirement A gene (*htrA*), and 56-kDa type-specific antigen gene (*tsa*) to the qPCR Orien16S–positive samples (Appendix Table 1, https://wwwnc.cdc.gov/EID/article/26/9/20-0918-App1.pdf). We sequenced PCR amplicons for both DNA strands using Sanger sequencing method (Psomagen Inc., https://psomagen.com). Two independent investigators analyzed the chromatogram of each sequence and aligned them using BioEdit version 7.0.5.3 (*17*) Sequences from these scrub typhus patients in Chile were submitted to GenBank under accession no. MK329247 (*rrs*), MN231837 (*rrs*), MT435057 (*rrs*), MK343091 (*htrA*), and MT431624 (*htrA*).

Phylogenetic Analysis

We compared *Orientia* DNA sequences from the 2016–2019 scrub typhus patients with DNA from the first *Orientia* scrub typhus patient in Chile from 2006 and that of distinct *Orientia* species, including *O. tsutsugamushi* and *Candidatus* O. chuto, different *Rickettsia* species, and other microorganisms retrieved from GenBank and aligned using ClustalW (http://www.clustal.org). We used MEGAX software (https://www.megasoftware.net) to infer phylogenetic analyses by the maximum-likelihood method (*18*) and to perform the search for the most appropriate model of nucleotide substitution for phylogenetic analysis according to the Bayesian information criterion. For the maximum-likelihood method, we obtained initial trees for the heuristic search automatically by applying neighbor-joining and Bio neighbor-joining algorithms to a matrix of pairwise distances estimated using the maximum composite likelihood approach and then selecting the topology with superior log likelihood value. We based the support of the topology on a bootstrapping of 1,000 replicates; the positions equivalent to gaps or missing data were deleted.

Comparison of Nucleotide Diversity

We created consensus sequences of the generated amplicons after alignment in BioEdit version 7.0.5.3, which we compared with respective sequences of *O. tsutsugamushi* and *Candidatus* O. chuto strains as well as the first *Orientia* case from Chile, obtained from GenBank. A sequence identity matrix was constructed in BioEdit version 7.0.5.3. The selected databases and algorithms used for alignment and comparison of sequences were in accordance with current recommendations for the taxonomical characterization of prokaryote strains (*19*).

Results

Cases

The 18 investigated scrub typhus cases were acquired in 3 regions currently known to be endemic for scrub typhus (*15*), Biobío, Los Lagos, and Aysen, which span >1,120 km (latitude 38°03′S to 47°47′S) in Chile; 5 of the 18 cases were from Chiloé Island (Los Lagos), where the initial case was reported (Table 1). At the time they sought treatment, all but 1 patient exhibited the 3 clinical signs characteristic of scrub typhus: fever, maculopapular rash, and inoculation eschar. The presence of *Orientia* genomic DNA was confirmed in all cases by qPCR Orien16S from buffy coat or eschar material (Table 1). All of the patients recovered from scrub typhus without sequelae, 16 after treatment with doxycycline, 1 after treatment with azithromycin, and 1 without specific antimicrobial therapy. Further epidemiologic and clinical details of some of the patients have been published elsewhere (*9*,*15*,*20*).

DNA Sequences and Phylogenetic Analyses

We successfully amplified fragments of *rrs* from 18 cases and *htrA* from17 cases; the primers for *tsa* failed to produce amplicons. For all assays, we successfully amplified a well-defined *Orientia* strain (Kawasaki clade) from South Korea as a positive control (*6*). The lengths of clean reads were 886 nt for *rrs* and 950 nt for *htrA*. Sequences of the isolates showed a high nucleotide identity (99.7%–100%) for both genes (Appendix Table 1), with a maximum divergence of 2 nucleotides. We were able to distinguish 3 distinct *rrs* genotypes (1, 2, and 3) and 2 genotypic variants of *htrA* (a and b) (Appendix Table 2). *HtrA* variants, although determined by only 1 nucleotide, led to distinct DNA codons with leucine versus phenylalanine. The genotype 1a samples (n = 10) derived from Los Lagos (continental and Chiloé Island), Biobío, and Aysén regions, whereas genotypes 2b (n = 3) occurred in the continental Los Lagos region, 3a (n = 1) in Chiloé Island, and genotype 3b (n = 3) in the Los Lagos region, both continental and Chiloé Island. For 1 genotype 2 strain, we could not amplify *htrA* (Appendix Table 2). Phylogenetic analyses of both genes from the DNA specimens from Chile formed a unique cluster separate from the 14 *O. tsutsugamushi* strains included in the analysis as well as from

Table 1. Epidemiologic, clinical, and diagnostic features of 18 scrub typhus patients, southern Chile, 2016–2019*

Patient		Patient	Exposure		Clinical signs			qPCR results		
no.	Isolate no.	age, y/sex	Date	Region	Fever	Rash	Eschar	Buffy coat	Eschar	Ref.
1	BM2016-I	55/M	2016 Feb	Los Lagos†	Yes	Yes	Yes	Positive	ND	(*9*)
2	LC2016-I	42/M	2016 Feb	Los Lagos†	Yes	No	Yes	ND	Positive	(*30*)
3	MS2016-M	43/M	2016 Mar	Aysén	Yes	Yes	Yes	Positive	Positive	(*15*)
4	IS2017-M	56/M	2017 Feb	Los Lagos	Yes	Yes	Yes	Positive	Positive	(*15*)
5	NV2017-I	73/M	2017 Feb	Los Lagos†	Yes	Yes	Yes	ND	Positive	(*30*)
6	AE2018-M	25/M	2018 Feb	Los Lagos	Yes	Yes	Yes	ND	Positive	(*15*)
7	FC2018-M	22/F	2018 Feb	Los Lagos	Yes	Yes	Yes	Positive	Positive	(*15*)
8	AF2018-M	39/M	2018 Feb	Los Lagos	Yes	Yes	Yes	Positive	Positive	(*15*)
9	EC2018-M	28/M	2018 Feb	Biobío	Yes	Yes	Yes	Positive	Positive	(*15*)
10	VP2018-M	21/F	2018 Mar	Los Lagos	Yes	Yes	Yes	Positive	Positive	(*15*)
11	SH2018-M	49/F	2018 Dec	Los Lagos	Yes	Yes	Yes	Negative	Positive	(*30*)
12	GM2019-I	30/F	2019 Feb	Los Lagos†	Yes	Yes	Yes	ND	Positive	(*30*)
13	JC2019-I	54/M	2019 Feb	Los Lagos†	Yes	Yes	Yes	ND	Positive	(*30*)
14	CC2019-M	63/M	2019 Feb	Los Lagos	Yes	Yes	Yes	ND	Positive	(*30*)
15	CV2019-M	23/F	2019 Feb	Los Lagos	Yes	Yes	Yes	ND	Positive	(*30*)
16	MA2019-M	53/M	2019 Feb	Los Lagos	Yes	Yes	Yes	ND	Positive	(*30*)
17	MV2019-M	54/F	2019 Feb	Los Lagos	Yes	Yes	Yes	ND	Positive	(*30*)
18	SG2019-M	41/M	2019 Feb	Los Lagos	Yes	Yes	Yes	ND	Positive	(*30*)

*ND, not done; ref., reference.
†Chiloé Island.

Candidatus O. chuto (Figures 1, 2). However, the *rrs* sequence from the 2016–2019 samples grouped together with that from the first scrub typhus case in Chile (Figure 1) (*8*).

Details of discrepancies in the nucleotide sequences were evaluated by identity matrices. For *rrs* from the isolates from Chile, identity of the consensus sequence ranged from 96.5% to 97.0% compared with *O. tsutsugamushi* and *Candidatus* O. chuto (Table 2, https://wwwnc.cdc.gov/EID/article/26/9/20-0918-T2.htm). A higher diversity was observed for *htrA*, with sequence identity of 88.2%–88.8% compared with *O. tsutsugamushi* and 85.2% with *Candidatus* O. chuto (Table 3, https://wwwnc.cdc.gov/EID/article/26/9/20-0918-T3.htm). We observed a GTA insertion (valine) in position 28 of *htrA* in all 18 samples, similar to *Candidatus* O. chuto, but this substitution was not observed in *O. tsutsugamushi* strains.

Species Designation

The *rrs* sequences we analyzed showed a divergence of ≥3% from known *Orientia* species, indicating that the isolates from Chile constitute a novel species within the genus *Orientia* (family *Rickettsiaceae*, order Rickettsiales, class Alphaproteobacteria). Our designation of the bacteria as a new species was corroborated by the divergence of *htrA* and our inability to generate amplicons with primers of *O. tsutsugamushi* type-specific antigen gene *tsa*. Until a type strain is cultivated and characterized, we propose the designation *Candidatus* Orientia chiloensis for the novel species, after the Chiloé Archipelago (Los Lagos Region, Chile) where the pathogen was first identified (*8*,*9*).

Discussion

Because of new diagnostic tools and increasing clinical awareness, our knowledge of rickettsial infections has increased over recent decades (*23*,*24*). For scrub typhus, which has been considered the most important rickettsiosis in Asia and Australasia, the discovery of new endemic regions outside of the traditional tsutsugamushi triangle raises questions about established paradigms (*25*). Since 2006, multiple patients with scrub typhus have been reported in southern Chile, >12,000 km away from known endemic regions (*8*,*9*,*15*). In addition, a case of scrub typhus caused by a novel species, *Candidatus* O. chuto, was diagnosed on the Arabian Peninsula (*7*). These findings, together with serologic and molecular data from sub-Saharan Africa and Europe, suggest that scrub typhus caused by various *Orientia* species might have a much wider than previously known, possibly global, distribution (*4*,*26*,*27*).

Most clinicoepidemiologic and ecologic aspects of scrub typhus in South America are currently unknown. A recent study on Chiloé Island suggested that trombiculid mites of the genus *Herpetacarus*, which were found to be infected with *Orientia*-species bacteria, might serve as vectors (*28*); preliminary phylogenetic analyses showed that the mite-associated strains were 99%–100% identical to those from patients (*29*). Clinically, the >40 patients with scrub typhus diagnosed in southern Chile during 2015–2019 sought treatment for conditions similar to those for scrub typhus from the Asia Pacific region—fever, generalized rash, and inoculation eschar—and, similarly, had a rapid response to treatment with tetracycline or azithromycin (*30*). Early molecular and

serologic data suggest that the *Orientia* species in Chile diverge from those in the Asia-Pacific region (*8*,*9*,*15*), but whether they represent distinct *O. tsutsugamushi* strains or a new species remained inconclusive. Our phylogenetic analyses of larger DNA segments from 2 conserved genes support the conclusion that the

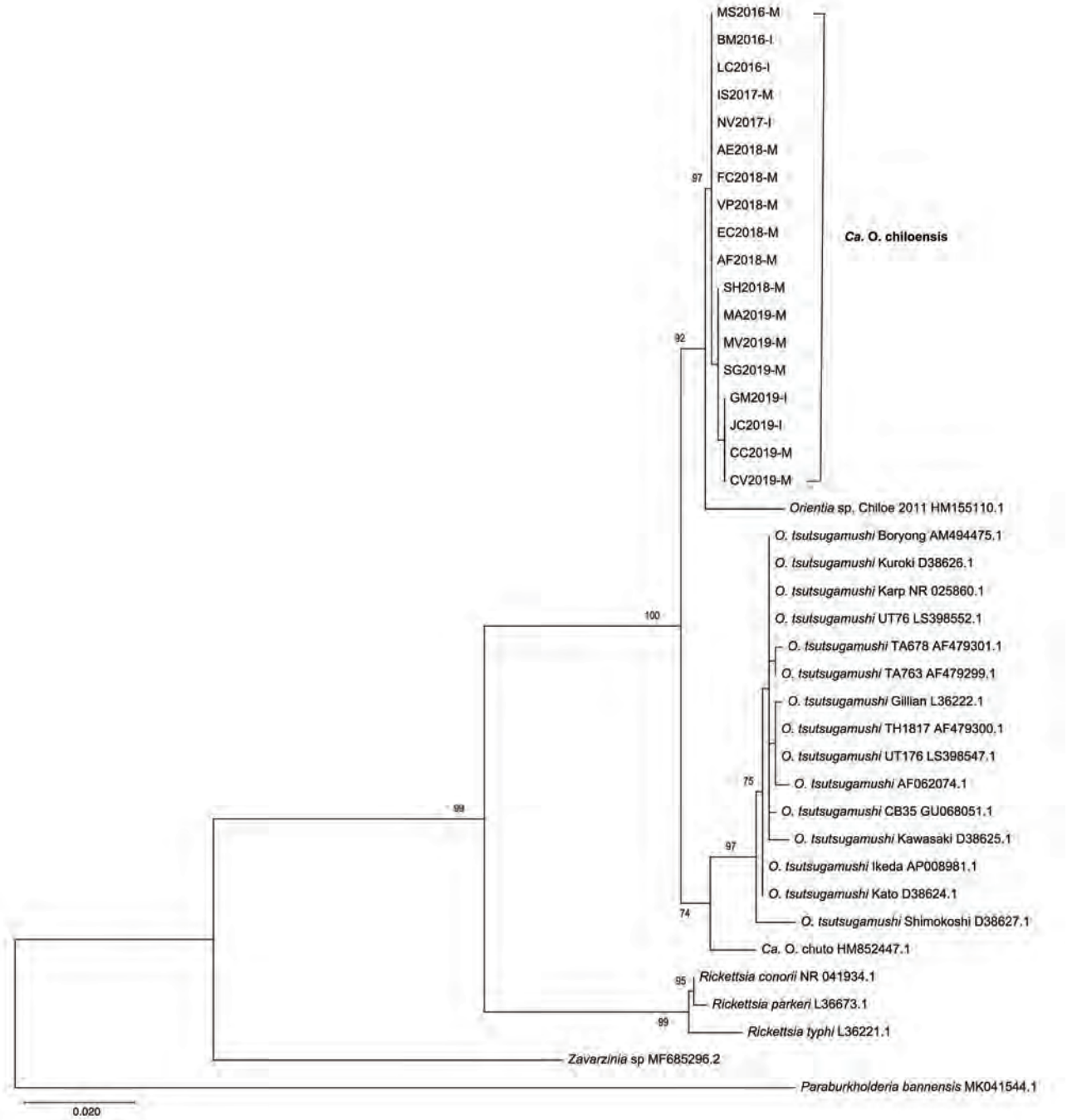

Figure 1. Phylogenetic analyses of sequences of the 16S rRNA gene (*rrs*) from scrub typhus cases in Chile compared with those from different *Orientia* and *Rickettsia* species and other microorganisms. We inferred the evolutionary history by using the maximum-likelihood method based on the Kimura 2-parameter model (*21*), according to the Bayesian information criterion for these sequences. The analysis involved 39 nt sequences and a total of 875 positions in the final dataset. The trees is drawn to scale, with branch lengths measured in the number of substitutions per site. All positions containing gaps and missing data were eliminated. For isolates from the cases in this study, the suffix "M" indicates an origin in mainland Chile and "I" an origin on Chiloé Island; these isolates clustered into a proposed new species provisionally named *Candidatus* Orientia chiloensis. GenBank accession numbers are indicated for reference sequences. Scale bar indicates nucleotide divergence.

isolates from patients in Chile cluster outside known *Orientia* species and represent a distinct species.

Culture-independent sequencing techniques play an important role in prokaryotic taxonomy, especially for strictly intracellular bacteria (*31*,*32*). For the description of new species, sequence analyses of the 16S rRNA gene (*rrs*) are paramount. A ≥3% divergence of *rrs* sequences from those in known species is the accepted threshold suggesting a novel species (*19*), although corrected levels of ≥1.30%–1.35% have been suggested (*33*,*34*). Isolates with *rrs* sequence differences of >5%–6% might belong to a distinct genus, if they display unique phenotypic differences (*35*). Distinct, lower thresholds have been developed for *Rickettsia* spp. (*31*), but this approach remains controversial among rickettsiologists (*36*). As should be the case for all molecularly defined novel species and genera, we have classified this proposed species as

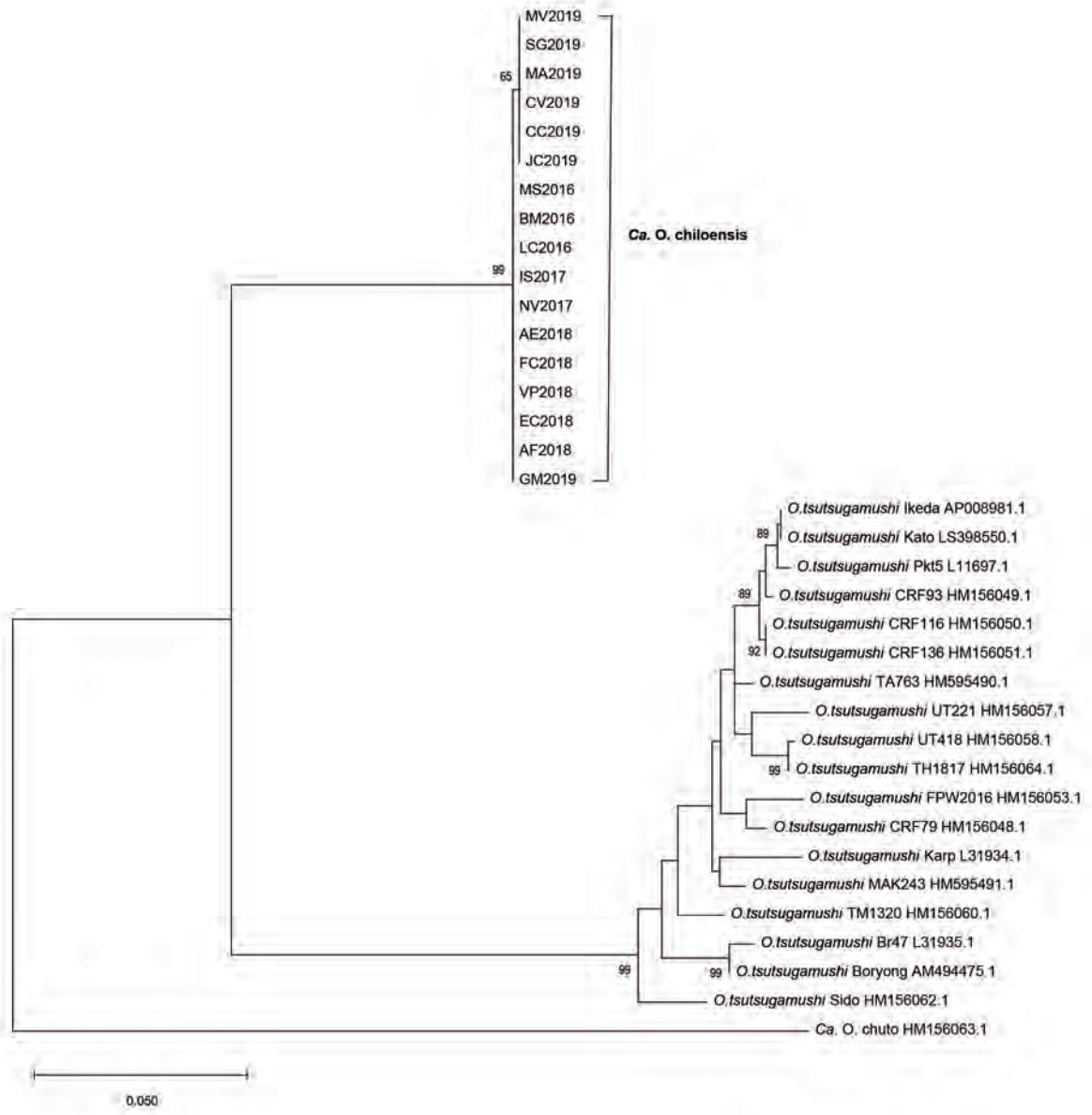

Figure 2. Phylogenetic analyses of sequences of the 47-kDa gene (*htrA*) from scrub typhus cases from Chile in comparison to different *Orientia* species. For the phylogenetic tree, the maximum-likelihood method based on the Hasegawa-Kishino-Yano model was applied (*22*). A discrete gamma distribution was used to model evolutionary rates differences among sites. The analysis involved 37 nucleotide sequences and a total of 736 positions in the final dataset. The tree is drawn to scale, with branch lengths measured in the number of substitutions per site. All positions containing gaps and missing data were eliminated. Isolates from the cases in this study clustered into a proposed new species provisionally named *Candidatus* Orientia chiloensis. GenBank accession numbers are indicated for reference sequences. Scale bar indicates nucleotide divergence.

Table 2. Identity matrix of 16S rRNA gene (*rrs*) showing percentage of pairwise identity of 886 nt consensus sequence of 18 recent *Candidatus* Orientia chiloensis cases in Chile with the first *Orientia* case from Chile in 2006, 16 *O. tsutsugamushi* strains, and *Candidatus* Orientia chuto

Sequences*†	1	2	3	4	5	6	7	8	9	10	11	12	13	14	15	16	17
1 Chiloensis																	
2 Chiloe 2006	98.0																
3 Chuto	97.0	95.8															
4 Boryong	96.7	95.7	97.7														
5 Kuroki	96.7	95.7	97.7	100													
6 Gilliam	96.5	95.4	97.5	99.7	99.7												
7 Karp	96.8	95.8	97.8	99.8	99.8	99.6											
8 Kawasaki	96.7	95.7	97.1	99.2	99.2	99.2	99.3										
9 Ikeda	96.9	95.9	97.9	99.7	99.7	99.5	99.8	99.2									
10 Kato	96.9	95.9	97.9	99.7	99.7	99.5	99.8	99.2	100								
11 Shimokoshi	96.9	96.1	96.9	98.4	98.4	98.4	98.5	98.6	98.6	98.6							
12 CB35	96.7	95.7	97.9	99.7	99.7	99.5	99.8	99.2	99.7	99.7	98.4						
13 TA678	96.6	95.6	97.6	99.6	99.6	99.4	99.7	99.0	99.6	99.6	98.3	99.6					
14 TA763	96.5	95.4	97.5	99.5	99.5	99.3	99.6	98.9	99.5	99.5	98.1	99.5	99.6				
15 TH1817	96.5	95.6	97.5	99.5	99.5	99.5	99.6	98.9	99.5	99.5	98.1	99.5	99.4	99.3			
16 UT176	96.8	95.8	97.6	99.6	99.6	99.6	99.7	99.3	99.6	99.6	98.5	99.6	99.5	99.4	99.6		
17 UT76	96.8	95.8	97.8	99.8	99.8	99.6	100	99.3	99.8	99.8	98.5	99.8	99.7	99.6	99.6	99.7	
18 Litchfield	96.6	95.6	97.1	99.2	99.2	99.2	99.3	98.9	99.2	99.2	98.5	99.2	99.0	98.9	99.2	99.5	99.3

*All sequences from strains of *O. tsutsugamushi* except 1 consensus sequence *Candidatus* Orientia chiloensis; 2 *Orientia* species; and 3 *Candidatus* Orientia chuto.
†Numbers in the column headers (top row) indicate the same sequences as those associated with the same numbers in the first column.
GenBank accession numbers: 2, HM 15510.1; 3, HM852447.1; 4, AM494475.1; 5, D38626.1; 6, L36222.1; 7, NR_025860.1; 8, D38625.1; 9, AP008981.1; 10, D38624.1; 11, D38627.1; 12, GU068051.1; 13, AF479301.1; 14, AF479299.1; 15, AF479300.1; 16, LS398547.1; 17, LS398552.1; 18, AF062074.1.

Candidatus, until type strains can be cultivated and fully described (*37*).

The novel *Orientia* species presented here fulfills the *rrs* gene criteria described in the previous sections. Our designation of a novel species was affirmed by a high divergence of another genomic marker, *htrA*, which diverged >11% from *O. tsutsugamushi* and of >14% from *Candidatus* O. chuto (Table 3). This conserved gene diverges only <3.7% among *O. tsutsugamushi* isolates (*38*). The *O. tsutsugamushi* type-specific antigen gene, *tsa*, which has a much higher diversity than *htrA* (*1*), was not amplifiable from isolates from Chile using primers designed for *O. tsutsugamushi*. This suggests that the *Candidatus* O. chiloensis *tsa* is unique, requiring the assessment of additional primers, possibly based on results from a future WGS.

Table 3. Identity matrix of 47-kDa high temperature requirement A gene (*htrA*) showing percentage of pairwise identity of 950 nt consensus sequence of 17 *Candidatus* Orientia chiloensis cases from Chile with 18 strains of *O. tsutsugamushi* and *Candidatus* Orientia chuto

Sequences*†	1	2	3	4	5	6	7	8	9	10	11	12	13	14	15	16	17	18	19
1 Chiloensis																			
2 Chuto	85.2																		
3 Ikeda	88.5	83.7																	
4 Pkt5	88.3	83.5	99.7																
5 Kp47	88.2	83.7	97.5	97.3															
6 Br47	88.3	83.8	96.9	96.7	96.5														
7 Boryong	88.4	83.7	97.2	97.0	96.8	99.4													
8 CRF116	88.3	83.5	99.5	99.3	97.5	96.9	97.2												
9 FPW2016	88.3	83.5	98.0	97.8	97.5	97.1	97.6	98.0											
10 Kato	88.5	83.7	100	99.7	97.5	96.9	97.2	99.5	98.0										
11 MAK243	88.8	84.2	98.5	98.3	98.0	97.5	97.8	98.5	98.0	98.5									
12 CRF79	88.3	83.7	98.7	98.5	97.7	96.9	97.2	98.7	98.7	98.7	98.5								
13 TM1320	88.6	83.4	98.4	98.2	97.0	97.4	97.7	98.2	97.8	98.4	97.9	97.6							
14 UT221	88.8	84.1	98.5	98.3	96.9	97.1	97.3	98.5	97.4	98.5	98.2	98.0	97.5						
15 UT418	88.4	84.1	98.5	98.3	97.5	96.9	97.2	98.5	97.5	98.5	98.2	98.4	97.4	98.4					
16 Sido	88.7	83.6	96.9	96.7	96.0	96.7	97.2	96.7	97.3	96.9	97.2	96.7	97.2	96.9	96.3				
17 CRF93	88.5	83.7	99.6	99.4	97.5	96.9	97.2	99.6	98.3	99.6	98.5	98.7	98.2	98.4	98.6	96.9			
18 CRF136	88.3	83.5	99.5	99.3	97.5	96.9	97.2	100	98.0	99.5	98.5	98.7	98.2	98.5	98.5	96.7	99.6		
19 TA763	88.6	83.8	99.1	98.9	97.8	97.1	97.6	99.1	98.3	99.1	98.7	98.9	97.7	98.5	98.7	97.0	99.0	99.1	
20 TH1817	88.3	84.0	98.5	98.3	97.4	96.8	97.1	98.5	97.4	98.5	98.0	98.3	97.3	98.4	99.7	96.1	98.4	98.5	98.7

*All sequences from strains of *O. tsutsugamushi* except 1 consensus sequence *Candidatus* Orientia chiloensis; 2 *Orientia* species; and 3 *Candidatus* Orientia chuto.
†Numbers in the column headers (top row) indicate the same sequences as those associated with the same numbers in the first column.
GenBank accession numbers: 2, HM156063.1; 3, AP008981.1; 4, L11697.1; 5, L31934.1; 6, L31935.1; 7, AM494475.1; 8, HM156050.1; 9, HM156053.1; 10, LS398550.1; 11, HM595491.1; 12, HM156048.1; 13, HM156060.1; 14, HM156057.1; 15, HM156058.1; 16, HM156062.1; 17, HM156049.1; 18, HM156051.1; 19, HM595490.1; 20, HM156064.1.

Currently, no *Orientia* culture isolate from Chile is available.

Surprisingly, the *rrs* and *htrA* sequences from the 18 *Orientia* samples from Chile were almost identical, showing a maximum variability of only 2 nucleotides. This genetic homogeneity over a wide geographic range is in sharp contrast to *O. tsutsugamushi* (*38*). As a unique characteristic among obligate intracellular pathogens, this species displays a dramatic genomic and phenotypic heterogeneity (*1*), which might be related to homologous recombination and lateral gene transfer (*39*). Among *O. tsutsugamushi* isolates, for example, the divergence of reported *rrs* sequences are up to 1.5% and for *htrA* sequences up to 3.6% (*1*,*38*), compared with ≤0.3% observed among isolates from *Orientia* DNA from Chile.

The most frequently applied phenotypic and molecular marker of *O. tsutsugamushi* strain heterogeneity is the highly variable 56-kDa TSA. This *Orientia*-specific surface protein is also known to be an important determinant of strain-specific pathogenicity and immunity (*1*). As we mentioned, we were not able to generate amplicons of strains from Chile with the applied *tsa* PCR or with *tsa* qPCR (*41*) or other commonly used primers (e.g., r56_2057). In a previous report, short *tsa* sequences were produced from 2 samples, but only after prolonged amplification cycles (*9*). These findings strongly suggest that *tsa* of *Candidatus* O. chiloensis is highly divergent from those of other *Orientia* species. Becaue the TSA surface protein is the main antigenic determinant, such divergence might explain the low serologic cross-reactivity, which was observed in patients with scrub typhus and in seroprevalence studies in Chile using *O. tsutsugamushi* whole-cell or recombinant antigens (*9*,*41*).

In conclusion, our results indicate that scrub typhus in Chile is caused by a novel *Orientia* species, suggesting an ancient origin of the disease in South America, rather than recent introduction. However, after obtaining cultured isolates of *Candidatus* O. chiloensis and larger gene sequences including from WGS, deeper comparative studies of the 3 *Orientia* species and their vectors are necessary to understand the ecology and evolution of these emerging intracellular pathogens, including the mechanisms responsible for the differences in strain variability and surface proteins.

Acknowledgments

We acknowledge Katia Velasquez and all other physicians who participated in identifying the scrub typhus cases included in this study. We also thank Teresa Azócar and Romina Alarcón for their technical help in processing the clinical samples.

This work was supported by a grant from the Fondo Nacional de Desarrollo Científico y Tecnológico (FONDECYT N° 1130817 and N° 1170810) and the Armed Forces Health Surveillance Branch and its Global Emerging Infections Surveillance and Response (GEIS) Section (funding year 2018, ProMIS ID P0017_19_NM_02 NMRC work unit number A0047).

The views expressed in this article reflect the results of research conducted by the authors and do not necessarily reflect the official policy or position of the Department of the Navy, Department of Defense, or the United States Government.

About the Author

Dr. Abarca is a pediatric infectious diseases specialist and professor at the School of Medicine, Pontificia Universidad Católica de Chile in Santiago, Chile. Her main research interests include vectorborne zoonoses and rickettsial infections as well as vaccine development.

References

1. Kelly DJ, Fuerst PA, Ching WM, Richards AL. Scrub typhus: the geographic distribution of phenotypic and genotypic variants of *Orientia tsutsugamushi.* Clin Infect Dis. 2009; 48(Suppl 3):S203–30. https://doi.org/10.1086/596576
2. Kim G, Ha NY, Min CK, Kim HI, Yen NT, Lee KH, et al. Diversification of *Orientia tsutsugamushi* genotypes by intragenic recombination and their potential expansion in endemic areas. PLoS Negl Trop Dis. 2017;11:e0005408. https://doi.org/10.1371/journal.pntd.0005408
3. Paris DH, Shelite TR, Day NP, Walker DH. Unresolved problems related to scrub typhus: a seriously neglected life-threatening disease. Am J Trop Med Hyg. 2013;89:301–7. https://doi.org/10.4269/ajtmh.13-0064
4. Xu G, Walker DH, Jupiter D, Melby PC, Arcari CM. A review of the global epidemiology of scrub typhus. PLoS Negl Trop Dis. 2017;11:e0006062. https://doi.org/10.1371/journal.pntd.0006062
5. Bonell A, Lubell Y, Newton PN, Crump JA, Paris DH. Estimating the burden of scrub typhus: a systematic review. PLoS Negl Trop Dis. 2017;11:e0005838. https://doi.org/10.1371/journal.pntd.0005838
6. Weitzel T, Aylwin M, Martínez-Valdebenito C, Jiang J, Munita JM, Thompson L, et al. Imported scrub typhus: first case in South America and review of the literature. Trop Dis Travel Med Vaccines. 2018;4:10. https://doi.org/10.1186/s40794-018-0070-8
7. Izzard L, Fuller A, Blacksell SD, Paris DH, Richards AL, Aukkanit N, et al. Isolation of a novel *Orientia* species (*O. chuto* sp. nov.) from a patient infected in Dubai. J Clin Microbiol. 2010;48:4404–9. https://doi.org/10.1128/JCM.01526-10
8. Balcells ME, Rabagliati R, García P, Poggi H, Oddó D, Concha M, et al. Endemic scrub typhus–like illness, Chile. Emerg Infect Dis. 2011;17:1659–63. https://doi.org/10.3201/eid1709.100960
9. Weitzel T, Dittrich S, López J, Phuklia W, Martinez-Valdebenito C, Velásquez K, et al. Endemic scrub

typhus in South America. N Engl J Med. 2016;375:954–61. https://doi.org/10.1056/NEJMoa1603657
10. Maina AN, Farris CM, Odhiambo A, Jiang J, Laktabai J, Armstrong J, et al. Q fever, scrub typhus, and rickettsial diseases in children, 2011–2012 Kenya. Emerg Infect Dis. 2016;22:883–6. https://doi.org/10.3201/eid2205.150953
11. Horton KC, Jiang J, Maina A, Dueger E, Zayed A, Ahmed AA, et al. Evidence of *Rickettsia* and *Orientia* infections among abattoir workers in Djibouti. Am J Trop Med Hyg. 2016;95:462–5. https://doi.org/10.4269/ajtmh.15-0775
12. Kocher C, Jiang J, Morrison AC, Castillo R, Leguia M, Loyola S, et al. Scrub typhus in the Peruvian Amazon. Emerg Infect Dis. 2017;23:1389–91. https://doi.org/10.3201/eid2308.170050
13. Luce-Fedrow A, Lehman ML, Kelly DJ, Mullins K, Maina AN, Stewart RL, et al. A review of scrub typhus (*Orientia tsutsugamushi* and related organisms): then, now, and tomorrow. Trop Med Infect Dis. 2018;3:pii E8. https://doi.org/10.3390/tropicalmed3010008
14. Abarca K, Weitzel T, Martínez-Valdebenito C, Acosta-Jamett G. Scrub typhus, an emerging infectious disease in Chile [in Spanish]. Rev Chilena Infectol. 2018;35:696–9. https://doi.org/10.4067/S0716-10182018000600696
15. Weitzel T, Martínez-Valdebenito C, Acosta-Jamett G, Jiang J, Richards AL, Abarca K. Scrub typhus in continental Chile, 2016–2018. Emerg Infect Dis. 2019;25:1214–7. https://doi.org/10.3201/eid2506.181860
16. Jiang J, Martínez-Valdebenito C, Weitzel T, Abarca K, Richards AL. Development of an *Orientia* genus-specific quantitative real-time PCR assay and the detection of *Orientia* species in DNA preparations from *O. tsutsugamushi*, *Candidatus* Orientia chuto, and *Orientia* species from Chile. In: Abstracts of the 29th Meeting of the American Society for Rickettsiology; Milwaukee, WI, USA; 2018 Jun 16–19. Abstract no. 46.
17. Hall TA. Bioedit: a user-friendly biological sequence alignment editor and analysis program for Windows 95/98/NT. Nucleic Acids Symp Ser. 1999;41:95–8.
18. Kumar S, Stecher G, Li M, Knyaz C, Tamura K. MEGA X: molecular evolutionary genetics analysis across computing platforms. Mol Biol Evol. 2018;35:1547–9. https://doi.org/10.1093/molbev/msy096
19. Tindall BJ, Rosselló-Móra R, Busse HJ, Ludwig W, Kämpfer P. Notes on the characterization of prokaryote strains for taxonomic purposes. Int J Syst Evol Microbiol. 2010;60:249–66. https://doi.org/10.1099/ijs.0.016949-0
20. Weitzel T, Acosta-Jamett G, Martínez-Valdebenito C, Richards AL, Grobusch MP, Abarca K. Scrub typhus risk in travelers to southern Chile. Travel Med Infect Dis. 2019;29:78–9. https://doi.org/10.1016/j.tmaid.2019.01.004
21. Kimura M. A simple method for estimating evolutionary rates of base substitutions through comparative studies of nucleotide sequences. J Mol Evol. 1980;16:111–20. https://doi.org/10.1007/BF01731581
22. Hasegawa M, Kishino H, Yano T. Dating of the human-ape splitting by a molecular clock of mitochondrial DNA. J Mol Evol. 1985;22:160–74. https://doi.org/10.1007/BF02101694
23. Merhej V, Angelakis E, Socolovschi C, Raoult D. Genotyping, evolution and epidemiological findings of *Rickettsia* species. Infect Genet Evol. 2014;25:122–37. https://doi.org/10.1016/j.meegid.2014.03.014
24. Richards AL. Worldwide detection and identification of new and old rickettsiae and rickettsial diseases. FEMS Immunol Med Microbiol. 2012;64:107–10. https://doi.org/10.1111/j.1574-695X.2011.00875.x
25. Walker DH. Scrub typhus—scientific neglect, ever-widening impact. N Engl J Med. 2016;375:913–5. https://doi.org/10.1056/NEJMp1608499
26. Jiang J, Richards AL. Scrub typhus: no longer restricted to the tsutsugamushi triangle. Trop Med Infect Dis. 2018;3:pii E11. PubMed https://doi.org/10.3390/tropicalmed3010011
27. Elliott I, Pearson I, Dahal P, Thomas NV, Roberts T, Newton PN. Scrub typhus ecology: a systematic review of *Orientia* in vectors and hosts. Parasit Vectors. 2019;12:513. https://doi.org/10.1186/s13071-019-3751-x
28. Acosta-Jamett G, Martínez-Valdebenito C, Beltrami E, Silva-de La Fuente MC, Jiang J, Richards AL, et al. Identification of trombiculid mites (Acari: Trombiculidae) on rodents from Chiloé Island and molecular evidence of infection with *Orientia* species. PLoS Negl Trop Dis. 2020;14:e0007619. https://doi.org/10.1371/journal.pntd.0007619
29. Martínez-Valdebenito C, Silva-de la Fuente MC, Acosta-Jamett G, Weitzel T, Jiang J, Richards AL, Abarca K. Molecular detection of *Orientia* spp. in trombiculid mites collected from rodents on Chiloé Island, Chile. In: Conference Book of the 2nd Asia Pacific Rickettsia Conference; Chiang Rai, Thailand; 2019 Nov 3–6. Abstract no. 33. p. 66.
30. Abarca K, Kuijpers S, Velásquez K, Martínez-Valdebenito C, Acosta-Jamett G, Weitzel T. Demographic, clinical, and laboratory features of South American scrub typhus in southern Chile, 2015–2019. In: Conference Book of the 2nd Asia Pacific Rickettsia Conference; Chiang Rai, Thailand; 2019 Nov 3–6. Abstract no. 26. p. 33.
31. Fournier PE, Raoult D. Current knowledge on phylogeny and taxonomy of *Rickettsia* spp. Ann N Y Acad Sci. 2009;1166:1–11. https://doi.org/10.1111/j.1749-6632.2009.04528.x
32. Parks DH, Chuvochina M, Waite DW, Rinke C, Skarshewski A, Chaumeil PA, et al. A standardized bacterial taxonomy based on genome phylogeny substantially revises the tree of life. Nat Biotechnol. 2018;36:996–1004. https://doi.org/10.1038/nbt.4229
33. Stackebrandt E, Ebers J. Taxonomic parameters revisited: tarnished gold standards. Microbiol Today. 2006;33:152–5.
34. Kim M, Oh HS, Park SC, Chun J. Towards a taxonomic coherence between average nucleotide identity and 16S rRNA gene sequence similarity for species demarcation of prokaryotes. Int J Syst Evol Microbiol. 2014;64:346–51. https://doi.org/10.1099/ijs.0.059774-0
35. Qin QL, Xie BB, Zhang XY, Chen XL, Zhou BC, Zhou J, et al. A proposed genus boundary for the prokaryotes based on genomic insights. J Bacteriol. 2014;196:2210–5. https://doi.org/10.1128/JB.01688-14
36. Walker DH. Rickettsiae and rickettsial infections: the current state of knowledge. Clin Infect Dis. 2007;45(Suppl 1):S39–44. https://doi.org/10.1086/518145
37. Raoult D, Fournier PE, Eremeeva M, Graves S, Kelly PJ, Oteo JA, et al. Naming of rickettsiae and rickettsial diseases. Ann N Y Acad Sci. 2005;1063:1–12. https://doi.org/10.1196/annals.1355.002
38. Jiang J, Paris DH, Blacksell SD, Aukkanit N, Newton PN, Phetsouvanh R, et al. Diversity of the 47-kD HtrA nucleic acid and translated amino acid sequences from 17 recent human isolates of *Orientia.* Vector Borne Zoonotic Dis. 2013;13:367–75. https://doi.org/10.1089/vbz.2012.1112
39. Fleshman A, Mullins K, Sahl J, Hepp C, Nieto N, Wiggins K, et al. Comparative pan-genomic analyses of *Orientia tsutsugamushi* reveal an exceptional model of

bacterial evolution driving genomic diversity. 2018;4:e000199. https://doi.org/10.1099/mgen.0.000199
40. Jiang J, Chan TC, Temenak JJ, Dasch GA, Ching WM, Richards AL. Development of a quantitative real-time polymerase chain reaction assay specific for *Orientia tsutsugamushi*. Am J Trop Med Hyg. 2004;70:351–6. https://doi.org/10.4269/ajtmh.2004.70.351
41. Weitzel T, Acosta-Jametta, G, Jiang J, Martínez-Valdebenito C, Farris C, Richards AL, et al. Human seroepidemiology of *Rickettsia* and *Orientia* species in Chile—a cross-sectional study in 5 regions. Ticks Tick Borne Dis. 2020;11:101503. https://doi.org/10.1016/j.ttbdis.2020.101503

Address for correspondence: Thomas Weitzel, Laboratorio Clínico, Clínica Alemana de Santiago, Av. Vitacura 5951, Santiago, Chile; email: thomas.weitzel@gmail.com; and Katia Abarca, Departamento de Enfermedades Infecciosas e Inmunología Pediátricas, Pontificia Universidad Católica de Chile, Santiago, Chile; email: katia@med.puc.cl

etymologia

Aline E. Santana, Fábio P. Sellera

Dermatophyte [dur′mə-to-fit″]

From the Greek *derma* (skin) + *phyton* (plant), dermatophytes are a group of 3 genera of filamentous fungi (*Microsporum*, *Epidermophyton*, and *Trichophyton*) that have the ability to invade keratinized tissues and cause superficial infections in humans and animals. Dermatophytes were improperly assigned to the Plantae kingdom until 1969, when they were then classified into the Fungi kingdom.

Dermatophytosis is also referred to as ringworm or tinea (Latin for "worm") because it can cause ring-shaped patches that are usually red, itchy, and have worm-like borders. In 1910, Raymond Jacques Adrien Sabouraud, a French dermatologist, was the first to report the morphologic characteristics of dermatophytes. During the decades that followed, taxonomy of dermatophytes has gone through revolutionary changes, mostly due to the advent of molecular diagnosis. Although studies performed in the 21st century have resulted in further classification changes and consolidation of new species, debates regarding the taxonomy of dermatophyte agents persist.

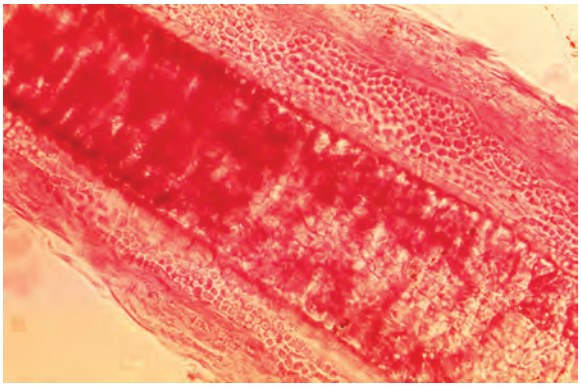

Figure. Photomicrograph of a guinea pig hair shaft specimen revealed ultrastructural features exhibited at the site of a ringworm infection by the dermatophyte, *Trichophyton mentagrophytes*. Note that the sporangia were confined to the outer region of the hair shaft, known as an exothrix infection. Original magnification ×430. CDC/Dr. Lucille K. Georg, 1968.

Sources

1. Borman AM, Summerbell RC. *Trichophyton, Microsporum, Epidermophyton*, and agents of superficial mycoses. In: Carroll KC, Pfaller MA, Landry ML, McAdam A, Patel R, Richter SS, et al., editors. Manual of clinical microbiology. Vol. 2, 12th ed. Washington: ASM Press; 2019. p. 2208–33.
2. de Hoog GS, Dukik K, Monod M, Packeu A, Stubbe D, Hendrickx M, et al. Toward a novel multilocus phylogenetic taxonomy for the dermatophytes. Mycopathologia. 2017;182:5–31. https://doi.org/10.1007/s11046-016-0073-9
3. Sabouraud R. The moths [in French]. Paris: Masson; 1910.
4. Whittaker RH. New concepts of kingdoms or organisms. Evolutionary relations are better represented by new classifications than by the traditional two kingdoms. Science. 1969;163:150–60. https://doi.org/10.1126/science.163.3863.150

Author affiliation: Universidade de São Paulo, São Paulo, Brazil

Address for correspondence: Fábio P. Sellera, Department of Internal Medicine, School of Veterinary Medicine and Animal Science, Universidade de São Paulo, São Paulo SP- 05508-270, Brazil; email: fsellera@usp.br

DOI: https://doi.org/10.3201/eid2609.ET2609

Clinicopathologic and Immunohistochemical Findings from Autopsy of Patient with COVID-19, Japan

Takuya Adachi, Ja-Mun Chong, Noriko Nakajima, Masahiro Sano, Jun Yamazaki, Ippei Miyamoto, Haruka Nishioka, Hidetaka Akita, Yuko Sato, Michiyo Kataoka, Harutaka Katano, Minoru Tobiume, Tsuyoshi Sekizuka, Kentaro Itokawa, Makoto Kuroda, Tadaki Suzuki

An autopsy of a patient in Japan with coronavirus disease indicated pneumonia lung pathology, manifested as diffuse alveolar damage. We detected severe acute respiratory syndrome coronavirus 2 antigen in alveolar epithelial cells and macrophages. Coronavirus disease is essentially a lower respiratory tract disease characterized by direct viral injury of alveolar epithelial cells.

Coronavirus disease (COVID-19), which was first reported in December 2019 in Wuhan, China, has been spreading rapidly and on a global scale. The causative virus is severe acute respiratory syndrome coronavirus 2 (SARS-CoV-2) (*1*). The World Health Organization declared the outbreak of COVID-19 to be pandemic on March 11, 2020, and had reported 693,282 laboratory-confirmed cases and 33,106 deaths globally as of March 30 (*2*). Numerous studies of the clinical features of COVID-19 and the virologic characteristics of SARS-CoV-2 have been conducted in China to date (*3*,*4*). Postmortem examination will provide valuable information required to elucidate the pathogenesis of COVID-19; however, only 2 studies have been published on COVID-19 pathology thus far (*5*,*6*). Further, the distribution of SARS-CoV-2 in a patient and identification of which cells are infected by SARS-CoV-2 have yet to be reported.

We describe the clinical course and the pathologic and virologic findings upon autopsy of a passenger on a cruise ship who died from COVID-19. The ship departed the port of Yokohama, Japan, on January 20, 2020, with a total of 3,711 passengers and crew; 712 (19%) of the persons on board were laboratory confirmed as having COVID-19. Of those, 12 had died as of March 31 (*7*).

Affiliations: Toshima Hospital, Tokyo, Japan (T. Adachi, J.-M. Chong, M. Sano, J. Yamazaki, I. Miyamoto, H. Nishioka, H. Akita); National Institute of Infectious Diseases, Tokyo, Japan (N. Nakajima, Y. Sato, M. Kataoka, H. Katano, M. Tobiume, T. Sekizuka, K. Itokawa, M. Kuroda, T. Suzuki)

DOI: https://doi.org/10.3201/eid2609.201353

Case Report

The passenger, an 84-year-old woman from Japan who had no notable medical history, had onset of fever (38.8°C) on February 5, followed by diarrhea (Table 1). On February 9, she went to the ship's medical office with shortness of breath, and a throat swab sample was taken. Three days later (illness day 8), she was admitted to Toshima Hospital (Tokyo, Japan) with dyspnea on exertion; body temperature was 38.2°C, pulse rate 70 beats/min, blood pressure 156/80 mm Hg, respiratory rate 16 breaths/min, and oxygen saturation 95% (with 2 L/min oxygen supplementation). A chest radiograph showed opacities in both lungs, and a computed tomography scan revealed ground glass opacities and consolidations, mainly in bilateral lower lung lobes (Figure 1, panels A–C). The diagnosis of COVID-19 was confirmed by real-time reverse transcription PCR on the throat swab and reported on illness day 9. On illness day 10, hypoxia progressed, even with 15 L/min oxygen supplementation. The patient expressly stated that she did not want mechanical ventilation. Ampicillin/sulbactam was administered intravenously, based on the identification of *Klebsiella pneumoniae* and methicillin-sensitive *Staphylococcus aureus* by sputum culture. Corticosteroids were added after the appearance of progressive hypoxemia and acute respiratory distress syndrome. On illness day 13, the antiretroviral

Table 1. Symptoms, signs, laboratory results, and treatment administered for an 84-year-old woman who died from coronavirus disease, by day of illness, cruise ship and Toshima Hospital, Tokyo, Japan, February 2020*

	Day of illness														
	Cruise ship							Hospital							
Characteristic	1	2	3	4	5	6	7	8	9	10	11	12	13	14	15	16
Symptom																
Temperature, °C	38.8				38.5		38.9	38.3	37.9	37.5	37.1	37.2	37.5	37.7	36.9	
Dyspnea†				+	+	+	+	++	++	++	++	+++	+++	+++	+++	+++
SaO_2, %								95–96	90–95	86–94	84–92	83–86	79–84	74–84	66–79	
Intervention																
O_2 (L/min)								2	5	15	15	15	15	15	15	15
ABPC/SBT											*	*	*	*	*	
MPSL, HYD										*	*	*		*	*	*
LPV/r													*	*	*	
Morphine														*	*	*
Blood test result																
Leukocytes, $10^3/\mu L$								3.7		4.2			12.4			
PLT, $10^4/\mu L$								13.4		14.0			22.8			
AST, U/L								53		58			46			
ALT, U/L								25		26			28			
CRE, mg/dL								0.71		0.64			0.63			
CRP, mg/dL								2.66		3.40			1.32			

*ABPC/SBT, ampicillin/sulbactam; ALT, alanine aminotransferase; AST, aspartate aminotransferase; CRE, creatinine; CRP, C-reactive protein; HYD, hydrocortisone; LPV/r, lopinavir/ritonavir; MPSL, methylprednisolone; PLT, platelet; SaO_2, oxygen saturation.
†Dyspnea severity indicated by +, mild; ++, moderate; +++, severe.

drug lopinavir/ritonavir was added orally. Despite all these treatment efforts, the dyspnea progressed and chest radiograph findings worsened (Figure 1, panel D). Intravenous morphine was initiated to alleviate breathing difficulties from illness on day 14. The patient died from respiratory failure on February 20 (illness day 16). The patient's family gave consent for an autopsy to be performed.

An autopsy was conducted 5 hours after death, with the exception of the brain and bone marrow. Macroscopically, the trachea and bronchi exhibited neither redness nor erosion; however, the lungs (left, 590 g; right, 690 g) were partially dark red, consolidated, and airless. The cut surface was slightly sticky. Specifically, both pleurae were slightly thickened, with pleural effusions of <1 mL in each pleural cavity. The heart (420 g) showed right ventricular dilatation, with 10 mL of cardiac effusion. We noted diffuse multiple punctate hemorrhages in the mucosa of the stomach and duodenum. Histologic analysis revealed that the lungs exhibited features of both exudative and organizing diffuse alveolar damage (DAD). The lung tissues in the exudative phase of DAD showed prominent hyaline membranes (Figure 2, panel A), and those in the organizing phase of DAD showed desquamation, squamous metaplasia of the epithelial cells (Figure 2, panel B), organizing hyaline membranes (Figure 2, panel C), and inflammatory cell infiltration with prominent plasma cells in the alveolar septa (Figure 2, panel D). We observed intra-alveolar hemorrhage, vascular congestion, and hyperplasia of type 2 pneumocytes. We also noted multinucleated syncytial cells. In addition, we detected hemophagocytosis in the lungs, spleen, and lymph nodes (Figure 2, panel E). The glomeruli of both kidneys were marked by microthrombi, suggesting early signs of disseminated intravascular coagulation (Figure 2, panel F). We observed no notable changes in the other organs.

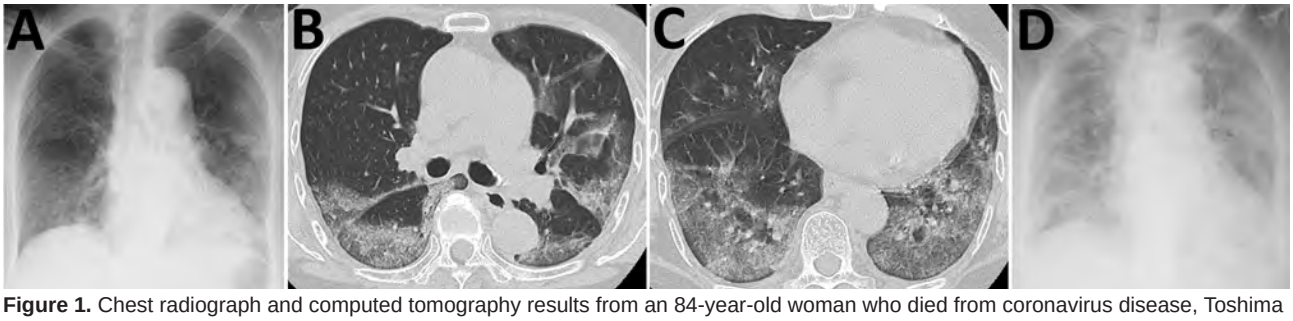

Figure 1. Chest radiograph and computed tomography results from an 84-year-old woman who died from coronavirus disease, Toshima Hospital, Tokyo, Japan, February 2020. A) Chest radiographs taken on admission (illness day 8), showing reticular shadows, mainly in bilateral lower lung fields. B, C) Chest computed tomography scan taken on illness day 8, indicating ground-glass opacities mainly located in posterior segments of the bilateral lower lobes, where the highest numbers of viral RNA copies were found on autopsy. D) Chest radiographs taken on illness day 14, with shadows spreading to almost entire lungs and exhibiting air bronchograms.

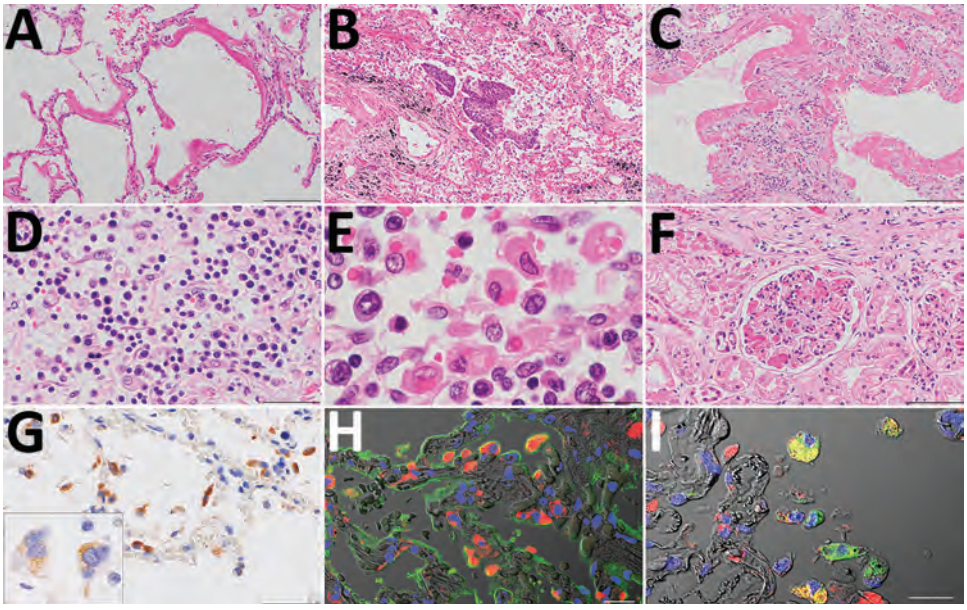

Figure 2. Pathologic findings for the lungs, lymph nodes, and kidneys in an autopsy of an 84-year-old woman who died from coronavirus disease, Toshima Hospital, Tokyo, Japan, February 2020. A) Marked diffuse alveolar damage in exudative phase with prominent hyaline membrane formation in lung tissues. Hematoxylin & eosin (H&E) staining. Scale bar indicates 200 μm. B, C) Desquamation and squamous metaplasia of the epithelium (B) and organized hyaline membranes (C), with septal fibrosis in the organizing phase lesions in lung sections. H&E staining. Scale bar indicates 200 μm. D) Inflammatory infiltrate comprised predominately of plasma cells in the alveolar septa. H&E staining. Scale bar indicates 50 μm. E) Obvious erythrophagocytic macrophages in the lymph nodes. H&E staining. Scale bar indicates 20 μm. F) Numerous microthrombi in the glomerulus in the kidneys. H&E staining. Scale bar indicates 100 μm. G) Immunostaining (brown) of severe acute respiratory syndrome coronavirus 2 antigen in alveolar epithelial cells. Scale bar indicates 50 μm. Inset: multinucleated syncytial cells; scale bar indicates 20 μm. H, I) Double immunofluorescence staining for severe acute respiratory syndrome coronavirus 2 (red) with epithelial cell marker (H; epithelial membrane antigen staining, green); macrophage marker (I; anti-CD68 antibody staining, green) in the same cell. TO-PRO-3 nucleic acid staining (blue) and differential contrast images are also shown. Scale bar indicates 20 μm.

To examine the distribution of SARS-CoV-2 antigens, we performed immunohistochemistry on all tissue sections by using rabbit polyclonal antibodies against the SARS-CoV nucleocapsid protein (*8*). We confirmed the reactivity of the antibody by using SARS-CoV-2–infected VeroE6/TMPRSS2 cells as a positive control and a mock-infected VeroE6/TMPRSS2 cells as a negative control (*9*). We detected SARS-CoV-2 antigens in the cytoplasm of alveolar epithelial cells in earlier-stage DAD lesions, with mild inflammation before formation of hyaline membranes (Figure 2, panel G) rather than progressed lesions. We also detected viral antigens detected in the cytoplasm of multinucleated syncytial cells (Figure 2, panel G, inset). We detected no signals in the trachea, intestine, or other extrapulmonary tissue sections. Double immunofluorescence staining revealed that the viral antigen was present in epithelial membrane antigen-positive alveolar epithelial cells and CD68 (clone PGM-1)–positive alveolar macrophages (Figure 2, panels H and I).

We determined copy numbers of SARS-CoV-2 RNA in various specimens by using real-time reverse transcription PCR to amplify a segment in the nucleocapsid protein–encoding region of SARS-CoV-2 RNA, using forward (5¢-GGCCGCAAATTGCACAAT-3¢) and reverse (5¢-CCAATGCGCGACATTCC-3¢) primers, and a labeled probe 5¢-(FAM)-CCCCCAGCGCTTCAGCGTTCT-(TAMRA)-3¢ (Table 2). We collected postmortem tissues by using a new set of forceps and scissors for each sample to avoid cross-contamination. We used the amount of human glyceraldehyde-3-phosphate dehydrogenase mRNA in the RNA extracted from each tissue as an internal reference for normalization. Although SARS-CoV-2 RNA loads in serum samples increased from illness day 8 to day 13, at the time of autopsy, we detected SARS-CoV-2 RNA at low levels in whole blood and feces but not in urine. The copy numbers of SARS-CoV-2 RNA detected in the swab samples collected during the autopsy were higher in the right bronchus than in the nasopharynx. In addition, SARS-CoV-2 RNA glyceraldehyde-3-phosphate dehydrogenase mRNA ratios in each tissue sample showed that viral loads in peripheral lung tissues were higher than those in trachea, bronchi, and upper respiratory tract tissues. We also detected low levels of SARS-CoV-2 RNA in nonrespiratory tract tissues, including the colon, liver, and spleen. Whole-genome sequencing of SARS-CoV-2 from the lung of the patient did not indicate substantial mutations except for a few single-nucleotide variations, including G11083T transversion compared with Wuhan-Hu-1 (GenBank accession no. MN908947; GISAID identification no. EPIISL402125), which is shared by the isolates obtained from the Diamond Princess cruise ship outbreak.

Table 2. Quantification of SARS-CoV-2 RNA in multiple specimens from an 84-year-old woman who died from coronavirus disease, Toshima Hospital, Tokyo, Japan, February 2020*

Day of illness	Specimen type or site	SARS-CoV-2 RNA	SARS-CoV-2, copies/reaction	GAPDH, copies/reaction	SARS-CoV-2 to GAPDH, ratio
Day 8 (admission)	Serum, copies/μL	2.7×10^1			
Day 10		6.2×10^1			
Day 13		2.8×10^2			
Day 16 (autopsy)	Whole blood, copies/μL	1.6×10^2			
	Urine, copies/μL	UDL			
	Feces, copies/μL	1.2×10^2			
	Swabs, copies in 1 μL medium				
	Nasopharynx	2.9×10^3			
	Trachea	1.5×10^2			
	Right bronchus	6.6×10^4			
	Left bronchus	1.3×10^2			
	Rectum	3.7×10^1			
	Frozen tissues				
	Pharynx		83	2,670	3.1×10^{-2}
	Tonsils		UDL	3,730	NA
	Epiglottis		43	13,000	3.3×10^{-3}
	Trachea		UDL	145	NA
	Right bronchus		840	421	2.0×10^0
	Right lung				
	Upper, S1/S2		76,600	1,570	4.9×10^1
	Upper, S3		584	82	7.1×10^0
	Middle, S5		11,900	3,000	4.0×10^0
	Lower, S6		37,100	1,230	3.0×10^1
	Lower, S8/S9		21,500	1,860	1.2×10^1
	Lower, S7/S10		17,100	221	7.7×10^1
	Left bronchus		67	93	7.2×10^{-1}
	Left lung				
	Upper, S1+2		56,500	2,300	2.5×10^1
	Upper, S3		26,300	12,600	2.1×10^0
	Upper, S4/S5		6,260	1,530	4.1×10^0
	Lower, S6		80,500	1,840	4.4×10^1
	Lower, S8/S9		1,000	325	3.1×10^0
	Lower, S10		22,900	977	2.3×10^1
	Heart		UDL	64,800	NA
	Liver		57	104,000	5.5×10^{-4}
	Kidney		UDL	5,910	NA
	Spleen		259	444,000	6.0×10^{-4}
	Pancreas		UDL	3,690	NA
	Colon		35	5, 030	7.0×10^{-3}

*GAPDH, glyceraldehyde-3-phosphate dehydrogenase; NA, not applicable; S, segment; SARS-CoV-2; severe acute respiratory syndrome coronavirus 2; UDL, under detection limit (<10 copies/reaction).

Conclusions

We report an autopsy of an 84-year-old cruise ship passenger who died from COVID-19. Lung pathology showed exudative and organizing phases of DAD, similar to what is observed in cases of severe acute respiratory syndrome (*10*–*13*). We detected SARS-CoV-2 antigen in alveolar epithelial cells and alveolar macrophages, also similar to what is observed in cases of severe acute respiratory syndrome (*14*,*15*). COVID-19 begins with upper respiratory tract symptoms (*3*) and ultimately becomes a lower respiratory tract disease in the later stages, based on the higher copy numbers of SARS-CoV-2 in the lower respiratory tract, relative to serum, whole blood, urine, feces, and rectal swab specimens taken during the clinical course and after death. COVID-19 is probably caused by direct injury of alveolar epithelial cells by SARS-CoV-2, accompanied by secondary damage to nonrespiratory organs. The high prevalence of SARS-CoV-2 infection on the cruise ship could not be attributed to specific genetic mutations of the virus.

Acknowledgments

Our deepest condolences go to the family of the patient, who was a caring mother and grandmother, and for whom a cruise ship vacation was a lifetime dream. We thank the patient's family, who generously offered us an opportunity to explore the pathology of this unknown disease, despite their grief at the loss of their family member. We also thank our nursing team at Toshima

Hospital for their diligent patient care; our pathology technicians, Asako Kusunoki, Yoko Shibasaki, and Misaki Hisawa, for their contributions to the autopsy; and Tsunekazu Hishima, Toru Motoi, and Masafumi Takimoto for their advice on pathologic diagnosis.

This study was supported in part by grants-in-aid from the Japan Agency for Medical Research and Development (AMED) to M.K. (grant nos. JP19fk0108104 and JP19fk0108103), T.S. (grant nos. JP19fk0108104, JP19fk0108110, and JP19fk0108082), and N.N. (grant no. JP19fk0108082).

About the Author

Dr. Adachi is the chief of the Department of Infectious Diseases at Toshima Hospital. His primary research interests include clinical management in an outbreak. He has been part of international outbreak response teams for Ebola disease, yellow fever, diphtheria, and cholera.

References

1. World Health Organization. Naming the coronavirus disease (COVID-19) and the virus that causes it [cited 2020 Mar 28]. https://www.who.int/emergencies/diseases/novel-coronavirus-2019/technical-guidance/naming-the-coronavirus-disease-(covid-2019)-and-the-virus-that-causes-it
2. World Health Organization. Coronavirus disease 2019 (COVID-19) situation report 67 [cited 2020 Mar 30]. https://www.who.int/emergencies/diseases/novel-coronavirus-2019/situation-reports
3. Chen N, Zhou M, Dong X, Qu J, Gong F, Han Y, et al. Epidemiological and clinical characteristics of 99 cases of 2019 novel coronavirus pneumonia in Wuhan, China: a descriptive study. Lancet. 2020;395:507–13. https://doi.org/10.1016/S0140-6736(20)30211-7
4. Lu R, Zhao X, Li J, Niu P, Yang B, Wu H, et al. Genomic characterisation and epidemiology of 2019 novel coronavirus: implications for virus origins and receptor binding. Lancet. 2020;395:565–74. https://doi.org/10.1016/S0140-6736(20)30251-8
5. Xu Z, Shi L, Wang Y, Zhang J, Huang L, Zhang C, et al. Pathological findings of COVID-19 associated with acute respiratory distress syndrome. Lancet Respir Med. 2020;8:420–2. https://doi.org/10.1016/S2213-2600(20)30076-X
6. Tian S, Hu W, Niu L, Liu H, Xu H, Xiao S-Y. Pulmonary pathology of early-phase 2019 novel coronavirus (COVID-19) pneumonia in two patients with lung cancer. J Thorac Oncol. 2020;15:700–4. https://doi.org/10.1016/j.jtho.2020.02.010
7. Japan Ministry of Health, Labor, and Welfare. Press release: current situation of the novel coronavirus infection, as of March 31 [in Japanese] [cited 2020 Mar 31]. https://www.mhlw.go.jp/stf/newpage_10636.html
8. Fukushi S, Mizutani T, Saijo M, Matsuyama S, Miyajima N, Taguchi F, et al. Vesicular stomatitis virus pseudotyped with severe acute respiratory syndrome coronavirus spike protein. J Gen Virol. 2005;86:2269–74. https://doi.org/10.1099/vir.0.80955-0
9. Matsuyama S, Nao N, Shirato K, Kawase M, Saito S, Takayama I, et al. Enhanced isolation of SARS-CoV-2 by TMPRSS2-expressing cells. Proc Natl Acad Sci U S A. 2020;117:7001–3. https://doi.org/10.1073/pnas.2002589117
10. Ding Y, Wang H, Shen H, Li Z, Geng J, Han H, et al. The clinical pathology of severe acute respiratory syndrome (SARS): a report from China. J Pathol. 2003;200:282–9. https://doi.org/10.1002/path.1440
11. Franks TJ, Chong PY, Chui P, Galvin JR, Lourens RM, Reid AH, et al. Lung pathology of severe acute respiratory syndrome (SARS): a study of 8 autopsy cases from Singapore. Hum Pathol. 2003;34:743–8. https://doi.org/10.1016/S0046-8177(03)00367-8
12. Hwang DM, Chamberlain DW, Poutanen SM, Low DE, Asa SL, Butany J. Pulmonary pathology of severe acute respiratory syndrome in Toronto. Mod Pathol. 2005;18:1–10. https://doi.org/10.1038/modpathol.3800247
13. Gu J, Korteweg C. Pathology and pathogenesis of severe acute respiratory syndrome. Am J Pathol. 2007;170:1136–47. https://doi.org/10.2353/ajpath.2007.061088
14. Nakajima N, Asahi-Ozaki Y, Nagata N, Sato Y, Dizon F, Paladin FJ, et al. SARS coronavirus-infected cells in lung detected by new in situ hybridization technique. Jpn J Infect Dis. 2003;56:139–41.
15. Nicholls JM, Butany J, Poon LLM, Chan KH, Beh SL, Poutanen S, et al. Time course and cellular localization of SARS-CoV nucleoprotein and RNA in lungs from fatal cases of SARS. PLoS Med. 2006;3:e27. https://doi.org/10.1371/journal.pmed.0030027

Address for correspondence: Tadaki Suzuki, Department of Pathology, National Institute of Infectious Diseases, 1-23-1, Toyama, Shinjuku-ku, Tokyo 162-8640, Japan; e-mail: tksuzuki@nih.go.jp

Detection of Severe Acute Respiratory Syndrome Coronavirus 2 RNA on Surfaces in Quarantine Rooms

Fa-Chun Jiang,[1] Xiao-Lin Jiang,[1] Zhao-Guo Wang, Zhao-Hai Meng, Shou-Feng Shao, Benjamin D. Anderson, Mai-Juan Ma

We investigated severe acute respiratory syndrome coronavirus 2 (SARS-CoV-2) environmental contamination in 2 rooms of a quarantine hotel after 2 presymptomatic persons who stayed there were laboratory-confirmed as having coronavirus disease. We detected SARS-CoV-2 RNA on 8 (36%) of 22 surfaces, as well as on the pillow cover, sheet, and duvet cover.

Severe acute respiratory syndrome coronavirus 2 (SARS-CoV-2) has rapidly spread globally and, as of May 2, 2020, had caused >3 million confirmed coronavirus disease cases (*1*). Although SARS-CoV-2 transmission through respiratory droplets and direct contact is clear, the potential for transmission through contact with surfaces or objects contaminated with SARS-CoV-2 is poorly understood (*2*). The virus can be detected on various surfaces in the contaminated environment from symptomatic and paucisymptomatic patients (*3*,*4*). Moreover, we recently reported detection of SARS-CoV-2 RNA on environmental surfaces of a symptomatic patient's household (*5*). Because SARS-CoV-2 remains viable and infectious from hours to days on surfaces (*6*,*7*), contact with a contaminated surface potentially could be a medium for virus transmission. In addition, high viral load in throat swab specimens at symptom onset (*8*,*9*) and peak infectiousness at 0–2 days for presymptomatic patients (*8*) suggest that presymptomatic patients may easily contaminate the environment. However, data are limited on environmental contamination of SARS-CoV-2 by patients who may be presymptomatic. Therefore, to test this hypothesis, we examined the presence of SARS-CoV-2 RNA in collected environmental surface swab specimens from 2 rooms of a centralized quarantine hotel where 2 presymptomatic patients had stayed.

The Study

Two Chinese students studying overseas returned to China on March 19 (patient A) and March 20 (patient B), 2020 (Table 1). On the day of their arrival in China, neither had fever or clinical symptoms, and they were transferred to a hotel for a 14-day quarantine. They had normal body temperatures (patient A, 36.3°C; patient B, 36.5°C) and no symptoms when they checked into the hotel. During the quarantine period, local medical staff were to monitor their body temperature and symptoms each morning and afternoon. On the morning of the second day of quarantine, they had no fever (patient A, 36.2°C; patient B, 36.7°C) or symptoms. At the same time their temperatures were taken, throat swab samples were collected; both tested positive for SARS-CoV-2 RNA by real-time reverse transcription PCR (rRT-PCR). The students were transferred to a local hospital for treatment. At admission, they remained presymptomatic, but nasopharyngeal swab, sputum, and fecal samples were positive for SARS-CoV-2 RNA with high viral loads (Table 1). In patient A, fever (37.5°C) and cough developed on day 2 of hospitalization, but his chest computed tomography images showed no significant abnormality during hospitalization. In patient B, fever (37.9°C) and cough developed on day 6 of

Author affiliations: Qingdao Municipal Center for Disease Control and Prevention, Qingdao, China (F.-C. Jiang, Z.-G. Wang, Z.-H. Meng, S.-F. Shao); Shandong Provincial Center for Disease Control and Prevention, Jinan, China (X.-L. Jiang); Global Health Research Center, Duke Kunshan University, Kunshan, China (B.D. Anderson); State Key Laboratory of Pathogen and Biosecurity, Beijing Institute of Microbiology and Epidemiology, Beijing, China (M.-J. Ma)

DOI: https://doi.org/10.3201/eid2609.201435

[1]These authors contributed equally to this article.

Table 1. Timeline from return to China by 2 persons with presymptomatic SARS-CoV-2 infection to results of environmental sampling of their rooms at a centralized quarantine hotel, 2020*

Characteristic	Patient A	Patient B
Date returned to China	19 Mar	20 Mar
Date entered quarantine	19 Mar	21 Mar
Date of SARS-CoV-2 RNA–positive detection	20 Mar	22 Mar
Date of environmental surface sampling	20 Mar	22 Mar
Symptoms at hospital admission	None	None
C_t for clinical samples at admission†		
Nasopharyngeal swab	24.72	27.87
Sputum	28.61	23.23
Fecal swab	33.12	NA
Symptoms during hospitalization	Fever, chills, cough	Fever, cough, sputum, sore throat
Disease severity	Mild	Moderate

*C_t, cycle threshold; NA, not available; rRT-PCR, real-time reverse transcription PCR; SARS-CoV-2, severe acute respiratory syndrome coronavirus 2.
†A lower C_t indicates a higher viral load. Only C_t values for open reading frame1ab (*ORF*ab1) gene of SARS-CoV-2 were provided in the table because the Ct values for nucleoprotein were similar to values of *ORF*ab1.

hospitalization, and her computed tomography images showed ground-glass opacities.

Approximately 3 hours after the 2 patients were identified as positive for SARS-CoV-2 RNA, we sampled the environmental surfaces of the 2 rooms in the centralized quarantine hotel in which they had stayed. Because of the SARS-CoV-2 outbreak in China, the hotel had been closed during January 24–March 18, 2020. Therefore, only these 2 persons had stayed in the rooms. We used a sterile polyester-tipped applicator, premoistened in viral transport medium, to sample the surfaces of the door handle, light switch, faucet handle, thermometer, television remote, pillow cover, duvet cover, sheet, towel, bathroom door handle, and toilet seat and flushing button. We also collected control swab samples from 1 unoccupied room. We collected each sample by swabbing each individual surface. We tested the samples with an rRT-PCR test kit (DAAN GENE Ltd, http://www.daangene.com) targeting the open reading frame 1ab (*ORF*1ab) and *N* genes of SARS-CoV-2. We interpreted cycle threshold (C_t) <40 as positive for SARS-CoV-2 RNA and $C_t \geq 40$ as negative.

We collected a total of 22 samples from the 2 rooms of the quarantine hotel (Table 2). Eight (36%) samples were positive for SARS-CoV-2 RNA. C_t values ranged from 28.75 to 37.59 (median 35.64). Six (55%) of 11 samples collected from the room of patient A were positive for SARS-CoV-2 RNA. Surface samples collected from the sheet, duvet cover, pillow cover, and towel tested positive for SARS-CoV-2 RNA, and surface samples collected from the pillow cover and sheet had a high viral load; C_t for *ORF*1ab gene from the pillow cover was 28.97 and from the sheet, 30.58. Moreover, the C_t values of these 2 samples correlated with those of patient A's nasopharyngeal (24.73) and fecal (33.12) swab samples at hospital admission. One surface sample from the faucet in patient B's room was positive for SARS-CoV-2 RNA; the C_t was 28.75 for the *ORF*1ab gene. Again, we detected SARS-CoV-2 RNA from the surface samples of the pillow cover; C_t was 34.57. All control swab samples were negative for SARS-CoV-2 RNA.

Conclusions

Our study demonstrates extensive environmental contamination of SARS-CoV-2 RNA in a relatively short time (<24 hours) in occupied rooms of 2 persons who were presymptomatic. We also detected SARS-CoV-2 RNA in the surface swab samples of the pillow cover, duvet cover, and sheet.

Evidence for SARS-CoV-2 transmission by indirect contact was identified in a cluster of infections at a shopping mall in China (*10*). However, no clear evidence of infection caused by contact with the contaminated environment was found. SARS-CoV-2 RNA has been detected on environmental surfaces in isolation rooms where the symptomatic or paucisymptomatic patients stayed for several days (*3*–*5*). In our study, we demonstrate high viral load shedding in presymptomatic patients, which is consistent with previous studies (*8*,*9*), providing further evidence for the presymptomatic transmission of the virus (*5*,*11*–*15*).

Table 2. Results of environmental sampling of 2 rooms at a centralized quarantine hotel occupied by 2 presymptomatic SARS-CoV-2–infected patients, China, 2020*

Environmental source†	Values‡	
	Patient A's room	Patient B's room
Door handle	0/1	0/1
Light switch	1/1 (37.59)	0/1
Faucet	0/1	1/1 (28.75)
Bathroom door handle	1/1 (36.02)	0/1
Toilet seat, flush handle	0/1	0/1
Thermometer	0/1	0/1
TV remote	0/1	0/1
Pillow cover	1/1 (28.98)	1/1 (34.57)
Duvet cover	1/1 (35.64)	0/1
Sheet	1/1 (30.58)	0/1
Towel	1/1 (36.98)	0/1
Total, no. (%)	6/11 (54.5)	2/11 (18.2)

*Values are no. positive/total (C_t) except as indicated. C_t, cycle threshold; rRT-PCR, real-time reverse transcription PCR; SARS-CoV-2, severe acute respiratory syndrome coronavirus 2.
†One swab was taken from each site except the light switch, from which 2 swabs were taken.
‡All samples taken from patients A and B after disinfection were negative and not included in this table. A lower C_t indicates a higher viral load. Only C_t values for open reading frame 1ab (ORFab1) gene of SARS-CoV-2 were provided because the C_t values for nucleoprotein were similar to those of *ORF*ab1.

In addition, presymptomatic patients with high viral load shedding can easily contaminate the environment in a short period.

Our results also indicate a higher viral load detected after prolonged contact with sheets and pillow covers than with intermittent contact with the door handle and light switch. The detection of SARS-CoV-2 RNA in the surface samples of the sheet, duvet cover, and pillow cover highlights the importance of proper handling procedures when changing or laundering used linens of SARS-CoV-2 patients. Thus, to minimize the possibility of dispersing virus through the air, we recommend that used linens not be shaken upon removal and that laundered items be thoroughly cleaned and dried to prevent additional spread.

The absence of viral isolation in our investigation was an obstacle to demonstrating the infectivity of the virus, but SARS-CoV-2 has been reported to remain viable on surfaces of plastic and stainless steel for up to 4–7 days (*6*,*7*) and 1 day for treated cloth (*7*). In summary, our study demonstrates that presymptomatic patients have high viral load shedding and can easily contaminate environments. Our data also reaffirm the potential role of surface contamination in the transmission of SARS-CoV-2 and the importance of strict surface hygiene practices, including regarding linens of SARS-CoV-2 patients.

This work was supported by the National Major Project for Control and Prevention of Infectious Disease of China (2017ZX10303401-006), the National Natural Science Foundation of China (81773494 and 81621005), and the Special National Project on investigation of basic resources of China (2019FY101502).

About the Author

Dr. Jiang is an epidemiologist in Qingdao Center for Disease Control and Prevention, Qingdao, Shandong Province, China. His primary research interests included infectious disease control and prevention and emerging infectious diseases.

References

1. World Health Organization. Coronavirus disease (COVID-19). Situation report—102 [cited 2020 May 1]. https://www.who.int/docs/default-source/coronaviruse/situation-reports/20200501-covid-19-sitrep.pdf
2. Centers for Disease Control and Prevention. Coronavirus disease 2019 (COVID-19). How COVID-19 spreads [cited 2020 May 2]. https://www.cdc.gov/coronavirus/2019-ncov/prevent-getting-sick/how-covid-spreads.html
3. Ong SWX, Tan YK, Chia PY, Lee TH, Ng OT, Wong MSY, et al. Air, surface environmental, and personal protective equipment contamination by severe acute respiratory syndrome coronavirus 2 (SARS-CoV-2) from a symptomatic patient. JAMA. 2020;323:1610. https://doi.org/10.1001/jama.2020.3227
4. Yung CF, Kam KQ, Wong MSY, Maiwald M, Tan YK, Tan BH, et al. Environment and personal protective equipment tests for SARS-CoV-2 in the isolation room of an infant with infection. Ann Intern Med. 2020 Apr 1 [Epub ahead of print]. PubMed https://doi.org/10.7326/M20-0942
5. Jiang XL, Zhang XL, Zhao XN, Li CB, Lei J, Kou ZQ, et al. Transmission potential of asymptomatic and paucisymptomatic SARS-CoV-2 infections: a three-family cluster study in China. J Infect Dis. 2020 Apr 22 [Epub ahead of print]. https://doi.org/10.1093/infdis/jiaa206
6. van Doremalen N, Bushmaker T, Morris DH, Holbrook MG, Gamble A, Williamson BN, et al. Aerosol and surface stability of SARS-CoV-2 as compared with SARS-CoV-1. N Engl J Med. 2020;382:1564–7. https://doi.org/10.1056/NEJMc2004973
7. Chin AWH, Chu JTS, Perera MRA, Hui KPY, Yen H-L, Chan MCW, et al. Stability of SARS-CoV-2 in different environmental conditions. Lancet Microbe. 2020;1:e10. https://doi.org/10.1016/S2666-5247(20)30003-3
8. He X, Lau EHY, Wu P, Deng X, Wang J, Hao X, et al. Temporal dynamics in viral shedding and transmissibility of COVID-19. Nat Med. 2020 Apr 15 [Epub ahead of print]. https://doi.org/10.1038/s41591-020-0869-5
9. Wölfel R, Corman VM, Guggemos W, Seilmaier M, Zange S, Müller MA, et al. Virological assessment of hospitalized patients with COVID-2019. Nature. 2020 Apr 1 [Epub ahead of print]. https://doi.org/10.1038/s41586-020-2196-x
10. Cai J, Sun W, Huang J, Gamber M, Wu J, He G. Indirect virus transmission in cluster of COVID-19 cases, Wenzhou, China, 2020. Emerg Infect Dis. 2020 Mar 12[Epub ahead of print]. https://doi.org/10.3201/eid2606.200412
11. Rothe C, Schunk M, Sothmann P, Bretzel G, Froeschl G, Wallrauch C, et al. Transmission of 2019-nCoV infection from an asymptomatic contact in Germany. N Engl J Med. 2020;382:970–1. https://doi.org/10.1056/NEJMc2001468
12. Yu P, Zhu J, Zhang Z, Han Y. A familial cluster of infection associated with the 2019 novel coronavirus indicating potential person-to-person transmission during the incubation period. J Infect Dis. 2020;221:1757–61. https://doi.org/10.1093/infdis/jiaa077
13. Tong ZD, Tang A, Li KF, Li P, Wang HL, Yi JP, et al. Potential presymptomatic transmission of SARS-CoV-2, Zhejiang province, China, 2020. Emerg Infect Dis. 2020;26:1052–4. https://doi.org/10.3201/eid2605.200198
14. Wei WE, Li Z, Chiew CJ, Yong SE, Toh MP, Lee VJ. Presymptomatic transmission of SARS-CoV-2—Singapore, January 23–March 16, 2020. MMWR Morb Mortal Wkly Rep. 2020;69:411–5. https://doi.org/10.15585/mmwr.mm6914e1
15. Kimball A, Hatfield KM, Arons M, James A, Taylor J, Spicer K, et al.; Public Health–Seattle & King County; CDC COVID-19 Investigation Team. Asymptomatic and presymptomatic SARS-CoV-2 infections in residents of a long-term care skilled nursing facility—King County, Washington, March 2020. MMWR Morb Mortal Wkly Rep. 2020;69:377–81. https://doi.org/10.15585/mmwr.mm6913e1

Address for correspondence: Mai-Juan Ma, State Key Laboratory of Pathogen and Biosecurity, Beijing Institute of Microbiology and Epidemiology, No. 20, Dongdajie St., Fengtai District, Beijing 100071, China; email: mjma@163.com

Large Outbreak of Coronavirus Disease among Wedding Attendees, Jordan

Dawood Yusef, Wail Hayajneh, Samah Awad, Suleiman Momany, Basheer Khassawneh, Shaher Samrah, Basil Obeidat, Liqaa Raffee, Ibrahim Al-Faouri, Ali Bani Issa, Heba Al Zamel, Enas Bataineh, Reem Qdaisat

In March 2020, a wedding in Jordan led to a large outbreak of coronavirus disease (COVID-19). We collected data on 350 wedding attendees, 76 who of whom developed COVID-19. Our study shows high communicability of COVID-19 and the enormous risk for severe acute respiratory syndrome 2 virus transmission during mass gatherings.

As of March 15, 2020, Jordan had only 1 confirmed case of coronavirus disease (COVID-19) (*1*). However, a wedding ceremony on March 13 led to a large outbreak of COVID-19 in northern Jordan. We believe the index case-patient was the bride's father, who arrived in Jordan from Spain, where local disease transmission was occurring (*2*), 4 days before the wedding. We describe characteristics of confirmed COVID-19 cases, symptoms, time from exposure to symptom onset, and other clinical features.

Methods

On March 13, a 2-hour wedding ceremony and party were held in an indoor venue designed to accommodate ≤400 guests. The exact number of attendees is unknown but estimated to be ≈360 based on discussions with the local health department. We identified 350 attendees and collected nasopharyngeal swabs for reverse transcription PCR (RT-PCR), regardless of the presence or absence of symptoms. Our study included persons who attended the wedding or had close contact with attendees and tested positive for severe acute respiratory syndrome coronavirus 2 (SARS-CoV-2), the causative agent of COVID-19. We collected data by using electronic medical records and direct phone calls with confirmed cases or their legal guardians. We performed RT-PCR on samples from 350 possible cases within 4 weeks of exposure at the wedding.

We collected demographic data, including age and gender; each person's general health status; symptoms at time of diagnosis; time from exposure to symptom onset or diagnosis, if asymptomatic; severity of symptoms, if present; and outcomes for confirmed cases. We analyzed data by using SPSS Statistics 21 (IBM, https://www.ibm.com) and used descriptive statistics to calculate means, medians, and ranges or counts and percentages. Jordan University of Science and Technology, Irbid, provided IRB approval (no. 233-2020)

The presumed index case-patient, the bride's father, is a 58-year-old man. He developed fever, cough, and a runny nose 2 days before the wedding. On March 15, he went to an emergency department and tested positive for SARS-CoV-2. He had no known exposure to persons with COVID-19 in Spain. When he arrived in Jordan, he had contact with his immediate family, other relatives, and the groom during the 4 days before the wedding.

Four weeks after the wedding, in addition to the index case-patient, 85 persons with a history of exposure related to the wedding tested positive for SARS-CoV-2. Of these, 76 (89.4%) attended the wedding; 9 (10.6%) did not attend the wedding but were close contacts of confirmed cases from the wedding. All confirmed COVID-19 case-patients were admitted to the hospital and strictly monitored daily, following national policy for the care of persons with confirmed cases.

Among 76 wedding attendees who tested positive for SARS-CoV-2, 40 (52.6%) were symptomatic and 36 (47.4%) were asymptomatic at diagnosis (Table 1). All were detected during surveillance performed by the public health authority of the ministry of health. One case-patient was pregnant and delivered a healthy full-term baby on the second day of hospital admission. Samples collected from

Author affiliation: Jordan University of Science and Technology, King Abdullah University Hospital, Irbid, Jordan

DOI: https://doi.org/10.3201/eid2609.201469

Table. Demographic and clinical features of 76 persons with confirmed coronavirus disease who attended a wedding, Jordan

Characteristics	No. (%)
Sex	
M	30 (39.5)
F	46 (60.5)
Relatives and friends of groom*	44 (57.9)
Relatives and friends of bride	32 (42.1)
Demographics	
Children <18 y	17 (22.4)
Adults ≥18 y	59 (77.6)
Age group, median 27 (range 2–80) y	
0–9	3 (3.9)
10–19	17 (22.4)
20–29	21 (27.6)
30–39	6 (7.9)
40–49	12 (15.8)
50–59	11 (14.5)
≥60	6 (7.9)
Symptoms at time of diagnosis	
Yes	40 (52.6)
No	36 (47.4)
Concurrent conditions†	
Yes	15 (19.8)
No	61 (80.2)

*Including the groom.
†Concurrent conditions included hypertension, diabetes mellitus, hypothyroidism, ischemic heart disease, and cancer.

the baby at birth and 48 hours of age tested negative for SARS-CoV-2 by RT-PCR.

Among symptomatic case-patients, the most common signs and symptoms were cough (70%), fever (60%), runny or congested nose (52.5%), headache (35%), sore throat (25%), fatigue or myalgia (17.5%), and shortness of breath (12.5%). Most (38) had mild symptoms, but 2 case-patients had serious or critical conditions. One, an 80-year-old woman with breast cancer, developed progressive pneumonia and respiratory failure and died 2 weeks after admission to the hospital for monitoring. We noted no statistical difference in the presence of concurrent conditions between symptomatic (15%) and asymptomatic (19%) case-patients ($p = 0.76$). The median time from exposure at the wedding and symptom onset was 5 days (range 2–13 days).

All 9 confirmed case-patients who did not attend the wedding were household contacts of wedding attendees. Among those, only 4 were symptomatic and developed initial symptoms 9, 11, 16, and 19 days after the wedding. The other 5 cases were asymptomatic and were detected during government surveillance. No further cases were confirmed at 4 weeks after the wedding.

Conclusions

COVID-19 is a serious pandemic disease and a public health threat. Our study shows a relatively high communicability of SARS-CoV-2. Among 350 identified wedding attendees, 76 tested positive by RT-PCR, an attack rate of 22%. Furthermore, those who were infected during the primary encounter became new sources for disease transmission, which was evident by confirmed cases among household contacts. The estimated basic reproduction number (R_0) for COVID-19 is 2–3.5, which means that 1 infected person can transmit the disease to 2–3 other susceptible persons (*3*,*4*). However, in closed and crowded social gatherings, the transmission rate can be much higher, as evidenced by this investigation. In Jordan, close physical contact, such as same-sex hugging, cheek-kissing, and hand shaking, are traditional wedding practices that convey congratulations to the host families. Also, immediate family members, especially parents of the bride and the groom, usually stand at the entrance of the wedding hall to receive congratulations from all guests. These factors, in addition to crowded dancing and close face-to-face communication, likely contributed to the large number of infections from this wedding.

We also noted a high rate (47.4%) of asymptomatic carriers among those infected. Asymptomatic carriers have been described in the literature (*5*–*7*), but their exact proportion in the community remains unknown. In addition, evidence suggests that asymptomatic SARS-CoV-2 carriers can transmit the virus to their contacts during the incubation period, which makes containing the disease more difficult (*8*,*9*). In our study, symptomatic case-patients reported symptom onset 2–13 days (median 5 days) after exposure, which coincides with the reported incubation period for COVID-19 (*3*). However, new data suggests a longer incubation period of ≤24 days is possible (*4*).

Our study has some limitations. We were not able to determine the total number of wedding attendees, which might have led us to overestimate the infectivity rate from this social gathering. Surveillance of asymptomatic persons might have missed some cases if viral shedding had not yet started or had ended before RT-PCR testing, which potentially caused us to miss some cases.

Before the outbreak from this wedding sparked a surge in COVID-19 disease, only 1 case, which was imported, had been reported in Jordan in early March. By April 10, the number of confirmed cases from the wedding constituted 24% of all COVID-19 cases in Jordan (*10*). The country has been under lockdown since March 14, and the city of Irbid, where the outbreak occurred, was isolated from the rest of the country to control the disease. No new wedding-related cases were detected by the fourth week after the event. Apart from the 1 fatality, all patients either

recovered or greatly improved, and most were discharged from the hospital.

Our study highlights the enormous risk for SARS-CoV-2 infection during mass social gatherings and the role such gatherings can play in the spread of COVID-19. In addition, it provides further evidence of asymptomatic SARS-CoV-2 transmission among secondary contacts. Communities should continue to discourage large gatherings, identify and test social contacts, and isolate confirmed cases to help control the global COVID-19 pandemic.

About the Author

Dr. Yusef is an associate professor of pediatric infectious diseases and the chairman of the Pediatric and Neonatology Department at Jordan University of Science and Technology, Jordan. His research interests include epidemiology, multidrug resistant organisms, and community and physician awareness in antimicrobial stewardship.

References:

1. World Health Organization. Coronavirus disease 2019 (COVID-19) situation report—55. Geneva: The Organization; 2020 Mar 15 [cited 2020 April 6]. https://www.who.int/docs/default-source/coronaviruse/situation-reports/20200315-sitrep-55-covid-19.pdf?sfvrsn=33daa5cb_8
2. World Health Organization. Coronavirus disease 2019 (COVID-19) situation report—49. Geneva: The Organization; 2020 Mar 9 [cited 2020 April 6]. https://www.who.int/docs/default-source/coronaviruse/situation-reports/20200309-sitrep-49-covid-19.pdf
3. Li Q, Guan X, Wu P, Wang X, Zhou L, Tong Y, et al. Early transmission dynamics in Wuhan, China, of novel coronavirus-Infected pneumonia. N Engl J Med. 2020;382:1199–207. https://doi.org/10.1056/NEJMoa2001316
4. Wang Y, Wang Y, Chen Y, Qin Q. Unique epidemiological and clinical features of the emerging 2019 novel coronavirus pneumonia (COVID-19) implicate special control measures. J Med Virol 2020 Mar 5 [Epub ahead of print]. https://doi.org/10.1002/jmv.25748
5. National Institute of Infectious Diseases, Japan. Field briefing: Diamond Princess COVID-19 cases 2020 Feb 19 [cited 2020 April 8]. https://www.niid.go.jp/niid/en/2019-ncov-e/9407-covid-dp-fe-01.html
6. Hu Z, Song C, Xu C, Jin G, Chen Y, Xu X, et al. Clinical characteristics of 24 asymptomatic infections with COVID-19 screened among close contacts in Nanjing, China. Sci China Life Sci. 2020;63:706–11. https://doi.org/10.1007/s11427-020-1661-4
7. Bai Y, Yao L, Wei T, Tian F, Jin DY, Chen L, et al. Presumed asymptomatic carrier transmission of COVID-19. JAMA. 2020;323:1406–7. https://doi.org/10.1001/jama.2020.2565
8. Yu X, Yang R. COVID-19 transmission through asymptomatic carriers is a challenge to containment. Influenza Other Respir Viruses; 2020 Apr 4 [Epub ahead of print]. PubMed https://doi.org/10.1111/irv.12743
9. Ye F, Xu S, Rong Z, Xu R, Liu X, Deng P, et al. Delivery of infection from asymptomatic carriers of COVID-19 in a familial cluster. Int J Infect Dis. 2020;94:133–8. https://doi.org/10.1016/j.ijid.2020.03.042
10. World Health Organization. Coronavirus disease 2019 (COVID-19) situation report—81. Geneva: The Organization; 2020 Apr 10 [cited 2020 Apr 10]. https://www.who.int/docs/default-source/coronaviruse/situation-reports/20200410-sitrep-81-covid-19.pdf

Address for correspondence: Dawood Yusef, Department of Pediatrics and Neonatology, Jordan University of Science and Technology, King Abdullah University Hospital, PO Box 3030, Irbid 22110, Jordan; email: dawood_hh@hotmail.com

Persistence of Severe Acute Respiratory Syndrome Coronavirus 2 in Aerosol Suspensions

Alyssa C. Fears, William B. Klimstra, Paul Duprex, Amy Hartman, Scott C. Weaver, Kenneth S. Plante, Divya Mirchandani, Jessica Ann Plante, Patricia V. Aguilar, Diana Fernández, Aysegul Nalca, Allison Totura, David Dyer, Brian Kearney, Matthew Lackemeyer, J. Kyle Bohannon, Reed Johnson, Robert F. Garry, Doug S. Reed,[1] Chad J. Roy[1]

We aerosolized severe acute respiratory syndrome coronavirus 2 and determined that its dynamic aerosol efficiency surpassed those of severe acute respiratory syndrome and Middle East respiratory syndrome coronaviruses. Although we performed experiments only once in each of several laboratories, our findings suggest retained infectivity and virion integrity for up to 16 hours in respirable-sized aerosols.

Severe acute respiratory syndrome coronavirus (SARS-CoV) 2, is a readily transmissible zoonotic pathogen and the etiologic agent of the coronavirus disease (COVID-19) pandemic (*1*). To determine aerosol stability of the virus, we measured the dynamic (short-term) aerosol efficiencies of SARS-CoV-2 and compared its efficiency with those of SARS-CoV and Middle East respiratory syndrome coronavirus (MERS-CoV).

The Study

We analyzed these 3 viruses' dynamic aerosol efficiencies using 3 nebulizers, the Collison 3-jet (C3), Collison 6-jet (C6) (http://www.chtechusa.com), and Aerogen Solo (AS) (https://www.aerogen.com), to generate viral aerosols (Appendix, https://wwwnc.cdc.gov/EID/article/26/9/20-1806-App1.pdf). We performed comparative efficiency experiments once in each of 4 aerobiology laboratories (Tulane University, New Orleans, LA, USA; National Institutes of Health Integrated Research Facility [NIH-IRF], Fort Detrick, MD, USA; US Army Medical Institute for Infectious Diseases, Fort Detrick, MD, USA; and University of Pittsburgh, Pittsburgh, PA, USA). The aerosol size distributions produced by the generators used, in mass median aerodynamic diameter, were 1–3 μm and had a geometric heterodispersity of ≈1.2–1.4. Aerosols were generated into 16-liter primate head-only exposure chambers (MERS-CoV or SARS-CoV-2) or a 30-liter rodent chamber (SARS-CoV), where the overall flow was ≈1 (Tulane) or 0.5 (NIH-IRF, US Army Medical Research Institute of Infectious Diseases, University of Pittsburgh) air changes per minute. Use chamber and corresponding flow rates enabled us to determine the dynamic efficiencies of the virus in aerosols during a short residence time. Samples were continuously collected and integrated throughout the initiation of respective nebulizers into the chamber during aerosol generation events of 10–30 min. We calculated the dynamic aerosol efficiency or spray factor (*Fs*) as a unitless quotient of initial titer (PFU/L in liquid stock) to the resulting aerosol (PFU/L aerosol) providing a quantitative indicator for comparing airborne fitness (*2*,*3*).

We determined *Fs* for all 3 viruses after <1 min of chamber residence after aerosolization (Figure 1). When we compared both MERS-CoV and SARS-CoV to SARS-CoV-2 aerosols generated with a C3 nebulizer across 3 laboratories, we noted a small but significant improvement in *Fs* for SARS-CoV-2 but not

Author affiliations: Tulane University School of Medicine, New Orleans, Louisiana, USA (A.C. Fears, R.F. Garry, C.J. Roy): University of Pittsburgh, Pittsburgh, Pennsylvania, USA (W.B. Klimstra, P. Duprex, A. Hartman, D.S. Reed); University of Texas Medical Branch, Galveston, Texas, USA (S.C. Weaver, K.S. Plante, D. Mirchandani, J.A. Plante, P.V. Aguilar, D. Fernández); US Army Medical Research Institute of Infectious Diseases, Fort Detrick, Maryland, USA (A. Nalca, A. Totura, D. Dyer, B. Kearney); National Institute of Allergy and Infectious Diseases, National Institutes of Health, Fort Detrick, Maryland, USA (M. Lackemeyer, J.K. Bohannon, R. Johnson)

DOI: https://doi.org/10.3201/eid2609.201806

[1]These authors contributed equally to this article.

for SARS-CoV (p = 0.02) or MERS-CoV (p = 0.01). Because SARS-CoV was aerosolized into a different chamber/volume than MERS-CoV and SARS-CoV-2, we cannot rule out chamber effects for the difference in *Fs* between SARS-CoV and SARS-CoV-2. Our comparison of nebulizers showed improved *Fs* for SARS-CoV-2 with the C6 (p = 0.006) and the AS (p = 0.01) over the C3 but no difference between the C6 and AS (p = 0.46).

Further studies with SARS-CoV-2 at Tulane preliminarily assessed the long-term stability of airborne virus. We used a custom-built rotating (Goldberg) drum to provide an environment in which rotational drum speed overcomes the terminal settling velocity of the 2–3-μm particles, providing a static aerosol suspension of known volume (*4*–*6*). We timed aerosol samples from the drum at 10 min and 30 min and at 2 h, 4 h, and 16 h after initiation of rotation/suspension. The entire drum volume (10.7 L) was evacuated at each sampling interval and represented a discrete aerosol generation event. We quantified virus contents by plaque assay and quantitative reverse transcription PCR (qRT-PCR). We also conducted scanning electron microscopy on the collected aerosol samples as a complimentary qualitative assessment of virion integrity after longer-term aerosol suspension (Appendix). We measured environmental parameters but did not control them during the aerosol suspension experiments. The prevailing ambient environmental conditions were 23°C SD ± 2°C and 53% SD ± 11% relative humidity throughout the aerosol stability experiments. No ultraviolet light source was used within the cavity of the drum during suspensions. After initial generation of viral bioaerosols into the drum reached steady-state concentration, the drum was sealed and maintained as a static aerosol. We conducted all sampling time points once in this set of experiments.

We graphed plaque assay and qRT-PCR results and applied nonlinear least-squares regression analysis single-order decay with no outlier detection, resulting in a poor curve fit, which typically results from a lack of replicate samples. We detected infectious SARS-CoV-2 at all time points during the aerosol suspension stability experiment (Figure 2). A minor but constant fraction of SARS-CoV-2 maintained replication-competence at all time points (Figure 2, panel A), including when sampled after 16 h of aerosol suspension. This finding resulted in a remarkably flat decay curve when measured for infectivity and failed to provide a biologic half-life ($\kappa = 2.93 \times 10^{-6}$; $t_{1/2} = 2.36 \times 10^{5}$; $\tau = 3.40 \times 10^{5}$). The curve (Figure 2, panel B) from the results of split sample analysis as

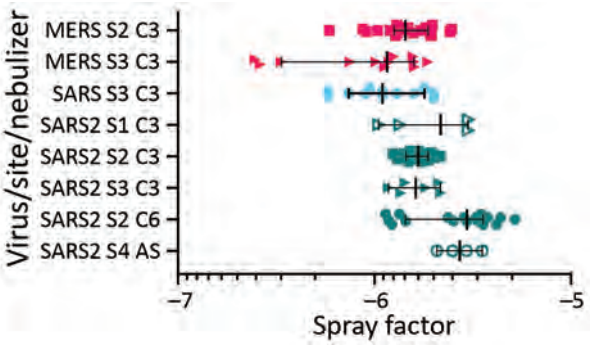

Figure 1. Aerosol efficiency of MERS-CoV, SARS-CoV and SARS-CoV-2 at different sites. Graph shows the spray factor (i.e., ratio of nebulizer concentration to aerosol concentration) for MERS-CoV (red), SARS-CoV (blue), and SARS-CoV2 (green). Aerosols were performed at 4 sites and with different nebulizers. AS, Aerogen Solo nebulizer; C3, Collison 3-jet nebulizer; C6, Collison 6-jet nebulizer; MERS-Cov, Middle East respiratory syndrome coronavirus; S1, Tulane University, New Orleans, LA, USA; S2, National Institutes of Health Integrated Research Facility, Fort Detrick, MD, USA; S3, US Army Medical Institute for Infectious Diseases, Fort Detrick, MD, USA; S4, University of Pittsburgh, Pittsburgh, PA, USA; SARS-CoV, severe acute respiratory syndrome coronavirus; SARS-CoV-2, severe acute respiratory syndrome coronavirus 2.

quantified by qRT-PCR showed minimal decreases in aerosol concentration measured in viral genome copies across all of time points sampled and approximated the decay curve of the infectious virus fraction (Figure 2, panel A), including similar decay curve characteristics ($\kappa = 6.19 \times 10^{-3}$; $t_{1/2} = 111.9$; $\tau = 161.4$).

We also performed a qualitative assessment of virion integrity after longer-term aerosol suspension (Appendix). Scanning electron microscopy (SEM) imaging of SARS-CoV-2 revealed virions that were heterogeneous in shape, either ovoid (Appendix Figure, panel A) or spherical (Appendix Figure, panel B). The minor:major axis ratio of oval virions was ≈0.7, which is consistent with prior SEM analyses of SARS-CoV-2 (https://www.flickr.com/photos/niaid/albums/72157712914621487). Airborne SARS-CoV-2 maintained the expected morphologies, size, and aspect ratios up to 16 h. Specifically, virions aged for 10 min (Appendix Figure, panels C, D) or 16 h (Appendix Figures, panels E, F) were similar in shape and general appearance to virions examined in samples of viral inoculum collected before aerosolization, which is consistent with the retention of replication-competence and suggests the potential to be infectious after long-term aging in aerosol suspension.

Conclusions

The comparison of short-term aerosol efficiencies of 3 coronaviruses showed SARS-CoV-2 approximates

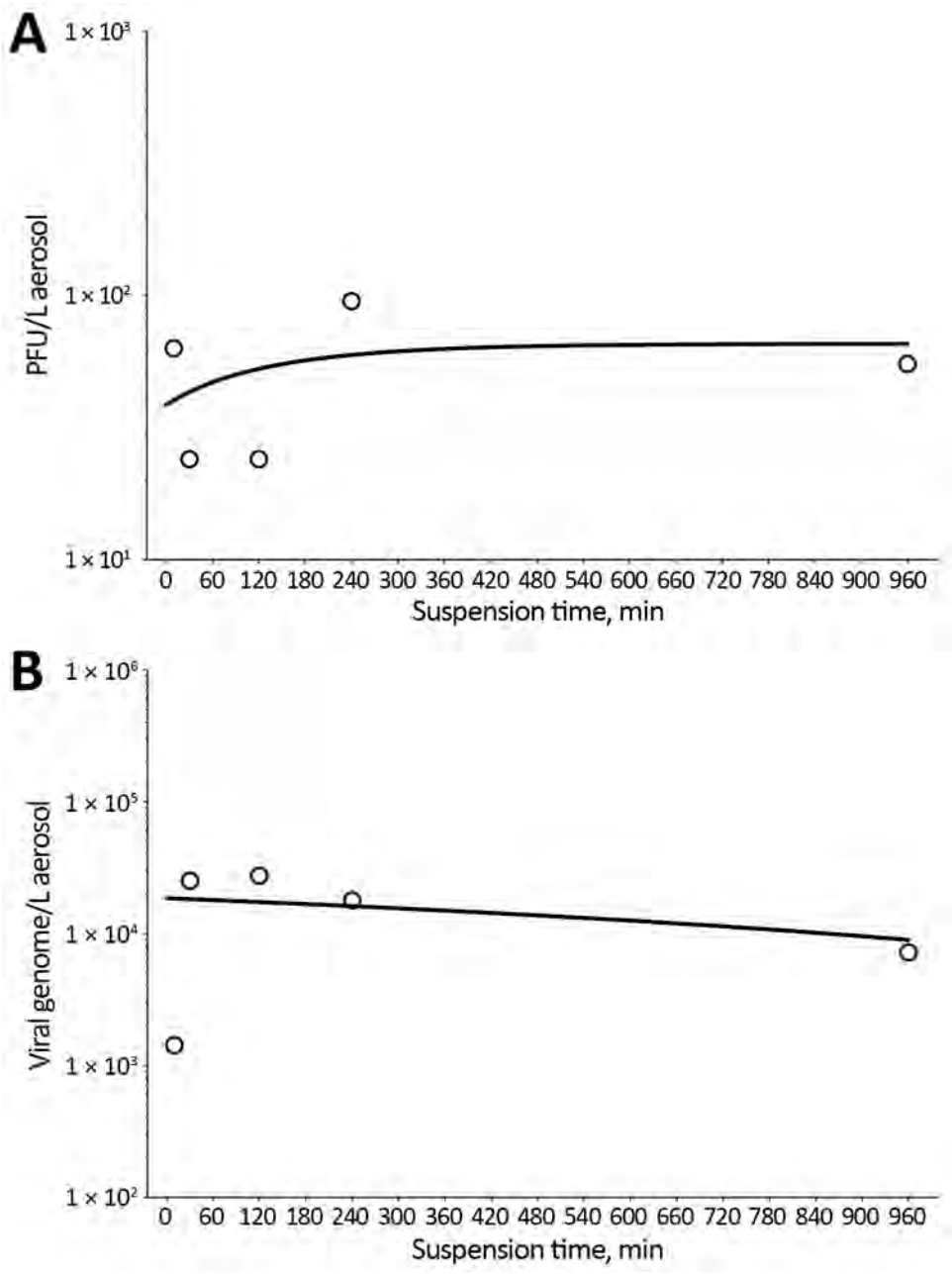

Figure 2. Decay curves of severe acute respiratory syndrome coronavirus 2 (SARS-CoV-2) in aerosol suspension. A) Aerosol concentration of infectious SARS-CoV-2 as measured by plaque assay found in impinger samples collected at 5 time points of increased aging in aerosol suspension. B) Corresponding aerosol concentration of SARS-CoV-2 in time-matched impinger samples as a function of viral genome copies as measured by reverse transcription quantitative PCR. Both time point virus estimates were graphed, and nonlinear least-squares regression analysis single-order decay with no outlier detection was performed, resulting in a poor curve fit by either method of viral quantitation resulting from number and lack of iterative samples in this analysis.

or exceeds the efficiency estimates of SARS-CoV and MERS-CoV. Some efficiency determinations for SARS-CoV-2 ranged to $-5.5^{\log 10}$ (Figure 1), a full log difference from MERS-CoV. The higher efficiencies across independent laboratories strengthens this observation. These data suggest that SARS-CoV-2 generally maintains infectivity at a respirable particle size over short distances, in contrast to either betacoronavirus. Aerosol suspension results suggest that SARS-CoV-2 persists longer than would be expected when generated as this size particle (2-μm mass median aerodynamic diameter). This finding is notable because decay and loss in the infectious fraction of airborne virus would be expected on the basis of prior susceptibility studies with other environmentally hardy viruses, such as monkeypox virus (*5*). A recent study (*6*) showing only a slight reduction of infectivity in aerosol suspensions with approximately similar particle sizes also suggested minimal effects on SARS-CoV-2 airborne degradation.

Collectively, these preliminary data suggest that SARS-CoV-2 is resilient in aerosol form, agreeing with conclusions reached in earlier studies of aerosol fitness (*6*). A limitation of our data is that we report

only 1 measurement of the 16-h time point; these findings must be replicated before definitive conclusions are reached. However, our results indicate that aerosol transmission of SARS-CoV-2 may be a more important exposure transmission pathway than previously considered (*7*). Our approach of quantitative measurement of infectivity of viral airborne efficiency augmented by assessment of virion morphology suggests that SARS-CoV-2 may be viable as an airborne pathogen. Humans produce aerosols continuously through normal respiration (*8*). Aerosol production increases during respiratory illnesses (*9*,*10*) and during louder-than-normal oration (*11*). A fraction of naturally generated aerosols falls within the size distribution used in our experimental studies (<5 μm), which leads us to conclude that SARS-CoV-2–infected persons may produce viral bioaerosols that remain infectious for long periods after production through human shedding and airborne transport. Accordingly, our study results provide a preliminary basis for broader recognition of the unique aerobiology of SARS-CoV-2, which might lead to tractable solutions and prevention interventions.

Acknowledgments

We thank Natalie Thornburg for providing 2019-nCoV/USA-WA1/2020 and Kathleen Gibson for obtaining the SARS-CoV-2 virus from the Centers for Disease Control and Prevention. We acknowledge the World Reference Center for Emerging Viruses and Arboviruses and BEI Resources, National Institute for Allergy and Infectious Diseases (NIAID), NIH, for providing MERS-CoV, EMC/2012, #NR-44260. We also thank Jenn Sword, Greg Kocher, and Dawn Gerhardt for providing all MERS-CoV and SARS-CoV-2 isolates.

This work was supported by the Intramural Research Program of the NIAID, NIH, and the Office of the Chancellor at the University of Pittsburgh. Work performed at Tulane National Primate Research Center (C.J.R., A.C.F.) was supported in part by NIH grant no. P51OD011104. R.F.G. was supported by NIH grant no. U19AI135995. Work at the University of Texas Medical Branch was supported by NIH grant no. R24AI120942. The Defense Health Program provided the funding for SARS-CoV-2 work in USAMRIID. The work at NIH-IRF was funded in part through NIAID, Division of Intramural Research and Division of Clinical Research, Battelle Memorial Institute's prime contract with NIAID under HHSN272200700016I and in whole or in part with federal funds from NIAID, NIH, US Department of Health and Human Services, HHSN272201800013C. J.K.B. performed this work as an employee of Battelle Memorial Institute. M.G.L. performed this work as an employee of Lovelace Respiratory Research Institute and Laulima Government Solutions, LLC.

About the Author

Ms. Fears is a doctoral candidate in the Biomedical Sciences Program, Department of Microbiology and Immunology, Tulane School of Medicine, Tulane University. Her primary research interests include infectious disease and immunopathogenesis of respiratory viral pathogens.

References

1. Zheng J. SARS-CoV-2: an emerging coronavirus that causes a global threat. Int J Biol Sci. 2020;16:1678–85. https://doi.org/10.7150/ijbs.45053
2. Roy CJ, Reed DS. Infectious disease aerobiology: miasma incarnate. Front Cell Infect Microbiol. 2012;2:163. https://doi.org/10.3389/fcimb.2012.00163
3. O'Malley KJ, Bowling JD, Barry EM, Hazlett KRO, Reed DS. Development, characterization, and standardization of a nose-only inhalation exposure system for exposure of rabbits to small-particle aerosols containing *Francisella tularensis*. Infect Immun. 2019;87:87. https://doi.org/10.1128/IAI.00198-19
4. Goldberg LJ, Watkins HM, Boerke EE, Chatigny MA. The use of a rotating drum for the study of aerosols over extended periods of time. Am J Hyg. 1958;68:85–93.
5. Verreault D, Killeen SZ, Redmann RK, Roy CJ. Susceptibility of monkeypox virus aerosol suspensions in a rotating chamber. J Virol Methods. 2013;187:333–7. https://doi.org/10.1016/j.jviromet.2012.10.009
6. van Doremalen N, Bushmaker T, Morris DH, Holbrook MG, Gamble A, Williamson BN, et al. Aerosol and surface stability of SARS-CoV-2 as compared with SARS-CoV-1. N Engl J Med. 2020;382:1564–7. https://doi.org/10.1056/NEJMc2004973
7. Pung R, Chiew CJ, Young BE, Chin S, Chen MI, Clapham HE, et al.; Singapore 2019 Novel Coronavirus Outbreak Research Team. Investigation of three clusters of COVID-19 in Singapore: implications for surveillance and response measures. Lancet. 2020;395:1039–46. https://doi.org/10.1016/S0140-6736(20)30528-6
8. Buonanno G, Stabile L, Morawska L. Estimation of airborne viral emission: quanta emission rate of SARS-CoV-2 for infection risk assessment. Environ Int. 2020;141:105794. https://doi.org/10.1016/j.envint.2020.105794
9. Proaño A, Bravard MA, López JW, Lee GO, Bui D, Datta S, et al.; Tuberculosis Working Group in Peru. Dynamics of cough frequency in adults undergoing treatment for pulmonary tuberculosis. Clin Infect Dis. 2017;64:1174–81. https://doi.org/10.1093/cid/cix039
10. Morawska L, Cao J. Airborne transmission of SARS-CoV-2: the world should face the reality. Environ Int. 2020; 139:105730. https://doi.org/10.1016/j.envint.2020.105730
11. Stadnytskyi V, Bax CE, Bax A, Anfinrud P. The airborne lifetime of small speech droplets and their potential importance in SARS-CoV-2 transmission. Proc Natl Acad Sci U S A. 2020;117:11875–7. https://doi.org/10.1073/pnas.2006874117

Address for correspondence: Chad J. Roy, Tulane National Primate Research Center, 18703 Three Rivers Rd, Covington, LA 70433, USA; email: croy@tulane.edu

Updated Estimates of Chronic Conditions Affecting Risk for Complications from Coronavirus Disease, United States

Mary L. Adams, David L. Katz, Joseph Grandpre

We updated estimates of adults at risk for coronavirus disease complications on the basis of data for China by using recent US hospitalization data. This update to our previous publication substitutes obesity for cancer as an underlying condition and increases adults reporting any of the conditions from 45.4% to 56.0%.

We had earlier reported estimates of any conditions affecting risk for complications from coronavirus disease (COVID-19) (hypertension, cancer, asthma, chronic obstructive pulmonary disease, diabetes, and cardiovascular disease) on the basis of mortality data from China (*1*). Recent US data on hospitalizations for COVID-19 (*2*) indicate that 89% had an underlying condition, but obesity was substituted for cancer in that list. We update those previous estimates of adults at risk (*1*) by using the US hospitalization data definition, which includes obesity instead of cancer.

The Study

Methods were described earlier (*1*) by using publicly available 2017 Behavioral Risk Factor Surveillance System data, which excludes nursing homes and prisons (*3*). Our key variable included adults reporting they were ever told they had diabetes, asthma (and still had it), chronic obstructive pulmonary disease, hypertension, cardiovascular disease (including heart disease or stroke) or they were obese with body mass index ≥30.0 kg/m^2 based on self-reported height and weight. Adults who reported ≥1 of the conditions were considered to be at risk for hospitalization for COVID-19 because of an underlying condition. New measures included the risk factors of ever smoking 100 cigarettes; sedentary lifestyle, defined as no leisure time physical activity in the past month; and inadequate fruit and vegetable consumption, defined as consuming the combination <5 times/day on the basis of responses to 5 questions. A measure of the number of risk factors (0–3) was also created. Demographic measures were the same as in the previous report (*1*) with the addition of census region (Northeast, Midwest, South, or West) (*4*).

Stata version 14.1 (StataCorp LP, https://www.stata.com) was used for analysis to account for the complex sample design of the Behavioral Risk Factor Surveillance System. Point estimates and 95% CIs are reported by using the weights, stratum, and PSU variables supplied in the dataset (*3*). Missing values were excluded from analysis.

The sample was described previously (*1*). Prevalence rates of the separate conditions were 8.5% for cardiovascular disease, 6.6% for chronic obstructive pulmonary disease, 9.1% for asthma, 10.8% for diabetes, 32.4% for hypertension, and 30.1% for obesity. We provide updated results (Table 1, https://wwwnc.cdc.gov/EID/article/26/9/20-2117-T1.htm) based on US hospitalizations, along with the results previously published (*1*), with the difference being the substitution of obesity for cancer as an underlying condition. Overall, 56.0% (95% CI 55.7%–56.4%) of respondents had ≥1 underlying conditions using the updated definition, compared with 45.4% using the previous definition, an increase of 23% over the previous rate. For the updated measure, 49.2% of employed or self-employed adults reported an underlying condition, and 18.7% of employed adults reported ≥2 underlying conditions. These results compare with 26.6% of all adults reporting ≥2 underlying conditions. Although

Author affiliations: On Target Health Data LLC, Suffield, Connecticut, USA (M.L. Adams); True Health Initiative, Derby, Connecticut, USA (D.L. Katz); Wyoming Department of Health, Cheyenne, Wyoming, USA; (J. Grandpre)

DOI: https://doi.org/10.3201/eid2609.202117

the percentage of adults with any of the conditions increased with age (Table 1), 60.7% of those with underlying conditions were <60 years of age when using the new definition, compared with 53.4% when using the earlier definition.

Prevalence rates for the risk factors were 40.4% for ever smoking, 26.6% for sedentary lifestyle, and 84.1% for inadequate fruit and vegetable consumption. Adults with each risk factor (or more risk factors) were more likely than those without the risk factor (or fewer) to report any underlying condition (Table 1). Among ever smokers, 40.7% currently smoke, resulting in a current smoking rate of 16.5%. Updated state rates ranged from 45.6% in the District of Columbia to

Table 2. Comparison of number of adults at risk for 2 studies of chronic conditions affecting risk for complications from coronavirus disease, United States*

State	Previous results		Updated results	
	No. adults at risk	% Total	No. adults at risk	% Total
AL	1,997,864	1.78	2,252,938	1.53
AK	237,208	0.21	291,023	0.23
AZ	2,351,799	2.10	2,655,251	2.13
AR	1,181,105	1.06	1,325,336	0.91
CA	12,240,142	10.93	13,490,767	11.97
CO	1,701,776	1.52	1,876,647	1.76
CT	1,239,597	1.11	1,329,957	1.1
DE	357,530	0.32	389,066	0.29
DC	213,357	0.19	233,818	0.23
FL	7,696,749	6.88	8,296,062	6.44
GA	3,541,358	3.16	3,974,293	3.09
HI	486,156	0.43	543,222	0.46
ID	534,533	0.48	631,470	0.53
IL	4,404,556	3.93	5,243,320	4.11
IN	2,428,188	2.17	2,790,038	2.08
IA	1,067,133	0.95	1,287,375	0.98
KS	983,323	0.88	1,124,218	0.86
KY	1,789,444	1.60	1,963,497	1.39
LA	1,806,330	1.61	1,996,887	1.44
ME	530,809	0.47	594,575	0.45
MD	2,054,758	1.84	2,323,720	1.83
MA	2,302,809	2.06	2,511,936	2.15
MI	3,749,235	3.35	4,175,950	3.13
MN	1,625,778	1.45	1,882,783	1.68
MS	1,150,036	1.03	1,306,805	0.92
MO	2,137,650	1.91	2,466,200	1.9
MT	356,113	0.32	387,405	0.34
NE	616,905	0.55	743,149	0.59
NV	1,048,591	0.94	1,167,736	0.93
NH	485,340	0.43	522,567	0.43
NJ	3,106,880	2.78	3,265,515	2.64
NM	701,585	0.63	804,730	0.64
NY	6,419,321	5.73	7,093,023	6.13
NC	3,713,582	3.32	4,186,911	3.15
ND	243,096	0.22	298,972	0.24
OH	4,268,748	3.81	4,881,408	3.66
OK	1,461,941	1.31	1,665,703	1.18
OR	1,418,689	1.27	1,573,562	1.28
PA	4,738,414	4.23	5,340,392	4.15
RI	393,069	0.35	426,186	0.33
SC	1,912,134	1.71	2,189,219	1.58
SD	281,110	0.25	333,818	0.27
TN	2,610,800	2.33	2,863,321	2.09
TX	8,977,387	8.02	10,449,000	8.24
UT	796,721	0.71	915,321	0.86
VT	226,397	0.20	246,641	0.20
VA	2,921,171	2.61	3,295,289	2.63
WA	2,464,452	2.20	2,711,697	2.25
WV	827,193	0.74	907,986	0.59
WI	1,949,872	1.74	2,269,999	1.82
WY	194,544	0.17	220,916	0.18
Total	111,943,278	100	125,717,620	100

*Previous results were based on mortality data from China (*1*), and underlying conditions include cardiovascular disease, diabetes, chronic obstructive pulmonary disease, asthma, hypertension, or cancer other than skin. Updated results are based on US hospitalization data (*2*), and obesity is substituted for cancer as an underlying condition.

68.8% in West Virginia, which was several percentage points higher but over a similar range of states compared with earlier estimates. State results obtained directly from Stata (Table 2) list the number of adults in each state at increased risk for hospitalizations and the percentage that number represents among all states, again showing both previously published and updated results.

Conclusions

We estimate that 56.0% of US adults, with a wide range across age groups and states, have ≥1 underlying conditions that increase risk for hospitalization caused by COVID-19. Our previous estimate of adults at risk for complications from COVID-19 (*1*) that included cancer and excluded obesity based on data for China, where obesity is much less prevalent (*5*), resulted in an estimate of 45.4%. Thus, the 23% increase appears to be the result of including of obesity as an underlying condition. In addition, although rates increase with increasing age group, over 60% of adults with underlying conditions by this new definition are <60 years of age. The underlying condition rate of 49.2% among the employed has potential implications as persons return to work. Also, the 26.6% of all adults who reported ≥2 underlying conditions, including 18.7% of the employed, might be at even greater risk for hospitalization based on results from other studies (*6*). Taken together, these results suggest that risk stratification based on age or number of underlying conditions might be considered as a means of more safely phasing in returning to work.

All the underlying conditions used in our updated measure are conditions for which behavioral risk factors have been well established (*7,8*). In unadjusted results each selected risk factor was associated with increased likelihood of reporting any of the 6 underlying conditions. In addition, the results for increasing number of risk factors indicate a stepwise increase in the percentage of adults reporting any of the underlying conditions with each additional risk factor (Table 1). These results suggest the potential for lowering risk for COVID-19 hospitalizations by reducing any or all of these 3 risk factors. In addition, being older, male, or African American also increased the likelihood of reporting an underlying condition, which are all groups that hospitalization data (*2*) suggested were disproportionately affected by COVID-19. These results suggest that observation might be caused by increased rates of underlying conditions among these groups. In addition, living in either the Midwest or South increased the likelihood of reporting an underlying condition compared with living in the West. This result is consistent with studies showing that obesity rates are also highest in these regions (*9*).

Our study does not address possible differences in contracting the disease, only the risk for hospitalization among those with COVID-19, based on US results for underlying conditions (*2*). Because only noninstitutionalized adults were surveyed, 1.3 million adults in nursing homes (*10*) were excluded, which almost certainly underestimates those with underlying conditions who were included in hospitalization data. Data are self-reported, and reliability and validity can vary for different measures tested (*11*). However, as long as a respondent was told they had a chronic condition, validity has been shown to be high. Age groups used for analysis did not match those used for weighting data, but that factor should have a minimal effect on results. Low response rates could introduce bias but, as noted, validity appears high for most measures used in this study.

We estimate 56.0% of US adults are at risk for needing hospitalization for COVID-19 because of underlying conditions, representing a 23% increase from the 45.4% earlier estimates, which excluded obesity. These underlying conditions are, in turn, associated with modifiable risk factors, including ever smoking, being sedentary, and inadequate fruit and vegetable consumption. These results suggest the potential for policies for opening businesses based on risk stratification of the population and for possible improvement of risk status through lifestyle change. A national focus on, and support for, a health promotion campaign would be timely.

Collection, analysis, and interpretation of data for this study were supported by the Centers for Disease Control and Prevention Grant/Cooperative Agreement no. 1U58DP006069-01.

About the Author

Ms. Adams is a consultant at On Target Health Data LLC, Suffield, CT. Her primary research interest is chronic diseases (including dementia) and their risk factors.

References

1. Adams ML, Katz DL, Grandpre J. Population-based estimates of chronic conditions affecting risk for complications from coronavirus disease, United States. Emerg Infect Dis. 2020 Apr 23 [Epub ahead of print]. https://doi.org/10.3201/eid2608.200679
2. Garg S, Kim L, Whitaker M, O'Halloran A, Cummings C, Holstein R, et al. Hospitalization rates and characteristics of patients hospitalized with laboratory-confirmed coronavirus disease 2019—COVID-NET, 14 States, March 1–30, 2020.

MMWR Morb Mortal Wkly Rep. 2020;69:458–64. https://doi.org/10.15585/mmwr.mm6915e3
3. Behavioral Risk Factor Surveillance System (BRFSS). Survey data and documentation [cited 2020 Mar 3]. https://www.cdc.gov/brfss/data_documentation/index.htm
4. US Census Bureau. Geographic terms and concepts: census divisions and census regions [cited 2020 Jan 27]. https://www.census.gov/geo/reference/gtc/gtc_census_divreg.html
5. Wu Y. Overweight and obesity in China. BMJ. 2006;333:362–3. https://doi.org/10.1136/bmj.333.7564.362
6. Sambamoorthi U, Tan X, Deb A. Multiple chronic conditions and healthcare costs among adults. Expert Rev Pharmacoecon Outcomes Res. 2015;15:823–32. https://doi.org/10.1586/14737167.2015.1091730
7. Adams ML, Grandpre J, Katz DL, Shenson D. The impact of key modifiable risk factors on leading chronic conditions. Prev Med. 2019;120:113–8. https://doi.org/10.1016/j.ypmed.2019.01.006
8. Adams ML, Grandpre J, Katz DL, Shenson D. Linear association between number of modifiable risk factors and multiple chronic conditions: results from the Behavioral Risk Factor Surveillance System. Prev Med. 2017;105:169–75. https://doi.org/10.1016/j.ypmed.2017.09.013
9. Centers for Disease Control and Prevention. Overweight and obesity: obesity prevalence maps, 2018 [cited 2020 Apr 29]. https://www.cdc.gov/obesity/data/prevalence-maps.html
10. Centers for Disease Control and Prevention. National Center for Health Statistics; Nursing Home Care [cited 2020 Jun 16]. https://www.cdc.gov/nchs/fastats/nursing-home-care.htm
11. Pierannunzi C, Hu SS, Balluz L. A systematic review of publications assessing reliability and validity of the Behavioral Risk Factor Surveillance System (BRFSS), 2004–2011. BMC Med Res Methodol. 2013;13:49. https://doi.org/10.1186/1471-2288-13-49

Address for correspondence: Mary L. Adams, On Target Health Data LLC, 247 N Stone St, West Suffield, CT 06093, USA; email: madams.ontargethealthdata@gmail.com

Clusters of Coronavirus Disease in Communities, Japan, January–April 2020

Yuki Furuse,[1] Eiichiro Sando,[1] Naho Tsuchiya,[1] Reiko Miyahara,[1] Ikkoh Yasuda,[1] Yura K. Ko,[1] Mayuko Saito, Konosuke Morimoto, Takeaki Imamura, Yugo Shobugawa, Shohei Nagata, Kazuaki Jindai, Tadatsugu Imamura, Tomimasa Sunagawa, Motoi Suzuki, Hiroshi Nishiura, Hitoshi Oshitani

We analyzed 3,184 cases of coronavirus disease in Japan and identified 61 case-clusters in healthcare and other care facilities, restaurants and bars, workplaces, and music events. We also identified 22 probable primary case-patients for the clusters; most were 20–39 years of age and presymptomatic or asymptomatic at virus transmission.

Coronavirus disease (COVID-19) typically causes febrile illness with respiratory symptoms (*1*,*2*), and many countries worldwide have been affected. Before characterizing COVID-19 as a pandemic in March 2020 (*3*), the World Health Organization advised countries to take measures to reduce spread of the virus, including identifying cases and clusters, isolating patients, tracing contacts, and preventing community transmission (*4*). Several countries have reported on the characteristics of a small number of clusters of COVID-19 cases (*5*,*6*). However, few comprehensive reports provide an overview of clusters of COVID-19 cases in communities and the significance of such clusters. We analyzed 61 COVID-19 clusters among various communities in Japan and identified 22 probable primary cases that might have contributed to the disease incidence in clusters.

Author affiliations: Kyoto University, Kyoto, Japan (Y. Furuse, K. Jindai); Nagasaki University, Nagasaki, Japan (E. Sando, I. Yasuda, K. Morimoto); Tohoku University, Sendai, Japan (N. Tsuchiya, Y.K. Ko, M. Saito, T. Imamura, S. Nagata, H. Oshitani); National Center for Global Health and Medicine, Tokyo, Japan (R. Miyahara); Niigata University, Niigata, Japan (Y. Shobugawa); Japan International Cooperation Agency, Tokyo (T. Imamura); National Institute of Infectious Diseases, Tokyo (T. Sunagawa, M. Suzuki); Hokkaido University, Sapporo, Japan (H. Nishiura)

DOI: https://doi.org/10.3201/eid2609.202272

The Study

We analyzed COVID-19 cases in Japan reported during January 15–April 4, 2020. All COVID-19 cases confirmed by reverse transcription-PCR in Japan must be reported to the Ministry of Health, Labour and Welfare. Through case interviews, local health authorities collected demographic and epidemiologic information, such as possible source of infection and contact and travel history. During the study period, a total of 3,184 laboratory-confirmed COVID-19 cases, including 309 imported cases, were reported. Among cases of local transmission, 61% (1,760/2,875) had epidemiologic links to known cases (Figure 1, panel A). We excluded 712 cases detected on a cruise that was anchored at Yokohama Port, Japan, from February 3 through March 1 (*7*).

We defined a cluster as ≥5 cases with primary exposure reported at a common event or venue, excluding within-household transmissions. Our definition also excluded cases with epidemiologic links to secondary transmission. For example, in the following scenario we would exclude cases A and B: boy A is a friend of boy B whose grandmother C contracted nosocomial COVID-19 in a nursing home from which ≥5 cases were reported; although all 3 have symptoms develop and are diagnosed with COVID-19, we would consider only grandmother C part of a cluster from the nursing home.

By investigating the epidemiologic links among cases, we identified 61 COVID-19 clusters in various communities. We observed clusters of COVID-19 cases from 18 (30%) healthcare facilities; 10 (16%) care facilities of other types, such as nursing homes and day care centers; 10 (16%) restaurants or bars; 8 (13%) workplaces; 7 (11%) music-related events, such as live music concerts, chorus group rehearsals, and karaoke parties; 5 (8%) gymnasiums; 2 (3%) ceremonial

[1]These authors contributed equally to this article.

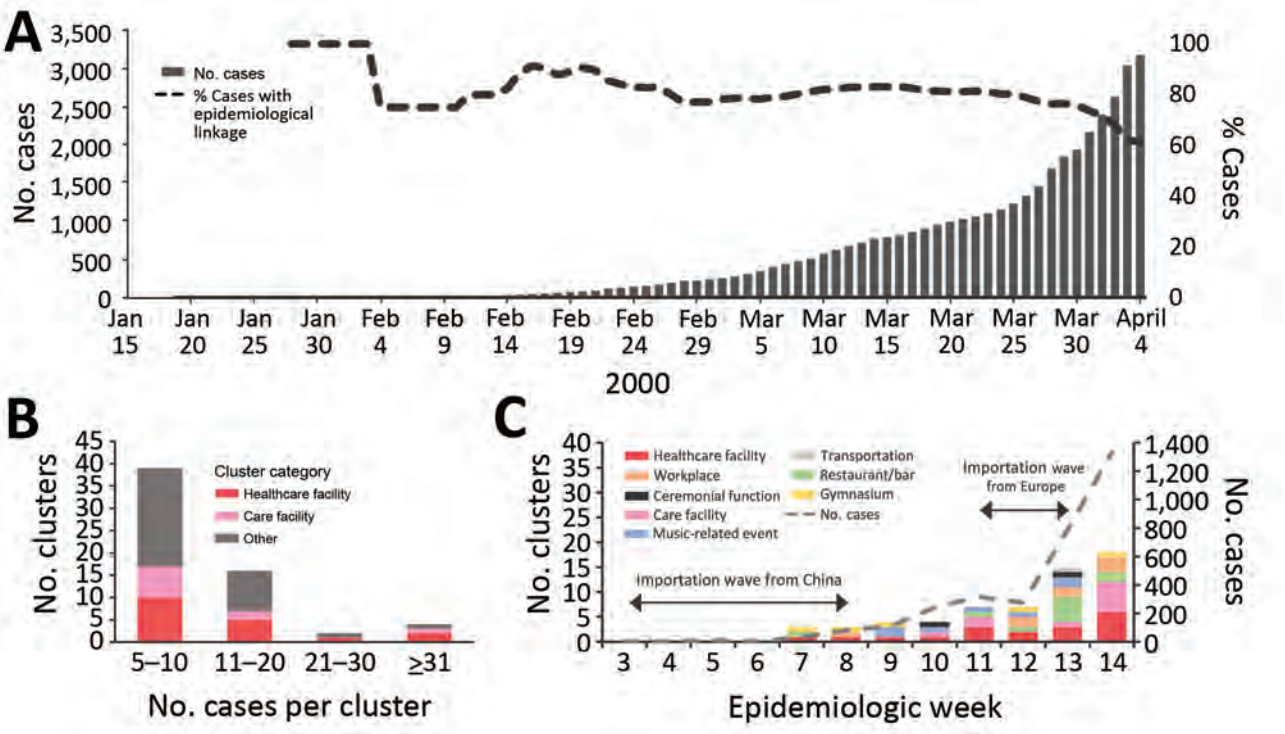

Figure 1. Analysis of 61 clusters of coronavirus disease (COVID-19) cases in communities in Japan, January 15–April 4, 2020. A) Cumulative number of COVID-19 cases, including the proportion of local cases with epidemiologic links to known confirmed cases. B) Distribution of clusters by number of cases in a cluster by category. C) Incidence of clusters of cases according to epidemiologic week as determined by date of confirmation of the first case in a cluster. Incidence of COVID-19 cases (weekly number of newly reported cases) in Japan and timing of two importation waves are also displayed. Epidemiologic week 3 corresponds to January 15, 2020, in panel A. The data and trend of imported cases were previously reported and described by Furuse et al. (*8*).

functions; and 1 (2%) transportation-related incident in an airplane. Most (39/61; 64%) clusters involved 5–10 cases (Figure 1, panel B). The largest cluster involved >100 cases in a hospital, including nosocomial infections and staff infections. The largest non–healthcare-related cluster we observed was among >30 persons who attended a live music concert, including performers, audience members, and event staff. Healthcare and care facilities accounted for >50% of clusters at epidemiologic weeks 11 and 14 (Figure 1, panel C).

We identified 22 probable primary case-patients who had symptoms develop before they had contact with other case-patients in a cluster or who had prior epidemiologic links before contact with a cluster. We did not identify probable primary cases for nosocomial clusters. We believe these 22 case-patients contributed to the incidence of clusters. Demographic data show that 9 (41%) probable primary case-patients were female and 13 (59%) were male. The most frequently observed age groups among probable primary cases were 20–29 years (n = 6; 27%) and 30–39 years (n = 5, 23%) (Figure 2, panel A). For 16 clusters, we determined the date of transmission from probable primary case-patients to other case-patients in a cluster and found 41% (9/22) of probable primary case-patients were presymptomatic or asymptomatic at the time of transmission; only 1 had a cough at the time of transmission (Figure 2, panel B). Of the 22 probable primary case-patients, 45% (10/22) had cough at the time of diagnosis. Of the 16 probable primary case-patients with the determined date of transmission, transmission occurred one day before illness onset for 5 (31%) case-patients and on the same day of illness onset for 4 (25%) case-patients (Figure 2, panel C). All age groups demonstrated presymptomatic or asymptomatic transmission.

Conclusions

We investigated clusters of COVID-19 cases and probable primary cases in Japan during January 15–April 4, 2020. We found that healthcare facilities, such as hospitals, and care facilities, such as nursing homes, were the primary sources of clusters, some of which had >100 cases. Japan experienced 2 waves of imported COVID-19 cases, after which local transmission occurred and the epidemic grew (*8*). Of note, clusters of COVID-19 cases at healthcare and care facilities predominated

at epidemiologic weeks 11 (March 9–15) and 14 (March 30–April 4), which corresponds to ≈3 weeks after the 2 waves of imported cases (Figure 1, panel C). Healthcare and care facilities might be located at the end of the local transmission chain because clusters in those facilities only became evident several weeks after community transmission persisted.

We noted many COVID-19 clusters were associated with heavy breathing in close proximity, such as singing at karaoke parties, cheering at clubs, having conversations in bars, and exercising in gymnasiums. Other studies have noted such activities can facilitate clusters of infection (*9*,*10*). Japan's Prime Minister's Office and the Ministry of Health, Labour and Welfare announced 3 situations that could increase the risk for COVID-19 cases and advised the population to avoid the "Three Cs": closed spaces with poor ventilation, crowded places, and close-contact settings (*11*).

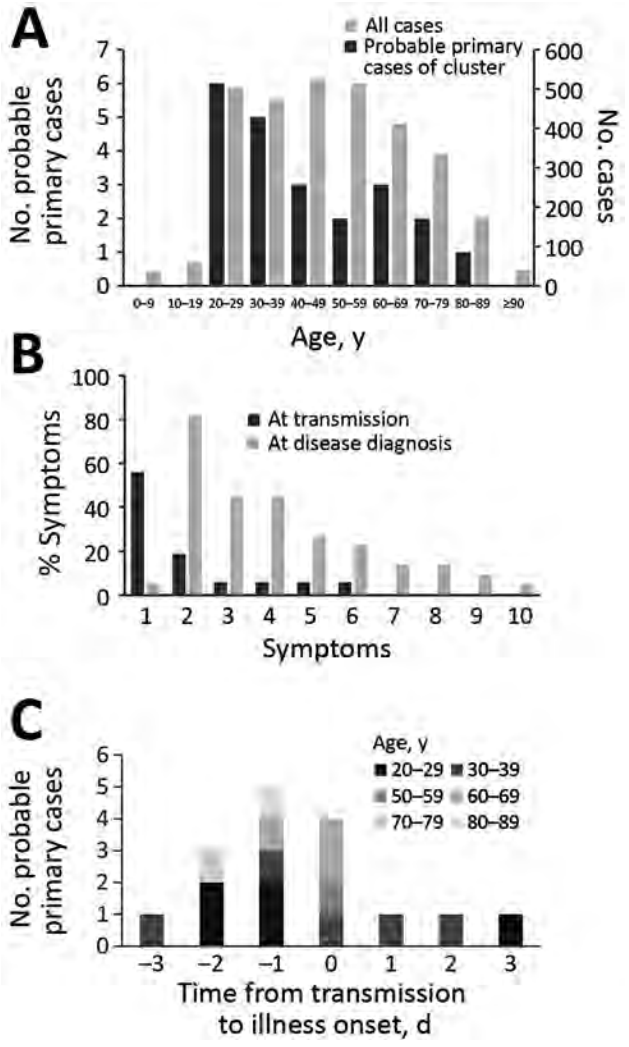

Figure 2. Analysis of probable primary cases of coronavirus disease (COVID-19) among 22 clusters in communities, Japan. A) Age ranges of probable primary COVID-19 cases in clusters. Age distribution among all COVID-19 cases in Japan is provided as reference. B) Proportions of symptoms among probable primary cases of COVID-19 clusters at transmission (n = 16) and among at laboratory confirmed diagnosis (n = 22). 1, Asymptomatic; 2, fever; 3, fatigue; 4, cough; 5, sore throat; 6, headache; 7, arthralgia or myalgia; 8, runny nose; 9, diarrhea; 10, difficulty breathing. C) Distribution of probable primary cases of COVID-19 clusters by time of transmission compared with illness onset by age groups (n = 16). Six cases were excluded because the time of transmission was undetermined.

Among the probable primary COVID-19 cases we identified from non-nosocomial clusters, half (11/22) were 20–39 years of age, which is younger than the age distribution of all COVID-19 cases in Japan (Figure 2, panel A). We do not know whether social, biological, or both factors play a role in the difference in transmission patterns between the younger and older persons. We also noted probable primary COVID-19 case-patients appear to transmit the virus and generate clusters even in the absence of apparent respiratory symptoms, such as cough.

Our study has some limitations. The epidemiologic investigation mostly relied on voluntary cooperation. Because some case-patients could not disclose contact history, epidemiologic links and clusters of cases might have missed. Recall bias is likely because Japan did not use digital devices for contact tracing and information was obtained only through interviews. In addition, we could not calculate a secondary attack rate from probable primary cases because data were unavailable for denominator, such as the number of persons present in the places where clusters of cases were detected.

Active case finding and investigation are key to establishing links to other cases or transmission events. Detecting clusters of cases can lead to effective quarantine of close contacts and to the identification of risk factors for the formation of such clusters (*12*). Our findings provide further information and insight on clusters of COVID-19 cases in communities that can aid in the ongoing efforts to curb the global pandemic.

Acknowledgments

We thank local governments, public health centers and institutes, and the National Institute of Infectious Diseases, Japan, for surveillance, laboratory testing, epidemiological investigations, and data collection. We also thank all members of National Task Force for COVID-19 and volunteers in the Cluster Response Team who supported data management, including Kozue Amemiya, Kayako Chishima, Aya Fujiwara, Yoko Hamasaki, Naomi Ikeda, Keiya Inoue, Sachi Ishida, Mariko Kanamori, Tsuyoki Kawashima, Tomoe Mashiko, Rie Masuda, Yoshifumi

Nin, Kota Ninomiya, Yukiyo Nitta, Akiko Sakai, Kazuaki Sano, Asako Sato, Akiko Sayama, Ayaka Takeuchi, Hiroto Tanaka, Fumie Tokuda, Shogo Yaegashi, Yoko Yamagiwa, Lisa Yamasaki, and Fumi Yoshimatsu.

This study was supported in part by grants from the Ministry of Education, Culture, Sport, Science and Technology in Japan (no. 16809810) and the Japan Agency for Medical Research and Development (no. 19fk0108104h1101).

About the Author

Dr. Furuse is an assistant professor at Institute for Frontier Life and Medical Sciences and Hakubi Center for Advanced Research, Kyoto University, Japan. His primary research interests include the public health, epidemiology, bioinformatics, and molecular biology of viral diseases.

References

1. Zhu N, Zhang D, Wang W, Li X, Yang B, Song J, et al.; China Novel Coronavirus Investigating and Research Team. A novel coronavirus from patients with pneumonia in China, 2019. N Engl J Med. 2020;382:727–33. https://doi.org/10.1056/NEJMoa2001017
2. Huang C, Wang Y, Li X, Ren L, Zhao J, Hu Y, et al. Clinical features of patients infected with 2019 novel coronavirus in Wuhan, China. Lancet. 2020;395:497–506. https://doi.org/10.1016/S0140-6736(20)30183-5
3. World Health Organization. WHO Director-General's opening remarks at the mission briefing on COVID-19—11 March 2020 [cited 2020 Jun 6]. https://www.who.int/dg/speeches/detail/who-director-general-s-opening-remarks-at-the-media-briefing-on-covid-19---11-march-2020
4. World Health Organization. WHO Director-General's opening remarks at the mission briefing on COVID-19—26 February 2020 [cited 2020 May 3]. https://www.who.int/dg/speeches/detail/who-director-general-s-opening-remarks-at-the-mission-briefing-on-covid-19---26-february-2020
5. Pung R, Chiew CJ, Young BE, Chin S, Chen MI, Clapham HE, et al. Investigation of three clusters of COVID-19 in Singapore: implications for surveillance and response measures. Lancet. 2020;395:1039–46. https://doi.org/10.1016/S0140-6736(20)30528-6
6. Shim E, Tariq A, Choi W, Lee Y, Chowell G. Transmission potential and severity of COVID-19 in South Korea. Int J Infect Dis. 2020;93:339–44. https://doi.org/10.1016/j.ijid.2020.03.031
7. Ministry of Health, Labour and Welfare. About coronavirus disease 2019 (COVID-19) press conference June 2, 2020 [cited 2020 Jun 6]. https://www.mhlw.go.jp/stf/seisakunitsuite/bunya/newpage_00032.html
8. Furuse Y, Ko YK, Saito M, Shobugawa Y, Jindai K, Saito T, et al. Epidemiology of COVID-19 outbreak in Japan, January–March 2020. Jpn J Infect Dis. 2020 Apr 30 [Epub ahead of print]. PubMed https://doi.org/10.7883/yoken.JJID.2020.271
9. Jang S, Han SH, Rhee J-Y. Coronavirus disease cluster associated with fitness dance classes, South Korea. Emerg Infect Dis. 2020 May 15 [Epub ahead of print]. https://doi.org/10.3201/eid2608.200633
10. Hamner L, Dubbel P, Capron I, Ross A, Jordan A, Lee J, et al. High SARS-CoV-2 attack rate following exposure at a choir practice—Skagit County, Washington, March 2020. MMWR Morb Mortal Wkly Rep. 2020;69:606–10. https://doi.org/10.15585/mmwr.mm6919e6
11. Prime Minister's Office of Japan; Ministry of Health, Labour and Welfare. Avoid the "three Cs"! [cited 2020 May 27]. https://www.mhlw.go.jp/content/10900000/000615287.pdf
12. Frieden TR, Lee CT. Identifying and interrupting superspreading events—implications for control of severe acute respiratory syndrome coronavirus 2. Emerg Infect Dis. 2020;26:1059–66. PubMed https://doi.org/10.3201/eid2606.200495

Address for correspondence: Hitoshi Oshitani, Department of Virology, Tohoku University Graduate School of Medicine, 2-1 Seiryo-machi, Aoba-ku, Sendai, 980-8575, Japan; email: oshitanih@med.tohoku.ac.jp

Toxigenic *Corynebacterium diphtheriae*–Associated Genital Ulceration

Frieder Fuchs, Derya Markert, Isabel V. Wagner, Max C. Liebau, Anja Berger, Alexandra Dangel, Andreas Sing, Mario Fabri, Georg Plum

In October 2016, an adolescent boy sought care for acute genital ulceration in Cologne, Germany. We presumed a sexually transmitted infection, but initial diagnostic procedures yielded negative results. He was hospitalized because swab samples from the lesion grew toxigenic *Corynebacterium diphtheriae*, leading to the diagnosis of possibly sexually transmitted cutaneous diphtheria.

Members of the genus *Corynebacterium* colonize the upper respiratory tract and healthy skin and are frequently found in clinical specimens without clinical significance. Three species, *C. diphtheriae*, *C. ulcerans*, and *C. pseudotuberculosis*, can cause serious infections by acquiring the ability to produce the diphtheria toxin manifesting clinically as cutaneous or respiratory diphtheria. Because vaccination is widely used in industrialized countries, diphtheria is rare, but it remains endemic to several countries of Africa, Asia, the Eastern Pacific region, and Eastern Europe. During 2001–2016, a total of 80 cases of toxigenic *Corynebacterium* spp. infections were notified in Germany (*1*).

Case Report

In October 2016, a 16-year-old boy from Ethiopia sought care at the University Hospital of Cologne (Cologne, Germany) with 3 papules at the glans and a slightly bleeding, painful ulceration at the dorsal shaft of his penis. He complained about local pruritus and had swollen, painful inguinal nodules on the left side. On clinical examination, the ulcer appeared to have coalesced from a few smaller lesions with an erythematous base and a yellow to purulent exudate. The boy denied having lesions before the ulcer. Specific history could not be clarified satisfactorily: the boy had an undefined status of residence and lived in an accommodation facility for asylum seekers. Given that he was an unaccompanied minor refugee, the examiners considered traumatic sexual experiences when the boy was unwilling to share further details especially about his sexual history. General physical examination was unremarkable. Pubertal development was normal.

We presumed a sexually transmitted infection. Because we considered herpes simplex virus and chancroid as likely diagnoses, the boy started on empiric outpatient treatment with valaciclovir and azithromycin. Serologic screening for syphilis and herpes simplex virus PCR yielded negative results. Toxigenic *C. diphtheriae* was cultured from the ulcer, and the boy was hospitalized 7 days after initial consultation because of cutaneous diphtheria. Toxigenicity of the isolate was verified by real-time PCR for *tox* gene and the modified Elek test in the German National Consulting Laboratory for Diphtheria. On the day of hospitalization the lesions showed only minor signs of resolution. Blood test analysis did not detect any systemic inflammation. No other swab of the genital lesions or the uninflammed tonsils grew pathogens. Because the boy's vaccination history was unclear, we used an enzyme immunoassay to determine the serum level of diphtheria toxin antibodies, and the results indicated seroprotection (4.69 IU/mL).

The patient was isolated and treated with intravenous penicillin (6 million U/d). When susceptibility testing revealed penicillin resistance, his antimicrobial drug regimen was changed to ciprofloxacin (1,200

Author affiliations: Institute for Medical Microbiology, Immunology and Hygiene, University of Cologne, Medical Faculty and University Hospital of Cologne, Cologne, Germany (F. Fuchs, D. Markert, G. Plum); University of Cologne, Medical Faculty and University Hospital of Cologne, Cologne (I.V. Wagner, M.C. Liebau, M. Fabri); Center for Molecular Medicine Cologne, University of Cologne, Faculty of Medicine, Cologne (M.C. Liebau); Bavarian Health and Food Safety Authority, National Consulting Laboratory for Diphtheria, Oberschleißheim, Germany (A. Berger, A. Dangel, A. Sing)

DOI: https://doi.org/10.3201/eid2609.180830

mg/d). After 4 days of inpatient treatment, the patient was discharged. Follow-up visits confirmed full recovery; repeat swab sample testing of throat and penis were culture- and PCR-negative. The patient completed antimicrobial drug therapy 10 days after discharge.

In contact tracing, initiated by the local health department, 2 persons were determined to be at risk because they shared a room with the patient at the accommodation facility. Swab samples from tonsils and suspicious skin lesions (including 1 penile wound) of the contacts were negative for *C. diphtheriae*. Consequently, we discussed public health actions with them; chemoprophylaxis or vaccination were not considered necessary.

Conclusions

Only few cases of cutaneous diphtheria are reported in Germany, and they are strongly associated with defined risk factors, especially contact, during endemic circulation, associated with traveling (*2*), migration (*3*), zoonotic reservoirs (*4*), or poor socioeconomic conditions (*5*). In this case, the clinical manifestion of the genital ulcer with typical symptoms of sexually transmitted infections, such as painful unilateral inguinal nodules, supports the likelihood of sexually transmitted diphtheria, although we were not able to verify the patient's medical or sexual history. We did not isolate any other pathogen, in contrast with another case of male urethritis in which toxigenic *C. diphtheriae* was part of a polymicrobial infection and sexual transmission was assumed (*6*). This case shows that unusual manifestations of diphtheria are conceivable on various body sites. Clinicians should consider this easily overlooked disease in the differential diagnosis for similar cases. This awareness might lead to an increase in confirmed cases, improve outcomes, and prevent disease through subsequent public health actions.

Acknowledgments

We thank Jeannine Wohlgemuth and the other technicians of the Institute for Medical Microbiology, Immunology and Hygiene, University of Cologne Medical Faculty and University Hospital of Cologne, for their excellent work in the diagnosis of this case.

About the Author

Dr. Fuchs is in his fourth year in clinical microbiology at the University Hospital of Cologne. His primary research interests are infectious diseases and antimicrobial resistance.

References

1. Robert Koch Institute. Infectious disease epidemiology annual report 2017 [in German] [cited 2019 Oct 10]. https://www.rki.de/DE/Content/Infekt/Jahrbuch/Jahrbuch_2017.pdf
2. Sing A, Heesemann J. Imported cutaneous diphtheria, Germany, 1997–2003. Emerg Infect Dis. 2005;11:343–4. https://doi.org/10.3201/eid1102.040560
3. Meinel DM, Kuehl R, Zbinden R, Boskova V, Garzoni C, Fadini D, et al. Outbreak investigation for toxigenic *Corynebacterium diphtheriae* wound infections in refugees from northeast Africa and Syria in Switzerland and Germany by whole genome sequencing. Clin Microbiol Infect. 2016;22:1003.e1-1003.e8.
4. Berger A, Boschert V, Konrad R, Schmidt-Wieland T, Hörmansdorfer S, Eddicks M, et al. Two cases of cutaneous diphtheria associated with occupational pig contact in Germany. Zoonoses Public Health. 2013;60:539–42. https://doi.org/10.1111/zph.12031
5. Lowe CF, Bernard KA, Romney MG. Cutaneous diphtheria in the urban poor population of Vancouver, British Columbia, Canada: a 10-year review. J Clin Microbiol. 2011;49:2664–6. https://doi.org/10.1128/JCM.00362-11
6. Berger A, Lensing C, Konrad R, Huber I, Hogardt M, Sing A. Sexually transmitted diphtheria. Sex Transm Infect. 2013;89:100–1. https://doi.org/10.1136/sextrans-2011-050418

Address for correspondence: Frieder Fuchs, Institute for Medical Microbiology Immunology and Hygiene, Goldenfelsstraße 19, 50935 Cologne, Germany; email: frieder.fuchs@uk-koeln.de

Duration of Carbapenemase-Producing *Enterobacteriaceae* Carriage in Hospital Patients

Yin Mo,[1] Anastasia Hernandez-Koutoucheva,[1] Patrick Musicha, Denis Bertrand, David Lye, Oon Tek Ng, Shannon N. Fenlon, Swaine L. Chen, Moi Lin Ling, Wen Ying Tang, Timothy Barkham, Niranjan Nagarajan, Ben S. Cooper, Kalisvar Marimuthu

To determine the duration of carbapenemase-producing *Enterobacteriaceae* (CPE) carriage, we studied 21 CPE carriers for ≈1 year. Mean carriage duration was 86 days; probability of decolonization in 1 year was 98.5%, suggesting that CPE-carriers' status can be reviewed yearly. Prolonged carriage was associated with use of antimicrobial drugs.

Rapid global dissemination of carbapenemase-producing *Enterobacteriaceae* (CPE) poses a public health threat (*1*). To prevent the spread of CPE in healthcare settings, international guidelines advocate for early identification, isolation, and contact precautions (*2*,*3*). To provide information helpful for the design of rational infection control policies, we estimated CPE carriage duration in a hospital cohort and identified risk factors for prolonged carriage.

The Study

During October 2016–February 2018, we conducted a prospective cohort study involving CPE carriers from 2 tertiary care centers in Singapore. CPE carriers were identified by routine collection of rectal swab samples in accordance with local infection control policies. We included patients who were >21 years of age and had the capacity to provide consent (Appendix Figure 1, https://wwwnc.cdc.gov/EID/article/26/9/19-0592-App1.pdf). We retrieved from medical records of enrolled patients the latest dates of CPE-negative rectal swab samples before the first positive sample. We collected fecal samples from participants at the time of enrollment, weekly for 4 weeks, monthly for 5 months, and bimonthly for 6 months. We recorded demographic characteristics, healthcare contact history, and medication history.

The fecal samples were inoculated onto selective chromogenic agar (CHROMID CARBA SMART; bioMérieux, https://www.biomerieux-diagnostics.com), and species identification was performed with matrix-assisted laser desorption/ionization time-of-flight mass spectrometry (Bruker, https://www.bruker.com). Antimicrobial susceptibility testing was performed by using VITEK-2 (bioMérieux). All *Enterobacteriaceae* isolates with a MIC of ≥2 mg/L for meropenem or ≥1.0 mg/L for ertapenem underwent PCR to detect $bla_{\text{NDM-1}}$, bla_{KPC}, $bla_{\text{OXA-48}}$, $bla_{\text{IMI-1}}$, and bla_{IMP} genes (*4*). All CPE isolates and fecal DNA underwent sequencing on an Illumina HiSeq 4000 sequencer (https://www.illumina.com). We used the Shannon diversity index to measure α-diversity for fecal microbial communities (https://cran.r-project.org/web/packages/vegan/vegan.pdf).

We analyzed data by using Bayesian multistate Markov models to account for interval censoring (Appendix). First, we estimated the overall transmission rates by considering patients to be in either CPE colonized or noncolonized states. Second, we considered CPE colonization on the species level and included as separate states carbapenemase-producing (CP)–*Escherichia coli* (CP-EC) colonized, CP–*Klebsiella pneumoniae*

Author affiliations: National University Hospital, Singapore (Y. Mo); Mahidol-Oxford Tropical Medicine Research Unit, Bangkok, Thailand (Y. Mo, A. Hernandez-Koutoucheva, P. Musicha, B.S. Cooper); National University of Singapore, Singapore (Y. Mo, D. Lye, S.L. Chen, N. Nagarajan, K. Marimuthu); Genome Institute of Singapore, Singapore (D. Bertrand, S.N. Fenlon, S.L. Chen, N. Nagarajan); University of Oxford, Oxford, UK (P. Musicha, B.S. Cooper); Nanyang Technological University (D. Lye, O.T. Ng); National Centre for Infectious Diseases, Singapore (D. Lye, O.T. Ng, K. Marimuthu); Tan Tock Seng Hospital, Singapore (D. Lye, W.Y. Tang, T. Barkham, K. Marimuthu); Singapore General Hospital, Singapore (M.L. Ling)

DOI: https://doi.org/10.3201/eid2609.190592

[1]These authors contributed equally to this article.

(CP-KP) colonized, and CP-EC/KP co-colonized (Appendix Figure 2). All analyses were performed by using R version 3.4.4 (https://www.R-project.org) and RStan (http://mc-stan.org).

We enrolled 21 patients (Table). Mean (± SD) follow-up period was 294 (± 77) days, and each participant provided 12 (± 1.5) samples. Throughout follow-up, 15 (71.4%) participants carried >1 species of CPE, and only 3 (14.3%) carried >1 type of carbapenemase gene (χ^2 of difference in proportions = 14.8, simulated p = 0.0005) (Appendix Table 1). The most common species carried were *K. pneumonia*e (18 [85.7%]) and *E. coli* (16 [76.2%]). The most frequently observed carbapenemase genes were $bla_{\text{OXA-48}}$ (11 [52.4%]) and bla_{KPC} (8 [38.1%]). We obtained 76 CP-KP isolates from the samples; the most common sequence type (25 [32.9%]) was 307. Among the 83 CP-EC isolates, the most common sequence type (22 [26.5%]) was 131. Sample positivity was continuous until clearance for most (17 [81.0%]) of the 21 participants. For 4 participants, negative samples were followed by positive samples; the longest period was 3 negative samples over 3 consecutive weeks (Appendix Figure 5).

The estimated mean duration of CPE carriage was 86 (95% credible interval [CrI] 60– 122) days. The probability of decolonization in 1 year was 98.5% (95% CrI 95.0%–99.8%), assuming a constant decolonization rate within the time interval. The longest observed carriage duration was 387 days. We performed a sensitivity analysis that included 16 participants who became decolonized during follow-up (i.e., the last sample collected was negative for CPE). This analysis gave a mean carriage time of 77 (95% CrI 53–108) days and a 98.8% (95% CrI 96.5%–99.9%) probability of decolonization within 1 year.

As time-fixed covariates, we analyzed age, co-colonization with other multidrug-resistant organisms, presence of a urinary catheter, antimicrobial drug use during follow-up, Charlson Comorbidity Index score, and readmission; as a time-varying covariate, we used the Shannon Diversity Index score to explore the covariates' association with decolonization (Appendix Figure 3). The only factor associated with prolonged CPE carriage was antimicrobial drug use during the follow-up period (hazard ratio 0.48, 95% CrI 0.20–0.93). The rate of decolonization for CP-EC was lower than that for CP-KP (0.018 [95% CrI 0.007–0.031] per day vs. 0.030 [95% CrI 0.016–0.049] per day) (Appendix Table 2, Figure 4).

Conclusions

CPE infections are typically preceded by asymptomatic carriage, especially in vulnerable patients such as those who are immunocompromised and critically ill (*5*). To prevent transmission, active surveillance to identify CPE carriers is essential but may be associated with a high cost:benefit ratio if implemented without knowledge of the natural history of CPE carriage.

Previously reported CPE carriage durations vary widely; median durations range from 43 to 387 days (*5*–*7*). These variations probably result from differences in follow-up schedules, microbiological and molecular methods used to identify CPE, and criteria to define clearance. Studies that reported longer carriage duration tended to adopt an opportunistic sampling strategy and considered both clinical and fecal samples to determine carriage (*7*). Opportunistic sampling may lead to selection bias because patients with more healthcare contacts would have more samples collected. Infrequent and inconsistent sampling is more likely to misclassify recolonization from a new transmission event as continuous colonization, resulting in perceived longer duration of carriage.

Of note, the participants carried more species of CPE than types of carbapenemase genes. Although this observation may be the result of new acquisition events, it is more parsimoniously explained by active interspecies horizontal gene transfer, especially

Table. Demographics for 21 participants in study of duration of carbapenemase-producing *Enterobacteriaceae* carriage in hospital patients, Singapore*

Characteristic	No. (%)
Sex	
M	15 (71.4)
F	6 (28.6)
Ethnicity	
Chinese	15 (71.4)
Malay	3 (14.3)
Indian	2 (9.5)
Other	1 (4.8)
Ambulatory status	
Independently performs ADL	12 (57.1)
Requires assistance in ADL	4 (19.0)
Wheelchair bound	3 (14.3)
Bed bound	2 (9.5)
Recent surgery†	15 (71.4)
Colonization or infection with another MDRO in the year preceding enrollment	4 (19.0)
Hospitalization in past year	11 (52.4)
Antibiotic intake during follow-up period	13 (61.9)
Readmission during follow-up period	10 (47.6)
Recent overseas travel	13 (61.9)

*Median age (interquartile range) was 60.0 (50.0–69.0) y; median Charlson Morbidity Index (interquartile range) 3.0 (2.0–5.0). ADL, activities of daily living; MDRO, multidrug-resistant organisms, including methicillin-resistant *Staphylococcus aureus*, vancomycin-resistant *Enterococcus*, carbapenem-resistant *Enterobacteriaceae*, carbapenem-resistant *Acinetobacter baumanii*, and carbapenem-resistant *Pseudomonas aeruginosa*, recorded from surveillance and clinical cultures taken in the year before study enrollment.
†Gastrointestinal surgeries (n = 7), skin and soft tissue surgeries (n = 4), neurosurgery (n = 2), removal of Tenckhoff catheter (n = 1), and urologic procedure (n = 1).

in a low-transmission setting such as Singapore. Differential rates of clearance of CP-KP and CP-EC can be related to colonizing affinity of the species and fitness cost of carbapenemase genes, which vary widely among different species (*8*). Further studies incorporating between-host and within-host transmission dynamics of resistance may shed light on the roles of bacterial clones and plasmids in spreading and maintaining resistance.

Our study has limitations. First, because the participants were screened after hospital admission, the time of initial colonization could not be confidently determined. However, our multistate Markov models assume a constant rate of decolonization. Our sensitivity analysis used the latest CPE-negative swab samples, so carriage duration estimates were similar to those calculated without the last known CPE-negative swab samples, suggesting that our modeling assumptions were reasonable. Second, our sample size was small and drawn from a single population, and the extent to which our findings can be extrapolated to other populations is uncertain. However, our study was rigorously conducted in terms of frequency of fecal sample collection, duration of follow-up, and number of participants in a nonoutbreak setting. The use of multistate models has been shown to preserve power with modest sample size given more frequent follow-ups (*9*).

Our systematic sampling and robust methods for identifying CPE enabled us to closely follow participants' carriage status. Using combined detection methods of culture on carbapenem-resistance selective media, antibiotic susceptibility testing, and PCR, we found that 4 (19.0%) patients had intervening negative samples, 1–3 weeks apart. This finding suggests that a patient should have ≥2 negative samples 4–6 weeks apart before considering CPE to be eliminated. The finding that the probability of decolonization is 98.5% in 1 year suggests that a policy of reviewing CPE carrier status yearly may be appropriate for this population. Further health economics analysis is needed to make institution-specific recommendations for rescreening frequency. Given the finding that antimicrobial drug use was the most important factor associated with prolonged CPE carriage, use of antimicrobial drugs in these patients should be avoided if not clinically indicated.

The study is primarily supported by the Singapore Biomedical Research Council–Economic Development Board Industry Alignment Fund (grant no. IAF311018). M.Y. is supported by the Singapore National Medical Research Council (NMRC) Research Fellowship (grant no. NMRC/Fellowship/0051/2017). B.S.C. is supported by the UK Medical Research Council/Department for International Development (grant no. MR/K006924/1). P.M. is supported by the Joint Programming Initiative on Antimicrobial Resistance (MODERN) (grant no. C-17-0014). A.H. is supported by Wellcome Trust (grant no. 212630/Z/18/Z). The Mahidol-Oxford Tropical Medicine Research Unit is part of the Wellcome-Trust Major Overseas Programme in Southeast Asia (grant no. 106698/Z/14/Z). Additional grant support was provided by the NMRC Clinician-Scientist Individual Research Grant (grant no. NMRC/CIRG/1463/2016 and NMRC/CIRG/1467/2017); the Singapore Ministry of Education Academic Research Fund Tier 2 grant, New Delhi Metallo-Beta-Lactamase, a global multi-centre, whole-genome study (grant no. MOE2015-T2-2-096); an NMRC collaborative grant, Collaborative Solutions Targeting Antimicrobial Resistance Threats in Health Systems (grant no. NMRC CGAug16C005); and an NMRC Clinician Scientist Award (grant no. NMRC/CSA-INV/0002/2016).

About the Author

Dr. Mo is an infectious diseases physician and senior lecturer at the National University of Singapore. Her research interests are antimicrobial resistance and infection control. She is pursuing a PhD degree with the University of Oxford and leading a multicenter clinical trial in Asia on shortening duration of antimicrobial drug use for patients with ventilator-associated pneumonia.

References

1. Logan LK, Weinstein RA. The Epidemiology of carbapenem-resistant *Enterobacteriaceae*: the impact and evolution of a global menace. J Infect Dis. 2017;215(suppl_1) :S28–36. https://doi.org/10.1093/infdis/jiw282
2. Magiorakos AP, Burns K, Rodríguez Baño J, Borg M, Daikos G, Dumpis U, et al. Infection prevention and control measures and tools for the prevention of entry of carbapenem-resistant *Enterobacteriaceae* into healthcare settings: guidance from the European Centre for Disease Prevention and Control. Antimicrob Resist Infect Control. 2017;6:113. https://doi.org/10.1186/s13756-017-0259-z
3. Centers for Disease Control and Prevention. Healthcare-associated infections [cited 2019 Mar 7]. https://www.cdc.gov/hai/organisms/cre/cre-toolkit/index.html
4. Teo JWP, La M-V, Krishnan P, Ang B, Jureen R, Lin RTP. *Enterobacter cloacae* producing an uncommon class A carbapenemase, IMI-1, from Singapore. J Med Microbiol. 2013;62:1086–8. https://doi.org/10.1099/jmm.0.053363-0
5. Tischendorf J, de Avila RA, Safdar N. Risk of infection following colonization with carbapenem-resistant *Enterobactericeae*: a systematic review. Am J Infect Control. 2016;44:539–43. https://doi.org/10.1016/j.ajic.2015.12.005
6. Bar-Yoseph H, Hussein K, Braun E, Paul M. Natural history and decolonization strategies for ESBL/carbapenem-resistant

Enterobacteriaceae carriage: systematic review and meta-analysis. J Antimicrob Chemother. 2016;71:2729–39. https://doi.org/10.1093/jac/dkw221
7. Zimmerman FS, Assous MV, Bdolah-Abram T, Lachish T, Yinnon AM, Wiener-Well Y. Duration of carriage of carbapenem-resistant *Enterobacteriaceae* following hospital discharge. Am J Infect Control. 2013;41:190–4. https://doi.org/10.1016/j.ajic.2012.09.020
8. Cerqueira GC, Earl AM, Ernst CM, Grad YH, Dekker JP, Feldgarden M, et al. Multi-institute analysis of carbapenem resistance reveals remarkable diversity, unexplained mechanisms, and limited clonal outbreaks. Proc Natl Acad Sci U S A. 2017;114:1135–40. https://doi.org/10.1073/pnas.1616248114
9. Cassarly C, Martin RH, Chimowitz M, Peña EA, Ramakrishnan V, Palesch YY. Assessing type I error and power of multistate Markov models for panel data–a simulation study. Commun Stat Simul Comput. 2017; 46:7040–61. https://doi.org/10.1080/03610918.2016.1222425

Address for correspondence: Mo Yin, National University Hospital, Division of Infectious Disease, 5 Lower Kent Ridge Rd, Singapore; email: yin_mo@nuhs.edu.sg

Chromobacterium haemolyticum Pneumonia Associated with Near-Drowning and River Water, Japan

Hajime Kanamori, Tetsuji Aoyagi, Makoto Kuroda, Tsuyoshi Sekizuka, Makoto Katsumi, Kenichiro Ishikawa, Tatsuhiko Hosaka, Hiroaki Baba, Kengo Oshima, Koichi Tokuda, Masatsugu Hasegawa, Yu Kawazoe, Shigeki Kushimoto, Mitsuo Kaku

We report a severe case of *Chromobacterium haemolyticum* pneumonia associated with near-drowning and detail the investigation of the pathogen and river water. Our genomic and environmental investigation demonstrated that river water in a temperate region can be a source of *C. haemolyticum* causing human infections.

Chromobacterium is a genus of gram-negative, facultative anaerobic bacteria; application of 16S rRNA gene sequencing into bacterial taxonomy is expanding its species (*1*–*5*). Most *Chromobacterium* infections in humans have been caused by *C. violaceum* (*6*). Recently, exceptionally rare cases of *C. haemolyticum* infections have been described (*2*,*4*,*7*–*9*), but environmental sources of this pathogen have not been well investigated. We describe a case of *Chromobacterium*-associated pneumonia due to near-drowning and environmental investigation of a river site of the near-drowning. We used whole-genome sequencing (WGS) to identify the *Chromobacterium* species causing pneumonia associated with near-drowning and investigate molecular features, including antimicrobial resistance, virulence, and genetic relatedness of clinical and environmental isolates of *C. haemolyticum*.

The Study

This study was approved by the institutional review board of Tohoku University Graduate School of Medicine (IRB no. 2018-1-716). In June 2018, a man in his 70s was transported to our emergency center. He had altered consciousness and hypothermia at admission. He had fallen down a bank and into a river in the Tohoku region of Japan while intoxicated from alcohol and was found immersed in the river. He had respiratory failure and required intubation and mechanical ventilation. He had multiple fractures and a cervical cord injury. He had a history of hypertension, diabetes, and benign prostatic hyperplasia but was not immunodeficient. We diagnosed severe aspiration pneumonia and sepsis and treated the patient empirically with intravenous meropenem plus levofloxacin. We detected a nonpigmented, β-hemolytic gram-negative bacillus from both sputum and blood cultures. *C. violaceum* was identified by a matrix-assisted laser desorption/ionization time-of-flight mass spectrometry (VITEK MS; bioMérieux, https://www.biomerieux.com) with a confidence value of 99.9%. We changed the antimicrobial drug regimen to intravenous ceftazidime plus levofloxacin based on antimicrobial susceptibility testing pattern (Appendix 1 Table, https://wwwnc.cdc.gov/EID/article/26/9/19-0670-App1.pdf). After 3 weeks of intravenous therapy and critical care, the patient showed clinical improvement and had negative blood and sputum cultures. He was transferred to a community hospital for further rehabilitation and completed an additional 2 months of oral levofloxacin.

In mid-August, we conducted an environmental investigation of the river water in the area where the patient was found. We collected 500 mL samples of river water, 2 samples at the site where the patient was found and 1 sample 4 km upstream, where he likely fell into the river. We filtered samples through a

Authors affiliations: Tohoku University Graduate School of Medicine, Sendai, Japan (H. Kanamori, T. Aoyagi, M. Katsumi, K. Ishikawa, T. Hosaka, H. Baba, K. Oshima, K. Tokuda, M. Hasegawa, Y. Kawazoe, S. Kushimoto, M. Kaku); National Institute of Infectious Diseases, Tokyo, Japan (M. Kuroda, T. Sekizuka)

DOI: https://doi.org/10.3201/eid2609.190670

polyethersulfone filter membrane with a pore size of 0.22 μm. We placed the membrane filters on sheep blood agar plates and incubated for 24 hours at 35°C. We recovered a nonpigmented, β-hemolytic colony similar to clinical isolates from each of the cultures, which we identified as *C. violaceum*. We performed antimicrobial susceptibility testing by using a MicroScan WalkAway 96 plus (Beckman Coulter, https://www.beckmancoulter.com; Appendix 1) and assessed antimicrobial susceptibility patterns of *Chromobacterium* isolates (Appendix 1 Table).

We performed WGS on the 3 environmental and 2 clinical isolates (Appendix 1). For comparative genomic analysis, we used additional 16 genome sequences of *Chromobacterium* spp. from wastewater treatment plants in Tokyo and 52 publicly available genome sequences of *Chromobacterium* spp. from the NCBI Assembly database (https://www.ncbi.nlm.nih.gov/assembly) (Figure 1; Appendix 1; Appendix 2 Table 1, https://wwwnc.cdc.gov/EID/article/26/9/19-0670-App2.xlsx). We identified 19 strains of *C. haemolyticum* with 252,974 single-nucleotide variants by core-genome phylogenetic analysis (Figure 1; Appendix 2 Table 2). Metagenomic analysis of a river water sample collected from the site of the patient's near-drowning revealed that the relative abundance of *Chromobacterium* is 0.07% (Figure 2). We deposited the complete genomic sequence of *C. haemolyticum* CH06-BL in GenBank (accession no. AP019312).

Conclusions

This severe case of drowning-associated pneumonia and bacteremia due to *C. haemolyticum* was successfully treated with appropriate antimicrobial therapy. Previously, 5 clinical cases of *C. haemolyticum* infections had been reported, including sputum colonization, necrotizing fasciitis with bacteremia, proctocolitis, pneumonia, and pediatric bacteremia (*2*,*4*,*7*–*9*). All patients, including the patient we report, survived after antimicrobial treatment. Intravenous antimicrobial therapy, such as meropenem or fluoroquinolone, is recommended for *C. haemolyticum* infections (*7*,*9*). The role of prolonged therapy for *C. haemolyticum* infections remains unclear, but in *C. violaceum* infections, an oral agent such as trimethoprim-sulfamethoxazole, tetracycline, or fluoroquinolone for 2–3 months can be used to prevent relapse (*6*).

As seen in the case we report, identification of *Chromobacterium* species is challenging. *C. violaceum* can produce a violet pigment (violacein) in most strains, and nonpigmented strains rarely have been

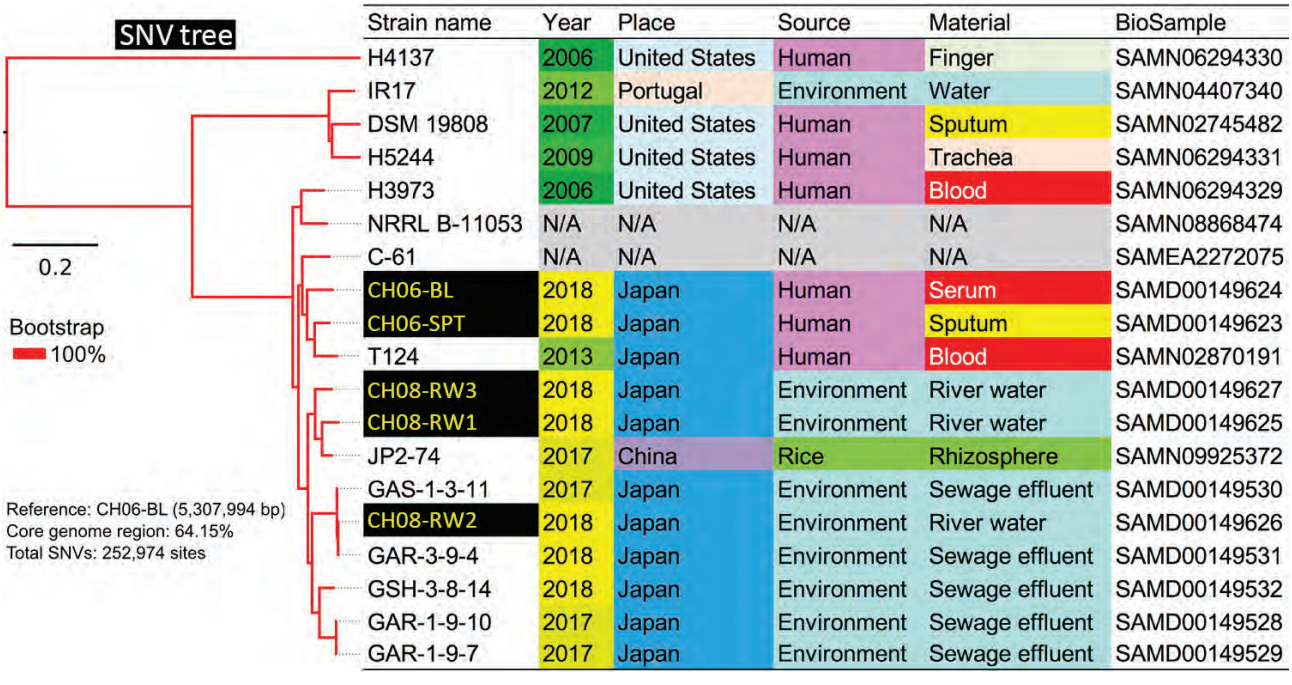

Strain name	Year	Place	Source	Material	BioSample
H4137	2006	United States	Human	Finger	SAMN06294330
IR17	2012	Portugal	Environment	Water	SAMN04407340
DSM 19808	2007	United States	Human	Sputum	SAMN02745482
H5244	2009	United States	Human	Trachea	SAMN06294331
H3973	2006	United States	Human	Blood	SAMN06294329
NRRL B-11053	N/A	N/A	N/A	N/A	SAMN08868474
C-61	N/A	N/A	N/A	N/A	SAMEA2272075
CH06-BL	2018	Japan	Human	Serum	SAMD00149624
CH06-SPT	2018	Japan	Human	Sputum	SAMD00149623
T124	2013	Japan	Human	Blood	SAMN02870191
CH08-RW3	2018	Japan	Environment	River water	SAMD00149627
CH08-RW1	2018	Japan	Environment	River water	SAMD00149625
JP2-74	2017	China	Rice	Rhizosphere	SAMN09925372
GAS-1-3-11	2017	Japan	Environment	Sewage effluent	SAMD00149530
CH08-RW2	2018	Japan	Environment	River water	SAMD00149626
GAR-3-9-4	2018	Japan	Environment	Sewage effluent	SAMD00149531
GSH-3-8-14	2018	Japan	Environment	Sewage effluent	SAMD00149532
GAR-1-9-10	2017	Japan	Environment	Sewage effluent	SAMD00149528
GAR-1-9-7	2017	Japan	Environment	Sewage effluent	SAMD00149529

Figure 1. Core genome single-nucleotide variations in a phylogenetic analysis of 19 strains of *Chromobacterium haemolyticum* in a case of pneumonia associated with near-drowning in river water, Japan. In total, 252,974 SNV sites were detected in core genome region among 19 strains. The phylogenetic analysis with SNV data was constructed by maximum likelihood method. Two clinical isolates (CH06-BL and CH06-SPT) and 3 environmental isolates (CH08-RW1, CH08-RW2, and CH08-RW3) of *C. haemolyticum* in this study were discordant (27,867–29,491 SNVs). Scale bar indicates nucleotide substitutions per site. SNV, single nucleotide variant.

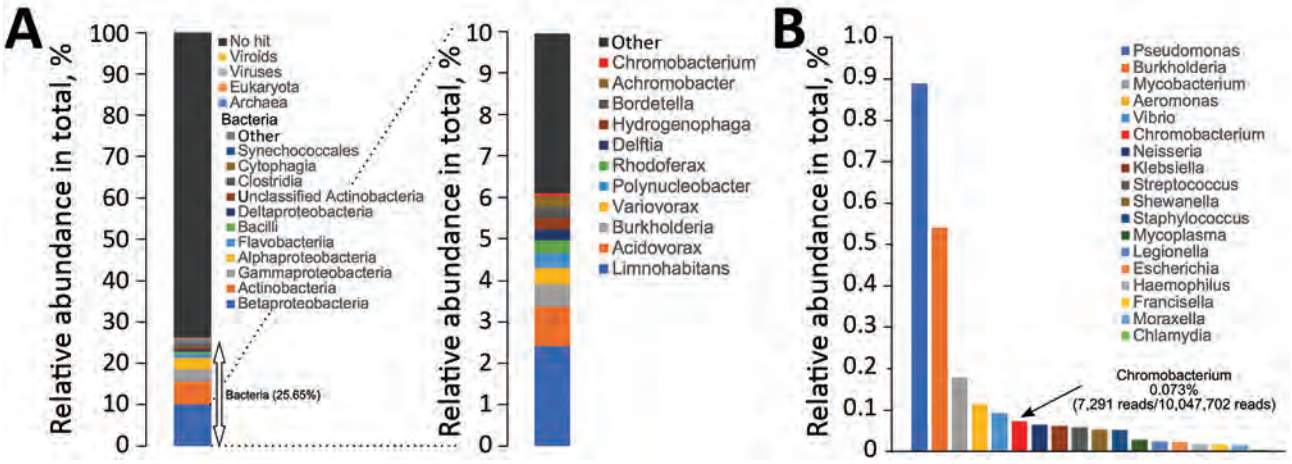

Figure 2. Metagenomic analysis of river water sample collected from the site of near-drowning of a patient with *Chromobacterium haemolyticum* pneumonia, Japan. A) Relative abundance of superkingdom, class of bacteria, and genus of betaproteobacteria in river water sample. The relative abundance of bacteria is 25.65%; the 10 most observed class and genus are summarized in cumulative bar charts. B) Comparison of relative abundance of bacteria causing pneumonia associated with drowning in genus level in the river water sample. The relative abundance of *Chromobacterium*, a Betaproteobacteria, is 0.073%.

described (*10*). *C. haemolyticum* does not produce violacein and is characterized by strong hemolytic activity on sheep blood agar (*2*,*4*). Only *C. violaceum* is currently available in the genus *Chromobacterium* on the mass spectrometry database of species identification. Differentiation between *C. haemolyticum* and *C. violaceum* is crucial because *C. haemolyticum* has greater resistance to antimicrobial drugs, such as β-lactams (*2*,*7*). Although *C. aquaticum* is a nonpigmented, β-hemolytic strain phenotypically similar to *C. haemolyticum*, 16S rRNA sequencing might not determine either *C. haemolyticum* or *C. aquaticum* because of artificial separation of both species (*4*). Thus, WGS is a useful tool for accurate identification of *Chromobacterium* species to avoid misidentification of *C. haemolyticum* (*1*–*5*).

C. haemolyticum CH06-BL and other clinical and environmental isolates in this study possessed $bla_{\text{CRH-1}}$ in the chromosome (Appendix 2 Table 1), but we did not identify mobile elements in the surrounding area. In a previous study, a class A β-lactamase, CRH-1 from *C. haemolyticum* was closely related to *Klebsiella pneumoniae* carbapenemase 2 (*11*). As seen in acquired resistance among other gram-negative bacilli, aquatic environments can be a reservoir (*11*,*12*).

The etiology of infections caused by *Chromobacterium* has not been fully elucidated. Of note, *Chromobacterium* accounted for only a small portion of the bacteria found in our metagenomics analysis of the river water, but this organism was isolated from the patient and was involved in human infection, despite presence of other potential pathogens in the river, such as *Pseudomonas*, *Aeromonas*, *Legionella*, that can cause pneumonia associated with drowning (Figure 2) (*13*). Our study isolates also had type III secretion system (T3SS) encoded by *Chromobacterium* pathogenicity island 1 and 1a (Cpi-1/-1a) (Appendix 1 Figure 2), which is known as a major virulence factor in *C. violaceum* (*14*). These results highlight the need for further research on antimicrobial resistance and virulence in *Chromobacterium* spp.

C. violaceum is widely distributed in natural aquatic environments and can be observed in water and soil sources, especially in tropical and subtropical areas (*6*). *C. haemolyticum* strains with genetic heterogeneity have been detected from lake water in a tropical region (*15*), but the bacterium's habitat in temperate regions remains unknown. Our comparative genomic analysis revealed that clinical and environmental isolates of *C. haemolyticum* were discordant (27,867–29,491 single-nucleotide variants), although there was no standard definition for its clonality.

Only 2 reports of cases with *C. haemolyticum* infections in temperate regions of Japan have been published (*7*,*9*). One study reported necrotizing fasciitis associated with exposure to river water after injury. The other described pneumonia caused by accidental aspiration of runoff water after a fall in a ditch and identification of the pathogen in the water and discordant results with clinical isolates by pulsed-field gel electrophoresis. However, detailed environmental investigations of the rivers as a source of the pathogen were not conducted in either article.

In summary, our genomic and environmental study demonstrates that *C. haemolyticum* in a local river, a natural habitat of this pathogen in Japan, caused

this human infection. Clinicians should remain aware that river water in temperate regions can be a source of *C. haemolyticum* infection.

Acknowledgments

We thank David J. Weber for his careful review of the manuscript.

This work was supported in part by a grant for the Research on Emerging and Re-emerging Infectious Diseases and Immunization (grant no. H30 Shinkogyosei-Ippan-002) from the Ministry of Health, Labour and Welfare, Japan, and a grant from the Research Program on Emerging and Re-emerging Infectious Diseases from the Japan Agency for Medical Research and Development (grant nos. JP18fk0108048 and JP18fk0108019).

About the Author

Dr. Kanamori is an infectious disease physician at Tohoku University Hospital, Sendai, Japan. His primary research interests are antimicrobial resistance, environmental hygiene, and healthcare epidemiology.

References

1. Blackburn MB, Farrar RR Jr, Sparks ME, Kuhar D, Mitchell A, Gundersen-Rindal DE. *Chromobacterium sphagni* sp. nov., an insecticidal bacterium isolated from Sphagnum bogs. Int J Syst Evol Microbiol. 2017;67:3417–22. https://doi.org/10.1099/ijsem.0.002127
2. Han XY, Han FS, Segal J. *Chromobacterium haemolyticum* sp. nov., a strongly haemolytic species. Int J Syst Evol Microbiol. 2008;58:1398–403. https://doi.org/10.1099/ijs.0.64681-0
3. Bajaj A, Kumar A, Yadav S, Kaur G, Bala M, Singh NK, et al. Isolation and characterization of a novel Gram-negative bacterium *Chromobacterium alkanivorans* sp. nov., strain IITR-71T degrading halogenated alkanes. Int J Syst Evol Microbiol. 2016;66:5228–35. https://doi.org/10.1099/ijsem.0.001500
4. Harmon N, Mortensen JE, Robinette E, Powell EA. Pediatric bacteremia caused by *Chromobacterium haemolyticum*/*Chromobacterium aquaticum*. Diagn Microbiol Infect Dis. 2016;86:108–11. https://doi.org/10.1016/j.diagmicrobio.2016.05.021
5. Zhou S, Guo X, Wang H, Kong D, Wang Y, Zhu J, et al. *Chromobacterium rhizoryzae* sp. nov., isolated from rice roots. Int J Syst Evol Microbiol. 2016;66:3890–6. https://doi.org/10.1099/ijsem.0.001284
6. Yang CH, Li YH. *Chromobacterium violaceum* infection: a clinical review of an important but neglected infection. J Chin Med Assoc. 2011;74:435–41. https://doi.org/10.1016/j.jcma.2011.08.013
7. Okada M, Inokuchi R, Shinohara K, Matsumoto A, Ono Y, Narita M, et al. *Chromobacterium haemolyticum*-induced bacteremia in a healthy young man. BMC Infect Dis. 2013;13:406. https://doi.org/10.1186/1471-2334-13-406
8. Tanpowpong P, Charoenmuang R, Apiwattanakul N. First pediatric case of *Chromobacterium haemolyticum* causing proctocolitis. Pediatr Int. 2014;56:615–7. https://doi.org/10.1111/ped.12301
9. Takenaka R, Nureki S, Ueno T, Shigemitsu O, Miyazaki E, Kadota J, et al. *Chromobacterium haemolyticum* pneumonia possibly due to the aspiration of runoff water. Jpn J Infect Dis. 2015;68:526–9. https://doi.org/10.7883/yoken.JJID.2014.285
10. Yang CH. Nonpigmented *Chromobacterium violaceum* bacteremic cellulitis after fish bite. J Microbiol Immunol Infect. 2011;44:401–5. https://doi.org/10.1016/j.jmii.2010.04.004
11. Gudeta DD, Bortolaia V, Jayol A, Poirel L, Nordmann P, Guardabassi L. *Chromobacterium* spp. harbour Ambler class A β-lactamases showing high identity with KPC. J Antimicrob Chemother. 2016;71:1493–6. https://doi.org/10.1093/jac/dkw020
12. Tacão M, Correia A, Henriques IS. Low prevalence of carbapenem-resistant bacteria in river water: resistance is mostly related to intrinsic mechanisms. Microb Drug Resist. 2015;21:497–506. https://doi.org/10.1089/mdr.2015.0072
13. Ender PT, Dolan MJ. Pneumonia associated with near-drowning. Clin Infect Dis. 1997;25:896–907. https://doi.org/10.1086/515532
14. Miki T, Okada N. Draft genome sequence of *Chromobacterium haemolyticum* causing human bacteremia infection in Japan. Genome Announc. 2014;2:e01047–14. https://doi.org/10.1128/genomeA.01047-14
15. Lima-Bittencourt CI, Costa PS, Barbosa FA, Chartone-Souza E, Nascimento AM. Characterization of a *Chromobacterium haemolyticum* population from a natural tropical lake. Lett Appl Microbiol. 2011;52:642–50. https://doi.org/10.1111/j.1472-765X.2011.03052.x

Address for correspondence: Hajime Kanamori; Department of Infectious Diseases, Internal Medicine, Tohoku University Graduate School of Medicine, 1-1 Seiryo-machi, Aoba-ku, Sendai 980-8574, Japan; email: kanamori@med.tohoku.ac.jp

Anicteric Leptospirosis-Associated Meningitis in a Tropical Urban Environment, Brazil

Scott A. Nabity, Guilherme C. Araújo, José E. Hagan, Alcinéia O. Damião, Mitermayer G. Reis, Albert I. Ko, Guilherme S. Ribeiro

While studying aseptic meningitis in Salvador, Brazil, we diagnosed anicteric leptospirosis in 1.7% (5/295) of patients hospitalized for aseptic meningitis. Leptospirosis-associated meningitis patients had lower mean cerebrospinal fluid cell counts and protein than other-cause aseptic meningitis ($p<0.05$). Clinicians must consider leptospirosis-associated meningitis in appropriate clinical-epidemiologic contexts.

The clinical signs of leptospirosis can vary widely, which complicates timely diagnosis and targeted therapy. Aseptic meningitis associated with *Leptospira* infection, hereafter termed leptospirosis-associated meningitis (LAM), has been well described (*1*–*3*). However, clinicians diagnose atypical forms of leptospirosis less frequently, particularly in the absence of classic signs (i.e., renal insufficiency or hepatitis). Detection requires a high level of clinical suspicion, and even then imperfect diagnostics for leptospirosis limit timely confirmation.

Leptospirosis causes ≈1 million illnesses annually; this figure does not include LAM (*4*). Despite the high global burden of leptospirosis and early knowledge that anicteric LAM is underappreciated (*1*), few existing studies delineate the proportion of aseptic meningitis caused by *Leptospira* sp. infection in settings in which it is endemic. We performed surveillance for aseptic meningitis in an area of high transmission of urban leptospirosis. Hospital Couto Maia, the Oswaldo Cruz Foundation, and Yale University provided ethics approval for this study.

Author affiliations: Massachusetts General Hospital, Boston, Massachusetts, USA (S.A. Nabity); Instituto Gonçalo Moniz, Salvador, Brazil (G.C. Araújo, A.O. Damião, M.G. Reis, A.I. Ko, G.S. Ribeiro); Yale University, New Haven, Connecticut, USA (J.E. Hagan, M.G. Reis, A.I. Ko); Universidade Federal da Bahia, Salvador, Brazil (M.G. Reis, G.S. Ribeiro)

DOI: https://doi.org/10.3201/eid2609.191001

The Study

We conducted the study at a public referral hospital for infectious diseases in Salvador, Brazil, April 18–October 18, 2012, during a period of seasonal increased risk for severe leptospirosis such as Weil's disease (*5*) and severe pulmonary hemorrhagic syndrome (*6*). We enrolled consecutive patients ≥5 years of age who had a diagnosis of aseptic meningitis, defined by clinical meningitis (fever with severe headache or meningismus); nonturbid, nonpurulent cerebrospinal fluid (CSF) containing 10–2,000 cells/m^3, protein ≤150 mg/dL, glucose ≥40 mg/dL; and negative results for bacterial meningitis on Gram stain, culture isolation, and latex agglutination tests. From the patients with aseptic meningitis, we aimed to select those most likely to elicit clinical suspicion for leptospirosis; a selection requirement was ≥1 epidemiologic risk factor for classic leptospirosis in the 30 days before symptom onset for leptospirosis testing. Risk factors were contact with floodwater, sewer water, or mud; rats at home or work; and residence or employment in a high-risk environment (i.e., slum community or animal farm) (*7*). We confirmed LAM by either *Leptospira* blood culture on EMJH media using 150 μL inoculum, or by reactive microagglutination test (MAT) by ≥1 of the following criteria: ≥4-fold acute-convalescent titer rise; seroconversion (undetectable acute-phase titer and convalescent-phase titer ≥1:200); or sample titer ≥1:800.

The public hospital received regional referrals for lumbar puncture and CSF analysis for suspected meningitis as standard practice; CSF showing >10 cells/mm^3 required inpatient observation. At enrollment, we obtained demographic, epidemiologic, and clinical data from patients. We followed the patients during hospitalization to ascertain outcomes. We compared clinical characteristics between leptospirosis-confirmed and unconfirmed patients ≥15 years of age to avoid age confounding. Comparisons were made using Fisher exact test (2-tailed, $\alpha = 0.05$) and Wilcoxon rank-sum test (2-tailed exact, $\alpha = 0.05$).

We identified 295 patients with aseptic meningitis ≥5 years of age at admission. Of these, 22 (7.5%) had ≥1 epidemiologic risk factor for classic leptospirosis and therefore met criteria for leptospirosis diagnostic testing. Five (23%, 95% CI 7%–44%) of the 22 had confirmed LAM. Among all 295 patients, noting that 22 of these were tested for leptospirosis, the proportion LAM-confirmed was 1.7% (95% CI 0.5%–3.9%). MAT titers were highest against *L. interrogans* serogroup Canicola for 2 patients and *L. interrogans* serogroup Icterohaemorrhagiae for 2 others with paired serum specimens (Table 1, https://wwwnc.cdc.gov/EID/article/26/9/19-1001-T1.htm). A fifth patient confirmed by an acute titer ≥1:800 had mixed highest titers against *L. interrogans* serogroup Icterohaemorrhagiae and *L. kirschineri* serogroup Cynopteri. None had a positive hemoculture for *Leptospira*, and none had clinical jaundice, which we defined as anicteric.

No patient was suspected to have leptospirosis at initial evaluation. However, 1 (patient 3) was subsequently suspected to have leptospirosis within 24 hours of hospitalization when a successive clinician noted mild respiratory distress with bilateral infiltrates on chest radiograph. Three confirmed patients ultimately had antimicrobial drug treatment (Table 1); none required admission to the intensive care unit or died, and all left the hospital at neurologic baseline. LAM patients had lower CSF cell counts and protein than patients with meningitis from other causes (Table 2).

Conclusions

The overall frequency of anicteric LAM among aseptic meningitis patients appeared low, despite being measured during Salvador's highest rainfall season. We increased diagnostic yield to 23% with elementary risk stratification for classic leptospirosis. Because this process was likely to miss LAM that did not meet our inclusion criteria for testing, we probably underestimated the true frequency of LAM.

Lower cell counts and CSF protein levels distinguished LAM from other causes of aseptic meningitis, although the small sample size of our study limits their reliability. CSF pleiocytosis accompanies most cases of leptospirosis, particularly during the secondary immune phase of classic disease (*2*,*3*), even without clinical meningeal signs. Although typical CSF chemistries for LAM are well known (i.e., slightly elevated cell count and protein; normal-low glucose) (*2*,*3*), only 1 previous report showed direct comparison between the CSF of anicteric LAM and nonleptospirosis aseptic meningitis (*8*). However, the report did not include epidemiologic information and the CSF data were presented in a way that limited statistical comparison.

Two of 5 cases of LAM had the highest MAT titer against serogroup Canicola, which is associated with canine reservoirs (*9*). Serogroup Icterohaemorrhagiae predominates for classic leptospirosis in this setting (≈90%) and is typically associated with rat (*Rattus norvegicus*) reservoirs (*5*). Thus, our findings suggest that

Table 2. Characteristics of patients with leptospirosis-associated and non-leptospirosis meningitis, Salvador, Brazil*

Characteristic	Confirmed leptospirosis-associated meningitis		Nonleptospirosis aseptic meningitis		
	No. patients	No. (%) or mean ± SD (range)	No. patients†	No. (%) or mean ± SD (range)	p value
Age, y	5	30.8 ± 9.9 (18–42)	13	28.6 ± 13.4 (16–51)	0.746‡
No. days of symptoms before hospital care	5	6.4 ± 1.8 (2–8)	13	6.2 ± 5.3 (2–20)	0.922‡
Symptom profile§					
Emesis	5	4 (80.0)	13	8 (61.5)	0.615
Photophobia	5	1 (20.0)	13	0	0.278
Nuchal rigidity	5	1 (20.0)	13	5 (38.5)	0.615
Abdominal pain	5	2 (40.0)	13	2 (15.4)	0.533
Diarrhea	5	2 (40.0)	13	2 (15.4)	0.533
Myalgia/arthralgia	5	4 (80.0)	13	6 (46.2)	0.314
Total peripheral eukocytes,10^3/mL	5	9.8 ± 4.2 (4.9–15.5)	13	9.2 ± 1.2 (5.2–20.4)	0.800‡
Platelets, 10^3/μL	5	214.8 ± 98.6 (108–336)	13	262.8 ± 52.6 (178–350)	0.193‡
Plasma chemistries					
Potassium, meq/L	4	4.5 ± 0.5 (4.1–5.2)	11	4.3 ± 0.5 (3.6–5.2)	0.504‡
Creatinine, mg/dL	5	1.1 ± 0.5 (0.6–1.8)	12	1.1 ± 0.3 (0.5–1.6)	0.910‡
ALT, U/L	4	42.8 ± 23.0 (25–76)	10	33.6 ± 9.5 (12–49)	0.297‡
Cerebrospinal fluid profile					
Nucleated cells, 10^6/L	5	67.6 ± 48.2 (28–150)	13	351.3 ± 402.6 (17–1500)	0.025¶
Glucose, mg/dL	4	61.0 ± 13.7 (46–77)#	12	60.9 ± 11.6 (44–84)	0.991‡
Protein, g/L	5	35.4 ± 8.8 (23–46)	12	66.3 ± 31.3 (34–141)	0.014¶

*ALT, alanine aminotransferase.
†Analysis restricted to patients ≥15 y of age to avoid confounding of biochemical parameters by age.
‡2-sample *t*-test using pooled variance.
§All patients had severe headache and none had a seizure.
¶Wilcoxon sum-rank nonparametric test.
#Excludes 1 patient with type 2 diabetes who had a blood glucose of 298 and a cerebrospinal fluid glucose of 143.

there may be notable differences in the epidemiology of LAM and of classic leptospirosis as well as differential pathogenic mechanisms among these serogroups (*10*). Various serogroups have been implicated in anicteric LAM; they include Icterohaemorrhagiae (*8*,*11*–*13*) and Canicola (*11*,*12*,*14*) from differing epidemiologic settings over time.

We selected our screening criteria to affirm leptospirosis risk based on our epidemiologic understanding of classical leptospirosis. Criteria less grounded in classical leptospirosis risk exposures in this setting (e.g., including exposure to dogs), may help stratify aseptic meningitis patients for diagnostic testing. Similarly, CSF analysis alone is unlikely to properly identify candidates for leptospirosis diagnostic investigation. We did not culture CSF for *Leptospira*, nor could we attempt PCR on CSF; these limitations may have reduced diagnostic yield.

We ascertained leptospirosis as the cause of meningitis in a setting of high endemic transmission of urban leptospirosis, where severe disease forms are a predominant clinical presentation, but little information has been obtained for aseptic meningitis. Our findings support the development and validation of risk stratification strategies for systematic assessments of aseptic meningitis aiming to detect LAM in regions in which leptospirosis occurs endemically or epidemically. Such strategies, perhaps expanded to include nonrodent animal exposures, would not only help to guide diagnostic work-up but may also direct early introduction of antimicrobial drugs in settings without laboratories capable of diagnosing leptospirosis. Until there is an effective approach to differentiate anicteric LAM from other-cause aseptic meningitis at clinical presentation in low-resource environments, clinicians must maintain a robust and enduring index of suspicion for leptospirosis when evaluating patients with aseptic meningitis.

Acknowledgments

We thank the staff of Couto Maia Hospital in Salvador, notably Ronaldo Ribeiro, Ana Veronica Mascarenhas, and Ceuci Nunes, for their collaboration. We also thank Nivison Nery and Renan Rosa for assistance with data curation, Jaqueline Cruz for diagnostic laboratory work, and the patients who consented to participate.

This work was supported by the National Institutes of Health (grant nos. R44 AI072856, U01 AI088752, R01 AI121207, D43 TW00919), the Fogarty International Clinical Research Scholars Program, the Duke Global Health Institute, and the Brazilian National Council for Scientific and Technological Development (CNPq). The funders had no role in study design, data collection and analysis, decision to publish, or preparation of the manuscript. M.G.R. and G.S.R. had scholarships from CNPq.

About the Author

Dr. Nabity is a medical epidemiologist who at the time of this study was with Massachusetts General Hospital, Boston, Massachusetts. His research involves the prevention, control, and elimination of infectious diseases.

References

1. Walch-Sorgdrager B. Leptospiroses. Bull Heal Organ (League Nations). 1939;8:143-386.
2. Coyle PK, Dattwyler R. Spirochetal infection of the central nervous system. Infect Dis Clin North Am. 1990;4:731–46.
3. Farr RW. Leptospirosis. Clin Infect Dis. 1995;21:1–8. https://doi.org/10.1093/clinids/21.1.1
4. Costa F, Hagan JE, Calcagno J, Kane M, Torgerson P, Martinez-Silveira MS, et al. Global morbidity and mortality of leptospirosis: a systematic review. PLoS Negl Trop Dis. 2015;9:e0003898. https://doi.org/10.1371/journal.pntd.0003898
5. Ko AI, Galvão MG, Ribeiro CMD, Johnson WD Jr, Riley LW; Salvador Leptospirosis Study Group. Urban epidemic of severe leptospirosis in Brazil. Lancet. 1999;354:820–5. https://doi.org/10.1016/S0140-6736(99)80012-9
6. Gouveia EL, Metcalfe J, de Carvalho AL, Aires TS, Villasboas-Bisneto JC, Queirroz A, et al. Leptospirosis-associated severe pulmonary hemorrhagic syndrome, Salvador, Brazil. Emerg Infect Dis. 2008;14:505–8. https://doi.org/10.3201/eid1403.071064
7. Nabity SA, Hagan JE, Araújo G, Damião AO, Cruz JS, Nery N, et al. Prospective evaluation of accuracy and clinical utility of the Dual Path Platform (DPP) assay for the point-of-care diagnosis of leptospirosis in hospitalized patients. PLoS Negl Trop Dis. 2018;12:e0006285. https://doi.org/10.1371/journal.pntd.0006285
8. Costa E, Costa Y, Santos RR, Silva HR, Silva NG, Silva IC, et al. Leptospirosis: a cause of aseptic meningitis [in Portuguese]. Rev Med Bahia. 1977;23:107–18.
9. Bharti AR, Nally JE, Ricaldi JN, Matthias MA, Diaz MM, Lovett MA, et al.; Peru-United States Leptospirosis Consortium. Leptospirosis: a zoonotic disease of global importance. Lancet Infect Dis. 2003;3:757–71. https://doi.org/10.1016/S1473-3099(03)00830-2
10. Ko AI, Goarant C, Picardeau M. Leptospira: the dawn of the molecular genetics era for an emerging zoonotic pathogen. Nat Rev Microbiol. 2009;7:736–47. https://doi.org/10.1038/nrmicro2208
11. Beeson PB, Hankey DD. Leptospiral meningitis. AMA Arch Intern Med. 1952;89:575–83. https://doi.org/10.1001/archinte.1952.00240040054007
12. Galvão PAA, Scheinberg MA, Pereira Jr W, Fucs M, Sonnewend JPAS, Farhat CK, et al. Leptospirosis of childhood [in Portuguese]. Pediatr Prat. 1968;39:155-160.
13. Amato Neto V, de Avila CA, Kawarabayashi M. Leptospira meningitis: cases reported in the city of São Paulo, during an epidemic outbreak of meningococcal disease [in Portuguese]. Rev Inst Med Trop Sao Paulo. 1982;24:322–5.
14. Hubbert WT. Leptospirosis in California. Public Health Rep. 1967;82:429–33. https://doi.org/10.2307/4593034

Address for correspondence: Guilherme Sousa Ribeiro, Instituto Gonçalo Moniz, Fundação Oswaldo Cruz, Rua Waldemar Falcão, 121, Candeal, 40296-710, Salvador, Bahia, Brazil; email: guilherme.ribeiro@fiocruz.br

Lyme Borreliosis with Scalp Eschar Mimicking Rickettsial Infection, Austria

Mateusz Markowicz, Anna-Margarita Schötta, Michiel Wijnveld, Gerold Stanek

We report on a patient in Austria with scalp eschar and neck lymphadenopathy. Rickettsial etiology was excluded by culture, PCR, and serologic tests. *Borrelia afzelii* was identified from the eschar swab by PCR. Lyme borreliosis can mimic rickettsiosis; appropriate tests should be included in the diagnostic workup of patients with eschars.

Scalp eschar and neck lymphadenopathy (SENLAT) is frequently caused by *Rickettsia slovaca* and *R. raoultii*. Reports on other etiologic agents have expanded the knowledge about the cause of this clinical entity (*1*,*2*). In some cases the causative agents remain undetermined. We report a case of SENLAT in a patient from Austria with serologic and molecular evidence for infection with *Borrelia burgdorferi* sensu lato (s.l.).

The Patient

A 61-year-old woman was referred to the outpatient department of the Institute for Hygiene and Applied Immunology, Medical University of Vienna (Vienna, Austria), because of fatigue, muscle pain, and elevated body temperature (37.7°C) of 1 week's duration. Before the onset of symptoms she reported having a tick bite on her head, and she noticed a palpable crust at the site of the bite. The patient was healthy, aside from having arterial hypertension and hypothyroidism, and she reported having contact with ticks and horses. She stated that ticks were highly abundant in her garden and frequently infested the horses. The physical examination revealed a crusty lesion measuring 0.5 cm, compatible with an eschar (Figure); lymph nodes in the neck were enlarged. The clinical picture and the history of tick exposure suggested a rickettsial infection.

Basic laboratory tests showed cell counts and liver function parameters within reference ranges, elevated lactate dehydrogenase (341 U/L, reference <247 U/L), and moderately elevated C-reactive protein (0.59 mg/dL, reference <0.5 mg/dL). Serologic tests for tickborne diseases using Anti-*Borrelia* plus VlsE ELISA for IgG and Anti-*Borrelia* ELISA for IgM (Euroimmun, https://www.euroimmun.com), *Rickettsia* IFA IgG (Focus Diagnostics, https://www.focusdx.com), and Weil-Felix agglutination assay (DiaMondial, http://www.diamondial.com) all showed results below the cutoff levels and were interpreted as negative. In addition, we obtained material from the scalp eschar for PCR and culture by removing the crust with sterile tweezers. We used parts of the crust for testing, together with a swab taken directly from the skin underneath the crust. We isolated DNA from the swab and crust parts using the PeqGOLD Tissue DNA Mini Kit (Peqlab, https://de.vwr.com/cms/life_science), according to the manufacturer's instructions. We used real-time PCR to target the *gltA* gene of *Rickettsia* spp. (*3*). We also attempted to culture *Rickettsia* spp. as previously described (*4*). We placed tissue from the eschar site directly into a tick cell-culture vial containing a layer of BME/CTVM2 cells. The cell line was provided by Lesley Bell-Sakyi, The Tick Cell Biobank, Institute of Infection and Global Health, University of Liverpool (Liverpool, UK), and cultivated as described previously (*5*,*6*). We supplemented the L-15 medium (Leibovitz's L-15 medium; GIBCO, Thermo Fisher Scientific, https://www.thermofisher.com) with an antibiotic–antimycotic mixture (GIBCO) to prevent unwanted contamination of bacterial or fungal origin. We prepared cytocentrifuge smears weekly from culture samples (≈100 μL) and stained them using the Shandon Kwik-Diff kit (Thermo Fisher Scientific).

The rickettsial PCR was negative, and cultivation was not successful. To confirm the negative culture, we took samples containing supernatant and cells after 2 months' incubation and tested them with the aforementioned real-time PCRs for *B. burgdorferi* s.l.

Author affiliation: Medical University of Vienna, Vienna, Austria

DOI: https://doi.org/10.3201/eid2609.191256

and *Rickettsia* spp. but also received negative results. At the patient's initial admission, we started treatment with doxycycline 200 mg for 10 days. and the patient reported a rapid improvement of her symptoms.

Three weeks after we began treatment, we repeated the serologic tests for the respective tickborne pathogens and measured high concentrations of antibodies against *B. burgdorferi* s.l.: IgG 44 U/mL (positive cutoff >22 U/mL) and IgM >200 U/mL (positive cutoff >22 U/mL). We used an immunoblot (Anti-*Borrelia* Euroline-RN-AT, Euroimmun) as a confirmatory test: for IgM, we observed strong reactivity for antigens p41, p39, and OspC; for IgG, we found strong reactivity for p41 and OspC and weak reactivity for VlsE. Levels of antibodies against *Rickettsia* spp. remained negative.

These findings confirmed that the patient had an infection with *B. burgdorferi* s.l.; therefore, we further analyzed the DNA extract from the swab to search for borrelial DNA. We used 2 real-time PCRs based on the 16S rRNA gene (*7*) and the flagellin gene (*3*); the 16S PCR gave a positive result. We used a nested PCR targeting the 5S–23S intergenic spacer region (*8*,*9*) for genospecies identification and purified the obtained amplicon using the QIAGEN Gel Extraction Kit (https://www.qiagen.com) before bidirectional sequencing (Microsynth, https://www.microsynth.ch). Comparison with known sequences available at the National Center for Biotechnology Information (https://blast.ncbi.nlm.nih.gov/Blast.cgi) yielded a 100% match to various *B. afzelii* strains.

Figure. Scalp eschar of a woman in Austria who was found to be infected with *Borrelia afzelii*.

Conclusions

The most common skin manifestation of Lyme borreliosis is solitary erythema migrans (EM) (*10*); multiple EM, borrelial lymphocytoma, and acrodermatitis chronica atrophicans occur less frequently. Eschar formations are local necrotic skin alterations covered by a crust and occur at the site of a tick bite after infection with tickborne rickettsial species. Enlargement of local lymph nodes, skin rash, and malaise are additional symptoms that may be observed (*11*). Diagnosis for patients with EM is based on the clinical picture only; no laboratory support is needed in most cases. *Rickettsia* spp. can be easily identified by PCR, either from skin tissue obtained from the eschar or by taking a swab from the same site for PCR testing. Serologic tests may be helpful if PCR is not available. A 2-step increase of the antibody titer in consecutive samples in an immunofluorescence assay is needed for confirmation of infection. Treatment with doxycycline is effective for both diseases.

Ixodes ricinus ticks are capable of transmitting several pathogenic species of the *B. burgdorferi* s.l. complex; it is the most common tick species that feeds on humans in central Europe. *B. afzelii* has been recognized as the most frequent genotype associated with EM in Europe. In a study in Slovenia, 89% of *Borrelia* species detected from skin biopsies of EM patients were *B. afzelii* (*12*). Similarly, *B. afzelii* was the most prevalent *Borrelia* species found in ticks in Austria (*13*). In a recent study we showed that 56% of all *I. ricinus* ticks positive for *B. burgdorferi* sl harbored *B. afzelii* (*13*). The range of tick vectors of *Rickettsia* spp. is much more diverse; *Dermacentor reticulatus* and *D. marginatus* ticks are known to transmit *R. slovaca* and *R. raoultii* (*11*). We asked the patient to collect ticks from the area where she lives for identification of the tick species abundant there. The morphological examination of ticks collected from vegetation revealed only the presence of

I. ricinus ticks; thus, it is unlikely that a species of *Dermacentor* tick transmitted the infection.

Identification of *B. afzelii* from the eschar of our patient was unexpected. Ni et al. have shown that eschar formations can occur after borrelial infection in patients with concomitant EM (*14*); however, it is not known whether those patients were also infected with *Rickettsia* spp. A molecular identification of *B. burgdorferi* s.l. in a tick from a patient with SENLAT has been reported (*2*), and our case study provides clear evidence that the spirochete can be detected directly in the scalp eschar. Moreover, we are not aware of any other report of molecular identification of *B. afzelii* from a skin swab and superficial skin material. Inclusion of *B. burgdorferi* in the differential diagnosis of patients with SENLAT appears justified, particularly if testing for *Rickettsia* spp. is not successful.

About the Author

Dr. Markowicz is a medical specialist in general medicine and hygiene and microbiology at the Medical University of Vienna, Vienna, Austria. His primary research interests are Lyme borreliosis and other bacterial tickborne diseases. He is also an unpaid member of the Executive Committee of ESGBOR, the ESCMID Study Group on Lyme Borreliosis.

References

1. Angelakis E, Pulcini C, Waton J, Imbert P, Socolovschi C, Edouard S, et al. Scalp eschar and neck lymphadenopathy caused by *Bartonella henselae* after tick bite. Clin Infect Dis. 2010;50:549–51. https://doi.org/10.1086/650172
2. Dubourg G, Socolovschi C, Del Giudice P, Fournier PE, Raoult D. Scalp eschar and neck lymphadenopathy after tick bite: an emerging syndrome with multiple causes. Eur J Clin Microbiol Infect Dis. 2014;33:1449–56. https://doi.org/10.1007/s10096-014-2090-2
3. Leschnik M, Khanakah G, Duscher G, Wille-Piazzai W, Hörweg C, Joachim A, et al. Species, developmental stage and infection with microbial pathogens of engorged ticks removed from dogs and questing ticks. Med Vet Entomol. 2012;4:440–6. https://doi.org/10.1111/j.1365-2915.2012.01036.x
4. Wijnveld M, Schötta A-M, Pintér A, Stockinger H, Stanek G. Novel *Rickettsia raoultii* strain isolated and propagated from Austrian *Dermacentor reticulatus* ticks. Parasit Vectors. 2016;9:567. https://doi.org/10.1186/s13071-016-1858-x
5. Bell-Sakyi L. *Ehrlichia ruminantium* grows in cell lines from four ixodid tick genera. J Comp Pathol. 2004;130:285–93. https://doi.org/10.1016/j.jcpa.2003.12.002
6. Alberdi MP, Nijhof AM, Jongejan F, Bell-Sakyi L. Tick cell culture isolation and growth of *Rickettsia raoultii* from Dutch *Dermacentor reticulatus* ticks. Ticks Tick Borne Dis. 2012;3:349–54. https://doi.org/10.1016/j.ttbdis.2012.10.020
7. Tsao JI, Wootton JT, Bunikis J, Luna MG, Fish D, Barbour AG. An ecological approach to preventing human infection: vaccinating wild mouse reservoirs intervenes in the Lyme disease cycle. Proc Natl Acad Sci U S A. 2004;101:18159–64. https://doi.org/10.1073/pnas.0405763102
8. Postic D, Assous MV, Grimont PA, Baranton G. Diversity of *Borrelia burgdorferi* sensu lato evidenced by restriction fragment length polymorphism of rrf (5S)-rrl (23S) intergenic spacer amplicons. Int J Syst Bacteriol. 1994;44:743–52. https://doi.org/10.1099/00207713-44-4-743
9. Wilhelmsson P, Fryland L, Börjesson S, Nordgren J, Bergström S, Ernerudh J, et al. Prevalence and diversity of *Borrelia* species in ticks that have bitten humans in Sweden. J Clin Microbiol. 2010;48:4169–76. https://doi.org/10.1128/JCM.01061-10
10. Stanek G, Wormser GP, Gray J, Strle F. Lyme borreliosis. Lancet. 2012;379:461–73. https://doi.org/10.1016/S0140-6736(11)60103-7
11. Parola P, Paddock CD, Socolovschi C, Labruna MB, Mediannikov O, Kernif T, et al. Update on tick-borne rickettsioses around the world: a geographic approach. Clin Microbiol Rev. 2013;26:657–702. https://doi.org/10.1128/CMR.00032-13
12. Ruzić-Sabljić E, Maraspin V, Lotric-Furlan S, Jurca T, Logar M, Pikelj-Pecnik A, et al. Characterization of *Borrelia burgdorferi* sensu lato strains isolated from human material in Slovenia. Wien Klin Wochenschr. 2002;114:544–50.
13. Schötta AM, Wijnveld M, Stockinger H, Stanek G. Approaches for reverse line blot-based detection of microbial pathogens in *Ixodes ricinus* ticks collected in Austria and impact of the chosen method. Appl Environ Microbiol. 2017;83:e00489-17. https://doi.org/10.1128/AEM.00489-17
14. Ni X-B, Jia N, Jiang B-G, Sun T, Zheng Y-C, Huo Q-B, et al. Lyme borreliosis caused by diverse genospecies of *Borrelia burgdorferi* sensu lato in northeastern China. Clin Microbiol Infect. 2014;20:808–14. https://doi.org/10.1111/1469-0691.12532

Address for correspondence: Mateusz Markowicz, Institute for Hygiene and Applied Immunology, Center for Pathophysiology, Infectiology and Immunology, Medical University of Vienna, Kinderspitalgasse 15, 1090 Vienna, Austria; email: mateusz.markowicz@meduniwien.ac.at

Assessing 3 Outbreak Detection Algorithms in an Electronic Syndromic Surveillance System in a Resource-Limited Setting

Emily Alsentzer,[1] Sarah-Blythe Ballard,[1] Joan Neyra, Delphis M. Vera, Victor B. Osorio, Jose Quispe, David L. Blazes, Luis Loayza

We evaluated the performance of X-bar chart, exponentially weighted moving average, and C3 cumulative sums aberration detection algorithms for acute diarrheal disease syndromic surveillance at naval sites in Peru during 2007–2011. The 3 algorithms' detection sensitivity was 100%, specificity was 97%–99%, and positive predictive value was 27%–46%.

Syndromic surveillance uses prediagnostic health-related data to signal probable outbreaks warranting public health response (*1*). Alerta and Vigila are internet-based syndromic surveillance systems successively implemented by Peru's navy (*2*–*4*). Among other disease syndromes, individual cases of acute diarrheal disease (ADD) are self-reported to healthcare workers at sites providing care for service members, dependents, and civilian employees. We assessed the performance of 3 ADD aberration detection algorithms in this resource-limited setting: X-bar chart, exponentially weighted moving average (EWMA), and Early Aberration Reporting System (EARS) C3 cumulative sums (CUSUM) models (*5*–*9*).

The Study

We defined ADD as ≥3 loose stools within 24 hours lasting <14 days, epidemic threshold as the incidence of cases in excess of normal for a given period, outbreak as the detection of ADD incidence above the epidemic threshold, true outbreak as an outbreak identified by the system with confirmation by trained field personnel (e.g., enteropathogen isolation), and epidemiological silence as a period during which no cases were reported. We performed descriptive analysis of ADD cases by using data from all reporting sites during 2007–2011, then conducted subsequent analyses by using data on nonbloody ADD. We calculated ADD incidence from weekly reports from Alerta and Vigila during 2007–2011 for naval bases with population denominator data available. We compared the number of site-weeks during which ≥1 ADD case was reported on shore-based sites with those of sea-based sites and nonbloody ADD incidence in summer with incidence in nonsummer months by using a Mann-Whitney test.

Sites with <4 months of epidemiologic silence during 2007–2011 (60 months) were included for outbreak detection analysis. We aggregated nonbloody ADD case counts by epidemiologic week and performed a timeseries analysis by using X-bar chart, EWMA, and modified EARS C3 CUSUM aberration detection algorithms to flag potential outbreak weeks (*8*). Algorithm details are provided in the Appendix (https://wwwnc.cdc.gov/EID/article/26/9/19-1315-App1.pdf).

To account for seasonal variability, nonbloody ADD cases for each week during 2009–2011 (36 months) were compared with an 8-week sliding historical baseline calculated from the current and previous 2 years (*10*,*11*). We excluded signals from weeks with <5 cases to minimize false signals associated with epidemiologic silence. Because of

Author affiliations: Massachusetts Institute of Technology, Cambridge, Massachusetts, USA (E. Alsentzer); Uniformed Services University of the Health Sciences, Bethesda, Maryland, USA (E. Alsentzer, S.B. Ballard, D.L. Blazes); Johns Hopkins Bloomberg School of Public Health, Baltimore, Maryland, USA (S.-B. Ballard); Naval Medical Research Unit No. 6, Callao, Peru (S.B. Ballard, D.M. Vera, V.B. Osorio, J. Quispe); Marina de Guerra del Perú, Callao (L. Loayza)

DOI: https://doi.org/10.3201/eid2609.191315

[1]These first authors were co–principal investigators and contributed equally to this article.

ADD's <1-week incubation period, we did not consider buffer intervals, except when implementing the C3 CUSUM-like algorithm, which sums positive differences in cases from the mean for the past 3 periods. We optimized X-bar k, EWMA k and λ, and CUSUM k and h by exploring X-bar and EWMA k and CUSUM h values ranging from 2 to 6, CUSUM k values 1 to 3.5, and λ values 0.25 to 0.5, choosing parameters to maximize specificity and positive predictive value (PPV) while maintaining perfect sensitivity in predicting outbreaks at a randomly selected site (Policlínico Naval Ancón) (*7*). We calculated algorithm sensitivity, specificity, and PPV and compared each model's performance by using pairwise exact McNemar tests with Bonferroni correction, using data from 5 sites capable of confirming true outbreaks through epidemiologic links (517 site-weeks). We performed all analyses in R version 3.6.3 (https://cran.r-project.org/bin/windows/base/old/3.6.3); p values <0.05 were considered statistically significant.

During 2007–2011, a total of 144 sites reported 48,409 ADD cases, 98% of which were nonbloody. A total of 8,860 nonbloody cases were reported from 91 sites in 2007, 10,775 cases from 101 sites in 2008, 9,347 cases from 107 sites in 2009, 9,698 cases from 120 sites in 2010, and 8,588 cases from 118 sites in 2011. Of all these cases, 87% occurred in persons ≥5 years of age, 9% in children 1–4 years of age, and 4% in children <1 years of age. During 2007–2011, nonbloody ADD incidence peaked in 2008 at 305.2 cases/1,000 population (Figure 1). Seasonal incidence was higher during Peru's summer months (median 14.3 cases/1,000 population), January through March, compared with other months (median 12.5 cases/1,000 population; p = 0.0003).

The median proportion of weeks during which a site reported ≥1 ADD case was 19% (interquartile range [IQR] 5%–44%), and the median length of epidemiologic silence was 58 weeks (IQR 13–147 weeks). We observed no statistically significant difference in the proportion of weeks with ≥1 ADD case between sea-based and shore-based sites (p = 0.55).

We established the aberration detection algorithm by using 6,962 site-weeks of data from the 45 sites with <4 months of epidemiologic silence during 2007–2011 (Table). These reporting sites consisted of 15 ships and 30 land bases from 20 districts within 14 provinces. Site populations ranged from 35 to 10,000 (median 210, IQR 93.75–450). Algorithm parameter sensitivity analysis yielded optimal results when X-bar k = 4.5, EWMA k = 4 and λ = 0.25, and CUSUM k = 1.5 and h = 3 (Appendix Figures 1–3).

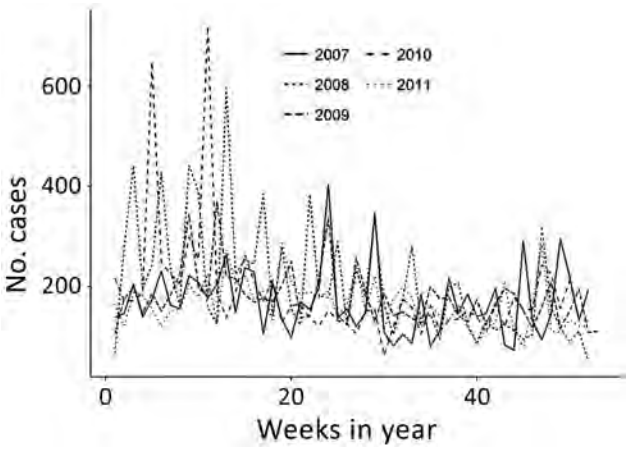

Figure 1. Epidemic curve for nonbloody acute diarrheal disease cases, by week, captured by the Alerta and Vigila Systems, Peru, 2007–2011.

We estimated algorithm sensitivity, specificity, and PPV by categorizing 785 weeks of data into positive and negative outbreak weeks and comparing each algorithm's outbreak predictions with data from the 5 sites capable of confirming true outbreaks during 2009–2011 (Figure 2). X-bar produced 13 signals, EWMA 13 signals, and CUSUM 20 signals. Six true outbreaks occurred (Table); all were detected by X-bar, EWMA, and CUSUM algorithms, corresponding to 100% sensitivity for each algorithm. Algorithm specificity across the 5 sites was 99.1% for X-bar, 99.1% for EWMA, and 98.2% for CUSUM. PPV was 46.2% for X-bar, 46.2% for EWMA, and 30% for CUSUM. X-bar and EWMA each produced 7 false-positives, and CUSUM produced 14 false-positives. The performance differences were not statistically significant.

Conclusions

X-bar, EWMA, and C3 CUSUM aberration detection algorithms identified all ADD outbreaks during 2009–2011, and approximately one third to one half of algorithm outbreak signals corresponded to true outbreaks. These findings suggest that these algorithms can usefully inform outbreak asset deployment, particularly in resource-limited settings.

Overall, X-bar and EWMA performed marginally better than CUSUM (PPV 46% vs. 30%). CUSUM frequently produced false-positives in the weeks after large outbreaks (e.g., after the 76-case outbreak at Policlínico Naval Ancón) (Table). X-bar's successful detection of ADD in the context of weekly reporting schedules and short disease incubation periods is consistent with its design, which favors detection of events lasting 1 epidemiologic period. In contrast,

Table. Nonbloody acute diarrheal disease case count and incidence, 2007–2011, and true outbreak detection data and algorithm performance, 2009–2011, for the 45 naval surveillance sites in Peru, analyzed by using X-bar chart, exponentially weighted moving average, and Early Aberration Reporting System C3 cumulative sums models*

Surveillance site	Total cases, 2007–2011	Average cases/week/1,000 population, 2007–2011	Date of true outbreak detection, case count, incidence, 2009–2011	Average outbreak detection algorithm performance, 2009–2011
BAP Aguirre	393	13.45	2009 Jan 24, 25 cases, 109/1,000 population	Sensitivity 100%, specificity 97.4%, PPV 20.0%
BAP Bolognesi	334	11.04	‡	‡
BAP Carvajal	581	14.56	‡	‡
BAP Eten	129	27.95	‡	‡
BAP Grau	887	9.04	‡	‡
BAP Mariátegui	490	16.64	‡	‡
BAP Montero	321	12.39	‡	‡
BAP Paita	185	†	‡	‡
BAP Palacios	1,118	27.16	‡	‡
BAP Pisagua	224	55.04		
BAP Pisco	283	†		
BAP Quiñones	289	9.17		
BAP Sánchez Carrión	156	39.90	‡	‡
BAP Velarde	114	36.54	2011 Sep 5, 12 cases, 250 cases/1,000 population	Sensitivity 100%, specificity 100%, PPV 100%
BAP Villavicencio	251	9.20	‡	‡
Base Aeronaval	991	4.19	‡	‡
Base Naval Chimbote	349	4.90	‡	‡
Base Naval Nanay	596	4.54	‡	‡
Base Naval San Juan	313	25.74	‡	‡
BCT Aguaytia	214	39.81	‡	‡
BCT Contamana	261	†		
BCT Huipoca	154	46.81	‡	‡
BCT San Alejandro	118	26.22	‡	‡
Capitanía Puerto Mollendo	171	19.52	‡	‡
Capitanía Puerto Puno	246	26.74	‡	‡
Centro Instrucción Técnica Naval	829	3.48	‡	‡
Clínica Naval de Iquitos	3,269	1.84	‡	‡
Comandancia Primera Zona Naval	244	21.02	‡	‡
Comandancia Tercera Zona Naval	625	21.48	2010 Aug 14, 31 cases, 207 cases/1,000 population	Sensitivity 100%, specificity 99.4%, PPV, 50.0%
Dirección de Capitanías y Guardacostas	293	5.77	‡	‡
Dirección de Hidrografía y Navegación	385	8.09	‡	‡
Escuela Naval	988	4.84	‡	‡
Estación Naval Isla San Lorenzo	449	24.34	‡	‡
Estación Naval Mollendo	343	6.42	‡	‡
Estación Naval Paita	796	8.93	‡	‡
Estación Naval Pucallpa	2,098	15.22	‡	‡
Estación Naval Submarinos	734	16.33	2010 Feb 8, 21 cases, 100 cases/1,000 population	Sensitivity 100%, specificity 99.1%, PPV 42.9%
Estación Naval de la Comandancia General	1,260	†	‡	‡
Hospital Base Naval del Callao	4,132	1.62	‡	‡
Policlínico Naval Ancón	2,019	5.24	2010 Feb 11, 33 cases 18 cases/1,000 population; 2010 Feb 20, 22 cases, 12 cases/1,000 population	Sensitivity 100%, specificity 98.1%, PPV 40.0%
Policlínico Naval San Borja	2,892	134.51	‡	‡
Posta Naval de Ventanilla	1,110	113.15	‡	‡
Villa Naval de Tumbes–El Salto	710	†	‡	‡

*BAP, Buque de la Armada Peruana (Peru Navy ship); BCT, Base Contraterrorist (Counter-terrorist base); PPV, positive predictive value.
†No denominator data available.
‡True outbreak data not available because of lack of on-site capability to establish epidemiologic link.

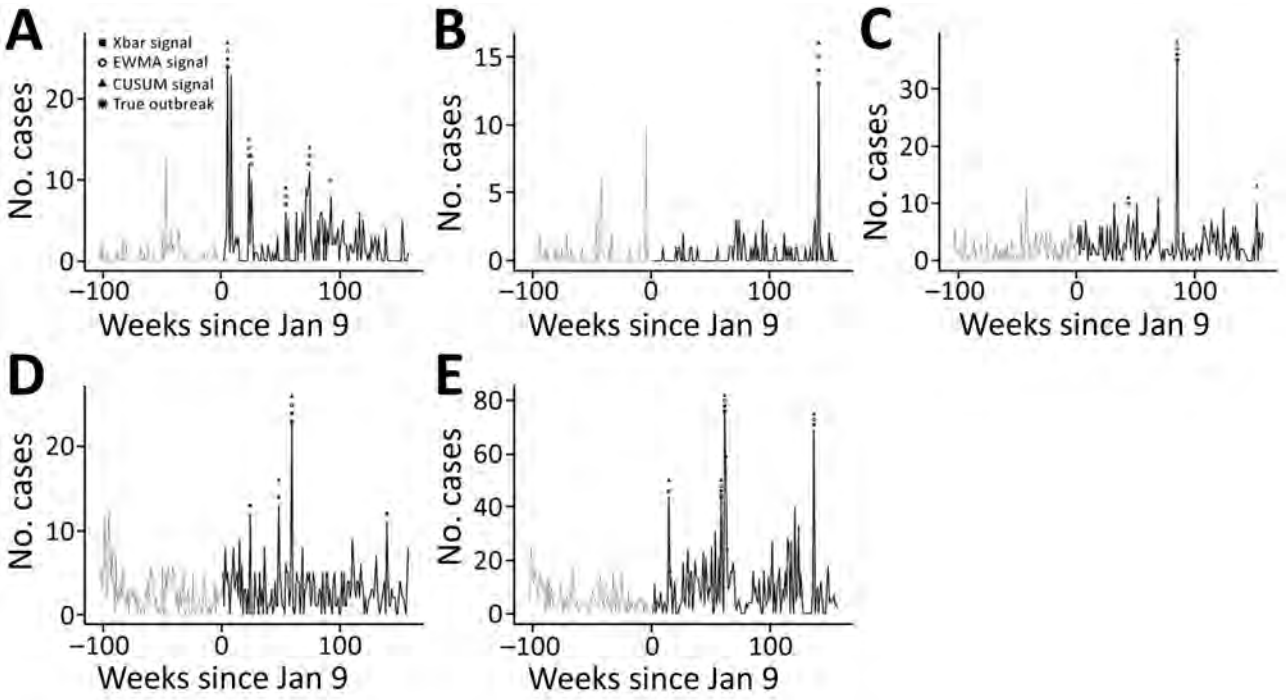

Figure 2. Epidemic curves for nonbloody acute diarrheal disease over time, demonstrating outbreaks identified by the Alerta and Vigila Systems, by identifying algorithm and surveillance site, Peru, 2009-2011. A) Buque de la Armada Peruana Aguirre; B) BAP Velarde; C) Comandancia Tercera Zona Naval; D) Estación Naval Submarinos; and E) Policlínico Naval Ancón. Shapes correspond with identifying algorithms; asterisks indicate outbreaks confirmed through epidemiologic links (i.e., true positives). CUSUM, C3 cumulative sums; EWMA, exponentially weighted moving average.

EWMA and CUSUM were designed for earlier detection of consecutive small baseline deviations (*12*). Whereas EWMA can be tuned to favor shorter outbreaks through its weighting parameter (λ), the C3 CUSUM algorithm is more rigid. In the context of weekly ADD reporting, EWMA and CUSUM algorithm performance might improve by counting consecutive weeks with outbreak signals as a single alert.

Our study has limitations, including the number of sites capable of confirming outbreaks, which reduced the statistical power to detect differences between algorithms, and the inability to distinguish a lack of reporting versus a lack of ADD cases to report during periods of epidemiologic silence. Combined, these factors limited the evaluation to 3,925 site-weeks of observation, reducing the reliability of algorithm parameter estimates. Furthermore, model parameters were established on only 1 of the 5 evaluation sites; a larger development set would better optimize model parameters while avoiding overfitting.

Characterizing algorithm parameter tradeoffs might aid system capability alignment with health priorities. Lower detection thresholds are advantageous for high-risk diseases with distinct syndromes, such as cholera, Ebola, and Middle East respiratory syndrome. Conversely, changing parameters, such as changing EWMA's weighting parameter (λ), can affect algorithm PPV (increasing to >60% during sensitivity analysis). Context-focused exploration could inform which parameters should be tuned to improve PPV, sensitivity, or specificity. Because smaller populations and stable disease baselines improve algorithm performance, tuning algorithm parameters for specific sites during implementation by using historical data might improve overall system performance, as might periodic evaluation of model assumptions, parameter tuning, and model performance.

The views expressed in this article are those of the authors and do not necessarily reflect the official policy or position of the Department of the Navy, Department of Defense, nor the governments of the United States or Peru.

About the Author

Ms. Alsentzer is a PhD student in the Harvard–MIT Program in Health Science and Technology. Her background is in computer science and biomedical informatics, and her research focuses on machine learning applications to healthcare. Dr. Ballard is a medical epidemiologist in the Epidemic Intelligence Service at the Centers for Disease Control and Prevention. Her background is in tropical diseases, surveillance, and global public health.

References

1. Henning KJ. Overview of syndromic surveillance: what is syndromic surveillance? MMWR Morb Mortal Wkly Rep. 2004;53(Suppl):5–11.
2. Margevicius KJ, Generous N, Abeyta E, Althouse B, Burkom H, Castro L, et al. The Biosurveillance Analytics Resource Directory (BARD): facilitating the use of epidemiological models for infectious disease surveillance. PLoS One. 2016; 11:e0146600. https://doi.org/10.1371/journal.pone.0146600
3. Blazes DL, Lewis SH. Disease surveillance: technological contributions to global health security. Boca Raton (Florida): CRC Press; 2016. p. 120–1.
4. Soto G, Araujo-Castillo RV, Neyra J, Fernandez M, Leturia C, Mundaca CC, et al. Challenges in the implementation of an electronic surveillance system in a resource-limited setting: Alerta, in Peru. BMC Proc. 2008; 2(Suppl 3):S4. https://doi.org/10.1186/1753-6561-2-s3-s4
5. Burkom H. Development, adaptation, and assessment of alerting algorithms for biosurveillance. Johns Hopkins APL Tech Dig. 2003;24:335–42 [cited 2020 Apr 4]. https://www.jhuapl.edu/content/techdigest/pdf/v24-n04/24-04-burkom.pdf
6. Hutwagner L, Thompson W, Seeman GM, Treadwell T. The bioterrorism preparedness and response Early Aberration Reporting System (EARS). J Urban Health. 2003;80(Suppl 1):i89–i96.
7. Fricker RD Jr, Hegler BL, Dunfee DA. Comparing syndromic surveillance detection methods: EARS' versus a CUSUM-based methodology. Stat Med. 2008;27:3407–29. https://doi.org/10.1002/sim.3197
8. Fricker R. Introduction to statistical methods for biosurveillance: with an emphasis on syndromic surveillance. Cambridge: Cambridge University Press; 2013. p. 178–215.
9. Hutwagner LC, Thompson WW, Seeman GM, Treadwell T. A simulation model for assessing aberration detection methods used in public health surveillance for systems with limited baselines. Stat Med. 2005;24:543–50. https://doi.org/10.1002/sim.2034
10. Murphy SP, Burkom H. Recombinant temporal aberration detection algorithms for enhanced biosurveillance. J Am Med Inform Assoc. 2008;15:77–86. https://doi.org/10.1197/jamia.M2587
11. Mathes RW, Lall R, Levin-Rector A, Sell J, Paladini M, Konty KJ, et al. Evaluating and implementing temporal, spatial, and spatio-temporal methods for outbreak detection in a local syndromic surveillance system. PLoS One. 2017;12:e0184419. https://doi.org/10.1371/journal.pone.0184419
12. Lombardo J. Disease surveillance: a public health approach. Hoboken (NJ): John Wiley & Sons, Inc.; 2007. p. 158.

Address for correspondence: Sarah-Blythe Ballard, Centers for Disease Control and Prevention, 1600 Clifton Rd NE, Mailstop H24-3, Atlanta, GA 30029-4027, USA; email: sballar3@jhu.edu

Human *Borrelia miyamotoi* Infection, Austria

Selma Tobudic, Heinz Burgmann, Gerold Stanek, Stefan Winkler, Anna-Margarita Schötta, Markus Obermüller, Mateusz Markowicz, Heimo Lagler

We report a human case of *Borrelia miyamotoi* infection diagnosed in Austria. Spirochetes were detected in Giemsa-stained blood smears. The presence of *B. miyamotoi* in the patient's blood was confirmed by PCR, and phylogenetic analysis identified an infection with a strain from Europe.

Borrelia miyamotoi is a relapsing fever spirochete transmitted by the same genus of ticks that transmits *B. burgdorferi* sensu lato (s.l.), *Anaplasma phagocytophilum*, *Babesia* species, and tickborne flaviviruses (*1*–*3*). *B. miyamotoi* has been documented in ticks from the United States and in numerous countries in Europe (including Russia), as well as in Japan (*1*,*4*–*6*). *B. miyamotoi* also has been found in *Ixodes scapularis* ticks in the northeastern and north-central United States and adjoining areas of Canada, in *I. pacificus* ticks in the far western United States and British Columbia, in *I. ricinus* ticks in Europe, and in *I. persulcatus* ticks in Europe and Asia (*1*,*7*,*8*). *I. pavlovskyi* and *I. ovatus* ticks in northern Asia are 2 other species that have been shown to carry *B. miyamotoi* (*9*). Endemic areas of *B. miyamotoi* in *Ixodes* ticks overlap with those of *B. burgdorferi* s.l. but with 10-fold lower prevalence (*4*). Co-infection of *Ixodes* ticks with both spirochetes also has been identified (*9*).

Unlike Lyme borreliosis, patients with *B. miyamotoi* disease typically do not have skin lesions but instead have a nonspecific febrile illness, potentially associated with leukopenia, thrombocytopenia, and elevated liver function parameters (*10*). Highly immunocompromised patients might have chronic meningitis (*2*). Untreated patients with *B. miyamotoi* disease might experience a limited number of recurrent episodes of fever, similar to other relapsing fevers caused by *Borrelia* infections (*6*). The same antibiotic regimens used to treat Lyme borreliosis (e.g., 10-14-day courses of oral doxycycline or amoxicillin) are effective for *B. miyamotoi* disease. Parenteral therapy with ceftriaxone would be preferred for patients with meningitis (*3*).

Diagnosis of *B. miyamotoi* disease should be considered in any patient who has fever attacks and resides in or has spent time during tick season in a region where Lyme borreliosis is endemic. Diagnosis requires confirmation using PCR. If the density of spirochetes in the blood is $\geq 10^4$/mL, spirochetes might be identified by examining several high-power fields of the blood smear or centifuged sample of cerebrospinal fluid stained with Giemsa or Wright stain (*10*). Several PCR assays can detect *B. miyamotoi* in whole blood, plasma, and cerebrospinal fluid by using primers specific for 16S ribosomal RNA and for the *flaB* and *glpQ* genes (*2*,*3*,*8*). Serologic testing based on glycerophosphodiester phosphodiesterase antigen of *B. miyamotoi* that is not found in *B. burgdorferi* s.l. is highly sensitive but only on convalescent-phase serum specimens (*11*).

The Case-Patient

A 51-year-old woman who had a long medical history of seropositive rheumatoid arthritis treated with rituximab sought care at our outpatient clinic for relapsing fever that started 3 months before. Fever episodes occurred every 5 days, and duration ranged from 2 to 3 days. Four weeks before the onset of symptoms, the patient had returned from a 3-week trip through the United States, where, as a tourist, she visited the East and West Coasts and stayed in several national parks. She reported several insect bites and 1 tick bite without erythema migrans that occurred while she was in the United States but did not notice any tick bites before or after her travel. After her return, the patient did not travel abroad again but spent her time in her home in lower Austria.

Author affiliations: Division of Infectious Diseases and Tropical Medicine, Medical University of Vienna, Vienna, Austria (S. Tobudic, H. Burgmann, S. Winkler, M. Obermüller, H. Lagler); Institute for Hygiene and Applied Immunology, Center for Pathophysiology, Infectiology and Immunology, Medical University of Vienna, Vienna (G. Stanek, A.-M. Schötta, M. Markowicz)

DOI: https://doi.org/10.3201/eid2609.191501

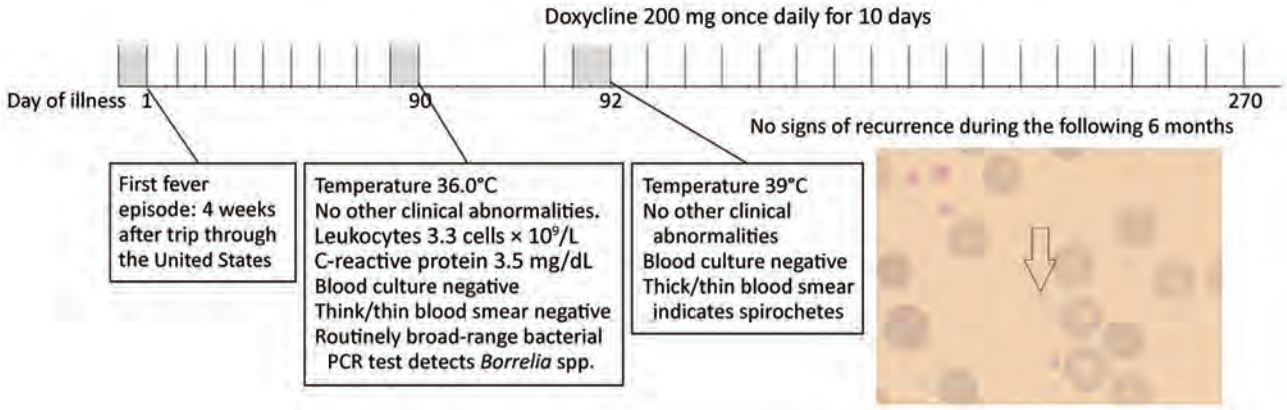

Figure 1. Timeline of the course of symptoms and treatment, including laboratory test results, for a patient with *Borrelia miyamotoi* infection (including Giemsa stain of thin blood smear on day 92), Austria. Arrows indicate spirochetes. Original magnification × 100.

Figure 2. Phylogenetic tree based on the 16S rRNA gene of *Borrelia miyamotoi* from a patient in Austria (Bm4667; arrow) and reference sequences. This phylogenetic tree was constructed by using the maximum-likelihood method based on the general time reversible model. The tree is drawn to scale, with bootstrap values shown at the nodes of the tree, inferred from 600 replicates. A total of 1,199 bp of *B. miyamotoi* 16S rRNA gene sequences was used in the final dataset, which involved 34 nt sequences and in which gaps and missing data were deleted. Evolutionary analyses were conducted in MEGA7 (https://www.megasoftware.net). The patient isolate clustered together with strains found in ticks from Europe. Information of the source and country for reference isolates is shown in parentheses after strain designation. Scale bar indicates substitutions per site.

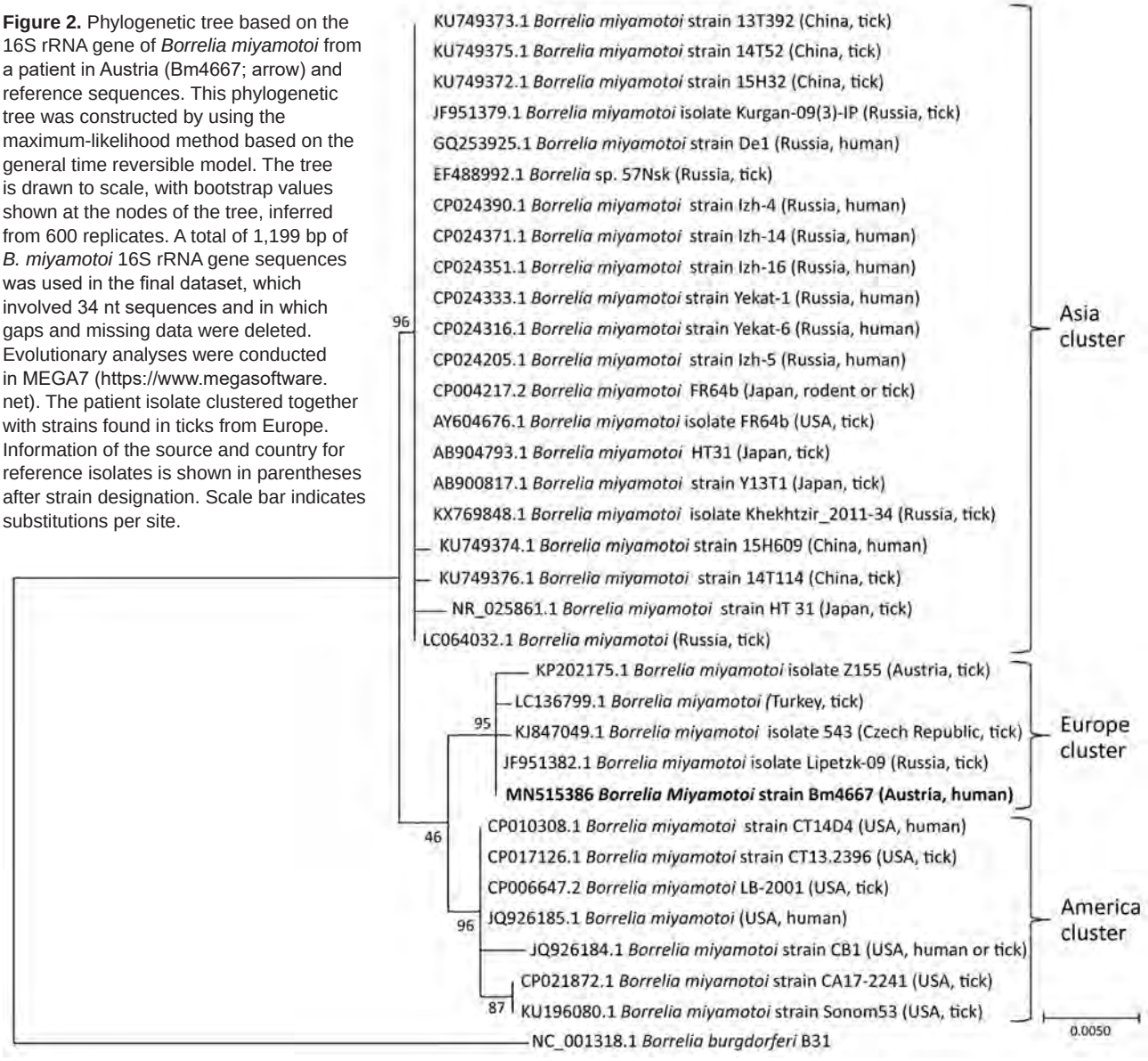

No abnormal findings were observed on physical examination; in particular, no apparent rash on the skin was noted. Routine laboratory tests performed were normal (including kidney and liver function tests), except for the evidence of leukopenia with 3.3 × 10^9 cells/L (reference range 4–10 × 10^9 cells/L) and slightly elevated C-reactive protein of 3.5 mg/dL (reference range <0.5 mg/dL). Multiple blood and urine cultures were negative (Figure 1). An initial peripheral Giemsa-stained blood smear was performed during an afebrile period without any result, but when the test was repeated during the next fever episode, spirochetes were detected between blood cells (Figure 1). Detection of spirochetes in blood smear, which is not typical in cases of *B. miyamotoi* infection, could be attributable to prolonged spirochetemia likely associated with rituximab therapy. *Borrelia* spp. was identified in a routinely broad-range bacterial 16S gene-based PCR test (SepsiTest-UMD; Molzym GmbH & Co. KG, https://www.molzym.com). DNA was extracted from EDTA blood, and a real-time PCR assay specific for *B. miyamotoi* targeting the *glpQ* gene (*5*) was positive. To confirm the genospecies present in the patient's blood, further PCRs targeting the 16S–23S internal transcribed spacer region (*12*,*13*), 16S rRNA, and *glpQ* gene (*14*,*15*) were performed, and amplicons were sent to a laboratory for bidirectional sequencing (Microsynth, Vienna, Austria). All PCRs confirmed the presence of *B. miyamotoi* in the patient's blood, and all yielded 100% identity to various *B. miyamotoi* strains in the GenBank database. Using MEGA7 (https://www.megasoftware.net), we constructed a phylogenetic tree for our isolate Bm4667 on the basis of the obtained 16S rRNA gene sequence (Figure 2). All 3 sequences obtained during this investigation were submitted to GenBank (accession no. MN515386 for the 16S rRNA gene, MT396940 for the *glpQ* gene, and MT396941 for the 16S–23S internal transcribed spacer region).

The patient was treated with 200 mg doxycycline once daily for 2 weeks. On the first day of antibiotic administration, the patient was admitted to our hospital for observation in case of potential Jarisch–Herxheimer reaction. However, during the therapy, no reaction or adverse effects were detected. The patient recovered successfully, and no signs of recurrence were observed in the following 6 months.

Conclusions

We describe a human case of *B. miyamotoi* infection diagnosed in Austria. Although the patient's report of a tick bite in the United States suggested that this infection was an imported case, the phylogenetic analysis of the *B. miyamotoi* strain clearly indicates an infection with a strain from Europe (and possibly Austria). Clinicians should be aware of the possibility of these infections.

Acknowledgment

We thank the patient for providing consent to publish information about her case.

About the Author

Dr. Tobudic is an internal medicine specialist at the Department of Infection Diseases and Tropical Medicine, Medical University of Vienna. Her research interest includes yeast infections, biofilm research, pathomechanism of antimicrobial resistance, and research of tickborne illness.

References

1. Fukunaga M, Takahashi Y, Tsuruta Y, Matsushita O, Ralph D, McClelland M, et al. Genetic and phenotypic analysis of *Borrelia miyamotoi* sp. nov., isolated from the ixodid tick *Ixodes persulcatus*, the vector for Lyme disease in Japan. Int J Syst Bacteriol. 1995;45:804–10. https://doi.org/10.1099/00207713-45-4-804
2. Gugliotta JL, Goethert HK, Berardi VP, Telford SR III. Meningoencephalitis from *Borrelia miyamotoi* in an immunocompromised patient. N Engl J Med. 2013;368:240–5. https://doi.org/10.1056/NEJMoa1209039
3. Hovius JW, de Wever B, Sohne M, Brouwer MC, Coumou J, Wagemakers A, et al. A case of meningoencephalitis by the relapsing fever spirochaete *Borrelia miyamotoi* in Europe. Lancet. 2013;382:658. https://doi.org/10.1016/S0140-6736(13)61644-X
4. Crowder CD, Carolan HE, Rounds MA, Honig V, Mothes B, Haag H, et al. Prevalence of *Borrelia miyamotoi* in *Ixodes ticks* in Europe and the United States. Emerg Infect Dis. 2014;20:1678–82. https://doi.org/10.3201/eid2010.131583
5. Reiter M, Schötta AM, Müller A, Stockinger H, Stanek G. A newly established real-time PCR for detection of *Borrelia miyamotoi* in *Ixodes ricinus* ticks. Ticks Tick Borne Dis. 2015;6:303–8. https://doi.org/10.1016/j.ttbdis.2015.02.002
6. Platonov AE, Karan LS, Kolyasnikova NM, Makhneva NA, Toporkova MG, Maleev VV, et al. Humans infected with relapsing fever spirochete *Borrelia miyamotoi*, Russia. Emerg Infect Dis. 2011;17:1816–23. https://doi.org/10.3201/eid1710.101474
7. Scoles GA, Papero M, Beati L, Fish D. A relapsing fever group spirochete transmitted by *Ixodes scapularis* ticks. Vector Borne Zoonotic Dis. 2001;1:21–34. https://doi.org/10.1089/153036601750137624
8. Richter D, Schlee DB, Matuschka FR. Relapsing fever-like spirochetes infecting European vector tick of Lyme disease agent. Emerg Infect Dis. 2003;9:697–701. https://doi.org/10.3201/eid0906.020459
9. Takano A, Toyomane K, Konnai S, Ohashi K, Nakao M, Ito T, et al. Tick surveillance for relapsing fever spirochete *Borrelia miyamotoi* in Hokkaido, Japan. PLoS One. 2014;9:e104532. https://doi.org/10.1371/journal.pone.0104532
10. Krause PJ, Fish D, Narasimhan S, Barbour AG. *Borrelia miyamotoi* infection in nature and in humans. Clin Microbiol Infect. 2015;21:631–9. https://doi.org/10.1016/j.cmi.2015.02.006

11. Schwan TG, Schrumpf ME, Hinnebusch BJ, Anderson DE Jr, Konkel ME. GlpQ: an antigen for serological discrimination between relapsing fever and Lyme borreliosis. J Clin Microbiol. 1996;34:2483–92. https://doi.org/10.1128/JCM.34.10.2483-2492.1996
12. Bunikis J, Garpmo U, Tsao J, Berglund J, Fish D, Barbour AG.Sequence typing reveals extensive strain diversity of the Lyme borreliosis agents *Borrelia burgdorferi* in North America and *Borrelia afzelii* in Europe. Microbiology. 2004;150:1741–55. https://doi.org/10.1099/mic.0.26944-0
13. Wilhelmsson P, Fryland L, Börjesson S, Nordgren J, Bergström S, Ernerudh J, et al. Prevalence and diversity of *Borrelia species* in ticks that have bitten humans in Sweden. J Clin Microbiol. 2010;48:4169–76. https://doi.org/10.1128/JCM.01061-10
14. Fomenko NV, Livanova NN, Borgoiakov VI, Kozlova IV, Shulaĭkina IV, Pukhovskaia NM, et al. Detection of Borrelia miyamotoi in ticks Ixodes persulcatus from Russia [in Russian]. Parazitologiia. 2010;44:201–11.
15. Fukunaga M, Hamase A, Okada K, Inoue H, Tsuruta Y, Miyamoto K, et al. Characterization of spirochetes isolated from ticks (*Ixodes tanuki*, *Ixodes turdus*, and *Ixodes columnae*) and comparison of the sequences with those of *Borrelia burgdorferi* sensu lato strains. Appl Environ Microbiol. 1996;62:2338–44. https://doi.org/10.1128/AEM.62.7.2338-2344.1996

Address for correspondence: Selma Tobudic, Department of Internal Medicine I, Division of Infectious Diseases and Tropical Medicine, Währinger Gürtel 18-20, A-1090 Vienna, Austria; email: selma.tobudic@meduniwien.ac.at

Role of Wildlife in Emergence of Ebola Virus in Kaigbono (Likati), Democratic Republic of the Congo, 2017

Sophie Gryseels,[1] Placide Mbala-Kingebeni,[1] Innocent Akonda, Roger Angoyo, Ahidjo Ayouba, Pascal Baelo, Daniel Bamuleka Mukadi, Elie Bugentho, Trenton Bushmaker, Christelle Butel, Sébastien Calvignac-Spencer, Eric Delaporte, Birgit De Smet, Ariane Düx, François Edidi-Atani, Robert Fischer, Corneille Kahandi, Jimmy Kapetshi, Servet Kimbonza Sumba, Léonce Kouadio, André Malekani Bendeke, Claude Mande, Guy Midingi Sepolo, Joseph Moudindo, Eitel Mpoudi Ngole, Prescott Musaba, Patrick Mutombo, Innocent Ndong Bass, Casimir Nebesse, Steve Ngoy, Simon-Pierre Ndimbo Kumogo, Stephanie N. Seifert, Jacques Tanzito, Dudu Akaibe, Nicaise Amundala, Kevin K. Ariën, Guy-Crispin Gembu, Fabian H. Leendertz, Herwig Leirs, Jean-Claude Mukinzi, Vincent Munster, Jean-Jacques Muyembe-Tamfum, Martine Peeters, Erik Verheyen, Steve Ahuka-Mundeke

Author affiliations: University of Arizona, Tucson, Arizona, USA (S. Gryseels); KU Leuven, Leuven, Belgium (S. Gryseels); University of Antwerp, Antwerp, Belgium (S. Gryseels, H. Leirs, E. Verheyen); Université de Montpellier, Montpellier, France (P. Mbala-Kingebeni, A. Ayouba, C. Butel, E. Delaporte, J. Moudindo, E. Mpoudi Ngole, I. Ndong Bass, M. Peeters); Institut National de Recherche Biomédicale, Kinshasa, Democratic Republic of the Congo (P. Mbala-Kingebeni, F. Edidi-Atani, J. Kapetshi, S. Kimbonza Sumba, G. Midingi Sepolo, D. Bamuleka Mukadi, S.P. Ndimbo Kumogo, J.J. Muyembe-Tamfum, S. Ahuka-Mundeke); Division Provinciale de la Sante, Buta (Bas-Uele), Democratic Republic of the Congo (I. Akonda); Programme National de Lutte Contre le Sida, Buta (I. Akonda); Centre de Surveillance de la Biodiversité, Kisangani, Democratice Republic of the Congo (R. Angoyo, P. Baelo, E. Bugentho, C. Kahandi, A. Malekani Bendeke, C. Mande, P. Musaba, P. Mutombo, C. Nebesse, S. Ngoy, J. Tanzito, D. Akaibe, N. Amundala, G.C. Gembu, J.C. Mukinzi); National Institutes of Health, Hamilton, Montana, USA (T. Bushmaker, R. Fischer, S.N. Seifert, V. Munster); Robert Koch Institute, Berlin, Germany (S. Calvignac-Spencer, A. Düx, L. Kouadio, D. Bamuleka Mukadi, F.H. Leendertz); Institute of Tropical Medicine, Antwerp (B. De Smet, K.K. Ariën); Laboratoire Central de la Pathologie Animale, Bingerville, Côte d'Ivoire (L. Kouadio); University of Kisangani, Kisangani (C. Mande, P. Musaba, C. Nebesse, D. Akaibe, N. Amundala, G.C. Gembu, J.C. Mukinzi); Centre de Recherches sur les Maladies Émergentes, Re-émergentes et la Médecine Nucléaire, Yaoundé, Cameroon (J. Moudindo, E. Mpoudi Ngole, I. Ndong Bass); Royal Belgian Institute of Natural Sciences, Brussels, Belgium (E. Verheyen)

DOI: https://doi.org/10.3201/eid2609.191552

After the 2017 Ebola virus (EBOV) outbreak in Likati, a district in northern Democratic Republic of the Congo, we sampled small mammals from the location where the primary case-patient presumably acquired the infection. None tested positive for EBOV RNA or antibodies against EBOV, highlighting the ongoing challenge in detecting animal reservoirs for EBOV.

The animal reservoir(s) for Ebola virus (EBOV) remain unclear. Although substantial evidence suggests several bat species can host EBOV and other filoviruses (*1*–*8*), it cannot be ruled out that other, less frequently surveyed mammal groups could also host these viruses or play a role in their ecology (*9*). An EBOV outbreak in humans implies that EBOV had been circulating among wildlife where the primary case-patient contracted the infection. If the primary case-patient and his or her activities before becoming ill are known, this information provides an opportunity for EBOV wildlife surveillance closely focused in space and season.

In late March 2017, signs and symptoms of hemorrhagic fever developed in an inhabitant of Kaigbono, a village in Likati district in northern Democratic Republic of the Congo (Figure 1, panel A) (*10*). In subsequent weeks, 2 probable and 5 confirmed cases of Ebola virus disease followed in nearby villages (Figure 1, panel B) (*10*,*11*). The World Health Organization officially declared this outbreak over on July 2, 2017. Our team

[1]These authors contributed equally to this article.

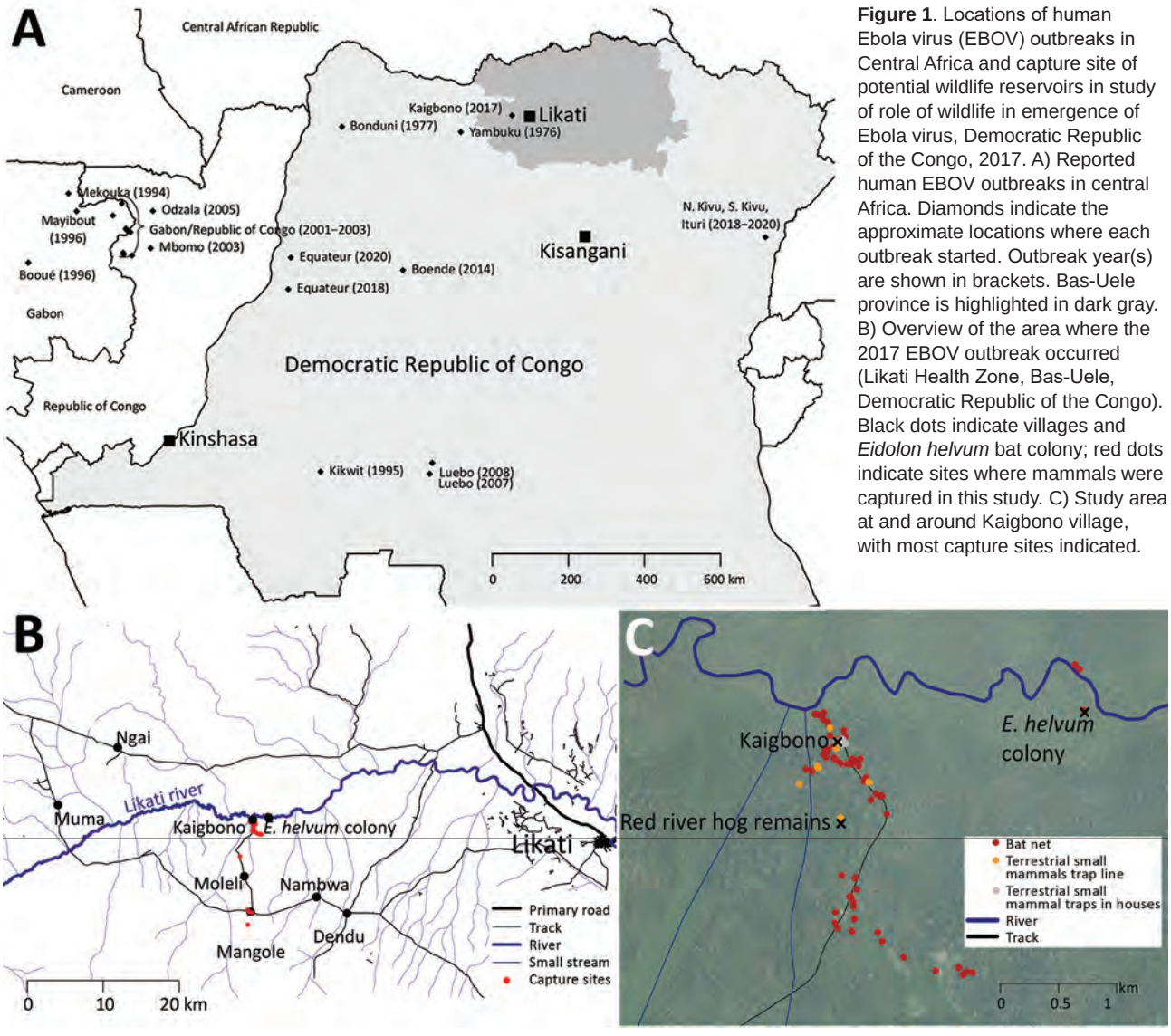

Figure 1. Locations of human Ebola virus (EBOV) outbreaks in Central Africa and capture site of potential wildlife reservoirs in study of role of wildlife in emergence of Ebola virus, Democratic Republic of the Congo, 2017. A) Reported human EBOV outbreaks in central Africa. Diamonds indicate the approximate locations where each outbreak started. Outbreak year(s) are shown in brackets. Bas-Uele province is highlighted in dark gray. B) Overview of the area where the 2017 EBOV outbreak occurred (Likati Health Zone, Bas-Uele, Democratic Republic of the Congo). Black dots indicate villages and *Eidolon helvum* bat colony; red dots indicate sites where mammals were captured in this study. C) Study area at and around Kaigbono village, with most capture sites indicated.

arrived in Kaigbono on July 5, 2017, to investigate potential EBOV circulation among local wildlife.

The Study

The primary case-patient spent the weeks preceding his illness in and around his home village of Kaigbono, a settlement of <50 inhabitants near the Likati River (Figure 1). The village is accessible only via the Likati River or narrow forest paths. The primary case-patient often collected fish from fishermen along the river and transported it to the village.

This primary case-patient ate cooked meat from a red river hog (*Potamochoerus porcus*) ≈13 days before symptom onset. Other persons had found the dead hog in the forest ≈700 m from the village. Up to 4 Kaigbono villagers (none of whom became ill) collected the meat around the upward shoulder area of the hog, reportedly leaving the rest of the carcass because the meat touching the ground and the internal organs had already decomposed. Two of these persons prepared and cooked the meat, which subsequently was shared by ≈10–20 persons in Kaigbono, including the primary case-patient (the only person in whom febrile illness developed). On July 10 we retrieved a skull of a red river hog at the site described as the location where the abovementioned hog was found (Figure 1, panel C). Another potential zoonotic exposure occurred ≈7 days before symptom onset in the primary case-patient when he brought home a large bat. Other persons had hunted and killed the bat, probably at the site of a large seasonal colony of straw-colored fruit bats at the Likati River (*Eidolon helvum*; Figure 1, panels B, C). Villagers

reported that the colony arrives annually in March and leaves in July; we observed that most of the *E. helvum* bats left the site during July 16–19. Given the colony's large size (at least several thousand), most bats hunted during this season probably belong to *E. helvum*. However, we observed that *Hypsignathus monstrosus* and *Epomops franqueti*, other bat species in which EBOV RNA has been documented (*3*), also might have been occasionally hunted. The primary case-patient's wife prepared (removed its internal organs) and grilled the bat. Only the primary case-patient ate the bat. His wife did not report a fever.

From July 6, 2017 through August 18, 2017, we trapped 476 small mammals (rodents, shrews, and bats) and acquired samples from 11 mammals hunted by local inhabitants. None of the animals showed signs of illness. Of these animals, we euthanized and collected organ samples (preserved in RNALater) of 388 (when possible, we also collected dried blood spots and oral, urogenital, and/or rectal swab specimens from these animals); collected only dried blood spots and oral, urogenital, and/or rectal swab specimens of 79; and did not sample 20. We collected bat fecal samples from plastic sheets fixed to trees underneath the *E. helvum* bat colony (Figure 1, panels B, C). We also swabbed the exterior of the skull of the abovementioned red river hog and extracted its molars.

We extracted RNA from ≥1 organ, blood, and/or fecal samples of 419 of the 467 sampled animals and from samples swabbed from the skull and the molar pulp remains of the red river hog. We performed multiplex quantitative reverse transcription PCR (qRT-PCR) targeting EBOV and Sudan virus L gene, as previously described (*12*). We further tested RNA extract from 91 fecal samples and 1 urine sample collected at the *E. helvum* bat colony, although 47 of these samples showed signs of PCR inhibition. None of the samples of the total of 465 individual animals or environmental feces were qRT-PCR positive (Figure 2; Appendix Table, https://wwwnc.cdc.gov/EID/article/26/9/19-1552-App1.pdf).

We used a 10-antigen Luminex assay (Luminex Corporation, https://www.luminexcorp.com) to test dried blood spots of 272 animals and 92 fecal samples for antibodies against EBOV, as previously described (*2*,*13*). None of these samples could be considered positive for antibodies against EBOV (Appendix Figure).

Cytochrome b, 16S, or 12S gene PCR was attempted and Sanger sequenced on a subset (n = 334) of specimens for host species confirmation. We deposited sequences in GenBank under accession nos. MN597466–MN597893.

We distinguished 47 different mammal species (4 could not be assigned to a known species catalogued in GenBank) from 34 different genera across 359 specimens. For 268 of these, genetic information was necessary to identify the species, as species identification was not possible or not done correctly in the field (Appendix Table). Most species had low sample sizes with little power to detect low virus prevalences (Figure 2; Appendix). For an additional 67 nongenotyped animals, the genus could be unambiguously determined based on field morphology. We did not determine a genus or species for 62 animals.

Conclusions

Before his illness, the primary case-patient of the 2017 EBOV outbreak in Likati had eaten prepared meat from a red river hog and a fruit bat, probably *E. helvum*. He had contact with the uncooked carcass of the bat but not of the hog. The meat of the bat and the hog were prepared by others who had not fallen ill but whose serologic status is unknown. The hog had been dead for several days before butchering and cooking, causing us to question the infectiousness of any virus present in the meat. The susceptibility of

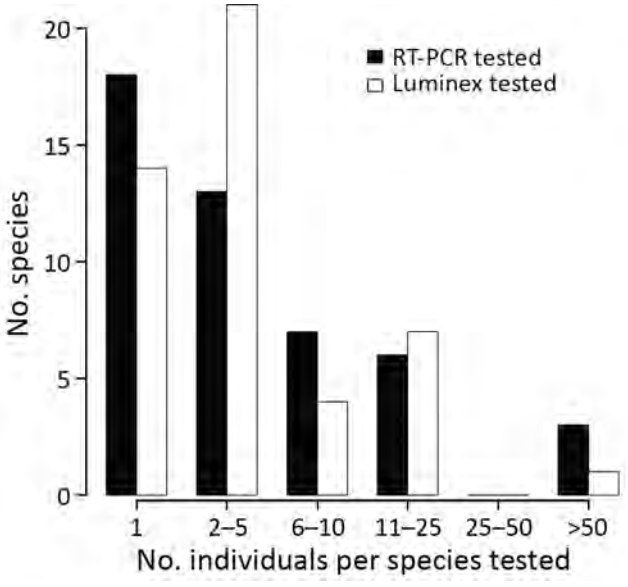

Figure 2. Abundance distribution of mammal species tested for Ebola virus and Sudan virus RNA using quantitative RT-PCR and for antibodies against ebolaviruses using the Luminex assay (Luminex Corporation, https://www.luminexcorp.com), for the set of specimens sampled in and around Kaigbono (Likati Health Zone, the Democratic Republic of the Congo) in 2017 that were determined to the species level. Each successfully tested environmental fecal sample is assumed to represent a single *Eidolon helvum* bat specimen (full descriptions available in Appendix Table, https://wwwnc.cdc.gov/EID/article/26/9/19-1552-App1.pdf). RT-PCR, reverse transcription PCR.

the bat species *E. helvum* to EBOV is also questionable because experimental data suggests EBOV could be refractory in *E. helvum* cells (*14*). Thus, we can neither exclude nor confirm which or if either of these animals sparked the Likati 2017 EBOV outbreak.

We started collecting wildlife specimens ≈3 months after the onset of the human outbreak, a time lag potentially important to local natural transmission dynamics yet still within similar seasonal conditions. We ceased sampling 6 weeks later when seasonal changes occurred (e.g., emigration of the *E. helvum* bat colony). Despite this directed sampling, we did not find evidence for EBOV RNA (n = 465 animals tested) or antibodies against EBOV (n = 364) in any wildlife specimen. Because we used a qRT-PCR specific to EBOV and Sudan virus, we cannot exclude the presence of RNA of other filoviruses in the samples. However, the Luminex assay would have revealed any antibodies against related filoviruses.

As noted in previous surveillance studies following an EBOV outbreak (*15;* reference *1* in Appendix), the high mammal species diversity in the Congo basin rainforest, combined with the remoteness of the outbreak site, complicates the collection of a sufficient sample size for all potentially relevant taxa (Figure 2; Appendix). Furthermore, many small mammals are difficult to identify at a species or genus level on the basis of morphology alone (Appendix). Therefore, we emphasize that EBOV and other virus surveillance in small mammals requires molecular identification of the host species.

Because all human EBOV outbreaks start from a spillover event from wildlife, knowledge on exactly which wildlife species are involved in EBOV natural ecology would provide a more precise geographical and seasonal risk map for human EBOV disease outbreaks. Therefore, despite the challenges highlighted by this study, investing in increased surveillance of African forest wildlife to find EBOV reservoirs could greatly benefit public health preparedness for the devastating disease caused by this virus.

Acknowledgments

We thank Lieselotte Cnops for logistic support and 3 anonymous reviewers for useful comments on the manuscript.

This work was supported by funds from the VLIR-UOS University Development Cooperation (Institutional University Cooperation); University of Antwerp; the Intramural Research Program of the National Institute of Allergy and Infectious Diseases, National Institutes of Health; Institut National de la Santé et de la Recherche Médicale/Ebola Task Force; REACTing (REsearch and ACTion targeting emerging infectious diseases); EBO-SURSY project funded by European Union; Christophe Mérieux Prize 2015 awarded to J.J.M.T.; Institut de Recherche pour le Développement; German Research Council (grant no. LE1813/7-1); the Global Health Protection Programme supported by the Federal Ministry of Health on the basis of a decision by the German Bundestag; and the Department of Economy, Science and Innovation EWI from the Flemish Government (Belgium). S.G. was supported by an OUTGOING [PEGASUS]^2 Marie Skłodowska-Curie fellowship of the Research Foundation–Flanders (grant no. 12T1117N). E.V. was financially supported by the Operational Directorate of Taxonomy and Phylogeny and Capacities for Biodiversity and Sustainable Development at the Royal Belgian Institute of Natural Sciences. K.K.A. was supported by a grant from Flanders Innovation & Entrepreneurship.

About the Author

Dr. Mbala-Kingebeni is a researcher at the Institut National de Recherche Biomédicale and University of Kinshasa, Democratic Republic of Congo. His research interests include characterization of hosts that harbor zoonotic pathogens.

References

1. Pourrut X, Souris M, Towner JS, Rollin PE, Nichol ST, Gonzalez JP, et al. Large serological survey showing cocirculation of Ebola and Marburg viruses in Gabonese bat populations, and a high seroprevalence of both viruses in *Rousettus aegyptiacus*. BMC Infect Dis. 2009;9:159. https://doi.org/10.1186/1471-2334-9-159
2. De Nys HM, Kingebeni PM, Keita AK, Butel C, Thaurignac G, Villabona-Arenas CJ, et al. Survey of Ebola viruses in frugivorous and insectivorous bats in Guinea, Cameroon, and the Democratic Republic of the Congo, 2015–2017. Emerg Infect Dis. 2018;24:2228–40. https://doi.org/10.3201/eid2412.180740
3. Leroy EM, Kumulungui B, Pourrut X, Rouquet P, Hassanin A, Yaba P, et al. Fruit bats as reservoirs of Ebola virus. Nature. 2005;438:575–6. https://doi.org/10.1038/438575a
4. Towner JS, Amman BR, Sealy TK, Carroll SA, Comer JA, Kemp A, et al. Isolation of genetically diverse Marburg viruses from Egyptian fruit bats. PLoS Pathog. 2009; 5:e1000536. https://doi.org/10.1371/journal.ppat.1000536
5. Negredo A, Palacios G, Vázquez-Morón S, González F, Dopazo H, Molero F, et al. Discovery of an ebolavirus-like filovirus in Europe. PLoS Pathog. 2011;7:e1002304. https://doi.org/10.1371/journal.ppat.1002304
6. He B, Feng Y, Zhang H, Xu L, Yang W, Zhang Y, et al. Filovirus RNA in fruit bats, China. Emerg Infect Dis. 2015;21:1675–7. https://doi.org/10.3201/eid2109.150260
7. Goldstein T, Anthony SJ, Gbakima A, Bird BH, Bangura J, Tremeau-Bravard A, et al. The discovery of Bombali virus

adds further support for bats as hosts of ebolaviruses. Nat Microbiol. 2018;3:1084–9. https://doi.org/10.1038/s41564-018-0227-2
8. Yang XL, Tan CW, Anderson DE, Jiang RD, Li B, Zhang W, et al. Characterization of a filovirus (Měnglà virus) from *Rousettus* bats in China. Nat Microbiol. 2019;4:390–5. https://doi.org/10.1038/s41564-018-0328-y
9. Leendertz SA, Gogarten JF, Düx A, Calvignac-Spencer S, Leendertz FH. Assessing the evidence supporting fruit bats as the primary reservoirs for Ebola viruses. Ecohealth. 2016;13:18–25. https://doi.org/10.1007/s10393-015-1053-0
10. Nsio J, Kapetshi J, Makiala S, Raymond F, Tshapenda G, Boucher N, et al. Outbreak of Ebola virus disease in northern Democratic Republic of Congo. J Infect Dis. 2017;2019:3. https://academic.oup.com/jid/article/221/5/701/5426903
11. World Health Organization. Ebola Virus Disease Democratic Republic of Congo. External situation report 10. 2017 May 23. [cited 2017 May 23]. https://apps.who.int/iris/bitstream/handle/10665/255565/EbolaDRC-24052017.pdf.
12. de Wit E, Rosenke K, Fischer RJ, Marzi A, Prescott J, Bushmaker T, et al. Ebola laboratory response at the Eternal Love Winning Africa campus, Monrovia, Liberia, 2014–2015. J Infect Dis. 2016;214(suppl 3):S169–76. https://doi.org/10.1093/infdis/jiw216
13. Ayouba A, Touré A, Butel C, Keita AK, Binetruy F, Sow MS, et al. Development of a sensitive and specific serological assay based on Luminex technology for detection of antibodies to Zaire Ebola virus. J Clin Microbiol. 2016;55:165–76. https://doi.org/10.1128/JCM.01979-16
14. Ng M, Ndungo E, Kaczmarek ME, Herbert AS, Binger T, Kuehne AI, et al. Filovirus receptor NPC1 contributes to species-specific patterns of ebolavirus susceptibility in bats. eLife. 2015;4:4. https://doi.org/10.7554/eLife.11785.
15. Leirs H, Mills JN, Krebs JW, Childs JE, Akaibe D, Woollen N, et al. Search for the Ebola virus reservoir in Kikwit, Democratic Republic of the Congo: reflections on a vertebrate collection. J Infect Dis. 1999;179(Suppl 1):S155–63. https://doi.org/10.1086/514299

Address for correspondence: Sophie Gryseels, Clinical and Epidemiological Virology, Rega Institute, KU Leuven, Herestraat 49, 3000 Leuven, Belgium; email: sophiegryseels@gmail.com

Sequence Type Changes Associated with Decreasing Macrolide-Resistant *Mycoplasma pneumoniae*, Japan

Miyuki Morozumi, Takeshi Tajima, Megumi Sakuma, Michi Shouji, Hidenori Meguro, Kota Saito, Satoshi Iwata, Kimiko Ubukata

We compared sequence types (STs) of *Mycoplasma pneumoniae* isolates from Japan during 2002–2019. ST3 and ST14 dominated during 2002–2016, and ST7 and ST33 dominated during 2018–2019. These STs were associated with a decrease in macrolide-resistant strains after an epidemic of infection with *M. pneumoniae* during 2011–2012.

Mycoplasma pneumoniae is a major cause of community-acquired pneumonia, and macrolide-resistant *M. pneumoniae* is a serious concern in Asia (*1*–*3*). Throughout Japan, an outbreak of macrolide-resistant *M. pneumoniae* infection occurred during 2011–2012 (*2*). After this outbreak, the number of drug-resistant strains decreased for every year from 2013 through 2019. In contrast, China and South Korea still showed a high rate of macrolide resistance in *M. pneumoniae* during 2014–2018 (*1*,*3*). We determined antimicrobial drug susceptibility and performed analysis by using multilocus sequence typing (MLST), clonal complexes (CCs), and P1 gene typing for *M. pneumoniae* isolated from children to identify trends concerning this bacterium in Japan.

The Study

We obtained nasopharyngeal swab samples from patients who had pneumonia or bronchitis at 21 medical institutions throughout Japan during October 2018–July 2019. We collected samples after obtaining informed consent from patients or their family members (Ethics Committee approval no. 2016–0015, Keio University School of Medicine, Tokyo, Japan).

We suspended samples in 0.5 mL of pleuropneumonia-like organism broth (Difco, https://www.fishersci.com). We then performed DNA extraction by using a described protocol (*4*). We used a Cycleave PCR Kit (Takara Bio, https://www.takarabio.com) to detect *M. pneumoniae*. For confirmed cases of infection with *M. pneumoniae*, we used a Cycleave PCR to distinguish between macrolide-susceptible and macrolide-resistant strains (*5*). Cultures were grown in pleuropneumonia-like organism broth, according to previously described methods (*6*).

We determined MICs for antimicrobial resistance of isolates by using microdilution methods (*6*). We performed MLST analysis based upon sequencing of 8 housekeeping genes (*ppa*, *pgm*, *gyrB*, *gmk*, *glyA*, *atpA*, *arcC*, and *adk*) according to the method described in the MLST database (https://pubmlst.org/mpneumoniae). To determine relationships between sequence types (STs), we performed CC analysis by using global optimal eBURST (http://www.phyloviz.net/goeburst). Typing of the P1 adhesin gene in *M. pneumoniae* was performed as described (*7*).

During the 2018–2019 study period, 105 samples were received (mean patient age 8 years). *M. pneumoniae* was confirmed by real-time PCR in 83 (79.0%), and culturing was successful in 53 (50.5%). Of these 53 isolates, only 6 (11.3%) were macrolide-resistant *M. pneumoniae*. All of these macrolide-resistant strains had an A2063G mutation in the 23S rRNA gene.

We provide yearly changes in macrolide-resistant *M. pneumoniae* during 2002–2019 (except for 2014 and 2017) in Japan (Table). Data from the earlier years beginning in 2002 were reported previously (*2*,*6*,*7*). Our study group results from the earlier periods

Author affiliations: Keio University School of Medicine, Tokyo, Japan (M. Morozumi, M. Sakuma, S. Iwata, K. Ubukata); Hakujikai Memorial Hospital, Tokyo (T. Tajima); National Center for Global Health and Medicine, Tokyo (M. Shouji); Meguro Clinic, Chiba, Japan (H. Meguro); Saito Pediatric Clinic, Saitama, Japan (K. Saito); National Cancer Center Hospital, Tokyo (S. Iwata)

DOI: https://doi.org/10.3201/eid2609.191575

Table. Yearly changes in macrolide-susceptible and macrolide-resistant *Mycoplasma pneumoniae*, Japan, 2002–2019*

Macrolide susceptibility†	2002–2005	2006–2009	2010–2013	2015–2016	2018–2019	Total
Susceptible	241 (93.1)	161 (62.6)	45 (13.8)	86 (43.7)	47 (88.7)	580
Resistant	18 (6.9)	96 (37.4)	281 (86.2)	111 (56.3)	6 (11.3)	512
Total	259	257	326	197	53	1,092

*Values are no. (%).
†Macrolide susceptibility was distinguished on the basis of a mutation in the 23S rRNA gene and results of susceptibility measurements.

indicated macrolide-resistance rates of 6.9% (18/259) during 2002–2005; a total of 37.4% (96/257) during 2006–2009; a total of 86.2% (281/326) during 2010–2013, including the epidemic years 2011–2012; and 56.3% (111/197) during 2015–2016 compared with 11.3% (6/53) during 2018–2019. These resistance rates have decreased rapidly beginning in 2018, and the MICs for quinolone and tetracycline have remained unchanged; no drug-resistant strains were identified.

We determined relationships observed between STs and 279 macrolide-susceptible *M. pneumoniae* versus 191 macrolide-resistant *M. pneumoniae* during 2002–2019 (Figure 1). ST3 and ST14 accounted for most macrolide-susceptible *M. pneumoniae* during 2002–2016; these STs have been largely replaced by ST7 (n = 30, 56.6%) and ST33 (n = 13, 24.5%) during 2018–2019. ST33 first appeared in this study in 2018, and ST14 was more prevalent among macrolide-susceptible *M. pneumoniae* during 2002–2016 but was rarely detected during 2018–2019. Differences in STs during 2002–2016 and during 2018–2019 were highly significant ($p<0.001$). Conversely, most macrolide-resistant *M. pneumoniae* isolates belonged to ST3, as in previous years.

We determined relationships between CC and STs according to goeBURST (Figure 2). The data include 470 strains from our study and 62 strains registered in the MLST database from other countries. Of the 2 CC clusters, the CC1 centered on ST3, and CC2 centered on ST2. ST7 and ST33, which were prevalent during 2018–2019, belonged to CC2. Although ST14 was the most prevalent member of CC2 until 2016, ST33 replaced it and increased during 2018. Both ST14 and ST33 were derived from ST15 and showed a single-locus variant of the *adk* gene. We registered ST34, which was derived from ST33, as a new ST.

Results for P1 typing of *M. pneumoniae* showed that STs belonging to CC1 were type 1 and STs belong to CC2 were type 2. ST14, ST15, ST33, and ST34 belonged to type 2a, a subtype of P1 type 2.

Conclusions

In Japan, prevalence of macrolide-resistant *M. pneumoniae* has decreased recently and rapidly. Other study groups have reported similar trends (*8*). However, in countries in Asia other than Japan, the resistance rate has remained high in China (*3*) and South Korea (*1*). In the European Union, the overall rate is low, but has varied by country. Macrolide-resistant *M. pneumoniae* was not detected in Sweden during 1996–2013 (*9*), and the rate has been consistently low in Germany (1.9%–3.6%) (*10*). Because of tight control of antimicrobial drug prescriptions, Sweden shows extremely low use of macrolides (*11*) compared with for more frequent use in countries in Asia (*12*), where excessive use of macrolides is likely to affect selection and increase of drug-resistant strains.

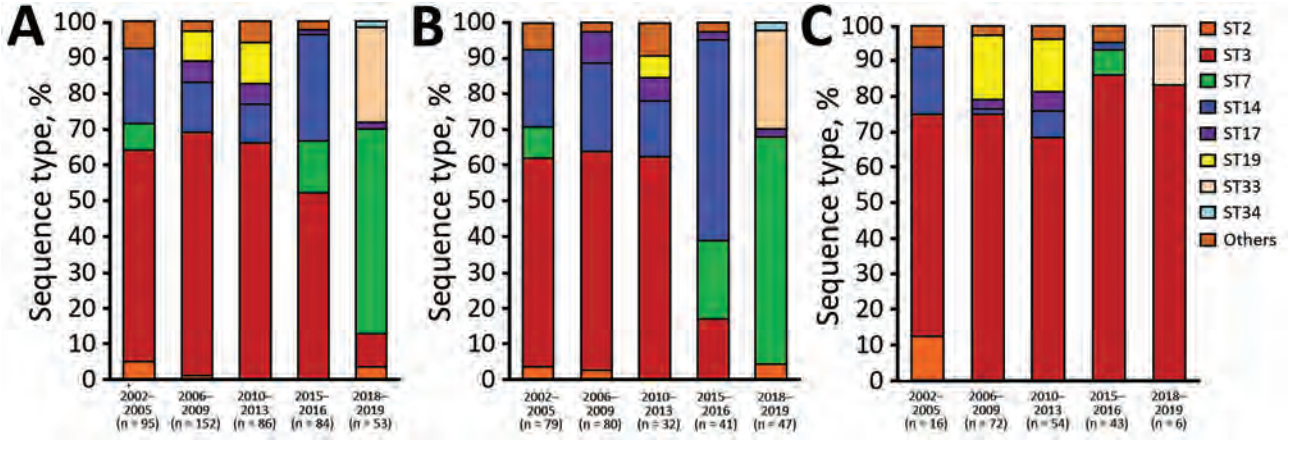

Figure 1. Relationships between year of isolation and STs among 279 macrolide-susceptible *M. pneumoniae* and 191 macrolide-resistant *M. pneumoniae* from children in Japan, 2002–2019. A) All strains tested; B) macrolide-susceptible strains; C) macrolide-resistant strains. Others includes ST13 (2005), ST15 (2002, 2016), ST16 (2002, 2010), ST18 (2010), ST20 (2004), ST21 (2011), ST 22 (2003, 2006, 2016), ST29 (2016), and ST30 (2016). ST, sequence type.

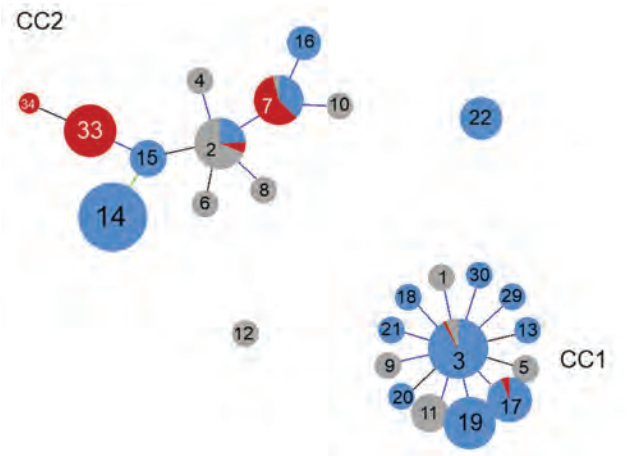

Figure 2. Relationships between CCs and STs for *Mycoplasma pneumoniae* isolates determined by goeBURST (http://www.phyloviz.net), Japan. Data were obtained from isolates including 470 strains from Japan during 2002–2019 and 62 strains isolated in the United Kingdom, the United States, China, and France. Blue circles indicate isolates from Japan during 2002–2016; red circles indicate isolates from Japan during 2018–2019; and gray circles indicate isolates from the United Kingdom during 1967–2010, the United States during 1944–1994, China during 2014, and France during 1981. Among all isolates, 26 STs were identified. CC, clonal complex; ST, sequence type.

In Japan, macrolide consumption has decreased gradually after the 2011–2012 outbreak of macrolide-resistant *M. pneumoniae* infections (http://amrcrc.ncgm.go.jp/surveillance/index.html), which may have contributed to the decrease in drug-resistant strains. In addition, the outbreak was followed by approval of tosufloxacin, a quinolone agent, for children with macrolide-resistant *M. pneumoniae* infection who fail to respond clinically to macrolides within 3 days. Approval of tosufloxacin as a treatment for these *M. pneumoniae* infections might have also contributed to the decrease in the macrolide resistance rate.

Our MLST results showed that predominant STs during 2018–2019 differed from those during 2016. *M. pneumoniae* could not be collected for our survey during 2017. This factor was a serious limitation because changes in STs might have occurred at that time. During 2018, strains identified as ST7 and ST33 were almost all susceptible and represented a major difference from previous findings. ST33, which contained a single-locus variant of the *adk* gene in ST15, was identified in Japan during 2018 and displaced ST14, the major ST among susceptible strains isolated during 2015–2016. The cause of ST replacement might have been acquisition of specific antibodies against epidemic *M. pneumoniae* in children and teenagers, which gave rise to a single-locus variant in its place.

CC1 is a circular clonal complex that spread from ST3 at the center toward different STs showing a single-locus variant. CC2 has extended from its original center at ST2 to include other STs with 1 or more mutated allele. STs belonging to CC2 seen to be more diverse than STs of CC1. Diversification has also been observed in type 2 of the P1 gene, corresponding to CC2 (*13*).

In conclusion, STs in *M. pneumoniae* isolates differed by area and year in Japan (*1*,*7*,*14*). Thus, MLST analysis is helpful in understanding worldwide trends among pathogenic *M. pneumoniae*.

Acknowledgments

We thank the pediatricians who actively participated in the *M. pneumoniae* Study Group (Toshiyuki Hikita, Junichi Ishikawa, Hirokazu Kutsuma, Masaaki Kobayashi, Eiichi Nakayama, Keita Matsubara, Osamu Kakuta, Kazuoki Kubota, Yosuke Mori, Hiroyoshi Ebara, Satoshi Koyama, Hiroaki Shiraishi, Shigeru Ohnari, Meiwa Shibata, Hidehisa Shinohara, Kensuke Nagai, Yasuo Kondo, and Takashige Okada); and Madoka Naito and Shinji Masuyoshi for providing laboratory assistance.

About the Author

Dr. Morozumi is an assistant professor at Keio University School of Medicine, Tokyo, Japan. Her research interests include molecular epidemiology and severe infections caused by *Streptococcus agalactiae* and *M. pneumoniae*.

References

1. Lee JK, Lee JH, Lee H, Ahn YM, Eun BW, Cho EY, et al. Clonal expansion of macrolide-resistant sequence type 3 *Mycoplasma pneumoniae*, South Korea. Emerg Infect Dis. 2018;24:1465–71. https://doi.org/10.3201/eid2408.180081
2. Okada T, Morozumi M, Tajima T, Hasegawa M, Sakata H, Ohnari S, et al. Rapid effectiveness of minocycline or doxycycline against macrolide-resistant *Mycoplasma pneumoniae* infection in a 2011 outbreak among Japanese children. Clin Infect Dis. 2012;55:1642–9. https://doi.org/10.1093/cid/cis784
3. Zhao F, Li J, Liu J, Guan X, Gong J, Liu L, et al. Antimicrobial susceptibility and molecular characteristics of *Mycoplasma pneumoniae* isolates across different regions of China. Antimicrob Resist Infect Control. 2019;8:143. https://doi.org/10.1186/s13756-019-0576-5
4. Morozumi M, Nakayama E, Iwata S, Aoki Y, Hasegawa K, Kobayashi R, et al. Simultaneous detection of pathogens in clinical samples from patients with community-acquired pneumonia by real-time PCR with pathogen-specific molecular beacon probes. J Clin Microbiol. 2006;44:1440–6. https://doi.org/10.1128/JCM.44.4.1440-1446.2006
5. Liu Y, Ye X, Zhang H, Wu Z, Xu X. Rapid detection of *Mycoplasma pneumoniae* and its macrolide-resistance mutation by Cycleave PCR. Diagn Microbiol Infect Dis. 2014;78:333–7. https://doi.org/10.1016/j.diagmicrobio.2013.12.002
6. Morozumi M, Hasegawa K, Kobayashi R, Inoue N, Iwata S, Kuroki H, et al. Emergence of macrolide-resistant

Mycoplasma pneumoniae with a 23S rRNA gene mutation. Antimicrob Agents Chemother. 2005;49:2302–6. https://doi.org/10.1128/AAC.49.6.2302-2306.2005
7. Ando M, Morozumi M, Adachi Y, Ubukata K, Iwata S. Multilocus sequence typing of *Mycoplasma pneumoniae,* Japan, 2002–2016. Emerg Infect Dis. 2018;24:1895–901. https://doi.org/10.3201/eid2410.171194
8. Tanaka T, Oishi T, Miyata I, Wakabayashi S, Kono M, Ono S, et al. Macrolide-resistant *Mycoplasma pneumoniae* infection, Japan, 2008–2015. Emerg Infect Dis. 2017;23:1703–6. https://doi.org/10.3201/eid2310.170106
9. Gullsby K, Bondeson K. No detection of macrolide-resistant *Mycoplasma pneumoniae* from Swedish patients, 1996–2013. Infect Ecol Epidemiol. 2016;6:31374. https://doi.org/10.3402/iee.v6.31374
10. Dumke R, Ziegler T. Long-term low rate of macrolide-resistant *Mycoplasma pneumoniae* strains in Germany. Antimicrob Agents Chemother. 2019;63:e00455-19. https://doi.org/10.1128/AAC.00455-19
11. Adriaenssens N, Coenen S, Versporten A, Muller A, Minalu G, Faes C, et al.; ESAC Project Group. European Surveillance of Antimicrobial Consumption (ESAC): outpatient macrolide, lincosamide and streptogramin (MLS) use in Europe (1997–2009). J Antimicrob Chemother. 2011;66(Suppl 6):vi37–45. https://doi.org/10.1093/jac/dkr190
12. Wushouer H, Tian Y, Guan XD, Han S, Shi LW. Trends and patterns of antibiotic consumption in China's tertiary hospitals based on a 5 year surveillance with sales records, 2011–2015. PLoS One. 2017;12:e0190314. https://doi.org/10.1371/journal.pone.0190314
13. Gullsby K, Olsen B, Bondeson K. Molecular typing of *Mycoplasma pneumoniae* strains in Sweden from 1996 to 2017 and the emergence of a new P1 cytadhesin gene, variant 2e. J Clin Microbiol. 2019;57:57. https://doi.org/10.1128/JCM.00049-19
14. Brown RJ, Nguipdop-Djomo P, Zhao H, Stanford E, Spiller OB, Chalker VJ. *Mycoplasma pneumoniae* epidemiology in England and Wales: a national perspective. Front Microbiol. 2016;7:157. https://doi.org/10.3389/fmicb.2016.00157

Address for correspondence: Kimiko Ubukata, Department of Infectious Diseases, Keio University School of Medicine, 35 Shinanomachi, Shinjuku-ku, Tokyo 160-8582, Japan; email: ubukatak@keio.jp

Hepatitis E Virus Genotype 7 RNA and Antibody Kinetics in Naturally Infected Dromedary Calves, United Arab Emirates

Victor M. Corman, Peter Nagy, Stefanie Ostermann, Jacqueline Arloth, Anne Liljander, Rajib Barua, Aungshuman Das Gupta, Fatima Hakimuddin, Judit Juhasz, Ulrich Wernery, Christian Drosten

Orthohepevirus A genotype 7 is a novel zoonotic variant of hepatitis E virus. To clarify infection in the animal reservoir, we virologically monitored 11 dromedary dam–calf pairs. All calves became infected during the first 6 months of life and cleared the virus after an average of 2 months. Dams did not become infected.

Infection with hepatitis E viruses (HEVs) is one of the major causes of acute hepatitis in humans (*1*). Most HEV strains infecting humans belong to the virus species *Orthohepevirus A* (HEV-A) (*2*). HEV-A comprises 8 genotypes; genotypes 1–4 and 7 are found in humans. HEV-A genotypes 1 and 2 seem to be restricted to humans. The other 3 genotypes have also been detected in animals, including pigs (genotypes 3 and 4) and camelids (genotype 7) (*1*).

The most likely source of human zoonotic HEV infection is consumption of contaminated food. Typically, human HEV infections lead to acute and self-limiting disease or asymptomatic seroconversion, but chronic hepatitis E has also been reported, mainly in transplant recipients (*3*,*4*). Infection with camel-associated HEV-A genotype 7 was reported in a patient from the United Arab Emirates with chronic hepatitis after liver transplantation (*4*,*5*). This infection was likely acquired through consumption of contaminated camel products. Despite the risk for zoonotic transmission, data about shedding and immunity of HEV-A genotype 7 infection in naturally infected dromedaries are scarce.

Author affiliations: Charité-Universitätsmedizin Berlin, Berlin, Germany. (V.M. Corman, C. Drosten); German Centre for Infection Research, Berlin (V.M. Corman, C. Drosten); Emirates Industries for Camel Milk and Products, Dubai, United Arab Emirates (P. Nagy, R. Barua, A. Das Gupta, J. Juhasz); Institute of Experimental Immunology, Lübeck, Germany (S. Ostermann, J. Arloth, A. Liljander); Central Veterinary Research Laboratory, Dubai (F. Hakimuddin, U. Wernery)

DOI: https://doi.org/10.3201/eid2609.191758

The Study

We investigated HEV-A RNA and specific antibody levels in dromedary calves and corresponding dams from 1 farm at monthly intervals over the course of the calves' first year of life. We included serum samples from 11 dam–calf pairs in the United Arab Emirates. The farm contained ≈4,500 camels. The 11 dam–calf pairs investigated in this study were kept in different fenced compartments within 100–150 m of each other but were housed together with other dam–calf pairs in the same paddock throughout lactation (*6*). All calves were born during June 2014. Serum samples were obtained during the first week and then at monthly intervals until 1 year after birth.

We tested samples for HEV RNA by using 2 reverse transcription PCRs (RT-PCRs) and for HEV antibodies by an HEV-A genotype 7 IgG ELISA (Appendix, https://wwwnc.cdc.gov/EID/article/26/9/19-1758-App1.pdf). In the studied cohort, all calves were naturally infected by HEV-A, as confirmed by RNA detection in serum samples, or seroconversion. In 9 of the 11 calves (#1–#9) (Figure 1), HEV-A RNA was detected in ≥1 serum sample. In 2 calves (#10 and #11) no RNA was detected, but an increase in ELISA ratio, equivalent to seroconversion, confirmed recent HEV-A infection.

The average age for infection of calves was 4.6 months (range 1–6 months). All HEV-A–RNA positive calves cleared the virus from their blood and showed accompanying seroconversion (Figure 1). Average viremia was 2.1 months (range 1–4 months). Viral RNA concentrations in serum samples ranged from 6.6×10^2 IU/mL to 2.3×10^6 IU/mL (mean 4.6×10^5 IU/mL).

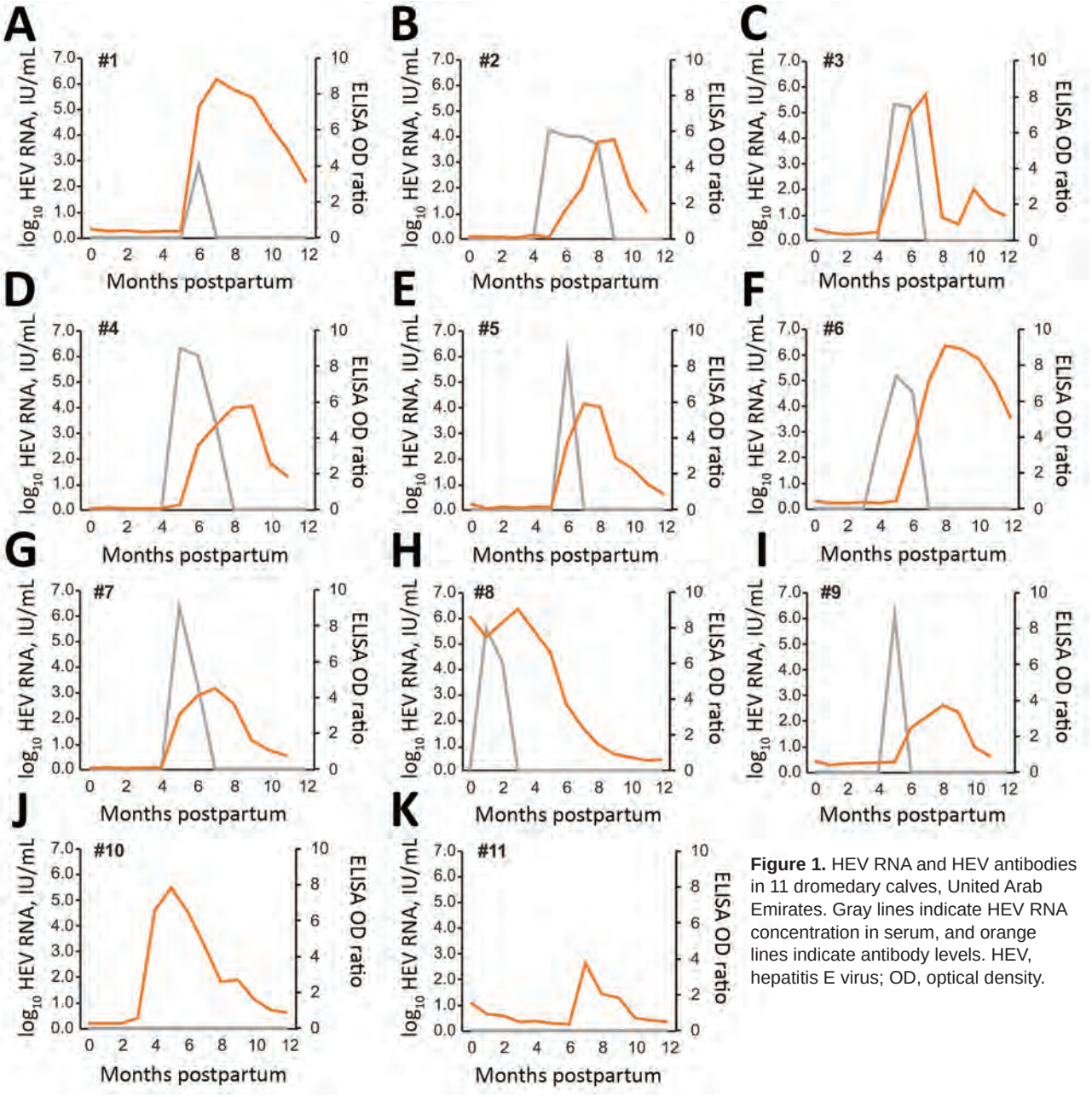

Figure 1. HEV RNA and HEV antibodies in 11 dromedary calves, United Arab Emirates. Gray lines indicate HEV RNA concentration in serum, and orange lines indicate antibody levels. HEV, hepatitis E virus; OD, optical density.

Phylogenetic analysis of partial open reading frame 1 region sequences confirmed that all strains belong to HEV-A genotype 7 (Figure 2). Sequences described clustered with a clade of HEV-A sequences obtained from camels and a human patient, all from the United Arab Emirates. All new sequences were highly similar and had 0–3 nt exchanges in the 283-nt fragment, which is consistent with the epidemiologic link of all infections and might indicate a common source of infection on this farm.

We compared novel sequences with all other camel associated HEV-A genotype 7 sequences available in GenBank (as of June 1, 2019). The novel sequences differ by 6.0% to 20.6% nt content within the partial open reading frame 1 region.

We found that none of the corresponding serum samples from dams were positive for HEV-A-RNA at any time or showed seroconversion during the study. We also found that 6/9 dams showed reactivity at the time of parturition by using the applied HEV-A genotype 7 ELISA and remained reactive through the year,

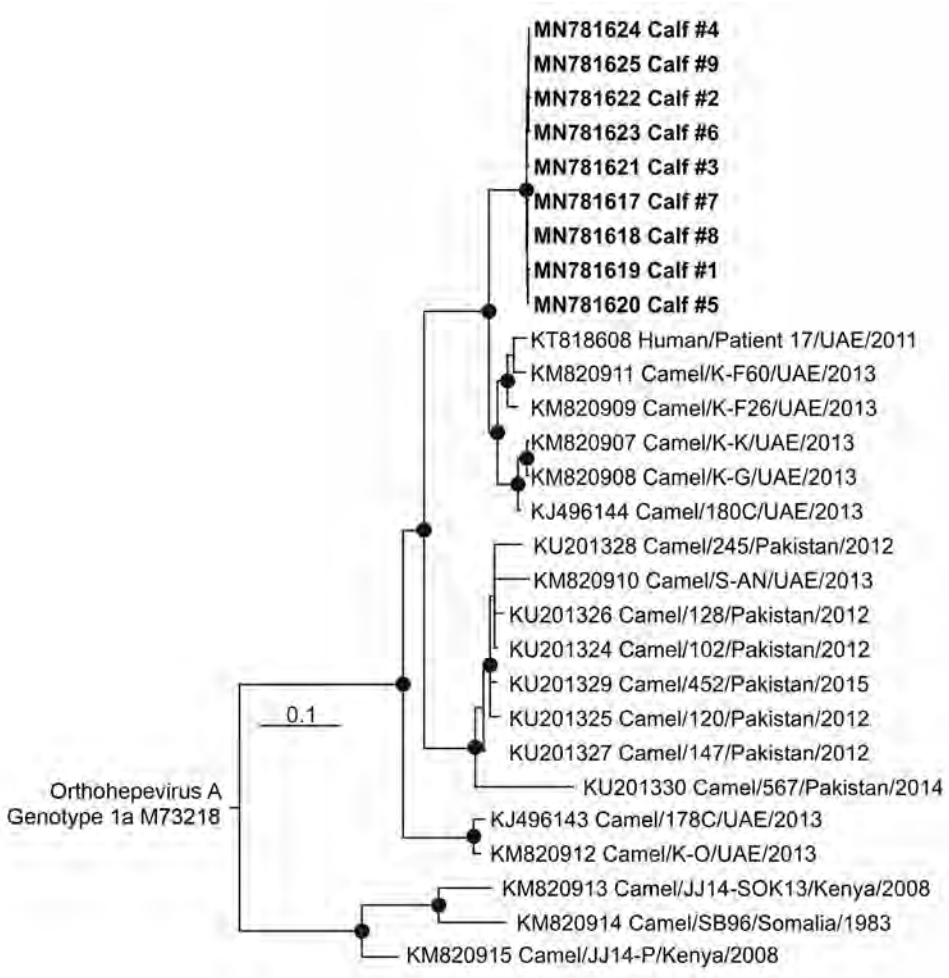

Figure 2. Phylogenetic tree of open reading frame 1 of HEV RNA sequences from 11 camel calves (bold), United Arab Emirates, and other *Orthohepevirus A* genotype 7 sequences available in GenBank as of May 1, 2019. The tree was calculated by using MrBayes (http://mrbayes.sourceforge.net) and a generalized time reversible substitution model. One million generations were sampled every 500 steps, and 20% of trees were discarded as burn-in. Bold indicates sequences obtained during this study. An *Orthohepevirus A* genotype 1 sequence (GenBank accession no M73218) was used as the outgroup. Taxon names of all reference sequences include GenBank accession number, strain, country of origin, and year of sampling. GenBank accession numbers for sequences obtained in this study are MN781617–25. Scale bar indicates nucleotide substitutions per site.

and the other 3 dams remained nonreactive during the study.

ELISA reactivity for all calves decreased after infection, and 2 of the 11 calves became negative (#8 and #11) (Figure 1). These 2 calves were the ones that had earliest infection date and the longest time span between infection and last available serum sample. To what extent the decrease of antibody levels is associated with a decreasing immunity against HEV-A genotype 7 was not investigated but should be the subject of future studies.

The observed natural course of HEV-A genotype 7 infection in camels is similar to that for HEV-A genotype 3 in pigs. Pigs represent the zoonotic source of most human HEV infections in the Northern Hemisphere (*7*). In piglets, HEV-A genotype 3 infection usually occurs at the age of 2–3 months, coinciding with the decrease in levels of maternal antibodies (*8*). HEV-A RNA is present in blood for ≈1 2 weeks, but longer periods ≤12 weeks have been described (*9*). Similarly, in our study of camels, all calves became infected within the first 6 months, and the duration of the viremia was an average of 8 weeks. Prevalence of HEV RNA in pigs at slaughter, which usually takes place at the age of 5–8 months, was found to be high, with ≤10% viral RNA detection in blood and ≤50% viral RNA detection in feces (*7*,*10*,*11*). As camels are slaughtered at higher age (≈2 years of age even in industrial farming) (*12*), a lower risk for HEV transmission associated with meat production might apply to camels in comparison with pigs.

The absence of RNA detection in dams suggests immunity in adult animals. The lack of detected HEV infection in 3 seronegative dams, despite close contact with their infected calves, points to additional factors, such as a T-cell–mediated immunity that might protect against HEV infection. This hypothesis is emphasized by simultaneous detection of antibodies and virus RNA in some calves and suggests that not all antibodies provide sterile immunity. This finding becomes essential when one considers intervention strategies, such as vaccination. Nevertheless, the time of seroconversion coincides with the time of decreasing viremia and infection clearance. A similar pattern of virus versus antibody findings has been found for pigs, humans, and hares (*8*,*13*–*15*).

The observation that all investigated calves were infected in the first year of life indicates a highly active enzootic infection pattern. The virus seems to be widespread in the studied herd and could therefore be widely associated with dromedaries. Because calves have contact with other calves on farms, the infection cycle is probably maintained by calf-to-calf transmission. This factor is relevant because humans are rarely in contact with camel calves but make intensive use of adult animals and derived products. However, our study was conducted in an industrial farming context. Different infection patterns with infection at higher age might be observed in husbandries that involve lower densities of animals and might also vary in other husbandry practices.

Conclusions

We provide essential information regarding age of infection, virus shedding, and immunity for camel-associated, zoonotic HEV-A genotype 7. Knowledge about the distribution of a zoonotic virus in its animal reservoir is needed to mitigate risks of acquisition along the husbandry and production chain. Intervention by vaccination will need to target calves at a time when they are still coreared with dams. Risks for the general human population seem to be low because humans are rarely in contact with camel calves unless directly involved in camel breeding. Future studies should investigate age-associated infection patterns in less industrialized forms of camel husbandry and the actual risk for transmission to humans when animals are slaughtered.

Acknowledgments

We thank Tobias Bleicker, Sebastian Brünink, and Philip El-Duah for providing excellent assistance.

This study was supported by the German Federal Ministry of Health (grant ZMVI1-2518FSB705 to V.M.C.) and a grant from the German Federal Ministry for Economic Cooperation and Development (contract no. 81195004 to V.M.C. and A.L.).

About the Author

Dr. Corman is a physician and virologist at the Institute of Virology, Charité-Universitätsmedizin Berlin, Berlin, Germany. His research interests are characterization of emerging viruses and development of diagnostic tools.

References

1. Rasche A, Sander AL, Corman VM, Drexler JF. Evolutionary biology of human hepatitis viruses. J Hepatol. 2019;70:501–20. https://doi.org/10.1016/j.jhep.2018.11.010
2. Purdy MA, Harrison TJ, Jameel S, Meng XJ, Okamoto H, Van der Poel WH, et al.; ICTV Report Consortium. ICTV virus taxonomy profile: *Hepeviridae*. J Gen Virol. 2017;98:2645–6. https://doi.org/10.1099/jgv.0.000940
3. Behrendt P, Steinmann E, Manns MP, Wedemeyer H. The impact of hepatitis E in the liver transplant setting. J Hepatol. 2014;61:1418–29. https://doi.org/10.1016/j.jhep.2014.08.047
4. Lee GH, Tan BH, Teo EC, Lim SG, Dan YY, Wee A, et al. Chronic infection with camelid hepatitis E virus in a liver-transplant recipient who regularly consumes camel meat and milk. Gastroenterology. 2016;150:355–7.
5. Rasche A, Saqib M, Liljander AM, Bornstein S, Zohaib A, Renneker S, et al. Hepatitis E virus infection in dromedaries, north and east Africa, United Arab Emirates, and Pakistan, 1983–2015. Emerg Infect Dis. 2016;22:1249–52. https://doi.org/10.3201/eid2207.160168
6. Meyer B, Juhasz J, Barua R, Das Gupta A, Hakimuddin F, Corman VM, et al. Time course of MERS-CoV infection and immunity in dromedary camels. Emerg Infect Dis. 2016;22:2171–3. https://doi.org/10.3201/eid2212.160382
7. Pavio N, Doceul V, Bagdassarian E, Johne R. Recent knowledge on hepatitis E virus in Suidae reservoirs and transmission routes to human. Vet Res (Faisalabad). 2017;48:78. https://doi.org/10.1186/s13567-017-0483-9
8. Salines M, Andraud M, Rose N. From the epidemiology of hepatitis E virus (HEV) within the swine reservoir to public health risk mitigation strategies: a comprehensive review. Vet Res (Faisalabad). 2017;48:31. https://doi.org/10.1186/s13567-017-0436-3
9. Sanford BJ, Dryman BA, Huang YW, Feagins AR, Leroith T, Meng XJ. Prior infection of pigs with a genotype 3 swine hepatitis E virus (HEV) protects against subsequent challenges with homologous and heterologous genotypes 3 and 4 human HEV. Virus Res. 2011;159:17–22. https://doi.org/10.1016/j.virusres.2011.04.010
10. Leblanc D, Ward P, Gagné MJ, Poitras E, Müller P, Trottier YL, et al. Presence of hepatitis E virus in a naturally infected swine herd from nursery to slaughter. Int J Food Microbiol. 2007;117:160–6. https://doi.org/10.1016/j.ijfoodmicro.2007.03.008
11. Krog JS, Larsen LE, Breum SO. Tracing hepatitis E virus in pigs from birth to slaughter. Front Vet Sci. 2019;6:50. https://doi.org/10.3389/fvets.2019.00050
12. Kadim IT, Mahgoub O, Faye B, Farouk MM. Camel meat and meat products. Wallingford (UK): Centre for Agricultural and Bioscience International; 2013.
13. Baylis SA, Crossan C, Corman VM, Blümel J, Scobie L, Dalton HR. Unusual serological response to hepatitis E virus in plasma donors consistent with re-infection. Vox Sang. 2015;109:406–9. https://doi.org/10.1111/vox.12294
14. Schlosser J, Eiden M, Vina-Rodriguez A, Fast C, Dremsek P, Lange E, et al. Natural and experimental hepatitis E virus genotype 3-infection in European wild boar is transmissible to domestic pigs. Vet Res (Faisalabad). 2014;45:121. https://doi.org/10.1186/s13567-014-0121-8
15. Corman VM, Hilgensloh L, Voigt U, Marklewitz M, Siebert U, Drosten C, et al. Hepatitis E virus infection in European brown hares, Germany, 2007–2014. Emerg Infect Dis. 2019;25:1233–5. https://doi.org/10.3201/eid2506.181618

Address for correspondence: Victor M. Corman, Institute of Virology, Charité-Universitätsmedizin Berlin, Helmut-Ruska-Haus Charitéplatz 1, Berlin 10117, Germany; email: victor.corman@charite.de

Carbapenemase-Producing Gram-Negative Bacteria in Andalusia, Spain, 2014–2018

Inmaculada López-Hernández, Mercedes Delgado-Valverde, Felipe Fernández-Cuenca, Lorena López-Cerero, Jesús Machuca, Álvaro Pascual

The emergence and spread of carbapenemase-producing gram-negative bacteria is a major public health concern. We used data collected from microbiology laboratories as part of the PIRASOA program during 2014–2018 to study the epidemiology of carbapenemase-producing bacteria in Andalusia, Spain. Our findings highlight the importance of ongoing surveillance and epidemiologic studies for these bacteria.

There are 3 common carbapenemase classes: class A includes *Klebsiella pneumoniae* carbapenemase (KPC); class B is metallo-β-lactamases (MBL), including Verona integron-encoded metallo-β-lactamase (VIM), New Delhi metallo-β-lactamase (NDM) and imipenemase (IMP); and class D includes oxacillinases (OXA), including OXA-48–like carbapenemases. In Spain, all 3 of these classes have been reported in recent studies (*1*–*4*). A multicenter study of *Enterobacterales* carbapenemase-producing gram-negative bacteria (CPGNB), isolated from urine specimens, found a prevalence of 1.6%. OXA-48 was the most prevalent, followed by KPC and MBL (*5*).

In Andalusia, a region in the south of Spain with a population of ≈8.4 million people, The PIRASOA (https://www.iavante.es/es/programa-pirasoa) program was designed to prevent and control healthcare-associated infections and promote the appropriate use of antimicrobials, covering the entire area of the Andalusia public healthcare system, which includes 34 hospitals in 8 provinces. Data collected through PIRASOA during 2014–2018 provided an opportunity for us to study and understand the epidemiology of carbapenemase-producing bacteria in Andalusia.

Author affiliations: Laboratorio PIRASOA, Hospital Universitario Virgen Macarena, Seville, Spain (I. Lopez-Hernandez, M. Delgado-Valverde, F. Fernández-Cuenca, L. López-Cerero, J. Machuca, Á. Pascual); Instituto de Biomedicina de Sevilla IBIS, Hospital Universitario Virgen Macarena, Consejo Superior de Investigaciones Científicas, Universidad de Sevilla, Seville (I. López-Hernández, M. Delgado-Valverde, F. Fernández-Cuenca, L. López-Cerero, J. Machuca, Á. Pascual); Red Española de Investigación en Patología Infecciosa (REIPI RD16/0016), Instituto de Salud Carlos III, Madrid, Spain (I. López-Hernández, M. Delgado-Valverde, F. Fernández-Cuenca, L. López-Cerero, J. Machuca, Á. Pascual); Universidad de Sevilla, Seville (Á. Pascual).

DOI: https://doi.org/10.3201/eid2609.191772

The Study

During January 2014–December 2018, microbiology laboratories in the hospitals included in the PIRASOA program voluntarily submitted CPGNB detected according to EUCAST screening criteria (*6*) to the PIRASOA reference laboratory. We identified the isolates using MALDI-TOF Biotyper (Bruker Daltonics, https://www.bruker.com). Antimicrobial susceptibility testing was performed by microdilution (Microscan; Beckman Coulter, https://www.beckmancoulter.com) and interpreted according to EUCAST breakpoints (*7*). We determined the inhibition of carbapenemase activity by using inhibitors (dipicolinic acid, phenyl-boronic acid, and cloxacillin). In addition, we tested all the isolates with the β-CARBA test (Bio-Rad, https://www.bio-rad.com) and, from January 2018, also with the NG-test CARBA 5 (NG Biotech, https://ngbiotech.com). All isolates with a positive or indeterminate result from phenotypic screening were tested by PCR and sequencing (Macrogen, https://dna.macrogen.com) (bla_{KPC}, bla_{OXA-48}, bla_{VIM}, bla_{IMP}, bla_{NDM}, $bla_{OXA-23,24/40,58}$) or by whole genome sequencing on a MiSeq system (Illumina, https://www.illumina.com), which became available in October 2017. We evaluated genetic relatedness by pulsed-field gel electrophoresis (CHEF DR-II system; Bio-Rad); isolates of <2 bands difference were assigned to the same cluster. We determined

multilocus sequence typing using PCR and sequencing or whole-genome sequencing data (https://cge.cbs.dtu.dk/services/MLST).

During the study period, we analyzed 2,005 gram-negative isolates of which 1,243 (62%) were carbapenemase producers. Among those 1,243 isolates, clinical specimens (64%, 791/1,243) comprised the predominant source, followed by surveillance (31%, 387/1,243) and environmental samples (5%, 65/1,243). The most common species were *K. pneumoniae* (45%, 560/1,243), *Acinetobacter baumannii* (34%, 425/1,243), and *K. oxytoca* (7%, 83/1,243).

KPC-3 was the most common carbapenemase we found (249; 20%); 96% of the KPC-3 was detected in *K. pneumoniae* belonging to clones sequence type (ST) 512 or ST258. In contrast, KPC-2, which comprised only 1.8% (23), was found in multiple species. Among OXA-48–like carbapenemases, which comprised 19% (254) of carbapenemases, 87% (221/254) were found in *K. pneumoniae*, 70% (155/221) of those in clones ST11, ST15, ST392, or ST307.

Over the course of the study period, we observed an increase in MBL carbapenemases, with a noteworthy increase in 2018 (Table 1; Figure 1). *Klebsiella* was most prevalent MBL, comprising 53% (157/294), almost equally distributed between *K. pneumoniae* and *K. oxytoca,* followed by *Pseudomonas aeruginosa* (20%, 60/294) and *Enterobacter cloacae* (14%, 42/294). The distribution of each MBL enzyme type varied significantly. We found 39% (77/197) of VIM in *K. oxytoca*, 80% (45/56) of NDM in *K. pneumoniae*, and 73% (30/41) of IMP in *P. aeruginosa*. OXA-23 (49%, 208/425) was the most common carbapenemase producer in *A. baumannii*, followed by OXA-58 (38%, 162/425), and OXA-24/40 (13%, 55/425). OXA-23 and OXA 24/40 isolates belonged predominantly to clone ST2. OXA-58 producers were detected in multiple clones. We summarize the distribution of carbapenemases among CPGNB in this study in Table 2.

Geographically, carbapenemase producers were found in 32 hospitals distributed throughout 8 provinces of the region, with KPC detected in 26 hospitals,

Table 1. Distribution of carbapenemase-producing gram-negative bacteria by year, Andalusia, Spain, 2014–2018

Carbapenemase	Bacteria	Year				
		2014	2015	2016	2017	2018
VIM	*Klebsiella pneumoniae*	0	0	9	9	15
	K. oxytoca	1	13	12	19	32
	Escherichia coli	0	2	1	3	2
	Enterobacter cloacae	0	4	4	10	15
	Citrobacter freundii	0	1	3	2	2
	C. amalonaticus	0	0	1	0	0
	Pseudomonas aeruginosa	1	0	0	0	29
	P. putida	0	0	0	3	3
	Acinetobacter spp	0	0	0	1	0
IMP	*K. pneumoniae*	0	0	0	0	2
	E. coli	0	0	0	0	1
	E. cloacae	0	0	0	2	5
	C. freundii	0	1	0	0	0
	P. aeruginosa	0	2	0	10	18
NDM	*K. pneumoniae*	0	0	1	7	37
	E. coli	0	0	1	1	3
	E. cloacae	0	0	2	0	0
	Acinetobacter spp	0	0	0	0	1
	A. baumannii	0	0	0	2	1
KPC	*K. pneumoniae*	35	71	61	54	38
	K. oxytoca	0	0	0	0	2
	E. coli	0	0	0	0	3
	E. cloacae	0	0	2	3	2
	C. freundii	0	0	0	1	0
OXA-48	*K. pneumoniae*	35	26	39	77	44
	K. oxytoca	0	0	0	1	3
	E. coli	6	3	0	1	3
	E. cloacae	1	1	0	0	5
	C. freundii	0	1	0	1	3
	K. aerogenes	0	0	0	0	4
OXA-23	*A. baumannii*	38	30	19	67	54
OXA-58	*A. baumannii*	15	25	46	38	36
OXA-24/40	*A. baumannii*	1	33	12	7	1
IMI	*E. cloacae*	0	0	0	0	1

IMP, imipenemase; KPC, *Klebsiella pneumoniae* carbapenemase; MBL, metallo-β-lactamases; NDM, New Delhi metallo-beta-lactamase; OXA, oxacillinases; VIM, Verona integron-encoded metallo-β-lactamase.

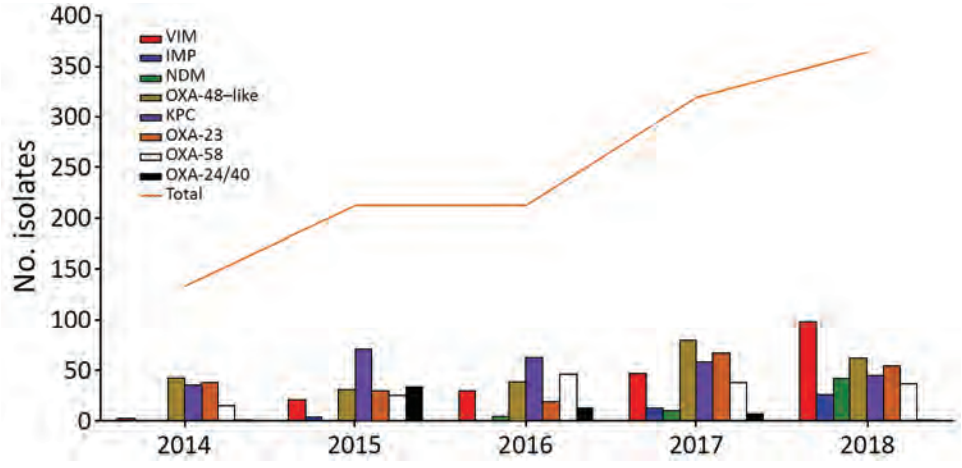

Figure 1. Distribution of carbapenemase types recovered in Andalusia, 2014–2018. IMP, imipenemase; KPC, *Klebsiella pneumoniae* carbapenemase; MBL, metallo-β-lactamases; NDM, New Delhi metallo-beta-lactamase; OXA, oxacillinases; VIM, Verona integron-encoded metallo-β-lactamase.

followed by OXA-48–like in 23 and MBL in 18 (Appendix Figure). Sequence type was available for 1,181 of 1,243 (95%) isolates. Some circulating high-risk clones were detected in *K. pneumoniae*, *E. cloacae*, *Escherichia coli*, *A. baumannii*, and *P. aeruginosa*. The combinations of species, carbapenemase variants, and sequence types are listed in the Appendix Table.

Six isolates (0.5%) produced 2 types of carbapenemase: Five isolates combined VIM-1 with either OXA-48 (*K. oxytoca* ST206 and *E. cloacae* ST114), OXA-245 (*Citrobacter freundii* ST63), IMP-8 (*E. cloacae* ST242), or NDM-1 (*C. freundii* ST170). The remaining isolate was *E. coli* ST617 harboring NDM-5 and OXA-48. According to pulsed-field gel electrophoresis, 765 of 1,243 isolates (62%) were included in 23 clusters submitted from 22 hospitals (Figure 2).

Conclusions

Our results provide an overview of the molecular epidemiology of CPGNB in Andalusia. The predominance of *K. pneumoniae* as a producer of all classes of carbapenemases is noteworthy, reflecting its role in disseminating carbapenemases in the region. KPC-3 and OXA-48 were the carbapenemases most frequently detected. KPC-3 was almost exclusively associated with *K. pneumoniae* and importantly with high-risk clones ST512 and ST258 considered endemic in other European countries (*8*–*10*). Like KPC-3, OXA-48 was predominantly found in *K. pneumoniae*, but it began appearing in other species in 2018, which raises concerns about the control of this carbapenemase in the region. In addition, the high-risk clones of OXA-48–producing *K. pneumoniae*, ST11, ST15, ST392, ST307,

Table 2. Distribution of carbapenemases by species, Andalusia, Spain, 2014–2018*

	Species										
	K. p.	*K. o.*	*E. coli*	*Enterobacter cloacae*	*C. f.*	*C. a.*	*Pseudomonas aeruginosa*	*P. putida*	*Acinetobacter* spp.	*A. baumannii*	*K. a.*
VIM-1	33	77	8	33	8	1	1	5	1	0	0
VIM-2	0	0	0	0	0	0	29	1	0	0	0
IMP-8	2	0	1	6	1	0	14	0	0	0	0
IMP-16	0	0	0	0	0	0	9	0	0	0	0
IMP-23	0	0	0	0	0	0	7	0	0	0	0
NDM-1	6	0	0	2	0	0	0	0	1	3	0
NDM-7	39	0	1	0	0	0	0	0	0	0	0
NDM-5	0	0	4	0	0	0	0	0	0	0	0
IMP-22	0	0	0	1	0	0	0	0	0	0	0
KPC-3	248	0	0	1	0	0	0	0	0	0	0
KPC-2	10	2	3	6	1	0	0	0	0	0	0
OXA-48	205	4	12	7	4	0	0	0	0	0	4
OXA-23	0	0	0	0	0	0	0	0	0	208	0
OXA-58	0	0	0	0	0	0	0	0	0	160	0
OXA-24/40	0	0	0	0	0	0	0	0	0	54	0
OXA-245	15	0	1	0	1	0	0	0	0	0	0
OXA-181	1	0	0	0	0	0	0	0	0	0	0
KPC-31	1	0	0	0	0	0	0	0	0	0	0
IMI-1	0	0	0	1	0	0	0	0	0	0	0
Total	560	83	30	57	15	1	60	6	2	425	4

**C. f.*, *Citrobacter freundii*; *C. a.*, *Citrobacter amalonaticus*; *E.*, *Escherichia*; *K. a.*, *Klebsiella aerogenes*; *K. o.*, *K. oxytoca*; *K. p.*, *Klebsiella pneumoniae*. IMP, imipenemase; KPC, *Klebsiella pneumoniae* carbapenemase; MBL, metallo-β-lactamases; NDM, New Delhi metallo-beta-lactamase; OXA, oxacillinases; VIM, Verona integron-encoded metallo-β-lactamase.

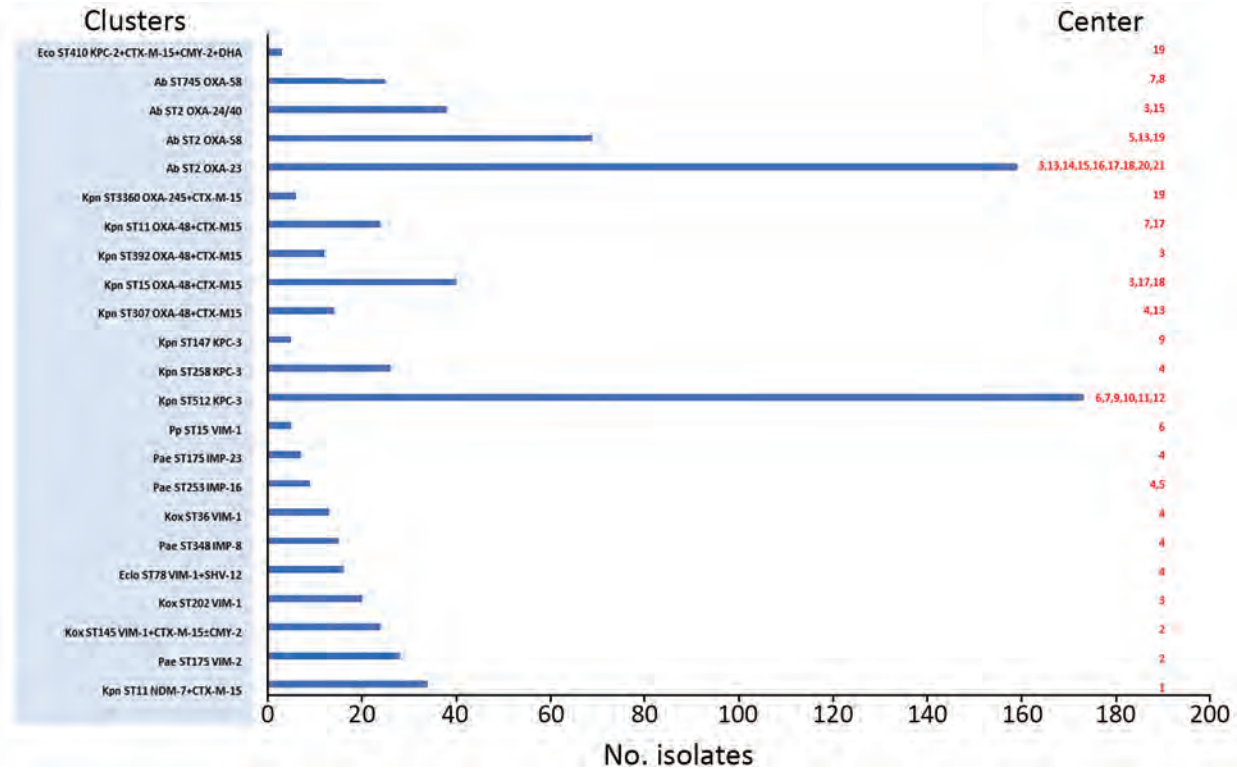

Figure 2. Characteristics of clusters of carbapenemase-producing gram negative bacteria, Andalusia, 2014–2018. Hospitals are identified by number: Almería ,1, 2, 5; Cádiz, 7, 8, 9; Córdoba, 6, 11, 12; Granada, 4, 13; Huelva, 20; Jaén, 10, 21; Málaga, 17, 18, 19; Sevilla, 3, 14, 15, 16. Ab, *Acinetobacter baumannii*; CTX-M, Cefotaximase-Munich; Eclo, *Enterobacter cloacae*; IMP, imipenemase; Kox, *Klebsiella oxytoca*; KPC, *Klebsiella pneumoniae* carbapenemase; Kpn, *Klebsiella pneumoniae*; MBL, metallo-β-lactamases; NDM, New Delhi metallo-beta-lactamase; OXA, oxacillinases; Pae, *Pseudomonas aeruginosa*; Pp, *Pseudomonas putida*; ST, sequence type; VIM, Verona integron-encoded metallo-β-lactamase.

differed from those for KPC-3, showing that specific clones have a role in the dissemination of specific carbapenemases in this region.

We found a significant temporal change in the epidemiology of MBL with a clear upward trend associated with several outbreaks in 2018. Findings from recent studies from Spain reflect the emergence of MBL in different CPGNB species (*4*,*11*,*12*). VIM was the MBL most frequently detected and, most of the VIM-producing bacteria were detected as part of clusters. IMP was almost exclusively found in *P. aeruginosa* isolates, showing the importance of this species in the dissemination of this carbapenemase; it was associated with different clusters in a single hospital and each variant was associated with a specific clone: IMP-8/ST348, IMP-23/ST175 and IMP-16/ST253. An increase in NDM was observed in 2018 associated with a large outbreak produced by *K. pneumoniae* ST11 NDM-7 in a single hospital.

In *A. baumanni*, OXA-23 and OXA-58 were the most common carbapenemases. ST2 was the predominant clone according to previous studies (*13*). A remarkable finding was the detection of *A. baumannii* ST85 harboring NDM-1 for the first time in Spain (*14*). The increase of carbapenemases in *E. coli* is a finding that could have epidemiologic significance because *E. coli* spread in the community more readily than other species and could begin to establish carbapenemases in the community. It is also remarkable that 7 of 23 clusters were detected in the same hospital, reflecting the burden of antimicrobial resistance in this hospital. This issue remains serious, and additional efforts for infection control should be made.

One limitation of this work is that, because submission of isolates is not mandatory, underreporting is likely. Nevertheless, we have evidence that most relevant isolates are routinely submitted. Furthermore, this study reinforces the importance of submitting all multidrug-resistant isolates to a reference laboratory because the information provided using molecular techniques makes the rapid detection of clusters and high-risk clones possible, which in turn, contributes to the success of infection prevention and control programs.

In summary, our study shows dissemination and establishment of CPGNB in Andalusia, including high-risk clones of different species. These findings demonstrate the importance of continuing surveillance programs and epidemiologic studies to detect and investigate the spread of carbapenemase-producing bacteria, particularly in Andalusia, which is a region predisposed to the introduction of new lineages because of tourism and migration pathways.

About the Author

Dr. López-Hernández is a clinical microbiologist in the Unit of Infectious Diseases and Clinical Microbiology of the Virgen Macarena University Hospital, Seville, Spain. Her research interest is antimicrobial resistance mechanisms in bacteria.

References

1. Pérez-Vazquez M, Oteo-Iglesias J, Sola-Campoy PJ, Carrizo-Manzoni H, Bautista V, Lara N, et al.; Spanish Antibiotic Resistance Surveillance Program Collaborating Group. Characterization of carbapenemase-producing *Klebsiella oxytoca* in Spain, 2016–2017. Antimicrob Agents Chemother. 2019;63:e02529–18. https://doi.org/10.1128/AAC.02529-18
2. Arana DM, Ortega A, González-Barberá E, Lara N, Bautista V, Gómez-Ruíz D, et al.; Spanish Antibiotic Resistance Surveillance Programme Collaborating Group. Carbapenem-resistant *Citrobacter* spp. isolated in Spain from 2013 to 2015 produced a variety of carbapenemases including VIM-1, OXA-48, KPC-2, NDM-1 and VIM-2. J Antimicrob Chemother. 2017;72:3283–7. https://doi.org/10.1093/jac/dkx325
3. Del Barrio-Tofiño E, Zamorano L, Cortes-Lara S, López-Causapé C, Sánchez-Diener I, Cabot G, et al.; GEMARA-SEIMC/REIPI Pseudomonas study Group. Spanish nationwide survey on *Pseudomonas aeruginosa* antimicrobial resistance mechanisms and epidemiology. J Antimicrob Chemother. 2019;74:1825–35. https://doi.org/10.1093/jac/dkz147
4. Nowak J, Zander E, Stefanik D, Higgins PG, Roca I, Vila J, et al.; MagicBullet Working Group WP4. High incidence of pandrug-resistant *Acinetobacter baumannii* isolates collected from patients with ventilator-associated pneumonia in Greece, Italy and Spain as part of the MagicBullet clinical trial. J Antimicrob Chemother. 2017;72:3277–82. https://doi.org/10.1093/jac/dkx322
5. García-Castillo M, García-Fernández S, Gómez-Gil R, Pitart C, Oviaño M, Gracia-Ahufinger I, et al.; iCREST Study Group. Activity of ceftazidime-avibactam against carbapenemase-producing Enterobacteriaceae from urine specimens obtained during the infection-carbapenem resistance evaluation surveillance trial (iCREST) in Spain. Int J Antimicrob Agents. 2018;51:511–5. https://doi.org/10.1016/j.ijantimicag.2018.01.011
6. EUCAST Guidelines for detection of resistance mechanisms and specific resistances of clinical and/or epidemiological importance, version 2.0 [cited 2 Jan 2018]. http://www.eucast.org/fileadmin/src/media/PDFs/EUCAST_files/Resistance_mechanisms/EUCAST_detection_of_resistance_mechanisms_170711.pdf
7. EUCAST. Breakpoint tables for interpretation of MICs and zone diameters, version 8.0, 2018 [cited 11 July 2017]. http://www.eucast.org/fileadmin/src/media/PDFs/EUCAST_files/Breakpoint_tables/v_8.1_Breakpoint_Tables.pdf
8. David S, Reuter S, Harris SR, Glasner C, Feltwell T, Argimon S, et al.; EuSCAPE Working Group; ESGEM Study Group. Epidemic of carbapenem-resistant *Klebsiella pneumoniae* in Europe is driven by nosocomial spread. Nat Microbiol. 2019;4:1919–29. https://doi.org/10.1038/s41564-019-0492-8
9. Ferrari C, Corbella M, Gaiarsa S, Comandatore F, Scaltriti E, Bandi C, et al. Multiple *Klebsiella pneumoniae* KPC clones contribute to an extended hospital outbreak. Front Microbiol. 2019;10:2767. https://doi.org/10.3389/fmicb.2019.02767
10. Becker L, Kaase M, Pfeifer Y, Fuchs S, Reuss A, von Laer A, et al. Genome-based analysis of carbapenemase-producing *Klebsiella pneumoniae* isolates from German hospital patients, 2008–2014. Antimicrob Resist Infect Control. 2018;7:62. https://doi.org/10.1186/s13756-018-0352-y
11. Espinal P, Miró E, Segura C, Gómez L, Plasencia V, Coll P, et al. First description of bla_{NDM-7} carried on an IncX4 plasmid in *Escherichia coli* ST679 isolated in Spain. Microb Drug Resist. 2018;24:113–9. https://doi.org/10.1089/mdr.2017.0039
12. Villa J, Carretero O, Viedma E, Lora-Tamayo J, Mingorance J, Chaves F. Emergence of NDM-7-producing multi-drug-resistant *Enterobacter hormaechei* sequence type ST-78 in Spain: a high-risk international clone. Int J Antimicrob Agents. 2019;53:533–4. https://doi.org/10.1016/j.ijantimicag.2018.11.009
13. Hamidian M, Nigro SJ. Emergence, molecular mechanisms and global spread of carbapenem-resistant *Acinetobacter baumannii*. Microb Genom. 2019;5:5. https://doi.org/10.1099/mgen.0.000306
14. Fernández-Cuenca F, Pérez-Palacios P, Galán-Sánchez F, López-Cerero L, López-Hernández I, López Rojas R, et al. First identification of bla_{NDM-1} carbapenemase in bla_{OXA-94}-producing *Acinetobacter baumannii* ST85 in Spain. Enferm Infecc Microbiol Clin. 2020;38:11–5. https://doi.org/10.1016/j.eimc.2019.03.008

Address for correspondence: I. López-Hernández, Department of Microbiology, School of Medicine, Av Sánchez Pizjuán s/n, 41009, Seville, Spain; email: inlopezh@us.es

Identification of *Streptococcus suis* Meningitis by Direct Triplex Real-Time PCR, Burkina Faso

Mahamoudou Ouattara, Mamadou Tamboura, Dinanibe Kambire, Mahamoudou Sanou, Kalifa Ouattara, Malika Congo, Adama Kaboré, Soufiane Sanou, Elie Kabré, Sable Sharpley, Theresa Tran, Stephanie Schwartz, Soumeya Ouangraoua, Abdoul-salam Ouedraogo, Lassana Sangaré, Rasmata Ouedraogo-Traore, Cynthia G. Whitney, Bernard Beall

Meningitis confirmation in Burkina Faso uses PCR for detecting *Streptococcus pneumoniae*, *Neisseria meningitidis*, or *Hemophilus influenzae*. We identified 38 cases of meningitis among 590 that were PCR-positive for 3 nonpneumococcal streptococcal pathogens, including 21 cases of *Streptococcus suis.* Among the country's 13 regions, 10 had *S. suis*–positive cases.

Streptococcus suis is a commensal organism of the upper respiratory tract of pigs that can occasionally cause severe invasive infections in these animals (*1*,*2*). The bacterium also can infect humans who have close contact with pigs or pork products, leading to serious diseases such as meningitis, endocarditis, and sepsis (*3*). *S. suis* can survive in dust, manure, and pig carcasses for days or even weeks under optimal conditions; therefore, the working environments in slaughterhouses and farms can be a source of human infection (*3*,*4*). Meningitis is the most common clinical manifestation of *S. suis* infection in humans and has an estimated case-fatality rate of 3% (*2*). Whereas this zoonotic pathogen is among the leading causes of adult meningitis in some countries of Southeast Asia (*5*), its incidence in Africa is largely unknown. We report 21 retrospectively confirmed cases of *S. suis* meningitis in Burkina Faso.

Author affiliations: Centers for Disease Control and Prevention, Atlanta, Georgia, USA (M. Ouattara, S. Sharpley, T. Tran, S. Schwartz, C.G. Whitney, B. Beall); Centre Hospitalier Universitaire Pédiatrique Charles de Gaulle, Ouagadougou, Burkina Faso (M. Tamboura, D. Kambire, M. Sanou, R. Ouedraogo-Traore); Centre Hospitalier Universitaire Yalgado Ouédraogo, Ouagadougou (K. Ouattara, M. Congo, L. Sangaré); Centre Hospitalier Universitaire Sanon-Sourô, Bobo-Dioulasso, Burkina Faso (A. Kaboré, S. Sanou, A-s, Ouedraogo); Centre-Muraz, Bobo-Dioulasso (E. Kabré, S. Ouangraoua)

DOI: https://doi.org/10.3201/eid2609.200203

The Study

Burkina Faso conducts nationwide case-based surveillance for bacterial meningitis. Cerebrospinal fluid (CSF) samples collected from patients with suspected meningitis are sent to 1 of 5 national laboratories for confirmation by culture and real-time PCR testing (*6*). Because of multiple challenges encountered by the laboratories in isolating bacteria from CSF, the confirmation of meningitis cases relies heavily on molecular detection (*6*). The real-time PCR assay currently used at the national laboratories only detects *Streptococcus pneumoniae*, *Neisseria meningitidis*, and *Haemophilus influenzae*. Between 2015 and 2018, the national laboratories tested 7,174 CSF samples from patients with suspected meningitis nationwide. Of these, 4,930 (68.7%) were PCR-negative for *S. pneumoniae*, *N. meningitidis*, and *H. influenzae*. To further investigate suspected meningitis cases that were PCR-negative after testing for the 3 pathogens, a subset of specimens was selected for additional screening based on leukocytes counts ≥50 cells/mm^3. In total, 912 PCR-negative specimens were available for the study; among these, 590 fit the selection criteria. The specimens were retested by using a triplex direct real-time PCR that was designed for the simultaneous detection of *Streptococcus agalactiae* (group B *Streptococcus* [GBS]), *S. pyogenes* (group A *Streptococcus* [GAS]), and *S. suis*. The nucleotide sequences and final concentrations of the primers and probes used in this assay (Table 1) were identical to those used in singleplex real-time PCR methods (*7*–*10*), with the exception that FAM was replaced by HEX as the reporter dye for *cfb*-specific probes for the GBS target and by Cy5 as the reporter dye for *spy*-specific probes for the GAS target. Each reaction was prepared in a final volume of 25 μL, including 1 μL of each primer and probe, 2 μL of CSF as DNA template, 12.5 μL of PerfeCta MultiPlex qPCR ToughMix mastermix (QuantaBio, https://www.quantabio.com),

Table 1. Sequences and concentrations of primers and probes used to detect *Streptococcus suis*, *S. agalactiae*, and *S. pyogenes*, Burkina Faso*

Target gene	Forward primer, 5′ → 3′	Reverse primer, 5′ → 3′	Probe, 5′ → 3′	Concentration of oligo per reaction, nM†
cfb (*7*), GBS	GGGAACAGATTATGAAAAACCG	AAGGCTTCTACACGACTACCAA	AGACTTCATTGCGTGCCAACCCTGAGAC 5′-HEX; 3′-BHQ1	200/200/200
fbpS (*8*), *S. suis*	TCCRATRCTGCTCTGCCATT	TGATAGTAGAAGTCCAGCARACT	AATAGCCC"T"GAAAAMCAGCCACWYTTTGARA 5′-FAM; 3′-SpC6; "T" = BHQ1	200/200/100
spy (*9*), GAS	GCACTCGCTACTATTTCTTACCTCAA	GTCACAATGTCTTGGAAACCAGTAAT	CCGCAAC"T"CATCAAGGATTTCGTTACCA 5′-Cy-5; 3′- SpC6; "T" = BHQ2	300/300/100
RNaseP (*10*)	AGATTTGGACCTGCGAGCG	GAGCGGCTGTCCCACAAGT	TTCTGACCTGAAGGCTCTGCGCG 5′-FAM; 3′-BHQ1	400/400/100

*GAS, group A *Streptococcus* (*Streptococcus pyogenes*); GBS, group A *Streptococcus* (*S. agalactiae*); RNaseP, human ribonuclease P.
†Concentration of forward primer/reverse primer/probe.

and 1.5 μL of PCR-grade water. The thermal profile for the real-time PCR runs was 1 cycle of 55°C for 5 min, 1 cycle of 95°C for 10 min, then 40 cycles of 95°C for 15 s and 60°C for 1 min. All specimens were tested by real-time PCR for the presence of the human ribonuclease P (RNaseP) gene to check for the presence of inhibitors. A specimen was considered positive if the cycle threshold (C_t) for 1 of the bacterial targets was ≤35 and was considered negative if the C_t was ≥40 for all bacterial targets with C_t ≤35 for RNaseP. If C_t was between 35 and 40 for the bacterial targets and ≤35 for RNaseP, the specimen is retested; if the result was reproducible, it was considered positive. The lower limits of detection (LLDs) were determined as previously described (*11*). The LLD of the direct triplex assay (3 CFU/μL for *S. suis*, 28 CFU/μL for GBS, and 26 CFU/μL for GAS) were compared with the LLD of the triplex assay conducted on DNA extracted from the same serial dilutions (2 CFU/μL for *S. suis*, 5 CFU/μL for GBS, and 3 CFU/μL for GAS).

Among the specimens tested, 21 were positive for *S. suis*, 13 for GAS, and 4 for GBS (Table 2). Of the 21 *S. suis*–positive case-patients, 1 was 4 years of age, 3 were 5–14 years of age, 2 were 15–29 years of age, 9 were 30–49 years of age, and 6 were ≥50 years of age; 16 (76.2%) were male and 5 (23.8%) were female. Two (9.5%) patients died, 14 recovered, and the outcome for 5 was unknown. Eight (61.5%) of the GAS-positive case-patients were <5 years of age and 5 were 5–14 years of age; 1 (7.7%) patient died, 5 recovered, and the outcome for 7 was unknown. All the GBS-positive case-patients were ≤6 months of age and all recovered. Median time from symptom onset to CSF collection was 2 days (range 1–10 days) for all the patients.

S. suis–positive cases were found among specimens from rural districts in 10/13 regions of the country with 28% (6/21) from the Centre-Est Region and 19% (4/21) from the Plateau Central Region. All adults with *S. suis* were farmers. Because of the retrospective detection of the etiology, the extent of any direct exposure of the *S. suis*–positive patients to pigs or pork products was unknown and attempts to collect additional information from the patients or their families were unsuccessful.

Table 2. Characteristics of patients with meningitis caused by *Streptococcus suis*, *S. pyogenes*, and *S. agalactiae*, Burkina Faso, 2015–2018*

Characteristics	Patients infected, no. (%)			All patients, no. (%), n = 590
	S. suis, n = 21	*S. pyogenes*, n = 13	*S. agalactiae*, n = 4	
Age, y				
<5	1 (4.8)	8 (61.5)	4 (100)	307 (52)
5–14	3 (14.3)	5 (38.5)	0	168 (28.5)
15–29	2 (9.5)	0	0	64 (10.8)
30–49	9 (42.8)	0	0	37 (6.3)
≥50	6 (28.6)	0	0	14 (2.4)
Sex				
M	16 (76.2)	9 (69.2)	2 (50)	332 (56.3)
F	5 (23.8)	4 (30.8)	2 (50)	258 (43.7)
Year CSF collected				
2015	5 (23.8)	1 (7.7)	0	87 (14.7)
2016	2 (9.5)	2 (15.4)	0	104 (17.6)
2017	6 (28.6)	3 (23.1)	2 (50)	195 (33.1)
2018	8 (38.1)	7 (53.8)	2 (50)	204 (34.6)
Median leukocytes, cells/mm^3 (range)	400 (51–6,250)	1,000 (53–8,000)	1,100 (800–2,400)	920 (50–8,000)
Median C_t (range)	26.1 (18.13–35.52)	25.33 (14.78–34.71)	23.47 (17.24–24.23)	25.33 (14.78–35.52)

*CSF, cerebrospinal fluid; C_t, cycle threshold.

Small-scale pig farming is a major economic activity in most parts of Burkina Faso. Although porcine-related occupations, undercooked pork consumption, and exposure to pigs have been identified as major risk factors for *S. suis* infection (*5*), its occurrence in a wide range of animal species have been reported (*2*).

DNA extracted from the *S. suis*–positive specimens were used for a multiplex conventional PCR for serotype detection (*12*). All the specimens were serotype 2 or 1/2 because the method used here could not clearly differentiate serotypes 2 and 1/2. Bacterial isolates from these cases were not available for further characterization. Serotype 2 is believed to cause 74%–95% of human cases of *S. suis* infections reported worldwide, but serotype 1/2 has not been reported to cause disease in humans (*1*,*2*).

Conclusions

Limited data are available regarding the incidence of streptococcal infections in Africa, and the disease burden likely is underestimated, especially for disease caused by *S. suis*. Two reported studies conducted in Togo identified 16 human cases of *S. suis* meningitis during 2010–2015 caused by serotype 2 (*13*,*14*). Another recent study in Madagascar described 2 human cases of *S. suis* meningitis, also caused by serotype 2 (*15*).

Our study reports 21 cases of *S. suis* meningitis from 2015–2018 in Burkina Faso. *S. suis* infections more commonly are observed in adult males and are directly correlated with occupational exposure to pigs or pork products (*2*,*13*,*15*). All adult cases reported here were farmers, although their exposure to pigs or pork was unknown. The presence of children among the patients in this study and in previous studies (*13*) indicates that older children also should be considered at risk. Finding 21 cases of this outbreak-prone zoonotic pathogen in this study raises concern about the incidence of *S. suis* disease in Burkina Faso and in other parts of Africa where pigs are raised. Prospective surveillance for *S. suis* could help identify farming communities where measures to prevent disease and its potential socioeconomic damages are needed.

About the Author

Dr. Ouattara is a microbiologist in the *Streptococcus* Laboratory, National Center for Immunization and Respiratory Diseases, Centers for Disease Control and Prevention, Atlanta, Georgia, USA. His primary research interests include meningitis, invasive streptococcal diseases, bacterial pathogenesis, and global laboratory capacity building.

References

1. Goyette-Desjardins G, Auger JP, Xu J, Segura M, Gottschalk M. *Streptococcus suis*, an important pig pathogen and emerging zoonotic agent-an update on the worldwide distribution based on serotyping and sequence typing. Emerg Microbes Infect. 2014;3:e45. https://doi.org/10.1038/emi.2014.45
2. Dutkiewicz J, Sroka J, Zając V, Wasiński B, Cisak E, Sawczyn A, et al. *Streptococcus suis*: a re-emerging pathogen associated with occupational exposure to pigs or pork products. Part I—epidemiology. Ann Agric Environ Med. 2017;24:683–95. https://doi.org/10.26444/aaem/79813
3. Gottschalk M, Xu J, Calzas C, Segura M. *Streptococcus suis*: a new emerging or an old neglected zoonotic pathogen? Future Microbiol. 2010;5:371–91. https://doi.org/10.2217/fmb.10.2
4. Strangmann E, Fröleke H, Kohse KP. Septic shock caused by *Streptococcus suis*: case report and investigation of a risk group. Int J Hyg Environ Health. 2002;205:385–92. https://doi.org/10.1078/1438-4639-00165
5. Mai NTH, Hoa NT, Nga TVT, Linh LD, Chau TTH, Sinh DX, et al. *Streptococcus suis* meningitis in adults in Vietnam. Clin Infect Dis. 2008;46:659–67. https://doi.org/10.1086/527385
6. Kambiré D, Soeters HM, Ouédraogo-Traoré R, Medah I, Sangare L, Yaméogo I, et al.; MenAfriNet Consortium. Nationwide trends in bacterial meningitis before the introduction of 13-valent pneumococcal conjugate vaccine–Burkina Faso, 2011–2013. PLoS One. 2016;11:e0166384. https://doi.org/10.1371/journal.pone.0166384
7. Diaz MH, Waller JL, Napoliello RA, Islam MS, Wolff BJ, Burken DJ, et al. Optimization of multiple pathogen detection using the TaqMan array card: application for a population-based study of neonatal infection. PLoS One. 2013;8:e66183. https://doi.org/10.1371/journal.pone.0066183
8. Srinivasan V, McGee L, Njanpop-Lafourcade BM, Moïsi J, Beall B. Species-specific real-time PCR assay for the detection of *Streptococcus suis* from clinical specimens. Diagn Microbiol Infect Dis. 2016;85:131–2. https://doi.org/10.1016/j.diagmicrobio.2016.02.013
9. Kodani M, Yang G, Conklin LM, Travis TC, Whitney CG, Anderson LJ, et al. Application of TaqMan low-density arrays for simultaneous detection of multiple respiratory pathogens. J Clin Microbiol. 2011;49:2175–82. https://doi.org/10.1128/JCM.02270-10
10. Emery SL, Erdman DD, Bowen MD, Newton BR, Winchell JM, Meyer RF, et al. Real-time reverse transcription-polymerase chain reaction assay for SARS-associated coronavirus. Emerg Infect Dis. 2004;10:311–6. https://doi.org/10.3201/eid1002.030759
11. Ouattara M, Whaley MJ, Jenkins LT, Schwartz SB, Traore RO, Diarra S, et al. Triplex real-time PCR assay for the detection of *Streptococcus pneumoniae, Neisseria meningitidis* and *Haemophilus influenzae* directly from clinical specimens without extraction of DNA. Diagn Microbiol Infect Dis. 2018. https://doi.org/10.1016/j.diagmicrobio.2018.10.008
12. Kerdsin A, Akeda Y, Hatrongjit R, Detchawna U, Sekizaki T, Hamada S, et al. *Streptococcus suis* serotyping by a new multiplex PCR. J Med Microbiol. 2014;63:824–30. https://doi.org/10.1099/jmm.0.069757-0
13. Tall H, Njanpop-Lafourcade BM, Mounkoro D, Tidjani L, Agbenoko K, Alassani I, et al. Identification of *Streptococcus suis* meningitis through population-based surveillance, Togo, 2010–2014. Emerg Infect Dis. 2016;22:1262–4. https://doi.org/10.3201/eid2207.151511

14. Prince-David M, Salou M, Marois-Créhan C, Assogba K, Plainvert C, Balogou KA, et al. Human meningitis due to *Streptococcus suis* in Lomé, Togo: a case report. BMC Infect Dis. 2016;16:651. https://doi.org/10.1186/s12879-016-2006-0
15. Raberahona M, Rasoanandrasana S, Rahajamanana VL, Ranaivo-Rabetokotany F, Andriananja V, Rakotomalala FA, et al. Novel *Streptococcus suis* sequence type 834 among humans, Madagascar. Emerg Infect Dis. 2018;24:391–2. https://doi.org/10.3201/eid2402.171138

Address for correspondence: Mahamoudou Ouattara, Centers for Disease Control and Prevention, 1600 Clifton Rd NE, Mailstop H18-B, Atlanta, GA 30329-4027, USA; email: mouattara1@cdc.gov

Enterovirus D68 Subclade B3 in Children with Acute Flaccid Paralysis in West Africa, 2016

Amary Fall, Ndack Ndiaye, Kevin Messacar, Ousmane Kebe, Mamadou Malado Jallow, Hamid Harouna, Davy Evrard Kiori, Sara Sy, Déborah Goudiaby, Mohamed Dia, Mbayame Ndiaye Niang, Kader Ndiaye, Ndongo Dia

We tested for enterovirus D68 in fecal samples collected during June–September 2016 from 567 patients with acute flaccid paralysis in 7 West Africa nations. Children <5 years old comprised 64.3% of enterovirus D68 positive patients. Our findings emphasize the need for active surveillance for acute flaccid myelitis.

Until 2014, enterovirus D68 (EV-D68) infections had been identified only sporadically after its discovery in 1962, but since 2014, the virus has emerged to cause large outbreaks of respiratory disease worldwide. In recent years, EV-D68 has been reported in outbreaks in the United States, Canada, Europe, Asia, and Africa, affecting ≥2,287 persons worldwide (*1*–*4*).

The 2014 EV-D68 outbreak coincided temporally and geographically with increases in cases of acute flaccid myelitis (AFM), a subtype of acute flaccid paralysis (AFP), described by the Centers for Disease Control and Prevention as acute-onset flaccid weakness, combined with spinal cord lesions confirmed by magnetic resonance imaging, largely restricted to the gray matter, and spanning ≥1 spinal segments (*5*). In 2014, a total of 120 AFM cases in the United States (*4*,*6*) and ≥6 in Europe were associated with EV-D68 outbreaks. Subsequent biennial circulation of EV-D68 was associated with surges in AFM cases in the United States in 2016 and 2018 (*7*). In addition, 29 EV-D68–associated AFM cases were reported in Europe in 2016 (*8*). Africa, unlike Europe and the United States, has no active AFM surveillance. However, a 2016 study in Senegal reported 4 cases of paralysis associated with EV-D68 identified in fecal samples from children with AFP (*2*). With no AFM- or AFP-specific surveillance data available, we analyzed fecal samples collected for polio surveillance to better understand the extent of EV-D68 associated with AFP in West Africa and the genetic diversity of identified strains.

Author affiliations: Institute Pasteur Dakar, Senegal (A. Fall, N. Ndiaye, O. Kebe, M.M. Jallow, D.E. Kiori, S. Sy, D. Goudiaby, M. Dia, M.N. Niang, K. Ndiaye, N. Dia); University of Colorado, Aurora, Colorado, USA (K. Messacar); Ministère de la Santé Publique, Niamey, Niger (H. Harouna)

DOI: https://doi.org/10.3201/eid2609.200312

The Study

We retrospectively tested for EV-D68 in fecal samples from patients <15 years old with AFP. The samples were collected during June–September 2016 as part of routine poliomyelitis surveillance in Niger, Senegal, Guinea, Mauritania, Gambia, Guinea-Bissau, and Cape Verde. Specimens were collected 24–48 hours apart and ≤14 days of paralysis onset. We inoculated fecal specimens onto human rhabdomyosarcoma cells after using chloroform for EV isolation according to the procedures described in the laboratory manual for the World Health Organization's Global Polio Laboratory Network (http://polioeradication.org/wp-content/uploads/2017/05/Polio_Lab_Manual04.pdf). We used a QIAmp Viral RNA Mini Kit (QIAGEN, https://www.qiagen.com) to extract RNA from 200 µL clarified fecal suspensions pretreated with

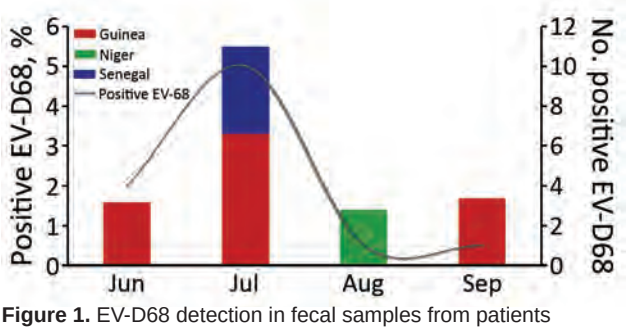

Figure 1. EV-D68 detection in fecal samples from patients with acute flaccid paralysis in 3 West Africa countries, June to September 2016. EV-D68, enterovirus D68.

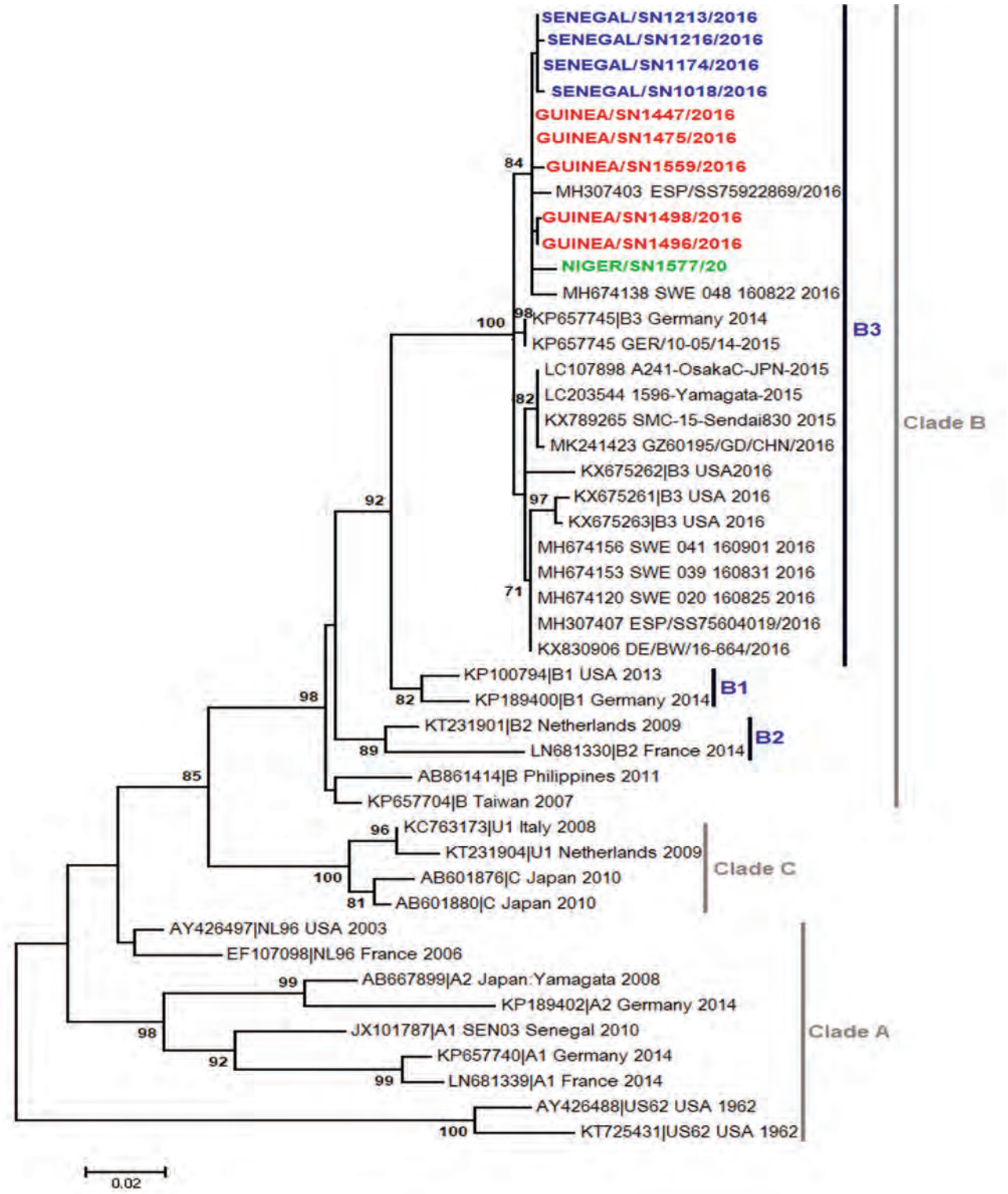

Figure 2. Phylogenetic relationships among EV-D68 strains detected in Guinea (red), Niger (green), and Senegal (blue), June–September 2016. We used the maximum-likelihood method based on the Tamura-Nei model method in MEGA7 (http://www.megasoftware.net) to generate the phylogenetic tree constructed on the viral protein 1 region of EV-D68 strains. Sequences are identified by GenBank accession number, country, and period of detection. The phylogenetic tree is rooted by the oldest EV-D68 sequence in GenBank, the Fermon strain. We performed 1,000 bootstrap replications to determine the consensus tree; support for nodes present in >70% of the trees are annotated. EV-D68, enterovirus D68.

chloroform. After RNA extraction, we screened all samples for EV-D68 by real time reverse transcription PCR as described elsewhere (*2*). For molecular characterization, the viral protein 1 region was amplified by a nested PCR and sequenced as described elsewhere (*2*). The alignment and phylogenic analyses of sequences obtained after cleaning were performed using MEGA 7.0 software (https://www.megasoftware.net).

We tested for EV-D68 in 567 fecal samples collected from 7 countries in West Africa: Cape Verde (n = 1), Gambia (n = 6), Guinea-Bissau (n = 5), Guinea Conakry (n = 391), Mauritania (n = 20), Niger (n = 85), and Senegal (n = 59), during June–September 2016. EV-D68 was detected in 16 (2.8%) patients from 3 countries: Guinea (11/391), Niger (1/85), and Senegal (4/59). The detection of EV-D68 in fecal samples from AFP patients in West Africa countries is consistent with case reports and case series from the United States, South America, Asia, and Europe during the same period (*7*–*11*).

The first EV-D68–associated AFP case was detected in Guinea in June 2016. Most cases (10/16) in West Africa in 2016 were detected during July (Figure 1), similar to the seasonality that has been observed in several other countries, including the United States (*12*), the Netherlands (*13*), and Senegal (*3*). Most EV-D68–positive patients (64.3%) were children <5 years old, consistent with our previous report from Senegal (*2*,*3*). BLAST analysis (https://blast.ncbi.nlm.nih.gov/Blast.cgi) showed that all sequenced EV-D68 strains shared >98% homology with strains detected in Spain, Sweden, Germany, Japan, and China. Phylogenetic analysis of the viral protein 1 fragment revealed that all sequences from West Africa belonged to clade B, subclade B3 (Figure 2). Indeed, EV-D68 subclade B3 was the predominant strain reported in several global regions during the same period (*9*–*14*). Moreover, results from phylogenetic testing showed that EV-D68 strains in West Africa clustered with strains circulating in Spain (GenBank accession no. MH307403) and Sweden (accession no. MH674138), with a bootstrap value of 97.

Our study has some limitations. One ongoing issue is the inability to accurately describe the flaccid paralysis syndrome. Radiography imaging will probably help distinguish AFM from other AFP conditions. In addition, detecting EV-D68 in feces does not prove a causal relationship with AFM, although in this study all of the fecal samples tested negative for poliovirus and other enteroviruses, ruling out those possible alternative diagnoses. The absence of EV-D68 positive patients from the other West Africa countries may be due to the small number of samples collected and screened during the study period. EV-D68 prevalence in West Africa might be higher if respiratory samples, known to yield higher EV-D68 counts than fecal samples, were used for screening (*6*,*14*). Recently, the Pan American Health Organization and the World Health Organization provided updated recommendations to include respiratory sampling in suspected AFP cases (*15*).

Conclusions

This study provides evidence of more widespread EV-D68 circulation in West Africa in 2016 than previously reported. Enhanced surveillance for EV-D68, including collecting respiratory specimens from patients with confirmed cases of AFM, is needed to improve our understanding of this disease and its burden. Phylogeographic and phylodynamic studies based on full genomes are needed to better understand the introduction of EV-D68 in Africa during these different outbreaks.

Acknowledgments

We thank Mohamed Salif Sylla, Dabo Moustapha, Djenou Sompare, and Kathleen Victoir (DI-IPP) and acknowledge the US Centers for Disease Control and Prevention for its unwavering support.

This study was supported by the US Department of Health and Human Services through grant number IDSEP140020-01-00 via the International Division of Pasteur Institutes.

About the Author

Dr. Fall is a postdoctoral student in the Department of Virology at the Pasteur Institute of Dakar. His research interest is the molecular characterization of noninfluenza respiratory viruses (mainly enterovirus, rhinoviruses, and respiratory syncytial virus) in pediatric populations in Senegal.

References

1. Kubi JA, Mutocheluh M, Bonney JHK, Ampofo WK, Odoom JK. Molecular detection of enterovirus D68 among children with acute respiratory tract infection in Ghana. Afr J Lab Med. 2019;8:732. https://doi.org/10.4102/ajlm.v8i1.732
2. Fall A, Ndiaye N, Jallow MM, Barry MA, Touré CSB, Kebe O, et al. Enterovirus D68 subclade B3 circulation in Senegal, 2016: detection from influenza-like illness and acute flaccid paralysis surveillance. Sci Rep. 2019;9:13881. https://doi.org/10.1038/s41598-019-50470-z

3. Fall A, Jallow MM, Kebe O, Kiori DE, Sy S, Goudiaby D, et al. Low circulation of subclade A1 enterovirus D68 strains in Senegal during 2014 North America outbreak. Emerg Infect Dis. 2019;25:1404–7. https://doi.org/10.3201/eid2507.181441
4. Dyda A, Stelzer-Braid S, Adam D, Chughtai AA, MacIntyre CR. The association between acute flaccid myelitis (AFM) and enterovirus D68 (EV-D68)—what is the evidence for causation? Euro Surveill. 2018;23. https://doi.org/10.2807/1560-7917.ES.2018.23.3.17-00310
5. Centers for Disease Control and Prevention. Revision to the standardized surveillance and case definition for acute flaccid myelitis. 2018 [cited 2020 May 25]. https://wwwn.cdc.gov/nndss/conditions/acute-flaccid-myelitis/case-definition/2018
6. Sejvar JJ, Lopez AS, Cortese MM, Leshem E, Pastula DM, Miller L, et al. Acute flaccid myelitis in the United States, August–December 2014: results of nationwide surveillance. Clin Infect Dis. 2016;63:737–45. https://doi.org/10.1093/cid/ciw372
7. Messacar K, Asturias EJ, Hixon AM, Van Leer-Buter C, Niesters HGM, Tyler KL, et al. Enterovirus D68 and acute flaccid myelitis—evaluating the evidence for causality. Lancet Infect Dis. 2018;18:e239–47. https://doi.org/10.1016/S1473-3099(18)30094-X
8. Knoester M, Helfferich J, Poelman R, Van Leer-Buter C, Brouwer OF, Niesters HGM; 2016 EV-D68 AFM Working Group. Twenty-nine cases of enterovirus-D68–associated acute flaccid myelitis in Europe 2016: a case series and epidemiologic overview. Pediatr Infect Dis J. 2019;38:16–21. https://doi.org/10.1097/INF.0000000000002188
9. Ruggieri V, Paz MI, Peretti MG, Rugilo C, Bologna R, Freire C, et al. Enterovirus D68 infection in a cluster of children with acute flaccid myelitis, Buenos Aires, Argentina, 2016. Eur J Paediatr Neurol. 2017;21:884–90. https://doi.org/10.1016/j.ejpn.2017.07.008
10. Hu YL, Chang LY. Current status of enterovirus D68 worldwide and in Taiwan. Pediatr Neonatol. 2019. https://doi.org/10.1016/j.pedneo.2019.09.007
11. Chen IJ, Hu SC, Hung KL, Lo CW. Acute flaccid myelitis associated with enterovirus D68 infection: a case report. Medicine. 2018;97:e11831. https://doi.org/10.1097/MD.0000000000011831
12. Wang G, Zhuge J, Huang W, Nolan SM, Gilrane VL, Yin C, et al. Enterovirus D68 subclade B3 strain circulating and causing an outbreak in the United States in 2016. Sci Rep. 2017;7:1242. https://doi.org/10.1038/s41598-017-01349-4
13. Knoester M, Schölvinck EH, Poelman R, Smit S, Vermont CL, Niesters HG, et al. Upsurge of enterovirus D68, the Netherlands, 2016. Emerg Infect Dis. 2017;23:140–3. https://doi.org/10.3201/eid2301.161313
14. Carballo CM, Erro MG, Sordelli N, Vazquez G, Mistchenko AS, Cejas C, et al. Acute flaccid myelitis associated with enterovirus D68 in children, Argentina, 2016. Emerg Infect Dis. 2019;25:573–6. https://doi.org/10.3201/eid2503.170897
15. Pan American Health Organization/World Health Organization. Epidemiological alert: acute flaccid myelitis associated with enterovirus D68. Washington (DC): The Organizations; 2017 Nov 1 [cited 2020 May 28]. https://www.paho.org/hq/dmdocuments/2017/2017-nov-01-epi-update-EV-D68.pdf

Address for correspondence: Ndongo Dia, Institut Pasteur Dakar, 36, Avenue Pasteur, B.P. 220, Dakar, Senegal; email: ndia@pasteur.sn

Fatal Measles Inclusion-Body Encephalitis in Adult with Untreated AIDS, France

Christophe Rodriguez, Meriadeg Ar Gouilh, Nicolas Weiss, Sébastian Stroer, Karima Mokhtari, Danielle Seilhean, Bertrand Mathon, Vanessa Demontant, Melissa N'Debi, Guillaume Gricourt, Paul-Louis Woerther, Jean-Michel Pawlotsky, Karl Stefic, Julien Marlet, Pierre-François Dequin, Antoine Guillon, Valérie Pourcher, David Boutolleau, Astrid Vabret, Sonia Burrel

We report a fatal case of measles inclusion-body encephalitis occurring in a woman from Romania with AIDS. After an extensive but unsuccessful diagnostic evaluation, a pan-pathogen shotgun metagenomic approach revealed a measles virus infection. We identified no mutations previously associated with neurovirulence.

We report a fatal case of measles inclusion-body encephalitis in a 28-year-old woman from Romania living in France who had untreated AIDS. She was initially admitted to the hospital on September 22, 2018 (day 0), for afebrile generalized motor seizure that began focally in the right lower limb. Results of magnetic resonance imaging (MRI) were initially unremarkable, but electroencephalogram (EEG) results showed slight abnormalities related to slow frontal activity. The patient recovered fully and was discharged with antiepileptic therapy. Of note, the patient had stopped antiretroviral therapy (ART) 1 year earlier and declined to restart therapy after this hospital admission.

Author affiliations: Henri Mondor Hospital, Assistance Publique des Hôpitaux de Paris, University of Paris-Est, Créteil, France (C. Rodriguez, V. Demontant, M. N'Debi, G. Gricourt, P.-L. Woerther, J.-M. Pawlotsky); National Reference Laboratory for Measles, Mumps, and Rubella, University Hospital of Caen, Normandie Université, Caen, France (M. Ar Gouilh, A. Vabret); Pitié-Salpêtrière Hospital, Assistance Publique des Hôpitaux de Paris, Sorbonne-Université, Paris, France (N. Weiss, S. Stroer, K. Mokhtari, D. Seilhean, B. Mathon, V. Pourcher, D. Boutolleau, S. Burrel); National Reference Center for Herpesviruses, Paris (D. Boutolleau, S. Burrel); University Hospital of Tours, University of Tours, Tours, France (K. Stefic, J. Marlet, P.-F. Dequin, A. Guillon); National Reference Center for HIV, Tours (K. Stefic, J. Marlet)

DOI: https://doi.org/10.3201/eid2609.200366

In the next week, she had several relapses of focal seizures, requiring hospital readmission on day 7. Despite antiepileptic therapy adjustments, the myoclonic seizures persisted and became resistant to high doses of anticonvulsants and clonazepam add-on therapy (day 31). Consequently, the patient was hospitalized in intensive care unit. EEG results showed a pattern of frontal-lobe epilepsy. MRI results showed hyperintense cortical signals in frontal and left temporal cortex without hemorrhage lesions and without any signs of cerebral venous thrombosis. Biologic investigation revealed HIV replication and 26/mm^3 CD4 T-cell count at day 35. We initiated antiretroviral medications on day 43.

During her hospitalization, the patient showed a gradual impairment of consciousness (Glasgow coma score 6 on day 61) and was mechanically ventilated. MRI results showed increase of the cortical hyperintensities, and EEG results showed diffuse encephalopathy pattern (Figure 1). We analyzed cerebrospinal fluid (CSF) samples taken on days 37, 62, and 64 for pathogens: viruses (herpes simplex virus, varicella zoster virus, enterovirus, cytomegalovirus, Epstein-Barr virus, human herpesvirus 6, HIV, and polyomavirus JC), bacterial and mycobacteria, fungi (*Aspergillus* spp., *Cryptococcus neoformans*), and parasites (*Toxoplasma gondii*); no pathogens were detected. All CSF were paucicellular with protein and glucose levels within reference levels. Results of testing for autoimmune antibodies were also negative.

We performed a brain biopsy of the left frontal lobe on day 71 to determine the cause of encephalitis by the underlying neurologic symptoms, abnormal imaging features, and biologic findings. Neuropathology analysis revealed scarce inflammatory activation of glial cells (Figure 2). Because all the first-line microbiology testing assays remained negative on the

biopsy, we considered using shotgun metagenomic (SMg) for panpathogen RNA/DNA detection to analyze the clinical samples with an unbiased approach. In brief, we performed an extraction combining bead beating and chemical and enzymatic lysis before library preparation. We performed sequencing on NextSeq500 with High Output Kit version 2.5 (300 cycles) (Illumina, https://www.illumina.com) (*1*). We analyzed sequencing data using MetaMIC software, which performed microorganism identification, genome reconstruction, and variant calling (*1*). A total of 5 samples were tested by SMg: CSF (day 61), bronchoalveolar lavage (days 63 and 76), brain biopsy (day 71), and whole blood (day 68). Only the brain

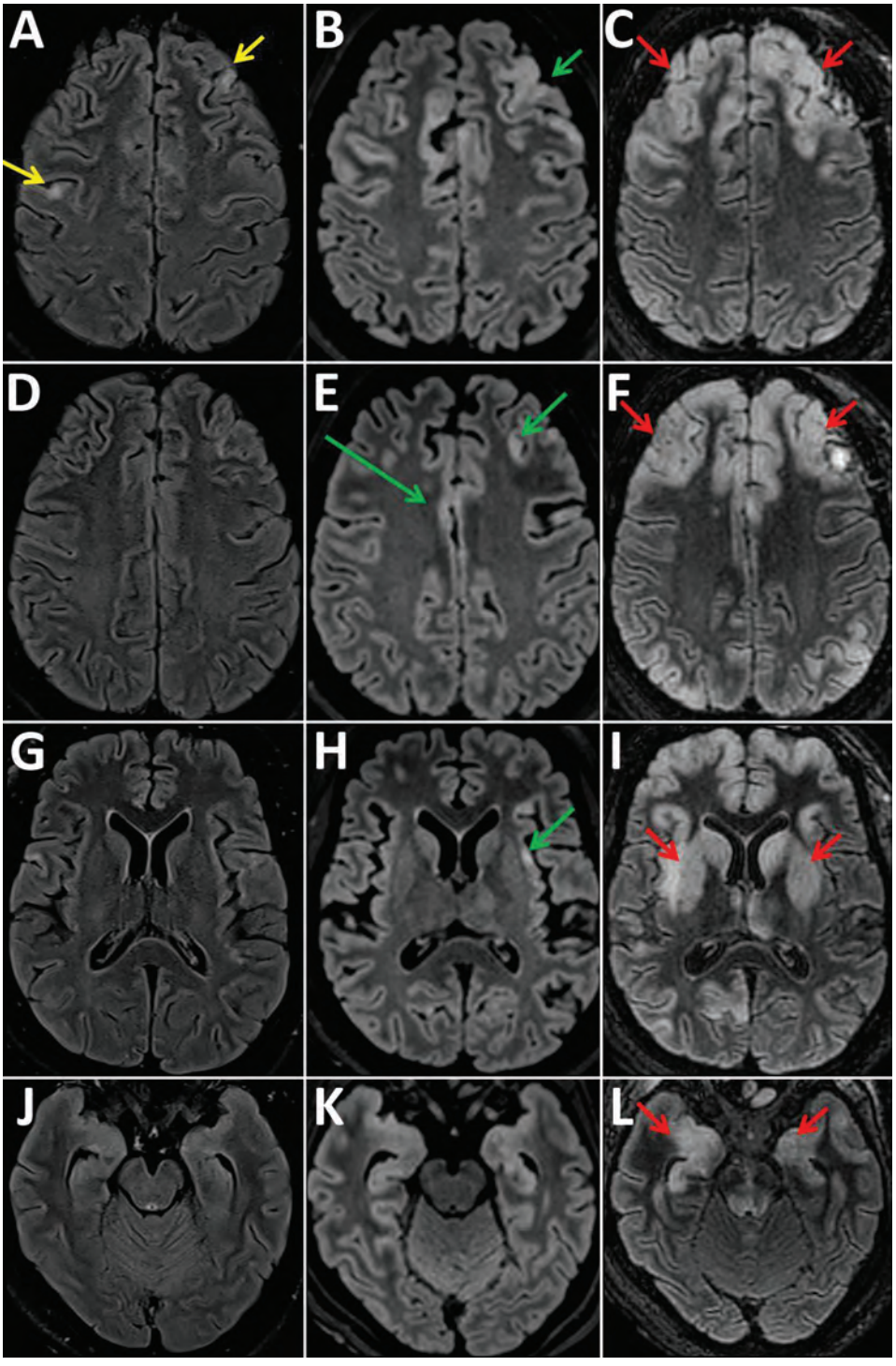

Figure 1. Fluid-attenuated inversion recovery images of magnetic resonance examinations of the brain in a 28-year-old woman from Romania with untreated AIDS and measles inclusion-body encephalitis. Images were taken 1 week (A, D, G, J), 2 weeks (B, E, H, K), and 5 weeks (C, F, I, L) after hospital admission, at the same brain levels. The first examination shows focal cortical hyperintensities (yellow arrows) in the left and right frontal cortex. After 2 weeks, these cortical hyperintensities have widened and are spreading to the cingulum and the insula (green arrows). At 5 weeks, cortical hyperintensities involve a larger part of the neocortex, but also spread to the basal ganglia, amygdala (red arrows), and hippocampus (the hippocampus changes may also be induced by status epilepticus) and to the posterior areas of the pons.

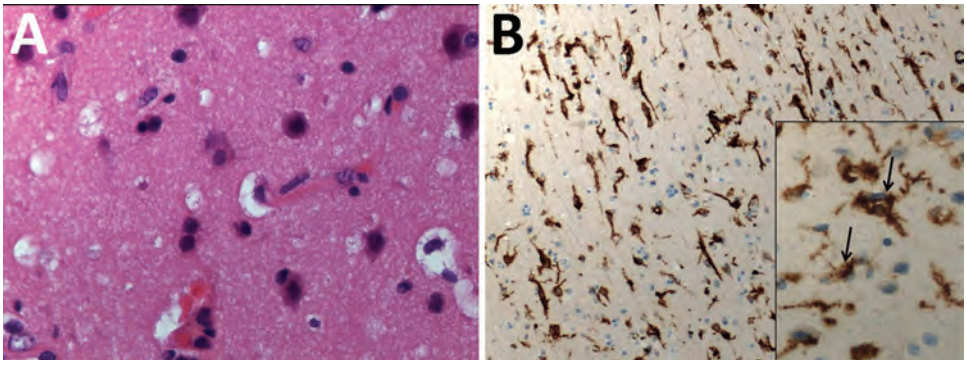

Figure 2. Histology and immunohistochemical staining of the cerebral cortex in a 28-year-old woman from Romania with untreated AIDS and measles inclusion-body encephalitis. A) Histology shows moderate increased cellular density and absence of nuclear inclusion bodies. Hematoxylin and eosin stain; original magnification ×100. B) Immunohistochemical staining microglial activation with high CD163 immunoreactivity Anti-human CD163 monoclonal antibody; original magnification ×100 and (inset) ×400.

biopsy sample was found to be positive for measles virus (MeV); >4,800,000 of 2 × 150 paired reads were assigned to the virus. These results were confirmed by specific MeV real-time reverse transcription PCR.

The detected MeV sequences in the brain biopsy enabled the reconstruction of a nearly-complete genome assembly (99.5% with a median depth coverage >25,000; GenBank accession no. MN893225). BLAST analysis (https://blast.ncbi.nlm.nih.gov/Blast.cgi) showed this MeV exhibited 99.3% identity (15,762/15,876 nt) with the closest available fully sequenced B3 genotype (MVs/California.USA/05.14/[B3]; GenBank accession no. KY969477). These results excluded infection by a MeV vaccine strain and oriented toward a European lineage origin. However, it was not possible to determine the precise origin of the virus because a high number of MeV harboring an identical C-terminal hypervariable domain (450 nt) of the nucleoprotein N gene N-450, the only genetic data available on the World Health Organization Measles Nucleotide Surveillance database (http://www.who-measles.org) (*2*), were co-circulating in Europe at the time (data not shown) (*3*–*6*). In addition, we identified no previously reported mutations suspected for neurovirulence (*7*,*8*).

We observed a mutational hotspot within the virus-encoded matrix protein (M). Of interest, the F1 5¢ end of the fusion protein (F) contained the most variable sites found along the genome. This hydrophobic F1 part is associated with hyperfusogenicity and neurodegenerative disorders (data not shown) (*7*,*8*).

Several characteristics supported a diagnosis of measles inclusion-body encephalitis (MIBE): an immunocompromised patient, undetectable MeV RNA with no intrathecal synthesis of MeV antibodies in CSF (MeV-specific IgG were detected in serum), and scarce inflammatory infiltrates on brain biopsy despite the absence of characteristic inclusions or multinucleated giant cells (*9*). Moreover, the retrospective clinical investigation revealed that the patient, who was not vaccinated against measles, had close contact with a sibling who was acutely ill with measles in April 2018 in Romania. Because of late MIBE diagnosis and despite supportive treatment, the patient's neurologic status continued to deteriorate rapidly, and she died at day 109 with severe brain damage exemplified by pejorative MRI evolution (Figure 1), showing bilateral, symmetric, and diffuse distribution of lesions during days 59–94.

Ongoing measles resurgence may lead to an increase of measles-induced encephalitis cases with life-threatening outcomes. We report here a fatal case in a woman with AIDS who had an encephalitic syndrome with no initial clear etiologic diagnosis, retrospectively tagged as MIBE. The patient did not receive ribavirin therapy (*10*) for MeV infection because the first-line extensive diagnostic testing was unsuccessful. As a last resort, a SMg approach detected MeV in a brain biopsy, despite the known result that CSF MeV detection in MIBE is often negative (*9*–*11*). Of interest, the brain biopsy did not reveal histopathologic features consistent with MIBE; we observed no immunoreactive inclusions or multinucleated giant cells within glial cells or neurons (*10*,*11*). However, MIBE lesions are scanty and can be missed in a small biopsy sample. Unfortunately, there was no material available for electron microscopy, and an autopsy was not done.

The encephalitic syndrome developed in this unvaccinated patient ≈6 months after a close contact with a documented measles case-patient; however, she did not report any rash or clinical symptoms of measles infection. It is noteworthy that MeV real-time reverse transcription PCR performed on the brain biopsy sample could have been sufficient to detect the virus. However, in this case, the advantage of SMg for the diagnosis of encephalitis is that, aside from pathogen identification, it was possible to generate

full genome sequence for B3-genotype MeV. In conclusion, this case highlights the advantage to have a reliable pan-pathogen SMg tool to diagnose atypical encephalitis with no clear etiology on an early brain biopsy sampling.

Acknowledgments

We thank the World Health Organization Measles Nucleotide Surveillance database administrator, curators, and national reference labs that contribute to this global surveillance system, especially Kevin Brown, Luiza Ustea, Mihaela Lazar, Jeff Connel, and Fabio Magurano.

About the Author

Dr. Rodriguez is an assistant professor in the Department of Microbiology at Henri Mondor Hospital, University of Paris-Est-Créteil, Créteil, France, and the head of the institution's genomics platform. He has implemented a clinical metagenomics technique in diagnostic routine and is working on the exploration of complex infectious diseases using this tool.

References

1. Rodriguez C, Jary A, Hua C, Woerther P-L, Bosc R, Desroches M, et al.; Multidisciplinary Necrotizing Fasciitis Study Group. Pathogen identification by shotgun metagenomics of patients with necrotizing soft-tissue infections. Br J Dermatol. 2019; https://doi.org/10.1111/bjd.18611
2. Rota PA, Brown K, Mankertz A, Santibanez S, Shulga S, Muller CP, et al. Global distribution of measles genotypes and measles molecular epidemiology. J Infect Dis. 2011;204(Suppl 1):S514–23. https://doi.org/10.1093/infdis/jir118
3. Katoh K, Standley DM. MAFFT multiple sequence alignment software version 7: improvements in performance and usability. Mol Biol Evol. 2013;30:772–80. https://doi.org/10.1093/molbev/mst010
4. Drummond AJ, Rambaut A. BEAST: Bayesian evolutionary analysis by sampling trees. BMC Evol Biol. 2007;7:214. https://doi.org/10.1186/1471-2148-7-214
5. Drummond AJ, Ho SYW, Phillips MJ, Rambaut A. Relaxed phylogenetics and dating with confidence. PLoS Biol. 2006;4:e88. https://doi.org/10.1371/journal.pbio.0040088
6. Darriba D, Taboada GL, Doallo R, Posada D. jModelTest 2: more models, new heuristics and parallel computing. Nat Methods. 2012;9:772. https://doi.org/10.1038/nmeth.2109
7. Hashiguchi T, Fukuda Y, Matsuoka R, Kuroda D, Kubota M, Shirogane Y, et al. Structures of the prefusion form of measles virus fusion protein in complex with inhibitors. Proc Natl Acad Sci USA. 2018;115:2496–501. https://doi.org/10.1073/pnas.1718957115
8. Plattet P, Alves L, Herren M, Aguilar HC. Measles virus fusion protein: structure, function and inhibition. Viruses. 2016;8:112. https://doi.org/10.3390/v8040112
9. Fisher DL, Defres S, Solomon T. Measles-induced encephalitis. QJM. 2015;108:177–82. https://doi.org/10.1093/qjmed/hcu113
10. Baldolli A, Dargère S, Cardineau E, Vabret A, Dina J, de La Blanchardière A, et al. Measles inclusion-body encephalitis (MIBE) in a immunocompromised patient. J Clin Virol. 2016;81:43–6. https://doi.org/10.1016/j.jcv.2016.05.016
11. Bitnun A, Shannon P, Durward A, Rota PA, Bellini WJ, Graham C, et al. Measles inclusion-body encephalitis caused by the vaccine strain of measles virus. Clin Infect Dis. 1999;29:855–61. https://doi.org/10.1086/520449

Address for correspondence: Dr. Sonia Burrel, Assistance Publique—Hopitaux de Paris, La Pitie Salpetriere, University Hospital, Virology Department, 83 boulevard de l'hopital Paris, Île-de-France 75013, France; email: sonia.burrel@aphp.fr

Oxacillinase-181 Carbapenemase-Producing *Klebsiella pneumoniae* in Neonatal Intensive Care Unit, Ghana, 2017–2019

Appiah-Korang Labi, Karen L. Nielsen, Rasmus L. Marvig, Stephanie Bjerrum, Christabel Enweronu-Laryea, Marc Bennedbæk, Mercy J. Newman, Prosper K. Ayibor, Leif P. Andersen, Jørgen A.L. Kurtzhals

We sequenced 29 carbapenemase-producing *Klebsiella pneumoniae* isolates from a neonatal intensive care unit in Ghana. Twenty-eight isolates were sequence type 17 with $bla_{OXA-181}$ and differed by 0–32 single-nucleotide polymorphisms. Improved surveillance and infection control are needed to characterize and curb the spread of multidrug-resistant organisms in sub-Saharan Africa.

Carbapenems are antimicrobial drugs of last resort for infections caused by multidrug-resistant gram-negative bacteria. Therefore, the global spread of carbapenemase-producing *Enterobacteriaceae*, which are resistant to carbapenems, is troubling (*1*,*2*). Because of the high number of deaths associated with infections caused by these bacteria, the World Health Organization classifies *Enterobacteriaceae* as priority organisms for which new antimicrobial drugs are urgently needed (*3*).

Oxacillinase (OXA)-48–like carbapenemases are among the most common carbapenemases in Enterobacterales; of the OXA-48–like enzymes, OXA-181 is the second most common type (*2*). OXA-48 *Klebsiella pneumoniae* is considered endemic to North Africa and the Middle East; OXA-181 *Klebsiella pneumoniae* is endemic to the Indian subcontinent. However, nosocomial outbreaks of OXA-181 have occurred in sub-Saharan Africa (*2*). We describe the epidemiology and clonal spread of OXA-181–producing *Klebsiella pneumoniae* in a neonatal intensive care unit (NICU) in Ghana. The Institutional Review Board of the Korle-Bu Teaching Hospital granted ethics approval (no. IRB/0025/2017) for this study.

Author affiliations: Korle-Bu Teaching Hospital, Accra, Ghana (A.-K. Labi); Copenhagen University Hospital, Rigshospitalet, Copenhagen, Denmark (A.-K. Labi, K.L. Nielsen, R.L. Marvig, M. Bennedbæk, L.P. Andersen, J.A.L. Kurtzhals); University of Copenhagen, Copenhagen (A.-K. Labi, S. Bjerrum, J.A.L. Kurtzhals); University of Ghana Medical School, Accra (C. Enweronu-Laryea, M.J. Newman); 37 Military Hospital, Accra (P.K. Ayibor)

DOI: https://doi.org/10.3201/eid2609.200562

The Study

We whole-genome sequenced 29 carbapenemase-producing *K. pneumoniae* isolates: 18 from neonatal carriage (isolates from swabs of neonates) (*4*), 3 from the NICU environment (cots and trolley handles), and 8 from neonatal bloodstream infections. These samples were isolated from the NICU of Korle-Bu Teaching Hospital (Accra, Ghana) from September 2017 through February 2019 (*5*) (Table; Appendix, https://wwwnc.cdc.gov/EID/article/26/9/20-0562-App1.pdf).

Twenty-eight of the 29 isolates were sequence type (ST) 17 and capsular type KL25. We excluded 1 isolate from further analysis that was ST48 and KL64. Core-genome phylogeny showed a close genetic relationship of all ST17 isolates (0–32 single-nucleotide polymorphism [SNP] differences; median 5 SNP differences), suggesting a localized outbreak (Figure 1). We estimated that the most recent common ancestor of the outbreak emerged in April 2017 (year 2017.3; 95% highest posterior density interval 2017.0–2017.6) with an estimated mean substitution rate of 2.1×10^{-6} SNPs/site/year (9.9 SNPs/year) (Appendix Figure).

All isolates were resistant to amoxicillin/clavulanic acid, gentamicin, amikacin, cefuroxime, ceftriaxone, ceftazidime, tazobactam/piperacillin, and ciprofloxacin. The isolates were susceptible to colistin and had MICs of ≤1 μg/mL. All outbreak isolates harbored the carbapenemase $bla_{OXA-181}$ and extended-spectrum β-lactamase $bla_{CTX-M-15}$ in addition to other β-lactamases (bla_{TEM-1B}, bla_{SHV-94}). We also found several genes encoding resistance to

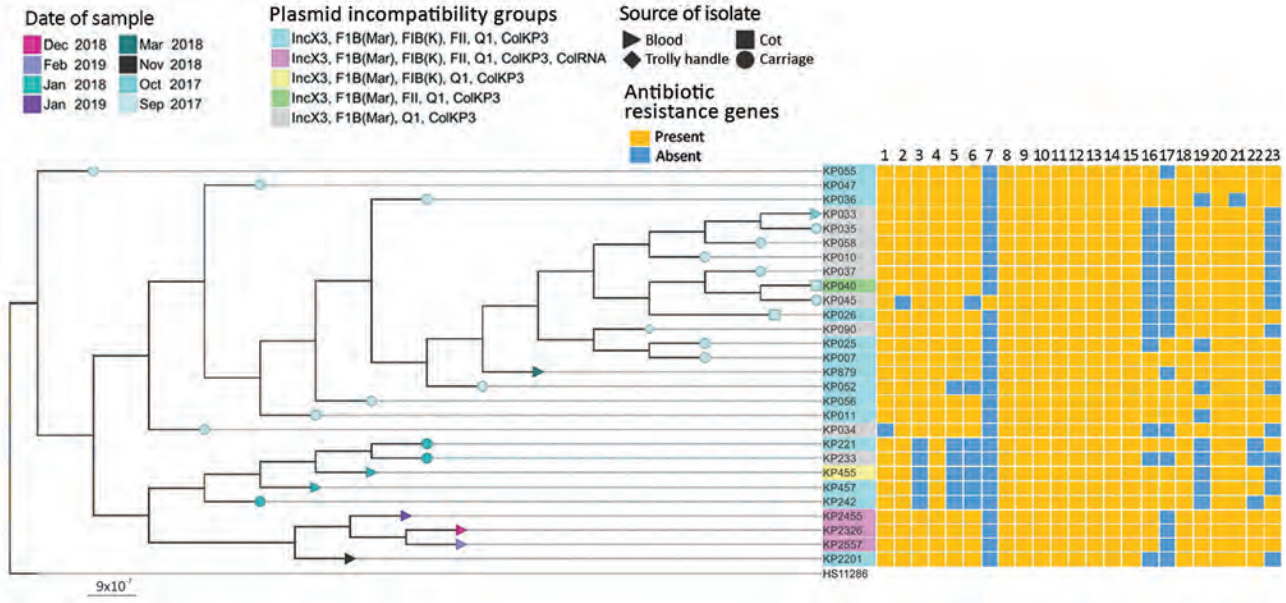

Figure 1. Phylogenetic tree of 28 carbapenemase-producing *Klebsiella pneumoniae* isolates and their acquired resistance genes from the neonatal intensive care unit at Korle-Bu Teaching Hospital, Accra, Ghana, 2017–2019. The tree was produced by analysis of single-nucleotide polymorphisms (SNPs) of core genomes. Maximum genetic distance was between isolates KP2201 and KP026, which differed by 32 SNPs. Tree used genome of *K. pneumoniae* reference strain HS11286 as outgroup. Lane 1, rmtB; lane 2, aph(3")-Ib; lane 3, aph(3')-Ia; lane 4, aph(6)-Id; lane 5, aac(3)-IId; lane 6, aadA2; lane 7, aadA2b; lane 8, blaOXA-181; lane 9, blaTEM-1B; lane 10, blaSHV-94; lane 11, blaCTX-M-15; lane 12, qnrS; lane 13, oqxA; lane 14, oqxB; lane 15, fosA; lane 16, mph(A); lane 17, catA2; lane 18, sul2; lane 19, sul1; lane 20, tetA; lane 21, tetG; lane 22, dfrA12; lane 23, drfA14. Scale bar indicates substitutions per site.

other antimicrobial drugs: aminoglycosides (*rmt*B, *aph(3'')-Ib*, *aph(3')-Ia*, *aph(6)-Id*, *aac(3)-IId*, *aadA2*, *aadA2b*); fluoroquinolones (*qnrS*, *oqxA*, *oqxB*); fosfomycin (*fosA*); macrolide (*mph (A)*); phenicols (*catA2*); sulphonamides (*sul2*, *sul1*); tetracyclines (*tetA*, *tetG*); and trimethoprim (*dfrA12*, *dfrA14*) (Figure 1).

All isolates contained 4 common plasmid incompatibility (Inc) groups (IncX3, IncF1B (Mar), IncQ1, IncColKP3). Eighteen isolates also contained incompatibility groups IncFIB (K) and IncFII, and 3 contained additional IncColRNA (Figures 1, 2). Further analysis revealed that recently recovered isolates had more plasmid Inc groups than did older isolates (Figure 1). The accessory genome of the isolates showed large variation in gene content (Figure 2). These data illustrate that this variation existed at the time of the first sampling in September 2017, when the isolates formed 3 distinct clusters (Figure 2). The clustering is associated with differences in plasmid content of the isolates and represents the uptake or loss of 205 genes. On the basis of the phylogeny and metadata, we hypothesize that 4 major evolutionary events caused changes in Inc groups and the ancestor of the cluster of isolates with Inc groups IncX3, IncFIB, IncQ1 and ColKP3 (Figure 2).

A study in South Africa identified a fully closed plasmid carrying $bla_{\text{OXA-181}}$ (*6*). Using the short-read sequencing applied in this study, we cannot determine whether $bla_{\text{OXA-181}}$ is carried on a plasmid or located in the chromosome. Mapping of raw reads toward the fully closed plasmid reveals complete coverage across the whole plasmid for 24 of the 28 isolates; the remaining 4 most recent isolates had reads covering the whole plasmid (except for 4 genes). This finding might indicate these isolates have a similar plasmid containing $bla_{\text{OXA-181}}$, although we cannot rule out that these reads might belong to other related plasmids and not the previously reported plasmid (*6*).

Conclusions

We identified an outbreak of ST17 *K. pneumoniae* carrying $bla_{\text{OXA-181}}$ in a NICU in Ghana. Outbreak isolates were resistant to all antimicrobial drugs commonly used to treat neonatal infections (although it was susceptible to colistin). Similar outbreaks of ST17 OXA-181–producing *K. pneumoniae* have been documented in South Africa (*7*), further confirming the spread of this type of resistance into nonendemic regions (*2*). Time-based phylogenetic analysis showed the outbreak isolates share

a recent ancestor (approximately April 2017). This finding suggests that the outbreak strain had been introduced recently into the NICU or that the outbreak strain had limited genetic diversity because of a recent bottleneck or selective sweep in the outbreak strain population.

K. pneumoniae is an entry point of antimicrobial resistance into the family *Enterobacteriaceae* (*8*). Thus, carbapenemase-producing *K. pneumoniae* in the NICU might transmit resistance to other *Enterobacteriaceae* species. Other studies have associated $bla_{OXA-181}$ with the insertion sequence element ISEcp1, which can spread cephalosporinases and extended-spectrum β-lactamases (*9*). In our study, all isolates possessed the IncX3 plasmid. This plasmid is self-transmissible and associated with worldwide dissemination of New Delhi metallo-β-lactamases 1 and 5 (*10*,*11*). Recent studies from countries in Africa have found $bla_{OXA-181}$ carried on the IncX3 plasmid in *Enterobacteriaceae* species, including *K. pneumoniae* (*2*,*6*,*7*).

In Europe, the spread of carbapenem-resistant *K. pneumoniae* has been driven by 4 carbapenemase-positive clonal lineages that are often transmitted in hospitals (*8*). The isolates from the NICU were genetically diverse, especially in the plasmid content of the accessory genome. This diversity indicates the genome evolved rapidly, similar to isolates from an outbreak of *K. pneumoniae* in Beijing, China. In the outbreak in China, the isolates underwent rapid genotypic evolution mainly through rearrangement (including the gain and loss of genes) in the accessory genome (*12*). Antimicrobial pressure in hospitals might lead to adaptation and resistance transmission of *K. pneumoniae* in the hospital environment (*8*).

From our data, we infer the background transmission of carbapenemase-producing *K. pneumoniae* in the NICU before its detection. Neonatal carriage or environmental contamination by carbapenemase-producing *K. pneumoniae* might have started or maintained the outbreak. Improved surveillance of multidrug-resistant organisms, buttressed with improved infection prevention and control activities, are required to detect and control outbreaks in low-resource settings.

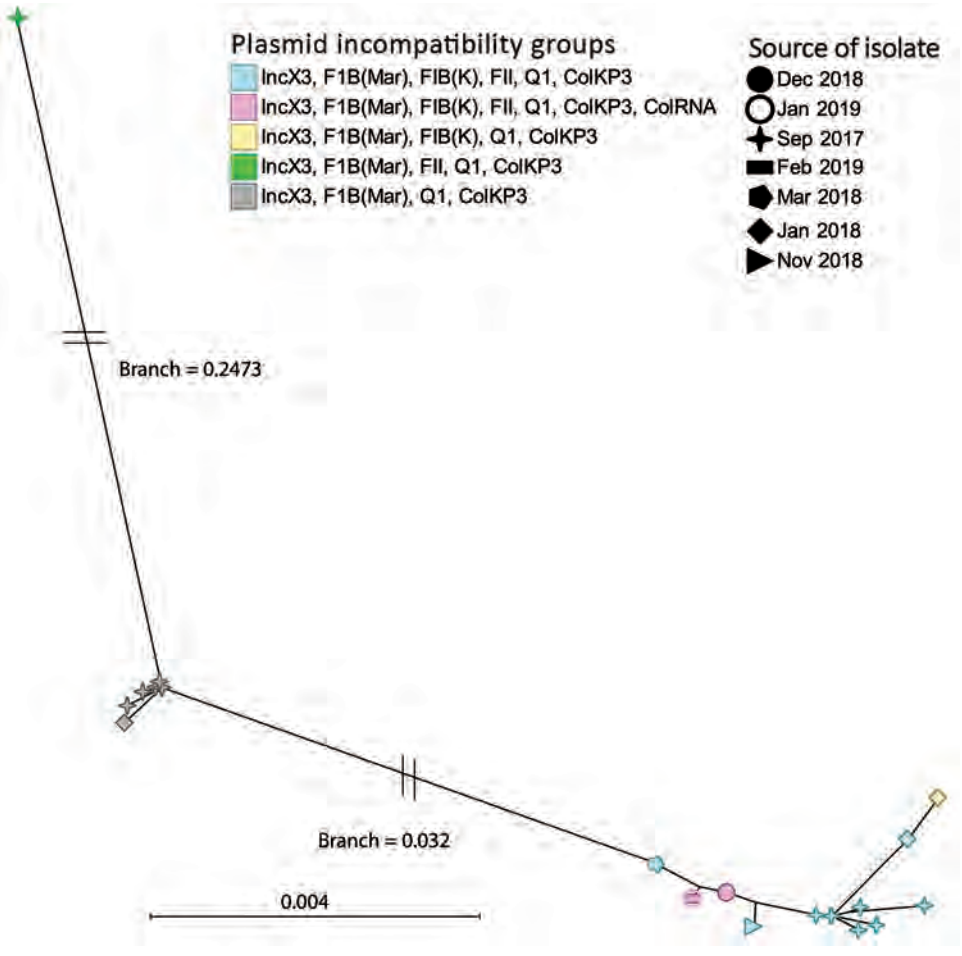

Figure 2. Binary rational tree illustrating genetic diversity (presence–absence of genes) of the accessory genome of carbapenemase-producing *Klebsiella pneumoniae* isolates from the neonatal intensive care unit at Korle-Bu Teaching Hospital, Accra, Ghana, 2017–2019. Different shapes represent different dates of organism isolation. Blue and green shapes evolved from the gray; pink and yellow evolved from the blue. Scale bar indicates genetic differences per site.

The study falls under the HAI-Ghana Project funded by the Danish Ministry of Foreign Affairs (grant no. 16-PO1-GHA). M.B. and R.L.M. are supported by the Danish National Research Foundation (grant no. 126). K.L.N. is supported by Mica-foundation.

About the Author

Dr. Labi is a doctoral student at the Centre for Medical Parasitology in the Department of Immunology and Microbiology at the University of Copenhagen. His research interests are antimicrobial resistance and stewardship and healthcare-associated infections.

References

1. Lee C-R, Lee JH, Park KS, Kim YB, Jeong BC, Lee SH. Global dissemination of carbapenemase-producing *Klebsiella pneumoniae*: epidemiology, genetic context, treatment options, and detection methods. Front Microbiol. 2016;7:895. https://doi.org/10.3389/fmicb.2016.00895
2. Pitout JDD, Peirano G, Kock MM, Strydom K-A, Matsumura Y. The global ascendency of OXA-48-type carbapenemases. Clin Microbiol Rev. 2019;33:e00102–19. https://doi.org/10.1128/CMR.00102-19
3. Tacconelli E, Carrara E, Savoldi A, Harbarth S, Mendelson M, Monnet DL, et al.; WHO Pathogens Priority List Working Group. Discovery, research, and development of new antibiotics: the WHO priority list of antibiotic-resistant bacteria and tuberculosis. Lancet Infect Dis. 2018;18:318–27. https://doi.org/10.1016/S1473-3099(17)30753-3
4. Labi A-K, Bjerrum S, Enweronu-Laryea CC, Ayibor PK, Nielsen KL, Marvig RL, et al. High carriage rates of multidrug-resistant gram-negative bacteria in neonatal intensive care units from Ghana. Open Forum Infect Dis. 2020;7:ofaa109.
5. Clinicaltrials.gov. Neonatal sepsis at neonatal intensive care units in Ghana [cited 2019 Nov 22]. https://clinicaltrials.gov/ct2/show/NCT03755635
6. Lowe M, Kock MM, Coetzee J, Hoosien E, Peirano G, Strydom K-A, et al. *Klebsiella pneumoniae* ST307 with $bla_{OXA-181}$, South Africa, 2014-2016. Emerg Infect Dis. 2019;25:739–47. https://doi.org/10.3201/eid2504.181482
7. Strydom KA, Chen L, Kock MM, Stoltz AC, Peirano G, Nobrega DB, et al. *Klebsiella pneumoniae* ST307 with OXA-181: threat of a high-risk clone and promiscuous plasmid in a resource-constrained healthcare setting. J Antimicrob Chemother. 2020;75:896–902. https://doi.org/10.1093/jac/dkz550
8. David S, Reuter S, Harris SR, Glasner C, Feltwell T, Argimon S, et al.; EuSCAPE Working Group; ESGEM Study Group. Epidemic of carbapenem-resistant *Klebsiella pneumoniae* in Europe is driven by nosocomial spread. Nat Microbiol. 2019;4:1919–29. https://doi.org/10.1038/s41564-019-0492-8
9. Potron A, Nordmann P, Lafeuille E, Al Maskari Z, Al Rashdi F, Poirel L. Characterization of OXA-181, a carbapenem-hydrolyzing class D β-lactamase from *Klebsiella pneumoniae*. Antimicrob Agents Chemother. 2011;55:4896–9. https://doi.org/10.1128/AAC.00481-11
10. Sonnevend A, Al Baloushi A, Ghazawi A, Hashmey R, Girgis S, Hamadeh MB, et al. Emergence and spread of NDM-1 producer *Enterobacteriaceae* with contribution of IncX3 plasmids in the United Arab Emirates. J Med Microbiol. 2013;62:1044–50. https://doi.org/10.1099/jmm.0.059014-0
11. Yang Q, Fang L, Fu Y, Du X, Shen Y, Yu Y. Dissemination of NDM-1-producing *Enterobacteriaceae* mediated by the IncX3-type plasmid. PLoS One. 2015; 10:e0129454. https://doi.org/10.1371/journal.pone.0129454
12. van Dorp L, Wang Q, Shaw LP, Acman M, Brynildsrud OB, Eldholm V, et al. Rapid phenotypic evolution in multidrug-resistant *Klebsiella pneumoniae* hospital outbreak strains. Microb Genom. 2019;5:e000263. https://doi.org/10.1099/mgen.0.000263

Address for correspondence: Appiah-Korang Labi, Korle-Bu Teaching Hospital, PO Box KB 945, Accra, Ghana; email: guylabi2@gmail.com

Japanese Encephalitis Virus as Cause of Acute Encephalitis, Bhutan

Sonam Wangchuk, Tshewang Dorji Tamang, Jit Bahadur Darnal, Sonam Pelden, Karma Lhazeen, Mimi Lhamu Mynak, G. William Letson, Shalini Khare, Brandon Troy Leader, Anthony A. Marfin, Susan L. Hills

In 2011, Bhutan's Royal Centre for Disease Control began Japanese encephalitis (JE) surveillance at 5 sentinel hospitals in widespread locations in Bhutan. During 2011–2018, a total of 20 JE cases were detected, indicating JE virus causes encephalitis in Bhutan. Maintaining JE surveillance will help improve understanding of JE epidemiology in this country.

Japanese encephalitis virus (JEV), a mosquitoborne flavivirus, is a common cause of encephalitis in Asia (*1*). Japanese encephalitis (JE) causes considerable illness and death, particularly in children <15 years of age (*2*). No specific treatment exists, but JE is preventable by vaccination.

JEV is maintained in an enzootic cycle between mosquitoes and amplifying vertebrate hosts, primarily pigs and wading birds (*2*). *Culex* mosquitoes are the principal vectors, especially *Cx. tritaeniorhynchus*, and commonly breed in rice fields and other stagnant water collections (*2*). JEV transmission occurs predominantly in rural agricultural areas (*2*).

In Bhutan, JEV vectors are prevalent in many southern districts and in some interior districts. Five *Culex* mosquito species have been identified: *Cx. tritaeniorhynchus*, *Cx. vishnui*, *Cx. pseudovishnui*, *Cx. gelidus*, and *Cx. quinquefasciatus*. In particular, *Cx. tritaeniorhynchus* mosquitoes have been documented in the southern districts of Chukha, Samtse, Sarpang, and Samdrup Jonghkar. In much of the country, rice fields and other mosquito breeding sites are common (G.M. Yeshey et al., unpub. data, https://www.researchgate.net/publication/277224776_Effect_of_mineral_fertilizers_on_rice_productivity_in_Punakha-Wangdue_Valley), and pigs and wading birds can be found. At least 18,800 pigs were reported in Bhutan in 2017 and reared in centralized government breeding farms, with up to several hundred pigs, or in backyard farms, typically with ≤5 pigs (*3*,*4*). About two thirds of the country's ≈750,000 persons live in rural areas (*5*). In consideration of the favorable conditions for JEV transmission and proximity to other JE-endemic countries, in 2011, the Royal Centre for Disease Control, Ministry of Health, implemented surveillance to investigate JE presence among humans in Bhutan.

The Surveillance

Bhutan's landscape ranges from lowland plains in the south to the Himalayan mountains in the north (*6*). The climate varies with elevation: very cold year-round in the north, temperate in the midlands, and subtropical in the south. Monsoon season spans mid-July through September. Bhutan has 20 administrative districts each with ≥1 general hospital. The regional referral hospital in Sarpang district in the south serves the central region and the referral hospital in Mongar district in the east serves the eastern region. The national referral hospital in the capital Thimphu also serves as the regional referral hospital for the western region.

The Royal Centre for Disease Control has conducted sentinel site–based JE surveillance at 5 sites since 2011: the national and 2 regional referral hospitals, Phuntsholing hospital in Chukha district in the southwest, and Samdrup Jongkhar hospital in Samdrup Jongkhar district in the southeast (Figure). The Royal Centre for Disease Control staff based surveillance case definitions on those from the World Health Organization (WHO) JE surveillance

Author affiliations: Royal Centre for Disease Control Thimphu, Bhutan (S. Wangchuk, J.B. Darnal, S. Pelden); Department of Public Health, Thimphu (T.D. Tamang, K. Lhazeen); Jigme Dorji Wangchuk National Referral Hospital, Thimphu (M.L. Mynak); PATH, Seattle, Washington, USA (G.W. Letson, B.T. Leader, A.A. Marfin); PATH India, Delhi, India (S. Khare); Centers for Disease Control and Prevention, Fort Collins, Colorado, USA (S.L. Hills)

DOI: https://doi.org/10.3201/eid2609.200620

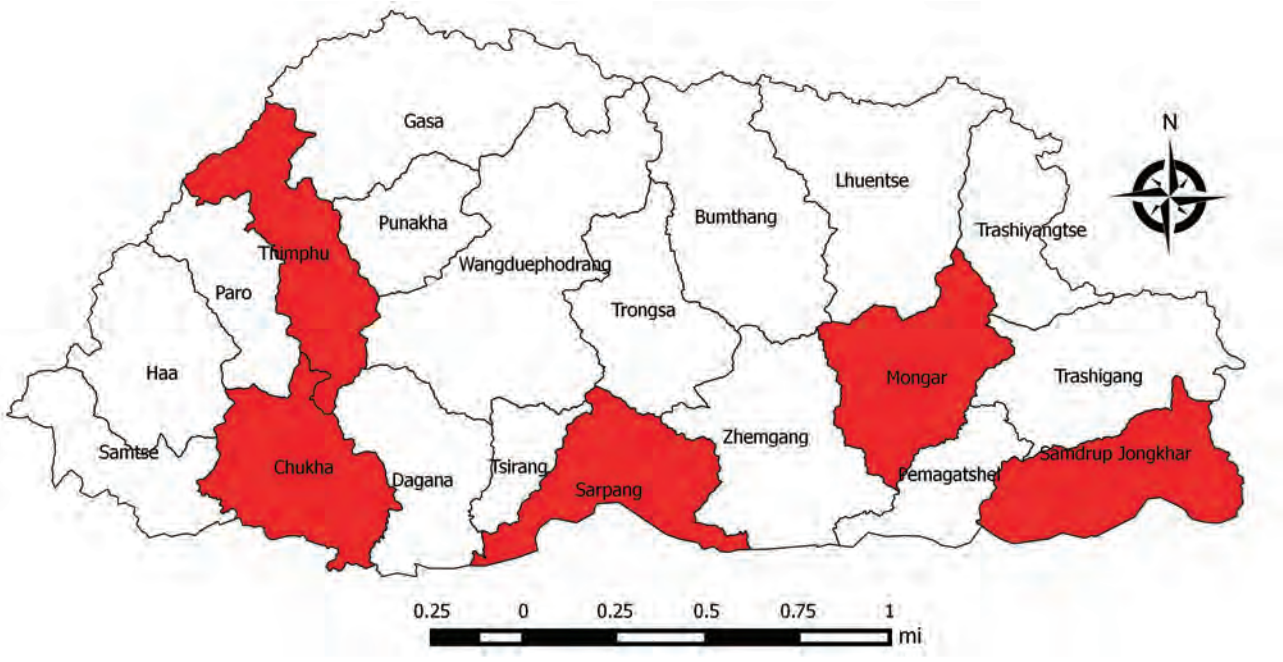

Figure. District locations of Japanese encephalitis sentinel surveillances sites (red shading), Bhutan.

standards (*7*). A clinical acute encephalitis syndrome (AES) case is illness in a person with acute onset of fever and ≥1 of the following: a change in mental status or new onset of seizures (excluding simple febrile seizures). A JE case is illness in a person with AES and laboratory evidence of JEV infection through detection of JEV IgM in serum or cerebrospinal fluid.

When an AES case is identified at a sentinel site, clinicians collect serum or cerebrospinal fluid samples from the affected person and send them to the Royal Centre for Disease Control laboratory for testing using JE IgM-capture ELISA; WHO provides the serologic assays (*8*). Since 2017, testing for dengue virus IgM in serum also has been conducted (*8*). Because the Royal Centre for Disease Control staff gathered data as part of routine public health surveillance activities, institutional review board review was not required.

We calculated incidence using Bhutan census annual estimates (*9*). Because the catchment population sizes of each sentinel hospital were unavailable, we could not calculate precise incidence estimates, and we based estimates on national population data.

During 2011–2018, among 680 AES patients for whom samples were tested, 20 (3%) had JEV infection based on IgM detection in serum (n = 15) or cerebrospinal fluid (n = 5). An annual median of 2.5 (range 0–5) JE cases were detected (Table). In 2017, after serum testing began for dengue, no dengue virus IgM was found in the 1 JEV IgM-positive patient tested. The regional referral hospital in Sarpang district reported 2 cases; the regional referral hospital in Mongar district, 4 cases; and the national referral hospital in Thimphu, 14 cases.

The median age of JE patients was 8.5 years (range 1.4–63.0 years). Fourteen (70%) cases were in children <15 years of age; in this age group, the median age was 5.8 years. The overall male:female ratio was 1:0.7; however, for children <15 years of age, the ratio was 1:1.3. The average annual incidence during the 8-year period was 0.3 (range 0–0.7) JE cases/100,000 population, and for children <15 years, 0.8 (range 0–1.7) cases/100,000 population (Table).

Table. Japanese encephalitis cases and incidence based on sentinel surveillance at 5 hospitals, Bhutan*

Cases and incidence	2011	2012	2013	2014	2015	2016	2017	2018
No. cases	3	0	2	2	5	4	3	1
Incidence/100,000 population*	0.4	0	0.3	0.3	0.7	0.5	0.4	0.1
No. cases in children <15 y	3	0	2	1	4	3	1	0
Incidence/100,000 children <15 y*	1.4	0	0.9	0.4	1.7	1.3	0.5	0

*Incidence calculations were based on the total population of Bhutan because sentinel hospital catchment population sizes were unavailable.

Conclusions

During 2011–2018, sentinel site–based surveillance detected 20 JE cases, indicating JEV as a cause of encephalitis in Bhutan. Similar to JE epidemiology in many other Asian countries, most (70%) cases occurred among children <15 years of age (*2*).

The average annual incidence estimates of 0.3 JE cases/100,000 total population and 0.8 cases/100,000 children <15 years of age most likely underestimate national disease incidence, because they are based on cases reported from 5 sentinel hospitals. These 5 hospitals are unlikely to capture JE cases from all of Bhutan's 20 districts, despite being geographically widespread, including where JEV transmission is probably highest; incorporating the country's 3 referral hospitals; and hospital staff reporting a high number of AES cases, suggesting good awareness of reporting requirements (*6*).

Our results are subject to limitations. Because cross-reactivity can occur between JEV and other flavivirus antibodies in serologic assays and no confirmatory testing was possible, ≥1 dengue or other flavivirus infection could have been misclassified as JEV infection. In addition, surveillance staff did not collect information about travel history; however, children, who represented 70% of all cases, are unlikely to have traveled to other JE-endemic countries.

To better elucidate JE epidemiology and refine incidence estimates, sentinel surveillance needs further strengthening, including possibly increasing the number of sites, improving epidemiologic data completeness, gathering patient outcome information, ensuring testing of both cerebrospinal fluid and serum samples whenever possible, and facilitating confirmatory testing at a reference laboratory. Collection of place of residence also would be useful, although most patients most likely reside in southern districts, where more JEV vectors are present.

Evidence of JEV transmission in Bhutan is not surprising, given the country's geographic location. JEV transmission has long been recognized in the bordering Indian states of Assam, West Bengal, and Arunachal Pradesh, which share similar ecologic conditions to southern and eastern Bhutan (*10*–*12*). All 3 Indian states have already established JE vaccination programs (*12*,*13*).

WHO recommends integration of JE vaccination into national immunization programs where JE is a public health priority. If case numbers are low, vaccination should be considered in areas with suitable animal reservoirs, ecologic conditions for transmission, and proximity to other JE-endemic countries (2). A vaccination program's costs and benefits should be considered (*14*); of the 3 WHO-prequalified JE vaccines, ≥1 is considered affordable for use in lower income countries (*1*).

Our findings will assist decision-making on JE vaccine introduction in Bhutan. Maintaining AES and JE surveillance and ensuring complete data collection and sample testing will enable improved understanding of JE epidemiology.

Acknowledgments

We thank Marc Fischer for his review of the manuscript.

The Bill & Melinda Gates Foundation provided funding support to PATH through grant #1873-640037-SUB of the Multi-Country JE vaccine Adoption Project and to the US Centers for Disease Control and Prevention through grant #OPPGH5333.

About the Author

Dr Wangchuk is the head of the Royal Centre for Disease Control, Department of Public Health, Ministry of Health, Bhutan. His main research interests are infectious and zoonotic diseases.

References

1. Hills S, Martin R, Marfin A, Fischer M. Control of Japanese encephalitis in Asia: the time is now. Expert Rev Anti Infect Ther. 2014;12:901–4. https://doi.org/10.1586/14787210.2014.929498
2. World Health Organization. Japanese encephalitis vaccines: WHO position paper—February 2015. Wkly Epidemiol Rec. 2015;90:69–87.
3. Ministry of Agriculture and Forests, Royal Government of Bhutan. Livestock statistics 2017 [cited 2019 Nov 8]. http://www.moaf.gov.bt/livestock-statistics-2018-available-online/
4. Monger VR, Stegeman JA, Koop G, Dukpa K, Tenzin T, Loeffen WL. Seroprevalence and associated risk factors of important pig viral diseases in Bhutan. Prev Vet Med. 2014;117:222–32. https://doi.org/10.1016/j.prevetmed.2014.07.005
5. World Bank and Royal Government of Bhutan. Bhutan Living Standards Survey Report 2017. [cited 2019 Oct 14]. http://www.nsb.gov.bt/publication/files/pub2yo10667rb.pdf
6. World Health Organization, Regional Office for South-East Asia. The Kingdom of Bhutan health system review. Health systems in transition. Vol. 7, no. 2 [cited 2019 Nov 8]. https://apps.who.int/iris/bitstream/handle/10665/255701/9789290225843-eng.pdf
7. World Health Organization. Vaccine preventable diseases surveillance standards. Japanese encephalitis [cited 2019 Nov 8]. https://www.who.int/immunization/monitoring_surveillance/burden/vpd/WHO_SurveillanceVaccinePreventable_10_JE_BW_R2.pdf
8. Johnson BW, Goodman CH, Jee Y, Featherstone DA. Differential diagnosis of Japanese encephalitis virus infections with the Inbios JE Detect™ and DEN Detect™ MAC-ELISA kits. Am J Trop Med Hyg. 2016;94:820–8. https://doi.org/10.4269/ajtmh.15-0631

9. National Statistics Bureau. Royal Government of Bhutan [cited 2020 Feb 21]. http://www.nsb.gov.bt/main/main.php
10. Chakravarty SK, Sarkar JK, Chakravarty MS, Mukherjee MK, Mukherjee KK, Das BC, et al. The first epidemic of Japanese encephalitis studied in India—virological studies. Indian J Med Res. 1975;63:77–82.
11. Chakraborty AK, Chakravarti SK, Chakravarty MS. Outbreak of Japanese encephalitis in two districts of Assam during 1980: some epidemiological features. Indian J Public Health. 1987;31:5–11.
12. Khan SA, Dutta P, Khan AM, Topno R, Chowdhury P, Borah J, et al. Japanese encephalitis epidemiology in Arunachal Pradesh, a hilly state in northeast India. Asian Pac J Trop Dis. 2011;1:119–22. https://doi.org/10.1016/S2222-1808(11)60050-9
13. Tiwari S, Singh RK, Tiwari R, Dhole TN. Japanese encephalitis: a review of the Indian perspective. Braz J Infect Dis. 2012;16:564–73. https://doi.org/10.1016/j.bjid.2012.10.004
14. World Health Organization. Principles and considerations for adding a vaccine to a national immunization programme: from decision to implementation and monitoring [cited 2020 May 5]. https://www.who.int/immunization/programmes_systems/policies_strategies/vaccine_intro_resources/nvi_guidelines/en/

Address for correspondence: Susan L. Hills, Centers for Disease Control and Prevention, 3156 Rampart Rd, Fort Collins, CO 80521, USA; email: shills@cdc.gov

Mycobacterial Testing Trends, United States, 2009–2015[1]

Samantha G. Dean, Emily E. Ricotta, Jonathan Fintzi, Yi Ling Lai,[2]
Sameer S. Kadri, Kenneth N. Olivier, Adrian Zelazny, D. Rebecca Prevots

We studied 31 US healthcare facilities to characterize trends in mycobacterial testing. During 2009–2015, testing for acid-fast bacilli increased 3.2% annually, and prevalence of pathogenic nontuberculous mycobacteria increased 4.5% annually. These increases were highest for subpopulations at high risk of infection, including older women, Asians, and patients with concurrent conditions.

Nontuberculous mycobacteria (NTM) are opportunistic environmental pathogens that can cause chronic lung disease (*1*,*2*). NTM are identified through laboratory testing for acid-fast bacilli, which test for all mycobacteria, including *Mycobacterium tuberculosis*. Multiple studies have described increasing NTM pulmonary disease (NTM PD) prevalence in the United States (*1*,*3*–*6*), a phenomenon that might be caused by true increase in disease rates, new efficient testing technologies, increased mycobacterial testing, or any combination of those. We assessed trends in mycobacterial testing rates and NTM PD prevalence from 2009 through 2015. We also analyzed factors associated with differential testing rates and prevalence across subpopulations.

The Study

The population for our study comprised persons whose medical encounters were represented in the Cerner HealthFacts Electronic Health Record database (https://sc-ctsi.org/resources/cerner-healthfacts). We extracted microbiological, demographic, and clinical data for all patient encounters at 31 facilities across the United States that continually reported microbiological data (Appendix, https://wwwnc.cdc.gov/EID/article/26/9/20-0749-App1.pdf) and that speciated mycobacterial culture results from 2009 through 2015. We included only microbiology data collected from pulmonary body sites and that used the words "AFB" and "culture" in the testing description (i.e., mycobacterial culture tests). For analyses of mycobacterial culture testing and pathogenic NTM culture positivity rates (Appendix), we used the number of unique inpatients and outpatients at the 31 facilities as the population denominator.

To estimate mycobacterial culture testing trends, we used Poisson regression models fit through quasi-likelihood methods, which enable overdispersion (*7*). We analyzed trends within the overall study population and subpopulations stratified by age, sex, race/ethnicity, concurrent conditions, facility size, region, and facility teaching status. To identify variables associated with the odds of mycobacterial culture testing per facility encounter and the odds of pathogenic NTM culture positivity per facility encounter, we fit 2 mixed-effect logistic regression models to the data. We adjusted these models for patient age, sex, interactions between age and sex, race/ethnicity, teaching facility status, facility census region, encounter year, and whether the patient had a pulmonary computed tomographic scan or radiograph during the study period. The following concurrent conditions have been associated with a higher risk for NTM PD and were included as predictors in the model: bronchiectasis (*4*,*8*), chronic obstructive pulmonary disease (*4*,*8*), cystic fibrosis (CF) (*9*), lung cancer (*4*,*5*,*8*), and rheumatoid arthritis (*8*). We included deidentified patient number as a random effect to account for clustering among an individual patient's multiple encounters.

Persons with mycobacterial culture tests were older and had more concurrent conditions than the overall population in the 31 study facilities: 20,670 (43%) of 48,563 persons with mycobacterial cultures were ≥65 years of age, compared with 1,984,443 (18%) of 10,802,134 persons in the overall study population (Table 1). Patients with the stated pulmonary conditions had higher rates of testing and NTM positivity than the overall study population. Bronchiectasis patients had mycobacterial culture tests (1,832/10,000 patients) and tested positive for NTM (339/10,000

Author affiliation: National Institutes of Health, Bethesda, Maryland, USA

DOI: https://doi.org/10.3201/eid2609.200749

[1]Preliminary results from this study were presented at the IDWeek Conference; October 2–6, 2019; Washington, DC, USA.

[2]Current affiliation: Kaiser Permanente, Oakland, California, USA.

Table 1. Rates of laboratory testing for AFB and pathogenic NTM positivity, United States, 2009–2015*

Variable	No. (%) patients†	No. (%) patients tested for AFB	Tests for AFB/10,000 patients‡	Pathogenic NTM cases/10,000 patients
Total	10,802,134 (100.0)	48,563 (100.0)	45.0	3.1
Sex				
F	5,599,841 (51.8)	22,975 (47.3)	41.0	3.0
M	4,545,803 (42.1)	25,585 (52.7)	56.3	3.6
Age, y				
<65	9,041,231 (83.7)	27,830 (57.3)	30.8	1.9
≥65	1,984,443 (18.4)	20,670 (42.6)	104.2	8.3
Sex and age, y				
F, <65	4,638,813 (42.9)	12,797 (26.4)	27.9	1.6
F, ≥65	1,089,079 (10.1)	10,144 (20.9)	94.6	8.8
M, <65	3,817,761 (35.3)	15,030 (30.9)	39.8	2.5
M, ≥65	816,161 (7.6)	10,526 (21.7)	131.0	8.6
Census region				
Midwest	2,112,964 (19.6)	11,866 (24.4)	56.2	4.7
Northeast	4,155,756 (38.5)	16,203 (33.4)	39.0	2.2
South	3,020,093 (28.0)	14,823 (30.5)	49.1	3.1
West	1,513,321 (14.0)	5,671 (11.7)	37.5	3.2
Race§				
African American	1,645,676 (15.2)	8,639 (17.8)	52.5	3.4
Asian	306,103 (2.8)	1,458 (3.0)	47.6	5.6
White	6,411,413 (59.4)	34,300 (70.6)	53.5	3.6
Concurrent conditions				
Lung cancer	56,719 (0.5)	3,729 (7.7)	657.5	24.9
Rheumatoid arthritis	52,004 (0.5)	711 (1.5)	136.7	6.7
Cystic fibrosis	3,835 (0.04)	865 (1.8)	2,255.5	276.4
Chronic obstructive pulmonary disease	165,107 (1.5)	4,301 (8.9)	260.5	19.9
Bronchiectasis	8,666 (0.1)	1,588 (3.3)	1,832.4	339.3
Teaching status indicator¶				
Nonteaching	2,094,368 (19.4)	7,815 (16.1)	37.3	3.3
Teaching	8,816,749 (81.6)	39,592 (81.5)	44.9	3.0

*AFB, acid-fast bacilli; NTM, nontuberculous mycobacteria.
†Stratified totals do not always add up to 100% because of missing data and patients' membership in multiple categories.
‡Patients with multiple tests or positive isolates are counted a single time.
§Racial/ethnic groups with small sample sizes and patients categorized as "Unknown" are not shown in stratified analysis.
¶Teaching status indicator refers to whether a facility visited by a patient is a teaching facility.

patients) at higher rates than any analyzed subpopulation (other than persons with CF). Although patients who identified as Asian were tested at a lower rate than patients who identified as White or African American (48/10,000 patients), their positivity rate of 5.6 per 10,000 patients was the highest of the 3 racial/ethnic groups examined in this study (Table 1).

From 2009 through 2015, the average annual increase in mycobacterial culture testing was 3.2% per year (95% CI 1.9%–4.5%) across all facilities. The average annual increase in pathogenic NTM positivity was 4.5% per year (95% CI 1.2%–7.9%) (Appendix Figure). Across subgroups, point estimates consistently showed an increase in testing and positivity (Figures 1, 2). Testing and positivity rates increased at a higher rate among persons who identified as Asian than among other racial/ethnic groups; among Asians, rates of culture testing increased 9.8% per year (95% CI 6.4%–13.4%), and culture positivity increased 20.1% per year (95% CI 7.6%–34.4%). Among persons with CF, rates of testing increased 26.6% per year (95% CI 15.2%–39.8%), and positivity increased 20.2% per year (95% CI 12.0%–29.3%). We observed decreasing trends in testing and positivity for patients in the Northeast census region; however, these trends were not significant (Figures 1, 2).

Using multivariable analysis we found male sex, Asian race/ethnicity, older age, concurrent pulmonary conditions, and admission to teaching facilities to be positively associated with mycobacterial culture testing and pathogenic NTM culture positivity. Encounters of women ≥65 years of age had 2.1-fold (95% CI 2.1–2.2) higher odds of mycobacterial culture testing compared with those for women <65 years of age. Encounters of persons who identified as Asian had 1.8-fold (95% CI 1.7–1.9) higher odds of mycobacterial culture testing compared with encounters of those who identified as White. All selected concurrent conditions were associated with increased odds of receiving a mycobacterial culture test. The highest odds were for persons with CF or bronchiectasis: compared with persons without these conditions, the odds of testing increased 18.4-fold (95% CI 16.6–20.3) for those with CF and 6.7-fold (95% CI 6.3–7.2) for those with bronchiectasis (Table 2).

Encounters of women ≥65 years of age had 3.2-fold (95% CI 2.7–3.8) higher odds of NTM positivity compared with those for women <65 years of age.

Persons who identified as Asian had 2.5-fold (95% CI 1.8–3.4) higher odds of culture positivity compared with those for persons who identified as white. Concurrent conditions increased the odds of testing 7.7-fold (95% CI 4.7–12.5) for patients with CF and 3.0-fold (95% CI 2.5–3.6) for patients with bronchiectasis (Table 2).

Conclusions

An important feature of our study is the analysis of both mycobacterial culture testing and NTM positivity data in a single population. We found that mycobacterial culture testing increased at an average of 3.2% per year (95% CI 1.9%–4.5%), whereas pathogenic NTM culture positivity increased an average of 4.5% per year (95% CI 1.2%–7.9%). This finding builds on previous work identifying an increase in prevalence of NTM PD (*1*,*3*–*6*). Increased testing might facilitate case identification and therefore might contribute to increasing NTM PD prevalence. Continued testing, particularly among populations at high risk, could advance understanding of NTM PD prevalence for improved clinical and public health planning.

Our analysis is consistent with prior studies showing the highest NTM PD prevalence among older women, Asians, and persons with CF, bronchiectasis, and chronic obstructive pulmonary disease (*1*). Our estimate of a 4.5% (95% CI 1.2%–7.9%) annual increase in NTM culture positivity is comparable with an estimated 7.5% (95% CI 6.7%–8.2%) annual increase in NTM PD prevalence from 2008 to 2015 made using a large managed care claims database (*6*). Further, many identified predictors of receiving a mycobacterial culture test are consistent with predictors of positivity, as identified in this and previous studies. This finding suggests that tests are being successfully focused toward groups such as older women and Asians that are at high risk for culture positivity (*1*).

Mycobacterial culture testing might be increasing because of greater awareness of NTM PD among groups at high risk. In 2012, the Cystic Fibrosis Foundation published guidelines recommending that CF patients be cultured annually for NTM (*10*). Furthermore, numerous studies published since 2010 have linked NTM PD to other concurrent conditions (*4*,*8*,*9*,*11*). These findings might contribute to improved awareness and increased testing, especially in populations at high risk for NTM PD.

This research was supported by the Intramural Research Program of the National Institutes of Health, National Institute of Allergy and Infectious Diseases.

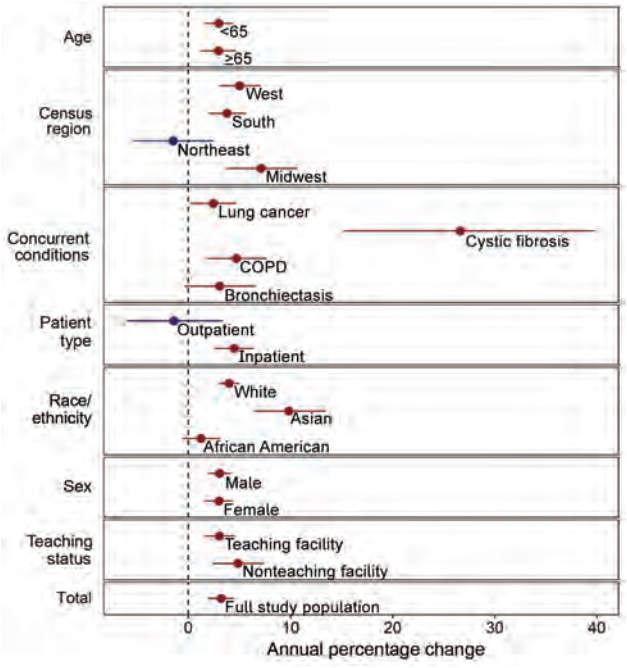

Figure 1. Annual percentage change in laboratory testing for acid-fast bacilli in 31 facilities, United States, 2009–2015. Red indicates increasing trends; blue indicates decreasing trends. Error bars indicate 95% CI. COPD, chronic obstructive pulmonary disease.

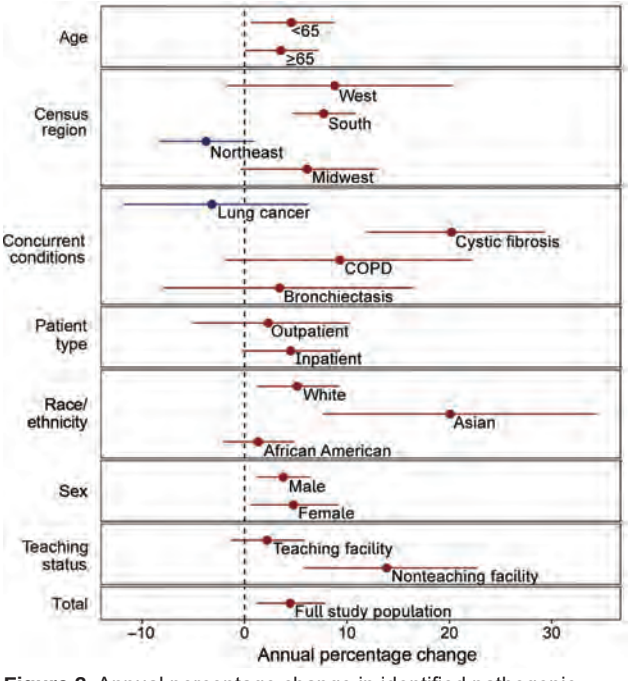

Figure 2. Annual percentage change in identified pathogenic nontuberculous mycobacteria (NTM) in 31 facilities, United States, 2009–2015. Red indicates increasing trends; blue indicates decreasing trends. Error bars indicate 95% CI. COPD, chronic obstructive pulmonary disease.

Table 2. Mixed-effect logistic regressions predicting laboratory testing for acid-fast bacilli and positivity for pathogenic nontuberculous mycobacteria, United States, 2009–2015*

Variable†	Testing for acid-fast bacilli, OR (95% CI)	Pathogenic nontuberculous mycobacteria positivity, OR (95% CI)
Sex‡		
M, age ≥65 y; ref: F, ≥65 y	1.5 (1.4–1.5)	1.1 (0.9–1.3)
M, age <65 y; ref: F, <65 y	1.7 (1.7–1.8)	1.8 (1.5–2.1)
Sex and age, y		
Age ≥65 y, M; ref: M, age <65 y	1.8 (1.7–1.8)	1.9 (1.6–2.3)
Age ≥65 y, F; ref: F, age <65 y	2.1 (2.1–2.2)	3.2 (2.7–3.8)
Race/ethnicity		
Asian; ref: white	1.8 (1.7–1.9)	2.6 (2.0–3.5)
African American; ref: white	1.0 (1.0–1.0)	1.0 (0.9–1.2)
Hispanic; ref: white	0.8 (0.7–0.8)	1.1 (0.7–1.6)
Concurrent conditions§		
Bronchiectasis	6.7 (6.3–7.2)	3.0 (2.5–3.6)
Chronic obstructive pulmonary disease	2.7 (2.6–2.8)	1.8 (1.6–2.1)
Cystic fibrosis	18.4 (16.6–20.3)	7.7 (4.7–12.5)
Lung cancer	4.5 (4.3–4.7)	1.3 (1.0–1.7)
Rheumatoid arthritis	1.4 (1.3–1.5)	0.7 (0.5–1.1)
Pulmonary computed tomographic scan or radiograph	3.3 (3.1–3.5)	1.5 (1.1–2.2)
Teaching facility; ref: nonteaching facility	1.6 (1.5–1.6)	1.4 (1.2–1.7)
Region		
Midwest; ref: Northeast	1.1 (1.1–1.1)	1.5 (1.3–1.8)
South; ref: Northeast	1.7 (1.6–1.7)	1.7 (1.4–2.0)
West; ref: Northeast	1.7 (1.7–1.8)	2 (1.5–2.5)

*OR, odds ratio; ref, referent.
†Model also adjusted for year as a potential confounder.
‡Age and sex odds ratios calculated with interaction term.
§Concurrent conditions were ascertained by codes from the International Classification of Diseases, 9th and 10th Revision. Computed tomographic scans and radiographs were identified through text searching procedure descriptions.

About the Author

Ms. Dean is an intramural research training award fellow at the National Institute of Allergy and Infectious Diseases. Her research interests include infectious disease epidemiology and methods.

References

1. Adjemian J, Daniel-Wayman S, Ricotta E, Prevots DR. Epidemiology of nontuberculous mycobacteriosis. Semin Respir Crit Care Med. 2018;39:325–35. https://doi.org/10.1055/s-0038-1651491
2. Novosad S, Henkle E, Winthrop KL. The challenge of pulmonary nontuberculous mycobacterial infection. Curr Pulmonol Rep. 2015;4:152–61. https://doi.org/10.1007/s13665-015-0119-3
3. Donohue MJ, Wymer L. Increasing prevalence rate of nontuberculous mycobacteria infections in five states, 2008–2013. Ann Am Thorac Soc. 2016;13:2143–50. https://doi.org/10.1513/AnnalsATS.201605-353OC
4. Prevots DR, Shaw PA, Strickland D, Jackson LA, Raebel MA, Blosky MA, et al. Nontuberculous mycobacterial lung disease prevalence at four integrated health care delivery systems. Am J Respir Crit Care Med. 2010;182:970–6. https://doi.org/10.1164/rccm.201002-0310OC
5. Adjemian J, Olivier KN, Seitz AE, Holland SM, Prevots DR. Prevalence of nontuberculous mycobacterial lung disease in U.S. Medicare beneficiaries. Am J Respir Crit Care Med. 2012;185:881–6. https://doi.org/10.1164/rccm.201111-2016OC
6. Winthrop KL, Marras TK, Adjemian J, Zhang H, Wang P, Zhang Q. Incidence and prevalence of nontuberculous mycobacterial lung disease in a large U.S. managed care health plan, 2008–2015. Ann Am Thorac Soc. 2020;17:178–85. https://doi.org/10.1513/AnnalsATS.201804-236OC
7. Hermansen TS, Ravn P, Svensson E, Lillebaek T. Nontuberculous mycobacteria in Denmark, incidence and clinical importance during the last quarter-century. Sci Rep. 2017;7:6696. https://doi.org/10.1038/s41598-017-06931-4
8. Prevots DR, Marras TK. Epidemiology of human pulmonary infection with nontuberculous mycobacteria: a review. Clin Chest Med. 2015;36:13–34. https://doi.org/10.1016/j.ccm.2014.10.002
9. Adjemian J, Olivier KN, Prevots DR. Epidemiology of pulmonary nontuberculous mycobacterial sputum positivity in patients with cystic fibrosis in the United States, 2010–2014. [Erratum in: Ann Am Thorac Soc. 2018;15:1114–5.] Ann Am Thorac Soc. 2018;15:817–26. https://doi.org/10.1513/AnnalsATS.201709-727OC
10. Floto RA, Olivier KN, Saiman L, Daley CL, Herrmann J-L, Nick JA, et al.; US Cystic Fibrosis Foundation and European Cystic Fibrosis Society. US Cystic Fibrosis Foundation and European Cystic Fibrosis Society consensus recommendations for the management of non-tuberculous mycobacteria in individuals with cystic fibrosis. Thorax. 2016;71(Suppl 1):i1–22. https://doi.org/10.1136/thoraxjnl-2015-207360
11. Winthrop KL, McNelley E, Kendall B, Marshall-Olson A, Morris C, Cassidy M, et al. Pulmonary nontuberculous mycobacterial disease prevalence and clinical features: an emerging public health disease. Am J Respir Crit Care Med. 2010;182:977–82. https://doi.org/10.1164/rccm.201003-0503OC

Address for correspondence: D. Rebecca Prevots, National Institute of Allergy and Infectious Diseases - Laboratory of Clinical Immunology and Microbiology 15B-1, 8 West Dr, Bethesda, MD 20852, USA; email: rprevots@niaid.nih.gov

Emergence of pstS-Null Vancomycin-Resistant *Enterococcus faecium* Clone ST1478, Canada, 2013–2018

Melissa McCracken, Robyn Mitchell, Stephanie Smith, Susy Hota, John Conly, Tim Du, John Embil, Lynn Johnston, Debbie Ormiston, Jennifer Parsonage, Andrew Simor, Alice Wong, George Golding, for the Canadian Nosocomial Infection Surveillance Program

Rates of vancomycin-resistant enterococci bloodstream infections have remained relatively low in Canada. We recently observed an increase of 113% in these infections rates, which coincided with emergence of *Enterococcus faecium pstS*-null sequence type 1478. The proportion of this sequence type increased from 2.7% to 38.7% for all tested isolates from 2013–2018.

Vancomycin-resistant enterococci (VRE) are major nosocomial pathogens that have been observed worldwide (*1*,*2*). VRE were identified in Canada in 1993 (*3*), but rates of colonization and infection have remained relatively low for years (*4*,*5*). VRE bloodstream infections (BSIs) are of particular concern because they are associated with increased illness, length of hospital stay, healthcare costs, and death (*6*–*8*). Furthermore, increased rates of VRE BSI have been reported (*8*).

Since 1999, the Canadian Nosocomial Infection Surveillance Program (CNISP) has conducted surveillance of VRE BSIs, which includes collection of patient epidemiologic data and laboratory analysis of blood isolates, including multilocus sequence typing (MLST) and antimicrobial drug susceptibility testing (*5*,*9*). The MLST scheme for *Enterococcus faecium* relies on the sequences of 7 essential housekeeping genes (*10*). However, in recent years, MLST nontypeable strains of *E. faecium* have emerged that do not harbor the *pstS* gene (*11*). These *pstS*-null sequence types (e.g., sequence type [ST] 1421 and ST1424) are believed to have occurred through multiple inversion events and have been reported to be rapidly spreading in Australia, Denmark, and the United Kingdom (*11*–*13*). We report emergence and molecular characterization of a *pstS*-null sequence type (ST1478) that is rapidly disseminating across acute care hospitals in Canada.

Author affiliations: Public Health Agency of Canada, Winnipeg, Manitoba, Canada (M. McCracken, T. Du, G. Golding); Public Health Agency of Canada, Ottawa, Ontario, Canada (R. Mitchell); University of Alberta, Edmonton, Alberta, Canada (S. Smith); Toronto General Hospital, Toronto, Ontario, Canada (S. Hota); University of Calgary Cumming School of Medicine, Calgary, Alberta, Canada (J. Conly); Health Sciences Centre, Winnipeg (J. Embil, D. Ormiston); Queen Elizabeth II Health Sciences Centre, Halifax, Nova Scotia, Canada (L. Johnston); University of Alberta Hospital, Edmonton (J. Parsonage); Sunnybrook Health Sciences Centre, Toronto (A. Simor); Saskatchewan Health Authority, Saskatoon, Saskatchewan, Canada (A. Wong)

DOI: https://doi.org/10.3201/eid2609.201576

The Study

CNISP is administered by the Public Health Agency of Canada and has conducted prospective surveillance for VRE infection and colonization since 1999 (*5*,*9*). CNISP is a partnership between the Centre for Communicable Disease and Infection Control and the National Microbiology Laboratory at the Public Health Agency of Canada and sentinel hospitals that participate as members of the Canadian Hospital Epidemiology Committee, a subcommittee of the Association of Medical Microbiology and Infectious Diseases Canada. Hospitalized patients with enterococcal bacteremia characterized as having vancomycin MICs ≥8 mg/L were eligible (*9*). A patient was included more than once if a positive VRE blood isolate was identified >14 days after completion of therapy for a previous infection and believed to be unrelated to previous infection in accordance with best clinical judgement (*9*). Epidemiologic data were collected and VRE BSI isolates were forwarded to the National Microbiology Laboratory for further characterization (*9*).

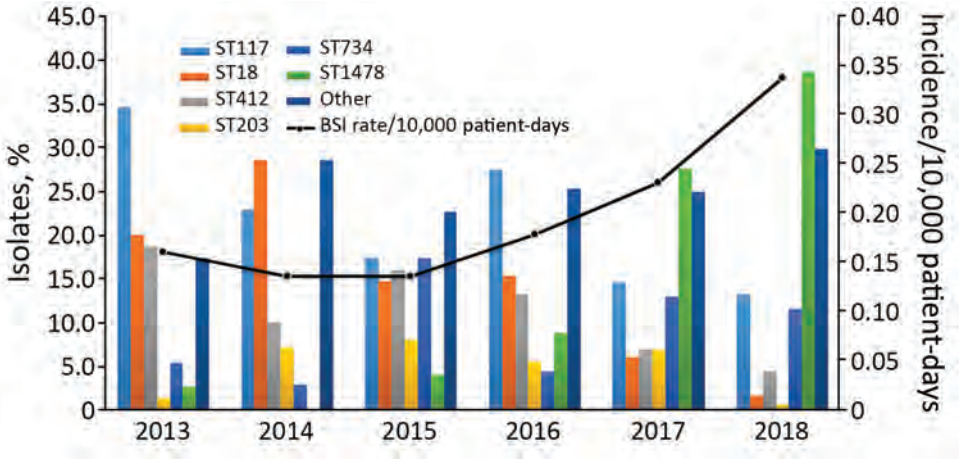

Figure. Increase in annual vancoymicin-resistant enterococci BSI rates and emergence of novel *pstS*-null sequence type ST1478, Canada, 2013–2018. BSI, bloodstream infection; ST, sequence type.

All isolates that failed to give a sequence type by conventional MLST (*10*) were subjected to whole-genome sequencing on the MiSeq Platform (Illumina, https://www.illumina.com). Assembled reads (contigs) were analyzed by using an in-house MLST tool based on 1 from the Center for Genomic Epidemiology website (https://cge.cbs.dtu.dk/services).

During 2013–2018, a total of 797 VRE BSI cases were reported among 62 participating acute care hospitals across 10 provinces for which 608 VRE BSI isolates were submitted. During this surveillance period, the rate of VRE BSI significantly increased from 0.16 cases/10,000 patient-days to 0.34 cases/10,000 patient-days (p<0.001) (Figure). These rates are much higher than those reported during 1999–2009 (0.005 cases/1,000 admissions during 1999 to 0.068 cases/1,000 admissions during 2009) (*5*). Of the 608 VRE BSI collected, different MLST types were identified, which included 4 of the newly reported *pstS*-null sequence types ST1478 (n = 115), ST1421 (n = 7), ST1424 (n = 2), and ST1612 (n = 1). The increase of ST1478 isolates from 2.7% in 2013 to 38.7% in 2018 coincides with the increase in VRE BSI rates (Figure). After emergence of ST1478, STs that once dominated (ST18, ST117, and ST412) dramatically decreased. This shift in clonal types is similar to what has been reported in other countries after identification of these *pstS*-null mutants (*12*).

As of 2018, ST1478 has been identified in 19 of 62 CNISP participating hospitals in 6 provinces. Of the 19 hospitals, 12 were from western Canada (British Columbia, Alberta, Saskatchewan, and Manitoba), 6 from central Canada (Ontario and Quebec), and 1 from eastern Canada (Newfoundland and Labrador, Prince Edward Island, New Brunswick, and Nova Scotia). Regionally, ST1478 represented 23.7% (65/274) of isolates tested from western Canada, 14.8% (49/332) of isolates tested from central Canada, and 50% (1/2) of isolates tested from eastern Canada during 2013–2018. Furthermore, among the VRE BSI identified in western Canada, a significantly higher proportion were

Table 1. Antimicrobial drug resistance results for ST1478 versus non-ST1478 isolates of vancoymicin-resistant enterococci, Canada, 2013–2018*

Antimicrobial drug	% ST1478, n = 115	% Non-ST1478, n = 493	p value
Ampicillin	100.0	100.0	1
Chloramphenicol	10.4	1	0.0001
Ciprofloxacin	100.0	100.0	1
Daptomycin	13.0	3.9	0.0014
Erythromycin	100.0	92.1	0.6068
HL gentamicin	80.0	13.6	0.0001
Levfloxacin	100.0	99.6	1
Linezolid	1.7	0.4	0.1669
Nitrofurantoin	16.5	35.9	0.002
Penicillin	100.0	100.0	1
Quinupristin/dalfopristin	0.9	8.5	0.0032
Rifampin	95.7	90.1	0.7104
HL streptomycin	15.7	39.8	0.0002
Tetracycline	91.3	46.0	0.0001
Tigecycline	0.9	0.4	0.4776
Vancomycin	100.0	97.2	0.8835

*HL, high level; ST, sequence type.

Table 2. Characteristics for patients with ST1478 versus non-ST1478 vancoymicin-resistant enterococci bloodstream infections, Canada, 2013–2018*

Characteristic	ST1478, n = 110	Non-ST1478, n = 492	p value
Mean age, y (SD)	58 (16.8)	59 (17.5)	0.89
Sex			
M	69/110 (62.7)	296/492 (60.2)	0.62
F	41/110 (73.3)	196/492 (39.8)	0.62
Central venous catheter	57/82 (69.5)	184/251 (73.3)	0.50
Solid organ transplant	24/97 (24.7)	42/325 (12.9)	0.005
Hemodialysis	15/70 (21.4)	47/223 (21.1)	0.95
Chemotherapy	11/70 (15.7)	54/223 (24.2)	0.14
ICU admission within 30 d of positive blood culture	11/91 (12.1)	60/332 (18.1)	0.18
30 d all-cause mortality rate	35/108 (32.4)	120/390 (30.8)	0.75

*Values are no. positive/no. tested (%) unless indicated otherwise. ICU, intensive care unit.

ST1478 (56.5%, 65/115) compared with non-ST1478 (42.4%, 209/493; p = 0.006).

The predominant *van* gene among ST1478 isolates was *vanA* (99.1%, n = 114); only 1 isolate harbored a *vanB* gene (0.9%). We determined resistance to antimicrobial drugs by using broth microdilution and GPALL1F Sensititer panels (Trek Diagnostics, http://www.trekds.com). We interpreted MICs by using breakpoints described by the Clinical and Laboratory Standards Institute (*14*). Antimicrobial drug susceptibility tests showed that ST1478 isolates have increased resistance to chloramphenicol (10.4%), daptomycin (13.0%), HL-gentamicin (80.0%), and tetracycline (91.3%) compared with non-ST1478 isolates (Table 1). We verified daptomycin nonsusceptibility by using Etest (bioMérieux, https://www.biomerieux.com). Clinically, increased daptomycin nonsusceptibility among the ST1478 isolates is of particular concern because daptomycin is 1 of the few remaining treatment options for VRE and resistance to it is an increasing clinical problem (*15*). CNISP surveillance data show a nonsignificant increase in the use of daptomycin to treat patients with VRE bloodstream infections. During 2015, a total of 53.7% of patients with a VRE BSI were given daptomycin, and during 2018, this proportion increased to 61.1% (p = 0.5).

During 2013–2018, we identified 115 ST1478 VRE BSI isolates among 110 patients. The median age of ST1478 patients was 58 years (interquartile range 52–69 years), and most (63.1%, 69/111) were male. The most commonly identified risk factors at the time of positive culture included use of a central venous catheter (69.5%, 57/82), solid organ transplant recipient (24.7%, 24/97), receiving hemodialysis (21.4%, 15/70), and receiving chemotherapy (15.7%, 11/70). A total of 31% (28/92) of ST1478 patients were already in an intensive care unit at the time of positive culture, and an additional 11 (12.1%) were admitted within 30 days of positive blood culture. The all cause 30-day mortality rate was 32.4%. Bacteremia patients with ST1478 VRE were similar with respect to age, sex, intensive care unit admission, and mortality rate compared with patients who had non-ST1478 VRE. Patients with ST1478 VRE were more likely to have undergone solid organ transplantation (24.7%) than patients with non-ST1478 VRE (12.9%; p = 0.005) (Table 2). However a VRE outbreak was reported by 1 center in their multiorgan transplant unit, which might explain this finding.

Conclusions

The emergence of the *pstS*-null mutant ST1478 identified in acute care hospitals in Canada coincides with a major increase in VRE BSI rates. This increase might be attributed to an increased virulence/fitness of this strain type or changes in VRE infection prevention and control practices.

Clinically, the increased proportion of daptomycin nonsusceptibility among this emerging strain type is of concern. Future work, including whole-genome sequencing, and collection of enhanced epidemiologic and infection prevention and control practices data are being undertaken to provide a better understanding of the transmission, clonal relatedness, and evolution of this strain type within and between hospitals across Canada. Clinicians should be aware of these drug-resistant bacteria.

Acknowledgments

We thank the physicians, epidemiologists, infection control practitioners, and laboratory staff at each participating hospital for their contributions to the study and Sean Ahmed and Ken Fakharuddin for providing expert technical assistance.

About the Author

Ms. McCracken is a microbiologist at the National Microbiology Laboratory in Winnipeg, Manitoba, Canada. Her primary research interests are vancomycin-resistant enterococci and methicillin-resistant *Staphylococcus aureus*.

References

1. Uttley AH, Collins CH, Naidoo J, George RC. Vancomycin-resistant enterococci. Lancet. 1988;1:57–8. https://doi.org/10.1016/S0140-6736(88)91037-9
2. Bonten MJ, Willems R, Weinstein RA. Vancomycin-resistant enterococci: why are they here, and where do they come from? Lancet Infect Dis. 2001;1:314–25. https://doi.org/10.1016/S1473-3099(01)00145-1
3. Kibsey PC, Willey B, Low DE, Cain D, Boychuk LR, Huele M. Vancomycin multiresistant *Enterococcus faecium*: first Canadian isolate. Presented at: 61st Conjoint Meeting on Infectious Diseases. Canadian Association for Clinical Microbiology and Infectious Diseases; Vancouver, British Columbia, Canada; November 8–10, 1993. Abstract K5.
4. Ofner-Agostini M, Johnston BL, Simor AE, Embil J, Matlow A, Mulvey M, et al.; Canadian Nosocomial Infection Surveillance Program. Vancomycin-resistant enterococci in Canada: results from the Canadian nosocomial infection surveillance program, 1999–2005. Infect Control Hosp Epidemiol. 2008;29:271–4. https://doi.org/10.1086/528812
5. McCracken M, Wong A, Mitchell R, Gravel D, Conly J, Embil J, et al.; Canadian Nosocomial Infection Surveillance Program. Molecular epidemiology of vancomycin-resistant enterococcal bacteraemia: results from the Canadian Nosocomial Infection Surveillance Program, 1999–2009. J Antimicrob Chemother. 2013;68:1505–9. https://doi.org/10.1093/jac/dkt054
6. Deshpande LM, Fritsche TR, Moet GJ, Biedenbach DJ, Jones RN. Antimicrobial resistance and molecular epidemiology of vancomycin-resistant enterococci from North America and Europe: a report from the SENTRY antimicrobial surveillance program. Diagn Microbiol Infect Dis. 2007; 58:163–70. https://doi.org/10.1016/j.diagmicrobio. 2006.12.022
7. Lu C-L, Chuang Y-C, Chang H-C, Chen YC, Wang JT, Chang SC. Microbiological and clinical characteristics of vancomycin-resistant *Enterococcus faecium* bacteraemia in Taiwan: implication of sequence type for prognosis. J Antimicrob Chemother. 2012;67:2243–9. https://doi.org/10.1093/jac/dks181
8. Prematunge C, MacDougall C, Johnstone J, Adomako K, Lam F, Robertson J, et al. VRE and VSE bacteremia outcomes in the era of effective VRE therapy: a systematic review and meta-analysis. Infect Control Hosp Epidemiol. 2016;37:26–35. https://doi.org/10.1017/ice.2015.228
9. Public Health Agency of Canada. Surveillance protocol for vancomycin-resistant *Enterococci* bloodstream infections in CNISP hospitals, 2019 [cited 2020 Apr 30]. https://ipac-canada.org/cnisp-publications.php
10. Homan WL, Tribe D, Poznanski S, Li M, Hogg G, Spalburg E, et al. Multilocus sequence typing scheme for *Enterococcus faecium*. J Clin Microbiol. 2002;40:1963–71. https://doi.org/10.1128/JCM.40.6.1963-1971.2002
11. Carter GP, Buultjens AH, Ballard SA, Baines SL, Tomita T, Strachan J, et al. Emergence of endemic MLST non-typeable vancomycin-resistant *Enterococcus faecium*. J Antimicrob Chemother. 2016;71:3367–71. https://doi.org/10.1093/jac/dkw314
12. Hammerum AM, Justesen US, Pinholt M, Roer L, Kaya H, Worning P, et al. Surveillance of vancomycin-resistant enterococci reveals shift in dominating clones and national spread of a vancomycin-variable *vanA Enterococcus faecium* ST1421-CT1134 clone, Denmark, 2015 to March 2019. Euro Surveill. 2019;24:1–5. https://doi.org/10.2807/1560-7917.ES.2019.24.34.1900503
13. Lemonidis K, Salih TS, Dancer SJ, Hunter IS, Tucker NP. Emergence of an Australian-like *pst*S-null vancomycin resistant *Enterococcus faecium* clone in Scotland. PLoS One. 2019;14:e0218185. https://doi.org/10.1371/journal.pone.0218185
14. Clinical and Laboratory Standards Institute. Performance standards for antimicrobial susceptibility testing: 20th Informational Supplement M100–S20. Wayne (PA): The Institute; 2018.
15. Kinnear CL, Patel TS, Young CL, Marshall V, Newton DW, Read AF, et al. Impact of an antimicrobial stewardship intervention on within- and between-patient daptomycin resistance evolution in vancomycin-resistant *Enterococcus faecium*. Antimicrob Agents Chemother. 2019;63:e01800-18. https://doi.org/10.1128/AAC.01800-18

Address for correspondence: Melissa McCracken, Public Health Agency of Canada, 1015 Arlington St, Winnipeg, MB R3C 4W1, Canada; email: melissa.mccracken@canada.ca

Buying Time with COVID-19 Outbreak Response, Israel

Eyal Leshem,[1] Arnon Afek,[1] Yitshak Kreiss

Author affiliations: Sheba Medical Center, Israel Ministry of Health, Tel Hashomer, Israel; Sackler School of Medicine, Tel Aviv University, Tel Aviv, Israel

DOI: https://doi.org/10.3201/eid2609.201476

Israel's response during the containment phase of the COVID-19 outbreak in early 2020 led to a delay in sustained community transmission and effective mitigation. During February–April 2020, a total of 15,981 confirmed cases resulted in 223 deaths. A total of 179,003 persons reported electronically to self-quarantine and were entitled to paid sick leave.

Countries' responses to the coronavirus disease (COVID-19) emergency have been determined by their geopolitical, societal, and healthcare system characteristics. A successful response results from early identification of effective interventions tailored for these specific characteristics. At the outset of the COVID-19 outbreak response, Israel's healthcare system faced a chronic shortage of healthcare resources; however, as Israel shifted from containment to mitigation, structural characteristics were leveraged to enhance the response. We describe Israel's healthcare system attributes as related to geopolitical and societal status and how these factors affected the outbreak response.

Israel's national healthcare system serves a population of 9.1 million (*1*). With 1.8 acute care hospital beds per 1,000 inhabitants and a national total of 758 licensed intensive care unit (ICU) beds, the healthcare system in Israel constantly lacks resources (*2*,*3*). In 2016, the average annual occupancy of internal medicine beds was 99% (monthly range 93%–107%) (*4*); during peak influenza season, overflow patients must receive mechanical ventilation in internal medicine wards. A shortage of surge ICU capacity during the early stages of the COVID-19 outbreak forced Israel to focus on early aggressive containment strategy.

Israel's life expectancy at birth of 82 years ranks eighth among Organization for Economic Cooperation and Development countries (*1*,*5*). Israel's National Health Insurance Law (NHIL) guarantees that every legal resident receives all ambulatory and urgent medical care with very low copayment. Robust community-based healthcare services reduce the need for emergency visits to acute care medical centers. When medically indicated, all urgent care referrals and hospitalizations are free of charge. The result of these policies was that patients with suspected COVID-19 were assessed, isolated, and treated without individual hesitancy or fear of medical expenses.

During a state of national emergency, the Ministry of Health (MoH) assumes control of hospital referrals and admissions, specifically ICU hospitalizations. Stockpiles of pandemic preparedness emergency equipment, including mechanical ventilators, personal protection equipment, and critical medication, are inventoried and managed at the national level. Throughout peak COVID-19 transmission, the MoH coordinated and diverted admissions of mechanically ventilated patients to avoid overwhelming ICU capacity.

Israel's land borders are infrequently traversed by international travels, and the country is functionally a geopolitical island. In 2019, of 4.6 million tourist entries into Israel, 88% were via international flights (*6*). Despite its culturally and politically diverse population, Israel's society shows social cohesion, resilience, and trust in public health and government institutions.

When the COVID-19 epidemic was first reported, Israel's MoH implemented a containment strategy that consisted of early travel restrictions to countries reporting COVID-19 transmission, as well as extensive testing and self-reported quarantine of returned travelers (Appendix Figures 1–3, https://wwwnc.cdc.gov/EID/article/26/9/20-1476-App1.pdf) (*7*). Patient contacts were identified through contact tracing and mobile phone surveillance. The MoH posted the whereabouts of confirmed cases on its website and through a mobile phone application. Persons could ascertain and report patient exposure electronically to the MoH and enter self-quarantine at home. Quarantined persons reporting electronically were issued a general statement of illness and became entitled to paid sick leave for the duration of quarantine time, enforced on employers by emergency MoH regulations and upheld by the Israel supreme court (*8*). Overall, by April 30, 2020, a total of 179,003 persons had self-reported to quarantine; 89,775 (50%) were returned travelers, and 89,228 (50%) were identified contacts of confirmed cases (*9*; Appendix Figure 4). To address increased transmission in ultra-Orthodox neighborhoods and in several Arab districts, focal lockdown measures were implemented in late April 2020. Cultural

[1]These authors contributed equally to this article.

characteristics and communal responsibility led to public adherence to these sometimes onerous requirements and contributed to civil obedience.

Altogether, Israel's containment measures proved successful in creating weeks of delay in peak transmission, more than those for some countries in Europe and cities in the United States (Figure). This delay afforded Israel's healthcare system and the MoH time to implement preparedness measures including medical staff training, emergency department preparation for suspected patient isolation, building isolated COVID-19 units, and shifting resources to compensate for the low number of ICU beds. For example, by April 9, Sheba Medical Center in Tel Hashomer had built 327 isolated COVID-19 ICU hospitalization beds with mechanical ventilation capacity, completely separated from its 71 general (non–COVID-19) ICU beds (*10*).

Moving from containment to mitigation, widescale social distancing measures were implemented (Appendix Table). These measures included school closure, movement and travel restrictions, discontinuation of nonessential work and commerce, and complete national curfew during the holidays of Passover and Independence Day. Local curfews were instituted in neighborhoods and cities with high COVID-19 incidence and in Muslim populations during Ramadan.

Taken together, these containment and mitigation steps may have contributed to the relatively low peak incidence, low mortality rate, and preservation of healthcare system function in Israel (Figure; Appendix Table). On the basis of these experiences to date, we recommend that countries fully leverage their particular geopolitical, social, and healthcare system characteristics as soon as possible in response to crises of such magnitude.

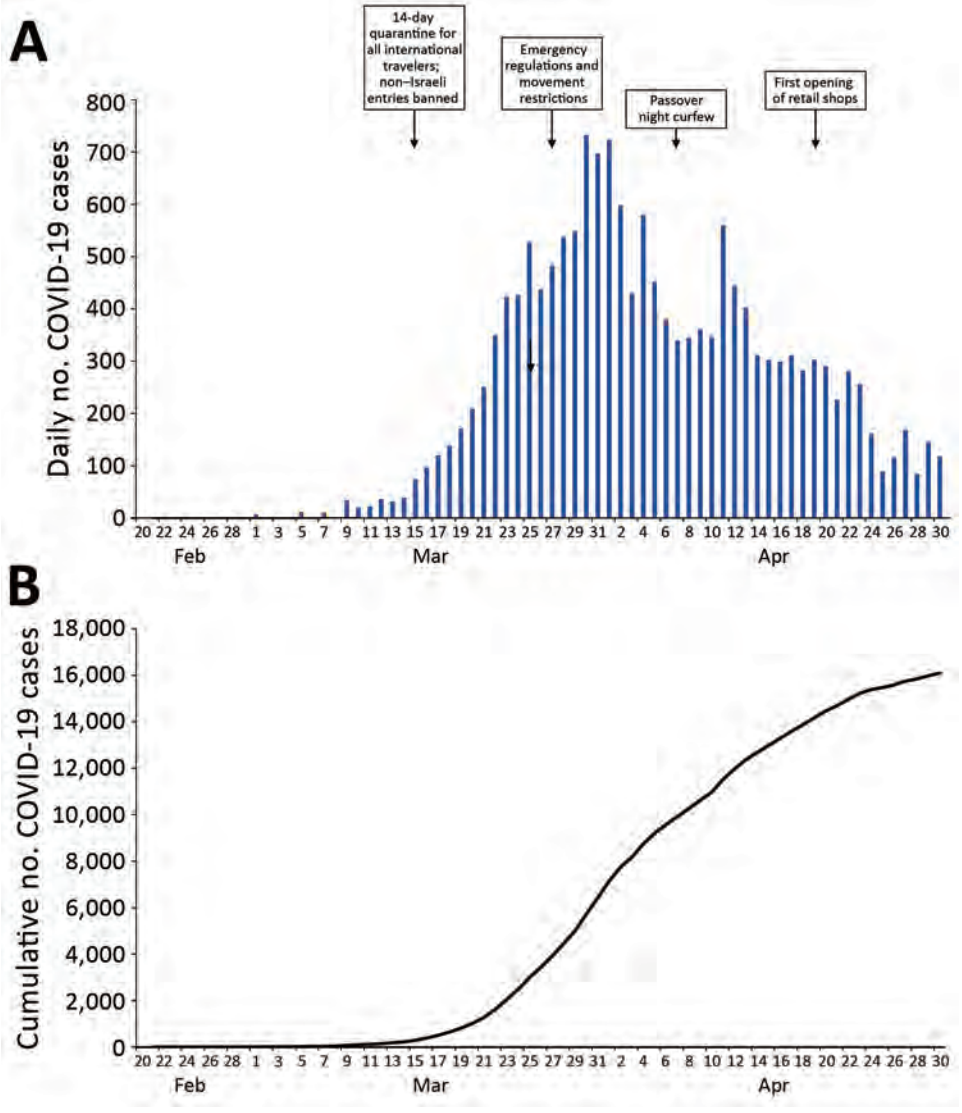

Figure. Numbers of COVID-19 cases and key public health interventions by date of implementation, Israel, February–April, 2020: A) daily numbers; B) cumulative totals.

About the Author

Dr. Leshem is a clinical associate professor at Tel Aviv University School of Medicine and the director of the Institute for Travel Medicine and Tropical Diseases at Sheba Medical Center in Tel Hashomer, Israel. His research interests include global health, epidemiology, and vaccine-preventable diseases.

References

1. Israel Central Bureau of Statistics. Population of Israel on the eve of 2020. 2019 [cited 2020 Mar 25]. https://www.cbs.gov.il/en/mediarelease/Pages/2019/Population-of-Israel-on-the-Eve-of-2020.aspx
2. Organization for Economic Cooperation and Development. OECD data: hospital beds. 2020 [cited 2020 Mar 22]. https://data.oecd.org/healtheqt/hospital-beds.htm
3. State of Israel Ministry of Health. Hospitalization beds in Israel, January 2020 [in Hebrew]. 2020 [cited 2020 Apr 12]. https://www.health.gov.il/UnitsOffice/HD/MTI/info/Pages/licensed_inpatient_hospital_beds.aspx
4. State of Israel Ministry of Health Information Division. Hospital occupancy by admission ward and month, 2016–2017 [in Hebrew]. 2017 [cited 2020 Mar 25] https://www.health.gov.il/UnitsOffice/HD/MTI/info/Pages/hospital_Beds.aspx
5. Chernichovsky D. Not "socialized medicine"—an Israeli view of health care reform. N Engl J Med. 2009;361:e46. https://doi.org/10.1056/NEJMp0908269
6. Israel Central Bureau of Statistics. Israel visitor arrivals in January–November 2019 [in Hebrew]. 2020 [cited 2020 Mar 25]. https://www.cbs.gov.il/he/mediarelease/DocLib/2019/367/28_19_367b.pdf
7. State of Israel Ministry of Health. HaMagen: the Ministry of Health app for fighting the COVID-19 outbreak. 2020 [cited 2020 May 12]. https://govextra.gov.il/ministry-of-health/hamagen-app/download-en
8. State of Israel Ministry of Health. A general statement of illness for isolated workers. 2020 [cited 2020 May 12]. https://govextra.gov.il/ministry-of-health/corona/corona-virus-en
9. State of Israel Ministry of Health . COVID-19 resources [in Hebrew]. 2020 [cited 2020 May 12]. https://data.gov.il/dataset/covid-19</eref>
10. Leshem E, Klein Y, Haviv Y, Berkenstadt H, Pessach IM. Enhancing intensive care capacity: COVID-19 experience from a tertiary center in Israel. Intensive Care Med. 2020 May 25 [Epub ahead of print]. PubMed https://doi.org/10.1007/s00134-020-06097-0

Address for correspondence: Eyal Leshem, Institute for Travel Medicine and Tropical Diseases, Sheba Medical Center, Tel Hashomer 52621, Israel; email: Eyal.Leshem@sheba.health.gov.il

Effectiveness of N95 Respirator Decontamination and Reuse against SARS-CoV-2 Virus

Robert J. Fischer, Dylan H. Morris, Neeltje van Doremalen, Shanda Sarchette, M. Jeremiah Matson, Trenton Bushmaker, Claude Kwe Yinda, Stephanie N. Seifert, Amandine Gamble, Brandi N. Williamson, Seth D. Judson, Emmie de Wit, James O. Lloyd-Smith, Vincent J. Munster

Author affiliations: National Institute of Allergy and Infectious Diseases, Hamilton, Montana, USA (R.J. Fischer, N. van Doremalen, S. Sarchette, M.J. Matson, T. Bushmaker, C.K. Yinda, S.N. Seifert. B.N. Williamson, E. de Wit, V.J. Munster); Princeton University, Princeton, New Jersey, USA (D.H. Morris); Marshall University, Huntington, West Virginia, USA (M.J. Matson); University of California, Los Angeles, Los Angeles, California, USA (A. Gamble, J.O. Lloyd-Smith), University of Washington, Seattle, Washington, USA (S.D. Judson)

DOI: https://doi.org/10.3201/eid2609.201524

The coronavirus pandemic has created worldwide shortages of N95 respirators. We analyzed 4 decontamination methods for effectiveness in deactivating severe acute respiratory syndrome coronavirus 2 virus and effect on respirator function. Our results indicate that N95 respirators can be decontaminated and reused, but the integrity of respirator fit and seal must be maintained.

The unprecedented pandemic of coronavirus disease has created worldwide shortages of personal protective equipment, in particular respiratory protection such as N95 respirators (*1*). Transmission of severe acute respiratory syndrome coronavirus 2 (SARS-CoV-2) occurs frequently in hospital settings; numerous reported cases of nosocomial transmission highlight the vulnerability of healthcare workers (*2*). The environmental stability of SARS-CoV-2 virus underscores the need for rapid and effective decontamination methods.

In general, N95 respirators are designed for one use before disposal. Extensive literature is available for decontaminating N95 respirators, of either bacterial spores, bacteria, or respiratory viruses (e.g. influenza A virus) (*3*–*6*). Effective inactivation methods for these pathogens and surrogates include UV light, ethylene oxide, vaporized hydrogen peroxide (VHP), gamma irradiation, ozone, and dry heat (A. Cramer et al., unpub data, https://doi.org/10.1101/2020.03.28.20043471) (*3*–*6*). The filtration efficiency and fit of N95 respirators has been less well explored, but reports

suggest that both filtration efficiency and N95 respirator fit can be affected by the decontamination method used (*7*; Appendix, https://wwwnc.cdc.gov/EID/article/26/9/20-1524-App1.pdf).

We analyzed 4 different decontamination methods, UV light (260–285 nm), 70°C dry heat, 70% ethanol, and VHP, for their ability to reduce contamination with infectious SARS-CoV-2 and their effect on N95 respirator function. The starting inoculum of SARS-CoV-2 has cycle threshold values of 20–22, similar to those observed in samples obtained from the upper and lower respiratory tract in humans. For each of the decontamination methods, we compared the normal inactivation rate of SARS-CoV-2 virus on N95 filter fabric to that on stainless steel. Using quantitative fit testing, we measured the filtration performance of N95 respirators after each decontamination run and 2 hours of wear, for 3 consecutive decontamination and wear sessions (Appendix). VHP and ethanol yielded extremely rapid inactivation both on N95 and on stainless steel (Figure, panel A). UV light inactivated SARS-CoV-2 virus rapidly from steel but more slowly on N95 fabric, probable because of its porous nature. Heat caused more rapid inactivation

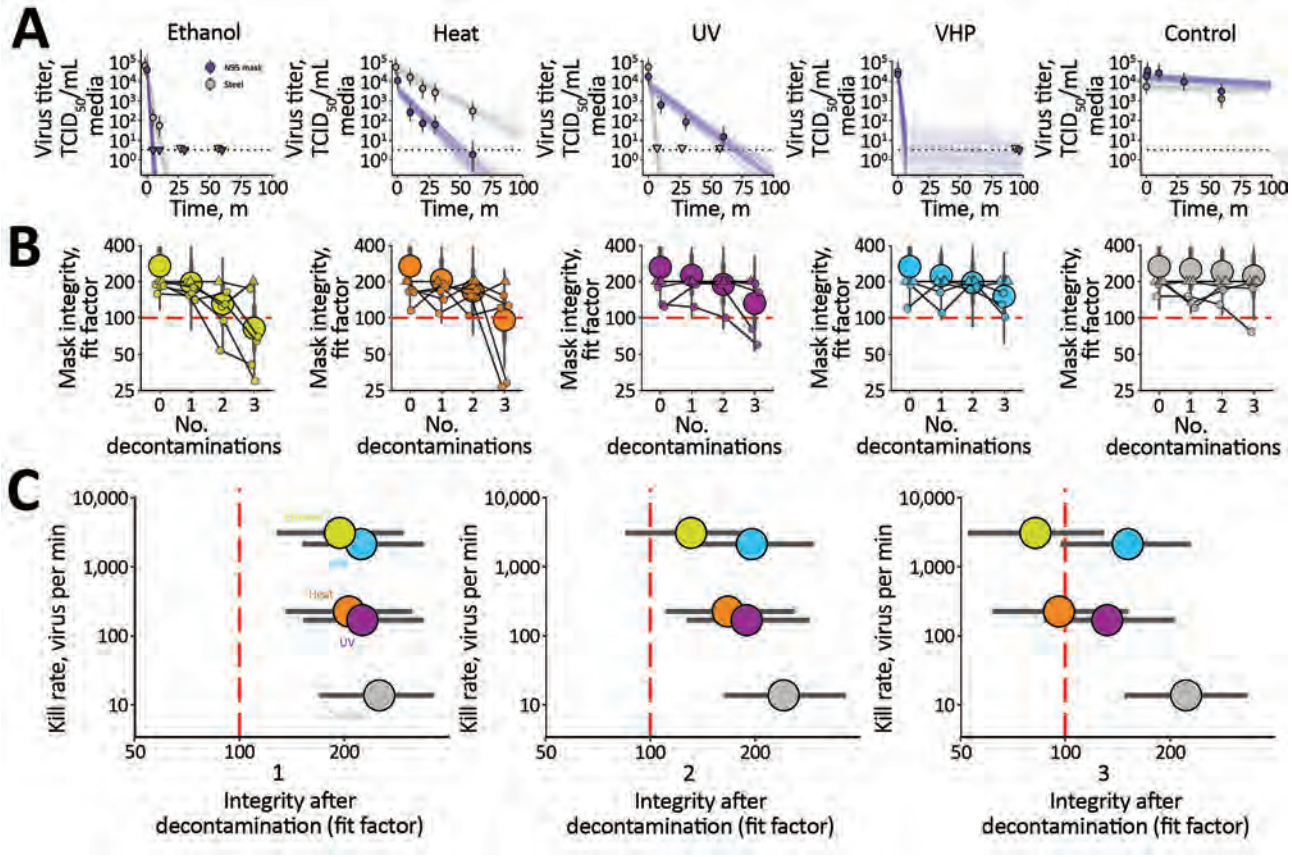

Figure. Results of decontamination of N95 respirators by 4 different methods. A) Inactivation of severe acute respiratory syndrome coronavirus 2 (SARS-CoV-2) virus (Appendix, https://wwwnc.cdc.gov/EID/article/26/9/20-1524-App1.pdf). Points indicate estimated mean viable titer across 3 replicates, circles the posterior median estimate of the mean, thick bars a 68% credible interval, and thin bars a 95% credible interval. Lines show predicted decay of virus titer over time and were generated by 50 random draws/replicate from the joint posterior distribution of the exponential decay rate (negative of the slope) and intercept (initial virus titer). Time points with no positive wells for any replicate are plotted as triangles at the approximate single-replicate LOD to indicate a plausible range of sub-LOD values. Black dotted line shows approximate LOD: $10^{0.5}$ $TCID_{50}$/mL media. Points at the LOD and at t = 0 for ethanol and heat methods applied to steel are offset slightly up and to the left to avoid overplotting. B) Mask integrity quantitative fit testing results after decontamination and 2 hours of wear for 3 consecutive runs. Data from 6 individual replicates (small circles and triangles) for each treatment are shown, in addition to estimated median fit factor (large circles), 68% range of underlying fit factors (thick bars), and 95% range (thin bars). Fit factors are a measure of filtration performance, the ratio of the concentration of particles outside the mask to the concentration inside. The measurement machine reports values ≤200; measured values of 200 are shown as upward-pointing triangles to indicate that true underlying values may be higher; other measured values are shown as circles. A minimal fit factor of 100 (red dashed line) is required for a mask to pass a fit test. See also Appendix Figure 3. C) SARS-CoV-2 decontamination performance after 1, 2, and 3 decontamination cycles, shown as kill rate vs. mask integrity after decontamination. Circles represent estimated median, bar length estimated 68% range. LOD, limit of detection; $TCID_{50}$, 50% tissue culture infective dose; VHP, vaporized hydrogen peroxide.

on N95 than on steel; inactivation rates on N95 were comparable to UV.

Quantitative fit tests showed that the filtration performance of the N95 respirator was not markedly reduced after a single decontamination for any of the 4 decontamination methods (Figure, panel B). Subsequent rounds of decontamination caused sharp drops in filtration performance of the ethanol-treated masks and, to a slightly lesser degree, the heat-treated masks. The VHP- and UV-treated masks retained comparable filtration performance to the control group after 2 rounds of decontamination and maintained acceptable performance after 3 rounds.

Our findings showed that VHP treatment had the best combination of rapid inactivation of SARS-CoV-2 virus and preservation of N95 respirator integrity under the experimental conditions (Figure, panel C). UV light killed the virus more slowly and preserved respirator function almost as well. Dry heat at 70°C killed the virus with similar speed to UV and is likely to maintain acceptable fit scores for 1–2 rounds of decontamination but should not be used for 3 rounds. Consistent with earlier findings (*8*), ethanol decontamination reduced N95 integrity and is not recommended.

All treatments, particularly UV light and dry heat, should be conducted for long enough to ensure sufficient reduction in virus concentration. The degree of required reduction depends upon the degree of initial virus contamination. Policymakers can use our estimated decay rates together with estimates of real-world contamination to choose appropriate treatment durations (Appendix).

Our results indicate that, in times of shortage, N95 respirators can be decontaminated and reused up to 3 times by using UV light and HPV and 1–2 times by using dry heat. Following nationally established guidelines for fit testing, seal check, and respirator reuse is critical (*9*,*10*). We recommend performing decontamination for sufficient time and ensuring proper function of the respirators after decontamination using readily available qualitative fit testing tools.

Acknowledgments

We thank Madison Hebner, Julia Port, Kimberly Meade-White, Irene Offei Owusu, Victoria Avanzato, and Lizzette Perez-Perez for excellent technical assistance.

This research was supported by the Intramural Research Program of the National Institute of Allergy and Infectious Diseases, National Institutes of Health. J.O.L.-S. and A.G. were supported by the Defense Advanced Research Projects Agency PREEMPT no. D18AC00031 and the UCLA AIDS Institute and Charity Treks, and J.O.L.-S. was supported by the US National Science Foundation (DEB-1557022), the Strategic Environmental Research and Development Program (RC-2635) of the US Department of Defense.

About the Author

Dr. Fischer is a member of the Virus Ecology Section at the Rocky Mountain Laboratories Division of Intramural Research, National Institute of Allergy and Infectious Diseases, National Institutes of Health. His research interests include the ecology of emerging viruses in their natural and spillover hosts, including SARS-CoV-2.

References

1. Ranney ML, Griffeth V, Jha AK. Critical supply shortages—the need for ventilators and personal protective equipment during the Covid-19 pandemic. N Engl J Med. 2020;382:e41. https://doi.org/10.1056/NEJMp2006141
2. McMichael TM, Currie DW, Clark S, Pogosjans S, Kay M, Schwartz NG, et al. Epidemiology of Covid-19 in a long-term care facility in King County, Washington. N Engl J Med. 2020; NEJMoa2005412. https://doi.org/10.1056/NEJMoa2005412
3. Batelle. Final report for the Bioquell hydrogen peroxide vapor (HPV) decontamination for reuse of N95 respirators. 2016 [cited 2020 May 22]. https://www.fda.gov/media/136386/download
4. Fisher EM, Shaffer RE. A method to determine the available UV-C dose for the decontamination of filtering facepiece respirators. J Appl Microbiol. 2011;110:287–95. https://doi.org/10.1111/j.1365-2672.2010.04881.x
5. Heimbuch BK, Wallace WH, Kinney K, Lumley AE, Wu CY, Woo MH, et al. A pandemic influenza preparedness study: use of energetic methods to decontaminate filtering facepiece respirators contaminated with H1N1 aerosols and droplets. Am J Infect Control. 2011;39:e1–9. https://doi.org/10.1016/j.ajic.2010.07.004
6. Lin TH, Tang FC, Hung PC, Hua ZC, Lai CY. Relative survival of *Bacillus subtilis* spores loaded on filtering facepiece respirators after five decontamination methods. Indoor Air. 2018;28:754–62. https://doi.org/10.1111/ina.12475
7. Lin TH, Chen CC, Huang SH, Kuo CW, Lai CY, Lin WY. Filter quality of electret masks in filtering 14.6–594 nm aerosol particles: effects of five decontamination methods. PLoS One. 2017; 12:e0186217. https://doi.org/10.1371/journal.pone.0186217
8. Viscusi DJ, Bergman MS, Eimer BC, Shaffer RE. Evaluation of five decontamination methods for filtering facepiece respirators. Ann Occup Hyg. 2009;53:815–827. https://doi.org/10.1093/annhyg/mep070
9. US Centers for Disease Control and Prevention. Decontamination and reuse of filtering facepiece respirators. 2020 [cited 2020 Apr 5]. https://www.cdc.gov/coronavirus/2019-ncov/hcp/ppe-strategy/decontamination-reuse-respirators.html
10. US National Institute for Occupational Safety and Health; US Centers for Disease Control and Prevention. Recommended guidance for extended use and limited reuse of N95 filtering facepiece respirators in healthcare settings. 2020 [cited 2020 May 22]. https://www.cdc.gov/niosh/topics/hcwcontrols/recommendedguidanceextuse.html

Address for correspondence: Vincent Munster, NIAID/NIH, Laboratory of Virology, Rocky Mountain Laboratories, 903S 4th St, Hamilton, MT 59840, USA; email: vincent.munster@nih.gov

Prolonged Infectivity of SARS-CoV-2 in Fomites

Boris Pastorino, Franck Touret, Magali Gilles, Xavier de Lamballerie, Rémi N. Charrel

Author affiliation: Unité des Virus Émergents, Marseille, France.

DOI: https://doi.org/10.3201/eid2609.201788

We spotted severe acute respiratory syndrome coronavirus 2 on polystyrene plastic, aluminum, and glass for 96 hours with and without bovine serum albumin (3 g/L). We observed a steady infectivity (<1 $\log_{10}$ drop) on plastic, a 3.5 $\log_{10}$ decrease on glass, and a 6 $\log_{10}$ drop on aluminum. The presence of proteins noticeably prolonged infectivity.

Severe acute respiratory syndrome coronavirus 2 (SARS-CoV-2) has spread worldwide, demonstrating a great potential for direct and indirect transmission between humans. Coronaviruses can keep their infectivity in fomites and thus can remain infectious on dry surfaces for hours (*1*,*2*). However, limited data are available for SARS-CoV-2 (*1*). Specifically, there are no data about the role of interfering substances such as proteins on SARS-CoV-2 infectivity in the environment. We evaluated the stability and infectivity of SARS-CoV-2 deposited on polystyrene plastic, aluminum, and glass for 96 hours at 45%–55% relative humidity (recommended for indoor living spaces by the American Society of Heating, Refrigeration and Air Conditioning Engineers) and 19°C –21°C temperature range using a 10^6 50% tissue culture infectivity dose ($TCID_{50}$)/mL inoculum.

We inoculated SARS-CoV-2 at a multiplicity of infection of 0.001 onto Vero E6 cells incubated at 37°C in 5% CO_2 for 72 h (Appendix, https://wwwnc.cdc.gov/EID/article/26/10/20-1788-App1.pdf). We collected the supernatant and clarified it by spinning at 1500 × *g* for 10 min. We prepared aliquots and stored them at -80°C before titration. We measured virus infectivity using $TCID_{50}$. We diluted the inoculum in cell culture medium containing 5% fetal bovine serum (FBS; final protein concentration 1.8 g/L) to 10^6 $TCID_{50}$/mL. For experiments with a higher protein concentration, we used a concentrated bovine serum albumin (BSA) solution (40 g/L) to result in a final protein concentration of 11.4 g/L. We measured virus infectivity sequentially on polypropylene plastic, aluminum, and glass slides. We deposited a 50-µL drop in triplicate on the various surfaces (≈1 cm^2 per piece) and recovered them sequentially to quantify viable infectious virions by endpoint titration on Vero E6 cells. The limit of detection for the assays was $10^{0.5}$ $TCID_{50}$/mL.

We conducted our experiments with and without BSA to mimic the protein content within body fluids of the respiratory system such as cough droplets, sputum, and airway mucosal secretions (*3*). Final protein concentration was 1.8 g/L without BSA conditions and 11.4 g/L with BSA conditions. We observed 3 different profiles, depending on surface type: a 3.5 $\log_{10}$ decrease over 44 h on glass (Figure 1, panel A), a steady infectivity with a <1 $\log_{10}$ drop over 92 h on polystyrene plastic (Figure 1, panel B), and a sharp 6 $\log_{10}$ drop in <4 h on aluminum (Figure 1 panel C). The probable adsorption of viral particles onto a plastic polystyrene surface was associated with prolonged infectivity, whereas a high drop on aluminum was observed as in previously published data on SARS-CoV, adenovirus, or poliovirus (*4*,*5*). Our results have also shown higher stability for SARS-CoV-2 on polystyrene plastic, with or without BSA, in comparison with a recent study (*1*); this variation could be explained by a different type of plastic used in the 2 studies. Regardless of the type of surface, virus infectivity decreased ≈1 $\log_{10}$ within 2 h (Table). To study SARS-CoV-2 stability in solution, we titrated cell culture supernatants containing 10^6 $TCID_{50}$/mL every 24 h for 96 h. We found that SARS-CoV-2 was very stable, showing an overall decreased infectivity <1.4 $\log_{10}$ reduction, results similar to those described for SARS-CoV (Appendix Figure) (*4*).

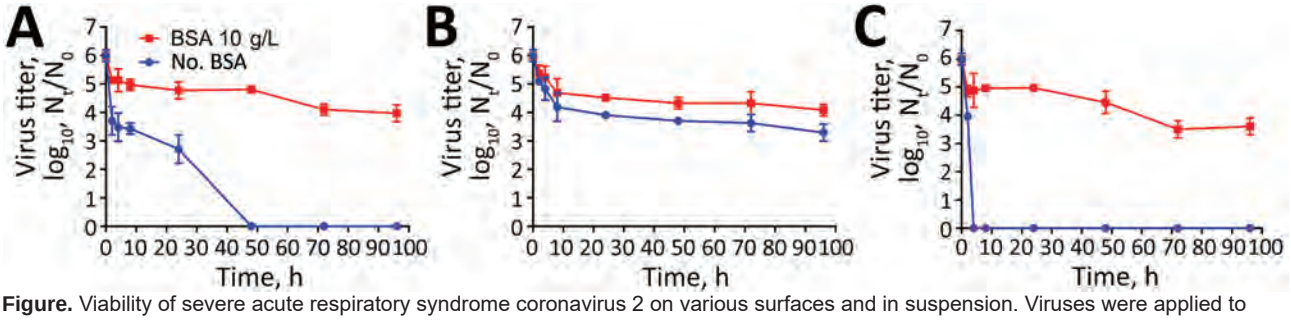

Figure. Viability of severe acute respiratory syndrome coronavirus 2 on various surfaces and in suspension. Viruses were applied to glass (A), polystyrene plastic (B), and aluminum (C) at 45%–55% relative humidity at 19°C–21°C for 96 h. The titer of viable virus is expressed as $TCID_{50}$/mL of collection medium. All samples were quantified by endpoint titration on Vero E6 cells with a limit of detection of ≈$10^{0.5}$ $TCID_{50}$/mL. $TCID_{50}$, 50% tissue culture infectivity dose.

Table. SARS-CoV-2 titer values for different materials*

	Material						
	Glass		Aluminum		Plastic		SARS-CoV-2 in
Time, h	No BSA	BSA 10 g/L	No BSA	BSA 10 g/L	No BSA	BSA 10 g/L	suspension
0				6 ± 0.2			
2	3.7 ± 0.5	5.1 ± 0.1	4 ± 0.1	4.8 ± 0.2	5.1 ± 0.1	5.4 ± 0.3	
4	3.5 ± 0.5	5.1 ± 0.4	ND	4.8 ± 0.5	4.8 ± 0.4	5.2 ± 0.4	
8	3.4 ± 0.2	4.9 ± 0.2	ND	4.9 ± 0.1	4.2 ± 0.5	4.6 ± 0.5	
24	2.7 ± 0.5	4.7 ± 0.3	ND	4.9 ± 0.1	3.8 ± 0.1	4.5 ± 0.1	5.99
48	ND	4.8 ± 0.1	ND	4.4 ± 0.4	3.7 ± 0.1	4.3 ± 0.2	4.99
72	ND	4.1 ± 0.2	ND	3.4 ± 0.3	3.6 ± 0.3	4.3 ± 0.4	3.99
96	ND	3.9 ± 0.3	ND	3.6 ± 0.3	3.3 ± 0.3	4.1 ± 0.2	3.99
Half-life	17	>96	2.5	>96	>96	>96	>96

*Values are mean value of 3 replicates ± SD. BSA, bovine serum albumin; ND, not detectable; SARS-CoV-2, severe acute respiratory syndrome coronavirus 2.

Our data showed that SARS-CoV-2 infectivity was remarkably preserved in the presence of proteins, regardless of the type of surface. A final concentration of 11.4 g/L of proteins, as used in our study, closely mimics that of respiratory fluids, which possess protein concentrations of a similar order of magnitude. However, the respiratory body fluids are complex media including not only proteins, but also enzymes and mucins (present in mucus) that may have a negative effect on virus infectivity. Regarding viral load measurement, the reason for avoiding the use of molecular techniques such as reverse transcription PCR is that despite that they allow quantification of RNA copies and determination of RNA decay, they cannot measure residual infectivity on various surfaces.

The protective effect of proteins had already been described for pandemic SARS-CoV or suggested for influenza A(H1N1) virus, but with less notable effects (*4*,*6*). As illustrated in other virus models (*7*), interfering substances such as proteins influenced the resistance of SARS-CoV-2 to drying and thus its persistence in the environment.

In conclusion, we showed that a moderate protein concentration in droplets markedly increased the infectivity of SARS-CoV-2, suggesting that a protein-rich medium like airway secretions could protect the virus when it is expelled and may enhance its persistence and transmission by contaminated fomites. Accordingly, it is plausible that fomites infected with SARS-CoV-2 play a key role in the indirect transmission of coronavirus disease (COVID-19). This finding supports surface cleaning as a necessary action that should be enforced and repeated becuase it may play a key role in halting SARS-CoV-2 transmission and mitigating the COVID-19 pandemic.

This study was funded in part by the European Virus Archive Global (EVA-GLOBAL) project H2020-INFRAIA-2019 program, project no. 871029, Preparedness and Response in an Emergency Contact to Pathogens of Medical and Veterinary Importance (PREPMedVet), Agence Nationale de la Recherche Franco-German Call on Civil Security/Global Security 2019 Edition, and the Inserm through the Reacting (REsearch and ACTion Targeting Emerging Infectious Diseases) initiative.

About the Author

Dr. Pastorino is research engineer with a PhD in virology. His primary research interests are biosafety aspects of Biosafety Level 3 viruses in the context of preparedness and response against epidemics.

References

1. van Doremalen N, Bushmaker T, Morris DH, Holbrook MG, Gamble A, Williamson BN, et al. Aerosol and surface stability of SARS-CoV-2 as compared with SARS-CoV-1. N Engl J Med. 2020;382:1564–7. https://doi.org/10.1056/NEJMc2004973
2. Ren S-Y, Wang W-B, Hao Y-G, Zhang H-R, Wang Z-C, Chen Y-L, et al. Stability and infectivity of coronaviruses in inanimate environments. World J Clin Cases. 2020;8:1391–9. https://doi.org/10.12998/wjcc.v8.i8.1391
3. Bansil R, Turner BS. The biology of mucus: composition, synthesis and organization. Adv Drug Deliv Rev. 2018;124:3–15. https://doi.org/10.1016/j.addr.2017.09.023
4. Rabenau HF, Cinatl J, Morgenstern B, Bauer G, Preiser W, Doerr HW. Stability and inactivation of SARS coronavirus. Med Microbiol Immunol (Berl). 2005;194:1–6. https://doi.org/10.1007/s00430-004-0219-0
5. Vasickova P, Pavlik I, Verani M, Carducci A. Issues concerning survival of viruses on surfaces. Food Environ Virol. 2010;2:24–34. https://doi.org/10.1007/s12560-010-9025-6
6. Kormuth KA, Lin K, Prussin AJ II, Vejerano EP, Tiwari AJ, Cox SS, et al. Influenza virus infectivity is retained in aerosols and droplets independent of relative humidity. J Infect Dis. 2018;218:739–47. https://doi.org/10.1093/infdis/jiy221
7. Firquet S, Beaujard S, Lobert P-E, Sané F, Caloone D, Izard D, et al. Survival of enveloped and non-enveloped viruses on inanimate surfaces. Microbes Environ. 2015;30:140–4. https://doi.org/10.1264/jsme2.ME14145

Address for correspondence: Remi Charrel, Unité des Virus Emergents, School of Medicine, 27 blvd Jean Moulin, Marseille 13005, France; remi.charrel@univ-amu.fr

Acute Cerebral Stroke with Multiple Infarctions and COVID-19, France, 2020

Souheil Zayet, Timothée Klopfenstein, Róbert Kovács, Silviu Stancescu, Beate Hagenkötter

Author affiliation: Nord Franche-Comté Hospital, Trévenans, France

DOI: https://doi.org/10.3201/eid2609.201791

We describe 2 cases in coronavirus disease patients in France involving presumed thrombotic stroke that occurred during ongoing anticoagulation treatment for atrial fibrillation stroke prophylaxis; 1 patient had positive antiphospholipid antibodies. These cases highlight the severe and unique consequences of coronavirus disease–associated stroke.

Coronavirus disease (COVID-19) is an infectious disease caused by severe acute respiratory syndrome coronavirus 2 (SARS-CoV-2). Evidence increasingly shows that SARS-CoV-2 is not always confined to the respiratory tract but can induce neurologic diseases (*1*). Several studies have reported that acute ischemic stroke can develop in COVID-19 patients (*1*–*6*). We describe 2 COVID-19 patients who had multiple cerebral infarctions; 1 patient had positive antiphospholipid antibodies.

On March 25, 2020, an 84-year-old man with a history of diabetes mellitus, arterial hypertension, coronary heart disease, peripheral arterial disease, and atrial fibrillation (treated with apixaban [2.5 mg orally 2×/d]) sought care for respiratory symptoms, including dyspnea and cough. At admission, physical examination revealed a blood pressure of 120/70 mm Hg, irregular heartbeat (100 beats/min), fever (39°C), and bilateral crackling sounds on pulmonary auscultation. Laboratory findings revealed low leukocyte count and lymphopenia (Appendix, https://wwwnc.cdc.gov/EID/article/26/9/20-1791-App1.pdf). Chest radiograph showed a bilateral interstitial infiltrate. Real-time reverse transcription PCR on a nasopharyngeal swab specimen confirmed COVID-19.

Supportive treatment began (oxygen support, antimicrobial drugs [ceftriaxone 1 g by intravenous (IV) infusion/d], and hydroxychloroquine [200 mg orally 2×/d]), and the same dosage of apixaban was continued. On April 3 (day 9 of hospitalization), dysarthria, left hemiplegia, and alteration of consciousness developed. Brain magnetic resonance imaging revealed acute ischemic stroke in multiple vascular areas (Figure). We switched the anticoagulation medication from apixaban to IV unfractionated heparin [18 UI/kg/h]). On April 6 (day 12), the patients Glasgow coma scale score was 3/15 (eye opening = 1, motor response = 1, verbal response = 1), and severe acute respiratory distress developed. No neurologic recovery occurred, and the patient did not undergo subsequent brain imaging. Mechanical ventilation was not possible (high Charlson comorbidity index), and the patient died on April 12 (day 18).

On April 3, a 74-year-old man with a history of multiple cardiovascular diseases, such as atrial fibrillation treated with rivaroxaban (20 mg orally 1×/d), sought care for influenza-like illness and confusion. His work colleagues had noticed disorientation during his activity as a truck driver. At admission, physical examination revealed hypertension (230/70 mm Hg) and irregular heartbeat (86 beats/min). He was febrile (38.3°C) and had crackling sounds on pulmonary auscultation. Neurologic examination showed nonfluent aphasia. COVID-19 was diagnosed from results of real-time reverse transcription PCR, microbiologic testing, and computed tomographic thoracic imaging (Appendix). Brain computed tomographic scan revealed many recent ischemic infarctions in different vascular areas, and magnetic resonance imaging of the brain confirmed this finding (Figure). As with patient 1, this patient had no non–central nervous system thrombotic events (e.g., pulmonary embolisms, abdominal visceral infarction). Treatment began with IV unfractionated heparin (18 UI/kg/h), hydroxychloroquine (200 mg orally 2×/d), and antimicrobial drugs (ceftriaxone 1g by IV infusion/d). The patient's aphasia regressed, and he was discharged on April 20.

Several factors can cause acute ischemic stroke, but the primary ones are arterial and cardiac embolism, arterial wall disease, and variants of those conditions. Both of these patients had concurrent cardiovascular conditions, particularly atrial fibrillation, although both were adequately treated with anticoagulants. Hematologic derangements, including lymphopenia and leukopenia, are associated with ischemic stroke and are predictors of worse prognosis with stroke (*7*). A systematic review and meta-analysis identified lymphopenia as one of the most prevalent laboratory results described in COVID-19 (35%–72%) (*8*), and we observed it in these 2 patients. Many infectious agents have been implicated as potential causes of cerebral stroke, such as herpes simplex virus, varicella zoster virus, *Treponema pallidum*, *Mycobacterium tuberculosis*, and *Aspergillus* spp.; acute bacterial meningitis has also been

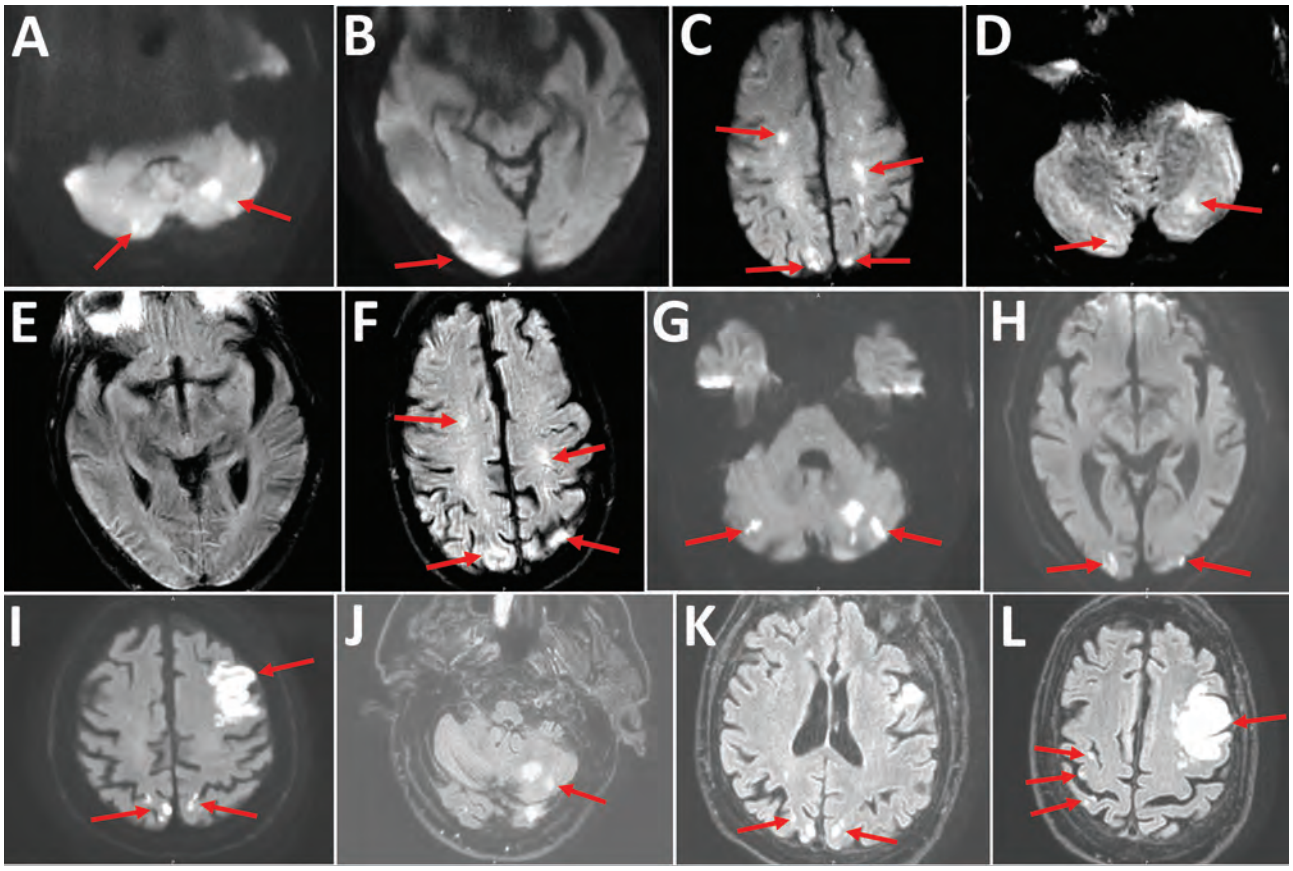

Figure. Cerebral magnetic resonance image (MRI) showing acute ischemic stroke in multiple vascular areas of 2 coronavirus disease patients, France. A–F) Patient 1. Diffusion weighted imaging (DWI) showed hyperintensive lesions of bilateral cerebellar hemispheres (arrows, A), right occipital cortex (arrows, B), bilateral centrum semiovale and bilateral parietal cortex (arrows, C). A part of the lesions are already hyperintensive in FLAIR (fluid-attenuated inversion recovery) sequences (arrows, D, F). Normal FLAIR sequence of the right occipital cortex; early stroke MRI (E). MRI quality is reduced because of dental artifact. G–L) Patient 2. Cerebral MRI showed multiple small ischemic infarctions with hyperintensive lesions (arrows) in bilateral cerebellar hemispheres (DWI [G], FLAIR [J; only left hemisphere]), bilateral occipital cortex (DWI [H], FLAIR [K]), main infarction in the left frontal lobe and small biparietal infarctions (DWI [I], FLAIR [L]).

implicated (*9*). Multiple brain localizations have previously been described with other viruses that lead to cerebrovascular complications through various mechanisms, including multifocal vasculopathy, focal infiltrative vasculitis and vasospasm, and direct vessel wall invasion and thrombus formation (*10*).

In this rapidly emerging epidemic, several cases have reported strokes in SARS-CoV-2–infected patients (*1*–*6*). However, the unique feature in the patients we report is multiple simultaneous strokes. These cases involved presumed thrombotic stroke that occurred during ongoing anticoagulation for atrial fibrillation stroke prophylaxis. Given the increasing realization that COVID-19 might be associated with hypercoagulability, the concurrent presence of anticoagulation with direct oral anticoagulants should not be reassuring as preventive.

Other authors suggest that the presence of antiphospholipid antibodies, such as anticardiolipin antibodies, as well as anti–β_2-glycoprotein I antibodies might rarely lead to multiple thrombotic cerebral events (*5*). In the patients we report, subsequent serologic testing showed anticardiolipin antibodies (IgM) in patient 1. We did not conduct functional testing (such as dilute Russell viper venom time). However, antiphospholipid antibody syndrome in cases of stroke cannot be diagnosed until positive antibodies persist after multiple months.

The association between cerebral stroke and COVID-19 requires more attention. Coagulability dysfunction and possibly antiphospholipid antibody syndrome may contribute to thromboembolic events in the central nervous system. Further investigation is required to determine the prognostic role of the presence of antiphospholipid antibodies in COVID-19.

Acknowledgments

We thank Vincent Gendrin for English language editing and his support and valuable feedback.

About the Author

Dr Zayet is a specialist in the Infectious Diseases Department of Nord Franche-Comte Hospital, France. His primary research interests focus on hepatitis and tuberculosis, especially in HIV-infected patients.

References

1. Mao L, Jin H, Wang M, Hu Y, Chen S, He Q, et al. Neurologic manifestations of hospitalized patients with coronavirus disease 2019 in Wuhan, China. JAMA Neurol. 2020 Apr 10 [Epub ahead of print]. https://doi.org/10.1001/jamaneurol.2020.1127
2. Oxley TJ, Mocco J, Majidi S, Kellner CP, Shoirah H, Singh IP, et al. Large-vessel stroke as a presenting feature of covid-19 in the young. N Engl J Med. 2020;382:e60. https://doi.org/10.1056/NEJMc2009787
3. Klok FA, Kruip MJHA, van der Meer NJM, Arbous MS, Gommers DAMPJ, Kant KM, et al. Incidence of thrombotic complications in critically ill ICU patients with COVID-19. Thromb Res. 2020 Apr 10 [Epub ahead of print]. https://doi.org/10.1016/j.thromres.2020.04.013
4. Lodigiani C, Iapichino G, Carenzo L, Cecconi M, Ferrazzi P, Sebastian T, et al.; Humanitas COVID-19 Task Force. Venous and arterial thromboembolic complications in COVID-19 patients admitted to an academic hospital in Milan, Italy. Thromb Res. 2020;191:9–14. https://doi.org/10.1016/j.thromres.2020.04.024
5. Zhang Y, Xiao M, Zhang S, Xia P, Cao W, Jiang W, et al. Coagulopathy and antiphospholipid antibodies in patients with covid-19. N Engl J Med. 2020;382:e38. https://doi.org/10.1056/NEJMc2007575
6. Griffin DO, Jensen A, Khan M, Chin J, Chin K, Parnell R, et al. Arterial thromboembolic complications in COVID-19 in low risk patients despite prophylaxis. Br J Haematol. 2020 May 6 [Epub ahead of print]. https://doi.org/10.1111/bjh.16792
7. Ren H, Liu X, Wang L, Gao Y. Lymphocyte-to-monocyte ratio: a novel predictor of the prognosis of acute ischemic stroke. J Stroke Cerebrovasc Dis. 2017;26:2595–602. https://doi.org/10.1016/j.jstrokecerebrovasdis.2017.06.019
8. Rodriguez-Morales AJ, Cardona-Ospina JA, Gutiérrez-Ocampo E, Villamizar-Peña R, Holguin-Rivera Y, Escalera-Antezana JP, et al.; Latin American Network of Coronavirus Disease 2019-COVID-19 Research (LANCOVID-19). Electronic address: https://www.lancovid.org. Clinical, laboratory and imaging features of COVID-19: A systematic review and meta-analysis. Travel Med Infect Dis. 2020;34:101623. https://doi.org/10.1016/j.tmaid.2020.101623
9. Shulman JG, Cervantes-Arslanian AM. Infectious etiologies of stroke. Semin Neurol. 2019;39:482–94. https://doi.org/10.1055/s-0039-1687915
10. Lin C-F, Hong C-T, Lee W-H, Wu D, Hu C-J, Chung C-C. Disseminated cutaneous herpes zoster and multiple cerebral infarcts in an adult with diabetes mellitus. J Neurovirol. 2020;26:130–2. https://doi.org/10.1007/s13365-019-00790-7

Address for correspondence: Souheil Zayet, Department of Infectious Disease, Nord Franche-Comte Hospital, 100 Route de Moval, 90400 Trevenans, France; email: souhail.zayet@gmail.com

Large SARS-CoV-2 Outbreak Caused by Asymptomatic Traveler, China

Jingtao Liu, Jiaquan Huang, Dandan Xiang

Author affiliations: Hubei University of Medicine, Shiyan, China (J. Liu); Huazhong University of Science and Technology, Wuhan, China (J. Liu, J. Huang, D. Xiang); Tongji Hospital, Wuhan (J. Huang, D. Xiang)

DOI: https://doi.org/10.3201/eid2609.201798

An asymptomatic person infected with severe acute respiratory syndrome coronavirus 2 returned to Heilongjiang Province, China, after international travel. The traveler's neighbor became infected and generated a cluster of ≥71 cases, including cases in 2 hospitals. Genome sequences of the virus were distinct from viral genomes previously circulating in China.

Coronavirus disease (COVID-19), caused by severe acute respiratory syndrome coronavirus 2 (SARS-CoV-2), has spread rapidly around the world since the first cases were reported in late 2019 (*1*,*2*). Prior to April 9, 2020, Heilongjiang Province, China, had not reported a new COVID-19 diagnosis since March 11, 2020. On April 9, SARS-CoV-2 was diagnosed in 4 patients. By April 22, ≥71 persons had been infected. The likely origin of this cluster is an imported case from an asymptomatic traveler.

We collected and analyzed epidemiologic data published on the website of the Health Commission of Heilongjiang Province for April 9–23, 2020 (*3*). We defined confirmed COVID-19 cases as persons who tested positive for SARS-CoV-2 and had clinical symptoms. We defined asymptomatic carriers as persons without clinical symptoms who tested positive for SARS-CoV-2. We refer to case-patients by a letter for each family (A–Z, AA–ZZ), then by the assumed transmission generation (1–2), and finally in sequential order of exposure to SARS-CoV-2–positive persons in generations 1–3 (Figure) (*4*).

On March 19, 2020, case-patient A0 returned to Heilongjiang Province from the United States; she was asked to quarantine at home. She lived alone during her stay in Heilongjiang Province. She had negative SARS-CoV-2 nucleic acid and serum antibody tests on March 31 and April 3.

Patient B1.1 was the downstairs neighbor of case-patient A0. They used the same elevator in the building but not at the same time and did not have close contact otherwise. On March 26, B1.1's mother, B2.2, and her mother's boyfriend, B2.3, visited and stayed in B1.1's

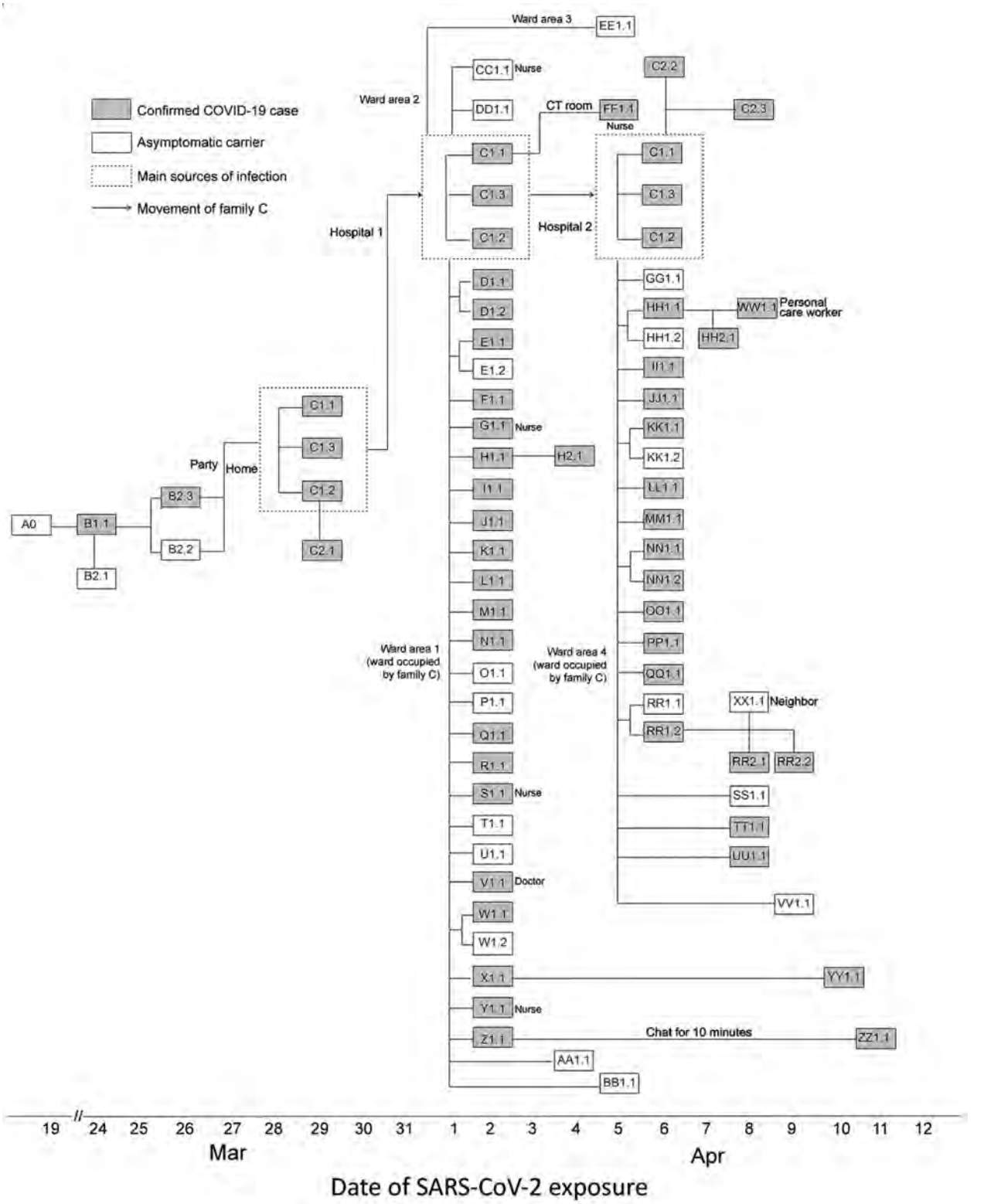

Figure. Timeline of exposure and connections between cases of severe acute respiratory syndrome coronavirus 2 (SARS-CoV-2) among persons in Heilongjiang Province, China. A0 returned from the United States on March 19, tested negative for SARS-CoV-2, and self-quarantined in her apartment and remained asymptomatic. However, SARS-CoV-2 serum IgM was negative and IgG was positive in later retests, indicating that A0 was previously infected with SARS-CoV-2 and likely was an asymptomatic carrier. B1.1, A0's downstairs neighbor, likely became infected by using the elevator in the building after A0 had used it.

home all night. On March 29, B2.2 and B2.3 attended a party with patient C1.1 and his sons, C1.2 and C1.3.

On April 2, C1.1 suffered a stroke and was admitted to hospital 1. His sons, C1.2 and C1.3, cared for him in ward area 1 of the hospital. Patient C1.1 shared the same clinical team and items, such as a microwave, with other patients in the ward. On April 6, patient C1.1 was transferred to hospital 2 because of fever; C1.2 and C1.3 accompanied him.

On April 7, patient B2.3 first noted symptoms of COVID-19. He tested positive for SARS-CoV-2 on April 9, the first confirmed case in this cluster. His close contacts, B1.1, B2.1, B2.2, and C1.1, subsequently tested positive for SARS-CoV-2 on April 9 or 10. Patient C1.1 was quarantined in hospital 2 when he tested positive on April 9. The epidemiologic investigation showed that none of these 5 persons had a history of travel or residence in affected areas with sustained transmission of SARS-CoV-2 during the 14 days before diagnosis, suggesting that SARS-CoV-2 came from contact with other persons.

During C1.1's admission at hospital 1, a total of 28 other persons, D1.1–BB1.1, were infected with SARS-CoV-2 in ward area 1. Because all patients in the ward could ambulate, 4 persons, CC1.1, DD1.1, EE1.1, and FF1.1, were infected in other wards and in the computed tomography room of hospital 1. Among hospital 1 staff, 5 nurses and 1 doctor were infected. In hospital 2, another 20 persons, GG1.1–VV1.1, were infected in the ward where C1.1 stayed (Figure).

On April 9, investigators also learned that A0, B1.1's neighbor, had returned on March 19 from the United States, where COVID-19 cases had been detected. Investigators performed SARS-CoV-2 serum antibody tests on A0 on April 10 and 11. SARS-CoV-2 serum IgM was negative but IgG was positive, indicating that A0 was previously infected with SARS-CoV-2 (*5*,*6*). Therefore, we believe A0 was an asymptomatic carrier (*7*,*8*) and that B1.1 was infected by contact with surfaces in the elevator in the building where they both lived (*9*). Other residents in A0's building tested negative for SARS-CoV-2 nucleic acids and serum antibodies.

On April 15, the Chinese Center for Disease Control and Prevention sequenced the entire genomes of 21 samples from the cluster. Viral genomes were identical in 18 cases and 3 other cases had a difference of 1–2 nucleotides, indicating that SARS-CoV-2 came from the same point of origin. The viral genome sequences from the cluster were distinct from the viral genomes previously circulating in China, indicating the virus originated abroad (*10*) and suggesting case A0 was the origin of infection for this cluster.

All persons associated with this cluster, including those who lived in the same community and had close contact with SARS-CoV-2–positive patients or visited the 2 hospitals during April 2–15, were tested for SARS-CoV-2 nucleic acids and serum antibodies. As of April 22, 2020, A0 remained asymptomatic, and a total of 71 SARS-CoV-2–positive cases had been identified in the cluster.

Our results illustrate how a single asymptomatic SARS-CoV-2 infection could result in widespread community transmission. This report also highlights the resources required for case investigation and challenges associated with containment of SARS-CoV-2. Continued measures to protect, screen, and isolate infected persons are essential to mitigating and containing the COVID-19 pandemic.

Acknowledgments

We thank the patients described in this report, the health care personnel who cared for them, the staff members of Health Commission of Heilongjiang Province, and the staff members of Heilongjiang Provincial Center for Disease Control and Prevention.

The opinions expressed by authors contributing to this journal do not necessarily reflect the opinions of the Chinese Centers for Disease Control and Prevention or the institutions with which the authors are affiliated.

About the Author

Mr. Liu is a PhD candidate in Huazhong University of Science and Technology. He also conducts research in Hubei University of Medicine. His primary research interest is neurodegenerative diseases.

Reference

1. Zhu N, Zhang D, Wang W, Li X, Yang B, Song J, et al.; China Novel Coronavirus Investigating and Research Team. A novel coronavirus from patients with pneumonia in China, 2019. N Engl J Med. 2020; 382:727–33. https://doi.org/10.1056/NEJMoa2001017
2. Holshue ML, DeBolt C, Lindquist S, Lofy KH, Wiesman J, Bruce H, et al.; Washington State 2019-nCoV Case Investigation Team. First case of 2019 novel coronavirus in the United States. N Engl J Med. 2020;382:929–36. https://doi.org/10.1056/NEJMoa2001191
3. Health Commission of Heilongjiang Province. China. Patient trajectory: release of new confirmed cases, asymptomatic infection trajectory on April 23, 2020 [in Chinese] [cited 2020 Apr 23]. http://yiqing.ljjk.org.cn/index/Patients/newslist
4. Ghinai I, Woods S, Ritger KA, McPherson TD, Black SR, Sparrow L, et al. Community transmission of SARS-CoV-2 at two family gatherings—Chicago, Illinois, February–March 2020. MMWR Morb Mortal Wkly Rep. 2020;69:446–50. https://doi.org/10.15585/mmwr.mm6915e1
5. To KK, Tsang OT, Leung WS, Tam AR, Wu TC, Lung DC, et al. Temporal profiles of viral load in posterior

oropharyngeal saliva samples and serum antibody responses during infection by SARS-CoV-2: an observational cohort study. Lancet Infect Dis. 2020;20:565–74. https://doi.org/10.1016/S1473-3099(20)30196-1
6. Jin Y, Wang M, Zuo Z, Fan C, Ye F, Cai Z, et al. Diagnostic value and dynamic variance of serum antibody in coronavirus disease 2019. Int J Infect Dis. 2020;94:49–52. https://doi.org/10.1016/j.ijid.2020.03.065
7. Pan Y, Long L, Zhang D, Yuan T, Cui S, Yang P, et al. Potential false-negative nucleic acid testing results for severe acute respiratory syndrome coronavirus 2 from thermal inactivation of samples with low viral loads. Clin Chem. 2020;66:794–801. https://doi.org/10.1093/clinchem/hvaa091
8. Li D, Wang D, Dong J, Wang N, Huang H, Xu H, et al. False-negative results of real-time reverse-transcriptase polymerase chain reaction for severe acute respiratory syndrome coronavirus 2: role of deep-learning-based CT diagnosis and insights from two cases. Korean J Radiol. 2020;21:505–8. https://doi.org/10.3348/kjr.2020.0146
9. Ong SWX, Tan YK, Chia PY, Lee TH, Ng OT, Wong MSY, et al. Air, surface environmental, and personal protective equipment contamination by severe acute respiratory syndrome coronavirus 2 (SARS-CoV-2) from a symptomatic patient. JAMA. 2020;323:1610. https://doi.org/10.1001/jama.2020.3227
10. Heilongjiang Province People's Government. 51st press conference on the progress of joint prevention and control of the new coronavirus pneumonia epidemic in Heilongjiang Province; April 28, 2020 [in Chinese] [cited 2020 Jun 1]. http://www.hlj.gov.cn/ftzb/system/ 2020/04/28/010925063.shtml

Address for correspondence: Dandan Xiang, Department of Infectious Diseases, Tongji Hospital, Tongji Medical College, Huazhong University of Science and Technology, 1095 Jiefang Avenue, Wuhan 430030, China; email: ddxiang2013@163.com

Antibody Responses after Classroom Exposure to Teacher with Coronavirus Disease, March 2020

Nicole E. Brown,[1] Jonathan Bryant-Genevier,[1] Uptala Bandy, Carol A. Browning, Abby L. Berns, Mary Dott, Michael Gosciminski, Sandra N. Lester, Ruth Link-Gelles, Daniela N. Quilliam, James Sejvar, Natalie J. Thornburg, Bernard J. Wolff, John Watson

DOI: https://doi.org/10.3201/eid2609.201802

Author affiliations: Centers for Disease Control and Prevention, Atlanta, Georgia, USA (N.E. Brown, J. Bryant-Genevier, M. Dott, S.N. Lester, R. Link-Gelles, J. Sejvar, N.J. Thornburg, B.J. Wolff, J. Watson); Rhode Island Department of Health, Providence, Rhode Island, USA (U. Bandy, C.A. Browning, A.L. Berns, M. Gosciminski, D.N. Quilliam); US Public Health Service Commissioned Corps, Rockville, Maryland, USA (M. Dott, R. Link-Gelles, J. Sejvar)

After returning from Europe to the United States, on March 1, 2020, a symptomatic teacher received positive test results for severe acute respiratory syndrome coronavirus 2. Of the 21 students exposed to the teacher in the classroom, serologic results suggested past infection for 2. Classroom contact may result in virus transmission.

In late February 2020, a teacher experienced headache, sore throat, myalgia, and fatigue while traveling in Europe, where community transmission of severe acute respiratory syndrome coronavirus 2 (SARS-CoV-2) was ongoing (*1*). After arriving back in the United States, the teacher returned to school February 24–27 while experiencing the same symptoms plus limited cough. An oropharyngeal swab sample collected on March 1 was positive for SARS-CoV-2 by reverse transcription PCR (cycle threshold values N1 = 35.05, N2 = 35.2; RNase P = 23.58). All students who attended classes with the infected teacher were instructed to quarantine themselves at home through March 12. After the quarantine period, we conducted a serologic survey to assess potential SARS-CoV-2 transmission in a classroom setting.

During February 24–27, the teacher taught 16 classes, all in the same room, each with ≤30 students. Of the 16 classes, 10 were discussion-based, in which the teacher reported walking around the room and speaking directly with students (interactive classes). For the other 6 classes, the teacher sat mostly in 1 location and close interactions with students were limited (noninteractive classes). On March 10, we contacted 120 students (48 [40%] enrolled in interactive classes, 72 [60%] enrolled in noninteractive classes) whose only known exposure was through classroom contact with the teacher and invited them to participate in our serologic survey; 21 (18%) students volunteered.

Median participant age was 17 years (range 5–18 years). Five (24%) participants had interactive classroom contact; mean in-class time was 108 minutes. Sixteen (76%) participants had noninteractive classroom contact only; mean in-class time was 50 minutes.

Participating students completed a questionnaire about symptoms experienced during the quarantine period and provided a blood specimen. On March 13,

[1]These first authors contributed equally to this article.

whole blood (3–5 mL) was collected and serum was separated before samples were frozen at –80°C for shipping. The Centers for Disease Control and Prevention tested the samples for antibodies by ELISA, as described previously (B. Freeman et al., unpub. data, https://www.biorxiv.org/content/10.1101/2020.04.24.057323v2). We considered reciprocal titers of ≥400 to be positive and reciprocal titers of ≥100 but <400 to be indeterminate.

Of the 5 students with interactive classroom contact, results for 2 (students A and B) were suggestive of previous SARS-CoV-2 infection; results for student A were positive and for student B indeterminate (Table). Students A and B were not in the classroom during the same period and sat in different locations in the classroom. Student A had a reciprocal titer of 400 and spent 135 minutes in interactive classes. Beginning February 26, this student experienced intermittent myalgia, rhinorrhea, and cough for 9 days. Student B had a reciprocal titer of 100, spent 90 minutes in the interactive classroom, and reported no symptoms. The remaining 3 students (students C–E) had reciprocal titers of <100. Student C spent 135 minutes in interactive classes and reported no symptoms. Students D and E each spent 90 minutes in interactive classes and reported limited symptoms. Student D reported subjective fever and headache lasting 1 day, and student E reported rhinorrhea lasting 1 day. Although no serologic evidence of previous infection was found for participants with noninteractive classroom contact only, 7 (44%) reported symptoms. The most common symptoms among participants with noninteractive classroom contact were sore throat (n = 3), headache (n = 3), rhinorrhea (n = 2), and myalgia (n = 2).

Although SARS-CoV-2 transmission from symptomatic persons to close contacts has been well established, risks associated with classroom contact are not well known. The positive results for student A suggest past infection with SARS-CoV-2. The meaning of the indeterminate result for student B is less clear in this context, but this result may be suggestive of past infection. We do not know whether results from student A or B are indicative of immunity to SARS-CoV-2 infection. The symptoms reported by both students are consistent with those reported by children and adolescents with mildly symptomatic and asymptomatic coronavirus disease (*2*,*3*).

This survey is subject to limitations. First, we based the definition of interactive classroom contact on reported usual behavior by the teacher; however, variability of contact for each participant was not defined. Second, reported symptoms might have been affected by students' expectation of the survey's intent, leading to social desirability bias. Third, because of low participation, the results may not be generalizable to all students who had contact with the teacher. Fourth, among students who chose to participate, participation might have been influenced by their perceived risk or symptoms experienced during the quarantine period, leading to selection bias. Fifth, potential infections may not have been detected because blood collection ≈14 days after exposure may have been too soon for development of SARS-CoV-2 antibodies. Last, the only known exposure for participating students was the infected teacher; however, students could have been exposed by unrecognized community transmission. The risk for transmission from mildly symptomatic or asymptomatic persons is not well known.

Widespread school closures have mostly eliminated the risk for classroom transmission of SARS-CoV-2. However, these results suggest that classroom interaction between an infected teacher and students might result in virus transmission.

Acknowledgments

We thank the principal and staff at the participating school, staff who conducted interviews and collected blood, laboratory staff who conducted testing, and Booker T. Daniels.

About the Author

Dr. Brown is an Epidemic Intelligence Service Officer in the Meningitis and Vaccine Preventable Diseases Branch, Division of Bacterial Diseases, National Center for Immunization and Respiratory Diseases, Centers for Disease Control and Prevention, in Atlanta, GA, USA. Her research interests include the epidemiology, control, and prevention of infectious diseases.

Table. Antibody responses, classroom time, and symptoms experienced among students who had had interactive classroom contact with a teacher with confirmed coronavirus disease, March 2020

Student	ELISA result reciprocal titer	ELISA result interpretation	Minutes spent in interactive classroom	Symptoms (duration, d)
A	400	Positive	135	Myalgia (1), rhinorrhea (1), cough (3)
B	100	Indeterminate	90	None
C	<100	Negative	135	None
D	<100	Negative	90	Subjective fever (1). headache (1)
E	<100	Negative	90	Rhinorrhea (1)

References

1. Kinross P, Suetens C, Gomes Dias J, Alexakis L, Wijermans A, Colzani E, et al.; ECDC Public Health Emergency Team. Rapidly increasing cumulative incidence of coronavirus disease (COVID-19) in the European Union/European Economic Area and the United Kingdom, 1 January to 15 March 2020. Euro Surveill. 2020;25. https://doi.org/10.2807/1560-7917.ES.2020.25.11.2000285
2. CDC COVID-19 Response Team. Coronavirus disease 2019 in children — United States, February 12–April 2, 2020. MMWR Morb Mortal Wkly Rep. 2020;69;422–426 [Epub ahead of print]. http://doi.org/10.15585/mmwr.mm6914e4
3. Castagnoli R, Votto M, Licari A, Brambilla I, Bruno R, Perlini S, et al. Severe acute respiratory syndrome coronavirus 2 (SARS-CoV-2) infection in children and adolescents: a systematic review. JAMA Pediatr. 2020 Apr 22 [Epub ahead of print]. https://doi.org/10.1001/jamapediatrics.2020.1467

Address for correspondence: Nicole E. Brown, Centers for Disease Control and Prevention, 1600 Clifton Rd NE, Mailstop H24-6, Atlanta, GA 30329–4027, USA; email: lvx6@cdc.gov

Severe Acute Respiratory Syndrome Coronavirus 2 among Asymptomatic Workers Screened for Work Resumption, China

Xiaoyu Han,[1] Xiong Wei,[1] Osamah Alwalid,[1] Yukun Cao, Yumin Li, Li Wang,[2] Heshui Shi[2]

Author affiliations: Union Hospital, Tongji Medical College, Wuhan, China (X. Han, O. Alwalid, Y. Cao, Y. Li, H. Shi); Hubei Province Key Laboratory of Molecular Imaging, Wuhan (X. Han, O. Alwalid, Y. Li, H. Shi); Wuhan Pingan Healthcare Diagnostic Center, Wuhan (X. Wei, L. Wang)

DOI: https://doi.org/10.3201/eid2609.201848

After the outbreak in Wuhan, China, we assessed 29,299 workers screened for severe acute respiratory syndrome coronavirus 2 by reverse transcription PCR. We noted 18 (0.061%) cases of asymptomatic infection; 13 turned negative within 8.0 days, and 41 close contacts tested negative. Among 6 contacts who had serologic tests, none were positive.

[1]These first authors contributed equally to this article.
[2]These senior authors contributed equally to this article.

As the population of Wuhan, China, returns to work, asymptomatic cases of severe acute respiratory syndrome coronavirus 2 (SARS-CoV-2) are being discovered among workers receiving health checkups for work resumption. Previous studies have shown that asymptomatic cases can be a public health threat and might lead to another outbreak (*1*,*2*). However, little is known about the clinical characteristics of asymptomatic infections. We report on cases of asymptomatic SARS-CoV-2 infection among persons during work resumption screening in Wuhan.

At Wuhan Pingan Healthcare Diagnostic Center, we reviewed 29,299 asymptomatic persons who were screened for SARS-CoV-2 by reverse transcription PCR (RT-PCR) and 22,633 asymptomatic persons tested for SARS-CoV-2 antibodies during March 13–April 25, 2020. Throat swab specimens were tested for SARS-CoV-2 by using Real-Time Fluorescent-PCR Kits (DAAN GENE Co., LTD, https://www.en.daangene.com; Appendix, https://wwwnc.cdc.gov/EID/article/28/9/20-1848-App1.pdf). We used colloidal gold-based immunochromatographic strip assay, Novel Coronavirus (SARS-CoV-2) IgM/IgG Antibody Detection Assay (Vazyme Biotech Co. Ltd., http://vazyme.bioon.com.cn) to perform antibody testing (Appendix). We recorded the demographic features, exposure history, RT-PCR and serology results, and imaging reports at the time of testing. We obtained follow-up data from persons screened by telephone.

Among 29,299 persons screened by RT-PCR, we confirmed 18 (0.061%) cases of SARS-CoV-2 infection. Of 22,633 persons tested for SARS-CoV-2 antibodies, 617 (2.7%) cases had positive IgG but negative IgM; 196 (0.87%) cases had positive IgG and IgM; and 40 (0.18%) cases had negative IgG but positive IgM.

The median age of 18 asymptomatic case-patients (10 male, 8 female) was 30.5 years (Table). Six (33.3%) cases had clear contact history with a confirmed case of SARS-CoV-2 infection. The median cycle threshold (C_t) values on the day of first positive RT-PCR were 38.2 (C_t range 37.2–39.3) for ORFa1b gene and 38.1 (C_t range 36.81–38.5) for N gene (Table). All antibody tests were obtained on the day of first positive RT-PCR except in 1 case (obtained 6 days later). Half (7/14) the cases had negative IgM and IgG; the other half had positive IgG but negative IgM results (Table). Among 8 case-patients who had computed tomography imaging of the chest, none had remarkable findings. We closely observed the cases for 3–41 (median 16.5) days; 13 cases had negative RT-PCR within a median of 8 (range 3–14) days (Table), and none had symptoms. Among 41 close contacts, all had 2 consecutive negative RT-PCR tests ≥24 hours apart.

Among 6 contacts who had serologic tests, none had positive results.

According to Wuhan Municipal Health Commission (*3*), 275,400 RT-PCR tests were performed for universal screening during April 9–15, 2020. Among those, 182 (0.066%) asymptomatic persons were identified as SARS-Cov-2–positive, which is consistent with our study. Half the cases in our study showed negative IgM and IgG at the time of positive RT-PCR, suggesting recent infections (≤14 days). Seven (50%) cases in our study had positive IgG but negative IgM, indicating a late stage infection, 4 of which had a long interval of exposure (30–75 days). In addition, 13 cases had negative RT-PCR assays ≤8 (range 3–14) days, suggesting a favorable prognosis for persons with asymptomatic infections.

Epidemiologic, virologic, and modeling evidence support the possibility of SARS-CoV-2 transmission from persons who are presymptomatic (SARS-CoV-2 detected before symptoms onset) or asymptomatic (never develop symptoms) (*4*). None of the 18 asymptomatic persons in our study developed symptoms. Recent reports showed that the viral load of SARS-CoV-2 infections in persons with no or mild symptoms was similar to the viral load of symptomatic patients (*5*,*6*), which could contribute to rapid transmissions (*5*). However, other studies demonstrated that asymptomatic patients had a lower viral load than symptomatic and presymptomatic patients (*7*,*8*,*9*), which might indicate less transmissibility from asymptomatic persons. The median cycle threshold values for the 18 cases were 38.2 for ORFa1b gene and 38.1 for the N gene, indicating a relatively low viral load. In addition, all 41 close contacts of the asymptomatic case-patients tested negative by RT-PCR. Possible explanations for this finding include that: the asymptomatic infected persons had relatively low viral load and were less infectious; that asymptomatic persons did not have clinical symptoms, such as sneezing or coughing, that could cause virus spread; and that, due to the strict isolation and preventive measures taken in Wuhan for ≥3 months, the population was generally protected from the spread of infection by mask-wearing and self-quarantine.

Table 1. Clinical characteristics of asymptomatic persons with detected severe acute respiratory syndrome coronavirus 2 infection, Wuhan, China*

Age, y/sex	Occupation	Underlying condition	Interval, d†	Exposure source	RT-PCR	C_t ORFa1b	C_t N	Interval, d‡	IgM	IgG	Chest CT	Interval, d§	Follow-up, d
29/M	Office worker	N	70	Family	+, –, –	37	38	5	–	+	Normal	0	41
32/M	Journalist	N	54	Bus passenger	+, +, –	39	38	9	–	+	Normal	0	41
27/M	Journalist	N	NA	Unclear	+, –	35	32	3	–	–	Normal	0	39
31/F	Researcher	N	61	Family	+, –, –, –, –	36	38	7	–	–	NA	NA	23
27/M	Office worker	N	75	Family	+, –, –, –	33	35	3	–	+	Normal	0	21
32/F	Housewife	N	NA	Unclear	+, –, –	38	37	14	–	–	NA	NA	17
37/F	Office worker	N	22	Family	+, –, –, –	40	39	8	NA	NA	NA	NA	16
57/M	Logistics dispatcher	Asthma	NA	Unclear	+, –, –	39	37	8	NA	NA	Normal	10	16
25/M	Banking	N	NA	Unclear	+, –, –	38	38	8	NA	A	NA	NA	16
26/M	Marketing	N	NA	Unclear	+	39	38	NA	–	–	NA	NA	17
23/M	Marketing	N	NA	Unclear	+, –	38	38	13	–	–	Normal	5	17
26/F	Office worker	N	NA	Unclear	+, –	38	40	14	NA	NA	NA	NA	17
60/F	Cleaner	N	NA	Unclear	+	37	37	NA	–	+	NA	NA	13
65/M	Cleaner	COPD	NA	Unclear	+	39	39	NA	–	–	Normal	0	13
28/F	Office worker	N	NA	Unclear	+	38	39	NA	–	+	NA	NA	8
33/F	Office worker	N	30	Family	+, –	39	37	12	–	+	Normal	0	14
30/F	Office worker	N	NA	Unclear	+, –	39	38	10	–	+	NA	NA	13
62/M	Worker	Hypertension	NA	Unclear	+	39	39	NA	–	–	NA	NA	3

*COPD, chronic obstructive pulmonary disease; CT, computed tomography; C_t ORFa1b, RT-PCR cycle threshold for the ORFa1b gene; C_t N, RT-PCR cycle threshold for the N gene; N, no; NA, not available; +, positive; –, negative.
†Days between last exposure and initial positive RT–PCR.
‡Days between first positive and first negative RT-PCR results
§Days between first positive RT-PCR and CT scan.

Our report has limitations. Our sample size of asymptomatic cases is small, and follow-up was short. Recall bias of exposure history is another limitation; in the absence of clear symptom onset, asymptomatic persons might be less likely to accurately recall exposures than persons with symptoms. Finally, that the study took a place during the post-peak period of the epidemic in Wuhan, so contacts could have been seropositive already; those tested were seronegative, but most contacts did not have serologic testing.

In conclusion, as the population returns to the workplace, asymptomatic SARS-CoV-2–infected persons could be among workers. Although we did not detect transmission among 41 contacts of persons who were SARS-CoV-2–positive, such transmission cannot be excluded. Therefore, continued testing, self-quarantine, and mask-wearing should be encouraged to reduce the risk for additional outbreaks.

Acknowledgments

We thank all our colleagues for helping us during the current study.

This study was supported by Zhejiang University special scientific research fund for COVID-19 prevention and control, the Huazhong University of Science and Technology (HUST) COVID-19 Rapid Response Call (grant no. 2020kfyXGYJ019).

About the Author

Dr. Han is a clinician in the Department of Radiology, Union Hospital, Tongji Medical College, Huazhong University of Science and Technology, Wuhan, China. Her research interests including image diagnosis of pneumonia and lung cancer.

References

1. Qiu J. Covert coronavirus infections could be seeding new outbreaks. Nature. 2020 Mar 20 [Epub ahead of print]. https://doi.org/10.1038/d41586-020-00822-x
2. Pan A, Liu L, Wang C, Guo H, Hao X, Wang Q, et al. Association of public health interventions with the epidemiology of the COVID-19 outbreak in Wuhan, China. JAMA. 2020;323:1–9. https://doi.org/10.1001/jama.2020.6130
3. Wuhan Municipal Health Commission. CN-HEALTHCARE: Hubei health, 2020 April 19 [in Chinese] [cited 2020 May 25]. https://www.cn-healthcare.com/articlewm/20200419/content-1105403.html
4. Furukawa NW, Brooks JT, Sobel J. Evidence supporting transmission of severe acute respiratory syndrome coronavirus 2 while presymptomatic or asymptomatic. Emerg Infect Dis. 2020 May 4 [Epub ahead of print]. https://doi.org10.3201/eid2607.201595
5. Arons MM, Hatfield KM, Reddy SC, Kimball A, James A, Jacobs JR, et al. Presymptomatic SARS-CoV-2 infections and transmission in a skilled nursing facility. N Engl J Med. 2020;382:2081–90. https://doi.org/10.1056/NEJMoa2008457
6. Zou L, Ruan F, Huang M, Liang L, Huang H, Hong Z, et al. SARS-CoV-2 viral load in upper respiratory specimens of infected patients. N Engl J Med. 2020;382:1177–9. https://doi.org/10.1056/NEJMc2001737
7. Kim SE, Jeong HS, Yu Y, Shin SU, Kim S, Oh TH, et al. Viral kinetics of SARS-CoV-2 in asymptomatic carriers and presymptomatic patients. Int J Infect Dis. 2020;95:441–3. https://doi.org/10.1016/j.ijid.2020.04.083
8. He D, Zhao S, Lin Q, Zhuang Z, Cao P, Wang MH, et al. The relative transmissibility of asymptomatic COVID-19 infections among close contacts. Int J Infect Dis. 2020;94:145–7. https://doi.org/10.1016/j.ijid.2020.04.034
9. Zhou R, Li F, Chen F, Liu H, Zheng J, Lei C, et al. Viral dynamics in asymptomatic patients with COVID-19. Int J Infect Dis. 2020;96:288–290. https://doi.org/10.1016/j.ijid.2020.05.03

Address for correspondence: Heshui Shui, Department of Radiology, Union Hospital, Tongji Medical College, Wuhan 430030, China; email: heshuishi@hust.edu.cn

Effects of Proactive Social Distancing on COVID-19 Outbreaks in 58 Cities, China

Zhanwei Du, Xiaoke Xu, Lin Wang, Spencer J. Fox, Benjamin J. Cowling, Alison P. Galvani, and Lauren Ancel Meyers

Author affiliations: The University of Texas at Austin, Austin, Texas, USA (Z. Du, S.J. Fox, L.A. Meyers); Dalian Minzu University, Dalian, China (X. Xu); University of Cambridge, Cambridge, UK (L. Wang); The University of Hong Kong, Hong Kong, China (B.J. Cowling); Center for Infectious Disease Modeling and Analysis, Yale School of Public Health, New Haven, Connecticut, USA (A.P. Galvani); Santa Fe Institute, Santa Fe, New Mexico, USA (L.A. Meyers)

DOI: https://doi.org/10.3201/eid2609.201932

Cities across China implemented stringent social distancing measures in early 2020 to curb coronavirus disease outbreaks. We estimated the speed with which these measures contained transmission in cities. A 1-day delay in implementing social distancing resulted in a containment delay of 2.41 (95% CI 0.97–3.86) days.

On December 31, 2019, a cluster of atypical pneumonia in Wuhan, China, was reported to the regional office of the World Health Organization (WHO). Its etiology was later identified as the novel severe acute respiratory syndrome coronavirus 2 (SARS-CoV-2). Coronavirus disease (COVID-19) spread rapidly across China and internationally (*1*); as of April 9, 2020, a total of 1,436,198 confirmed cases and 85,522 deaths had been reported in 209 countries (*2*). In the absence of pharmaceutical prophylactic options, the primary means of COVID-19 control are social distancing interventions, including school closures, work restrictions, shelter-in-place measures, and travel bans.

In late January, reported COVID-19 cases rose steeply in Hubei Province, and imported cases sparked outbreaks in many other cities throughout China. By February 14, 2020, the government had limited the movement of >500 million persons across 80 cities, many of which rapidly enacted multiple social distancing orders to slow the local spread of the virus, including restricting nonessential services and public transit (*3*–*6*). Given the substantial economic and societal costs of such measures (*7*), estimates of their effectiveness can serve as critical evidence for intervention policy decisions worldwide (*8*).

Using case data from online reports published by the Chinese Center for Disease Control and health commissions (Appendix Table 4, https://wwwnc.cdc.gov/EID/article/26/9/20-1932-App1.pdf), we estimated the time elapsed between the first reported case in a city and successful containment of the outbreak (χ). Technically, we consider an outbreak contained when the 95% CI of the instantaneous reproduction number (R_t) drops below 1. We analyzed the speed of COVID-19 containment for 58 cities in mainland China outside of Huebei Province that had ≥20 confirmed cases by February 14, 2020 (Figure; Appendix Tables 2, 3). Collectively, these cities deployed 7 different types of interventions over the course of their epidemics (*9*): bans on entertainment and public gatherings;

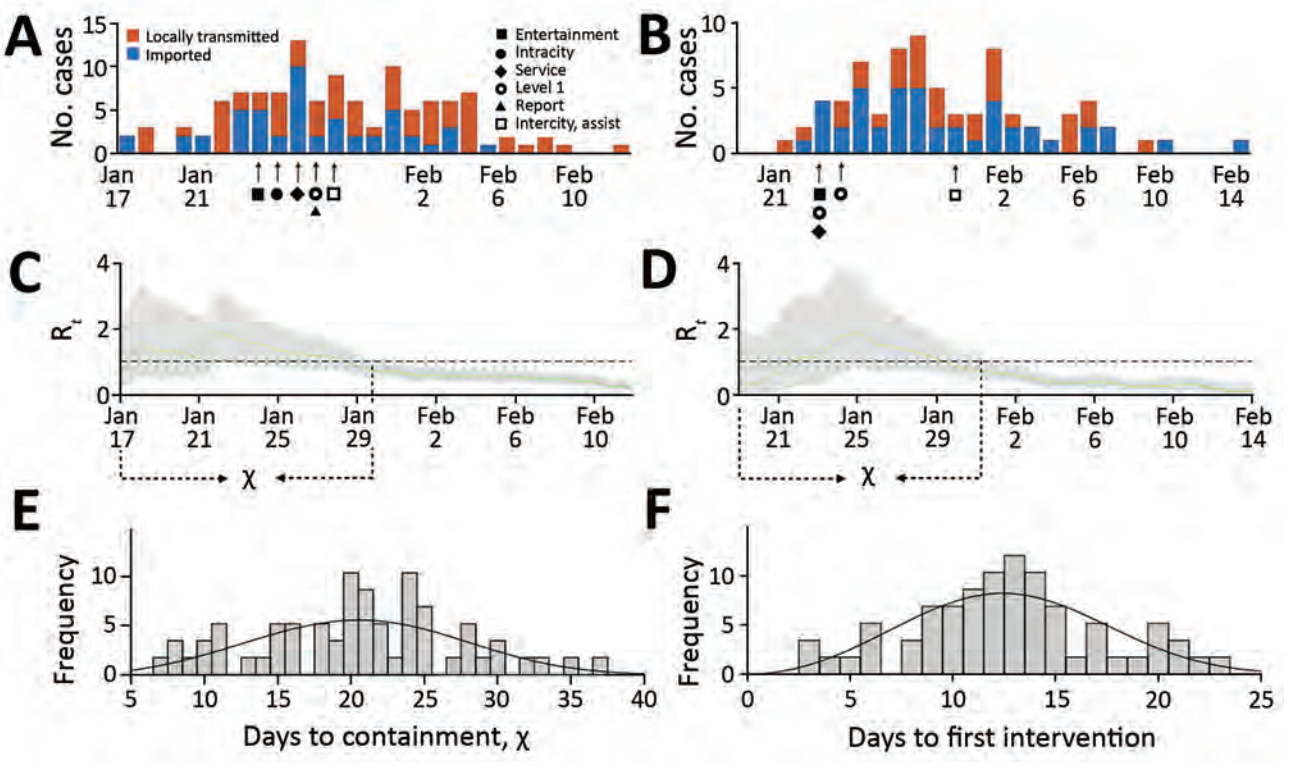

Figure. Coronavirus disease (COVID-19) introductions, transmission, and containment for 2 provincial capitals, China, before February 15, 2020. A) Estimated daily incidence of COVID-19 cases and the implementation of local social distancing measures in Xi'an. B) Estimated daily incidence of COVID-19 cases and the implementation of local social distancing measures in Nanjing. C, D) Estimated daily time-varying reproduction numbers (R_t). Green line indicates the median and gray shading 95% CI for R_t. We calculated the number of days from the first reported imported case until the upper 95% CI drops below 1 (χ) for (C) Xi'an and (D) Nanjing. E) The distribution of χ across 58 cities in mainland China. Mean duration of outbreaks is 21 days (SD ± 7). Based on an area under the curve comparison between gamma, log-normal, and Weibull distributions fitted via maximum-likelihood to the data, we found that the χ values are roughly Weibull distributed with scale 22.94 (95% CI 21.12–24.91) and shape 3.28 (95% CI 2.68–4.02), indicated by black line. F) The distribution of time between the first locally reported case and the first social distancing measure resembles a Weibull distribution with scale 14.24 (95% CI 13.01–15.60) and shape 2.98 (95% CI 2.44–3.65).

broad restrictions on public service including healthcare, schooling, shopping, and restaurants; initiation of a level 1 response entailing systematic testing and isolation of confirmed cases; suspension of intracity public transport; suspension of travel between cities; reporting of confirmed cases; recruitment of governmental staff and volunteers to enforce quarantine and social distancing. The mean (± SD) time between the first confirmed case and the implementation of the first social distancing measure was 13 (± 4.7) days. By the time these measures were enacted, the median cumulative reported cases in a city was 40, but the range was 9–248 across the 58 cities. The mean time until successful containment was 21 (± 7) days after the first reported case and 8 (± 6.8) days following the initiation of interventions. During the period of containment, the reproduction number (R_t) declined by an average of 54.3% (± 17.6%) (Appendix Figure 2).

Using a combination of linear regression and best-subsets model selection (*10*), we found that the timing of the first intervention and the initiation of level 1 response significantly predicted the speed of containment across the 36 cities that deployed all 7 interventions (R^2 = 0.27; p<0.001) (Appendix Figure 1). A delay of 1 day in implementing the first intervention is expected to prolong an outbreak by 2.41 (95% CI 0.96–3.86) days. In contrast, the timing of the level 1 response was inversely related to the speed of containment. Level 1 responses were initiated by the central government across mainland China over the course of 1 week, starting with the hardest hit areas in and near Hubei Province on the first day and working outwards toward more distant cities. Thus, the day of level 1 initiation within this 1-week period is a likely indicator for the initial severity of an outbreak and the corresponding difficulty of containment.

We have estimated the value of proactive social distancing interventions in terms of a reduction in days until successful containment. However, because most cities implemented multiple measures quickly and simultaneously, we are unable to disentangle the efficacies of individual modes of social distancing. We note that our estimates of R_t may be biased by the limited case report data available before February 14, 2020; we lack information about testing rates and priorities in China before February 14. As public health agencies around the globe struggle to determine when to implement potentially costly social distancing measures, these estimates highlight the potential long-term benefits of early and decisive action.

Acknowledgments

We thank Simon Cauchemez for helpful discussions.

Financial support was provided by US National Institutes of Health (grant no. U01 GM087719), the National Natural Science Foundation of China (grant no. 61773091), and Tito's Handmade Vodka.

About the Author

Dr. Du is a postdoctoral researcher in the Department of Integrative Biology at the University of Texas at Austin. He develops mathematical models to elucidate the transmission dynamics, surveillance, and control of infectious diseases.

References

1. Chen S, Yang J, Yang W, Wang C, Bärnighausen T. COVID-19 control in China during mass population movements at New Year. Lancet. 2020;395:764–6. https://doi.org/10.1016/S0140-6736(20)30421-9
2. World Health Organization. Coronavirus disease 2019 ([COVID-19)]: situation report 80. 2020 [cited 2020 Apr 9]. https://www.who.int/docs/default-source/coronaviruse/situation-reports/20200409-sitrep-80-covid-19.pdf
3. Chan JF-W, Yuan S, Kok K-H, To KK-W, Chu H, Yang J, et al. A familial cluster of pneumonia associated with the 2019 novel coronavirus indicating person-to-person transmission: a study of a family cluster. Lancet. 2020;395:514–23. https://doi.org/10.1016/S0140-6736(20)30154-9
4. Kraemer MUG, Yang C-H, Gutierrez B, Wu C-H, Klein B, Pigott DM, et al. The effect of human mobility and control measures on the COVID-19 epidemic in China. Science. 2020 Mar 25 [cited 2020 Mar 26]. https://science.sciencemag.org/content/early/2020/03/25/science.abb4218
5. Chinazzi M, Davis JT, Ajelli M, Gioannini C, Litvinova M, Merler S, et al. The effect of travel restrictions on the spread of the 2019 novel coronavirus (COVID-19) outbreak. Science. 2020;368:395–400. https://doi.org/10.1126/science.aba9757
6. Wu Z, McGoogan JM. Characteristics of and important lessons from the coronavirus disease 2019 (COVID-19) outbreak in China: summary of a report of 72,314 cases from the Chinese Center for Disease Control and Prevention. JAMA. 2020;323:1239–42. https://doi.org/10.1001/jama.2020.2648
7. Ayittey FK, Ayittey MK, Chiwero NB, Kamasah JS, Dzuvor C. Economic impacts of Wuhan 2019-nCoV on China and the world. J Med Virol. 2020;92:473–5. https://doi.org/10.1002/jmv.25706
8. Leung K, Wu JT, Liu D, Leung GM. First-wave COVID-19 transmissibility and severity in China outside Hubei after control measures, and second-wave scenario planning: a modelling impact assessment. Lancet. 2020;395:1382–93. https://doi.org/10.1016/S0140-6736(20)30746-7
9. Tian H, Liu Y, Li Y, Wu C-H, Chen B, Kraemer MUG, et al. An investigation of transmission control measures during the first 50 days of the COVID-19 epidemic in China. Science. 2020;368:638–42. https://doi.org/10.1126/science.abb6105
10. Yang H. The case for being automatic: introducing the automatic linear modeling (LINEAR) procedure in SPSS statistics. Multiple Linear Regression Viewpoints. 2013;39:27–37.

Address for correspondence: Lauren Ancel Meyers, Department of Integrative Biology, The University of Texas at Austin, 1 University Station C0990, Austin, TX 78712, USA; email: laurenmeyers@austin.utexas.edu

Parotitis-Like Symptoms Associated with COVID-19, France, March–April 2020

Jerome R. Lechien,[1] Annaelle Chetrit,[1] Younes Chekkoury-Idrissi, Lea Distinguin, Marta Circiu, Sven Saussez, Najete Berradja, Myriam Edjlali, Stephane Hans,[2] Robert Carlier[2]

Author affiliations: Foch Hospital, Paris, France (J.R. Lechien, Y. Chekkoury-Idrissi, L. Distinguin, M. Circiu, S. Hans); University of Mons, Mons, Belgium (J.R. Lechien, S. Saussez); University Hospital of Brussels (Saint-Pierre), Brussels, Belgium (J.R. Lechien, S. Saussez); Hôpitaux R. Poincaré–Ambroise Paré, Paris (A. Chetrit, N. Berradja, M. Edjlali, R. Carlier); Centre Hospitalier Sainte-Anne, Paris (M. Edjlali)

DOI: https://doi.org/10.3201/eid2609.202059

We report the clinical features of 3 patients in France who had parotitis (inflammation of the parotid salivary glands) as a clinical manifestation of confirmed coronavirus disease. Results from magnetic resonance imaging support the occurrence of intraparotid lymphadenitis, leading to a parotitis-like clinical picture.

The worldwide spread of coronavirus disease (COVID-19) is associated with the emergence of many clinical pictures of the disease. Patients might have nose and throat symptoms, such as loss of smell and taste (*1*). Many otolaryngologists have observed an increase in the number of patients with acute parotitis (inflammation of the parotid salivary glands), which could be related to COVID-19 (*2*). We report the clinical features of 3 outpatients who sought care at Foch Hospital (Paris, France) for parotitis-like symptoms in the context of COVID-19.

Three women sought care at the Department of Otolaryngology–Head and Neck Surgery of Foch Hospital for unilateral ear pain and retromandibular edema. The patients also reported general and otolaryngologic symptoms, including anorexia, arthralgia, myalgia, headache, fatigue, nasal obstruction, rhinorrhea, postnasal drip, sore throat, face pain, and loss of smell and taste (Table). Diagnosis of COVID-19 was confirmed by reverse-transcription PCR tests on nasopharyngeal swab specimens. The patients had no notable medical histories, and they were all vaccinated against mumps. The parotitis-like symptoms occurred at the onset of the disease in 2 patients and over the clinical course of the disease in the remaining patient. A clinical diagnosis of parotitis was made in all 3 cases. The otolaryngologist did not see any pus draining from the parotid duct.

Patients underwent magnetic resonance imaging (MRI), which indicated intraparotid lymphadenitis. In all three cases, we observed multiple unilateral or bilateral intraglandular lymph nodes in the deep and surface layers, in a relatively normal-sized gland. We preserved the lymph node architecture by using a preserved fatty hilum. We observed no juxtaglandular fat infiltration or thickening of the fascia. We also observed no intraglandular linear bands or cysts on the MRI (Appendix, https://wwwnc.cdc.gov/EID/article/26/9/20-2059-App1.pdf).

The 3 patients received 10–14 days of paracetamol (1 g 3–4×/d) for their COVID-19. The parotitis resolved over the next few days after diagnosis. The 3 patients had persistent loss of smell after the resolution of their general and parotitis-like symptoms.

The occurrence of acute parotitis related to COVID-19 has been suggested in a recent case report (*2*), corroborating the clinical observations of otolaryngologists. Our findings support the hypothesis that the parotitis-like symptoms might be attributable to intraparotid lymph node enlargement, which is different from a primary parotitis.

Infection with rubella, herpes, influenza, and human immunodeficiency viruses can result in salivary tropism (*3*,*4*), leading to diffuse parotitis. Our MRI findings mainly report diffuse enlargement of the gland without evidence of multiple intraglandular lymph nodes; however, the literature remains limited because the diagnosis is clinical and MRI is not often required. Mumps-related parotitis usually occurs in children and might be bilateral (*4*). In a patient with HIV infection, the parotid lesions appear as multiple and bilateral parotid lymphoepithelial cysts, which are bigger than lymph nodes (*5*). Moreover, cysts have T1 (hypo) and T2 (hyper) signals that are similar than those of the cerebrospinal fluid (*5*). In our patients, the MRI results did not indicate cysts.

The features we describe support the diagnosis of adenitis, which might impair the gland functioning. The adenitis and the parotid-related enlargement might block the main gland duct (Stenon's duct), leading to saliva retention and parotid tissue inflammation. The lack of saliva might be associated with sticky saliva and taste impairment. Intraparotid adenitis differs from primary diffuse parotitis, which was recently reported in an unique case of COVID-19 (*2*).

[1]These first authors contributed equally to this article.

[2]These senior authors contributed equally to this article.

Table. Demographic, clinical, and imaging characteristics of 3 patients who sought care for parotitis-like symptoms associated with coronavirus disease, Paris, France, March–April 2020*

Patient age, y/sex	Symptom type			Duration of symptoms	Treatment	MRI diagnosis
	General	ENT	Parotitis			
23/F	Anorexia, arthralgia, myalgia, fatigue, headache	Nasal obstruction, rhinorrhea, postnasal drip, sore throat, face pain, loss of smell and taste	Ear pain, retromandibular edema	10 d	Paracetamol	Intraparotid, lymphadenitis
31/F	Cough, arthralgia, myalgia, fatigue, headache, diarrhea, abdominal pain, urticaria, dyspnea	Nasal obstruction, rhinorrhea, postnasal drip, sore throat, face pain, loss of smell and taste	Ear pain, retromandibular edema, sticky saliva, pain during chewing	15 d	Paracetamol, vitamins	Intraparotid, lymphadenitis
27/F	Cough, fever, anorexia, arthralgia, myalgia, headache, fatigue	Rhinorrhea, face pain, sore throat, loss of smell	Ear pain, retromandibular edema	3 d	Paracetamol	Intraparotid, lymphadenitis

*Diagnoses were made in Foch Hospital (Paris, France) on the following dates: March 21 (patient 1), March 27 (patient 2), and April 2 (patient 3). ENT, ear, nose, and throat; MRI, magnetic resonance imaging.

Sanitation conditions and the difficulties in performing additional salivary gland examinations (e.g., sialography or MRI) complicate the characterization of parotitis. Thus, the main limitation of our report is the lack of functional examinations of the parotid during the clinical course of the disease. The assessment of the functioning of the saliva secretion and the detection of severe acute respiratory syndrome coronavirus 2 virus (SARS-CoV-2) in the saliva could provide further information about SARS-CoV-2 transmission through saliva.

Future studies are needed to characterize the parotid manifestations in COVID-19 patients. Although the findings of this study support the hypothesis that intraparotid lymphadenitis is a causal factor, the direct spread of SARS-CoV-2 into the parotid tissue might be theoretically possible regarding the presence of angiotensin converting enzyme 2 (the virus receptor) in the parotid tissue and the potential risk for excretion of virions through the saliva (*6*).

In conclusion, parotid inflammation might be encountered in COVID-19 patients and could be related to intraparotid lymphadenitis. Even in persons vaccinated against mumps, testing for viruses that cause a parotitis-like illness is important, including rubella virus, influenza virus, and SARS-CoV-2. Additional studies to characterize parotid manifestations in COVID-19 patients will help determine diagnosis and treatment.

Acknowledgments

We thank Isabelle Ducamp for the management of the patient appointments and Cynthia Knuts for proofreading the manuscript.

About the Author

Dr. Lechien is otolaryngologist–head and neck surgeon in Foch Hospital (Paris, France) and consultant in the University Hospital of Brussels (Saint-Pierre). He is vice-chairman of the clinical research committee of the World Otolaryngological Federation of Young Otolaryngologists.

References

1. Lechien JR, Chiesa-Estomba CM, Place S, Van Laethem Y, Cabaraux P, Mat Q, et al.; COVID-19 Task Force of YO-IFOS. Clinical and epidemiological characteristics of 1,420 European patients with mild-to-moderate coronavirus disease 2019. J Intern Med. 2020 Apr 30 [Epub ahead of print]. https://doi.org/10.1111/joim.13089
2. Acute parotitis: a possible precocious clinical manifestation of SARS-CoV-2 infection? Otolaryngol Head Neck Surg. 2020 May 5 [Epub ahead of print].
3. Elbadawi LI, Talley P, Rolfes MA, Millman AJ, Reisdorf E, Kramer NA, et al. Non-mumps viral parotitis during the 2014–2015 influenza season in the United States. Clin Infect Dis. 2018;67:493–501. https://doi.org/10.1093/cid/ciy137
4. Hviid A, Rubin S, Mühlemann K. Mumps. Lancet. 2008 ;371:932–44. https://doi.org/10.1016/S0140-6736(08)60419-5
5. Ihrler S, Steger W, Riederer A, Zietz C, Vogl I, Löhrs U. HIV-associated cysts of the parotid glands. An histomorphologic and magnetic resonance tomography study of formal pathogenesis [in German]. Laryngorhinootologie. 1996;75:671–6. https://doi.org/ 10.1055/-2007-997655
6. Xu J, Li Y, Gan F, Du Y, Yao Y. Salivary glands: potential reservoirs for COVID-19 asymptomatic infection. J Dent Res. 2020 Apr 9 [Epub ahead of print]. https://doi.org/10.1177/0022034520918518

Address for correspondence: Dr. Lechien, Department of Otorhinolaryngology–Head and Neck Surgery, Foch Hospital, School of Medicine, UFR Simone Veil, Université Versailles Saint-Quentin-en-Yvelines (Paris Saclay University), Rue Worth, 40, 92150, Paris, France; email: jerome.lechien@umons.ac.be

Clostridiodes difficile in COVID-19 Patients, Detroit, Michigan, USA, March–April 2020

Avnish Sandhu, Glenn Tillotson, Jordan Polistico, Hossein Salimnia, Mara Cranis, Judy Moshos, Lori Cullen, Lavina Jabbo, Lawrence Diebel, Teena Chopra

Author affiliations: Detroit Medical Center, Detroit, Michigan, USA (A. Sandhu, J. Polistico, H. Salimnia, M. Cranis, J. Moshos, L. Cullen, L. Jabbo, T. Chopra); Wayne State University School of Medicine, Detroit (A. Sandhu, J. Polistico, H. Salimnia, L. Diebel, T. Chopra); GST Micro LLC, Henrico, Virginia, USA (G. Tillotson)

DOI: https://doi.org/10.3201/eid2609.202126

We describe 9 patients at a medical center in Detroit, Michigan, USA, with severe acute respiratory syndrome coronavirus 2 and *Clostridiodes difficile*. Both infections can manifest as digestive symptoms and merit screening when assessing patients with diarrhea during the coronavirus disease pandemic. These co-infections also highlight the continued importance of antimicrobial stewardship.

Coronavirus disease (COVID-19), which is caused by infection with severe acute respiratory syndrome coronavirus 2 (SARS-CoV-2), predominantly includes pulmonary symptoms; however, <10% of cases also include gastrointestinal events, including abdominal pain, diarrhea, and vomiting (*1*–*4*). During the COVID-19 pandemic, clinicians must be vigilant of co-infections in patients with COVID-19.

Several studies have collected data on concomitant antibiotic use in patients with COVID-19. A single-center study of 52 critically ill patients cited hospital-acquired infection in only 7 (13.5%) patients, yet 49 (94%) patients received antibiotic therapy (*5*). Another study, which analyzed 113 deceased patients from a cohort of 799 moderate-to-severely ill COVID-19 patients during January 13–February 12, 2020, reported that 105 (93%) deceased patients and 144 (89%) survivors had received empiric antibacterial therapy with either moxifloxacin, cefoperazone, or azithromycin (*6*). These antibiotics are strongly associated with *C. difficile* infection (CDI) (*7*). We report an observation of CDI as a co-occurrence or sequalae of overuse of antibiotics in COVID-19 patients.

We conducted a clinical surveillance review of CDI for all laboratory-confirmed COVID-19 patients treated at any of the hospitals belonging to Detroit Medical Center (Detroit, Michigan, USA). We screened patients by using TheraDoc software (https://www.theradoc.com) during March 11–April 22, 2020. We abstracted data regarding baseline demographics, medical history, symptoms, laboratory values, microbiologic findings, concomitant antibiotic use, and treatment for CDI. We obtained institutional review board approval for this study.

We identified 9 cases of co-infection with SARS-CoV-2 and *C. difficile*. This cohort mainly included elderly patients who were predominantly female (Table). The rate of CDI at the center was 3.32/10,000 patient-days during January–February 2020 and increased to 3.6/10,000 patient-days during March–April 2020.

We noted prior CDI in 3 patients; these infections occurred 1–4 months before admission. All patients were confirmed to be positive for *C. difficile* by PCR and showed symptoms of diarrhea in addition to other characteristic signs and symptoms, such as abdominal pain, nausea, and vomiting. Two patients had diarrhea and were found to be positive for *C. difficile* at admission, whereas the remaining 7 had onset of diarrhea only after COVID-19 diagnosis; median duration from CDI diagnosis to COVID-19 diagnosis in these 7 patients was 6 days. This group of patients

Table. Baseline demographic and clinical characteristics of 9 patients with *Clostridium difficile* and severe acute respiratory syndrome coronavirus 2 co-infection, Detroit, Michigan, USA, March–April 2020*

Characteristic	Value
Age, y, median	75
Sex	
F	7
M	2
Race	
African American	6
Caucasian	1
Unknown	2
Hospitalization in prior 60 d	5
Required intensive care unit and vasopressors	4
ATLAS score, median†	6
Charlson comorbidity index score, median	8
Symptoms at admission	
Cough	4
Shortness of breath	3
Fever	4
Diarrhea and abdominal pain	2
Laboratory results	
Ferritin, ng/mL, median‡	1,459.4
Leukocyte count, x 10^3 cells/mm^3), average	12.0
Creatinine, mg/dL, average§	4.22
Microbiologic findings	
Blood culture positive	2
Respiratory culture positive	2

*Values indicate no. patients unless otherwise indicated. Some patients had >1 symptom.
†Scoring information available at https://www.mdcalc.com/atlas-score-clostridium-difficile-infection.
‡Ferritin was only obtained in 8 patients.
§Three patients were on dialysis.

were severely ill, having high ATLAS scores (https://www.mdcalc.com/atlas-score-clostridium-difficile-infection) and multiple underlying conditions; hypertension (n = 8) and diabetes (n = 5) were the most frequent of these conditions.

Three patients received antibiotics in the month before admission; 8 received antibiotics at admission. One patient was initiated on antibiotics on day 15; this patient was also receiving antibiotics the month before admission. The most commonly administered antibiotics were cefepime (n = 5), ceftriaxone (n = 3), meropenem (n = 2), and azithromycin (n = 2). Specific CDI therapies were oral vancomycin (n = 6); vancomycin and intravenous metronidazole (n = 1); no treatment (n = 1); and a combination of oral vancomycin, intravenous metronidazole, rectal vancomycin, fidaxomicin, and fecal microbiota transplantation (n = 1). One patient who did not receive antibiotics was considered to be colonized with *C. difficile*. Four (44.4%) patients died during hospital admission, 1 (11.1%) was discharged to hospice, 1 (11.1%) is still hospitalized, and 3 (33.3%) were discharged to a long-term care facility.

CDI is a challenging disease, with a recurrence rate of 15%–20% and a mortality rate of 5% (*8*). When CDI is present as a co-infection with COVID-19, CDI therapy can be difficult to monitor if diarrhea persists because of COVID-19.

These cases highlight the importance of judicious use of antibiotics for potential secondary bacterial infection in patients with COVID-19. Antibiotics are known to have unintended consequences, such as *C. difficile* infection. All 9 patients received antibiotics; the median duration of antibiotic use before PCR-positive CDI was 5 days. All patients in our cohort were elderly, an age group at higher risk for complications from overuse of antibiotics, such as adverse events, antibiotic resistance, and concomitant infections like CDI (*9*). Secondary infections on top of CDI can increase the risk for death in patients with severe COVID-19; in this cohort, 4 patients died and 1 was discharged to hospice. To prevent CDI co-infections during the COVID-19 pandemic, integrated use of antimicrobial stewardship is needed to monitor appropriate antibiotic use.

Symptoms of CDI can complicate diagnosis of COVID-19 because both conditions can have similar manifestations; in a study of 206 COVID-19 patients, 19.4% had diarrhea as the first symptom onset (*10*). Of the 2 patients who had CDI diagnosed at admission, 1 patient solely had gastrointestinal symptoms, which possibly led to delayed diagnosis of COVID-19. Both COVID-19 and CDI should be considered when evaluating patients with diarrhea during the COVID-19 pandemic. Distinguishing between actual CDI versus colonization also is vital; 1 patient in our cohort was colonized. A limitation of this study is the small number of cases. However, in the face of the COVID-19 pandemic and the extensive use of antibiotics, clinicians should remain aware of possible CDI and SARS-CoV-2 co-infection.

G.T. is a consultant to Melinta, Crestone, Ferring, AirMmax, and Shionogi. Other authors in the manuscript have no relevant conflict of interest or financial disclosure. No funding was needed for this manuscript.

About the Author

Dr. Sandhu is an infectious diseases–epidemiology fellow at Detroit Medical Center, Wayne State University School of Medicine. Her current research interest is in multidrug-resistant hospital-acquired infections.

References

1. US Centers for Disease Control and Prevention. Interim clinical guidance for management of patients with confirmed coronavirus disease (COVID-19) [cited 2020 May 1]. https://www.cdc.gov/coronavirus/2019-ncov/hcp/clinical-guidance-management
2. Guan WJ, Ni ZY, Hu Y, Liang WH, Ou CQ, He JX, et al.; China Medical Treatment Expert Group for Covid-19. Clinical characteristics of coronavirus disease 2019 in China. N Engl J Med. 2020;382:1708–20. https://doi.org/10.1056/NEJMoa2002032
3. Chen N, Zhou M, Dong X, Qu J, Gong F, Han Y, et al. Epidemiological and clinical characteristics of 99 cases of 2019 novel coronavirus pneumonia in Wuhan, China: a descriptive study. Lancet. 2020;395:507–13. https://doi.org/10.1016/S0140-6736(20)30211-7
4. Wang D, Hu B, Hu C, Zhu F, Liu X, Zhang J, et al. Clinical characteristics of 138 hospitalized patients with 2019 novel coronavirus-infected pneumonia in Wuhan, China. JAMA. 2020;323:1061–9. https://doi.org/10.1001/jama.2020.1585
5. Yang X, Yu Y, Xu J, Shu H, Xia J, Liu H, et al. Clinical course and outcomes of critically ill patients with SARS-CoV-2 pneumonia in Wuhan, China: a single-centered, retrospective, observational study. Lancet Respir Med. 2020;8:475–81. https://doi.org/10.1016/S2213-2600(20)30079-5
6. Chen T, Wu D, Chen H, Yan W, Yang D, Chen G, et al. Clinical characteristics of 113 deceased patients with coronavirus disease 2019: retrospective study. BMJ. 2020;368:m1091. https://doi.org/10.1136/bmj.m1091
7. Brown KA, Khanafer N, Daneman N, Fisman DN. Meta-analysis of antibiotics and the risk of community-associated *Clostridium difficile* infection. Antimicrob Agents Chemother. 2013;57:2326–32. https://doi.org/10.1128/AAC.02176-12
8. Guh AY, Mu Y, Winston LG, Johnston H, Olson D, Farley MM, et al.; Emerging Infections Program Clostridioides difficile Infection Working Group. Trends in US burden of *Clostridium difficile* infection and outcomes. N Engl J Med. 2020;382:1320–30. https://doi.org/10.1056/NEJMoa1910215

9. Biedron C, Chopra T. Issues surrounding antibiotic use in older adults. Curr Transl Geriatr Exp Gerontol Rep. 2013;2:151–8. https://doi.org/10.1007/s13670-013-0050-9
10. Han C, Duan C, Zhang S, Spiegel B, Shi H, Wang W, et al. Digestive symptoms in COVID-19 patients with mild disease severity: clinical presentation, stool viral RNA testing, and outcomes. Am J Gastroenterol. 2020 Apr 15 [Epub ahead of print]. https://doi.org/10.14309/ajg.0000000000000664

Address for correspondence: Teena Chopra, Wayne State University, Detroit Medical Center, 3990 John Rd, Detroit, MI 48201, USA; email: tchopra@med.wayne.edu

SARS-CoV-2 RNA Detection on Disposable Wooden Chopsticks, Hong Kong

Grace Lui, Christopher K.C. Lai, Zigui Chen, Sylvia L.Y. Tong, Wendy C.S. Ho, Apple C.M. Yeung, Siaw S. Boon, Rita W.Y. Ng, Paul K.S. Chan

Author affiliation: The Chinese University of Hong Kong Faculty of Medicine, Hong Kong, China

DOI: https://doi.org/10.3201/eid2609.202135

We detected severe acute respiratory syndrome coronavirus 2 (SARS-CoV-2) RNA on disposable wooden chopsticks used by 5 consecutive asymptomatic and postsymptomatic patients admitted for isolation and care at our hospital. Although we did not assess virus viability, our findings may suggest potential for transmission through shared eating utensils.

In late 2019, severe acute respiratory syndrome coronavirus 2 (SARS-CoV-2) emerged in China (*1*), spreading primarily through droplets and contact with respiratory secretions or fecal materials (*2*,*3*). It has been shown that SARS-CoV-2 remains viable on plastic and stainless steel for 72 hours (*4*), and SARS-CoV on wood for 60 hours (*5*). Chopsticks have been essential eating utensils for >3 millennia, particularly in Asia, and are made mainly of wood and plastic; metal chopsticks are found in some countries, such as South Korea. Personal chopsticks are often used to pick food from communal dishes. We investigated whether chopsticks could be a potential vehicle of transmission for SARS-CoV-2.

We recruited 5 consecutive patients admitted for isolation and care at our hospital: 1 patient who was asymptomatic, 2 whose symptoms had subsided, 1 with moderate coronavirus disease (COVID-19) caused by SARS-CoV-2 infection, and 1 with severe COVID-19. Before mealtimes, each patient was given a pair of wooden chopsticks packed in a sealed plastic bag. These chopsticks are widely available in Hong Kong, including in canteens of public hospitals. They are made of plain wood, not bamboo, and not painted with color or lacquer. After mealtimes, we collected the used chopsticks. We dipped the tips of the chopsticks in 1 mL of phosphate-buffered normal saline and shook them for 30 sec to release saliva and oral fluid. We detected SARS-CoV-2 RNA by quantitative reverse transcription PCR (*6*). We collected serial sputum samples and nasopharyngeal and throat swabs to document respiratory shedding and for comparison of viral RNA concentrations among specimen types. The Joint Chinese University of Hong Kong—New Territories East Cluster Research Ethics Committee approved this study.

Patient A, 47-year-old woman, was a close contact of a confirmed case-patient. Her diagnosis was based on a surveillance throat sample collected during quarantine. She was admitted to the hospital for isolation and appeared asymptomatic throughout her stay. A pair of chopsticks collected 2 days after admission (12 days after her last exposure) was positive for SARS-CoV-2 RNA (Figure). Two respiratory samples collected after admission were also positive. High-resolution computed tomography (HRCT) of her lungs revealed small consolidations and ground-glass opacities in both lower lobes, left upper lobe, and right middle lobe.

Patient B, a 22-year-old woman, had a runny nose, headache, and fever develop on the day she returned from Europe. Her symptoms subsided after admission. Two chopsticks collected 1–2 days after symptoms had subsided were positive for SARS-CoV-2 RNA (Figure). Viral RNA was detected from respiratory specimens until 8 days after symptoms had subsided. HRCT revealed small patchy ground-glass opacity in the anterior segment of the left upper lobe of the lungs.

Patient C, a 67-year-old man with hypertension and minor coronary artery disease, had fever, cough with whitish sputum, and loose bowel movements develop 2 days after returning from Europe. Chopsticks collected 5 and 7 days after illness onset were positive for SARS-CoV-2 RNA (Figure). All respiratory

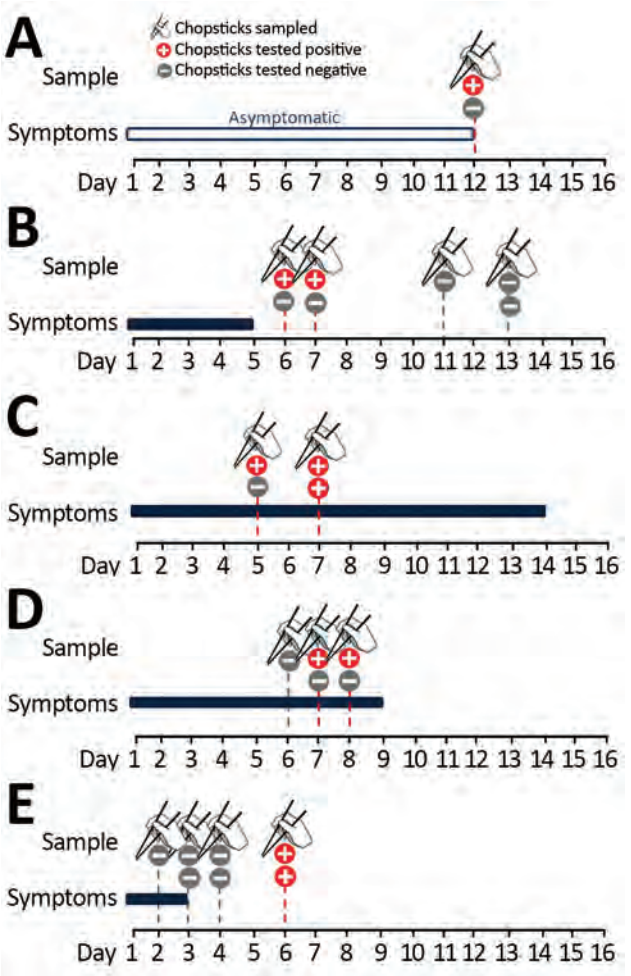

Figure. Timelines showing results of severe acute respiratory syndrome coronavirus 2 reverse transcription -PCR testing of chopsticks used by 5 patients in Hong Kong. The results of testing on serial respiratory specimens confirmed that all chopstick samples were collected when patients were shedding viruses from the respiratory tract. A) Patient A was asymptomatic. B) Patient B was postsymptomatic. C) Patient C had severe infection with pneumonia and desaturation. D) Patient D had moderate infection with pneumonia. E) Patient E was postsymptomatic.

samples were positive during this period. Chest radiograph revealed right lower lobe infiltrates; the patient's oxygen saturation fell, requiring supplemental oxygen for 2 days.

Patient D, a 59-year-old man with ankylosing spondylitis and osteoarthritis of both hip joints, had cough with whitish sputum, sore throat, hoarseness, and fever develop. He had no history of travel or contact with known COVID-19 case-patients. Two chopsticks collected 7 and 8 days after illness onset were positive for SARS-CoV-2 (Figure). All respiratory specimens collected during this period were also positive (Appendix Figure, https://wwwnc.cdc.gov/EID/article/26/9/20-2135-App1.pdf). HRCT of the lungs revealed right lower lobe consolidation.

Patient E, the last patient admitted in this study series, was a 26-year-old woman who had fever and headache develop 4 days after returning from Japan; chest radiograph revealed right lower lobe infiltrates. Her fever subsided soon after admission. She developed gastrointestinal upset after receiving lopinavir/ritonavir and was not eating well. Chopsticks collected 1–3 days after symptom onset were negative for SARS-CoV-2, but the 2 pairs collected 3 days after fever had subsided were positive for SARS-CoV-2 RNA (Figure). All respiratory specimens collected from patient E during the study period were positive.

Our study demonstrates frequent contamination of chopsticks with viruses shed from patients with different severity of SARS-CoV-2 infection, including asymptomatic and postsymptomatic patients. In 2 cases, chopsticks were positive after symptoms had subsided. Our main limitations were the small sample size and no attempt to investigate virus viability. Nevertheless, the possibility of chopsticks or other dining utensils as a vehicle for transmission of this novel coronavirus should not be ignored. Although restaurants often provide extra serving chopsticks for picking food from shared dishes, in practice it is easy to mix up personal and serving chopsticks during a meal. Furthermore, serving chopsticks are not commenly used when dining with family and close friends. Restrictions on communal meals should be implemented as part of social distancing strategies, especially in communities with a custom to share dishes. Chopsticks and other eating utensils used by patients should be handled and disposed of as infectious substances as a standard infection control practice.

About the Author

Dr. Lui is an infectious disease physician at the Faculty of Medicine, The Chinese University of Hong Kong, Hong Kong, China. Her primary research interest is emerging infections.

References:

1. Guan WJ, Ni ZY, Hu Y, Liang WH, Ou CQ, He JX, et al.; China Medical Treatment Expert Group for Covid-19. Clinical characteristics of coronavirus disease 2019 in China. N Engl J Med. 2020;382:1708–20. https://doi.org/10.1056/NEJMoa2002032
2. Wang W, Xu Y, Gao R, Lu R, Han K, Wu G, et al. Detection of SARS-CoV-2 in different types of clinical specimens. JAMA. 2020;323:1843–4. https://doi.org/10.1001/jama.2020.3786
3. Xiao F, Tang M, Zheng X, Liu Y, Li X, Shan H. Evidence for gastrointestinal infection of SARS-CoV-2. Gastroenterology. 2020;158:1831–3.e3. https://doi.org/10.1053/j.gastro.2020.02.055

4. van Doremalen N, Bushmaker T, Morris DH, Holbrook MG, Gamble A, Williamson BN, et al. Aerosol and surface stability of SARS-CoV-2 as compared with SARS-CoV-1. N Engl J Med. 2020;382:1564–7. https://doi.org/10.1056/NEJMc2004973
5. Duan SM, Zhao XS, Wen RF, Huang JJ, Pi GH, Zhang SX, et al.; SARS Research Team. Stability of SARS coronavirus in human specimens and environment and its sensitivity to heating and UV irradiation. Biomed Environ Sci. 2003;16:246–55.
6. Lui G, Ling L, Lai CK, Tso EY, Fung KS, Chan V, et al. Viral dynamics of SARS-CoV-2 across a spectrum of disease severity in COVID-19. J Infect. 2020 Apr 18 [Epub ahead of print]. https://doi.org/10.1016/j.jinf.2020.04.014

Address for correspondence: Paul K.S. Chan, Department of Microbiology, The Chinese University of Hong Kong, Prince of Wales Hospital, 30-32 Ngan Shing Street, Shatin, Hong Kong, China; email: paulkschan@cuhk.edu.hk

Effect of Environmental Conditions on SARS-CoV-2 Stability in Human Nasal Mucus and Sputum

M. Jeremiah Matson, Claude Kwe Yinda, Stephanie N. Seifert, Trenton Bushmaker, Robert J. Fischer, Neeltje van Doremalen, James O. Lloyd-Smith, Vincent J. Munster

Author affiliations: Marshall University Joan C. Edwards School of Medicine, Huntington, West Virginia, USA (M.J. Matson); Rocky Mountain Laboratories, National Institute of Allergy and Infectious Diseases, National Institutes of Health, Hamilton, Montana, USA (M.J. Matson, C. Kwe Yinda, S.N. Seifert, T. Bushmaker, R.J. Fischer, N. van Doremalen, V.J. Munster); Montana State University, Bozeman, Montana, USA (T. Bushmaker); University of California, Los Angeles, Los Angeles, California, USA (J.O. Lloyd-Smith)

DOI: https://doi.org/10.3201/eid2609.202267

We found that environmental conditions affect the stability of severe acute respiratory syndrome coronavirus 2 in nasal mucus and sputum. The virus is more stable at low-temperature and low-humidity conditions, whereas warmer temperature and higher humidity shortened half-life. Although infectious virus was undetectable after 48 hours, viral RNA remained detectable for 7 days.

Severe acute respiratory syndrome coronavirus 2 (SARS-CoV-2) is shed predominantly in upper and lower airway secretions (*1*), and transmission likely occurs predominantly through respiratory droplets, and potentially through direct contact and fomites. We describe SARS-CoV-2 stability in human nasal mucus and sputum under different environmental conditions.

We acquired pooled human nasal mucus and sputum commercially (Lee BioSolutions Inc., https://www.leebio.com) and mixed it with SARS-CoV-2 (SARS-CoV-2/human/USA/USA-WA1/2020) (*2*). We aliquoted 50 μL of each fluid containing 1×10^5 50% tissue culture infective dose/mL SARS-CoV-2 into sealed tubes (liquid setting) or onto polypropylene disks (surface setting), as previously described (*3*). We assessed stability under 3 environmental conditions: 4°C/40% relative humidity (RH), 21°C/40% RH, and 27°C/85% RH (RH applies only to exposed surface samples). We collected samples at specified timepoints and analyzed them for infectious virus by using endpoint titration. We extracted aliquots of collected surface samples by using the QIAGEN QIAamp Viral RNA Mini Kit (QIAGEN, https://www.qiagen.com) and analyzed them for the presence of viral RNA by using a quantitative reverse transcription PCR assay targeting the E gene (*4*). We fit linear regression models to $\log_{10}$-transformed titer data, calculated SARS-CoV-2 half-life ($t_{1/2}$) for each condition, and tested differences by using analysis of covariance. We report all experimental measurements as means of 3 replicates with SE. We considered differences with p values ≤0.05 statistically significant.

We observed no significant differences in SARS-CoV-2 $t_{1/2}$ between environmental conditions in liquid nasal mucus. In surface nasal mucus, SARS-CoV-2 $t_{1/2}$ was significantly shorter at 27°C/85% RH compared with 21°C/40% RH (p = 0.0023) and 4°C/40% RH (p = 0.0007). At 27°C/85% RH, SARS-CoV-2 $t_{1/2}$ also was significantly shorter in surface compared with liquid nasal mucus (p = 0.0101). Other comparisons of nasal mucus did not demonstrate significant differences in SARS-CoV-2 $t_{1/2}$ (Table; Figure, panel A, B).

SARS-CoV-2 $t_{1/2}$ was significantly longer in liquid sputum at 4°C than at 21°C (p = 0.0006) and 27°C (p<0.0001). In surface sputum, SARS-CoV-2 $t_{1/2}$ also was significantly longer at 4°C/40% RH than at 21°C/40% RH (p = 0.0042) and 27°C/85% RH (p = 0.0002). In addition, SARS-CoV-2 $t_{1/2}$ was significantly longer at 21°C/40% RH than 27°C/85% RH (p = 0.0027) in surface sputum. We observed no significant differences in SARS-CoV-2 $t_{1/2}$ between

liquid and surface sputum (Table; Figure, panel C, D). SARS-CoV-2 RNA remained detectable for ≥7 days in all surface samples, with a gradual increase in cycle threshold value (decrease in detected RNA) occurring only in nasal mucus at 27°C/85% RH (Figure, panel B, D).

We previously reported on the surface stability of SARS-CoV-2 in culture media at 21°C/40% RH (*3*). However, SARS-CoV-2 stability is affected by its surrounding matrix and environmental conditions. The $t_{1/2}$ we report here for SARS-CoV-2 in surface nasal mucus and sputum at 21°C/40% (Table) is considerably shorter than what we found in culture media under similar conditions ($t_{1/2}$ 6.8 [95% CI 5.6–8.2] hours) (*3*). In addition, we set out to determine SARS-CoV-2 stability in nasal mucus and sputum under environmental conditions that approximate temperate winter (4°C/40% RH), climate-controlled (21°C/40% RH), and temperate summer or tropical (27°C/85% RH) settings. SARS-CoV-2 was generally more stable at cooler temperatures and lower RH, and less stable at warmer temperatures and higher RH. Nevertheless, with our experimental protocol and initial titer, we predicted that SARS-CoV-2 would remain infectious in nasal mucus and sputum on surfaces for ≥10–12 hours even in warm, humid conditions. However, the amount of infectious SARS-CoV-2 shed and virus stability in relationship to infectious dose for humans are currently unknown, hampering conclusions regarding infectious duration and transmission. The general similarity in SARS-CoV-2 stability between liquid and surface samples suggests that in general temperature factored more heavily than humidity.

Table. Half-life ($t_{1/2}$) for SARS-CoV-2 in human nasal mucus and sputum under different environmental conditions*

Sample and exposure type	Environment	Half-life, h (95% CI)
Nasal mucus		
Liquid	4°C	4.9 (3.5–8.7)
	21°C	3.7 (3.1–4.7)
	27°C	3.1 (2.3–4.4)
Surface	4°C/40% RH	3.3 (2.6–4.4)
	21°C/40% RH	3.1 (2.5–4.1)
	27°C/85% RH	1.5 (1.2–1.9)
Sputum		
Liquid	4°C	7.0 (5.8–8.9)
	21°C	1.9 (1.3–3.2)
	27°C	1.3 (1.1–1.7)
Surface	4°C/40% RH	5.8 (4.8–7.3)
	21°C/40% RH	3.1 (2.3–4.6)
	27°C/85% RH	1.5 (1.1–2.4)

*RH, relative humidity; SARS-CoV-2, severe acute respiratory syndrome coronavirus 2.

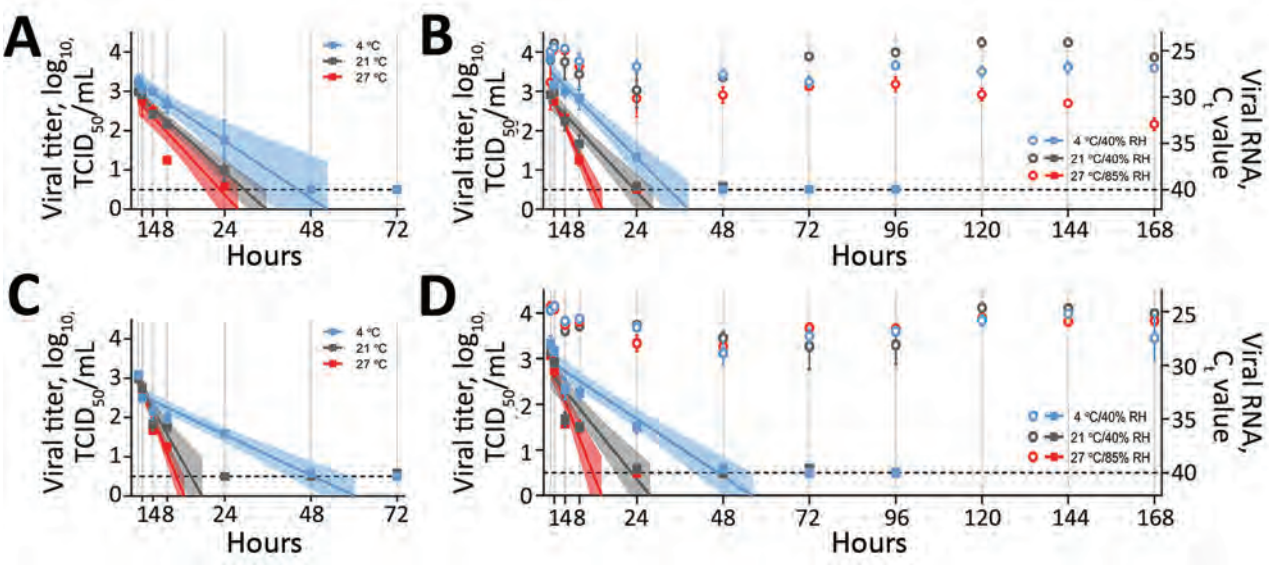

Figure. Stability of severe acute respiratory syndrome coronavirus 2 over time in human nasal mucus and sputum under different environmental conditions: liquid nasal mucus (A), surface nasal mucus (B), liquid sputum (C), and surface sputum (D). For panels B and D, the squares correspond to viral titer on the left y-axis, and the circles correspond to viral RNA (C_t value) on the right y-axis. We collected samples in 1 mL media for each condition at 0, 1, 4, 8, and 24 hours, then daily for 7 days and performed end-point titrations in quadruplicate on Vero E6 cells and made calculations using the Spearman-Kärber method. We $\log_{10}$-transformed and fit titers with linear regression models, including 95% CIs (shaded area around lines of best fit), by using GraphPad Prism 8 (https://www.graphpad.com). We extracted aliquots of collected surface samples by using the QIAamp Viral RNA Mini Kit (QIAGEN, https://www.qiagen.com) and analyzed them for the presence of viral RNA by using quantitative reverse transcription PCR targeting the E gene. For both viral titers and C_t values, plots show means of 3 replicates with SE. The limit of detection for each experimental condition was $10^{0.5}$ $TCID_{50}$/mL for viral titer and 40 for C_t value and is indicated by the dashed line. Relative humidity is not applicable to liquid samples (panels A and C), which were in sealed tubes. C_t, cycle threshold; RH, relative humidity; $TCID_{50}$/mL, 50% tissue culture infective dose/mL.

Community transmission of SARS-CoV-2 is widespread (*5*) and might be explained by contact with asymptomatic or presymptomatic (*6*) infected persons. Because of the surface stability of SARS-CoV-2, fomite transmission might also play a role. In addition, reduced surface stability of SARS-CoV-2 in human nasal mucus and sputum in warmer and more humid conditions might result in decreased virus transmission, and climatic influence on SARS-CoV-2 transmission rates might eventually drive seasonal outbreak dynamics in a postpandemic period (*7*), similar to other respiratory viruses (e.g., influenza A virus or human coronavirus OC43).

SARS-CoV-2 RNA has been detected on surfaces throughout clinical settings (*8*,*9*) and aboard a cruise ship for extended periods (*10*), but any correlation to infectious virus was previously unknown. In our study, infectious virus persisted in both nasal mucus and sputum on surfaces for ≈24 hours under climate-controlled conditions. However, viral RNA was consistently detectable for ≥7 days under various conditions in both nasal mucus and sputum on surfaces. These findings suggest that inferences regarding the presence of infectious virus from quantitative reverse transcription PCR data alone should be made with caution.

Acknowledgments

We thank Emmie de Wit, Brandi Williamson, and Jon Schulz for their technical assistance.

This research was supported by the Intramural Research Program of the National Institutes of Health, the National Institute of Allergy and Infectious Diseases, and the Defense Advanced Research Projects Agency's Preventing Emerging Pathogenic Threats Program (grant no D18AC00031).

About the Author

Mr. Matson is an MD/PhD student at the Marshall University Joan C. Edwards School of Medicine and is performing his dissertation research at the National Institute of Allergy and Infectious Diseases Virus Ecology Section. He is interested in emerging and reemerging viruses.

References

1. Zhu N, Zhang D, Wang W, Li X, Yang B, Song J, et al.; China Novel Coronavirus Investigating and Research Team. A novel coronavirus from patients with pneumonia in China, 2019. N Engl J Med. 2020;382:727–33. https://doi.org/10.1056/NEJMoa2001017
2. Harcourt J, Tamin A, Lu X, Kamili S, Sakthivel SK, Murray J, et al. Severe acute respiratory syndrome coronavirus 2 from patient with coronavirus disease, United States. Emerg Infect Dis. 2020;26:1266–73. https://doi.org/10.3201/eid2606.200516
3 van Doremalen N, Bushmaker T, Morris DH, Holbrook MG, Gamble A, Williamson BN, et al. Aerosol and surface stability of SARS-CoV-2 as compared with SARS-CoV-1. N Engl J Med. 2020;382:1564–7. https://doi.org/10.1056/NEJMc2004973
4. Corman VM, Landt O, Kaiser M, Molenkamp R, Meijer A, Chu DK, et al. Detection of 2019 novel coronavirus (2019-nCoV) by real-time RT-PCR. Euro Surveill. 2020;25. https://doi.org/10.2807/1560-7917.ES.2020.25.3.2000045
5. Liu J, Liao X, Qian S, Yuan J, Wang F, Liu Y, et al. Community transmission of severe acute respiratory syndrome coronavirus 2, Shenzhen, China, 2020. Emerg Infect Dis. 2020;26:1320–3. https://doi.org/10.3201/eid2606.200239
6. He X, Lau EHY, Wu P, Deng X, Wang J, Hao X, et al. Temporal dynamics in viral shedding and transmissibility of COVID-19. Nat Med. 2020;26:672–5. https://doi.org/10.1038/s41591-020-0869-5
7. Kissler SM, Tedijanto C, Goldstein E, Grad YH, Lipsitch M. Projecting the transmission dynamics of SARS-CoV-2 through the postpandemic period. Science. 2020;368:860–8. https://doi.org/10.1126/science.abb5793
8. Ong SWX, Tan YK, Chia PY, Lee TH, Ng OT, Wong MSY, et al. Air, surface environmental, and personal protective equipment contamination by severe acute respiratory syndrome coronavirus 2 (SARS-CoV-2) from a symptomatic patient. JAMA. 2020;323:1610. https://doi.org/10.1001/jama.2020.3227
9. Guo ZD, Wang ZY, Zhang SF, Li X, Li L, Li C, et al. Aerosol and surface distribution of severe acute respiratory syndrome coronavirus 2 in hospital wards, Wuhan, China, 2020. Emerg Infect Dis. 2020;26. https://doi.org/10.3201/eid2607.200885
10. Moriarty LF, Plucinski MM, Marston BJ, Kurbatova EV, Knust B, Murray EL, et al.; CDC Cruise Ship Response Team; California Department of Public Health COVID-19 Team; Solano County COVID-19 Team. Public health responses to COVID-19 outbreaks on cruise ships—worldwide, February–March 2020. MMWR Morb Mortal Wkly Rep. 2020;69:347–52. https://doi.org/10.15585/mmwr.mm6912e3

Address for correspondence: Vincent J. Munster, NIH/NIAID Rocky Mountain Laboratories, Laboratory of Virology, 903 S 4th St, Hamilton, MT 59840, USA; email: munstervj@niaid.nih.gov

Methemoglobinemia in Patient with G6PD Deficiency and SARS-CoV-2 Infection

Kieran Palmer, Jonathan Dick, Winifred French, Lajos Floro, Martin Ford

Author affiliation: King's College Hospital National Health Service Foundation Trust, London, UK

DOI: https://doi.org/10.3201/eid2609.202353

We report a case of intravascular hemolysis and methemoglobinemia, precipitated by severe acute respiratory syndrome coronavirus 2 infection, in a patient with undiagnosed glucose-6-phosphate dehydrogenase deficiency. Clinicians should be aware of this complication of coronavirus disease as a cause of error in pulse oximetry and a potential risk for drug-induced hemolysis.

Coronavirus disease is a novel infectious disease that primarily manifests as an acute respiratory syndrome but can also cause multiorgan dysfunction. Severe acute respiratory syndrome coronavirus 2 (SARS-CoV-2) infection has been documented to cause vasoocclusive crisis and acute chest syndrome in patients with sickle cell anemia (*1*). We report another potentially major complication of infection in a patient with a common enzymatic disorder.

Glucose 6-phosphate dehydrogenase (G6DP) deficiency is an X-linked enzymatic disorder that affects 400 million persons worldwide and has a high prevalence (5%–20%) in African and Asian populations (*2*). G6DP catalyzes the formation of nicotinamide adenine dinucleotide phosphate (NADPH) (*3*). NADPH maintains hemoglobin in the ferrous state by forming reduced glutathione, which prevents oxidative damage (*3*). G6DP deficiency increases the risk for intravascular hemolysis upon exposure to oxidative agents, such as fava beans, sulfonamides, and hydroxychloroquine, the subject of clinical trials for persons with SARS-CoV-2 infection.

G6PD deficiency can induce methemoglobinemia by inhibiting NADPH-flavine reductase, which prevents the reduction of methemoglobin. Methemoglobin is unable to bind to oxygen, and the remaining oxyhemoglobin develops heightened oxygen affinity and diminished delivery, leading to tissue hypoxia (*4*). Viral infections, including HIV, hepatitis viruses (A, B, and E), and cytomegalovirus, can precipitate intravascular hemolysis in patients with G6PD deficiency (*5*,*6*). Concurrent methemoglobinemia has also been reported in the context of viral-induced hemolysis (*5*).

A 62-year-old Afro-Caribbean man with a medical history of type 2 diabetes and hypertension came to the hospital for a 5-day history of fever, dyspnea, vomiting, and diarrhea. Auscultation of his chest showed bilateral crackles. He was tachycardic, hypotensive, and dehydrated, with a prolonged capillary refill time and dry mucous membranes.

Laboratory tests showed an acute kidney injury. Blood urea nitrogen was 140 mg/dL, creatinine 5.9 mg/dL (baseline 1.1 mg/dL), capillary blood glucose >31 mmol/L, and blood ketones 1.1 mmol/L. A chest radiograph showed bilateral infiltrates, and a result for a SARS-CoV-2 reverse transcription PCR specific for the RNA-dependent RNA polymerase gene was positive (validated by Public Health England, London, UK).

The patient was treated for SARS-CoV-2 pneumonitis and a hyperosmolar hyperglycemic state with crystalloid fluid, oxygen therapy, and an insulin infusion. His creatinine increased to 9.3 mg/dL, suspected secondary to hypovolemia and viremia, and acute hemodialysis was started. Results of a screen for other causes of acute kidney injury, including renal ultrasonography and autoimmune serologic analysis, was unremarkable.

On day 7 postadmission, his peripheral oxygen saturations decreased, and oxygen therapy was increased to 15 L/min by use of a nonrebreather mask to maintain saturations of 80%. Arterial blood gas analysis revealed a partial pressure of oxygen of 22 kPa and an oxygen saturation of 100%. Co-oximetry showed a methemoglobin level of 6.5%. Repeat laboratory tests showed hemolytic anemia; hemoglobin was 52 g/L, haptoglobin <0.1 mg/dL, and lactate dehydrogenase 1,566 U/L. A direct antiglobulin test excluded major immune-mediated hemolysis. A blood film for the patient showed normochromic normocytic erythrocytes and a few hemighost cells (Figure, panel A). A 2-stage G6DP assay confirmed G6DP deficiency (0.8 IU/g hemoglobin).

The patient was given 2 blood transfusions (Figure, panel B) and oxygen therapy. His medication history included amoxicillin/clavulanic acid, heparin, amlodipine, and metformin, which did not indicate a precipitant for the hemolytic crisis. The methemoglobinemia gradually resolved, and his oxygen requirements decreased. He recovered dialysis-independent renal function. He was given folic acid (5 mg/d) and discharged 22 days after admission.

The mechanism by which SARS-CoV-2 causes hemolysis is unknown. Other viral infections have been reported to produce reactive oxygen and nitrogen species, which impair intracellular proteins and DNA

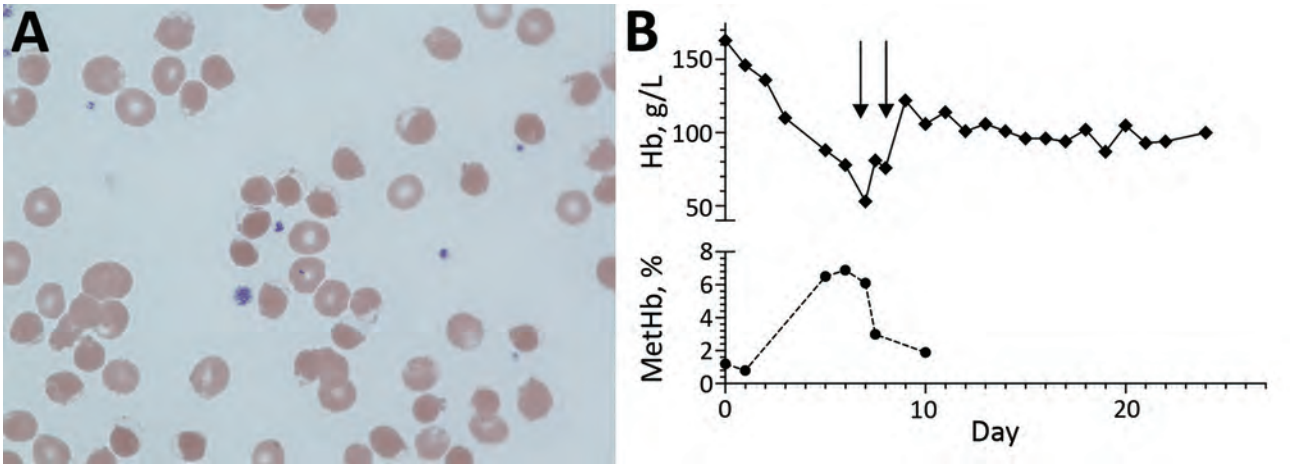

Figure. Testing of patient with G6PD deficiency and SARS-CoV-2 infection, United Kingdom. A) Blood film showing normochromic normocytic erythrocytes and a few hemighost cells. Hemighost cells are formed after oxidative hemolysis seen in G6DP deficiency. Hb is contracted to 1 pole of the cell, leaving an unfilled area enclosed by an intact membrane (original magnification ×100). B) Hb and metHb concentration during admission. Each arrow indicates a 3-unit erythrocyte transfusion. G6PD, glucose-6-phosphate dehydrogenase; Hb, hemoglobin; metHb, methemoglobin; SARS-CoV-2, severe acute respiratory syndrome coronavirus 2.

in cells with damaged antioxidant enzyme metabolism (*7*). The concurrent secondary methemoglobinemia in this case also suggests oxidative stress and impaired redox balance.

Patients with G6DP deficiency might be more vulnerable to SARS-CoV-2 infection (*8*). Infection of G6DP-deficient lung cells with human coronavirus 229E resulted in increased viral production and replication compared with normal cells (*9*). An increased susceptibility to infection and hemolysis with secondary tissue hypoxia might result in increased illness and death (*8*).

Hydroxychloroquine has been proposed as a treatment for SARS-CoV-2 infection and is considered safe in usual therapeutic doses in class II or III G6PD deficiency. However, caution is advised with higher doses because data for this setting are limited. Oxidative stress might contribute to the pathogenesis of severe SARS-CoV-2 infection (*10*). Evaluation of parameters of oxidative stress in SARS-CoV-2 are currently underway (ClinicalTrials.gov identifier NCT04375137) and might determine whether there is an increased risk for drug-induced hemolysis in patients with G6PD deficiency.

Treatment for methemoglobinemia with intravenous methylene blue is recommended if the blood methemoglobin level is >20%–30%. However, in G6DP deficiency, treatment with methylene blue is contraindicated because the reduction of methemoglobin is NADPH dependent. This finding might precipitate intravascular hemolysis and therapy with ascorbic acid or supportive treatment with oxygen as indicated instead. During the SARS-CoV-2 pandemic, clinicians must be aware of the possible increased susceptibility of patients with G6DP deficiency to severe hemolytic crises and the consequences for investigation and treatment.

About the Author

Dr. Palmer is an internal medicine trainee in the Renal Department, King's College Hospital NHS Foundation Trust, London, UK. His primary research interests are infectious diseases and general medicine.

References

1. Nur E, Gaartman AE, van Tuijn CF, Tang MW, Biemond BJ. Vaso-occlusive crisis and acute chest syndrome in sickle cell disease due to 2019 novel coronavirus disease (COVID-19). Am J Hematol. 2020;95:725–6. https://doi.org/10.1002/ajh.25821
2. Cappellini MD, Fiorelli G. Glucose-6-phosphate dehydrogenase deficiency. Lancet. 2008;371:64–74. https://doi.org/10.1016/S0140-6736(08)60073-2
3. Efferth T, Schwarzl SM, Smith J, Osieka R. Role of glucose-6-phosphate dehydrogenase for oxidative stress and apoptosis. Cell Death Differ. 2006;13:527–8, author reply 529–30. https://doi.org/10.1038/sj.cdd.4401807
4. Hassan KS, Al-Riyami AZ, Al-Huneini M, Al-Farsi K, Al-Khabori M. Methemoglobinemia in an elderly patient with glucose-6-phosphate dehydrogenase deficiency: a case report. Oman Med J. 2014;29:135–7. https://doi.org/10.5001/omj.2014.33
5. Au WY, Ngai CW, Chan WM, Leung RY, Chan SC. Hemolysis and methemoglobinemia due to hepatitis E virus infection in patient with G6PD deficiency. Ann Hematol. 2011;90:1237–8. https://doi.org/10.1007/s00277-011-1167-6
6. Araujo T, Katiyar V, Gonzales Zamora JA. Acute retroviral syndrome presenting with hemolytic anemia induced by G6PD deficiency. Trop Med Infect Dis. 2018;4:6. https://doi.org/10.3390/tropicalmed4010006

7. Aydemir D, Ulusu NN. Is glucose-6-phosphate dehy (COVID-19) infections and deaths? Pathog Glob Health. 2020; 114:109–10. https://doi.org/10.1080/20477724.2020.1751388
8. Kassi EN, Papavassiliou KA, Papavassiliou AG. G6PD and chloroquine: selecting the treatment against SARS-CoV-2? J Cell Mol Med. 2020;24:4913–4. https://doi.org/10.1111/jcmm.15312
9. Wu YH, Tseng CP, Cheng ML, Ho HY, Shih SR, Chiu DT. Glucose-6-phosphate dehydrogenase deficiency enhances human coronavirus 229E infection. J Infect Dis. 2008; 197:812–6. https://doi.org/10.1086/528377
10. Delgado-Roche L, Mesta F. Oxidative stress as key player in severe acute respiratory syndrome coronavirus (SARS-CoV) infection. Arch Med Res. 2020. Apr 30 [Epub ahead of print]. https://doi.org/10/1016/j.arcmed.2020.04.019.

Address for correspondence: Kieran Palmer, Renal Department, King's College Hospital National Health Service Foundation Trust, Denmark Hill, Brixton, London SE59RS, UK; email: kieran.palmer3@nhs.net

Asymptomatic SARS-CoV-2 Infection in Nursing Homes, Barcelona, Spain, April 2020

Blanca Borras-Bermejo,[1] Xavier Martínez-Gómez,[1] María Gutierrez-San Miguel, Juliana Esperalba, Andrés Antón, Elisabet Martin, Marta Selvi, María José Abadías, Antonio Román, Tomàs Pumarola, Magda Campins, Benito Almirante

Author affiliations: Vall d'Hebron Hospital Universitari, Barcelona, Spain (B. Borras-Bermejo, X. Martínez-Gómez, M. Gutierrez-San Miguel, J. Esperalba, A. Antón, M.J. Abadías, A. Román, T. Pumarola, M. Campins, B. Almirante); Universitat Autònoma de Barcelona, Bellaterra, Spain (X. Martínez-Gómez, A. Antón, A. Román, T. Pumarola, M. Campins, B. Almirante); Servei Atenció Primària Muntanya, Barcelona (E. Martin); Centre d'Atenció Primària Sant Andreu, Barcelona (M. Selvi)

DOI: https://doi.org/10.3201/eid2609.202603

During the coronavirus disease pandemic in Spain, from April 10–24, 2020, a total of 5,869 persons were screened for severe acute respiratory syndrome coronavirus 2 at nursing homes. Among residents, 768 (23.9%) tested positive; among staff, 403 (15.2%). Of those testing positive, 69.7% of residents and 55.8% of staff were asymptomatic.

As of April 2020, Spain was one of the countries accounting for the most coronavirus disease (COVID-19) deaths (*1*). More than half of those deaths occur in persons >80 years of age (*2*), which highlights the vulnerability of the elderly. Moreover, severe acute respiratory syndrome coronavirus 2 (SARS-CoV-2) can be easily spread within nursing homes, causing outbreaks with high associated mortality rate (*3*,*4*). By the beginning of April, the exponential increase of cases overwhelmed the healthcare system in Spain. In this context, rapid outbreak identification and early intervention in nursing homes was needed.

At Vall d'Hebron Hospital, a tertiary hospital in Catalonia, Spain, we conducted test-based screening as a containment measure to promptly implement effective prevention and control measures in nursing homes. We present the early results of a coordinated intervention with primary care teams in ≈6,000 residents and facility staff in nursing homes in our catchment area.

We evaluated 69 nursing homes that had a total census of 6,714 persons. We excluded previous laboratory-confirmed cases of COVID-19. During April 10–24, an integrated team of hospital and primary care staff obtained samples for SARS-CoV-2 testing from all residents and workers: nasopharyngeal and oropharyngeal swab samples both combined in the same collection tube with viral transport media. We used a commercial CE-IVD–marked, real-time reverse transcription PCR–based assay (Cobas SARS-CoV-2; Roche Diagnostics, https://www.roche.com) on a Cobas 6800 system.

Each nursing home director recorded any symptoms present at least 48 hours before the scheduled day of testing for all residents and staff. According to the World Health Organization case definition of a suspected case of COVID-19, a person was classified as symptomatic if fever or acute respiratory symptoms were present at any moment during the preceding 14 days. In the absence of either, the person was considered to be asymptomatic.

We obtained a total of 5,869 samples, 3,214 from residents and 2,655 from facility staff. Overall, 768 (23.9%) residents and 403 (15.2%) staff members tested positive for SARS-CoV-2 (Table). The presence of fever or respiratory symptoms during the preceding 14 days was recorded in 2,624 residents (81.6%) and 1,772 staff members (66.7%). Among those testing positive and for whom we had information about symptoms, 69.7% of the residents and 55.8% of staff were asymptomatic.

[1]These first authors contributed equally to this article.

Table. SARS-CoV-2 test results for residents and staff of 69 nursing homes, Barcelona, Spain, April 2020*

Patient status during the preceding 14 days	SARS-CoV-2 test results, no. (%)†			
	Residents		Staff	
	Positive, N = 768	Negative, N = 2,446	Positive, N = 403	Negative, N = 2,252
Asymptomatic	486 (69.7)	1,727 (89.6)	144 (55.8)	1,311 (86.6)
Symptomatic‡	211 (30.3)	200 (10.4)	114 (44.2)	203 (13.4)

*Results include all residents and staff who were in the facility the day of screening intervention. Testing was by reverse transcription PCR. SARS-CoV-2, severe acute respiratory syndrome coronavirus 2.
†Percentage calculated over those with symptom information available; it was missing for 590 (18.4%) residents and 883 (33.3%) staff members.
‡A person was considered symptomatic if fever or respiratory symptoms were present at time of assessment, or at any moment in the preceding 14 days.

On the basis of laboratory results, we planned specific infection prevention and control measures, adapted to facility characteristics in <72 hours. The most relevant measures applied included isolation of infected residents, establishing cohorted areas and designated staff, excluding infected staff from work, ensuring proper supply of personal protection equipment, and training staff about contact- and droplet-based precautions. We established coordinated follow-up evaluation with primary care teams and facility directors.

COVID-19 heavily affected nursing homes, causing uncountable deaths in Spain (*5*,*6*). Restriction policies for visitors in nursing homes were described as part of the state of emergency declared on March 14 (*7*), but a national guideline to reduce the risk for SARS-CoV-2 transmission in these settings was not available until March 24 (*8*). Moreover, despite knowledge of community transmission starting in late February, widespread testing for SARS-CoV-2 was not available until mid-April.

Our data show an overall high prevalence of SARS-CoV-2 infection in residents and staff, noting a high transmission in these settings. Specific aspects of nursing homes (shared rooms or bathrooms, physically or cognitively impaired residents requiring high-demand care, rotating staff working in different facilities) and a limited adoption of prevention and control measures as reported by our teams are some factors that may explain these results. Among those with known symptom status, we found a high proportion of asymptomatic cases: 69.7% of infected residents and 55.8% of infected staff.

Our study had several limitations. The ascertainment process could lead to misclassification due to atypical symptoms in the elderly. Furthermore, cross-sectional symptom assessment and testing did not allow us to differentiate between presymptomatic and asymptomatic cases. Nevertheless, these values are consistent with a study performed in a nursing facility in King County, Washington, USA, in which 56% of the residents testing positive were asymptomatic (*9*).

Given that presymptomatic and asymptomatic transmission has been demonstrated (*10*), our data suggest that asymptomatic cases could have had an important role in transmission dynamics. Symptoms-based approaches would have failed to correctly identify cases and therefore continued transmission. Furthermore, testing of facility staff should be included as part of the prevention and control measures, because they may contribute to sustained transmission.

In conclusion, the high prevalence of SARS-CoV-2 cases found in nursing homes highlights that this vulnerable population requires special attention and proactive interventions in coordination with the primary care teams. In the context of established community transmission of SARS-CoV-2, we recommend implementing test-based screening irrespective of symptomatology in nursing homes as the best approach to rapidly implement prevention and control measures.

Acknowledgments

We thank the Preventive Medicine and Epidemiology Department, Microbiology Department, and primary care teams, along with nursing home directors and staff, who actively collaborated in the implementation in a tight timeframe. We thank Friedel Laaf for the language review.

About the Author

Dr. Borras-Bermejo is a preventive medicine and public health physician working in the Preventive Medicine and Epidemiology Department in Vall d'Hebron University Hospital, Barcelona, Spain. Her research interests include vaccines and hospital infection prevention and control.

References

1. World Health Organization. Coronavirus disease (COVID-19) situation report 106. 2020 [cited 2020 June 4]. https://www.who.int/emergencies/diseases/novel-coronavirus-2019/situation-reports
2. Centro de Coordinación de Alertas y Emergencias Sanitarias. Dirección General de Salud Pública, Calidad e Innovación. Update 108. Coronavirus disease (COVID-19) [in Spanish]. 2020 May 17 [cited 2020 May 21]. https://bit.ly/2Ajvtt2
3. Comas-Herrera A, Zalakain J. Mortality associated with COVID-19 outbreaks in care homes: early international evidence. 2020 [cited 2020 May 21]. https://ltccovid.org/

2020/04/12/mortality-associated-with-covid-19-outbreaks-in-care-homes-early-international-evidence
4. Etard J-F, Vanhems P, Atlani-Duault L, Ecochard R. Potential lethal outbreak of coronavirus disease (COVID-19) among the elderly in retirement homes and long-term facilities, France, March 2020. Euro Surveill. 2020;25:8–10. https://doi.org/10.2807/1560-7917.ES.2020.25.15.2000448
5. Rada AG. Covid-19: the precarious position of Spain's nursing homes. BMJ. 2020;369:m1554. https://doi.org/10.1136/bmj.m1554
6. ECDC Public Health Emergency Team, Danis K, Fonteneau L, Georges S, Daniau C, Bernard Stoecklin S, et al. High impact of COVID-19 in long-term care facilities, suggestion for monitoring in the EU/EEA, May 2020. Euro Surveill. 2020;25:1–5. https://doi.org/10.2807/1560-7917.ES.2020.25.22.2000956
7. Ministerio de la Presidencia relaciones con las cortes y memoria democrática. Royal Decree 463/2020 (March 14) declaring the alarm state for the health crisis management situation caused by COVID-19. BOE no 67 from March 14, 2020 [in Spanish]. 2020 Mar 14;67(I):25390–400 [cited 2020 May 21]. https://www.boe.es/diario_boe/txt.php?id=BOE-A-2020-3692
8. Ministerio de Sanidad. Guideline for the prevention and control of COVID-19 in nursing homes and other residential social services [in Spanish]. 2020 [cited 2020 May 21]. https://www.mscbs.gob.es/profesionales/saludPublica/ccayes/alertasActual/nCov-China/documentos/Residencias_y_centros_sociosanitarios_COVID-19.pdf
9. Arons MM, Hatfield KM, Reddy SC, Kimball A, James A, Jacobs JR, et al.; Public Health–Seattle and King County and CDC COVID-19 Investigation Team. Presymptomatic SARS-CoV-2 infections and transmission in a skilled nursing facility. N Engl J Med. 2020;382:2081–90. https://doi.org/10.1056/NEJMoa2008457
10. He X, Lau EHY, Wu P, Deng X, Wang J, Hao X, et al. Temporal dynamics in viral shedding and transmissibility of COVID-19. Nat Med. 2020;26:672–5. https://doi.org/10.1038/s41591-020-0869-5

Address for correspondence: Magda Campins, Servei de Medicina Preventiva i Epidemiologia, Vall d'Hebron Hospital Universitari, Vall d'Hebron Barcelona Hospital Campus, Passeig Vall d'Hebron 119-129, 08035 Barcelona, Spain; email: mcampins@vhebron.net

Leuconostoc lactis and *Staphylococcus nepalensis* Bacteremia, Japan

Satoshi Hosoya, Satoshi Kutsuna, Daisuke Shiojiri, Saeko Tamura, Erina Isaka, Yuji Wakimoto, Hidetoshi Nomoto, Norio Ohmagari

Author affiliation: National Center for Global Health and Medicine, Tokyo, Japan

DOI: https://doi.org/10.3201/eid2609.191123

Leuconostoc lactis is a glycopeptide-resistant, gram-positive, facultative anaerobic coccus isolated from dairy products, whereas *Staphylococcus nepalensis* is coagulase-negative coccus that has not been identified as human pathogen. We report an instructive case of *L. lactis* and *S. nepalensis* bacteremia in a 71-year-old man who experienced Boerhaave syndrome after a meal.

Leuconostoc lactis is an intrinsically glycopeptide-resistant but ampicillin-susceptible, gram-positive, facultative anaerobic coccus (*1*) found in food products including dairy products, vegetables, and wine. *L. lactis* is a very rare pathogen associated with bloodstream infections (*2*). *Staphylococcus nepalensis* is a novobiocin-resistant coagulase-negative staphylococcus also found in food products, such as dry-cured ham and fish sauce, that has not been reported as a human pathogen (*3*–*5*). Neither *L. lactis* nor *S. nepalensis* is part of normal human bacterial flora (*2*,*3*).

A 71-year-old man with hypertension and hyperlipidemia sought care for upper abdominal pain and vomiting after a meal at his son's restaurant. A computed tomography (CT) scan showed collapse of the lower esophagus wall and expansion of the mediastinum; medical staff diagnosed a spontaneous esophageal rupture and performed emergency surgery. Surgical findings demonstrated a 5 cm perforation of the lower esophagus with no rupture to the thoracic and abdominal cavity. The final diagnosis included Boerhaave syndrome, esophageal hiatus hernia, and mediastinitis. Two sets of blood culture taken on day 1 were positive for gram-positive cocci, which we identified by matrix-assisted laser desorption/ionization time-of-flight (MALDI-TOF) mass spectrometry as *L. lactis* in an aerobic bottle (10.7 h to culture) and an anaerobic bottle (13.3 h to culture) and *S. nepalensis* in 1 anaerobic bottle (24.3 h to culture). The 2 bacteria were indications of true bacteremia; therefore, we escalated ampicillin/sulbactam (treatment to piperacillin/tazobactam for *L. lactis* (Appendix Table 1, https://wwwnc.cdc.gov/EID/

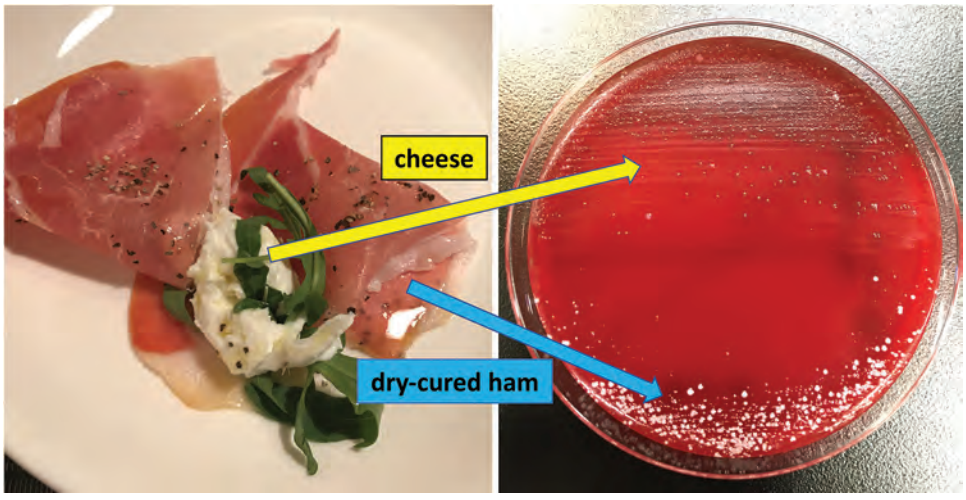

Figure. Culture of cheese and dry-cured ham on blood agar medium from investigation of patient with *Leuconostoc lactis* and *Staphylococcus nepalensis* bacteremia, Japan. The colonies, cultured from cheese, were identified as *L. lactis* by matrix-assisted laser desorption/ionization time-of-flight mass spectrometry mass spectrometry; however, the colonies derived from dry-cured ham were identified as *S. equorum* and *S. xylosus* but not as *S. nepalensis*.

article/26/9/19-1123-App1.pdf) and initiated vancomycin treatment for *S. nepalensis* on day 3 after admission (Appendix Table 2). We measured MICs in the microdilution method using the MicroScan WalkAway 96 SI system (Beckman Coulter, https://www.beckmancoulter.com) with a MICrofast7J panel and determined the susceptibility of *L. lactis* according to Clinical and Laboratory Standards Institute (CLSI) guidelines (*6*). On day 7, we deescalated piperacillin/tazobactam to ampicillin/sulbactam, referring to the MICs, and we obtained follow-up sets of blood culture. The culture results were negative. We discontinued vancomycin by day 14 but maintained the ampicillin/sulbactam regimen. A follow-up CT scan on day 28 showed a subsiding mediastinal abscess. Moreover, a pathological examination of the surgical biopsy demonstrated no esophageal cancer. On the basis of the clinical course of the disease, we strongly suspected a breakthrough of *L. lactis* and *S. nepalensis* through the ruptured esophagus into the bloodstream. To prove this relationship, we obtained permission from the patient's son to analyze samples of the food products his father consumed, including cheese, dry-cured ham, sauerkraut, pizza margherita, bianchetti (pasta with boiled young sardines), and red and white wine. We cultured samples from these products on blood agar medium; colonies of *L. lactis*, confirmed by MALDI-TOF mass spectrometry, were derived from cheese samples (Figure).

Approximately 20 cases of *L. lactis* bacteremia have been reported (*1*), mostly in immunosuppressed patients with malignancy including leukemia, diabetes, or impaired skin barrier function due to central venous catheter. Several entry routes to the bloodstream have been hypothesized, including the digestive tract or the skin in catheter-related bloodstream infections, or as a result of microbial substitution due to glycopeptide administration; however, no entry point has been definitively identified (*1*,*2*,*7*,*8*). In addition, *L. lactis* bacteremia caused by gastrointestinal tract perforation had not been reported. We concluded that *L. lactis* colonized cheese and entered the bloodstream through a perforation of the lower esophagus, and we were able to demonstrate that *L. lactis* can enter the bloodstream through a rupture of the digestive tract. Based on our findings, we may advise screening for gastrointestinal diseases, such as ulcer, perforation, and malignancy, in patients with *L. lactis* bacteremia.

S. nepalensis has not previously been reported as a human pathogen, nor has its pathogenicity been described. Because the results of the food sample cultures identified other coagulase-negative *Staphylococci* bacteria (*S. equorum* and *S. xylosus*), rather than *S. nepalensis*, from the dry-cured ham colonies, we could not conclusively demonstrate the entry of *S. nepalensis* to the bloodstream. Moreover, contamination with *S. nepalensis* was possible; only 1 anaerobic bottle of blood culture taken at admission was positive. However, because *S. nepalensis* is not normally found in the human microbial flora but is a part of the predominant flora in dry-cured ham together with *S. equorum* and *S. xylosus* (*4*), we suspect that the *S. nepalensis* bacteremia diagnosis was correct.

In conclusion, we demonstrate the point of entry for *L. lactis* into the human bloodstream and show results implying that *L. lactis* can be a pathogen of bacteremia, as previous reports have shown (*1*,*2*,*7*,*8*). Our report is also a suspected case of *S. nepalensis* bacteremia; further investigation is needed for confirmation.

About the Author

Dr. Hosoya was a junior resident of the Department of Disease Control and Prevention Center, National Center for Global Health and Medicine, Tokyo, Japan at the time of this work. He is an obstetrician-gynecologist with the National Center for Global Health and Medicine. His primary research interest is infectious disease in obstetrics and gynecology.

References

1. Matsuda K, Koya J, Toyama K, Ikeda M, Arai S, Nakamura F, et al. A therapeutic benefit of daptomycin against glycopeptide-resistant gram-positive cocci bloodstream infections under neutropenia. J Infect Chemother. 2017;23:788–90. https://doi.org/10.1016/j.jiac.2017.06.010
2. Yang C, Wang D, Zhou Q, Xu J. Bacteremia due to vancomycin-resistant *Leuconostoc lactis* in a patient with pneumonia and abdominal infection. Am J Med Sci. 2015;349:282–3. https://doi.org/10.1097/MAJ.0000000000000380
3. Nováková D, Pantůcek R, Petrás P, Koukalová D, Sedlácek I. Occurrence of *Staphylococcus nepalensis* strains in different sources including human clinical material. FEMS Microbiol Lett. 2006;263:163–8. https://doi.org/10.1111/j.1574-6968.2006.00408.x
4. Fulladosa E, Garriga M, Martín B, Guàrdia MD, García-Regueiro JA, Arnau J. Volatile profile and microbiological characterization of hollow defect in dry-cured ham. Meat Sci. 2010;86:801–7. https://doi.org/10.1016/j.meatsci.2010.06.025
5. Fukami K, Satomi M, Funatsu Y, Kawasaki K, Watabe S. Characterization and distribution of *Staphylococcus* sp. implicated for improvement of fish sauce odor. Fish Sci. 2004;70:916–23. https://doi.org/10.1111/j.1444-2906.2004.00887.x
6. Clinical and Laboratory Standards Institute. Methods for antimicrobial dilution and disk susceptibility testing of infrequently isolated or fastidious bacteria. 3rd ed. CLSI guideline M45. Wayne (PA): The Institute; 2016.
7. Lee MR, Huang YT, Lee PI, Liao CH, Lai CC, Lee LN, et al. Healthcare-associated bacteremia caused by *Leuconostoc* species at a university hospital in Taiwan between 1995 and 2008. J Hosp Infect. 2011;78:45–9. https://doi.org/10.1016/j.jhin.2010.11.014
8. Patel T, Molloy A, Smith R, Balakrishnan I. Successful treatment of *Leuconostoc* bacteremia in a neutropenic patient with tigecycline. Infect Dis Rep. 2012;4:e31. https://doi.org/10.4081/idr.2012.e31

Address for correspondence: Satoshi Kutsuna, Department of Disease Control and Prevention Center, National Center for Global Health and Medicine, 1-21-1, Toyama, Shinjuku-ku, Tokyo 162-8655, Japan; email: skutsuna@hosp.ncgm.go.jp

Latent Tuberculosis Screening Using Electronic Health Record Data

Jeffrey D. Jenks, Richard S. Garfein, Wenhong Zhu, Michael Hogarth

Author affiliation: University of California, La Jolla, California, USA

DOI: https://doi.org/10.3201/eid2609.191391

Screening for latent tuberculosis infection is recommended for foreign-born persons in the United States. We used proxy data from electronic health records to determine that 17.5% of foreign-born outpatients attending the UC San Diego Health clinic (San Diego, CA, USA) underwent screening. Ending the global tuberculosis epidemic requires improved screening.

The World Health Organization End TB Strategy aims to end the global tuberculosis (TB) epidemic by 2035 (*1*). The US Preventive Service Task Force (*2*) and Centers for Disease Control and Prevention (*3*) recommend screening for latent tuberculosis infection (LTBI) in populations at increased risk for infection or progression to TB disease, including foreign-born persons and former residents of countries with increased TB prevalence. Seventy-four percent of active TB cases in San Diego County, California, USA, occur among foreign-born persons, most of whom are from the Philippines, Vietnam, and Mexico; 80% result from reactivated LTBI (*5*). Therefore, TB elimination in the United States requires better diagnosis and treatment of LTBI, especially in foreign-born persons in areas with a low background prevalence of TB, such as San Diego County. However, the frequency of screening for LTBI in foreign-born persons is unknown.

Because medical records often lack information about country of birth, we assessed whether self-reported nationality plus preferred language is a good proxy variable for foreign birth. We used this proxy to determine LTBI screening, prevalence, and treatment rates in foreign-born persons seen at UC San Diego Health (UCSDH) Medical Center in San Diego. We searched the electronic health record (EHR) at UCSDH and validated this search by reviewing a subset of individual EHRs. The University of California San Diego Institutional Review Board approved this study.

We used the clinical data repository module of our EHR, EPIC (https://www.epic.com), to search the records of all patients who accessed care in the outpatient clinic at UCSDH at least once from March

31, 2018, through March 30, 2019, and who were determined to be at high risk for LTBI on the basis of birth country (*6*). We calculated the proportion of foreign-born persons screened for LTBI from the total number who met our search criteria, and we compared results using a χ^2 test with a 2-sided p value of <0.05. Self-reported nationality and preferred language was used as a proxy for birth country. For example, we used Mexican nationality and Spanish language as a proxy for being born in Mexico.

A total of 8,234 persons met our search criteria, most of whom were female, were Mexican, and identified Spanish as their primary language (Table). Overall, 1,437 (17.5%) underwent LTBI screening while receiving care at UCSDH, most with the Quantiferon-TB Gold test (QIAGEN, https://www.qiagen.com). Detailed review of 250 randomly selected patient EHRs from persons who underwent LTBI screening found that 209 (83.6%) had documentation of being born, living, or spending a considerable amount of time (including frequent travel) in a TB-endemic country. A higher proportion of men (19.3%) than women (16.4%) had been screened for LTBI; otherwise, persons who were and were not screened did not differ significantly. Of those screened for LTBI, 956 (66.5%) tested negative and 379 (26.4%) positive by tuberculin skin test or Quantiferon-TB Gold test. To validate LTBI status, we reviewed 250 randomly selected EHRs of patients screened for LTBI, of whom 174 (69.6%) were determined not to have LTBI, 73 (29.2%) had newly diagnosed LTBI, and 3 (1.2%) had pulmonary TB.

To determine the proportion of patients who had LTBI, we searched the EHRs of the 8,234 patients for isoniazid, rifampin, and rifapentine prescription patterns. This search identified 184 patients who had been prescribed rifampin or isoniazid and either had completed or were still undergoing treatment. To

Table. TB testing and treatment among foreign-born outpatients attending UC San Diego Health Medical Center, San Diego, California, USA, March 31, 2018–March 30, 2019*

Variable	TB tested, no. (%)		p value
	No, n = 6,797	Yes, n = 1,437	
Sex			
F	4,390 (64.6)	860 (59.8)	0.000
M	2,407 (35.4)	577 (40.2)	
Nationality or regionality			
Mexican	5,142 (75.7)	1,074 (74.7)	1.0
Chinese	732 (10.8)	186 (12.9)	
Vietnamese	635 (9.3)	91 (6.3)	
Filipino	186 (2.7)	44 (3.1)	
Guatemalan	43 (0.6)	12 (0.8)	
Asian Indian	18 (0.3)	6 (0.4)	
African	13 (0.2)	10 (0.7)	
Other	17 (0.3)	10 (0.7)	
Unknown	11 (0.2)	4 (0.3)	
Preferred language			
Spanish	5,215 (76.7)	1,094 (76.1)	0.097
Vietnamese	646 (9.5)	90 (6.3)	
Mandarin	384 (5.6)	108 (7.5)	
Chinese	265 (3.9)	68 (4.7)	
Tagalog	184 (2.7)	44 (3.1)	
Cantonese	82 (1.2)	15 (1.0)	
African†	11 (0.2)	12 (0.8)	
Telugu	2 (<1.0)	1 (<1.0)	
Haitian Creole	0	5 (0.3)	
Country of birth			
Unknown	6,745 (99.2)	1,362 (94.8)	1.0
Mexico	49 (0.7)	66 (4.6)	
Other	3 (<1.0)	9 (0.6)	
TB test			
QuantiFERON-TB Gold test‡	NA	1,340 (93.2)	NA
TST	NA	97 (6.8)	
TB test result			
Negative	NA	956 (66.5)	NA
Positive§	NA	379 (26.4)	
Equivocal/low mitogen	NA	102 (7.1)	

*Foreign-born is a proxy for outpatients at UC San Diego Health Medical Center with a self-reported nationality of Mexican, Chinese, Vietnamese, Filipino, Guatemalan, Asian Indian, African plus preferred language other than English. NA, not applicable, TB, tuberculosis; TST, tuberculin skin test.
†Includes Amharic, Somali, and Swahili.
‡QIAGEN, https://www.qiagen.com.
§QuantiFERON TB-Gold titer >0.35 IU/mL or reactive TST considered positive.

validate the EHR search we reviewed these records. A total of 135 (73.4%) patients had been treated for LTBI and 28 (15.2%) had been or were being treated for active pulmonary TB or an atypical mycobacterial infection. The remaining 23 (11.4%) had been prescribed isoniazid or rifampin for another reason, had previously been treated for LTBI and isoniazid or rifampin was documented as a historical medication, or refused treatment. No patients had been prescribed rifapentine. Of those who began treatment for LTBI, 101 (74.8%) completed or were still undergoing treatment at the time of the study, 5 (3.7%) stopped treatment, and treatment completion was unknown for 29 (21.6%).

In our tertiary/quaternary medical center, which serves a large population of foreign-born patients, we found self-reported nationality and preferred language to be a good proxy for foreign-born persons and others who meet the US Preventive Service Task Force and Centers for Disease Control and Prevention guidelines for LTBI screening. However, our single-center study is in a unique setting and so might not reflect findings in other settings. Our proposed screening strategy might miss persons who prefer speaking English but would otherwise meet criteria for LTBI screening. This study identified missed opportunities for screening and diagnosis of LTBI among foreign-born persons; of those who had a recent diagnosis of LTBI, most were successfully treated. Improved LTBI screening, possibly with the use of routine EHR tools, is needed to end the global TB epidemic.

The work was partially supported by the National Institutes of Health, grant UL1TR001442, of CTSA funding.

About the Author

Dr. Jenks is an assistant clinical professor in the Department of Medicine, University of California San Diego. His primary research interests include tuberculosis and invasive fungal infections.

References

1. World Health Organization. The End TB Strategy [cited 2019 Sep 5]. https://www.who.int/tb/post2015_strategy
2. Bibbins-Domingo K, Grossman DC, Curry SJ, Bauman L, Davidson KW, Epling JW Jr, et al.; US Preventive Services Task Force. Screening for latent tuberculosis infection in adults: US Preventive Services Task Force recommendation statement. JAMA. 2016;316:962–9. https://doi.org/10.1001/jama.2016.11046
3. Lewinsohn DM, Leonard MK, LoBue PA, Cohn DL, Daley CL, Desmond E, et al. Official American Thoracic Society/Infectious Diseases Society of America/Centers for Disease Control and Prevention clinical practice guidelines: diagnosis of tuberculosis in adults and children. Clin Infect Dis. 2017;64:111–5. https://doi.org/10.1093/cid/ciw778
4. Centers for Disease Control and Prevention. Latent TB infection in the United States [cited 2019 Sep 5]. https://www.cdc.gov/tb/statistics/ltbi.htm
5. San Diego County Department of Public Health. County of San Diego Tuberculosis Control Program. 2015 fact sheet [cited 2020 Sep 5]. https://www.sandiegocounty.gov/content/dam/sdc/hhsa/programs/phs/tuberculosis_control_program/Factsheet%202015.pdf
6. Centers for Disease Control and Prevention. Latent Tuberculosis Infection: A guide for primary health care providers [cited 2020 Sep 5]. https://www.cdc.gov/tb/publications/ltbi/appendixb.htm

Address for correspondence: Jeffrey D. Jenks, Department of Medicine, University of California San Diego, 330 Lewis St, Ste 301, San Diego, CA 92103, USA; email: jjenks@ucsd.edu

Putative Conjugative Plasmids with *tcdB* and *cdtAB* Genes in *Clostridioides difficile*

Gabriel Ramírez-Vargas, César Rodríguez

Author affiliation: Facultad de Microbiología and Centro de Investigación en Enfermedades Tropicales, Universidad de Costa Rica, San José, Costa Rica

DOI: https://doi.org/10.3201/eid2609.191447

The major toxins of *Clostridioides difficile* (TcdA, TcdB, CDT) are chromosomally encoded in nearly all known strains. Following up on previous findings, we identified 5 examples of a family of putative conjugative plasmids with *tcdB* and *cdtAB* in clinical *C. difficile* isolates from multilocus sequence typing clades C-I, 2, and 4.

Clostridioides difficile spores may differentiate in the colon of susceptible humans into vegetative cells and release 1 or 2 large clostridial cytotoxins (TcdA, TcdB) or a binary toxin with ADP-ribosyltransferase activity (CDT), or both, to cause colitis and diarrhea (*1*). When present, genes for TcdA, TcdB, and CDT are almost without exception encoded by 2 separate chromosomal loci known as PaLoc and CdtLoc (*2*). Recent discovery of clade C-I strains SA10-050 and

CD10-165 in France (*3*) and HSJD-312 and HMX-152 in Costa Rica (*4*) challenged this paradigm, as these strains carry a monotoxin *tcdB*$^{+}$ PaLoc next to a full CdtLoc on extrachromosomal molecules that resemble conjugative plasmids (*4*).

The Anaerobic Bacteriology Research Laboratory (LIBA) has been isolating and typing *C. difficile* in Costa Rica for nearly a decade and thereby generated an isolate collection with >800 records. We searched mobile genetic elements (MGEs) among whole-genome sequences from 150 of those bacteria, leading to the discovery of 5 new *tcdA*$^{-}$/*tcdB*$^{+}$/*cdtAB*$^{+}$ putative plasmids among isolates that were cultivated from loose fecal samples of patients under clinical suspicion for *C. difficile* infections (CDIs): LIBA-6656, LIBA-7194, LIBA-7602, LIBA-7678, and LIBA-7697. These materials were collected at 3 hospitals located within a 78.5 km^2 area in 2013 (LIBA-6656), 2016 (LIBA-7194), 2017 (LIBA-7602), and 2018 (LIBA-7678, LIBA-7697). Raw sequencing data can be retrieved from the European Nucleotide Archive (https://www.ebi.ac.uk/ena; LIBA-6656, run ERR467623) or from the MicrobesNG platform (https://microbesng.com/portal/projects/FB43968C-E9EF-4270-9D1A-054457CC9B54).

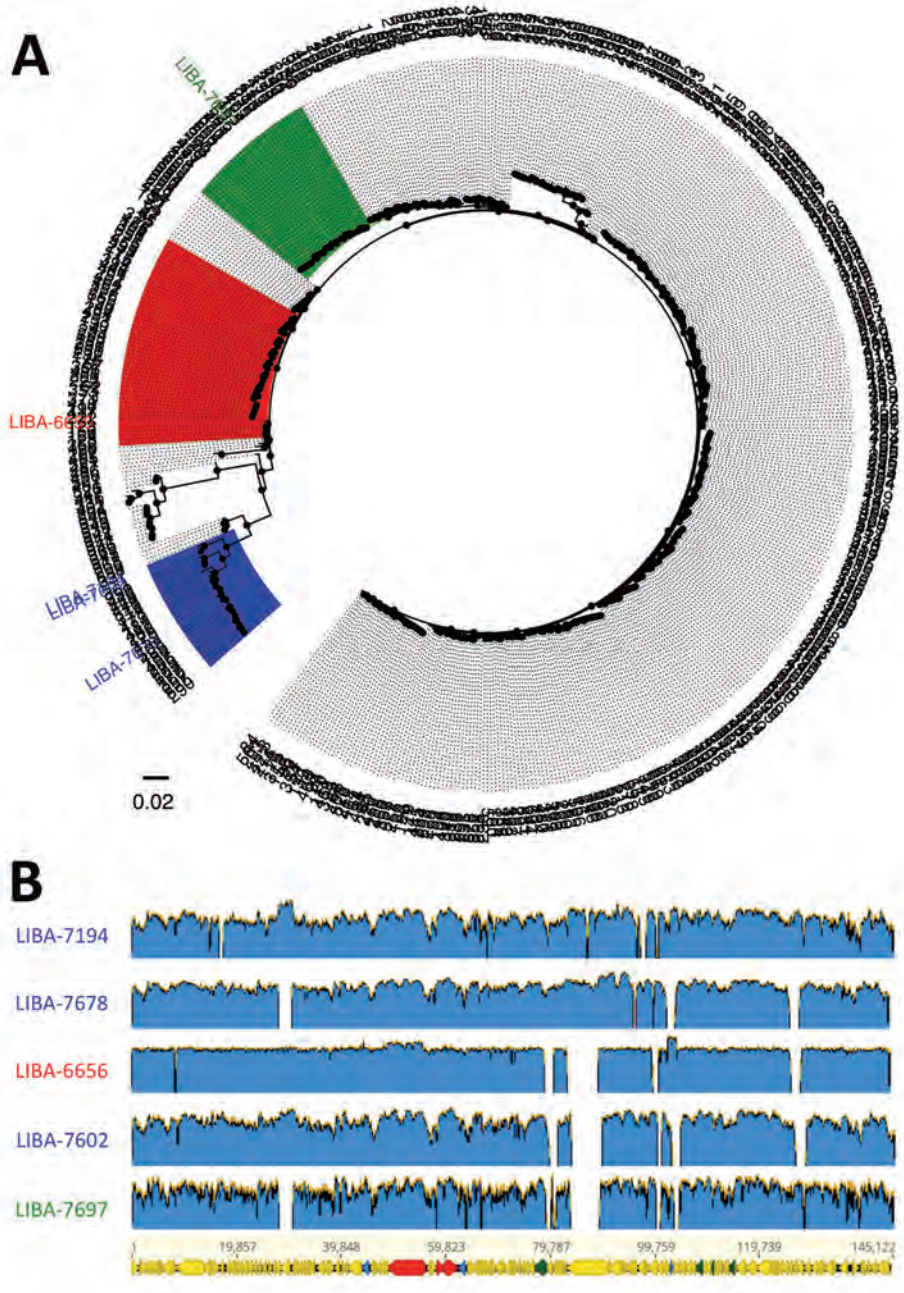

Figure. Multilocus sequence typing–based classification (A) and diversity of extrachromosomal circular sequences (B) of *Clostridioides difficile* strains with plasmid-encoded toxins. A) FastTree (http://www.microbesonline.org/fasttree) phylogenic tree derived from a MUSCLE (http://www.drive5.com/muscle) alignment of concatenated multilocus sequence typing alleles from all *C. difficile* sequence types deposited in the PubMLST database (https://pubmlst.org). Tip labels represent sequence types or strain names. Strains from clade C-I are highlighted in blue, from clade 2 in red, and from clade 4 in green. B) This graphic shows short reads from strains LIBA-7194, LIBA-7678, LIBA-7602 (clade C-I, blue), LIBA-6656 (clade 2, red), and LIBA-7697 (clade 4, green) mapped to the plasmid sequence of strain HSJD-312, which was obtained through hybrid PacBio (Pacific Biosciences, https://www.pacb.com) and Illumina (Illumina, https://www.illumina.com) sequencing and therefore used as a reference (145.1 kb, bottom). Arrows in the reference sequence represent annotated coding sequences. Genes for toxins are in red; for transposases, integrases, and recombinases are in blue, and for proteins from a putative conjugation machinery are in green.

A tree of aligned, concatenated, multilocus sequence typing allele combinations revealed that the new plasmid sequences were present in isolates assigned to clade C-I (LIBA-7194, LIBA-7602, LIBA-7678), clade 2 (LIBA-6656), and clade 4 (LIBA-7697) (Figure 1, panel A). This unexpected result expands the host range of this type of MGE to include *C. difficile* clades more commonly associated with human hosts. The 3 clade C-I strains were different, as confirmed by pairwise estimates of genomic MinHash (min-wise independent permutations locality sensitive hashing scheme) distances (0.022–0.049) calculated with MASH (https://mash.readthedocs.io/en/latest/index.html) and average nucleotide identities (94.15%–97.45%) calculated with FastANI (https://github.com/ParBLiSS/FastANI). Genome similarity showed a tendency to decrease with time (data not shown), suggesting that clade C-I strains are evolving.

Although our plasmid assemblies are awaiting confirmation by long-read sequencing, the size of 3 of the reconstructed plasmids (139.2–147.7 kb) closely matches that of known *C. difficile* toxin plasmids, such as pHSJD-312 (145.1 kb) (*4*). The toxin contigs of LIBA-7697 (53.2 kb) and LIBA-7194 (228.8 kb) were fragmented or likely misassembled, respectively. Read mapping to a high-quality hybrid assembly of pHSJD-312 showed 53.6%–93.7% identical sites in the alignment and 92%–98% reference sequence coverage, indicating that the new toxin plasmids are not the same molecule (Figure 1, panel B). We corroborated this result with a Panaroo (https://github.com/gtonkinhill/panaroo) pangenome analysis of pHSJD-312 and the plasmid sequences found in LIBA-6656, LIBA-7602, and LIBA-7678, because it classified only 135 (89%) of 152 genes as conserved. This core genome included toxin loci, agr loci, and potential conjugation systems. In contrast, mapping gaps corresponded to putative virulence factors (i.e., lectin-binding or cell wall–binding proteins), hypothetical proteins, and MGEs, such as class 2 introns and transposases (Figure 1, panel B). These findings imply that this group of chimeric molecules is undergoing nonhomologous recombination.

The MGE-associated *tcdB* sequence of LIBA-6656 (clade 2) could not be fully assembled. In the remaining 4 strains, this gene was highly conserved (99%–100% protein sequence identity) and expected to encode variant TcdBs that would cause a *Clostridium sordellii*–like cytopathic effect. Besides its plasmid-borne *tcdB*, LIBA-6656 carries a different *tcdB* allele on a chromosomal PaLoc. The contribution of each of these *tcdB* alleles to infection is unclear at this time. Yet, the coexistence of 2 PaLocs within a host is compatible with the suggested transition from ancient monotoxin PaLocs to modern bitoxin PaLocs (*3*). We also noted a high level of sequence identity for *cdtA* (≥99%) and *cdtB* (≥98%) in all 5 putative plasmids. However, it is difficult with such a small dataset to conclude whether the noted conservation of toxin gene sequences reflects stable coevolution or only the short evolutionary time after acquisition.

As previously seen in other clade C-I toxin plasmids, the toxin genes of the new putative plasmids are flanked by genes for a transposase and an integrase (*4*). Furthermore, we identified their PaLocs as lateral gene transfer events using Alien_Hunter software (Sanger Institute, https://www.sanger.ac.uk). Additional elements from this group of MGEs lack toxin genes (*4*), indicating that they are gained through lateral gene transfer.

Three of the 5 isolates that host new toxin plasmids would have remained undetected if we had not attempted *C. difficile* cultivation from TcdB$^-$ fecal samples or sequencing for isolates with negative results for *tcdC* and *tcdA* (LIBA-7194, LIBA-7602, LIBA-7678). We therefore anticipate that the frequency of *C. difficile* isolates with toxin plasmids has been underestimated and recommend that current diagnostic procedures be refined. Moreover, our results open avenues to explore whether similar plasmids are present in species other than *C. difficile* and are implicated in undiagnosed cases of antibiotic-associated diarrhea.

Acknowledgments

Thomas Riedel and Jörg Overmann generated the plasmid sequence that was used as a reference (pHJSD-312) in the context of the BMBF-MICITT project Cd-biOmics.

Vicerrectoría de Investigación/UCR funded this work.

About the Author

Dr. Ramírez-Vargas is a clinical microbiologist currently working at the Clinical Laboratory of the National Children's Hospital of Costa Rica. He has studied mobile genetic elements in *C. difficile* for over 5 years.

Dr. Rodríguez is a clinical bacteriologist based at the University of Costa Rica. He investigates the resistome and mobilome of anaerobic bacteria and the ecotoxicology of antibiotic resistance in clinical and extraclinical settings.

References

1. Balsells E, Shi T, Leese C, Lyell I, Burrows J, Wiuff C, et al. Global burden of *Clostridium difficile* infections: a systematic review and meta-analysis. J Glob Health. 2019;9:010407. https://doi.org/10.7189/jogh.09.010407

2. Knight DR, Elliott B, Chang BJ, Perkins TT, Riley TV. Diversity and evolution in the genome of *Clostridium difficile*. Clin Microbiol Rev. 2015;28:721–41. https://doi.org/10.1128/CMR.00127-14
3. Monot M, Eckert C, Lemire A, Hamiot A, Dubois T, Tessier C, et al. *Clostridium difficile*: new insights into the evolution of the pathogenicity locus. Sci Rep. 2015;5:15023. https://doi.org/10.1038/srep15023
4. Ramírez-Vargas G, López-Ureña D, Badilla A, Orozco-Aguilar J, Murillo T, Rojas P, et al. Novel Clade C-I *Clostridium difficile* strains escape diagnostic tests, differ in pathogenicity potential and carry toxins on extrachromosomal elements. Sci Rep. 2018;8:13951. https://doi.org/10.1038/s41598-018-32390-6

Address for correspondence: César Rodríguez, Universidad de Costa Rica, Facultad de Microbiología, Ciudad Universitaria Rodrigo Facio, San Pedro de Montes de Oca, 11501-2060, San José, Costa Rica; email: cesar.rodriguezsanchez@ucr.ac.cr

Information-Accessing Behavior during Zika Virus Outbreak, United States, 2016

Rachael Piltch-Loeb, David Abramson

Author affiliation: New York University, New York, New York, USA

DOI: https://doi.org/10.3201/eid2609.191519

We used latent class analysis to examine Zika virus–related information-accessing behavior of US residents during the 2016 international outbreak. We characterized 3 classes of information-accessing behavior patterns: universalists, media seekers, and passive recipients. Understanding these patterns is crucial to planning risk communication during an emerging health threat.

During the past 15 years, new media platforms have emerged as routine channels of health communication. Little is known about how persons navigate this dynamic and complex information landscape, especially during an emerging health threat with little scientific certainty and few or no medical countermeasures (*1*,*2*). The 2016 Zika virus outbreak provides for an examination of how people interact with this dynamic information landscape. As scientific understanding of the virus evolved, so did Zika risk communication strategies. Previous reports have identified public sources of Zika information but have not considered the public's information-accessing behavior (*3*,*4*). We used latent class analysis (LCA) to characterize and differentiate types of information-accessing behavior and identify how these behavioral patterns shifted during the 2016 Zika virus outbreak.

LCA identifies clusters within the population on the basis of participants' responses to observed variables (*5*,*6*). We collected and pooled data from 3 representative samples of US households drawn from fully replicated, single-stage, random-digit dialing samples of households supplemented by lists of randomly generated cell phone numbers. The survey had a 4%–6% response rate. We conducted the surveys in April–May (1,233 participants), July–August (1,231 participants), and October–November (1,234 participants) of 2016.

The survey analyzed access to 6 categories of information sources: news (online or print); television or radio; social media, such as Facebook, YouTube, Reddit, or other apps; personal physician; government agencies; and friends, family, or co-workers. We used these data to form 6 binary variables indicating access to each category of information source. We then used these variables to determine 3 classes of information-accessing behavior.

In accordance with the best practices suggested by Nylund et al. (*7*), we used 6 criteria to determine the optimal number of classes (Appendix, https://wwwnc.cdc.gov/EID/article/26/9/19-1519-App1.pdf). New York University's Institutional Review Board approved this research.

Our LCA results suggested that information-accessing behaviors could be grouped into 3 distinct classes: universalists, media seekers, and passive recipients. We sorted each participant into a class on the basis of the number of sources he or she had accessed (Figure). Class 1 comprised universalists, that is, participants who actively accessed information from all sources included in the survey. Class 2 comprised media seekers, that is, participants who primarily accessed information from mass media. Class 3 comprised passive recipients of information; these participants accessed the fewest number of sources and had the highest probability of seeking information from broadcast media. Class membership was not necessarily static; an individual participant might exhibit different information-accessing behaviors at different time points within the Zika outbreak.

The acquisition patterns of Zika information shifted across time. At the first time point (April–May 2016), universalists constituted 23.0% of the US population, media seekers 20.7%, and passive recipients 54.3%. At the second time point (July–August 2016),

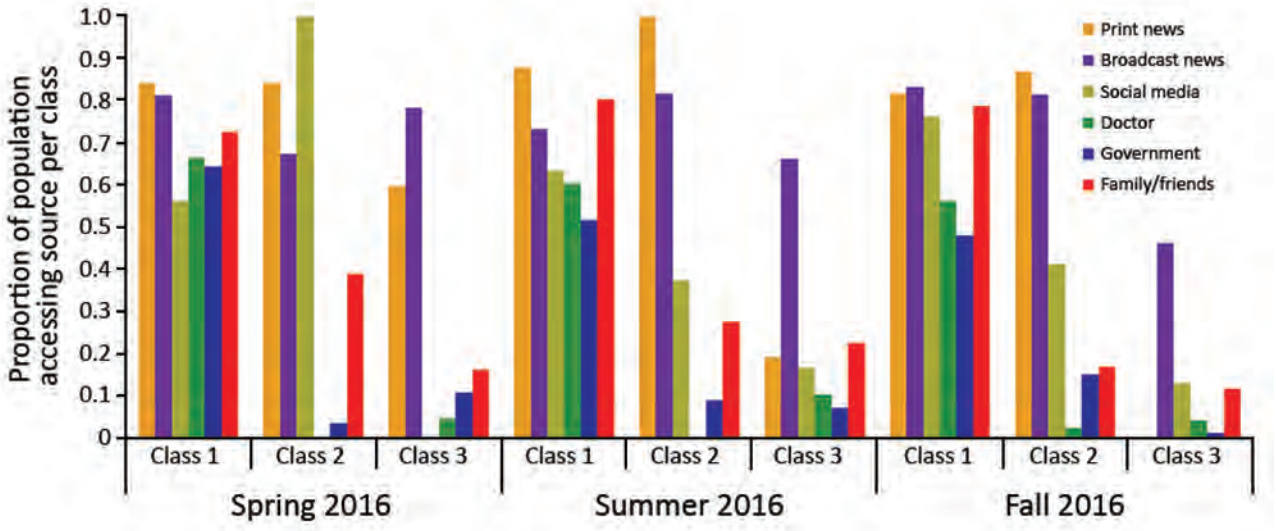

Figure. Latent classes of information access for Zika virus, United States, 2016. Proportion of the population that used a given category of information source in each class, across 3 time points of data collection.

universalists constituted 13.8% of the population, media seekers 51.5%; and passive recipients 34.8%. At the third time point (October–November 2016), universalists constituted 16.0% of the population, media seekers 52.0%, and passive recipients 32.0%.

As understanding of Zika virus evolved and media coverage shifted, the proportion of the population in each of the identified classes also shifted. Our finding that the proportion of the population in the universalist group was largest at the first time point suggests that in the earlier phases of the Zika outbreak, acquisition of information increased among the most highly attuned portions of the population. We hypothesize that as the mosquito season began, behavior patterns shifted from passive information acquisition to active information acquisition in the shift to media seeking (*8*). This hypothesis explains the shift from the large proportion of passive recipients at the first time point to the larger proportions of media seekers at the second and third time points.

These population shifts suggest large portions of the population were initially passive, perhaps uninterested, recipients of information about Zika. During the course of the surveys, a proportion of passive recipients and universalists may have become media seekers. In addition, we found that early adopters of emerging information could be retransmitters within their networks. Only universalists consistently accessed information from their own social network (including personal contacts and social media), the medical community, and government sources. Further exploration is needed to determine whether these findings are influenced by the actual lack of risk for Zika in the United States or whether they are reflective of larger behavioral patterns.

Our analysis is limited by the number of information source categories included in the survey and the lack of source specificity. However, our study took a unique approach in characterizing patterns of information-accessing behavior. These findings can be used to inform risk communication strategies designed for population segments with different information-accessing behavior patterns.

This study was funded by National Science Foundation under Rapid Response Research grant no. 1638545.

About the Authors

Dr. Piltch-Loeb is a Preparedness Fellow at the Harvard T.H. Chan School of Public Health. She completed this work as part of her doctorate in the department of Social and Behavioral Sciences at New York University Global Public Health. Her research interests include public health emergencies and risk communication.

Dr. Abramson is a clinical associate professor in the department of Social and Behavioral Sciences at New York University Global Public Health. His research interests include public health disaster science.

References

1. Anker AE, Reinhart AM, Feeley TH. Health information seeking: a review of measures and methods. Patient Educ Couns. 2011;82:346–54. https://doi.org/10.1016/j.pec.2010.12.008
2. Jacobs W, Amuta AO, Jeon KC. Health information seeking in the digital age: an analysis of health information seeking

behavior among US adults. Cogent Soc Sci. 2017;3:1302785. https://doi.org/10.1080/23311886.2017.1302785
3. Piltch-Loeb R, Merdjanoff AA, Abramson DM. How the US population engaged with and prioritized sources of information about the emerging Zika virus in 2016. Health Secur. 2018;16:165–77. https://doi.org/10.1089/hs.2017.0107
4. Sell TK, Watson C, Meyer D, Kronk M, Ravi S, Pechta LE, et al. Frequency of risk-related news media messages in 2016 coverage of Zika virus. Risk Anal. 2018;38:2514–24. https://doi.org/10.1111/risa.12961
5. Wolfe JH. Pattern clustering by multivariate mixture analysis. Multivariate Behav Res. 1970;5:329–50. https://doi.org/10.1207/s15327906mbr0503_6
6. Goodman LA. The analysis of systems of qualitative variables when some of the variables are unobservable. Part IA modified latent structure approach. The American Journal of Sociology. 1974;79:1179–259. https://doi.org/10.1086/225676
7. Nylund KL, Asparouhov T, Muthén BO. Deciding on the number of classes in latent class analysis and growth mixture modeling: a Monte Carlo simulation study. Struct Equ Modeling. 2007;14:535–69. https://doi.org/10.1080/10705510701575396
8. Agarwal NK. Information source and its relationship with the context of information seeking behavior. In: iConference 2011: proceedings of the 2011 iConference; 2011 Feb 8–11; Seattle, Washington, USA. New York: Association for Computing Machinery; 2011. p. 48–55.

Address for correspondence: Rachael Piltch-Loeb, New York University, Global Public Health, 715 Broadway Rm 1229, New York, NY 10003, USA; email: rpl5@nyu.edu

Severe Fever with Thrombocytopenia Syndrome Virus in Ticks and SFTS Incidence in Humans, South Korea

Jeong Rae Yoo,[1] Sang Taek Heo,[1] Sung Wook Song, Seung Geon Bae, Seul Lee, Sungho Choi, Chaehyun Lee, Sugyeong Jeong, Myeongseop Kim, Woojin Sa, Yeongrim Lee, Haseon Choi, Sun-Ho Kee, Keun Hwa Lee

DOI: https://doi.org/10.3201/eid2609.200065

[1]These authors contributed equally to this article.

Author affiliations: Jeju National University, Jeju, South Korea (J.R. Yoo, S.T. Heo, S.W. Song, S.G. Bae, S. Lee, S. Choi, C. Lee, S. Jeong, M. Kim, W. Sa, Y. Lee, H. Choi); Korea University, Seoul, South Korea (S.-H. Kee); Hanyang University College of Medicine, Seoul (K.H. Lee).

During 2016–2018, we collected 3,193 ticks from rural areas in South Korea to investigate the prevalence of severe fever with thrombocytopenia syndrome virus (SFTSV). We detected SFTSV in ticks at an infection rate (IR) of 11.1%. We noted increases in the human IR associated with the monthly SFTSV IR in ticks.

Severe fever with thrombocytopenia syndrome (SFTS) is a tickborne zoonosis caused by the SFTS virus (SFTSV) (*1*); >1,000 SFTS cases have been reported in South Korea (*2*). The SFTS prevalence rate was 2.26/100,000 inhabitants on the mainland and 13.66/100,000 inhabitants on Jeju Island, South Korea (*2*). SFTSV has been detected in several species of ticks, including *Haemaphysalis longicornis*, *Amblyomma testudinarium*, and *Ixodes nipponensis* (*3*). A previous study reported that the minimum infection rate of SFTSV in infected ticks was lower (0.37%) on Jeju Island than in other collection areas (1.97%) (*4*). However, 7%–14% SFTSV seropositivity was identified in domestic and wild animals (*4*–*5*), and 2%–5% SFTSV seropositivity was identified in a healthy population in South Korea (*6*). Therefore, our aim was to investigate the SFTSV infection rate (IR) in ticks in the region with the highest endemicity, Jeju Island, and to analyze the relationship between the geographic distribution of ticks and SFTSV and human cases of SFTS.

During June 2016–January 2019, well-equipped trained researchers collected ticks from the natural environment of Jeju Island. The tick sampling sites included 5 rural areas: Aewol-eup (AW); Seon Hul-ri (SH); Jeo Ji-ri (JJ); and Ha Do-ri (HD) and Bo Mok-ri (BM) (Figure). These 5 areas were chosen to compare SFTSV IR in ticks in areas with the highest rates of human SFTS cases, SH, HD, and AW, and SFTSV IR in ticks in areas with lower human SFTS rates, JJ and BM. Ticks were manually collected 2 times per month, during the first and third weeks, by dragging a white cloth in woodlands for 2 hours in each area. We morphologically identified tick species and developmental stages by using an Olympus SD-ILK-200–2 stereomicroscope (Olympus Corporation, https://www.olympus-lifescience.com) (*7*) and extracted viral RNA by using a QIAamp Viral RNA Mini kit (QIAGEN Inc., https://www.qiagen.com) according to the manufacturer's instructions (Appendix, https://wwwnc.cdc.gov/EID/article/26/9/20-0065-App1.pdf).

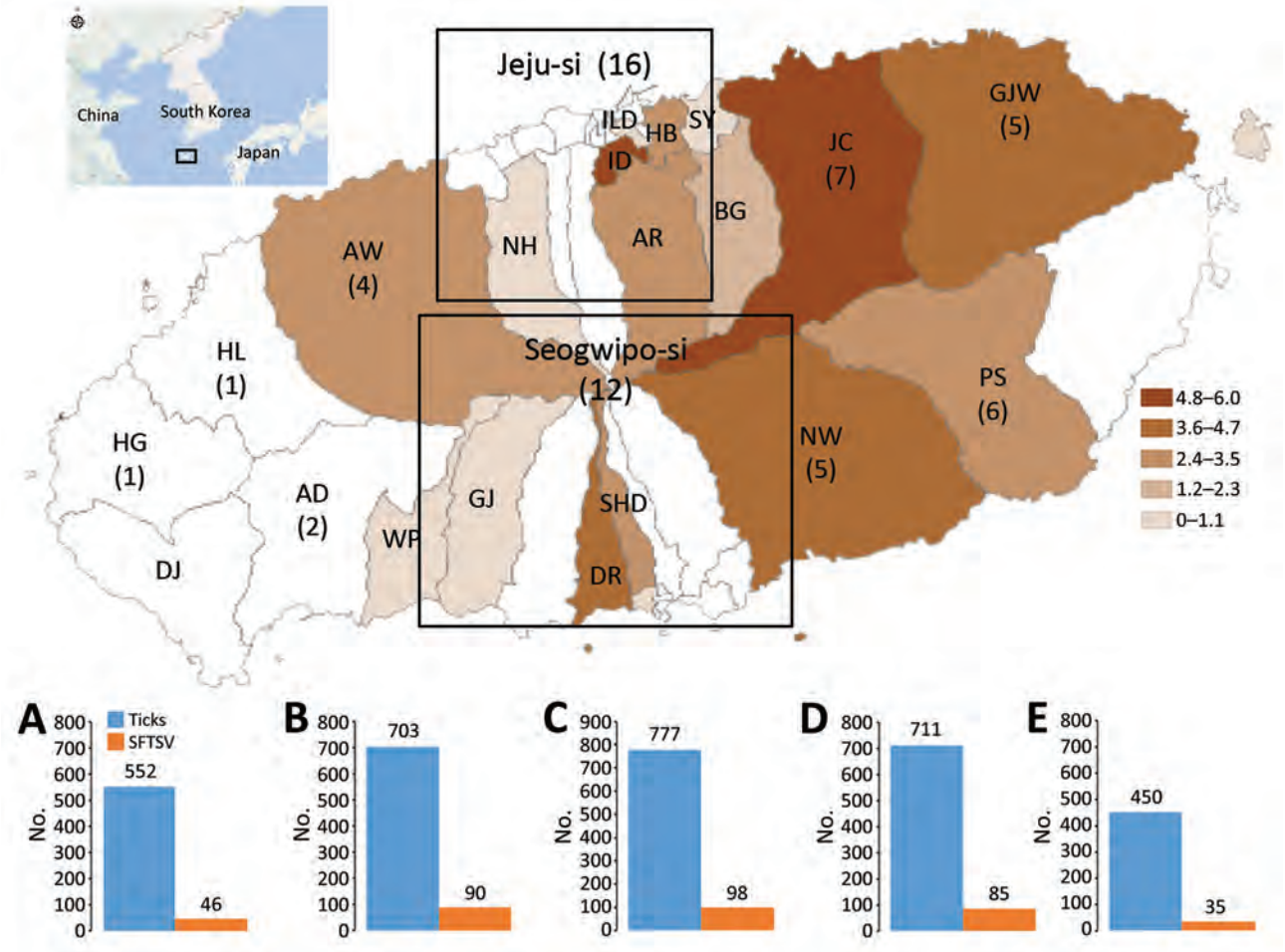

Figure. Geographic distribution of patients with severe fever with thrombocytopenia syndrome (SFTS) during January 2013–January 2019 and yearly incidence rates of SFTS virus (SFTSV) from June 2016–January 2019 on Jeju Island, South Korea. Inset shows location of Jeju Island near the coast of South Korea. Orange indicate regions of patients with SFTS in 2013–2019. Graphs show SFTSV detected in ticks and cases of human SFTS in A) Jeo Ji-ri; B) Aewol-eup; C) Seon Hul-ri; D) Ha Do-ri; and E) Bo Mok-ri. AR, Ara-dong; AW, Aewol-eup; BG, Bonggae-dong; BM, Bo Mok-ri; DR, Daeryun-dong; GJ, Ganjeong-dong; GJW, Gujwa-eup; HB, Hwabug-dong; HD, Ha Do-ri; ILD, Ildo-dong; ID, Ido-dong; JC, Jocheon-eup; JJ, Jeo Ji-ri; NH, Nohyeong-dong; NW, Nanwon-eup; PS, Pyoseon-myeon; SHO, Seohong-dong; SH, Seon Hul-ri; SY, Samyang-dong; WP, Wolpyeong-dong.

A total of 3,193 ticks were collected; most (99.9%) were *H. longicornis* and 81.3% of all ticks were nymphs. We detected SFTSV in 11.1% (354/3,193) of ticks (Appendix Table). Among the 5 areas, the average IR of SFTSV in ticks was 12.8% in AW, 12.6% in SH, 12.0% in HD, 8.3% in JJ, and 7.8% in BM. Adult ticks had a higher SFTSV IR (12.4%) than nymphs (9.5%). SFTSV was detected mainly in adult ticks (Appendix Table).

The monthly IR of SFTSV in ticks increased in May, peaked in July, and then slowly decreased (Appendix Figure 1). In addition, changes in the incidence of SFTS in patients were associated with increases in the monthly IR of SFTSV in ticks at a rate of 19.8% (95% CI 2.3%–40.2%) increase of SFTS in patients per 1% increase in monthly SFTSV IR in ticks (p = 0.02). SFTSV-infected ticks also were observed in the winter season. SFTSV sequences from infected ticks in our study and SFTS patients on Jeju Island were consistent with each other but differed from viruses in other regions of South Korea (Appendix Figure 2).

In a previous study, the prevalence of SFTSV in ticks was very low (0.2%), implying that ticks alone might not be sufficient to maintain SFTSV in nature (*8*). However, the high IR of SFTSV in ticks could explain why Jeju Island had one of the highest rates of human SFTS infection in South Korea. Changes in the incidence of patients with SFTS showed a pattern similar to that of monthly SFTSV IR in ticks. The IR of SFTSV in SH was the highest, along with HD and AW, where rates of human SFTS cases also were high.

In East Asia, humans most frequently acquire SFTS during May–July, and shrub, forest, and rainfed

cropland areas are associated with high risk for infection(*2*,*3*,*6*). Northeast Jeju Island, which includes SH, AW, and HD, has many farms and wetlands, and the IR of SFTSV in ticks peaked there in July, August, and September. In addition, SFTSV was detected in ticks in winter on Jeju Island, but no SFTS cases were reported in South Korea during winter. The 62 confirmed SFTS cases were statistically significantly associated with higher ambient temperature (22.5°C ±4.2°C) compared with patients with negative RT-PCR results for SFTSV (18.9°C ±5.7°C; p<0.001) (J.R. Yoo, unpub. data). The optimal temperature range for growth and reproduction of *H. longicornis* ticks is 20°–24°. Jeju Island maintains a temperature >20° during May–October and is largely a rural and natural environment. We consider this area to have the highest prevalence of SFTS cases and ticks with SFTSV in South Korea.

The results of this study showed that Jeju Island has the highest IR of SFTSV in ticks compared with other regions of South Korea and endemic countries. In addition, we found that the partial small segment of SFTSV in ticks was highly homologous to SFTSV in patients on Jeju Island and that Northeast Jeju Island, which includes SH, is a high-risk area for human SFTS infections.

Acknowledgments

We thank the members of department of microbiology, Jeju National University, Graduate College of Medicine and the Safety for Agricultural Injuries of Famers cohort study, Jeju National University Hospital for assistance in collecting tick samples in various regions of Jeju Island, South Korea.

This work was supported by a grant from the Korea Health Technology Research and Development Project through the Korea Health Industry Development Institute and funded by the Ministry of Health & Welfare, South Korea (grant no. HG18C0037).

About the Author

Dr. Yoo and Dr. Heo are professors in the Department of Internal Medicine, Jeju National University, College of Medicine, Jeju, South Korea. Their research interests are infectious diseases.

References

1. Yun SM, Lee WG, Ryou J, Yang SC, Park SW, Roh JY, et al. Severe fever with thrombocytopenia syndrome virus in ticks collected from humans, South Korea, 2013. Emerg Infect Dis. 2014;20:1358–61. https://doi.org/10.3201/eid2008.131857
2. Korea Centers for Disease Control and Prevention. Infectious disease surveillance 2019, public health weekly report [in Korean] [cited 2020 May 1]. https://is.cdc.go.kr
3. Im JH, Baek J, Durey A, Kwon HY, Chung MH, Lee JS. Current status of tick-borne diseases in South Korea. Vector Borne Zoonotic Dis. 2019;19:225–33. https://doi.org/10.1089/vbz.2018.2298
4. Oh SS, Chae JB, Kang JG, Kim HC, Chong ST, Shin JH, et al. Detection of severe fever with thrombocytopenia syndrome virus from wild animals and Ixodidae ticks in the Republic of Korea. Vector Borne Zoonotic Dis. 2016;16:408–14. https://doi.org/10.1089/vbz.2015.1848
5. Yu KM, Yu MA, Park SJ, Kim YI, Robles NJ, Kwon HI, et al. Seroprevalence and genetic characterization of severe fever with thrombocytopenia syndrome virus in domestic goats in South Korea. Ticks Tick Borne Dis. 2018;9:1202–6. https://doi.org/10.1016/j.ttbdis.2018.05.001
6. Yoo JR, Heo ST, Kim M, Song SW, Boo JW, Lee KH. Seroprevalence of severe fever with thrombocytopenia syndrome in the agricultural population of Jeju Island, Korea, 2015–2017. Infect Chemother. 2019;51:337–44. https://doi.org/10.3947/ic.2019.51.4.337
7. Goff ML, Loomis RB, Welbourn WC, Wrenn WJ. A glossary of chigger terminology (Acari: Trombiculidae). J Med Entomol. 1982;19:221–38. https://doi.org/10.1093/jmedent/19.3.221
8. Luo LM, Zhao L, Wen HL, Zhang ZT, Liu JW, Fang LZ, et al. *Haemaphysalis longicornis* ticks as Reservoir and Vector of Severe Fever with Thrombocytopenia Syndrome Virus in China. Emerg Infect Dis. 2015;21:1770–6. https://doi.org/10.3201/eid2110.150126

Address for correspondence: Keun Hwa Lee, Department of Microbiology, Hanyang University College of Medicine, 222 Wangsimni-ro Seongdong-gu, Seoul 04763, South Korea; email: yomust7@gmail.com

Typhus Group Rickettsiosis, Brazilian Amazon

Antonio H.H. Minervino, Marcelo B. Labruna, Salatiel R. Dias, Francisco B. Costa, Thiago F. Martins, Phablo N.S. da Silva, Álvaro A. Faccini-Martínez

Author affiliations: Federal University of Western Pará, Santarém, Brazil (A.H.H. Minervino, S.R. Dias, P.N.S. da Silva); University of São Paulo, São Paulo, Brazil (M.B. Labruna, T.F. Martins); Universidade Estadual do Maranhão, São Luís, Brazil (F.B. Costa); Asociación Colombiana de Infectología, Bogotá, Colombia (Á.A. Faccini-Martínez)

DOI: https://doi.org/10.3201/eid2609.201305

Rickettsia rickettsii infection is the only rickettsiosis included in the list of reportable diseases in Brazil, where typhus group rickettsioses, mainly murine typhus, have been underreported. We report a case of typhus group rickettsiosis with unique ecologic particularities in a patient from the Brazilian Amazon, where, to our knowledge, rickettsioses have not been reported.

Typhus group rickettsioses are vectorborne infectious diseases that include murine typhus, caused by *Rickettsia typhi*, and epidemic typhus, caused by *R. prowazekii* (*1*). *R. typhi* is maintained in an enzootic cycle involving small mammals (e.g., *Rattus* spp. rats and *Didelphis* spp. opossums) and their ectoparasites, mainly fleas (*2*). *R. typhi* is usually transmitted to humans by contamination of the bite site, mucosal or skin abrasions with rickettsia-containing ectoparasite feces, or inhalation in contaminated dust (*2*). *R. prowazekii* is transmitted mainly by feces of human clothing lice (*Pediculus humanus humanus*) or a sylvatic cycle in the United States by contact with ectoparasites of flying squirrels (*1*).

In Brazil, there have been few reports of murine typhus, mostly >60 years ago and all from human-modified landscapes in southeastern or southern regions, far from the Amazon (*3*). To our knowledge, Brazil has had only 1 case of recrudescent, epidemic typhus (Brill-Zinsser disease) in a refugee from Europe (*4*). Currently, Brazilian spotted fever (*R. rickettsii* infection), a tickborne disease, is the only rickettsiosis included in the list of notifiable diseases in Brazil (*3*). We report a new case of typhus group rickettsiosis in a patient from the Brazilian Amazon.

On August 27, 2019, a 37-year-old man was admitted to a hospital at Porto Trombetas District (Pará State, eastern Amazon region of Brazil) (Figure) because of 4 days of fever, chills, headache, malaise, and productive cough, associated with mild respiratory distress 72 hours after fever onset. His daily work consisted of outdoor herpetologic monitoring activities in Saracá-Taquera National Forest (35 km from Porto Trombetas) during the 2 weeks before disease onset. He reported that while in the forest, he removed an attached tick from his right thigh 10 days before disease onset.

Physical examination showed fever (temperature 38.3°C), tachycardia, tachypnea, O_2 saturation 91%, bilateral inguinal lymphadenopathy, no rash, and a furuncle lesion at the site of the tick bite on the right thigh, and no inoculation eschar. Blood analysis showed leukocytosis (15,000 cells/mm^3); neutrophilia (84%); standard platelet count (221,000 platelets/μL); and increased levels of alanine aminotransferase (50 U/L), aspartate aminotransferase (38 U/L), and C-reactive protein (20 mg/L). Chest radiograph showed bilateral interstitial pulmonary infiltrates. Presumptive diagnoses of Lyme borreliosis or Brazilian spotted fever was made and the patient was admitted.

Supplementary oxygen, ceftriaxone, chloramphenicol, and doxycycline were administered, and serologic tests for *Borrelia burgdorferi* and *Rickettsia* spp. were performed. Twenty-four hours later, the patient showed clinical stability, major improvement of respiratory status, and no fever. After 7 days of antimicrobial drug treatment, he was discharged with complete resolution of symptoms.

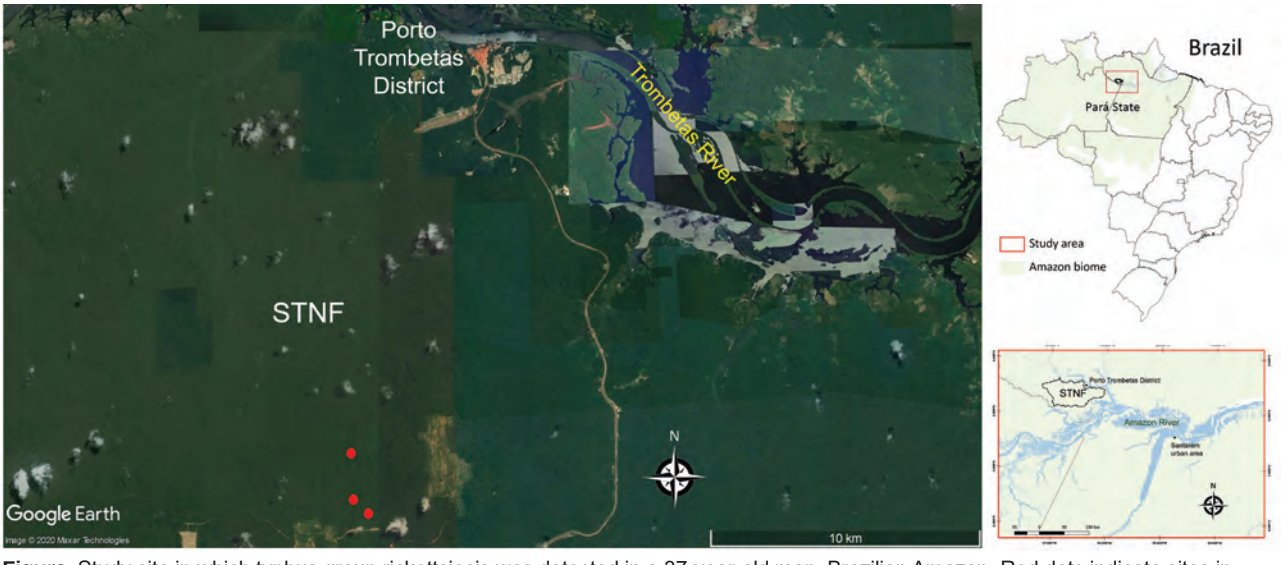

Figure. Study site in which typhus group rickettsiosis was detected in a 37-year-old man, Brazilian Amazon. Red dots indicate sites in STNF in which the patient worked during the day in the 2 weeks before disease onset. During this same period, he spent the night at his house in Porto Trombetas District, where he denied any rat infestation. Insets show location of STNF in Pará state and Brazil. STNF, Saracá-Taquera National Forest.

A serum sample collected on August 28 (5 days after disease onset) showed negative results by commercial ELISA for *B. burgdorferi* IgM and IgG. Results of indirect fluorescent antibody assays were nonreactive for *R. conorii* IgG but positive (titer 1:64) for *R. typhi* IgG.

To confirm a presumptive diagnosis of rickettsiosis, we collected a second serum sample 2 months later and showed by using an in-house indirect fluorescent antibody assays (*5*) negative results for IgG (titer <1:64) against 6 *Rickettsia* species: *R. felis*; *R. bellii*; and the spotted fever group agents *R. rickettsii*, *R. parkeri*, *R. amblyommatis*, and *R. rhipicephali*. This serum sample had a titer of 1:2,048 against *R. typhi* (Wilmington strain), confirming typhus group rickettsiosis.

There have been previous reports of typhus group rickettsiae in ticks from other areas (*6*,*7*). After we considered the tick bite history of the patient, during October 12–14, 2019, we went to areas in Saracá-Taquera National Forest that the patient visited and collected 170 ticks in 7 species. Attempts to detect rickettsial DNA in these ticks showed only *R. amblyommatis* in *Amblyomma cajennense* sensu stricto ticks (Appendix, https://wwwnc.cdc.gov/EID/article/26/9/20-1305-App1.pdf).

In a retrospective interview, the patient recalled 3 additional activities during the 2 weeks before disease onset: a daily rest in the forest for a few minutes after work, seeking work materials in a small mammal trap-storage at a facility within the natural forest, and 2 short visits to his mother's house in the urban area of Santarém municipality (Pará State). He denied rat infestation in his own house at Porto Trombetas but reported previous rat infestations in his mother's house.

Borreliosis and rickettsioses have not been confirmed in the Brazilian Amazon (*8*). The patient's tick bite history before onset of symptoms led clinicians to presume these diagnoses and initiate appropriate antimicrobial drug treatment (e.g., doxycycline) (*1*), with a successful outcome. Because *R. amblyommatis*, a possibly nonpathogenic species (*1*), was the only agent detected in collected ticks, we consider that the furuncle lesion at the site of the tick bite was a pyogenic, localized, skin infection, and not rickettsia related.

Because of similar clinical manifestations and serologic cross-reactions between typhus group rickettsiae (*1*), we could not confirm the typhus group etiologic agent of this case-patient. We presume *R. typhi* as a probable infection because he had potential occupational exposures with rodents or other small mammals and their ectoparasites, rather than clothing louse infestation (*1*), in addition to an absence of neurologic symptoms, which are more common for epidemic typhus than for murine typhus (*9*,*10*). Conversely, the fact that the patient had spent most of his time in a forest environment could also implicate a sylvatic cycle of typhus group rickettsia in the Amazon forest.

Acknowledgments

We thank Thiago Moreira and Osvaldo Nunes for providing assistance during tick sampling; Guilheme and Helder Batista for providing logistical support; and Carlos Pinheiro and all personnel from the Chico Mendes Institute for Biodiversity Conservation in Porto Trombetas for providing valuable assistance in expediting authorizations and logistic support in the field.

About the Author

Dr. Minervino is an associate professor at the Federal University of Western Pará, Santarém, Brazil. His research interests include epidemiology of tick-borne diseases.

References

1. Fang R, Blanton LS, Walker DH. Rickettsiae as emerging infectious agents. Clin Lab Med. 2017;37:383–400. https://doi.org/10.1016/j.cll.2017.01.009
2. Azad AF. Epidemiology of murine typhus. Annu Rev Entomol. 1990;35:553–69. https://doi.org/10.1146/annurev.en.35.010190.003005
3. Silva LJ, Papaiordanou PM. Murine (endemic) typhus in Brazil: case report and review. Rev Inst Med Trop São Paulo. 2004;46:283–5. https://doi.org/10.1590/S0036-46652004000500010
4. Meira JA, Jamra M, Lodovici J. Brill's disease: (epidemic typhus recrudescence) (in Portuguese). Rev Hosp Clin Fac Med Sao Paulo. 1955;10:237–46.
5. Angerami RN, Krawczak FS, Nieri-Bastos FA, Santos F, Medorima C, Ribeiro Resende M, et al. First report of African tick-bite fever in a South American traveler. SAGE Open Med Case Rep. 2018;6:2050313X18775301.
6. Medina-Sanchez A, Bouyer DH, Alcantara-Rodriguez V, Mafra C, Zavala-Castro J, Whitworth T, et al. Detection of a typhus group *Rickettsia* in *Amblyomma* ticks in the state of Nuevo Leon, Mexico. Ann N Y Acad Sci. 2005;1063:327–32. https://doi.org/10.1196/annals.1355.052
7. Dzul-Rosado K, Lugo-Caballero C, Tello-Martin R, López-Avila K, Zavala-Castro J. Direct evidence of *Rickettsia typhi* infection in *Rhipicephalus sanguineus* ticks and their canine hosts. Open Vet J. 2017;7:165–9. https://doi.org/10.4314/ovj.v7i2.14
8. Rodriguez-Morales AJ, Bonilla-Aldana DK, Idarraga-Bedoya SE, Garcia-Bustos JJ, Cardona-Ospina JA, Faccini-Martínez ÁA. Epidemiology of zoonotic tick-borne diseases in Latin America: are we just seeing the tip of the iceberg? F1000 Res. 2018;7:1988. https://doi.org/10.12688/f1000research.17649.1
9. Tsioutis C, Zafeiri M, Avramopoulos A, Prousali E, Miligkos M, Karageorgos SA. Clinical and laboratory characteristics, epidemiology, and outcomes of murine typhus: a systematic review. Acta Trop. 2017;166:16–24. https://doi.org/10.1016/j.actatropica.2016.10.018
10. Bechah Y, Capo C, Mege JL, Raoult D. Epidemic typhus. Lancet Infect Dis. 2008;8:417–26. https://doi.org/10.1016/S1473-3099(08)70150-6

Address for correspondence: Álvaro A. Faccini-Martínez, Asociación Colombiana de Infectología, Carrera 15 No.118-03, Bogotá, Colombia; email: afaccini@gmail.com

Rhabdomyolysis as Potential Late Complication Associated with COVID-19

Ying-Chao He, Feng Chen

Author affiliation: Fujian Provincial Hospital, Fuzhou, Fujian, China

DOI: https://doi.org/10.3201/eid2609.201463

To the Editor: We provide follow-up information on a case discussed in Emerging Infectious Diseases of a man with severe acute respiratory syndrome coronavirus 2 (SARS-CoV-2) infection who reportedly had late-onset rhabdomyolysis with lower limb pain and fatigue (*1*). After the patient was stabilized, he was transferred to Wuhan Union Hospital with medical support by Fujian Provincial Hospital, where he disclosed symmetric weakness (Medical Research Council grade 4/5) in both lower limbs with weakened deep tendon reflexes and decreased sensation to light touch and pinprick distally. Because weakness and paresthesia persisted after biochemistries normalized, we feel that these observations are not explained solely by rhabdomyolysis.

The patient was discharged 43 days after admission and was able to walk normally but with reduced endurance. Electromyography (day 120) showed motor and sensory fiber involvement in both lower extremities, presenting as axonal injury accompanied by demyelination (Tables 1, 2). Despite his 10-year history of diabetes, the patient reported no history of paresthesia or reduced motor endurance, which ruled against preexisting diabetic neuropathy or myopathy. We believe he developed peripheral neuropathy during his COVID-19 illness, which may have been missed during the acute phase. We are unsure what caused this neuropathy. In addition to hematologic or lymphatic spread, coronaviruses may directly invade the peripheral nerve terminals and interfere with subsequent synaptic transfer (*2*). Indirect causes, such as cytokine-mediated damage, should also be considered in this patient (*3*). Finally, thromboembolism has the potential to cause peripheral nerve ischemia and necrosis (*4*). However, the coagulation indices, including fibrinogen (7.95 g/L, reference 2–4 g/L), D-dimer (>20 mg/L, reference <0.5mg/L), and fibrinogen degradation products (80 μg/mL, reference <5 μg/mL), were at the highest level at the onset of rhabdomyolysis and gradually decreased with enoxaparin treatment. We cannot offer a definitive diagnosis and were limited by the lack of muscle biopsies and complete electromyography; however, several factors may have caused his peripheral neuropathy.

About the Authors

Dr. He is a neurologist and Dr. Chen is an emergency physician in Fujian Provincial Hospital, Fujian, China. During the COVID-19 outbreak, they worked as a support medical team in the isolation ward of Union Hospital, Tongji Medical College, Wuhan, China.

References

1. Jin M, Tong Q. Rhabdomyolysis as potential late complication associated with COVID-19. Emerg Infect Dis. 2020 Mar 20 [Epub ahead of print]. https://doi.org/10.3201/eid2607.200445

Table 1. Motor nerve conduction studies on a patient with rhabdomyolysis after severe acute respiratory syndrome coronavirus 2 infection, China

Location	Distal latency, ms	Amplitude, mV	Conduction velocity, m/s	F latency, ms
Left tibial nerve				
Ankle-abductor hallucis brevis	6.5 (reference ≤5.1)	0.825 (reference ≥4)	38 (reference ≥40)	51.4 (reference ≤56)
Popliteal fossa	15.4	0.755		
Right tibial nerve				
Ankle-abductor hallucis brevis	6.3 (reference ≤5.1)	5.4 (reference ≥4)	39 (reference ≥40)	49.4 (reference ≤56)
Popliteal fossa	15.0	4.46		
Left peroneal nerve				
Ankle-extensor digitorum brevis	5.1 (reference ≤5.5)	1.061 (reference ≥2)	35 (reference ≥42)	Not tested
Below fibula	11.6	1.022		
Right peroneal nerve				
Ankle-extensor digitorum brevis	3.8 (reference ≤5.5)	1.947 (reference ≥2)	33 (reference ≥42)	Not tested
Below fibula	10.7	1.328		

Table 2. Antidromic sensory nerve conduction studies on a patient with rhabdomyolysis after severe acute respiratory syndrome coronavirus 2 infection, China

Location	Amplitude, μV	Conduction velocity, m/s
Left superficial fibular nerve: lateral calf–lateral ankle	Absent	Absent
Right superficial fibular nerve: lateral calf–lateral ankle	5.879 (reference ≥6)	37 (reference ≥40)
Left sural nerve: calf–posterior ankle	Absent	Absent
Right sural nerve: calf–posterior ankle	4.225 (reference ≥6)	37 (reference ≥40)

2. Ding Y, He L, Zhang Q, Huang Z, Che X, Hou J, et al. Organ distribution of severe acute respiratory syndrome (SARS) associated coronavirus (SARS-CoV) in SARS patients: implications for pathogenesis and virus transmission pathways. J Pathol. 2004;203:622–30. https://doi.org/10.1002/path.1560
3. Ye Q, Wang B, Mao J. The pathogenesis and treatment of the "cytokine storm" in COVID-19. J Infect. 2020;80:607–13. https://doi.org/10.1016/j.jinf.2020.03.037
4. Wichmann D, Sperhake J-P, Lütgehetmann M, Steurer S, Edler C, Heinemann A, et al. Autopsy findings and venous thromboembolism in patients with COVID-19. Ann Intern Med. 2020 May 6 [Epub ahead of print]. https://doi.org/10.7326/M20-2003

Address for correspondence: Feng Chen, Emergency Department, Fujian Provincial Hospital, Fujian Provincial Clinical College of Fujian Medical University, Fuzhou, Fujian 350001, China; email: fjslchenfeng@126.com

COVID-19 Outbreak Associated with Air Conditioning in Restaurant, Guangzhou, China, 2020

Francis W. Moses, Ricardo Gonzalez-Rothi, Gene Schmidt

Author affiliations: Moses Engineering, Gainesville, Florida, USA (F.W. Moses); Florida State University, Tallahassee, Florida, USA (R. Gonzalez-Rothi); Schmidt Consulting Group, Pensacola, Florida, USA (G. Schmidt)

DOI: https://doi.org/10.3201/eid2609.201749

To the Editor: Lu et al. (*1*) describe the indoor airborne spread of COVID-19 (coronavirus disease) facilitated by a type of standard, wall-mounted, ductless air conditioner (AC) used in most countries. These units are low-cost in comparison to ducted AC units, which can cost 3 times as much to purchase, install, and operate. Ductless units cool and dehumidify indoor air but have little ability to filter or remove airborne contaminants.

A wall-mounted ductless system blows air directly onto those closest to it, potentially disseminating infectious droplets or aerosols along the airflow. Lu et al. use arrows to point out the airflows emanating from and returning to the AC unit, delineating a possible trajectory of putative airborne droplets. This trajectory coincides with the seating distribution of other persons at the restaurant who later became ill (*1*). We agree that the AC probably contributed to the upstream and downstream airborne spread of the virus.

The type of AC system required to mitigate airborne transmission is neither affordable nor architecturally feasible for many buildings or regions. To prevent the spread of coronavirus disease in indoor spaces, we need work-around solutions in addition to distancing and fresh air exchange. Viable, low-cost possibilities might include operating AC on low fan settings and installing units near the ceiling, which would channel airflow towards the ceiling instead of directly onto patrons. Other methods might include installing high-efficiency particulate air filters, ultraviolet germicidal irradiation (which can disinfect some airborne coronaviruses such as mouse hepatitis virus and Middle Eastern respiratory syndrome coronavirus) (*2*), or a combination of these methods.

References

1. Lu J, Gu J, Li K, Xu C, Su W, Lai Z, et al. COVID-19 outbreak associated with air conditioning in restaurant, Guangzhou, China, 2020. Emerg Infect Dis. 2020 Apr 2 [Epub ahead of print]. https://doi.org/10.3201/eid2607.200764
2. Bedell K, Buchaklian AH, Perlman S. Efficacy of an automated multiple emitter whole-room ultraviolet-C disinfection system against coronaviruses MHV and MERS-CoV. Infect Control Hosp Epidemiol. 2016;37:598–9. https://doi.org/10.1017/ice.2015.348

Address for correspondence: Ricardo Gonzalez-Rothi, 12702 NW 112th Ave, Alachua, FL 32615, USA; email: ricg23@gmail.com

Nonpharmaceutical Measures for Pandemic Influenza in Nonhealthcare Settings—International Travel-Related Measures

Jaspreet Pannu

Author affiliation: Leland Stanford Junior University, Stanford, California, USA

DOI: https://doi.org/10.3201/eid2609.201990

To the Editor: Ryu et al. reviewed international travel–related measures for pandemic influenza, including screening travelers for infection (*1*). Although the authors did not review the performance of individual screening tools, Ryu et al. reported that no evidence exists to indicate that screening has any substantial effect on preventing the spread of pandemic influenza.

However, government officials continue to call for international airport screening guidelines as a crucial measure to control coronavirus disease. Therefore, differentiating between screening tools with poor technical performance and those approved for fever detection is worthwhile. For example, the Food and Drug Administration (FDA) states that thermal scanners should not be used as standalone tools for fever detection (*2*). FDA instead recommends that officials use handheld infrared thermometers as screening tools.

Thermal scanners use long-wave infrared to generate heat map images of persons and objects. This technology records surface temperature; however, fever determination requires a measurement of core body temperature. A study with 1,109 participants showed a correlation with core temperature of merely $R^2 = 0.41$ for the most commonly used thermography region, the forehead (*3*). Performance of $R^2 = 0.69$ was achieved only with overlaid standard camera video and complex free-form deformation models. Participants were assessed individually, after being seated for 15 minutes, without topical cosmetics or eyewear, at a stable ambient temperature and humidity, and without nearby infrared radiation sources. These conditions are rarely, if ever, met in the airport setting.

Despite this evidence, costly thermal scanners have been deployed at airports in many countries. In contrast, inexpensive infrared thermometers are FDA approved for core temperature approximation. At their current performance, thermal scanners must be clearly distinguished from infrared thermometers, and thermal scanning should not be recommended for fever screening.

References

1. Ryu S, Gao H, Wong JY, Shiu EYC, Xiao J, Fong MW, et al. Nonpharmaceutical measures for pandemic influenza in nonhealthcare settings—international travel-related measures. Emerg Infect Dis. 2020;26:961–6. https://doi.org/10.3201/eid2605.190993
2. US Food and Drug Administration. Enforcement policy for telethermographic systems during the coronavirus disease 2019 (COVID-19) public health emergency. 2020 Apr 16 [cited 2020 May 1] https://www.fda.gov/regulatory-information/search-fda-guidance-documents/enforcement-policy-telethermographic-systems-during-coronavirus-disease-2019-covid-19-public-health
3. Zhou Y, Ghassemi P, Pfefer J, Casamento J, McBride D, Chen M, et al. Large-scale clinical study of 'point of care' thermal imaging for febrile patient detection: towards optimal non-contact diagnostics in disease pandemics. In: Gannot I, editor. Proceedings volume 10872: optical fibers and sensors for medical diagnostics and treatment applications XIX. SPIE BiOS 10872; 2019 Mar 4; San Francisco, CA, USA. Bellingham (WA): Society of Photo-Optical Instrumentation Engineers; 2019 [cited 2020 May 1] https://www.spiedigitallibrary.org/conference-proceedings-of-spie/10872/108720X/Large-scale-clinical-study-of-point-of-care-thermal-imaging/10.1117/12.2514766.short?SSO=1

Address for correspondence: Jaspreet Pannu, Leland Stanford Junior University, 300 Pasteur Dr, Stanford, CA 94305, USA; email: jassi@stanford.edu

Clostridioides difficile in COVID-19 Patients, Detroit, Michigan, USA, March–April 2020

Saraswathi Lakkasani, Kok Hoe Chan, Hamid S. Shaaban

Author affiliation: Saint Michael's Medical Center, New York Medical College, Newark, New Jersey, USA

DOI: https://doi.org/10.3201/eid2609.202505

To the Editor: Sandhu et al. (*1*) reported 9 patients who were co-infected with severe acute respiratory syndrome coronavirus 2 (SARS-CoV-2) and *Clostridioides difficile*. *C. difficile* infection (CDI) can be a co-occurrence or result of antimicrobial drug overuse and is potentially a complication of coronavirus disease (COVID-19). We report a 52-year-old man with hypertension who had fever, respiratory symptoms, abdominal pain, and diarrhea for 3 days. At admission to Saint Michael's Medical Center (Newark, New Jersey, USA), he had a temperature of 101.8°F but was otherwise hemodynamically stable. He had an elevated absolute lymphocyte count (700 cells/μL), indicating lymphopenia. He tested positive for SARS-CoV-2 RNA by reverse transcription PCR and had elevated inflammatory markers on blood profile. He tested positive for *C. difficile* toxin and antigen at admission. He did not

use antimicrobial drugs or proton pump inhibitors and had no known contacts with persons with diarrhea. He was mechanically ventilated and received oral vancomycin, intravenous metronidazole, and vasopressors. He died of respiratory failure and septic shock. In comparison to the patients described by Sandhu et al., the patient we report was younger and did not have a history of antimicrobial use.

SARS-CoV-2 has multifaceted presentations. Angiotensin-converting enzyme 2 receptor, which can act as a receptor for severe acute respiratory syndrome coronavirus, is expressed not only in alveolar cells but also in the gastrointestinal tract, including colonic cells (*2*,*3*). Diarrhea associated with COVID-19 might erode the normal microbial flora of the gut, leading to increased risk for CDI. Also, COVID-19 might weaken the immune system, leaving the patient vulnerable to CDI. COVID-19 patients produce inadequate interferon-γ and have defective macrophage activation and function, resulting in a dysregulated immune response (*4*). Interleukin-12 and interferon-γ are components of cell-mediated immunity. Interferon-γ produced by T-helper cells induces macrophages to destroy bacteria such as *C. difficile* (*5*).

The relationship between SARS-CoV-2 and CDI is still poorly understood. CDI might be a complication of COVID-19; however, we could not exclude the possibility of co-occurrence of CDI with COVID-19. Physicians should consider CDI when encountering a COVID-19 patient with diarrhea.

References

1. Sandhu A, Tillotson G, Polistico J, Salimnia H, Cranis M, Moshos J, et al. *Clostridiodes difficile* in COVID-19 patients, Detroit, Michigan, USA, March–April 2020. Emerg Infect Dis. 2020 May 22 [Epub ahead of print]. https://doi.org/10.3201/eid2609.202126
2. Li W, Moore MJ, Vasilieva N, Sui J, Wong SK, Berne MA, et al. Angiotensin-converting enzyme 2 is a functional receptor for the SARS coronavirus. Nature. 2003;426:450–4. https://doi.org/10.1038/nature02145
3. Hamming I, Timens W, Bulthuis MLC, Lely AT, Navis G, van Goor H. Tissue distribution of ACE2 protein, the functional receptor for SARS coronavirus. A first step in understanding SARS pathogenesis. J Pathol. 2004;203:631–7. https://doi.org/10.1002/path.1570
4. Blanco-Melo D, Nilsson-Payant BE, Liu WC, Uhl S, Hoagland D, Møller R, et al. Imbalanced host response to SARS-CoV-2 drives development of COVID-19. Cell. 2020; 181:1036–1045.e9. https://doi.org/10.1016/j.cell.2020.04.026
5. Cruz-Adalia A, Veiga E. Close encounters of lymphoid cells and bacteria. Front Immunol. 2016;7:405. https://doi.org/10.3389/fimmu.2016.00405

Address for correspondence: Kok Hoe Chan, Saint Michael's Medical Center, Newark, NJ 07101, USA; email: kchan2@primehealthcare.com

Zika Virus Infection, Philippines, 2012

Corazon Cerilla Buerano, Lady-Anne Suarez Pangilinan, Maria Terrese Alonzo Dimamay, Cynthia Abad Mapua, Mark Pierre Sijo Dimamay, Ronald Roll Matias, Filipinas Florendo Natividad, Maria Luisa de Guzman Daroy, Futoshi Hasebe, Kouichi Morita, Meng Ling Moi

Author affiliations: St. Luke's Medical Center, Quezon City, Philippines (C.C. Buerano, L.-A.S. Pangilinan, M.T.A. Dimamay, C.A. Mapua, M.P.S. Dimamay, R.R. Matias, F.F. Natividad); St. Luke's Medical Center College of Medicine, Quezon City (M.L.G. Daroy); WHO Collaborating Centre for Reference and Research on Tropical and Emerging Viral Diseases, Institute of Tropical Medicine (NEKKEN), Nagasaki, Japan (F. Hasebe, K. Morita, M.L. Moi)

DOI: https://doi.org/10.3201/eid2609.190896

To the Editor: Alera et al. described a 2012 case of Zika virus infection in the Philippines (*1*). In 2007, a Zika virus outbreak occurred in Yap, Micronesia, possibly caused by travelers from the Philippines (*2*). Zika virus infections were reported in the Philippines in 1953, 2012, and 2016 (*3*). Although frequent travel exchange between Yap and the Philippines could be a possible transmission route, no data on Zika virus infection were recorded in the Philippines between 1953 and 2012.

We detected Zika virus infection in 1 (0.75%) of 134 febrile, non–dengue infected patients at St. Luke's Medical Center (Quezon City, the Philippines) during 2010–2015 by subjecting patient serum samples to serological and molecular tests. Ethics clearance (reference no. 19042) for this study was given by St. Luke's Medical Center Institutional Ethics Review Committee. The only patient who tested positive for Zika virus was a 31-year-old woman diagnosed with an upper respiratory tract infection in 2010. Because of her work, she might not have traveled internationally. We obtained her serum sample on day 3 of fever. She did not have a rash or arthralgia. Although we did not isolate Zika virus according to guidelines (*4*), we confirmed infection using other techniques. The patient's serum sample tested positive for Zika virus RNA, IgM against Zika virus, and neutralizing antibodies against Zika virus by using a plaque reduction neutralization test to neutralize 50% of plaques ($PRNT_{50}$) ($PRNT_{50}$ Zika virus = 1:80, $PRNT_{50}$ dengue virus serotypes 1–4 <1:10). The sample tested negative for IgM against dengue and Japanese encephalitis viruses but

positive for IgG against Zika virus nonstructural protein 1. These results suggest local Zika virus infection in the Philippines since at least 2010, 2 years earlier than the previously reported infection (*1*).

This work was supported by the Agency for Research and Development (AMED) under grant no. AMED JP-20wm0125006, AMED Research on Emerging and Re-emerging Infectious Diseases (grant nos. 19fk0108109h0001, 20fk0108109h0001, 20fk0108123h1101) and the Joint Usage/Research Center on Tropical Disease, Institute of Tropical Medicine, Nagasaki University (grant no. 2020-Ippan-21). Partial support came from the Research and Biotechnology Group, St. Luke's Medical Center, Quezon City, Philippines (project no. 07-024).

References

1. Alera MT, Hermann L, Tac-An IA, Klungthong C, Rutvisuttinunt W, Manasatienkij W, et al. Zika virus infection, Philippines, 2012. Emerg Infect Dis. 2015;21:722–4. https://doi.org/10.3201/eid2104.141707
2. Musso D, Gubler DJ. Zika Virus. Clin Microbiol Rev. 2016;29:487–524. https://doi.org/10.1128/CMR.00072-15
3. Duong V, Dussart P, Buchy P. Zika virus in Asia. Int J Infect Dis. 2017;54:121–8. https://doi.org/10.1016/j.ijid.2016.11.420
4. Centers for Disease Control and Prevention. Testing for Zika virus infection. 2019 Jun 13 [cited 2020 Jun 11]. https://www.cdc.gov/zika/laboratories/types-of-tests.html

Address for correspondence: Meng Ling Moi, Department of Virology, Institute of Tropical Medicine, Nagasaki University, 1-12-4 Sakamoto Nagasaki, Nagasaki, Nagasaki 852-8523, Japan; email: sherry@nagasaki-u.ac.jp

CORRECTION

Correction: Vol. 26, No. 7

The name of author Xiankun Zeng was misspelled in in Changes in Approach to Cataract Surgery in an Ebola Virus Disease Survivor with Prior Ocular Viral Persistence (J.R. Wells et al.). The article has been corrected online (https://wwwnc.cdc.gov/eid/article/26/7/19-1559_article).

Artist Unknown. Relief showing Helios, sun god in the Greco-Roman mythology (detail) (c.390 BCE). Marble. 33.8 in × 33.9 in × 8 5/8 in/85.8 cm × 86.3 cm. From Wikimedia Commons. Holding institution: Pergamon-Museum, Berlin, Germany.

The Concept of the Crown and Its Potential Role in the Downfall of Coronavirus

Terence Chorba

Coronavirus virions are spherical or variable in shape and composed of an outer layer of lipid covered with a crown of club-shaped peplomers or spikes. Within each spike is a helical single-stranded RNA–containing structural protein. Although the term *corona* was first used in English in the 1500s, it was borrowed directly from the Latin word for "crown." *Corona* is derived from the Ancient Greek κορώνη *(korōnè),* meaning "garland" or "wreath," coming from a proto-Indo-European root, *sker- or ker-*, meaning "to turn" or "to bend."

In the 1967 initial description of an electron microscopic image of a human common cold virus, June Almeida (née Hart) and David Tyrrell described the surface of coronavirus particles as being "covered with a distinct layer of projections roughly 200Å [20 nm] long….[with] a narrow stalk

Author affiliation: Centers for Disease Control and Prevention, Atlanta, Georgia, USA

DOI: https://doi.org/10.3201/eid2609.AC2609

just in the limit of resolution of the microscope and a 'head' roughly 100Å across". In micrographs, the club-shaped spikes that stud the surface of coronaviruses are glycoproteins that give the appearance of a radiate crown.

Our modern-day *corona* conceptualization of club-shaped spikes on the coronavirus surface comes from traditional representations of crowns as radiate headbands, worn as symbols of sovereign power, to liken that power to that of the sun. Solar deities have been integral in the development of cultures across the world. In predynastic Egypt, Atum was a solar deity associated with the sun god Ra, and Horus was the god of the sky and sun. In Buddhist cosmology, the bodhisattva (one who is on the path toward Buddhahood) of the sun, *Sūryaprabha*, and the bodhisattva of the moon, *Candraprabha*, are both classically represented as human figures with a background of radiate halos. In traditional Western art, such a solar crown is often represented as a curved band of points representing rays. Representations with radiate crowns date from the 3rd century BCE onward, beginning with their frequent inclusion in representations of Alexander III of Macedon (commonly referred to as Alexander the Great), who was likened to the sun deity, Helios (Figure 1).

Throughout ancient world references, the character of Helios is featured favorably. In the 12th book of the Odyssey, Homer refers to Helios as a god "who gives joy to mortals." This month's *EID* cover features a rendition of a sculpted metope, a rectangular carved marble plaque in a Doric frieze that was excavated from the Temple of Athena at Troy/Ilion by Heinrich Schliemann in 1872. This metope, dating from 300–280 BCE, depicts Helios driving a quadriga which is a chariot drawn by four horses abreast. In a later depiction of Helios seen on this page, the deity is represented in a bronze bust with seven rays radiating from a head of long hair. Found at the beginning of the last century in Tripoli, this bust dates from the 1st century CE and may also have been intended to serve as a portrait of Alexander himself.

In ancient Rome, the linkage between the power of rulers and the power of the sun was also frequently depicted on coinage. For example, a sovereign wearing a radiate crown on the front (obverse) of the coin and a personification of the sun also wearing a radiate crown and sometimes driving a quadriga on the back (reverse) was common. Figure 2 is an example of such coinage from 274 CE, featuring the emperor Aurelian wearing a radiate crown on the obverse, and, on the reverse, a personification of the official sun god of the later Roman Empire, the *Sol Invictus* (Unconquered Sun), also wearing a radiate crown. In the modern era, positive artistic depictions of liberty and peace have also worn radiate crowns including the Statue of Liberty and the silver US Peace Dollar (1921–1935) that was featured on the March 2018 cover of this journal.

Figure 1. Bust of Helios, radiate (seven rays), with long hair, wearing a chlamys, a short cloak worn by men in ancient Greece. 1st century CE. Public domain image by Marie-Lan Nguyen. Holding institution: Louvre Museum, Paris, France.

Helios and crowns are associated with power and joy in Western art in ways contradictory to the reality of the tragic pandemic that we are now experiencing with a novel pathogen featuring surface projections that are likened visually to the life-saving rays of the sun. Most recently, two illustrators at the Centers for Disease Control and Prevention, Alissa Eckert and Dan Higgins, have immortalized those surface projections in a creative, colored representation of SARS-CoV-2 that itself has "gone viral" in print and digital media (Figure 3). These same spike glycoproteins undergo cleavage into two units: a receptor-binding unit (in the globular head of the spike) and a fusion unit (in the stalk of the spike). The receptor-binding unit is responsible for the initial binding of coronaviruses to angiotensin-converting enzyme 2 receptors on the surface of endothelial cells of the human respiratory

Figure 2. Antoninianus (2 denarii silvered bronze coin) of the Roman emperor Aurelian, 274–275 CE. Obverse: IMP AVRELIANVS AVG [Emperor Aurelian Augustus]. Crowned and cuirassed bust of Aurelian facing right. Reverse: ORIENS AVG [Eastern (rising) sun Augustus]. Crowned figure of *Sol Invictus* [Unconquered Sun] holding laurel branch and bow, stepping on conquered enemy. Private collection, Atlanta, Georgia. Photography by Will Breedlove.

epithelium and other tissues; the fusion unit mediatesthe subsequent fusion of the virus with endothelial cell membranes.

Protruding surface proteins have served as primary targets for successful vaccine development for viruses other than coronavirus, for example, the hemagglutinin of influenza A and the surface glycoprotein of Ebola virus. For COVID-19, vaccine trials have begun in which the goal is primarily induction of immunologic responses to the spike protein of the virus *corona*. As is the case with other viruses, interaction of SARS-CoV-2 surface proteins with host cell receptors has also been an important target in the planned development of therapeutic drugs to block viral interactions with host cells. In the face of the current raging COVID-19 pandemic, it is hoped that the spikes of the radiate corona of SARS-CoV-2 will herald its downfall. If these spikes become targets of successful therapeutic and prophylactic interventions, we may somehow resolve the paradox of the resemblance of the spikes of this pathogen to the welcome rays of Helios.

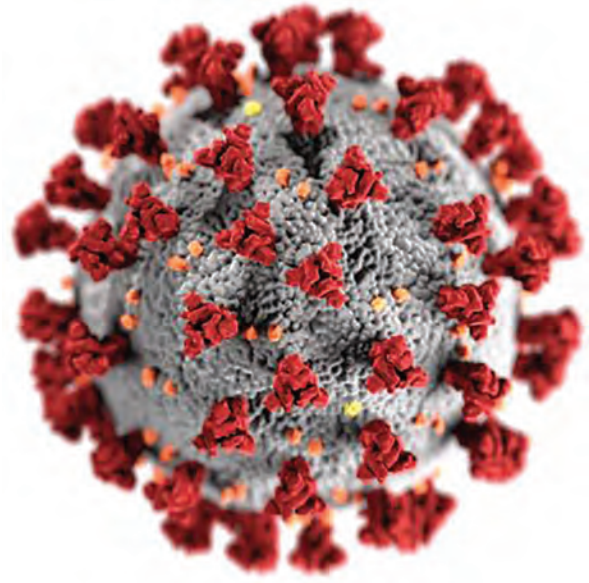

Figure 3. Illustration revealing ultrastructural morphology exhibited by coronaviruses. Note the spikes that adorn the outer surface of the virus, which impart the look of a corona surrounding the virion, when viewed electron microscopically. Public Health Image Library, CDC/Alissa Eckert, MSMI; Dan Higgins, MAMS.

Bibliography

1. Almeida JD, Tyrrell DA. The morphology of three previously uncharacterized human respiratory viruses that grow in organ culture. J Gen V irol. 1967;1:175–8. https://doi.org/10.1099/0022-1317-1-2-175
2. Chorba T. Peace, liberty, mycobacteria, and tuberculosis mortality. Emerg Infect Dis. 2018;24:611–2. https://doi.org/10.3201/eid2403.AC2403
3. Dhama K, Sharun K, Tiwari R, Dadar M, Malik YS, Singh KP, et al. COVID-19, an emerging coronavirus infection: advances and prospects in designing and developing vaccines, immunotherapeutics, and therapeutics.

Hum Vaccin Immunother. 2020;16:1232–8. https://doi.org/10.1080/21645515.2020.1735227
4. Giaimo C. The spiky blob seen around the world. New York Times, April 1, 2020 [cited 2020 Jul 23] https://www.nytimes.com/2020/04/01/health/coronavirus-illustration-cdc.html
5. Kam YW, Okumura Y, Kido H, Ng LF, Bruzzone R, Altmeyer R. Cleavage of the SARS coronavirus spike glycoprotein by airway proteases enhances virus entry into human bronchial epithelial cells in vitro. PLoS One. 2009;4:e7870. https://doi.org/10.1371/journal.pone.0007870
6. Li F. Structure, function, and evolution of coronavirus spike proteins. Annu Rev Virol. 2016;3:237–61. https://doi.org/10.1146/annurev-virology-110615-042301
7. Liu C, Zhou Q, Li Y, Garner LV, Watkins SP, Carter LJ, et al. Research and development on therapeutic agents and vaccines for COVID-19 and related human coronavirus diseases. ACS Cent Sci. 2020;6:315–31. https://doi.org/10.1021/acscentsci.0c00272
8. Orenstein JM, Banach B, Baker SC. Morphogenesis of coronavirus HCoV-NL63 in cell culture: A transmission electron microscopic study. Open Infect Dis J. 2008;2:52–8. https://doi.org/10.2174/1874279300802010052
9. Wikimedia Commons. File: Helios with chlamys Louvre AO7530.jpg [cited 2020 Jul23]. https://commons.wikimedia.org/wiki/File:Helios_with_chlamys_Louvre_AO7530.jpg
10. World Health Organization. Draft landscape of COVID-19 candidate vaccines [cited 2020 Jun 24]. https://www.who.int/publications/m/item/draft-landscape-of-covid-19-candidate-vaccines

Address for correspondence: Terence Chorba, Centers for Disease Control and Prevention, 1600 Clifton Rd NE, Mailstop US 12-4, Atlanta, GA 30329-4027, USA; email: tlc2@cdc.gov

EMERGING INFECTIOUS DISEASES®

Upcoming Issue

- Operating Protocols of a Community Treatment Center for Isolation of Patients with Coronavirus Disease, South Korea
- Community Treatment Centers for Isolation of Asymptomatic and Mildly Symptomatic Patients with Coronavirus Disease, South Korea
- Clinical Course of Asymptomatic and Mildly Symptomatic Patients with Coronavirus Disease Admitted to Community Treatment Centers, South Korea
- Investigations of Shiga Toxin–Producing *Escherichia coli* Outbreaks Linked to Leafy Greens, United States and Canada, 2009–2018
- Healthcare-Associated Legionnaires' Disease, Europe, 2008–2017
- Nationwide External Quality Assessment of SARS-CoV-2 Molecular Testing, South Korea
- Sequential Acquisition of Human Papillomavirus Infection at Genital and Anal Sites, Liuzhou, China
- Impact of Social Distancing Measures on Coronavirus Disease Healthcare Demand, Central Texas, USA
- Multicenter Prevelance Study Comparing Molecular and Toxin Assays for *Clostridioides difficile* Surveillance, Swtizerland
- Association between Shiga Toxin–Producing *Escherichia coli* O157:H7 Subtype and Disease Severity, England, 2009–2019
- Effect of Nonpharmaceutical Interventions on Transmission of Severe Acute Respiratory Syndrome Coronavirus 2, South Korea, 2020
- Rapid, Sensitive, Full-Genome Sequencing of Severe Acute Respiratory Syndrome Coronavirus 2
- Seoul Orthohantavirus in Wild Black Rats, Senegal, 2012–2013
- Emerging Sandfly-borne Phlebovirus in China
- Silent Circulation of Rift Valley Fever in Humans in Botswana
- Contact Tracing during Coronavirus Disease Outbreak, South Korea, 2020
- Main Routes of Entry and Genomic Diversity of SARS-CoV-2, Uganda
- High Proportion of Asymptomatic SARS-CoV-2 Infections in 9 Long-Term Care Facilities, Pasadena, California, USA, April 2020
- Coronavirus Disease among Persons with Sickle Cell Disease, United States, March 20–May 21, 2020
- Highly Pathogenic *Francisella hispaniensis* Infections Causing Multiple Organ Failure Related to Seawater Exposure
- Basic Reproduction Number of Chikungunya Virus Transmitted by Aedes Mosquitoes
- Limitations of Ribotyping as Genotyping Method for Corynebacterium ulcerans
- Polyester Vascular Graft Material and Risk for Intracavitary Thoracic Vascular Graft Infection
- COVID-19 in Patient with Sarcoidosis Receiving Long-Term Hydroxychloroquine Treatment, France, 2020
- Undetected Circulation of African Swine Fever in Wild Boar, Asia
- Review of Mental Health Response to COVID-19, China
- Viral RNA Load in Mildly Symptomatic and Asymptomatic Children with COVID-19, Seoul
- Q Fever Endocarditis and a New Genotype of *Coxiella burnetii*, Greece
- Antibody Responses to SARS-CoV-2 at 8 Weeks Postinfection in Asymptomatic Patients
- Disappearance of SARS-CoV-2 Antibodies in Infants Born to Women with COVID-19, Wuhan, China
- Relative Bradycardia in Patients with Mild-to-Moderate Coronavirus Disease, Japan
- Culture-Competent SARS-CoV-2 in Nasopharynx of Symptomatic Neonates, Children, and Adolescents
- Retrospective Screening for SARS-CoV-2 RNA in California, USA, Late 2019
- Coronavirus Disease Exposure and Spread from Nightclubs, South Korea

Complete list of articles in the October issue at http://www.cdc.gov/eid/upcoming.htm

Earning CME Credit

To obtain credit, you should first read the journal article. After reading the article, you should be able to answer the following, related, multiple-choice questions. To complete the questions (with a minimum 75% passing score) and earn continuing medical education (CME) credit, please go to http://www.medscape.org/journal/eid. Credit cannot be obtained for tests completed on paper, although you may use the worksheet below to keep a record of your answers.

You must be a registered user on http://www.medscape.org. If you are not registered on http://www.medscape.org, please click on the "Register" link on the right hand side of the website.

Only one answer is correct for each question. Once you successfully answer all post-test questions, you will be able to view and/or print your certificate. For questions regarding this activity, contact the accredited provider, CME@medscape.net. For technical assistance, contact CME@medscape.net. American Medical Association's Physician's Recognition Award (AMA PRA) credits are accepted in the US as evidence of participation in CME activities. For further information on this award, please go to https://www.ama-assn.org. The AMA has determined that physicians not licensed in the US who participate in this CME activity are eligible for AMA PRA Category 1 Credits™. Through agreements that the AMA has made with agencies in some countries, AMA PRA credit may be acceptable as evidence of participation in CME activities. If you are not licensed in the US, please complete the questions online, print the AMA PRA CME credit certificate, and present it to your national medical association for review.

Article Title

Invasive Infections with *Nannizziopsis obscura* Species Complex in 9 Patients from West Africa, France, 2004–2020

CME Questions

1. Your patient is a 58-year-old immunocompromised man from sub-Saharan West Africa who presents with nodular skin lesions and a mass on chest radiology. On the basis of the case series of 9 patients by Garcia-Hermoso and colleagues, which one of the following statements about clinical features of invasive fungal infection with *Nannizziopsis obscura* species complex is correct?

A. Most patients had B-cell immunocompromise
B. The most frequently involved sites clinically were kidney and liver
C. Most patients who were treated received mainly azole therapy
D. There were no known deaths

2. According to the case series by Garcia-Hermoso and colleagues, which one of the following statements about microbiological features of invasive fungal infection with *N. obscura* species complex is correct?

A. Few isolates had low minimum inhibitory concentrations for the 8 antifungal drugs tested
B. The human strains of N. obscura were the same as those isolated from reptiles, based on multilocus sequence analysis
C. Nannizziopsis spp. have specific features in culture
D. The most common finding at pathology or direct microbiological examination was the presence of nonspecific hyaline, septate, smooth-walled hyphae

3. On the basis of the case series by Garcia-Hermoso and colleagues, which one of the following statements about clinical implications of features of invasive fungal infection with *N. obscura* species complex is correct?

A. *N. obscura* infection is probably underestimated, as identification is possible only by sequencing, which requires a tissue biopsy
B. The study proves that the portal of entry is via breaks in the skin
C. The study proves that voriconazole is the initial treatment of choice
D. Pharmacotherapy is the only treatment option

Earning CME Credit

To obtain credit, you should first read the journal article. After reading the article, you should be able to answer the following, related, multiple-choice questions. To complete the questions (with a minimum 75% passing score) and earn continuing medical education (CME) credit, please go to http://www.medscape.org/journal/eid. Credit cannot be obtained for tests completed on paper, although you may use the worksheet below to keep a record of your answers.

You must be a registered user on http://www.medscape.org. If you are not registered on http://www.medscape.org, please click on the "Register" link on the right hand side of the website.

Only one answer is correct for each question. Once you successfully answer all post-test questions, you will be able to view and/or print your certificate. For questions regarding this activity, contact the accredited provider, CME@medscape.net. For technical assistance, contact CME@medscape.net. American Medical Association's Physician's Recognition Award (AMA PRA) credits are accepted in the US as evidence of participation in CME activities. For further information on this award, please go to https://www.ama-assn.org. The AMA has determined that physicians not licensed in the US who participate in this CME activity are eligible for AMA PRA Category 1 Credits™. Through agreements that the AMA has made with agencies in some countries, AMA PRA credit may be acceptable as evidence of participation in CME activities. If you are not licensed in the US, please complete the questions online, print the AMA PRA CME credit certificate, and present it to your national medical association for review.

Article Title

Q Fever Osteoarticular Infection in Children

CME Questions

1. Which one of the following statements regarding the laboratory diagnosis of *Coxiella burnetii* infection is most accurate?

A. The best way to identify *C. burnetii* is with standard cultures
B. Indirect immunofluorescence assay (IFA) is the preferred serology test for *C. burnetii*
C. Complement fixation test (CFT) has a higher sensitivity compared with IFA
D. Qualitative polymerase chain reaction (qPCR) for *C. burnetii* is not available yet

2. Which one of the following findings constitutes a definite criterion for the diagnosis of persistent Q fever osteoarticular infection (OAI)?

A. Positive blood PCR
B. Positive bone, synovial biopsy, or joint aspirate PCR
C. IgG I antibodies of at least 800 mg/dL
D. The presence of mono- or polyarthralgia

3. Which one of the following joints was affected by Q fever OAI in each of the 3 cases in the current study?

A. Hand/wrist
B. Ankle/foot
C. Knee
D. Hip

4. Which one of the following statements regarding the treatment of Q fever OAI among children is most accurate?

A. Beta-lactam antibiotics are preferred among children younger than 8 years
B. Tetracyclines are preferred among children younger than 8 years
C. The minimal treatment duration is 3 months
D. Surgical debridement may be necessary even with adequate antimicrobial therapy